A multiple endpoint approach to predict the hepatotoxicity of pharmaceuticals *in vitro*

Zur Erlangung des akademischen Grades eines

DOKTORS DER NATURWISSENSCHAFTEN

(Dr. rer. nat.)

Fakultät für Chemie und Biowissenschaften

Karlsruher Institut für Technologie (KIT) - Universitätsbereich

genehmigte

DISSERTATION

von

Dipl.-Ing. (FH) Germaine Loredana Truisi

aus

Weinheim

Dekan: Prof. Dr. Peter Roesky
Referent: PD Dr. Stefan O. Müller
Koreferent: Prof. Dr. Doris Wedlich
Tag der mündlichen Prüfung: 18. Juli 2014

Declaration of originality

I, Germaine Loredana Truisi, hereby declare that the intellectual content and writing of this thesis is product of my own work. I have used no other sources except as noted by citations. Any contribution by others, with whom I worked within the framework of the EU-project 'Predict-IV' or elsewhere, have been explicitly acknowledged as such. This thesis has not been published anywhere else or has been presented to any other examination board.

Limburgerhof, 24th May 2014	Germaine L. Truisi
Place, Date	Signature

Acknowledgement

I want to thank everyone for their support during my doctoral thesis.

Ai miei genitori
(To my parents)

Abstract

The rising costs and increasing attrition rates during drug development force the pharmaceutical industry to review and improve standard testing strategies. Hepatotoxicity is still the major cause for the failure of new drug candidates in pre-clinical and clinical phases. Therefore, there is an urgent need for more predictive models to identify the toxic potential of new drug candidates. More specifically, the role of drug-induced mitochondrial dysfunction is becoming an increasingly important mechanism to study in liver toxicity. To date, promising *in vitro* systems lack full acceptance, mainly because they deliver only discrete information on single endpoints.

In this work, a new testing strategy approach was evaluated to predict the hepatotoxic potential of pharmaceuticals. For this purpose, primary rat (PRH) and human hepatocytes (PHH) cultured in an optimised sandwich configuration (cells between two hydrated layers of collagen) were used; thus, allowing the long-term, repeat-dosing of drugs. The strategy based on a comprehensive evaluation of multiple endpoints, including cytotoxicity, biokinetic profiling, transcriptomics and proteomics. Pharmaceuticals with known toxicities and pharmacokinetic properties in rats and humans were used as model compounds, namely ibuprofen, chlorpromazine, cyclosporine A and amiodarone. The cell cultures were treated daily with two concentrations per compound for up to 14 days. After 1, 3 and 14 days of exposure, samples were prepared for global transcriptomics and proteomics analyses. At five specific time points on the first and last treatment day samples of cell lysate and medium supernatant were collected for biokinetics. To address drug-induced mitochondrial dysfunction directly, a second focus of the thesis was on the assessment of mitochondrial toxicity using functional assays. Therefore, adenosine triphosphate levels and cellular respiration were measured in PRH and the human hepatoma cell lines, HepG2 and HepaRG.

The determination of the compounds' biokinetic profiles showed that the *in vitro* bioavailability of the drugs was mainly influenced by biological factors e.g. cellular metabolism and/or enzyme inhibition/induction. Furthermore, the biokinetic data revealed species differences that were in accordance with the literature. Global transcriptomics provided compound-specific profiles which allowed the elucidation of their underlying mechanisms of toxicity. In addition, different susceptibilities of PHH from different human donors were identified. Here, basal CYP activities helped explain donor differences observed in the biokinetic and transcriptomic profiling; hence, supporting the assumption that CYP-mediated metabolism plays a central role in inter-donor variation. Proteomics mirrored the comprehensive transcriptomic profiling to some extent and complemented information known for the drugs. The experiments on mitochondrial function revealed that all compounds affected cellular respiration; albeit at concentrations greatly exceeding the human therapeutic concentrations.

In conclusion, the endpoints described here using primary hepatocytes provided valuable mechanistic information on altered cellular functions. This knowledge will ultimately advance

our understanding of drug-induced hepatotoxicity. Furthermore, the early identification of species differences would help to translate and interpret pre-clinical findings to the human situation.

Zusammenfassung

Steigende Ausgaben und die zunehmende Terminierung vieler Wirkstoffkandidaten während der Arzneimittelentwicklung stellen die pharmazeutische Industrie vor die Herausforderung, standardisierte Sicherheitsprüfungen zu überdenken. Da Hepatotoxizität nach wie vor die Hauptursache für das Scheitern neuer Wirkstoffe in präklinischen und klinischen Phasen ist, besteht die Notwendigkeit, neue prädiktive Modelle zu entwickeln, welche zur Bestimmung der Hepatotoxizität neuer Wirkstoffe herangezogen werden können. Weiterhin erlangt die arzneimittelinduzierte mitochondriale Toxizität als zugrundeliegender Mechanismus der Hepatotoxizität immer mehr an Bedeutung. Derzeitig mangelt es jedoch selbst vielversprechenden *in vitro* Systemen weitestgehend an Akzeptanz, hauptsächlich weil sie nur begrenzte Information zu einzelnen Endpunkten liefern.

Die vorliegende Arbeit beschäftigt sich mit der Bewertung einer neuen Teststrategie zur Vorhersage des hepatotoxischen Potenzials von Arzneimitteln. Hierfür wurden primäre Ratten- (PRH) und humane Hepatozyten (PHH) unter optimierten Kulturbedingungen im Sandwichformat (Zellen zwischen zwei hydratisierten Kollagenschichten) verwendet. Das sogenannte „Sandwichformat“ ermöglichte die Langzeitkultur und somit die wiederholte Substanzbehandlung der Zellen. Die Teststrategie basierte auf einer umfassenden Auswertung mehrerer Endpunkte, darunter Zytotoxizität, Biokinetik, Transcriptomics und Proteomics. Aufgrund der bekannten toxischen und pharmakokinetischen Eigenschaften in Ratte und Mensch dienten Ibuprofen, Chlorpromazin, Cyclosporin A und Amiodaron hierbei als Referenzsubstanzen. Über einen Zeitraum von insgesamt 14 Tagen wurden die Hepatozytenkulturen täglich mit zwei Konzentrationen der jeweiligen Substanz behandelt. Proben für Transcriptomics und Proteomics wurden nach 1-, 3- und 14-tägiger Behandlung aufgearbeitet. Des Weiteren wurden für die Analyse der Biokinetik Zelllysate und Überstände des Kulturmediums zu jeweils fünf spezifischen Zeitpunkten des ersten und letzten Behandlungstages entnommen. Zur Detektion einer arzneimittelinduzierten Dysfunktion der Mitochondrien lag der zweite Fokus der Arbeit darin, die mitochondriale Toxizität mittels funktioneller Experimente zu beurteilen. Zu diesem Zwecke wurden Adenosintriphosphat-Gehalte und zelluläre Atmung in PRH sowie in den humanen Hepatomzelllinien HepG2 und HepaRG gemessen.

Die biokinetischen Profile der einzelnen Substanzen zeigten, dass die Bioverfügbarkeit der Substanzen *in vitro* hauptsächlich durch biologische Eigenschaften wie beispielsweise zellulärer Metabolismus und/oder Enzyminhibition/-induktion beeinflusst wurde. Des Weiteren deckte die Biokinetik in der Literatur beschriebene Speziesunterschiede auf. Die Auswertung der Transcriptomics-Daten lieferte substanzspezifische Genexpressionsprofile, welche die zugrundeliegenden Mechanismen der Toxizität aufzeigte. Zusätzlich wurden unterschiedliche Empfindlichkeiten der PHH verschiedener Spender identifiziert. Die beobachteten Unterschiede

zwischen den Spendern gingen aus den Biokinetik- und Transcriptomics-Daten hervor und konnten meist mit basalen Zytochrom-P450-Monooxygenase (CYP)-Aktivitäten erklärt werden. Diese Beobachtung unterstützte die Annahme, dass CYP-vermittelter Metabolismus eine zentrale Rolle in der interindividuellen Variabilität spielt. Die Proteomics-Daten spiegelten die umfangreichen Transcriptomics-Profile teilweise wider und ergänzten Informationen zu den jeweiligen Substanzen. Zu guter Letzt zeigten die Experimente zur Funktionalität der Mitochondrien, dass alle getesteten Wirkstoffe die zelluläre Atmung beeinflussten, wobei dies erst bei Konzentrationen beobachtet wurde, welche die humane therapeutische Plasmakonzentration überschritten.

Zusammengefasst lieferten die in der vorliegenden Arbeit evaluierten Endpunkte wertvolle mechanistische Informationen über arzneimittelinduzierte Veränderung von Zellfunktionen, die zum besseren Verständnis der Hepatotoxizität pharmazeutischer Wirkstoffe beitragen. Weiterhin unterstützt die frühe Identifizierung von Speziesunterschieden die Übertragbarkeit von präklinischen Befunden auf den Menschen.

Table of contents

List of abbreviations[1]

2D-GE	Two-dimensional gel electrophoresis
2-ME	2-mercaptoethanol
3-MC	2-methylcholanthren
3 R	Reduction, Refinement, Replacement
ADME	Absorption, Distribution, Metabolism, Excretion
ADP	Adenosine diphosphate
AMI	Amiodarone
AMP	Adenosine monophosphate
ANOVA	Analysis of variance
Anti	Antimycin
AQUA	Absolute quantification
ATP	Adenosine triphosphate
BCRP	Breast cancer resistant protein
BH q-value	False discovery rate according to Benjamini and Hochberg
BMEL	Bundesministerium für Ernährung und Landwirtschaft
BSA	Bovine serum albumin
BSEP	Bile salt export pump
cDNA	Complementary DNA
C_{max}	Peak plasma concentration
CNT	Concentrative nucleoside transporter
CO_2	Carbon dioxide
CoA	Coenzyme A
COX	Cyclooxygenase
CPZ	Chlorpromazine
cRNA	Copy RNA
CsA	Cyclosporine A
CYP	Cytochrome P450-dependent monooxygenase
d	Day
Da	Dalton
DEPC	Diethylpyrocarbonat
Dex	Dexamethasone
DMan	D-mannitol
DME	Drug metabolising enzyme
DMEM	Dulbecco's modified eagle medium
e.g.	*Exempli gratia* (for example)
EDTA	Ethylenediaminetetraacetic acid

[1] Gene symbols are given in the text with the corresponding gene names provided in the appendix only. In agreement with the Guidelines for Nomenclature of Genes, Genetic Markers, Alleles, and Mutations in Mouse and Rat (MGI, 2014) gene symbols for rat begin with an uppercase letter, followed by all lowercase letters / Arabic numbers and are italicised (e.g. Cyp1a). Human gene symbols are designated by all uppercase letters or by a combination of uppercase letters and Arabic numbers and italicised (e.g. CYP1A) in accordance with the Guidelines for Human Gene Nomenclature (HGNC, 2014). In addition to the gene symbols proper names are italicised in the text. Protein designations follow the same rules as gene symbols but are not italicised (e.g. Cyp1a for rat and CYP1A for human protein).

EFPIA	European Federation of Pharmaceutical Industries and Associations
EMA	European Medicines Agency
EURL ECVAM	European Union Reference Laboratory for alternatives to animal testing
$FADH_2$	Flavin adenine dinucleotide
FBS	Fetal bovine serum
FC	Fold change
FCCP	Carbonyl cyanide 4-(trifluoromethoxy)phenylhydrazone
FDA	U.S. Food and Drug Administration
g	Gram
Gal	Galactose
Glu	Glucose
GSH	Glutathione
GST	Glutathion-S-transferase
h	Hour (3600 s)
HC	High concentration
HDL	High density lipoprotein
HEPES	4-(2-Hydroxyethyl)piperazine-1-ethanesulfonic acid
HGNC	HUGO Gene Nomenclature Committee
HIV	Human immunodeficiency virus
HPLC	High-performance liquid chromatography
HSDB	Hazardous Substances Data Bank
i.e.	*Id est* (that is)
IBU	Ibuprofen
ICH	International Conference on Harmonisation of Technical Requirements for Registration of Pharmaceuticals for Human Use
IPA®	Ingenuity Pathway Analysis®
iTRAQ	Isobaric tags for relative and absolute quantification
IVT	*In vitro* transcription
JRC	Joint Research Centre
k	Kilo (10^3)
K_{OW}	Octanol/water partition coefficient
L	Litre
LC	Low concentration
LC-MS/MS	Liquid chromatography-tandem mass spectrometry
LDH	Lactate dehydrogenase
LOD	Limit of detection
LOQ	Limit of quantification
LTKB	Liver toxicity knowledge base
µ	Micro (10^{-6})
m	Milli (10^{-3})
M	Molar concentration (mol/L)
m/z	Mass-to-charge
MAO	Monoamine oxidase
MAQC	MicroArray Quality Control
MATE	Multidrug and toxin extrusion transporter
MDR	Multidrug resistance protein

Met	Metformin
MFI	Median fluorescence intensity
MGI	Mouse Genome Informatics
min	Minute (60 s)
ML	Monolayer
mRNA	Messenger RNA
MRP	Multidrug resistance-associated protein
MTT	3-(4,5-dimethylthiazol-2-yl)-2,5-diphenyl tetrazolium bromide
n	Nano (10^{-9})
NADH	Nicotinamide adenine dinucleotide
nBCl	n-butyl chloride
NCBI	National Center for Biotechnology Information
NFAT	Nuclear factor of activated T‑cells
NGS	Next generation sequencing
NHS	N-hydroxysuccinimide
NOAEL	No-observed-adverse-effect-level
NOEC	No-observed-effect-concentration
NSAID	Non-steroidal anti-inflammatory drug
NTCP	Sodium-taurocholate cotransporting polypeptide
O_2	Oxygen
OAT	Organic anion transporter
OATP	Organic anion transporting polypeptide
OCR	Oxygen consumption rate
OCT	Organic cation transporter
OECD	Organisation for Economic Co-operation and Development
Oligo	Oligomycin
OXPHOS	Oxidative phosphorylation
PB	Phenobarbital
PBPK	Physiologically-based pharmacokinetic
PBS	Phosphate buffered saline
PCN	Pregnenolone-16α-carbonitrile
PE	Phycoerythrin
PHH	Primary human hepatocytes
PhRMA	Pharmaceutical Research and Manufacturers of America
pKa	Negative logarithm of the acid dissociation constant (Ka) (pKa = ‑log10 Ka)
PPAR	Peroxisome proliferator-activated receptor
PPi	Inorganic pyrophosphate
PRH	Primary rat hepatocytes
Q10	Coenzyme Q10
QGP2.0	QuantiGene® Plex 2.0
qRT-PCR	Quantitative real-time polymerase chain reaction
REACH	Registration, Evaluation, Authorisation and Restriction of Chemicals
RIN	RNA integrity number
RLT	Lysis buffer for use with the RNeasy Plus Kits (Qiagen internal naming)
ROS	Reactive oxygen species

Rot	Rotenone
RPE	Concentrated wash buffer for use with RNeasy Kits (Qiagen internal naming)
rpm	Rounds per minute
RT	Room temperature
RW1	Cash buffer for use with RNeasy Kits (Qiagen internal naming)
s	Second
SDS-PAGE	Sodium dodecyl sulfate polyacrylamide gel electrophoresis
SEQC	Sequencing Quality Control
SILAC	Stable isotope labelling with amino acids in cell culture
SOP	Standard operating procedure
SRC	Spare respiratory capacity
SULT	Sulfotransferase
SW	Sandwich
$t_{1/2}$	Half-life
TC	Toxic concentration
TCDD	Tetrachlorodibenzo-p-dioxin
TG	Technical guideline
U	Unit
UDP	Uridine diphosphate
UGT	Uridine 5'-diphospho-glucuronosyltransferase
% v/v	Percentage by volume

1 Introduction

1.1 Toxicology

Toxicology is the study of adverse effects of chemical, physical or biological agents on living organisms. The term toxicology, from the Greek *toxicon*, poison, and *logos*, science, was introduced in the 17th century. But the intuitiveness and knowledge of poisons dates back to the earliest times of human existence, when contact with animal and plant derived toxins was a matter of life and death.

In historical terms, toxicology was related to medicine, just as pharmacy and chemistry were. The toxicological observations made at that time involved trial and error experiences of remedies and cases of poisonings. It was not before the 19th century that toxicology became an independent scientific discipline. Eventually, with the growing chemical industry, the knowledge of artificially manufactured substances grew and went beyond that of pharmaceutical remedies (Milles, 1999).

When it comes to "the science of poisons", it appears inevitable to mention Paracelsus (born Philippus Theophrastus Aureolus Bombastus von Hohenheim, 1493 - 1541). Paracelsus, a physician who introduced chemicals into medicine (Borzelleca, 2000), phrased the statement that still today resembles a fundamental concept in toxicology:

"Was ist das nit gifft ist
alle ding sind gifft und nichts ohn gifft
Allein die dosis macht das ein ding kein gift ist."

Translated in brief, "the dose makes the poison", this nowadays is known as the dose-response relationship. What began as basic, more or less watchful waiting practice, developed to a highly sophisticated scientific field. The ongoing progress in analytical methods and molecular biology has led to an advanced knowledge of cellular functions. Consequently, adverse effects are now being elucidated through identification of underlying mechanisms of toxicity.

Today, toxicology can be found in many different areas, e.g. pharmaceutical, food, environmental, occupational, forensic and clinical toxicology. However, it is always concerned with compounds and physical processes (e.g. radiation) that adversely affect people, animals, and the environment. In the end, it is the task of toxicological research to determine the dose of a substance which is safe. For this purpose, dose finding and risk assessment studies are conducted, mainly using multiple expensive animal experiments (Figure 1), which are required by law in the pharmaceutical industry.

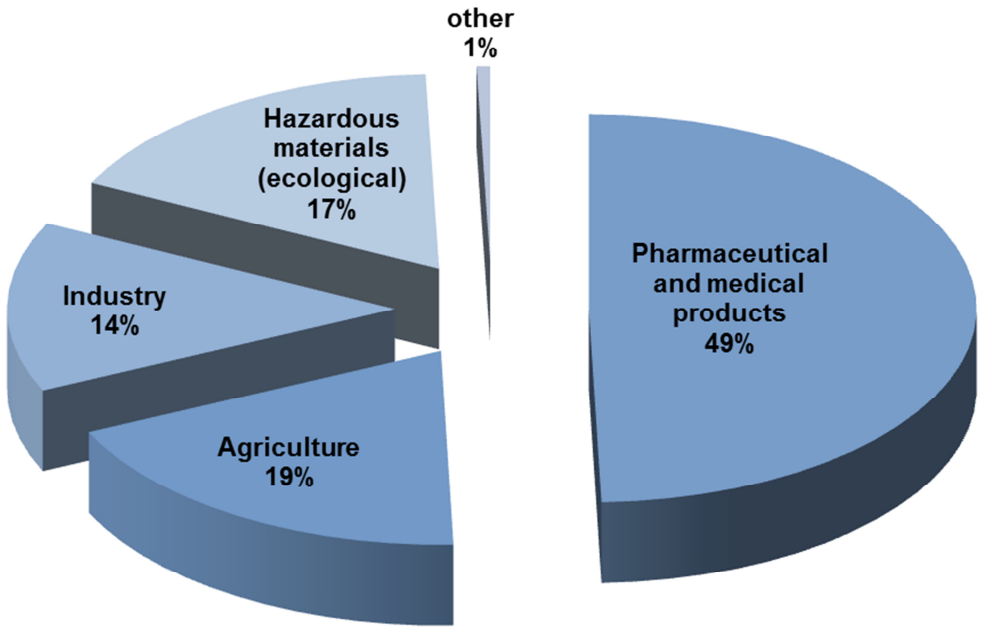

Figure 1. Percentage of animals used in different industrial sections for the assessment of compound toxicity and safety. The percentages are based on a universe of 174,656 animals and given for Germany in the year 2011. Source: BMEL (2013).

In 1959, the zoologist, William Russell, and the microbiologist, Rex Burch, published "The Principles of Humane Experimental Technique" (Russell and Burch, 1959). In this book, the concept of the *3 R* was proposed, which stands for the *Reduction*, *Refinement* and *Replacement* of animal experiments wherever possible. Briefly, the total number of animals can be reduced by maximising the information via e.g. consideration of multiple endpoints in one experiment. A continuous effort has to be made to minimise stress and pain throughout an animal's lifespan and thus refine the studies. Finally, alternative (*in silico*, *in vitro*) testing strategies should be constantly evaluated to attain an adequate replacement for *in vivo* studies. The *3 R* principle is widely accepted as an ethical code of behaviour. The chemical, cosmetics and pharmaceutical industries are permanently striving to develop and validate new animal-free testing strategies for the accurate prediction of human toxicities. The validation of non-animal testing strategies is actively supported by the European Union. The European Union Reference Laboratory for alternatives to animal testing (EURL ECVAM) was originally launched as ECVAM by the Joint Research Centre (Institute for Health and Consumer Protection) in 1991 (JRC, 2014a). The EURL ECVAM assists and promotes the development and validation of non-animal tests and further coordinates their evaluation at the European level.

1.2 Toxicology in drug discovery and development

Drug discovery and development describes the process a new drug candidate has to pass through successfully before eventually being launched to the market. This process is time and resource

consuming. The time from the discovery of a new molecular entity[2] to when it is available for the patient is 10 - 15 years, while in 2012 the estimated costs for research and development were ~ 1.2 billion US dollars per drug (EFPIA, 2014). Figure 2 illustrates the drug discovery and development process, including the pre-discovery or research phase. During pre-discovery, a solid knowledge base is built to understand the underlying molecular mechanisms of the disease of interest. This is the basis for the identification of a biological target, usually a gene or protein, which is "drugable", i.e. it must interact and be affected by a potential new drug candidate. After validating the target by proving its involvement in the disease, compounds must be tested for their ability to interact with the target. A possible way to select compounds at this early stage is to screen large compound libraries for their ability to alter the target activity. The latter is also known as "Hit Discovery", and can result in lists of > 100,000 compounds. *In silico* techniques are used to narrow down the choice of hits. Then, the compounds are ranked according to their potency for the target activity and the effective concentration should be relevant to potential achievable plasma concentrations. Further, early tests on efficacy (*in vivo*), absorption, distribution, metabolism, excretion (ADME; *in vitro* and *in vivo*) and toxicity (*in vitro*) guide the choice of lead compounds (10 - 100) to obtain a list of preclinical candidates (~ 1 - 5). In the preclinical phase (Phase 0), the compounds must pass more tests on efficacy, formulation development, safety pharmacology and toxicity (*in vivo*). The preclinical phase therefore serves to determine if a drug candidate is safe enough to enter human testing, i.e. clinical trials. In Phase I the candidate drug is tested in either healthy volunteers or patients (first-in-man) and mainly aims to deliver information on the tolerability (assessment of safety and side effects) and pharmacokinetics. With the knowledge of safe doses from Phase I, Phase II follows, involving a small group of patients (100 - 500, depending on the intended indication). Phase II serves as the proof of concept trial, where the therapeutic efficacy is explored. Finally, in Phase III, the therapeutic efficacy of the new candidate drug must be confirmed either by comparison to a reference drug or a placebo. In addition, the large group of patients (1,000 - 5,000) involved at this stage, allows the comprehensive assessment of the drug's safety, dose-response relationship and risk-benefit analyses. After successful completion of all phases and approval of the marketing application from the regulatory authority, the new medicine is launched onto the market, where it automatically enters Phase IV (post-marketing monitoring or pharmacovigilance).

[2] Technical term for new drugs frequently used by the U.S. Food and Drug Administration. Includes new chemical and biological entities.

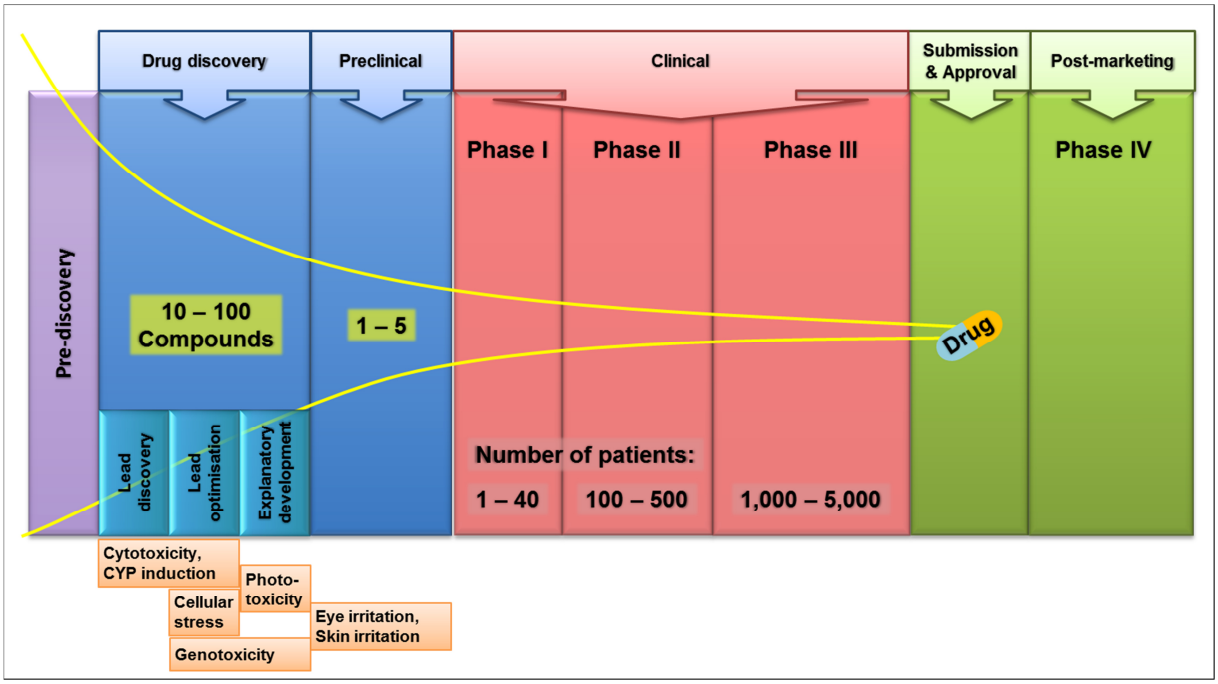

Figure 2. The drug discovery and development process. Consecutive phases from pre-discovery to post-marketing, whereas number of tested compounds decreases continuously. The drug discovery phase can be further divided into lead discovery, lead optimisation and exploratory development, as described in the text. *In vitro* methods (orange), supportive during drug discovery and preclinical development, are given along with their field of application that might vary across different pharmaceutical companies (adapted from PhRMA, 2014; modified).

1.2.1 Profiling a drug's toxicity

The main objective of toxicological studies during the drug discovery and development process is the determination of the new candidate's safety profile. Already during lead discovery in silico toxicology is used to screen the many hits. This approach makes use of structure activity relationships and computer-assisted prediction models (Simon-Hettich et al., 2006) to help prioritise and/or optimise hit towards lead compounds. Subsequently, *in vitro* toxicity studies support lead optimisation, exploratory development, preclinical development (Phase 0) and clinical phases. While more expensive, but also more informative, *in vivo* toxicity studies span from exploratory development onwards. It is important that the conducted studies are in accordance with the recommendations of regulatory authorities (European Medicines Agency (EMA), U.S. Food and Drug Administration (FDA)), which grant performance of clinical trials and marketing authorisation for new medicines. Thus, studies relevant for approval are performed according to existing and accepted guidelines, under either Good Laboratory Practice or other company specific quality procedures (e.g. Quality Management System at Merck KGaA) which ensure the traceability of data generated during drug development. Whereas International Conference on Harmonisation of Technical Requirements for Registration of Pharmaceuticals for Human Use (ICH) guidelines specifically describe testing methods for

pharmaceuticals, Organisation for Economic Co-operation and Development (OECD) guidelines are pertinent for chemicals (which can include drugs). An important ICH guideline is the "M3(R2) - Guidance on Nonclinical Safety Studies for the Conduct of Human Clinical Trials and Marketing Authorization for Pharmaceuticals" (ICH, 2009), which summarises the general approach how to support human clinical trials. It includes most of the important safety ICH guidelines, which are given in Table 1.

Table 1. List of International Conference on Harmonisation of Technical Requirements for Registration of Pharmaceuticals for Human Use (ICH) safety guidelines and corresponding endpoint.

ICH guideline	Study endpoint
S1	Carcinogenicity
S2	Genotoxicity
S3	Toxico- and pharmacokinetics
S4	Chronic toxicity
S5	Reproductive toxicology
S6	Preclinical evaluation for biotechnological products
S7	Safety pharmacology
S8	Immunotoxicity
S9	Nonclinical evaluation for anticancer drugs

In summary, the aims of pharmaceutical toxicology include (i) the characterisation of a drug's safety profile, (ii) the assessment of any risk associated with the use of the drug and (iii) the compliance to regulatory requirements. The aim is therefore to support the drug discovery and development process.

Drug attrition rates and withdrawals due to poor pharmacokinetics/bioavailability have decreased considerably over the last 10 - 20 years (accounting for only 10% of the attritions in 2000). However, safety issues (inacceptable toxicity and clinical safety concerns) still amount to approximately 30% of drug failures in 2000 (Kola and Landis, 2004). Drugs with new, complex pharmaceutical mechanisms are likely one reason for this negative trend. Between 2007/8 and 2010, failures due to safety concerns amounted to 19% in Phase II and 21% in Phase III and submission (Arrowsmith, 2011a; Arrowsmith, 2011b). The improvement in pharmacokinetics/bioavailability shifted the attritions (taken as a percentage) to the late phases of the process. A candidate drug with poor pharmacokinetics that would have been revealed in Phase I now enters advanced phases and tends to fail for other reasons (Kola and Landis, 2004). The pharmaceutical industry, which is under pressure to improve the current situation, invests a lot of effort into scientific innovations. Therefore, companies have also intensified their research in *in vitro* methods in order to develop screening strategies which enable a better assessment of a candidates' toxicological profile.

1.2.2 *In vitro* testing strategies

Regulatory authorities encourage the consideration of alternative methods and thus contribution to the *3 R* principle. For such ethical, but also economic reasons, research groups undertake constant efforts to develop *in vitro* assays that can be used as animal-free alternatives to current standard tests. To date, even well-established *in vitro* systems often lack full acceptance, simply because they lack validation studies.

However, there already exist several *in vitro* methods that are being successfully integrated by pharmaceutical companies in their drug discovery and development process. Figure 2 includes application of alternative methods that are being used to gain more knowledge on compound toxicity. While Table 2 lists examples of which *in vitro* assay can be used to cover corresponding endpoints, most pharmaceutical companies handle the type of assay and order differently.

Several *in vitro* methods have passed regulatory scrutiny and are integrated in official ICH guidelines. The ICH guideline S2(R1) contains several *in vitro* methods that are recommended to be incorporated in a standard test battery for the assessment of genotoxicity. First to mention is the bacterial reverse gene mutation test (Ames test), which is reported to have a weak sensitivity (45 - 60%) to predict rodent carcinogenicity (Kirkland et al., 2005). Further tests comprise (i) the chromosome aberration assay, (ii) micronucleus test and (iii) mouse lymphoma gene mutation assay, which are suitable to measure chromosomal damage. The corresponding practical application, interpretation of results and further procedures are delineated in the guideline. As confirmation of the *in vitro* findings, *in vivo* genotoxicity studies are still requested. These *in vivo* studies are suggested to be integrated into repeated-dose rat toxicity studies (ICH , 2011); hence, contributing to a reduction of animal experiments. A further *in vitro* assay included in the ICH safety guidelines is the 3T3 Neutral Red Uptake test for the assessment of phototoxicity potential of a compound. This assay is only requested if the compound absorbs wavelengths within the range of natural sunlight (290 - 700 nm). *In vitro* models to gain purely mechanistic information (e.g. transcriptomics, metabolomics) could be included also during clinical trials, however this is done on a case-by-case basis.

Table 2. *In vitro* assays used to assess corresponding endpoints. The underlined *in vitro* assays indicate those included in the indicated technical guidelines (TGs) of the Organisation for Economic Co-operation and Development (OECD).
Abbreviations: ATP - adenosine triphosphate; MTT - 3-(4,5-dimethylthiazol-2-yl)-2,5-diphenyl tetrazolium bromide; LDH - lactate dehydrogenase; CYP - cytochrome P450-dependent monooxygenase; mRNA - messenger RNA; GSH - glutathione.

Endpoint	*In vitro* assay	OECD
Cytotoxicity	ATP assay, MTT assay, LDH leakage	
CYP induction potential	mRNA induction, reporter gene assay	
Cellular/oxidative stress	GSH depletion, activation of Nrf2 antioxidant-response or heat shock response pathways, p53 activation	
Genotoxicity	Ames test chromosome aberration assay micronucleus test mouse lymphoma assay, Comet assay	TG471 TG473, 475, 483 TG487
Phototoxicity	3T3 Neutral Red Uptake	TG432
Eye irritation	Bovine Cornea Opacity Test Isolated chicken eye	TG437 TG438
Skin corrosion/ irritation	Human skin models (EpiSkin™, EpiDerm™)	TG431 TG439

A recent EU regulation, named REACH (Registration, Evaluation, Authorisation and Restriction of CHemicals) and aiming to protect the human health and environment, entered into force in June 2007. Before REACH, there was a vast discrepancy between the safety data for different chemicals, because the declaration of safety/risk information was not compulsory for chemicals on the market before 1981. Thus, REACH aims to introduce consistent safety information status for all chemicals manufactured in and imported into the EU. Within the framework of the REACH directive an increase in animal experiments was expected. Therefore, the chemical industry is encouraged to develop new alternative methods (*in vitro* and *in vivo*) in order to reduce the use of animals (*3 R* concept). Here, regulatory approved alternatives will be included in the corresponding OECD guidelines. The Institute for Health and Consumer Protection of the Joint Research Centre offers a system (TSAR[3]) to keep track on the approval status of alternative methods (JRC, 2014b). Generally, advances in the development of animal-free methods for the safety assessment of chemicals are likely to be also relevant for the testing of pharmaceuticals (see Table 2).

1.2.3 The utility of *Omics* technologies

The elucidation of mode of action and underlying mechanisms of toxicity is highly valuable to comprehensively understand the (adverse) effects mediated by a compound. Major advances in the field of *Omics* technologies offer great opportunities for this purpose. The traditional *Omics* include transcriptomics, proteomics and metabolomics, which address the analysis of global gene

[3] Tracking System for Alternative test methods Review, Validation and Approval in the Context of EU Regulations on Chemicals

expression, protein and metabolite abundance, respectively. In the following sections technologies of transcriptomics and proteomics are described.

The study of gene expression changes after exposure to toxic doses of a chemical, physical or biological agent is known as toxicogenomics. The basic assumption is that changes on the gene level occur before changes manifest on the protein level. In traditional toxicology, adverse effects on the cellular level are recorded using organ histopathology of animals from single- or repeated-dose studies. Hence, toxicogenomics has great potential to unveil adverse effects at earlier time points and lower compound concentrations. For a long time quantitative real-time PCR (qRT-PCR) was the classical method for gene expression analysis. In the mid-1990s, the microarray technology was first described by Schena et al. (1995). Since then, great progress was achieved in its development, eventually allowing the simultaneous measurement of tens of thousands of genes. Microarray technology soon became a very popular and widely accepted tool for studying gene expression changes, although forfeiting specificity and sensitivity. Therefore, qRT-PCR, being highly specific and sensitive, often served to confirm findings of the new microarray technology. The MicroArray Quality Control (MAQC) projects, launched by the FDA, studied the reproducibility and robustness of microarrays across platforms (MAQC-I; Shi et al., 2006). The results (fold changes) were in good accordance with results from qRT-PCR, which makes confirmation approaches nowadays obsolete (Canales et al., 2006). A more recent methodology, with the potential to substitute microarray technology, is next generation sequencing (NGS). NGS allows measurements with high sensitivity, accuracy and a wide dynamic range, i.e. also the detection of genes with low expression levels (Su et al., 2011). In contrast to the microarray technology, which detects pre-defined probes of annotated genes, in NGS every existing RNA transcript is sequenced and counted; hence, providing an unbiased approach. In response to this new technology, the FDA launched the third phase of MAQC, also known as Sequencing Quality Control (SEQC) in December 2008 (FDA, 2011).

In the course of scientific research, increasing knowledge has been gained in the complex process of gene regulation, making the “one gene one enzyme/polypeptide” hypothesis more and more untenable. Today, it is known that messenger RNA (mRNA) does not necessarily correlate with protein abundance (Anderson and Seilhamer, 1997; Gygi et al., 1999). Furthermore, silencing, alternative splicing on RNA level and post-translational modification of proteins are not detected by transcriptomics analysis, which makes proteomics an important complementary tool. In contrast to RNA nucleotides, proteins resemble a very heterogeneous class of endogenous molecules. This renders the accession of the complete cellular set of proteins for quantitative analyses extremely difficult, or even impossible. A large variety of technologies are available for proteomic analysis, for example, simple gel electrophoretic methodologies for separation (SDS-PAGE, 2D-GE). The more sophisticated technologies, which allow the identification and quantification of multiple proteins, involve the use of mass spectrometry. Mass spectrometric analysis require an appropriate fractionation (liquid chromatography) and

ionisation (electron spray ionisation, matrix-assisted laser desorption/ionisation or chemical ionisation) of the analytes. Isobaric tags for relative and absolute quantification (iTRAQ), stable isotope labelling with amino acids in cell culture (SILAC) and absolute quantification (AQUA) resemble technologies which specifically apply to the quantitative analysis of proteins.

For the presented work, the analysis of the proteome was conducted using the iTRAQ™ technology, which is based on labelling of peptides with isobaric tags (Zieske, 2006). This approach enables the parallel identification and quantification of proteins in different samples (up to 1,000 – depending on the separation method). The reproducible measurement gives rise to protein profiles per condition (sample) which allows conclusions to be drawn regarding the toxicity of pharmaceuticals. As illustrated in Figure 3, the tag (iTRAQ™ reagent) consists of a (i) Reporter Group, (ii) Balance Group and (iii) peptide reactive group – in (i) and (ii) the use of different isotopes is employed to generate molecules which are isobaric, i.e. have identical number of nucleons (molecular weights). This method enables the simultaneous analysis of up to eight samples (Lovric, 2011). The application of *Omics* analyses to *in vitro* systems is very appealing because they deliver broad and comprehensive information without or only a minimum (primary cells) requirement of animals. The use of human tissue and cells helps further to overcome interspecies differences, a major issue present in safety assessment. The joint interpretation of different *Omics* endpoints leads to a fundamental increase in knowledge, which serves to identify the overall picture of underlying molecular mechanisms.

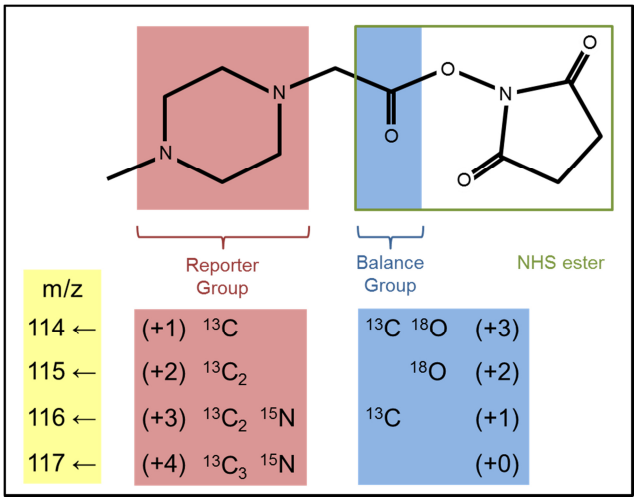

Figure 3 – Isobaric tags for relative and absolute quantification (iTRAQ™) reagent composition with the principle of *Reporter* and *Balance Group* generation. The peptide reactive group is depicted here as N-Hydroxysuccinimide (NHS) ester.

1.3 Liver - the main drug metabolising organ

1.3.1 Physiology and function of the largest gland

In healthy adults, the liver weighs 1.2 - 1.6 kg and is located on the right of the body under the lower ribs. The two primary lobes of the liver are of unequal size: a large right and small left lobe. The liver develops from the embryonic endoderm, as well as the gastro intestinal tract (without mouth, pharynx and rectum), pancreas, thyroid gland, thymus, respiratory tract, urinary bladder and urethra (Grapin-Botton, 2008). Liver parenchymal cells, i.e. hepatocytes, account for ~ 70% of the total organ mass (Zorn, 2008). The non-parenchymal cells of the liver include:

- Sinusoidal endothelial cells constitute the wall of the liver sinusoids. These cells lack a basal lamina and form a fenestrated surface, two characteristics unique to liver sinusoids (Iwakiri and Groszmann, 2007).
- Kupffer cells are liver-specific, resting tissue macrophages. They reside in the sinusoidal lumen and in the space of Dissé (space between the sinusoidal endothelial cells and hepatocyte plates). These cells play an important role in the first-line defence via phagocytosis of bacteria and viruses and are important mediators of the inflammatory response (Smedsrod et al., 1994).
- Pit cells are hepatic natural killer cells, which are known to have anti-tumour activity (Wisse et al., 1997).
- Ito cells, also known as hepatic stellate cells, resemble the main storage of vitamin A (80%; Senoo et al., 2007). Furthermore, these cells play a role during liver regeneration and the regulation of immune responses (Hellerbrand, 2013). During the pathological state of liver injury, the hepatic stellate cells are activated and start to express proinflammatory and profibrogenic genes (Hellerbrand, 2013).

Two vessels supply the liver with blood (Figure 4 A): the hepatic artery, which carries oxygen-rich blood from the heart and the portal vein, which carries nutrient-rich blood from the small intestine. Therefore, alimentary nutrients and exogenous xenobiotics absorbed from the intestine flow through the portal vein and pass through the liver before entering the systemic circulation. Together with the intrahepatic bile duct, the hepatic artery and portal vein build the so-called portal triad (Figure 4 B). The filtration of the blood and production of the bile takes place in a specific structural and functional unit, the liver lobule. There are two views of liver lobule organisation: the classical liver lobule (anatomical) and the liver acinus (functional). The classical liver lobule is confined by portal triads surrounding a central vein, which results in a hexagonal shape. By contrast, the liver acinus overlaps with the classic liver lobules, is rather diamond-shaped and involves two portal triads and two portal veins. It is divided in three zones: 1 - periportal, 2 - transitional, 3 - perivenous. The liver acinus model is important to be able to

understand the metabolic differences and pathophysiologies in hepatocytes between the portal triads and the central vein. As blood flows from the portal vein/hepatic artery to the hepatic vein and thus from zone 1 to 3, it becomes depleted of oxygen, nutrients and xenobiotics. The periportal hepatocytes (zone 1) exhibit increased rates of oxidative energy metabolism (rich in mitochondria), gluconeogenesis, urea synthesis and bile formation; while liponeogenesis, glutamine synthesis and xenobiotic metabolism predominate in the hepatocytes in the perivenous zone 3 (Katz, 1992). The passage of metabolic characteristics is fluent, i.e. hepatocytes in zone 2 have properties intermediate between the cells of zones 1 and 3.

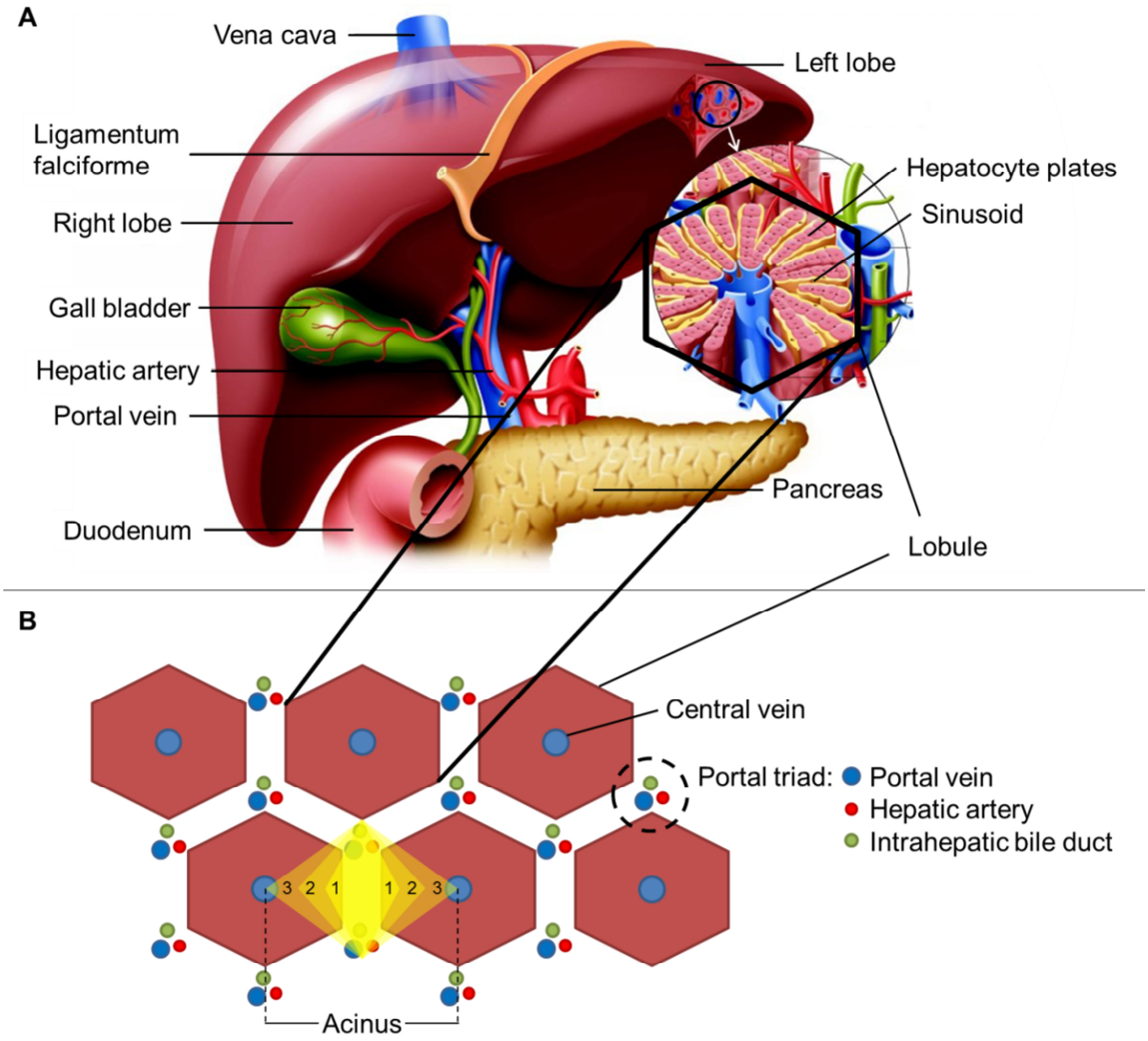

Figure 4. Anatomy of the liver (A left) and cellular architecture of a liver lobule in cross section (A right). Schematic arrangement of classic and anatomic view of the liver lobules in horizontal cross section with a portal triad at each corner of the hexagonal lobule (B). In addition, the functional unit of a liver acinus is shown with the 3 zones that align in the direction of blood flow along the connecting axis of two adjacent central veins (A: Wissen, 2014, modified).

The physiological functions of the liver include:

- Carbohydrate metabolism (glucose synthesis and storage in the form of glycogen)
- Cholesterol metabolism (cholesterol uptake and synthesis of very low density lipo protein)

- Blood homeostasis (synthesis of albumin and coagulation factors)
- First-line defence (interception of absorbed bacteria, viruses and their products)
- Bile homeostasis (bile formation and biliary secretion)
- Vitamin A storage
- Xenobiotic metabolism

1.3.2 The liver's role in xenobiotic metabolism

The anatomical location between the intestinal tract and the systemic circulation makes the liver the first organ to encounter enterally absorbed xenobiotics. This is presumably the main reason that the liver is fully equipped with a broad range of drug metabolising enzymes (DMEs) and thus, represents the main drug metabolising organ in the body. The transformation of exogenous and endogenous compounds is an essential process to enable the excretion of (potentially toxic) waste products. Biliary and urinary excretion are the two major elimination pathways for xenobiotics. Whereas hydrophilic molecules can be directly excreted via bile and urine, the excretion of lipophilic molecules is more difficult. In order to avoid the accumulation of lipophilic substances in the body, these compounds need to be transformed into hydrophilic derivatives, which are subsequently more easily removable via normal excretion pathways. The elimination of enterally absorbed compounds and metabolites from the blood during the first pass through the liver is called the "first pass effect". In pharmaceutical research, the "first pass effect" is an undesired effect of enterally (oral and rectal) applied drugs because their bioavailability, i.e. amount of drug that reaches the systemic circulation, is often dramatically reduced.

Xenobiotic metabolism can be classified into three, typically consecutive phases (Figure 5). Generally, a lipophilic xenobiotic is metabolised by DMEs in a so-called "functionalisation phase" (Phase I). In this phase the compound is activated by unmasking or introducing functional groups via oxidation, reduction or hydrolysis. Depending on the unmasked or introduced component, an electrophilic or nucleophilic metabolite is generated. Examples of typical functional groups are given in Figure 5, while Table 3 lists the main classes of Phase I - III enzymes. Subsequently, in a Phase II reaction the active metabolite is (enzymatically or non-enzymatically) conjugated to polar endogenous ligands such as glutathione (GSH) or glucuronic acid. Finally, Phase III refers to the elimination of the resulting hydrophilic metabolite from the hepatocytes by transporters. The hydrophilic metabolite can be easily excreted from the body via renal or biliary routes.

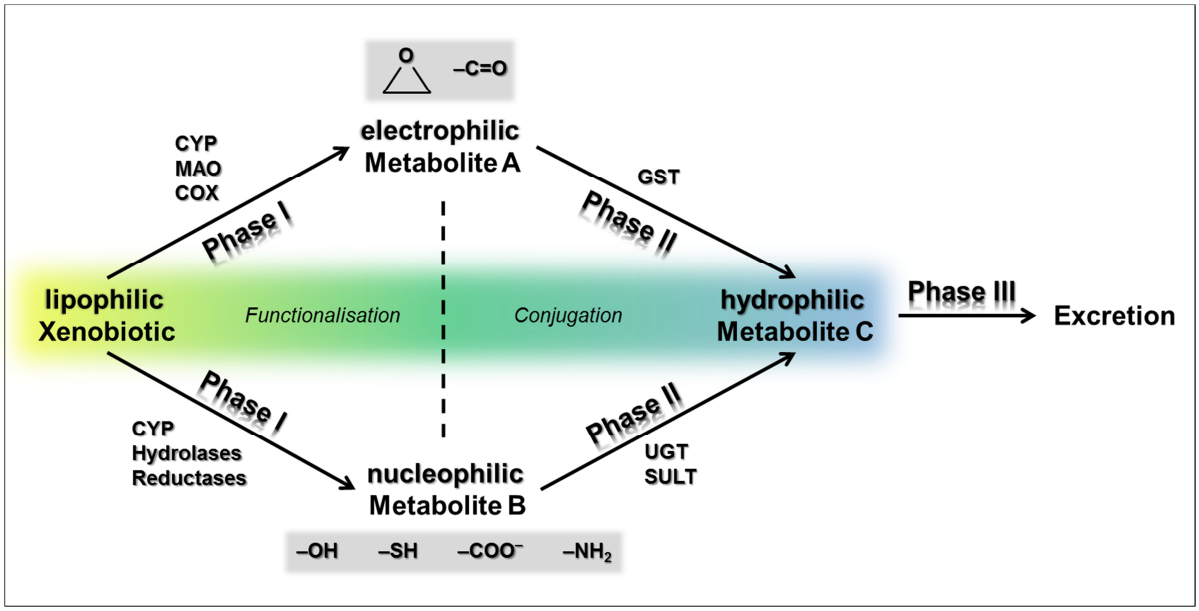

Figure 5. Classical phase model of xenobiotic metabolism. A lipophilic xenobiotic is metabolised to an electrophilic (e.g. epoxide functions, carbonyl groups) or nucleophilic (e.g. hydroxyl-, sulfhydryl-, carboxylic acid-, amino groups) metabolite in Phase I by phase I drug metabolising enzymes (including cytochrome P450-dependent monooxygenases (CYP), monoamine oxidases (MAO), cyclooxygenases (COX)). In Phase II, the functionalised metabolites are conjugated to polar molecules by phase II enzymes (including glutathione S-transferases (GST), uridine 5'-diphospho-glucuronosyltransferases (UGT), sulfotransferases (SULT)). In Phase III the resulting metabolite C is hydrophilic and thus eliminable via bile or urine (adapted from Oesch and Arand, 1999; modified).

Although xenobiotic metabolism aims to detoxify and excrete foreign compounds, metabolism sometimes leads to their toxification. Generally, Phase II reactions mostly yield non-reactive metabolites. By contrast, Phase I reactions can produce highly reactive intermediates, which bind to cellular macromolecules such as proteins, nucleic acids or lipids, before interacting with a Phase II enzyme. If the intracellular concentration of such reactive metabolites exceeds the threshold of inherent repair mechanisms, a compound-induced adverse effect manifests. Depending on the affected mechanisms this eventually results in a genotoxic or cytotoxic potential of the xenobiotic.

Table 3. Overview of main classes of Phase I and II drug metabolising enzymes. Phase III transporters are hepatic efflux transport proteins.
Abbreviations: CoA - coenzyme A; UDP - uridine diphosphate.

Phase I enzymes	Phase II enzymes	Phase III transporters
Cytochrome P450 enzymes	Glutathione S transferase	Multidrug resistance proteins
Flavin-dependent monooxygenases	Acyl-CoA aminoacid-N-aclytransferases	Multidrug resistance-associated proteins
Monoaminooxygenases	Sulfotransferases	Organic solute transporters
Cyclooxygenases	Acetyltransferases	P-glycoprotein
Alcohol dehydrogenases	UDP-Glucuronosyltransferases	Bile salt export pump
Aldehyde dehydrogenases	Methyltransferases	
Reductases		
Esterases		
Epoxydehydrolases		

Many Phase I catalysing enzymes belong to the cytochrome P450-dependent monooxygenase (CYP) superfamily of monooxygenases, which reside in the endoplasmatic reticulum membrane. The CYP genes originate from a common progenitor and various isoforms with specialised functions have developed during evolution (Eichelbaum and Schwab, 2009). The families, subfamilies and isoforms are classified based on the homology of their amino acid sequence. Briefly, all enzymes sharing > 40% homology are assigned to a family (denoted by the first number, e.g. CYP1); whereas, enzymes of one subfamily share > 55% homology (letter, e.g. CYP1A) (Eichelbaum and Schwab, 2009). The isoform corresponds to the individual gene of the subfamily and is designated as a number (e.g. CYP1A1). The major CYP isoforms involved in the metabolism of drugs are: 1A2, 2C9, 2C19, 2D6, 3A4 (Lamb et al., 2007).

Xenobiotic metabolism can be influenced by many factors and at different stages. Drugs, food ingredients and contaminants hold potential to (i) induce / inhibit an enzyme's activity or (ii) elevate / decrease its corresponding gene expression level. Of particular importance is the transcriptional regulation of DMEs, which is mainly controlled by transcription factors. Table 4 gives an overview of the transcription factors that influence the transcription of Phase I - III DMEs.

Table 4. Transcription factors involved in the transcriptional regulation of drug metabolising enzymes with examples of typical compounds known as inducers (agonists). The Phase I - III target genes (human: all uppercase letters; rat: uppercase letter, followed by all lowercase letters / Arabic numbers) are given with corresponding reference.
Abbreviations: PCN - pregnenolone-16α-carbonitrile; TCDD - tetrachlorodibenzo-p-dioxin.

Transcription factors	Typical inducers	Phase I, II and III target genes	Reference
Constitutive androstane receptor (CAR)	phenobarbital, rifampicin, carbamazepine, efavirenz, nevirapine	*CYP1A1* and *CYP1A2*	Yoshinari et al., 2010
		CYP3A4	Goodwin et al., 2002
		CYP2C9 and *CYP2C19*	Gerbal-Chaloin et al., 2002
		UGT1A1, *UGT1A6*	Sugatani et al., 2001
		MDR1	Geick et al., 2001
		MRP2	Kast et al., 2002
		MRP4	Assem et al., 2004
Pregnane-X receptor (PXR)	rifampicin (humans), PCN (rodents)	*CYP2B6* and *CYP3A4*	Maglich et al., 2002
		UGT1A1, *UGT1A6*	Sugatani et al., 2001
		MRP2	Kast et al., 2002
Peroxisome proliferator-activated receptor (PPAR)	palmitic acid, oleic acid, linoleic acid, arachidonic acid	*CYP4A11*	Omiecinski et al., 2011
		Sult2a	Fang et al., 2005
		UGT2B	Barbier et al., 2003
		Mdr2	Barbier et al., 2004
Aryl hydrocarbon receptor (AHR)	TCDD, benzo[a]pyrene, heterocyclic amines	*CYP1A1/2*	Omiecinski et al., 2011

However, elevated enzyme levels are not always dependent on transcriptional activation. The induction of CYP2E1, for example, is achieved via an increased translational efficiency and stabilisation of the protein from degradation (Novak and Woodcroft, 2000).

1.3.3 Drug-induced hepatotoxicity

The liver is the first organ confronted with enterally applied drugs and their metabolic products are absorbed from the intestines in high concentrations. These are potentially toxic as parent compound or toxified through metabolism, which takes place in the liver itself but also in the gut enterocytes which contain sufficient amounts of DMEs (Martignoni et al., 2006). To date, new candidate drugs still fail due to unacceptable hepatotoxicity in pre-clinical and clinical phases and it is estimated that 50% of acute liver failures are attributable to drug-induced hepatotoxicity (Dambach, 2005; FDA, 2009; Mandenius et al., 2011). In clinics, pathophysiological manifestations range from asymptomatic elevations of liver enzymes to severe liver dysfunction (Assis and Navarro, 2009). Generally, a variety of illnesses can affect the liver: hepatitis (liver inflammation), cholestasis (impairment of bile secretion), steatosis (fatty liver), liver fibrosis and cirrhosis (liver scarring), liver tumour (hepatocellular carcinoma). These liver pathologies can be caused by many diseases (e.g. hypertriglyceridemia, bacterial or viral infections), but also by chemicals and drugs. Today, new drugs are designed to address complex mechanisms of actions and thus, drug-induced hepatotoxicity can cause all forms of known liver pathologies.
State-of-the-art technologies can deliver in-depth knowledge on inherent compound properties, i.e. physicochemical properties, cytotoxic potential, metabolite profiling, CYP-induction potential, *et cetera*. However, drug-induced hepatotoxicity eventually needs to be regarded as a multifactorial event with the individual patient being the main uncertainty factor. Many risk factors are known to increase the susceptibility of drug-induced hepatotoxicity (Figure 6). For example, individuals who suffer from human immunodeficiency virus (HIV), Hepatitis B and C virus infections are known to have an increased susceptibility to drug-induced liver injury (Kaplowitz, 2004) or women who seem more vulnerable to acute liver failure (Ostapowicz et al., 2002). For the latter, sex differences in CYP enzymes, steroid hormone levels and immune response are thought to be responsible (Flynn and Ferguson, 2010).

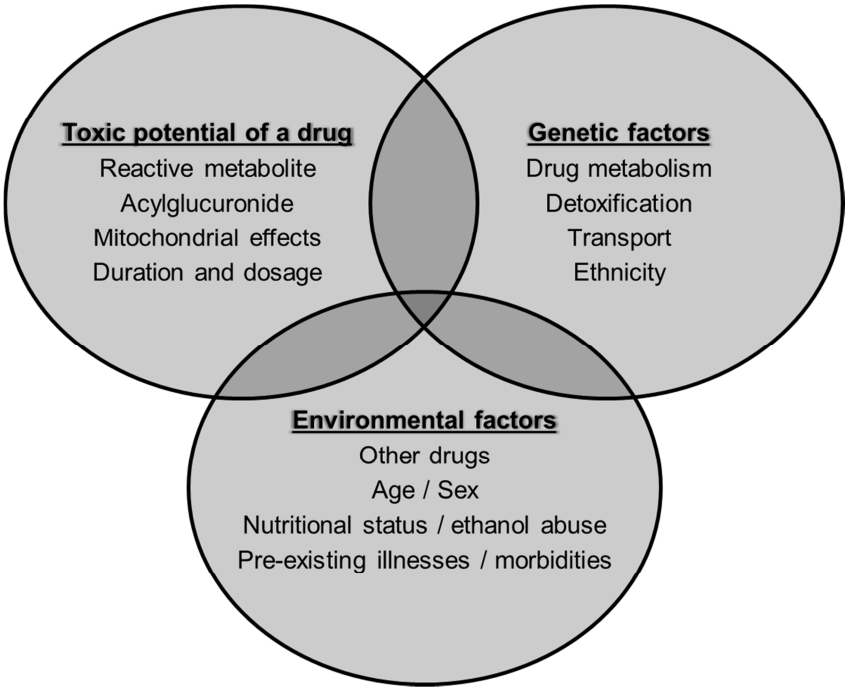

Figure 6. Venn diagram of risk factors contributing to an increased susceptibility to drug-induced hepatotoxicity (adapted from Kaplowitz, 2004; modified).

Drug-induced hepatotoxicity can be categorised as either (i) intrinsic (Type A) or (ii) idiosyncratic (Type B) reactions. Intrinsic hepatotoxicity can be predicted because it is dose-dependent and thus can be expected to occur in all patients. By contrast, idiosyncratic reactions are unpredictable events. They are often independent from the applied dose, evidence variable periods of latency and occur very rarely (one event in every 1000 - 100,000 patients) (Lee, 2003). For the latter case, regulatory studies fail to predict idiosyncratic toxicities, probably attributed more to statistical reasons, i.e. too few patients tested. In addition, the diagnosis of idiosyncratic hepatotoxicity in clinics is a challenge because its origins are not well understood (Assis and Navarro, 2009).

1.3.3.1 Molecular mechanisms of drug-induced hepatotoxicity

On the molecular level, drug-induced hepatotoxicity can be elicited via various mechanisms. As previously described, xenobiotic metabolism can lead to the production of reactive metabolites. The structural activation enables the metabolites to bind to intracellular macromolecules and thus impair cellular functions, and reactivity depends on the chemical structure. Potential consequences include mitochondrial dysfunction, alteration of calcium homeostasis, adenosine triphosphate (ATP) depletion, swelling and rupture of organelles and cell, release of pro-apoptotic factors; eventually leading to cell death. A further possibility is haptenation, by which an immune response is elicited through covalent binding of the metabolite (hapten) to liver proteins that are consequently perceived as foreign by immune cells. Lastly, the covalent binding to DNA molecules resembles a key feature of genotoxic carcinogens.

Some chemical structure motifs predestine a compound to produce reactive oxygen species (ROS) via redox cycling. The anticancer drug, doxorubicin, the antibiotic nitrofurantoin, but also chemicals like the herbicide, paraquat, are all known redox cycling agents (Rana et al., 2013). The production of ROS is also mediated by other mechanisms, for example, impairment of the mitochondrial respiratory chain, whereupon electron leakage leads to the reduction of oxygen. Independently from its source, increasing ROS (oxidative stress) results in (i) antioxidant reduction, (ii) lipid peroxidation, (iii) further mitochondrial injury and (iv) DNA damage; whereas, these events may also result in cell death or, in the latter case, genotoxicity (Gomez-Lechon et al., 2010).

The inhibition of transporter molecules is another mechanism that potentially leads to hepatotoxicity. Drugs inhibiting transporters needed for the excretion of endogenous (waste) products can do this either via covalent binding (irreversible) or through competitive inhibition (reversible). As a consequence, endogenous (e.g. bile salts) and exogenous (xenobiotics, metabolites) products accumulate to toxic concentrations and can lead to cell death or impaired bile salt secretion, which manifest *in vivo* as hepatitis or cholestasis, respectively.

Drug-induced liver injury frequently manifests as intra-hepatic cholestasis. This pathology is characterised by bile flow impairment via alterations of the hepatic transporters (Figure 7) (Padda et al., 2011).

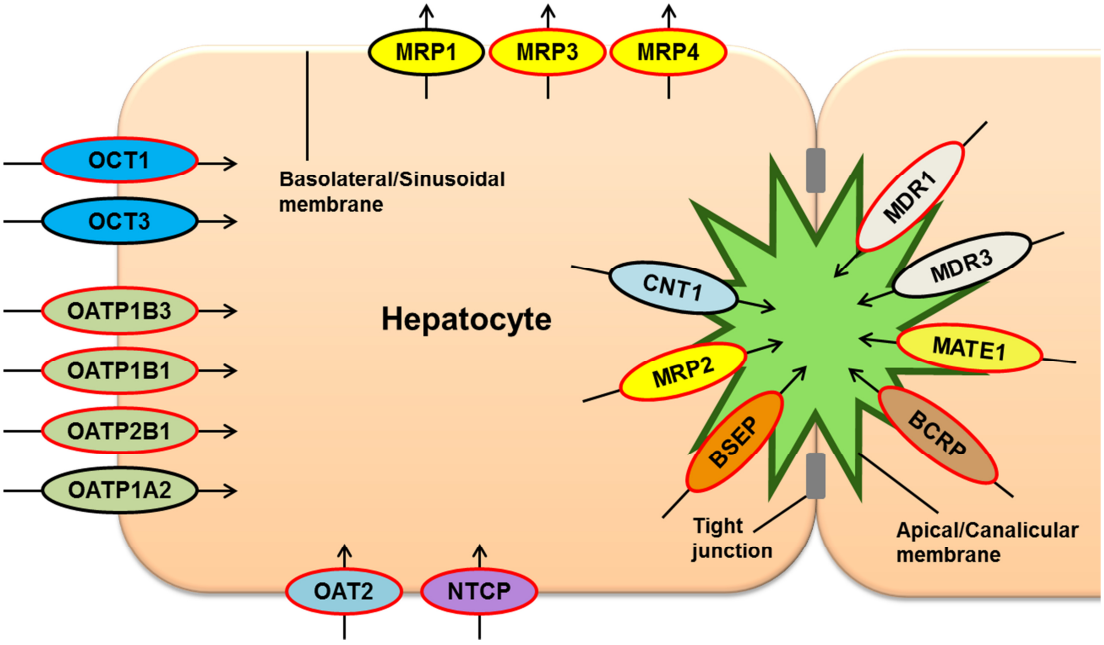

Figure 7. Schematic representation of sinusoidal and canalicular transporters in hepatocytes. The influx transporters at the sinusoidal membrane include organic cation transporters (OCTs), organic anion transporting polypeptides (OATPs), organic anion transporter (OAT) and Na^+-taurocholate cotransporting polypeptide (NTCP). The efflux transporters at the sinusoidal membrane include those of the multidrug resistance-associated proteins (MRPs). The canalicular efflux transporters shown are concentrative nucleoside transporter (CNT), MRP2, bile salt export pump (BSEP), multi drug resistance proteins (MDRs), multidrug and toxin extrusion transporter (MATE) and breast cancer resistance protein (BCRP). The red-rimmed transporter indicate those that can be involved in the development of cholestasis (figure adopted from Solvobiotech, 2014; modified).

The induction of transcription factors or covalent binding are potential mechanisms by which a drug induces or inhibits, respectively, an important DME. As a result the metabolism of the drug itself or concomitant applied drugs can be altered, the latter resulting in potential drug-drug interactions. An induction would lead to decreased peak plasma concentration (C_{max}) and half-life ($t_{1/2}$) of the parent compound and simultaneously increased plasma levels of the metabolite. Assuming that the parent compound exerts the pharmacological effect, the drug's efficacy is decreased. By contrast, enzyme inhibition would cause the opposite effect, with accumulation of the parent compound potentially evoking exaggerated adverse effects. Since drug-mediated CYP inhibition/induction leading to drug-drug interactions is a major risk factor for drug-induced hepatotoxicity, the assessment of a new candidate drug's potential to inhibit/induce different human CYPs *in vitro* and *in vivo* is requested by regulatory authorities (FDA, 2012).
The impairment of mitochondrial function reflects a further mechanism that will be discussed in detail below.

1.3.3.2 Importance of mitochondrial toxicity for drug-induced hepatotoxicity

Mitochondria generate most of the cell's ATP, which led to the alias "energy powerhouses of the cell". However, these organelles fulfil many functions that contribute to cellular homeostasis, including fatty acid oxidation, intrinsic apoptosis signalling, heme synthesis, steroid synthesis from cholesterol, thermogenesis, calcium homeostasis and replication of its own set of genetic material (mitochondrial DNA). Mitochondrial dysfunction is frequently the underlying cause for drug-induced liver injury. The antidiabetic drug, troglitazone, was withdrawn from the market due to hepatotoxicity that is very likely related to its potential to induce mitochondrial toxicity (Okuda et al., 2010). The complexity of this organelle is the basis for the multiple mechanisms through which a xenobiotic can act as mitotoxicant. Six molecular mechanisms contributing to mitochondrial toxicity are briefly outlined below.

1. *Inhibition of mitochondrial respiratory chain*. The mitochondrial respiratory chain is needed to maintain the electrochemical gradient (complex I - IV) and to produce ATP under oxygen consumption (complex V). Drugs can inhibit each of the five complexes involved in the oxidative phosphorylation, resulting in its partial or complete shutdown. Figure 8 shows the complexes of the respiratory chain including the corresponding inhibitors.

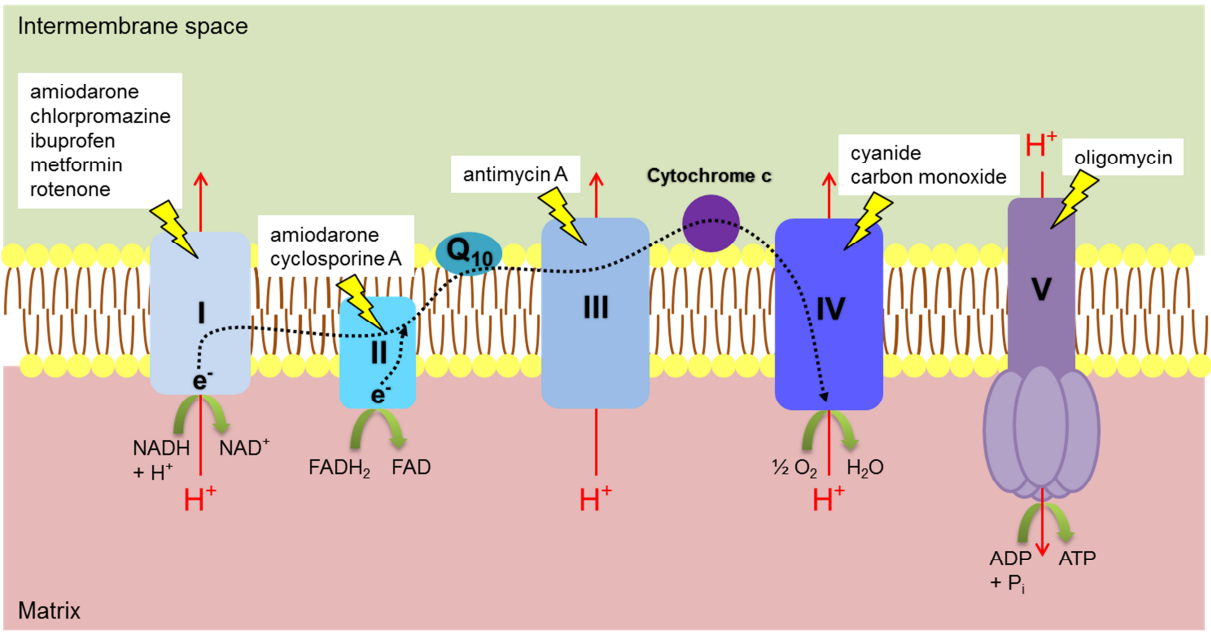

Figure 8. Mitochondrial respiratory chain. The electrons from oxidation of nicotinamide adenine dinucleotide (NADH) (at complex I (I)) or flavin adenine dinucleotide ($FADH_2$) (at complex II (II)) are transported via coenzyme Q10 (Q10), complex III (III) and cytochrome c to complex IV (IV) where oxygen (O_2) is reduced to water (H_2O). Complex V (V) exploits the proton gradient for adenosine triphosphate (ATP) production from adenosine diphosphate (ADP). Complex I - V with corresponding substances that inhibit their function are indicated in white boxes. Full names of the different complexes are: NADH-coenzyme Q10 oxidoreductase (complex I), succinate-Q oxidoreductase (complex II), Q-cytochrome c oxidoreductase (complex III), cytochrome c oxidase (complex IV), ATP-synthase (complex V).

2. *Reactive oxygen species generation*. The transfer of electrons through the electron transport chain (complex I - IV) is prone to electron leakage, also under normal conditions. The leaking electrons often results in the reduction of oxygen to superoxide anion, a ROS itself, but also precursor of other highly ROS able to damage proteins, phospholipids and DNA (Turrens, 2003). Complexes I and III are primarily involved in ROS generation (Adam-Vizi and Chinopoulos, 2006). Under pathological conditions, i.e. impaired oxidative phosphorylation, the production of ROS can be dramatically increased, resulting in oxidative stress that further damages the mitochondria; hence, a "*circulus vitiosus*" (Figure 9).

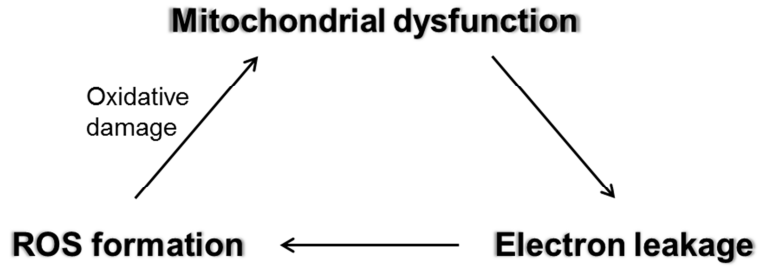

Figure 9. "*Circulus virtiosus*" of mitochondrial impairment. The dysfunction leads to electron leakage from the mitochondrial respiratory chain. Electrons reduce oxygen to superoxide, which is a precursor of many highly reactive oxygen species (ROS). These ROS react with adjacent proteins, phospholipids and DNA and consequently further aggravate the mitochondrial dysfunction.

3. *Uncoupling of oxidative phosphorylation*. The proton (pH) gradient across the inner mitochondrial membrane contributes to 10 - 20% of the electrochemical gradient, while the transmembrane potential (electrical component) contributes 80 - 90% (Wu et al., 1990). Complexes I, III and IV contribute to its maintenance, by permanent transport of protons from the matrix to the intermembrane space. Some compounds are capable of moving protons from the intermembrane space into the membrane bypassing complex V (F_0F_1-ATPase). Scientifically this event is termed "uncoupling" because proton translocation into the matrix is uncoupled from ATP synthesis; accordingly, these compounds are described as "uncouplers" or "protonophores". Uncoupling eventually results in the collapse of the mitochondrial membrane potential, increase in oxygen consumption and blockade of ATP synthesis. Many non-steroidal anti-inflammatory drugs (NSAIDs) are known to act as protonophores, such as diclofenac, indomethacin, naproxen and nimesulide.
4. *Opening of the mitochondrial permeability transition*. In normal physiology, the mitochondrial permeability transition pore, located between the inner and the outer membrane, contributes to mitochondrial homeostasis (Brenner and Moulin, 2012). The pores are normally closed, but opening can be triggered by endogenous factors such as high calcium, ROS, free fatty acids, bile salts and iron. The opening leads to the exchange of compounds (< 1.5 kDa) and thus the collapse of the electrochemical gradient. The accumulation of water eventually results in the expansion of the matrix and rupture of the outer membrane; consequently releasing pro-apoptotic factors that induce the programmed cell death pathway. Drugs known to induce irreversible opening of the mitochondrial permeability transition pore are diclofenac, nimesulide, troglitazone and gemfibrozil, while cyclosporine A is known to inhibit mitochondrial permeability transition pore opening (Brenner and Moulin, 2012).
5. *Inhibition of beta-oxidation*. The catabolism of fatty acids is an important source of energy and contributes to the homeostasis of triglycerides within the cell. Inhibition of mitochondrial beta-oxidation results in the accumulation of free fatty acids and triglycerides. Furthermore, acetyl-coenzyme A (acetyl-CoA) and reduction equivalents (nicotinamide adenine dinucleotide (NADH) and flavin adenine dinucleotide ($FADH_2$)), important components of the tricarboxylic acid cycle and oxidative phosphorylation, respectively, are not produced; consequently, ATP production is lowered. However, two distinctions are made at the pathophysiological level: Firstly, a severe inhibition of mitochondrial beta-oxidation, which results in microvesicular steatosis characterised by the intracellular accumulation of small lipid droplets. This pathology is known to result in life-threatening liver lesions associated with liver failure and possible death (Fromenty and Pessayre, 1995). Secondly, the mild inhibition of mitochondrial beta-oxidation shows a different pathology. In this case, single, large lipid vacuoles form in the cytoplasm of

hepatocytes, causing so-called “macrovacuolar steatosis”. Macrovacuolar steatosis can progress to steatohepatitis after several years, while in the short term it is considered to be a benign liver lesion (Labbe et al., 2008). Compounds known to inhibit mitochondrial fatty acid oxidation include amineptine (tricyclic antidepressant), amiodarone (anti-arrhythmic), ibuprofen (analgesic), perhexiline (antianginal) and valproic acid (anticonvulsant) (Begriche et al., 2011).

6. *Inhibition of mitochondrial DNA replication and protein synthesis*. In the matrix mitochondria possess their own DNA and DNA replication enzymes. The mitochondrial DNA comprises genes for 13 polypeptides, 22 different transfer RNAs and 2 ribosomal RNAs, whereas the polypeptides code for subunits of the respiratory chain (Nadanaciva and Will, 2009). An impaired oxidative phosphorylation can either be caused by the inhibition of mitochondrial DNA replication via inhibition of DNA polymerase gamma, or by affecting protein synthesis via inhibition of ribosomes. A further consequence is the secondary inhibition of mitochondrial beta-oxidation and the tricarboxylic acid cycle (Begriche et al., 2011). Drugs reported to act as transcriptional inhibitors include the class of nucleoside reverse transcriptase inhibitors (antivirals). Some antibiotics are known to inhibit ribosomal translation, which is attributed to the structural similarity between mitochondrial and bacterial ribosomes; examples are chloramphenicol and antibiotics from the groups of aminoglycosides, lincosamides and tetracyclines.

1.3.4 Prediction of drug-induced hepatotoxicity

As introduced above, drug-induced hepatotoxicity is a frequent cause of attritions in drug development and drug withdrawals post-marketing. The identification of a drug’s potential to induce liver toxicity in non-clinical phases is a major obstacle for pharmaceutical companies. This is because drug-induced hepatotoxicity, being mostly idiosyncratic in nature and host-dependent (Chen et al., 2014), is difficult to predict with current regulatory animal toxicity studies. By contrast, intrinsic (dose-related) hepatotoxicity correlates well across species but contributes only a small proportion of all cases (Bissell et al., 2001). To address this issue, the EMA published a *Non-Clinical Guideline on Drug-induced hepatotoxicity*. In this guideline a stepwise approach is described on how hepatotoxicity signals can be detected by an integrated risk assessment from standard non-clinical studies in two mammalian species (one rodent and one non-rodent). Depending on a positive outcome follow-up studies to characterise the hepatotoxic effect are recommended. These include monitoring of additional parameters from *in vivo* studies and *in vitro* models to elucidate mechanisms of liver toxicity induced by the investigational compound. Recommended *in vitro* human and animal systems in the guideline include those investigating the drug’s cytotoxic potential and up-regulation of detoxification and/or survival factors (EMA, 2008).

Acetaminophen and coumarin are two prominent examples of species-specific responses to the hepatotoxic potential of a compound. Different susceptibilities were observed in hepatocytes from hamster, mouse, rat and human treated with acetaminophen; whereas, hepatocytes from rat and human were less sensitive towards acetaminophen-induced toxicity. The sensitivities to acetaminophen-induced hepatotoxicity were attributed to the rate of N-acetyl-para-benzoquinoneimine formation, by CYP-mediated activation of the parent compound (Slikker et al., 2004; Tee et al., 1987). In the second example, coumarin, species-specific responses are due to differences in its metabolism. For example, coumarin 7-hydroxylation is mediated by human CYP2A6 but it is activated by 3,4-epoxidation by the rat orthologue (CYP2A1) (Lewis and Lake, 2002). In the latter example, the rat is more susceptible because of a slower detoxification rate compared to human and mouse (Uehara et al., 2008). Most importantly, Uehara et al. (2008) were able to reconstruct the species differences in a toxicogenomics approach using primary rat and human hepatocytes.

Generally, similarity in drug metabolism and pharmacokinetics, drug effects (pharmacodynamics) and mechanisms leading to toxicity appear essential factors by which the animal model (healthy or diseased) should be chosen (Dixit and Boelsterli, 2007). It is widely accepted that understanding the underlying mechanisms of toxicity and species differences is essential for the correct interpretation of the data. Nevertheless, many underlying mechanisms leading to species differences still need exploration. It is the aim of academic, industrial and governmental research groups to constantly acquire new insights into such discrepancies. This knowledge will then automatically improve the preclinical safety testing strategies and consequently improve the predictive value for human hazard assessment.

Recent advances in the field of hepatocyte alternative models contribute to continuous development in this area of research (for a comprehensive review see Godoy and Hewitt et al., 2013). It is widely accepted that cell culture systems using human cells are the best models to study toxic effects in humans. However, animal-derived cell culture systems have also proven useful to study drug metabolism, identify biological targets and toxic effects. *In vitro* systems may vary in their complexity, moving away from the *in vivo* situation with increasing ease of handling (from the complex isolated perfused liver model to simple monolayer culture of hepatoma-derived cell lines). Nonetheless, the benefit of less complex *in vitro* systems is that they allow a uniform, controlled culture and deliver results that are expected to be easy interpretable (Tuschl et al., 2008). Today, many hepatocyte *in vitro* models exist (Table 5). These *in vitro* models, including hepatic cell models, are frequently applied to deliver discrete pieces of information, e.g. on cytotoxicity or gene expression changes. The determination of multiple endpoints, allowing an integrated analysis of the data that is expected to be complementary was addressed by the EU-project Predict-IV.

Table 5. *In vitro* models with corresponding advantages and disadvantages used for the assessment of hepatotoxicity.
Abbreviations: m RNA - messenger RNA; PCLS - precision cut liver slices.

Liver *in vitro* model	Advantages	Disadvantages
Isolated perfused liver	Preserved liver physiology; metabolism is maintained; measurement of biliary excretion	Only short-term exposures (hours); sacrifice of animal required; limited availability of human material
Precision cut liver slices	Similar mRNA expression to liver tissue[4]; rat PCLS correctly predicted *in vivo* hepatotoxicity[5]	to date, maximum incubation of 96 h; sacrifice of animal required; limited availability of human material
Co-cultures	Mimic liver physiological condition; non-parenchymal cells regulate hepatocyte function	Difficult to establish due to different culture requirements by the different cell types
Bioartificial liver (3D models and microfluidic systems)	liver-like properties due to integration of liver microenvironment	Current strategies only partially mimic liver microenvironment
Isolated hepatocytes, cultured in sandwich conformation	Metabolism is maintained[6], repeated dosing feasible	2D culture; sacrifice of animal required; limited availability of human material
Isolated hepatocytes, cultured in conventional monolayer	Ease of use, metabolism is maintained	2D culture, sacrifice of animal required; limited availability of human material; maximum time in culture: 3 - 5 d

1.4 EU-project Predict-IV

The rising costs and increasing attrition rates is a problematic situation for the pharmaceutical industry. The failure of new drug candidates during development can mainly be attributed to lack of efficacy and unpredicted toxicity in animals and humans (Kola and Landis, 2004). To address these current challenges, the EU-funded collaborative project Predict-IV was initiated. Predict-IV is used as acronym (IV stands for *in vitro*) for the project's full title: "Profiling the toxicity of new drugs: a non-animal based approach integrating toxicodynamics and biokinetics" (Predict-IV website: www.predict-iv.toxi.uni-wuerzburg.de). The project ran from 2008 to 2013 and was funded by the EU's *Seventh Framework Programme for Research and Technological Development* (FP7) under the grant agreement number 202222. The Predict-IV project aimed to develop a novel *in vitro* testing strategy for the assessment of drug safety. The application in the early stage of development and late discovery phase should help to improve the early identification of inacceptable toxicity and pharmacokinetics.

A total of three target organs, namely liver, kidney and the central nervous system, were addressed within the project. Recent advances in *in vitro* technologies allowed the integration and optimisation of the most appropriate cell culture model for each target organ, i.e. it was not envisaged to develop new *in vitro* models. The Predict-IV strategy (Figure 10) included different toxicodynamic (toxicogenomics, proteomics, metabolomics, high content imaging) and *in vitro*

[4] Boess et al., 2003
[5] Elferink et al., 2008
[6] Tuschl et al., 2009

biokinetics endpoints. The generated data should lead to the establishment of a no-observed-effect-concentration (NOEC) *in vitro*, which can be translated into *in vivo* doses using physiologically-based pharmacokinetic (PBPK) modelling. Here, the determination of polymorphisms in the major DMEs was supposed to further help to integrate inter-individual susceptibilities. The difference between the predicted no-observed-adverse-effect-level (NOAEL) and reported therapeutic dose levels *in vivo* could then be used to deduce a margin of safety, which serves as benchmark to support drug candidate selection.

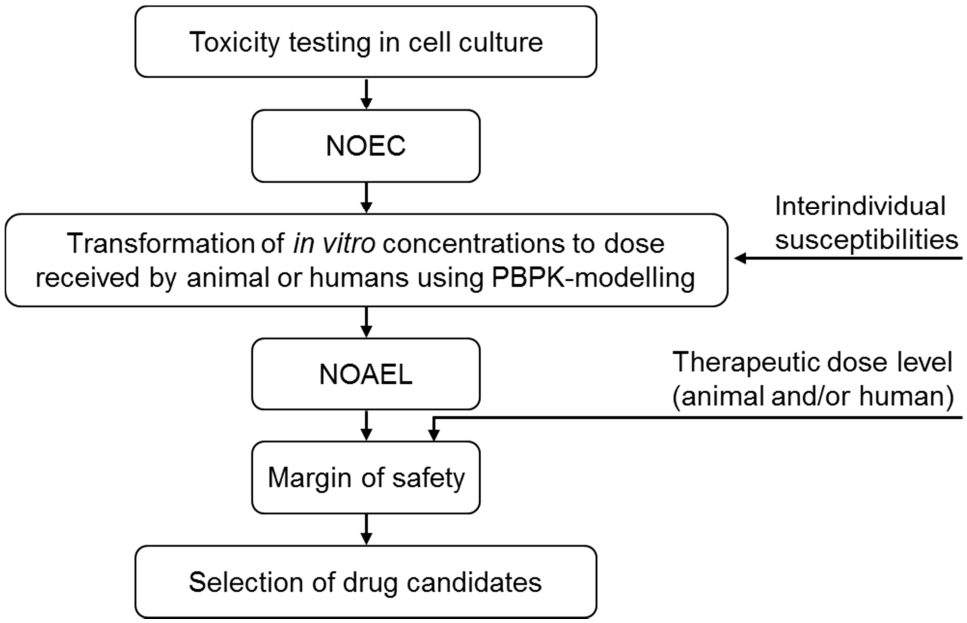

Figure 10. Proposed Predict-IV strategy for the use of the generated *in vitro* data for the assessment of drug safety. The integrated analysis of the results from cell culture assays and biokinetics measurements provide no-observed-effect-concentration (NOEC) *in vitro*. The NOEC will be translated into an *in vivo* no-observed-adverse-effect-level (NOAEL) using physiologically-based pharmacokinetic (PBPK) modelling. Comparison of the predicted NOAEL and the reported therapeutic dose level allows the calculation of a margin of safety, which helps the selection of new drug candidates.

The approach included the use of drugs with organ-specific toxicities in liver, kidney and the central nervous system. Well described toxicity and information on kinetics in animals and humans were criteria for the compound selection. This enabled the comparison of the *in vitro* results to existing *in vivo* data. Table 6 shows the final compound list specific for the different target organs.

Table 6. Final compound list for the assessment of organ-specific toxicities. Bold writing indicates compounds used in more than one organ system. Biokinetics was measured only for a subset of compounds (blue).

Liver	Kidney	Central nervous system
Acetaminophen	Acyclovir	Buflomedil
EMD 335823	Adefovir dipivoxil	Carbamazepine
Fenofibrate	Cadmium chloride	Ciprofloxacin
Metformin	Cidofovir	Diazepam
Rosiglitazone	**Cis-platinum**	**Cis-platinum**
Troglitazone	Ibandronate	Loperamide
Valproic acid	Iopromide	Nadolol
	Tenofovir	Ondansetron
Amiodarone	Vancomycin	**Amiodarone**
Chlorpromazine	Zoledronic acid	**Chlorpromazine**
Cyclosporine A	**Cyclosporine A**	**Cyclosporine A**
Ibuprofen		Propofol

Therefore, this project aimed to develop an integrated analysis of dynamic and kinetic endpoints to predict toxicity prior to pre-clinical animal testing. Along with elucidation of the compound's mode-of-action, this strategy should further enable the identification of relevant biomarkers of toxicity.

The Predict-IV consortium comprised a total of 21 partners from academia and industry, forming a multidisciplinary team with expertise in various scientific areas (analytical chemistry, biochemistry, cellular model development, toxicogenomics, proteomics, metabolomics, high content imaging, bioinformatics, kinetic modelling, toxicology and risk assessment). The work carried out and reported in this thesis was part of the Predict-IV project, contributing to the liver work package, which focussed in the prediction of liver toxicity. The liver work package included three hepatocyte systems, namely primary rat and human hepatocytes and the novel human hepatoma-derived cell line, HepaRG. Primary hepatocytes are considered as the gold standard for metabolism studies (Castell et al., 2006), while HepaRG cells represent a robust functioning hepatic cell line that is discussed as a potential surrogate for human hepatocytes (Aninat et al., 2006). Each hepatocyte system was cultured according to its optimal conditions and treated hepatotoxic compounds (Table 6). The analysis of the results deriving from the different hepatocyte systems should help to identify species differences. Furthermore, a direct comparison of the HepaRG cells with primary human hepatocytes should reveal benefits and limitations of this novel cell line for their use in future toxicity and drug metabolism studies.

1.5 Compounds - the good, the bad and the ugly

1.5.1 Pharmaceuticals with hepatotoxic potential

1.5.1.1 Ibuprofen

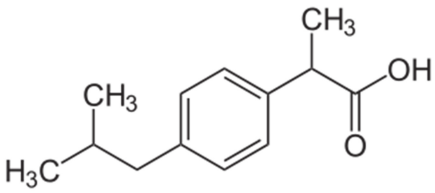

Ibuprofen (IBU) is a NSAID with analgesic, antipyretic and antiphlogistic properties that is frequently used for the treatment of mild to moderate pain and inflammatory diseases, such as rheumatoid arthritis and osteoarthritis (RxList - Motrin, 2007). At therapeutic concentrations, it non-specifically inhibits the cyclooxygenase enzymes (COX-1 and -2), thus preventing the synthesis of prostaglandins, which are involved in the development of pain, fever and inflammatory processes. IBU belongs to the class of 2'-arylpropionic acids, also known as profens, which contain a carboxylic acid moiety and a chiral centre at the 2' position of the propionic acid group. The inflammatory activity of IBU is associated with the (S)-(+)-enantiomer (Adams et al., 1976); whereas, chiral inversion of the (R)-(-)-IBU is observed not only *in vivo* (Knihinicki et al., 1990; Lee et al., 1985) but also *in vitro* (Tracy and Hall, 1991).

IBU was originally developed as an antirheumatic agent (Adams et al., 1967) in 1961. After proving its effectiveness and safety in clinical trials it was launched on the market as Brufen™ in 1969, before eventually being available as a prescription-free drug in 1983 (Rainsford, 1999).

Gastrointestinal adverse reactions are the most frequently reported side effects with IBU, with percentages ranging from 4 - 16% in clinical trials (RxList - Motrin, 2007). Gastric ulceration and perforation result from drug-induced inhibition of prostaglandins, which are physiologically important because they play a role in the protection of the gut's mucosal barrier from harmful agents (Lichtenstein et al., 1995; Shorrock and Rees, 1988). Further IBU-mediated adverse reactions include those to the (i) central nervous system (dizziness, headache), (ii) cutaneous reactions (rash, pruritus) and (iii) cardiovascular safety (edema, fluid retention) (Rx List - Motrin, 2007); however, these are considerably less severe compared to other NSAIDs. Specific liver toxicities are rarely reported with IBU; however, there are case reports of varying hepatopathies associated with exposure to IBU, including hepatitis (Laurent et al., 2000), hepatic cholestasis (Elkrief et al., 2007), hepatic failure (Rodriguez-Gonzalez et al., 2002) and vanishing bile duct syndrome (Taghian et al., 2004). Overall, IBU is considered to be a safe NSAID with rare incidences of liver toxicities (Bennett et al., 2009; Laurent et al., 2000; Rodriguez-Gonzalez et al., 2002).

The metabolism of IBU includes phase I and II metabolising enzymes. In humans, IBU is metabolised mainly by CYP2C9 and to a lower extent by CYP2C8 (Chang et al., 2008) forming the major metabolites, 2-hydroxy-IBU and carboxy-IBU, that are eliminated mainly via the urine (Hamman et al., 1997). The Cyp2c6 and Cyp2c11 enzymes are the rat orthologues of human

CYP2C9 (Daniel et al., 2006; Vecera et al., 2011) and hence thought to be involved in the transformation of IBU in the rat. UGT2B7 and UGT1A3 are the main enzymes contributing to the phase II metabolism of IBU in humans (Kuehl et al., 2005). Like most drugs with carboxylic acid moieties, IBU is conjugated to uridine diphosphate glucuronic acid, the cofactor used by uridine 5'-diphospho-glucuronosyltransferases (UGTs, phase II DMEs); hence forming acyl glucuronides. A further metabolite often produced from drugs possessing a carboxylic acid moiety is the corresponding CoA thioester. In recent years these two reactive metabolites (acyl glucuronide and CoA thioester) have been discussed as important mediators of drug-induced toxicity (Regan et al., 2010).

The urinary metabolite profiles revealed differences between human and rat. 2-Hydroxy-IBU-acyl glucuronide was the major metabolite in humans, while 2-hydroxy ibuprofen dominated in rats. The CYP-mediated transformation of IBU was 19% in humans and 37% in rats, while glucuronidation amounted to 41% in humans and 21% in rats (Sanoh et al., 2012). Taken together, phase II metabolism is more pronounced in humans, while phase I activation prevails in rats.

The inhibition of the beta-oxidation of fatty acids is an off-target effect of IBU. So far, there are three known mechanisms by which the drug exerts this inhibition. The beta-oxidation of fatty acids in mitochondria first requires the activation of fatty acids by coupling to the cofactor, CoA, a reaction that is catalysed by acyl-CoA-synthetases. During the metabolic inversion process of R-(-)-IBU to the pharmacologically active S-(+)-IBU, ibuprofenyl-CoA is formed; whereas, formation of CoA thioesters was found to be stereoselective for the (R)-Enantiomer (Knadler et al., 1990; Knights et al., 1988; Knihinicki et al., 1989). However, the stereoselective inhibition of beta-oxidation via CoA sequestration by R-(-)-IBU was shown to be dependent on the CoA concentration itself, such that inhibition was stronger at low CoA concentrations (Freneaux et al., 1990). Hence, this mechanism is more relevant *in vitro*, where CoA concentrations are reported to be lower compared to *in vivo* (liver cell cytosol concentration of 50 µM (Williamson and Corkey, 1979)). The medium- and long-chain, but not the short-chain fatty acyl-CoA-synthetases, are reported to be involved in the ibuprofenyl-CoA synthesis (Tracy et al., 1993). In summary, the inhibition of acyl-CoA-synthetases and sequestration of CoA by IBU hampers the activation and thus catabolism of fatty acids. Furthermore, IBU is reported to inhibit complex I of the mitochondrial respiratory chain (Sandoval-Acuna et al., 2012). This inhibition leads to the accumulation of NADH, which cannot transfer its electrons to coenzyme Q10 and thus, is not oxidised to NAD^+, a cofactor needed by the hydroxyacyl-CoA-dehydrogenase during beta-oxidation. In addition, the inhibition of the beta-oxidation leads to a reduced synthesis of $FADH_2$, which serves as an electron donor in the oxidative phosphorylation (at the level of complex II: succinate dehydrogenase). Consequently, beta-oxidation and oxidative phosphorylation are closely linked together.

To conclude, taking the frequent use of this over-the-counter analgesic into consideration, the potential of IBU to induce liver toxicity in humans can be considered minor; thus, making IBU a safe drug and represents a negative compound in this work.

1.5.1.2 Chlorpromazine

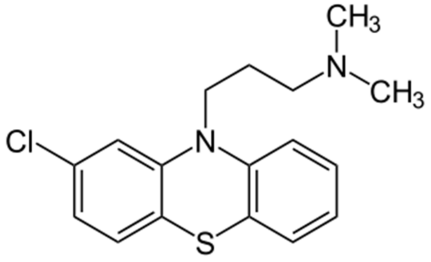

Chlorpromazine (CPZ) is a phenothiazine mainly prescribed for the treatment of psychotic disorders, but also for nausea and intractable hiccups. The molecular mechanisms by which CPZ exerts its pharmacological actions are still unclear. As a typical antipsychotic drug it acts primarily as an antagonist of dopamine D2 receptors. However, CPZ blocks multiple (different) neurotransmitter receptors, hence exhibiting a broad spectrum of action. The pharmacological actions include central-depressant and antipsychotic effects, but it also has antiemetic, local anaesthetic, ganglion-blocking, anti-adrenergic, anti-cholinergic, anti-histaminergic properties and impairs the bodies thermoregulation (anonymous 1967; Kopera and Armitage, 1954; Mutschler, 2013).

Synthesised in the laboratories of the French pharmaceutical company Rhône-Poulenc, CPZ was released onto the market in 1952 under the brand name *Largactil* (Ban, 2007). To date, CPZ remains the primary drug for treating schizophrenia (Liu and DeHaan, 2009).

Common adverse effects associated with the use of CPZ include those on the central nervous system, inducing dystonia, motor restlessness, pseudo-parkinsonism and tardive dyskinesia. Furthermore, adverse effects on the cardiovascular system are reported, mainly in the form of hypotension leading to drowsiness and tachycardia. After prolonged treatment periods depositions of fine particular matter in eye lenses and corneas lead to ophthalmic reactions and occur more often than dermatologic effects (skin pigmentation) (RxList - Thorazine, 2008).

Long-term therapy with CPZ results in elevated liver enzymes in up to 40% of patients, where some parameters (serum aminotransferases) tend to normalise without discontinuation of the drug (NIH - Chlorpromazine, 2014). Since its introduction in the 1950s, CPZ has always been associated with hepatotoxicity (Werther and Korelitz, 1957) comprising primarily cholestatic liver injury that potentially promotes to vanishing bile duct syndrome (Chitturi and George, 2002).

The metabolism of CPZ in the liver is extensive, including S-oxidation, N-oxidation, hydroxylation, desmethylation, and di-desmethylation (Hartmann et al., 1983). The resulting metabolites hold a distinct pharmacological and toxicological potential (Abernathy, 1977). In humans, CYP1A2, 2C19, 2D6 and 3A4 are involved in the metabolism of CPZ (Yoshii et al., 2000; Wójcikowski et al., 2010). A comparison of human and rat liver microsomes revealed that both species generate the same CPZ metabolites; although, to different extents. Whereas

7-hydroxylation and sulfoxidation rates were comparable, demethylation and oxidative deamination were lower in human compared to rat microsomes (Coccia and Westerfeld, 1967).
CPZ affects multiple cellular mechanisms, which results in a variety of pathological manifestations. It inhibits bile salt secretion, which eventually leads to the intra-hepatic cholestasis observed *in vivo*. *In vitro* studies have elucidated that the cholestatic pathology is initiated at the molecular level, where CPZ reduces the expression of canalicular bile salt transporters (*BSEP*, *MDR3*) (Antherieu et al., 2013). Furthermore, CPZ is known to inhibit peroxisomal beta-oxidation of long-chain fatty acids (Leighton et al., 1984; Vamecq, 1987). At the level of mitochondrial function, CPZ inhibits mitochondrial beta-oxidation. Furthermore, energy production via oxidative phosphorylation is reduced, because the drug inhibits complex I (Modica-Napolitano et al., 2003) and impairs the mitochondrial membrane potential (MacAllister et al., 2013). An impaired mitochondrial respiratory chain represents a source of ROS. In fact, ROS generation is considered to play an important role during CPZ-induced hepatotoxicity. As a cationic amphiphilic drug, CPZ is capable of inducing phospholipidosis (Brosnan et al., 1970), which so far has only been reported in animals. In controlled studies CPZ was found to increase cholesterol levels significantly (Clark et al., 1967; Mefferd et al., 1958).
In conclusion, although now rarely used, CPZ is known to cause acute and chronic cholestatic liver injury in humans which allows it to be used as a positive hepatotoxic drug in the present work.

1.5.1.3 Cyclosporine A

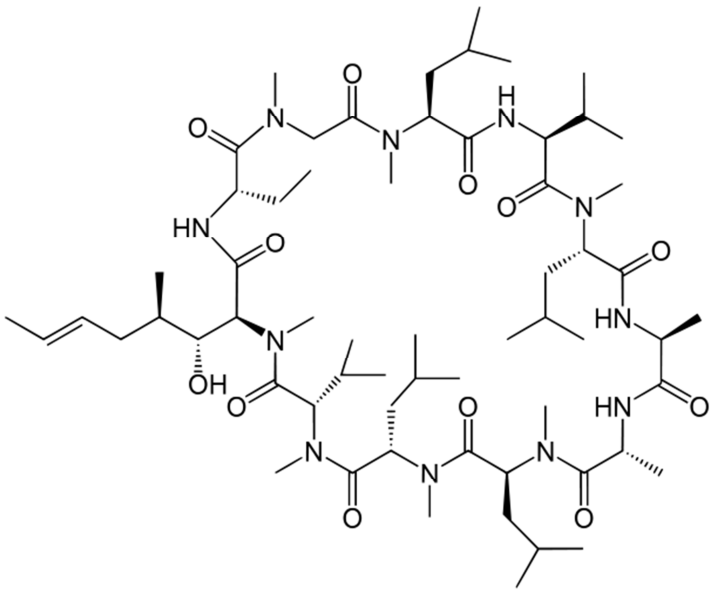

The cyclic polypeptide, cyclosporine A (CsA), consists of 11 amino acids and is a product of the fungus *Tolypocladium inflatum*. The drug is used to suppress humoral and cellular immune reactions required for organ transplantations and autoimmune diseases. CsA exerts its pharmacological action on T-cells where it binds to cyclophilin. The CsA-cyclophilin complex inhibits the phosphatase activity of the calcineurin-calmodulin complex, which normally activates the transcription factor, nuclear factor of activated T-cells (NFAT), after antigen binding. In the presence of CsA, the calcineurin-calmodulin complex fails to activate NFAT and thus the transcription of interleukin-2, which is needed for the maturation of T-cells to cytotoxic T-cells (Mutschler, 2013).

In 1983 Sandoz, now Novartis, introduced CsA to the market under the brand name *Sandimmune*®, which immediately became a standard therapy for the prevention of graft rejection (Staehelin, 1996).

The main side effects reported for CsA are renal dysfunction, tremor, hypertension and hirsutism[7] (RxList - Sandimmune, 2013). Nephrotoxicity is the most frequent and clinically important adverse effect of CsA. The drug induces time- and dose-dependent renal cell apoptosis, which is thought to be the main mechanism leading to chronic CsA-induced nephrotoxicity (Xiao et al., 2013). Reversible hepatotoxicity (elevated serum enzymes and bilirubin) occurred during controlled clinical trials in 4 - 7% of kidney, heart and liver transplant patients (RxList - Sandimmune, 2013). Case reports of acute liver injury are rare, while other more severe liver toxicities (chronic hepatitis, acute liver failure, vanishing bile duct syndrome) have not been reported (NIH - Cyclosporine, 2014). However, cholestatic effects have been shown to occur in rats treated with CsA (Chan and Shaffer, 1997).

The enzymes involved in the biotransformation of CsA are CYP3A4 and CYP3A5 in human (Zochowska et al., 1990) and Cyp3a1/2 in rat (Brunner et al., 1998). Phase I metabolism in the liver leads to a large number of metabolites, while Phase II metabolism was shown to play a minor role (Christians et al., 1991). The nomenclature of CsA metabolites follows a code system where the position of the biotransformation is considered, e.g. oxidation at site 1 η (8') or 4 γ

[7] Excessive facial and body hairiness.

corresponds to the metabolites AM1 or AM4, respectively (Kahan et al., 1990). The metabolites are transported via ABCB1 into the bile for excretion (Staatz, 2010). CsA metabolism studies in liver slices revealed a lower metabolic rate in rats (~ 81%) compared to human (Vickers et al., 1992). Furthermore, the profile of primary metabolites reflected the species differences *in vivo*, with metabolite M1 predominating in rat and M17 in human (Vickers et al., 1992).

At the molecular level, CsA and its metabolites are known to inhibit the canalicular bile salt transporters by simply being substrates (i.e. a competitive inhibitor). This competitive inhibition results in the intracellular accumulation of toxic bile salts. Furthermore, the impaired bile salt secretion and thus bile flow is linked to hepatic cholestasis, which is the hepatopathy observed *in vivo* (Chan and Shaffer, 1997). CsA inhibits enzymes involved in beta-oxidation (Illsinger et al., 2011), which leads to the intracellular accumulation of fatty acids and lipids. In line with this, the drug has been shown to induce lipid accumulation in *in vitro* assays using HepG2 cells (McMillian et al., 2001). A further consequence of an inhibited beta-oxidation is the impairment of oxidative phosphorylation and thus an increased electron leakage. This results in the generation of ROS, which is considered to be a cause of CsA-induced cytotoxicity *in vitro* (deArriba et al., 2013; Jennings et al., 2007; Rezzani, 2006). The pharmacological effect of CsA, i.e. immunosuppression, is considered as an intrinsic risk factor for patients to develop cancer and numerous case reports justify the listing of CsA as known human carcinogen (NTP - 12th RoC, 2011; Ryffel et al., 1992).

In conclusion, there are a number of reports of clinically apparent cholestatic liver injury caused by CsA (although it is rare); therefore, this drug was employed as a positive compound in these studies.

1.5.1.4 Amiodarone

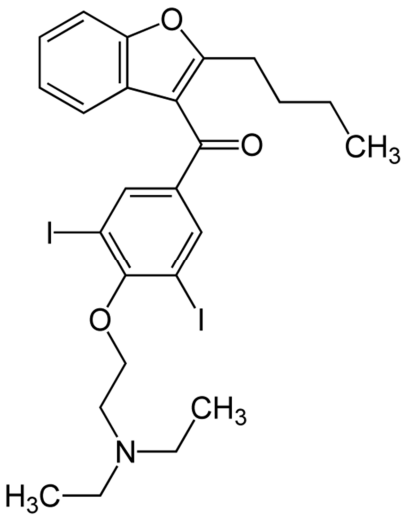

Amiodarone (AMI), an iodinated benzofuran derivative, is used for the treatment of supraventricular and ventricular cardiac arrhythmias (Mutschler, 2013). It is an antiarrhythmic drug with mainly Class III (Vaughan Williams' classification[8]) effects, but holds also mild Class I, II and IV effects (Sohns and Zabel, 2010). AMI exerts its main pharmacological action (Class III effect) by inhibition of potassium-channels, resulting in a prolonged action potential. In 1961, AMI was introduced by the Belgium company Labaz to treat angina pectoris. Its progenitor molecule is khellin, the active ingredient of *ammi visnaga* extract and known as a cardio effective glucoside.

AMI is known to accumulate in body tissues and has an extremely long half-life of 25 ± 12 days (DIDB - Amiodarone, 2014). The side effects of AMI therapy include worsening of the cardiovascular situation, pulmonary toxicity leading to lung fibrosis, thyroid dysfunction (hypo- and hyperthyreosis), ophthalmic and dermatological reactions (RxList - Cordarone, 2014). The ophthalmic side effects are attributed to accumulation of the compound in the cornea, while dermatological reactions occur due to pigmentation and photosensitivity (Rx List - Cordarone, 2014). Reported liver pathologies include phospholipidosis, steatohepatitis, liver inflammation and cirrhosis. AMI is reported to inhibit beta-oxidation and stimulate *de novo* lipogenesis (Massart et al., 2013), which in some patients manifests as macrovacuolar or serious microvesicular steatosis (Lewis et al., 1990).

Cyp3a2 and CYP3A4/2C8 are the main monooxygenases involved in the phase I metabolism of AMI in the rat (Shayeganpour et al., 2006) and human (Fabre et al., 1993; Ohyama et al., 2000), respectively. These CYP isoforms are highly expressed in the liver and mediate the deethylation of AMI, resulting in the major metabolites, mono-N-desethylamiodarone and di-N-desethylamiodarone, which are relevant to the observed toxicities after treatment with this drug.

Various *in vivo* and *in vitro* approaches revealed that AMI's hepatotoxicity is primarily due to adverse effects on the mitochondria (Fromenty and Pessayre, 1995). The effect on mitochondrial respiration is biphasic, starting with increased oxygen consumption due to uncoupling of the oxidative phosphorylation and followed by decreased respiration based on complex I and II inhibition (Fromenty et al., 1990b; Kaufmann et al., 2005; Spaniol et al. 2001; Waldhauser et al. 2006). The inhibition is observed only at higher concentrations (> 200 µM *in vitro*), i.e. when AMI accumulation in the mitochondrial matrix exceeds a concentration threshold (Fromenty et al., 1990b). Zahno et al. (2011) showed that the CYP3A4-derived metabolites, mono-N-

[8] Classification system for antiarrhythmic agents according to their electrophysiological and pharmacological action (Vaughan Williams, 1975). To date, four classes exist with the Class I further containing subclasses IA, IB and IC (Mutschler et al., 2013).

desethylamiodarone and di-N-desethylamiodarone, are more potent inhibitors of the respiratory chain compared to the parent compound and that CYP3A4 induction with rifampicin increased the cytotoxicity of AMI in primary human hepatocytes (PHH). In addition to the adverse effects upon cellular respiration, AMI disrupts mitochondrial fatty acid oxidation (beta-oxidation) (Fromenty et al. 1990a; Kaufmann et al., 2005; Spaniol et al. 2001; Waldhauser et al. 2006). AMI blocks beta-oxidation due to its ability to inhibit carnitine palmitoyltransferase-1, which plays a central role in the transport of long-chain fatty acids into the mitochondria (Kennedy et al., 1996) but also the acyl-CoA dehydrogenase activity was found to be decreased after treating isolated rat liver mitochondria with AMI (Kaufmann et al., 2005). Consequently, inhibition of beta-oxidation leads to accumulation of free fatty acids (Spaniol et al., 2003) and microvesicular steatosis *in vivo* (Fromenty and Pessayre, 1995).

Overall, inhibition of the electron transport chain and uncoupling of oxidative phosphorylation, either by AMI itself or accumulating free fatty acids that act as extrinsic uncouplers (Kadenbach, 2003), results in the generation of ROS due to electron leakage. ROS formation can induce mitochondrial permeability transition pore opening which results in mitochondrial swelling and disruption of the outer membrane (Green and Reed, 1998). Subsequently, release of cytochrome c and other apoptosis-inducing proteins leads to cell death. In keeping with this finding, mitochondrial swelling and cytochrome c release was observed in AMI treated isolated rat liver mitochondria (Kaufmann et al., 2005), and the induction of late apoptosis/necrosis was shown in primary rat hepatocytes (PRH) treated with AMI (Waldhauser et al., 2006). Golli-Bennour et al. (2012) were able to reduce AMI-mediated cytotoxicity by pre-treating HepG2 cells with the antioxidant, vitamin E. Taking the data from current literature together, it can be concluded that AMI exerts its cytotoxic effect *in vitro* via oxidative stress.

In conclusion, although usually mild, liver injury is a common side-effect of AMI, thus, this drug was employed as a positive compound in this work.

1.5.2 Compounds with and without mitochondrial toxic potency

The pharmaceuticals used in these studies are all reported to affect mitochondrial function. Therefore, an assay for the assessment of the mitochondrial toxicity was established, where effects on the cellular oxygen consumption was determined. For this purpose positive agents known to act toxic on mitochondrial respiration were included in the experiments (antimycin, carbonyl cyanide 4-(trifluoromethoxy)phenylhydrazone (FCCP), metformin, oligomycin, rotenone), as well as negative compounds (D-mannitol, n-butyl chloride).

Table 7. List of positive and negative controls used for the evaluation of the mitochondrial toxicity assay including the corresponding application and toxic effect on mitochondrial function.
Abbreviations: FCCP - carbonyl cyanide 4-(trifluoromethoxy)phenylhydrazone; ATP - adenosine triphosphate; NADH - nicotinamide adenine dinucleotide.

	Compound	Application	Toxic effect on mitochondria
Positive controls	Antimycin A (secondary metabolite of *Streptomyces* bacteria)	Active ingredient in fish poison (a piscicide) (Seipke and Hutchings, 2013)	Inhibition of complex III (cytochrome c oxidoreductase) by blocking the electron transfer from cytochrome b_H to a quinone within the cytochrome reductase (Schaegger et al., 1995)
	FCCP (chemical)	Synthetic proton ionophor	Uncoupling by transfer of protons from the mitochondrial inter-membrane space to the matrix, which results in the collapse of the pH gradient needed for ATP production.
	Metformin (pharmaceutical)	Treatment of non-insulin-dependent diabetes mellitus (developed in the 1950s)	Induction of mitochondrial biogenesis and thus increase energy metabolism (Kukidome et al., 2006)
	Oligomycin (product of *Streptomyces* species)	Antibiotic	Inhibition of the F_1/F_0 ATPase by binding to the F_0 subunit of the complex V, which results in a blocked proton transport through F_0 and therefore an inhibition of both ATP synthesis and hydrolysis (Pagliarani et al., 2013).
	Rotenone (produced by several plants, including species from the legume families (Cabezas et al., 2012))	Active ingredient in insecticide and piscicide	Inhibition of complex I (NADH:ubiquinone oxidoreductase) by impairing the electron transfer from NADH to the oxidised flavin mononucleotide (Horgan et al., 1968)
Negative controls	D-mannitol (sugar alcohol)	Clinical use: acute glaucoma (Shin et al., 2013), nephroprotection (Morgan et al., 2012) and treatment of Ciguatera Fish Poisoning (Friedman et al., 2008) In foods: sucrose substitute with very low glycaemic index (Livesey, 2003)	Inhibition of the mitochondrial permeability transition, thereby preventing mitochondrial swelling and a drop of the membrane potential (Sava et al., 2006). In sum, mitochondria protective and not toxic.
	n-butyl chloride (chemical)	Anthelmintic agent for veterinary deworming (HSDB - n-butyl chloride, 2003)	No adverse interaction with mitochondrial function reported.

1.6 Aim of work

The presented work in this thesis was part of the EU-project Predict-IV, which aimed to develop strategies to improve the assessment of drug safety in the early stage of development and late discovery phase.

The overall aim of this work was to evaluate multiple endpoints for the prediction of a drug's potential to induce liver toxicity. The evaluation involved an integrated approach using optimised cell models and advanced kinetic and dynamic endpoints (biokinetics, transcriptomics, proteomics and metabolomics). Therefore, the first part of this thesis focussed on data from studies using primary rat and human hepatocytes after short- and long-term repeated exposure to drugs with known toxicities and pharmacokinetics in animals and humans (namely IBU, CPZ, CsA and AMI). The *Omics* technologies should help to elucidate the mode of action of the drugs in a complementary manner. The hepatic culture systems employed allowed a long-term exposure to the compounds, thus mimicking repeated-dosing *in vivo*. Sequential sampling times on days 1, 3 and 14 should reveal potential time-dependent manifestations of the adverse effect(s). In addition, the application of a low and high treatment concentration was expected to allow discrimination between pharmacological and toxicological drug-induced effects, respectively. The use of rat and human hepatocytes should allow for the identification of potential species differences in response to drug treatment. Finally, the *in vitro* results need to be compared to existing *in vivo* data in order to comment on the suitability of the applied cell models for their prediction of liver toxicity.

All four compounds were reported to impair mitochondrial function. Hence, the second focus was on the implementation and evaluation of different approaches to analyse drug-induced mitochondrial toxicity. The assays employed included ATP measurement and two protocols for the measurement of cellular respiration (*MitoXpress O_2-sensitive probe respiration assay* and *Seahorse MitoStress assay*). For this purpose, PRH and the human hepatoma cell lines, HepG2 and HepaRG, were used. The susceptibility to mitochondrial toxins of the HepG2 cell line was increased further by adapting the cells to galactose-containing (glucose-free) cell culture medium; thus, forcing the cells to produce ATP via mitochondrial oxidative phosphorylation rather than via glycolysis. In order to estimate the potential of IBU, CPZ, CsA and AMI to act as mitochondrial toxicants, known positive and negative compounds were included in the different assays.

1.7 Personal contributions

This thesis was embedded in the EU-funded project Predict-IV, which represents a collaboration of partners with diverse scientific expertise. All generated data in this multidisciplinary team belongs to the Predict-IV consortium. With the consent of the consortium, internal and external generated data of the four pharmaceuticals (IBU, CPZ, CsA and AMI) was used for this thesis. In the following paragraphs a comprehensive overview on my personal contributions is given.

Dose finding studies for pharmaceutical compounds in the liver work package

I performed the dose-finding studies for IBU, CPZ, CsA and AMI in PRH, analysed and presented the results on my own responsibility. Furthermore, I was mainly involved in the decision making for the TC_{10} in PRH, and the other two hepatic systems PHH and HepaRG cells.

Sampling optimisation for kinetics and proteomics

During preparation of the cell lysate fractions, it was not possible to separate the cells from the surrounding collagen. However, the residual collagen negatively affected analytics. I considered and tested different strategies to remove excessive collagen from the cell lysate fraction, including collagenase digestion and the improved protein and RNA extraction protocol recently published by Heidebrecht et al. (2009). Finally, no removal strategy was applied, due to a lack of reproducibility.

Time point selection for kinetics experiments

My contribution included comprehensive literature search for the assigned compound CsA. Furthermore, I was mainly involved in the discussions on time point selection for all four biokinetic compounds.

Tissue culture and sample generation for final experiments

I conducted the final studies in PRH for IBU, CPZ, CsA and AMI, including sandwich culture preparation and daily treatment for up to 14 days. This included sample processing for transcriptomics, proteomics, metabolomics (NMR and MS) on day 1, 3 and 14. Furthermore, samples for biokinetics were collected on five specific time points on day 0 and day 13. A total of three biological replicates were completed for proteomics, metabolomics and biokinetics, while five biological replicates were completed for transcriptomics. For the characterisation of the different replicates, samples for CYP activity and CYP induction measurement were included.

Determination of the cell number per well

It was decided that the cell number per well should be used for normalisation of the cell lysate concentration measured for the biokinetic profiling. Based on the failed approach to use the DNA content for this purpose, I established a high content imaging-based cell count protocol for the long-term culture in PRH on my own initiative.

Data generation

The generated PRH samples were processed by me. This comprised RNA amplification and hybridisation for transcriptomics and the measurement of CYP induction using the QuantiGene® assay.

Statistical analysis of PRH and PHH transcriptomics data

I performed the statistical analysis of the global gene expression data used in my thesis.

Biological interpretation of results

My major task was the biological interpretation of biokinetics, transcriptomics and proteomics data for PRH and PHH treated with the four pharmaceuticals, as described above. The CYP activities (PRH and PHH) and CYP induction were considered, in order to account for inter-individual susceptibilities (human) and species differences.

Further contributions

I was responsible for data presentation during regular project meetings, as well as writing project deliverables and reports.

Mitochondrial toxicity

The experiments on mitochondrial toxicity were conducted as supplemental information beyond the Predict-IV project upon my own initiative and comprise the following actions:

- Pre-validation of MitoXpress assay
- Compound selection
- Implementation of MitoXpress O_2-sensitive probe and Seahorse MitoStress assay experiments
- Sample measurement
- Data analysis
- Biological interpretation

2 Materials and Methods

2.1 Materials

2.1.1 Consumables

Name	Manufacturer, Corporate headquarters
6-well Multiwell™, BD Falcon™	Becton Dickinson GmbH, Heidelberg, Germany
15 mL tubes, Cellstar®	Greiner Bio-One GmbH, Frickenhausen, Germany
50 mL tubes, Cellstar®	Greiner Bio-One GmbH, Frickenhausen, Germany
24-well cell culture plates, Cellstar®	Greiner Bio-One GmbH, Frickenhausen, Germany
96-well Microplates, black/clear, BD Falcon™	Becton Dickinson GmbH, Heidelberg, Germany
96-well Microplates, white/Clear, BD Falcon™	Becton Dickinson GmbH, Heidelberg, Germany
96-well polystyrene plates, round bottom, costar®	Corning Inc., Corning (NY), USA
Adhesive PCR Foil Seals, ABgene®	Thermo Fisher Scientific, Waltham (MA), USA
ART 10 REACH, disposable tips	Molecular BioProducts, San Diego (CA), USA
ART 20P, disposable tips	Molecular BioProducts, San Diego (CA), USA
ART 100E, disposable tips	Molecular BioProducts, San Diego (CA), USA
ART 200, disposable tips	Molecular BioProducts, San Diego (CA), USA
ART 300, disposable tips	Molecular BioProducts, San Diego (CA), USA
ART 1000E, disposable tips	Molecular BioProducts, San Diego (CA), USA
ART 1000G, disposable tips	Molecular BioProducts, San Diego (CA), USA
BeadChip Array RatRef-12 v1	Illumina Inc., San Diego (CA), USA
BeadChip Array HumanHT-12_v4	Illumina Inc., San Diego (CA), USA
BioRobotix™ Tips, 1000 µL	Molecular BioProducts, San Diego (CA), USA
BioRobotix™ Tips, 175 µL	Molecular BioProducts, San Diego (CA), USA
BioRobotix™ Tips, 50 µL	Molecular BioProducts, San Diego (CA), USA
BioRobotix™ Tips, 10 µL	Molecular BioProducts, San Diego (CA), USA
Bottle Top Filters - 1000 mL Capacity	Nalgene, Rochester (NY), USA
CASY®cup	Schaerfe System GmbH, Reutlingen, Germany
Cell counter, Fuchs-Rosenthal, bright-line	LO-Laboroptik, Lancing, UK
Cell culture flasks, 75 cm², Cellstar®	Greiner Bio-One GmbH, Frickenhausen, Germany
Cell culture flasks, 175 cm², Cellstar®	Greiner Bio-One GmbH, Frickenhausen, Germany
Cell Scrapers	Iwaki® cell biology, Asahi Techno Glass Corporation, Chiba, Japan
Multipette® tips 1 mL	Eppendorf AG, Hamburg, Germany
Multipette® tips 2.5 mL	Eppendorf AG, Hamburg, Germany
Multipette® tips 5 mL	Eppendorf AG, Hamburg, Germany
Multipette® tips 10 mL	Eppendorf AG, Hamburg, Germany
Parafilm® “M” Laboratory Film	Bemis® Company Inc., Neenah (WI), USA
pH-indicator paper pH 6.4 - 8.0 Special indicator	Merck KGaA, Darmstadt, Germany
Pipette Tips, 0.5 - 20 µL	Brand GmbH&Co. KG, Wertheim, Germany
Pipette Tips, 2 - 200 µL	Brand GmbH&Co. KG, Wertheim, Germany
Pipette Tips, 5 - 300 µL	Brand GmbH&Co. KG, Wertheim, Germany

Pipette Tips, 50 - 1000 µL	Brand GmbH&Co. KG, Wertheim, Germany
Protein LoBind tubes, 2 mL	Eppendorf AG, Hamburg, Germany
QIAshredder™ (250)	Qiagen, Hilden, Germany
Safe-lock tubes, 2 mL	Eppendorf AG, Hamburg, Germany
Safe-lock tubes, 1.5 mL	Eppendorf AG, Hamburg, Germany
Serological pipettes 5 mL, NUNC™	Thermo Fisher Scientific, Waltham (MA), USA
Serological pipettes 10 mL, NUNC™	Thermo Fisher Scientific, Waltham (MA), USA
Serological pipettes 25 mL, NUNC™	Thermo Fisher Scientific, Waltham (MA), USA
Serological pipettes 50 mL, NUNC™	Thermo Fisher Scientific, Waltham (MA), USA
Thermosprint™, 96-well PCR plates	Biovendis Ltd., Birmingham, UK
Thermosprint™, 10 mL tubes	Bilatec AG, Heidelberg, Germany
Transparent Sealing Tape PCR (adhesive)	Biovendis Ltd., Birmingham, UK
XF96 Cell Culture Microplates	Seahorse Bioscience, North Billerica (MA), USA
XF96 Sensor Cartridges	Seahorse Bioscience, North Billerica (MA), USA
XF96 Calibration Plates	Seahorse Bioscience, North Billerica (MA), USA

2.1.2 Chemicals and Reagents

Name	Manufacturer, Corporate headquarters
2-Mercaptoethanol	Sigma-Aldrich, Steinheim, Germany
Acetic acid 99 - 100%	Merck KGaA, Darmstadt, Germany
Agencourt® RNAclean XP	Beckman Coulter GmbH, Krefeld, Germany
Albumin Fraction V	Merck KGaA, Darmstadt, Germany
Albumin solution from bovine serum 35% in DPBS	Sigma-Aldrich, Steinheim, Germany
Amersham™ Cy™ 3-Streptavidin 1 mg	GE Healthcare UK Ltd, Buckinghamshine, UK
Ammonium Bicarbonate – ReagentPlus®	Sigma-Adrich, Steinheim, Germany
Block E1 Buffer	Illumina Inc., San Diego (CA), USA
Buffer RLT Plus (220 ml)	Qiagen, Hilden, Germany
Calcium chloride dehydrate	Merck KGaA, Darmstadt, Germany
CASY®ton	Roche Diagnostics GmbH, Mannheim, Germany
Collagen from rat tail tendon	Roche Diagnostics GmbH, Mannheim, Germany
DEPC treated Water, Ambion®	Life Technologies GmbH, Darmstadt, Germany
Dexamethasone	Sigma-Aldrich, Steinheim, Germany
Dimethyl sulfoxide Hybri-Max™	Sigma-Aldrich, Steinheim, Germany
DMEM/F-12, GlutaMAX™, Gibco®	Life Technologies GmbH, Darmstadt, Germany
DMEM/F-12, HEPES, Powder, Gibco®	Life Technologies GmbH, Darmstadt, Germany
DMEM/F-12, HEPES, Gibco®	Life Technologies GmbH, Darmstadt, Germany
DMEM, no Glucose, Gibco®	Life Technologies GmbH, Darmstadt, Germany
DMEM without sodium bicarbonate, powder	Sigma-Aldrich, Steinheim, Germany
DPBS (1x), Calcium, Magnesium, Gibco®	Life Technologies GmbH, Darmstadt, Germany
DPBS (1x), no calcium, no magnesium, Gibco®	Life Technologies GmbH, Darmstadt, Germany
EGTA	AppliChem GmbH, Darmstadt, Germany
Ethanol gradient grade for liquid chromatography LiChrosolv®	Merck Chemicals, Merck KGaA, Darmstadt, Germany

Foetal Bovine Serum, Lot. No. RSJ30856	HyClone® UK Ltd, Cramlington, UK
D(+)-Galactose, anhydrous	Sigma-Aldrich, Steinheim, Germany
Gentamycin, 50 mg/mL, liquid, Gibco®	Life Technologies GmbH, Darmstadt, Germany
D(+)-Glucose	Merck KGaA, Darmstadt, Germany
GlutaMAX™ 200 mM	Life Technologies GmbH, Darmstadt, Germany
Hepa-RG™ Thawing/Plating Medium Supplement, L/N: 1997168	Merck KGaA, Darmstadt, Germany
Hepa-RG™ Tox Medium Supplement, L/N: 2123677	Merck KGaA, Darmstadt, Germany
HEPES	Merck KGaA, Darmstadt, Germany
HEPES Buffer Solution 1 M, Liquid, Gibco®	Life Technologies GmbH, Darmstadt, Germany
High-Temperature Wash Buffer	Illumina Inc., San Diego (CA), USA
Hoechst 33342 trihydrochloride, trihydrate	Life Technologies GmbH, Darmstadt, Germany
Insulin solution human	Sigma-Aldrich, Steinheim, Germany
Insulin-Transferrin-Selenium-G Supplement (100X), Gibco®	Life Technologies GmbH, Darmstadt, Germany
Ketanest™ S 25 mg/mL	Pfizer Pharma GmbH, Berlin, Germany
Liberase TM	Roche Diagnostics GmbH, Mannheim, Germany
Magnesium sulphate heptahydrate, EMSURE®	Merck KGaA, Darmstadt, Germany
Methanol hypergrade for LC-MS LiChrosolv®	Merck KGaA, Darmstadt, Germany
MitoXpress-Xtra-HS	Luxcel Biosciences Ltd, Cork, Ireland
Nuclease-Free Water (not DEPC treated), Ambion®	Life Technologies GmbH, Darmstadt, Germany
Penicillin-Streptomycin (10,000 units Penicillin, 10mg Streptomycin per mL in 0.9% NaCl)	Sigma-Aldrich, Steinheim, Germany
Potassium chloride, EMSURE®	Merck KGaA, Darmstadt, Germany
Potassium dihydrogen phosphate	Merck KGaA, Darmstadt, Germany
RNAprotect™ Cell Reagent (250 mL)	Qiagen, Hilden, Germany
RNase AWAY™	Molecular BioProducts, San Diego (CA), USA
Rompun® Injection Solution 2%	Bayer Vital GmbH, Leverkusen, Germany
Sodium chloride – Suprapur®	Merck KGaA, Darmstadt, Germany
Sodium hydrogen carbonate	Merck KGaA, Darmstadt, Germany
Sodium hydroxide solution 1.0 N	Sigma-Aldrich, Steinheim, Germany
Sodium Pyruvate MEM 100 mM, Liquid, Gibco®	Life Technologies GmbH, Darmstadt, Germany
Trypan Blue 0.5% Solution	EuroClone S.p.A., Milan, Italy
Trypsin-EDTA solution (1X), 0.5 g trypsin and 0.2 g EDTA x 4 Na per L with phenol red	Sigma-Aldrich, Steinheim, Germany
Universal Human Reference RNA	Agilent Technologies, Waldbronn, Germany
Universal Rat Reference RNA	Agilent Technologies, Waldbronn, Germany
Wash E1 BC Buffer	Illumina Inc., San Diego (CA), USA
Williams' Medium E, no Glutamine, Gibco®	Life Technologies GmbH, Darmstadt, Germany
Williams' Medium E without sodium bicarbonate, powder	Sigma-Aldrich, Steinheim, Germany
XF Calibrant Solution	Seahorse Bioscience, North Billerica (MA), USA

2.1.3 Compounds

Name	Manufacturer, Corporate headquarters
Amiodarone hydrochloride	Sigma-Aldrich, Steinheim, Germany
Antimycin A	Sigma-Aldrich, Steinheim, Germany
Chlorpromazine	Sigma-Aldrich, Steinheim, Germany
Cyclosporine A, Calbiochem®	Merck KGaA, Darmstadt, Germany
carbonyl cyanide 4-(trifluoromethoxy)phenylhydrazone (FCCP)	Sigma-Aldrich, Steinheim, Germany
Ibuprofen	Sigma-Aldrich, Steinheim, Germany
Metformin, Calbiochem®	Merck KGaA, Darmstadt, Germany
Oligomycin A	Sigma-Aldrich, Steinheim, Germany
Rotenone	Sigma-Aldrich, Steinheim, Germany

2.1.4 Cells

Name	Manufacturer, Corporate headquarters
Cryopreserved HepaRG™, L/N: N1956555	Merck KGaA, Darmstadt, Germany
Human hepatoma HepG2, L/N: 58483209	LGC Standards, Teddington, UK

2.1.5 Kits

Name	Manufacturer, Corporate headquarters
Agilent RNA 6000 Nano Kit	Agilent Technologies, Waldbronn, Germany
CellTiter-Glo® Luminescent Cell Viability Assay	Promega Corporation, Madison (WI), USA
Illumina® TotalPrep™-96 RNA Amplification Kit, Ambion®	Life Technologies GmbH, Darmstadt, Germany
QuantiGene® Plex 2.0 Assay (rat, 17 Plex), Panel 31104, Panomics	Affymetrix®, Santa Clara (CA), USA
QuantiGene® Plex 2.0 Assay Kit (Magnetic Separation)	Affymetrix®, Santa Clara (CA), USA
QuantiGene® Sample Processing Kit for Cultured Cells	Affymetrix®, Santa Clara (CA), USA
RNeasy®Plus Mini Kit (250)	Qiagen, Hilden, Germany
XF Cell Mito Stress Test Kit	Seahorse Bioscience, North Billerica (MA), USA

Equipment

Name	Manufacturer, Corporate headquarters
Agilent 2100 Bioanalyzer	Agilent Technologies, Waldbronn, Germany
BeadArray Reader	Illumina Inc., San Diego (CA), USA
Bead Chip Cartridge	Illumina Inc., San Diego (CA), USA
CASY® Cell Counter Model TTC	Schaerfe System GmbH, Reutlingen, Germany
Cellomics® ArrayScan® VTI HCS Reader	Thermo Fisher Scientific, Waltham (MA), USA
Centrifuge 5415 R	Eppendorf AG, Hamburg, Germany
Eppendorf Pipettes	Eppendorf AG, Hamburg, Germany
Heraeus® HERAcell® CO_2 incubator	Thermo Fisher Scientific, Waltham (MA), USA
Heraeus® HERAsafe® Sterile bench	Thermo Fisher Scientific, Waltham (MA), USA
Heraeus Megafuge 1.0 R	Thermo Fisher Scientific, Waltham (MA), USA
HydroFlex™ microplate washer for 96-well format	Tecan Group Ltd, Maennedorf, Switzerland
Infinite® F500	Tecan Group Ltd, Maennedorf, Switzerland
Little Dipper Microarray Processor Model 650c	SciGene Corporation, Sunnyvale (CA), USA
Luminex® 200™ System	Life Technologies GmbH, Darmstadt, Germany
LUMIstar Galaxy	BMG LABTECH GmbH, Ortenberg, Germany
Mastercycler® gradient	Eppendorf AG, Hamburg, Germany
Microplate Spectro Photometer MWGt Discovery	Bio-Tek Instruments Inc., Winooski (VT), USA
Multipette® plus	Eppendorf AG, Hamburg, Germany
NanoDrop 2000	Thermo Fisher Scientific, Waltham (MA), USA
Olympus IX70 Fluorescence Microscope	Olympus Deutschland GmbH, Hamburg, Germany
QIAcube™	Qiagen, Hilden, Germany
PHMP Grant-bio Plate heater	Grant Instruments (Cambridge) Ltd, Cambridgeshire, UK
TECAN infinite F500	Tecan Group Ltd, Maennedorf, Switzerland
TheOnyx Liquid Performer	AVISO Trade GmbH, Gera, Germany
ThermoStat plus	Eppendorf AG, Hamburg, Germany
Titramax 101 platform shaker	Heidolph Instruments GmbH & Co. KG, Schwabach, Germany
VorTemp™ 56 Shaking Incubator	Labnet International Inc., Edison (NJ), USA
Vortex-Genie 2 Vortex Mixer	Scientific Industries Inc., Bohemia (NY), USA
Water bath 1002	GFL Gesellschaft für Labortechnik mbH, Burgwedel, Germany

2.1.6 Software

Name	Manufacturer, Corporate headquarters
Agilent 2100 Expert software version B.03.08.SI648	Agilent Technologies, Waldbronn, Germany
Genedata Analyst™ version 7.5	Genedata, Basel, Switzerland
Casy® measure version 1.5	Schaerfe System GmbH, Reutlingen, Germany
CellF Soft Imaging System version 2.4	Olympus Soft Imaging Solutions GmbH, Muenster, Germany
Cellomics® Scan Software version 7.6.2.4	Thermo Fisher Scientific, Waltham (MA), USA
GenomeStudio V2009.1	Illumina Inc., San Diego (CA), USA
GraphPad Prism® version 5.02	GraphPad Software, Inc., La Jolla (CA), USA
Illumina® BeadScan software version 3	Illumina Inc. San Diego (CA), USA
KC4™ Data Analysis Software version 3.4	Bio-Tek Instruments Inc., Winooski (VT), USA
LUMIstar Galaxy version 4.30-0	BMG LABTECH GmbH, Ortenberg, Germany
Magellan™ Data Analysis Software version 6.6	Tecan Group Ltd, Maennedorf, Switzerland
NanoDrop 2000 / 2000c Operating Software	Thermo Fisher Scientific, Waltham (MA), USA
Robo Manager THEONYX version 6.3.2	MWG BIOTECH AG, Ebersberg, Germany
XFe Wave 1.1.1 Software	Seahorse Bioscience, North Billerica (MA), USA
xPONENT® v3.1 Software	Life Technologies GmbH, Darmstadt, Germany

2.2 Cell culture techniques

The tissue culture procedures described in the following sections were conducted under sterile conditions. Cell cultures were incubated in an incubator maintained under a humidified atmosphere of 5% carbon dioxide (CO_2) / 95% air, at 37°C.

In the presented work primary hepatocytes were used. Generally, primary cells can be isolated from whole organs or organ sections by perfusing them with enzyme-containing buffers which digest the extra cellular matrix, namely collagen, to release single cells. In contrast to cell lines, which are tumour-derived and proliferate continuously, primary hepatocytes represent fully differentiated cells from which only a very low percentage undergo cell division (Francavilla et al., 1986). As a result, defined requirements are needed for primary cell cultures. The monolayer (ML) culture involves seeding the cells in an appropriate media into plates coated with a dried layer of collagen I (Figure 11 A). This culture format allows for short-term maintenance of the cells, i.e. a maximum of up to five days. Shortly after this time, the cells start to dedifferentiate and lose their liver-like properties (Grant et al., 1985; Tuschl et al., 2009). An alternative culture approach is the sandwich (SW) configuration in which the cells are embedded in between two layers of gelatinised collagen (Figure 11 B); hence making it possible to keep the cells alive and functional for up to four weeks (unpublished data). In the following sections, the preparation of both culture methods is described for the primary rat and human hepatocytes.

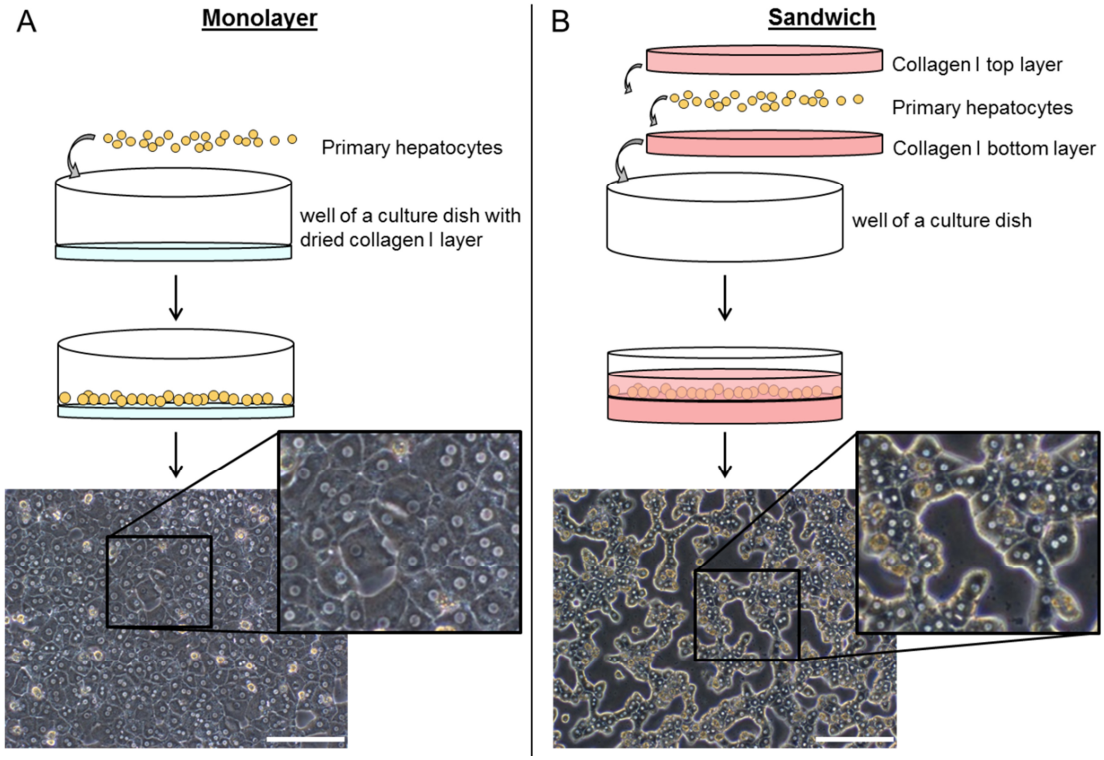

Figure 11. Scheme of primary hepatocytes cultures in monolayer (A) and sandwich (B) configuration. The pictures show the primary rat hepatocytes 24 h after seeding in the corresponding culture model. The white scale bar on the bottom right of each picture corresponds to 200 µm.

2.2.1 Experimental schedule for long-term cultures

The study described deals with *Omics* results from long-term cultures (14 days) of PRH and PHH treated daily with four pharmaceuticals, namely AMI, CPZ, CsA and IBU. The PRH were isolated and cultured at Merck Serono (Darmstadt, Germany), while the PHH were processed by the Predict-IV project partner, KaLy-Cell (Plobsheim, France). Figure 12 illustrates the time schedule for culture preparation, treatment and sampling of hepatocytes from these two species.

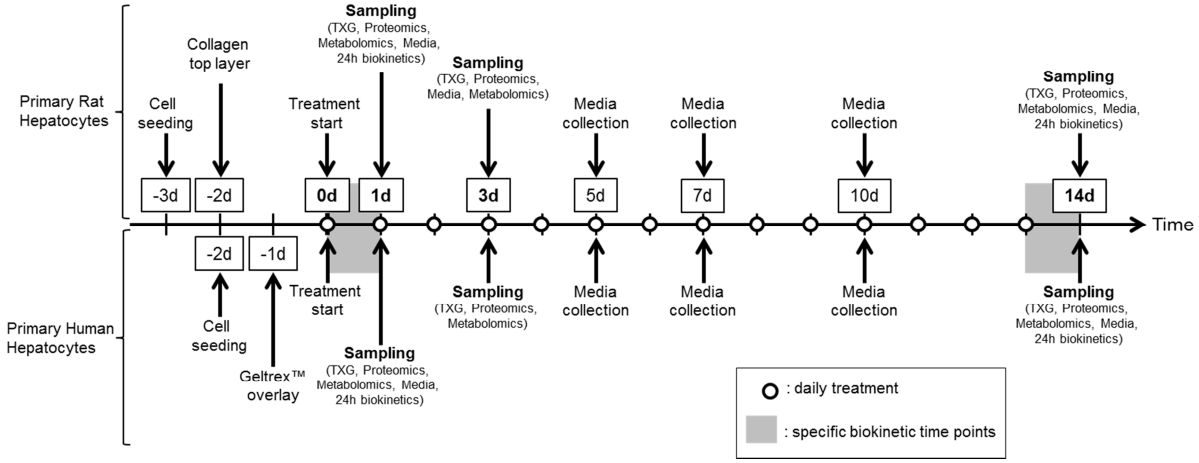

Figure 12. Timeline of experimental procedures, including cell culture preparation, treatment and sampling time points for primary rat and human hepatocytes. For both cell types, a total of three biological replicates were performed, whereas five biological replicates were performed for the toxicogenomics endpoint of the primary rat hepatocytes.

2.2.2 Primary rat hepatocytes cultures

2.2.2.1 Preparation of tissue culture plates for monolayer and sandwich cultures

Rat tail tendon collagen type I lyophilisate was dissolved in 0.2% acetic acid solution to a final concentration of 1 mg/mL. The preparation was allowed to dissolve for at least 2 h at room temperature (RT) or overnight at 4°C and kept refrigerated until needed.

For the ML 96-well and 6-well cultures, the collagen stock solution was further diluted in 0.2% acetic acid to 20 µg/mL and 100 µg/mL, respectively. Upon addition of 110 µL per well of a 96-well plate and 600 µL per well of a 6-well plate of the corresponding concentration the collagen solution dried under UV-light (non-permanent, i.e. pre-set daily cycle) in the sterile bench. These plates were kept under sterile conditions at RT until needed.

The bottom layer for the SW cultures was prepared freshly, i.e. on the same day of cell isolation and hence cell seeding. Dulbecco's modified eagle medium (DMEM)/F12 media (10x concentrated) was diluted 1:10 in collagen stock solution (1 mg/mL) and the acidic pH was adjusted with 1 N sodium hydroxide to 7.4 while keeping the solution chilled on ice. Neutralised collagen solution was added to wells and spread evenly over the surface in order to cover the entire growth area (250 µL and 75 µL per well of a 6-well and 24-well plate format,

respectively). To allow proper gelation, the collagen-coated cell culture plates were incubated for at least 1.5 h in the incubator.

2.2.2.2 Rat liver perfusion

The use of animals was in accordance of the national law and regulations, and procedures were performed by authorised staff only (Approval number from the local authorities: v54-19c20/15, DA4/Anz271E).

The isolation of primary hepatocytes from adult male Wistar rats was performed using a two-step enzymatic perfusion method, according to an in-house standard operating procedure (SOP), based on methods described previously by Seglen (1976) and Tuschl et al. (2009). Only hepatocyte preparations with an initial viability greater than 85% were used. The cells were plated in serum-containing seeding medium.

PRH seeding medium:	DMEM/F12 (GlutaMAX™) medium 10% (v/v) FBS 1 mM sodium pyruvate 100 U/mL penicillin 100 µg/mL streptomycin 5 µg/mL insulin

A density of 0.03, 0.25 or 1.5 x 10^6 cells per well and a volume of 100 µL, 500 µL or 1.5 mL in 96-, 24- and 6-well plates, respectively, was used.

2.2.2.3 Short-term cultures of PRH

Freshly isolated PRH were seeded in seeding media (see above) on a dried layer of collagen in 96- or 6-well plates (densities see above). After an attachment period of 4 - 5 h, the media was replaced with serum-free culture medium.

PRH culture medium:	DMEM/F12 (GlutaMAX™) medium 1 mM sodium pyruvate 100 U/mL penicillin 100 µg/mL streptomycin ITS-G (1x – corresponding to 17.241 mM insulin, 0.688 mM transferrin and 0.387 µM sodium selenite) 0.44 mg/mL BSA 100 nM dexamethasone

2.2.2.4 Long-term cultures of PRH

In order to enable the long-term culture of isolated PRH, these cells were cultured in a collagen SW format. For this culture format, the cells were seeded in seeding media on a gelatinised layer of collagen I and DMEM solution (see section 2.2.2.1) and after an attachment period of 4 - 5 h, the culture medium was replaced with fresh seeding medium (see section 2.2.2.3). Following

over-night incubation, the cells were washed with cold phosphate buffered saline (PBS; plus calcium and magnesium) and covered with a second layer of freshly prepared collagen-DMEM mixture. The second layer was added carefully to the monolayers and then allowed to gelatinise in the incubator prior to adding serum-free culture medium. A volume of 400 µL or 100 µL neutralised collagen solution was added per well of a 6-well or 24-well plate.

2.2.3 Primary human hepatocytes cultures

Experiments using PHH were conducted by the Predict-IV collaboration partner, KaLy-Cell. The PHH were isolated from liver resections from patients who had undergone partial liver hepatectomies for therapy of various pathologies (see Table 8). The biopsies (20 - 100 g) were healthy tissue dissected with a margin of safety proximity from the tumour or infection. All experiments were performed with permission of the National Ethics Committee (France) and regulatory authorities. PHH were isolated using a two-step liver perfusion method described previously by LeCluyse and Alexandre (2010). The cells were cultured as described by Parmentier et al. (2013) on collagen I coated tissue culture plates (BD BioCoat™) with or without a Geltrex™ (Invitrogen) overlay for long- or short-term cultures, respectively. Treatment was initiated the following day for the short-term experiments or two days after seeding for the long-term experiments (Figure 12).

Table 8. Background information on the different donors of liver sections used for human hepatocyte culture experiments within Predict-IV.

Donor	Sex	Age	Pathology	Medication
1	Male	42	Echinococcosis alveolaris	-
2	Male	75	Hepatic tumour	Atenolol, Kardegic, Ramipril, Inspra, Rasilez
3	Male	63	Hydatid Cyst	-

2.2.4 Compound treatment of primary hepatocyte long-term cultures

2.2.4.1 Dose finding studies

In the dose finding studies, the hepatocyte cultures were treated with AMI, CPZ, CsA, IBU and the corresponding solvent control. Methanol was used to dissolve AMI, while CPZ, CsA and IBU were dissolved in dimethyl sulfoxide (DMSO).

In order to get an estimate of the compounds' cytotoxicity, a broad concentration range was used to treat PRH cultures in 96-well plates ML configuration for 24 h (Table 9). For this purpose one biological replicate was used.

Table 9. Concentrations of ibuprofen (IBU), chlorpromazine (CPZ), cyclosporine A (CsA) and amiodarone (AMI). Compounds were applied to primary rat hepatocyte monolayer cultures in 96-well plate format for cytotoxicity testing after 24 h of treatment.

	Compound concentration in µM											
IBU	500	1000	1500	2000	3500	5000						
CPZ	1	10	15	20	25	30	40	50	60	70	80	100
CsA	5	10	25	50	75	100	200	300	400	500		
AMI	1	10	25	50	75	100	125	150	200	300		

Subsequently, a narrowed concentration range was taken to assess the cytotoxicity in 24-well plated SW long-term cultured hepatocytes (Table 10), which is considered to be more representative for the final experiments which were performed in 6-well plate SW format up to 14 days. Here, the highest concentration was set to the TC_{50} (concentration exerting 50% cytotoxicity) found in the cytotoxicity screen in 96-well plate ML. Samples were collected after 1, 3 and 14 days repeated treatment and a total of three biological replicates were carried out.

Table 10. Concentrations of ibuprofen (IBU), chlorpromazine (CPZ), cyclosporine A (CsA) and amiodarone (AMI). Compounds were applied to primary rat hepatocyte sandwich cultures in 24-well plate format for cytotoxicity testing after 1, 3 and 14 days of treatment.

	Compound concentration in µM						
IBU	500	1000	1500	2000	3500	5000	
CPZ	1	5	15	30	40	45	50
CsA	0.1	1	5	10	25	50	100
AMI	1	10	25	50	75	100	125

Finally, three concentrations around the TC_{10} (concentration exerting 10% cytotoxicity) calculated from the 24-well plate long-term culture experiments were tested in the 6-well plate SW culture format (Table 11). For confirmation purposes a single experiment was conducted, taking only the cytotoxic potential after 14 days repeated dosing into consideration.

Table 11. Concentrations of ibuprofen (IBU), chlorpromazine (CPZ), cyclosporine A (CsA) and amiodarone (AMI). Compounds were applied to primary rat hepatocyte sandwich cultures in 6-well plate format for cytotoxicity testing after 14 days of treatment.

	Compound concentration in µM		
IBU	10	500	1000
CPZ	15	20	25
CsA	0.1	1	10
AMI	1	10	25

The dose finding studies in PHH were performed by the Predict-IV partner KaLy-Cell in France. The determined TC_{10} were communicated personally (KaLy Cell (Parmentier)).

2.2.4.2 Final experiments

For the final experiments, the long-term cultures were treated daily with two concentrations of AMI, CPZ, CsA, and IBU, as well as the corresponding solvent control. Prior to each experiment, stock solutions were prepared freshly and aliquots were stored at -20°C for a maximum of three months. For daily treatment, the prepared stock solutions were diluted (1:500) in serum-free culture medium. Solvent control containing media were prepared freshly at a final concentration of 0.2%.

2.2.5 Cell culture for mitochondrial toxicity

2.2.5.1 Collagen coating of 96-well plates

Cells used to determine mitochondrial toxicity were seeded on collagen-coated cell culture vessels. The collagen-coating protocol used for these assays differed from the collagen-coating procedure described previously under section 2.2.2.1. Black and white 96-well plates and *XF Cell Culture Microplates* were all collagen-coated using the following protocol. The collagen I stock solution (1 mg/mL) was diluted to 20 µg/mL with 0.2% acetic acid. A volume of 110 µL of the diluted collagen solution was added to each well and incubated for 1 h at RT. After this time, the collagen solution was aspirated, and the wells were washed twice with PBS and subsequently air dried.

2.2.5.2 HepG2 cells

The human hepatoma HepG2 cell is a hepatocellular carcinoma-derived cell line frequently used in research due to their robustness and ease of use. These cells were purchased at ATCC and a large stock (with an initial passage number: 4) was prepared in-house in order to be able to use cells with a low passage number.

2.2.5.2.1 Thawing

In order to speed up the thawing procedure, a T75 culture flask (75 cm² growth area) was prepared by adding 10 mL DMEM-F12 culture media at RT.

HepG2 culture medium:	DMEM-F12 10% (v/v) FBS 1 mM sodium pyruvate 100 U/mL penicillin 100 µg/mL streptomycin 50µg/mL gentamycin

A cryovial containing ~ 5 - 7 x 10^6 viable HepG2 cells was taken out of the liquid nitrogen storage tank and immersed in a water bath warmed to 37°C to thaw the cells. Shortly before the medium/cells were completely thawed, the cell suspension was transferred using a pipette to the prepared culture flask. This T75 flask was denoted as passage number 1. The cells were spread evenly by gently shaking the flask alternately back/forth and left/right a few times before placing the vessel into the incubator. Following an attachment phase of 8 - 16 h the medium was replaced to remove any detached cells and residual DMSO from the freezing medium.

2.2.5.2.2 Culturing and Passaging

Once in culture, the medium was refreshed every 2 - 3 days. Once the cells had reached a confluence of approximately 80%, the cells were trypsinised and transferred to a T175 culture flask (175 cm²). To trypsinise the cells, they were first washed with PBS (calcium- and magnesium-free) and then incubated with enough Trypsin-ethylenediamineteraacetic acid (EDTA) solution to cover the entire growth area. Excessive trypsin was aspirated for a more controllable dissociation of the tight junctions between the cells. For optimal tryptic digestion, the cells were incubated in the incubator for 5 min. Detachment was monitored visually under the microscope before tapping the flask gently to completely remove the cells from the plastic surface. The enzymatic digestion was stopped by adding culture medium and the entire cell suspension volume was transferred to a T175 flask containing medium such that the total final volume was approximately 20 mL. After proper distribution of the cells, the culture vessel was placed into the incubator. Generally, HepG2 cells were passaged at a ratio of 1:8. The cells were used in endpoint experiments up to passage 16.

2.2.5.2.3 Adaptation to galactose-containing medium

In order to increase the sensitivity of cells to toxicants with mechanisms of action involving mitochondria, the glucose in the standard HepG2 culture medium was replaced with galactose (Gal) (Marroquin et al., 2007).

HepG2-Gal culture medium:	DMEM-F12 without glucose
	10% (v/v) FBS
	1 mM sodium pyruvate
	100 U/mL penicillin
	100 µg/mL streptomycin
	5 mM HEPES
	2 mM L-glutamine
	10 mM D-(+)-galactose

Initial conditioning of the HepG2 cells to the glucose-free medium was achieved by passaging the HepG2 cells (at 80 - 90% confluence) at a ratio of 1:5 into a T175 culture flask containing galactose culture medium. The final passage number of the galactose HepG2 cell cultures

therefore included the standard number of passages in glucose medium plus the number of passages in galactose medium. The first transfer to galactose medium was assigned to passage number 1, e.g. PXX-YY (X: number in glucose, Y: number in galactose). The maximal passage number of cells in galactose-containing medium was 12. The medium was replaced every 2 - 3 days. Generally, cells were cultured in galactose-containing medium for at least 3 passages prior to their use in experiments in order to metabolically adapt the HepG2 cells to the alternative sugar source.

2.2.5.2.4 Seeding

Table 12 summarises the cell seeding densities used for the different assays. For the *MitoXpress*® and ATP assays, the first column ("1") of each plate was left free of cells in order to include appropriate controls. In the *XF Cell Culture Microplates*, the wells in the corners of the plate were left without cells.

2.2.5.3 HepaRG™ cell line

This cell line exhibits many liver-like properties and is being tested extensively as a replacement hepatic model to carry out *in vitro* screening for the prediction of hepatotoxicants (Antherieu et al., 2012). HepaRG™ cells were evaluated for their suitability to predict mitochondrial toxicity. The seeding medium for HepaRG cells was supplemented Williams' E medium.

HepaRG seeding medium:	Williams' E medium GlutaMAX™ (1x) HepaRG™ Thawing/Plating Medium Supplement (one vial per 100 mL medium; the composition is proprietary)

An appropriate number of cryovials (each vial containing a minimum of 8 x 10^6 viable cells) was transferred from the liquid nitrogen storage tank and immersed in a water bath warmed to 37°C. Shortly before the medium/cells were entirely thawed, the cell suspension was transferred using a pipette to a *Falcon* tube containing a sufficient volume of culture medium (20 mL for three vials). The cell suspension was centrifuged at 400 x g (without brake) and RT for 2 min to pellet the cells. After centrifugation, the media was carefully aspirated. Multiple cell pellets were pooled in an appropriate volume of medium (approximately 12.5 mL for every three vials). Cell viability was assessed by trypan blue exclusion method, using the Fuchs-Rosenthal chamber. Cells were seeded at densities depending upon the assay carried out (Table 12) in 100 µL media per well. The cells were allowed to attach overnight before the media was changed to culture medium.

HepaRG culture medium:	Williams' E medium GlutaMAX™ (1x) HepaRG™ Tox Medium Supplement (one vial per 100 mL medium; the composition is proprietary)

On day 4 after seeding, the HepaRG™ cells were used for the different assays.

2.2.5.4 Primary rat hepatocytes

PRH are very close to the *in vivo* situation with respect to respiration because these cells contain functional mitochondria. These cells were seeded as described above in section 2.2.2.3 according to the endpoint measurement (Table 12).

Table 12. Seeding densities of different cell types used in different assays.

	***MitoXpress*® O_2 assay (black 96-well)**	**1 h ATP assay (white 96-well)**	***Seahorse XF extracellular flux* (*XF Cell Culture Microplate*)**
HepG2 – Glucose	80,000 cells/well	80,000 cells/well	25,000 cells/well
HepG2 – Galactose	80,000 cells/well	80,000 cells/well	16,000 cells/well
HepaRG	50,000 cells/well	50,000 cells/well	12,000 cells/well
PRH	35,000 cells/well	35,000 cells/well	12,000 cells/well

2.2.5.5 Compound treatment

For the *MitoXpress*® O_2 assay, 5 - 8 stock solutions per compound (Table 13) were prepared in DMSO or water (metformin) and aliquots were stored at -20°C until needed.

Table 13. Final concentrations of test compounds assessed for mitochondrial toxicity. Compounds marked (*) were tested only in the *MitoXpress*® O_2 assay, while metformin (**) was included only in the *Seahorse XF extracellular flux* assay. Abbreviation: FCCP - carbonyl cyanide 4-(trifluoromethoxy)phenylhydrazone.

	Final concentration in µM									
Ibuprofen	1	5	25	50	100	150	300	500	750	1000
Chlorpromazine	1	5	10	20	40	60	80	100	200	400
Cyclosporine A	0.05	0.5	5	10	15	20	50	75	100	200
Amiodarone	0.5	2	5	10	50	100	200	300	400	600
FCCP*	0.003	0.03	0.3	3	30	60	125			
Antimycin*	0.003	0.03	0.3	3	30	60	125	250		
Oligomycin*	0.003	0.03	0.3	3	30	60				
Metformin**	50	100	300	500	750	1000				
n-butyl chloride	5	50	150	500	1000					
D-mannitol	5	50	150	500	1000					

For detection of extracellular oxygen consumption, the treatment was started shortly before data acquisition (see section 2.3.8 for details).

Cytotoxicity was measured using ATP content after 1 h, which corresponds to the time at which *MitoXpress*® O_2 consumption was measured. Here, under non sterile conditions, 150 µL 37°C-

warm culture medium was added to triplicate wells together with 1 µL test compound stock solution. The plate was then incubated on the plate heater set to 37°C for 1 h. The ATP assay was performed as described in section 2.3.1.

The 10-fold stock solutions of test compounds (Table 13) evaluated in the *Seahorse XF extracellular flux* assay were prepared in basal DMEM and Williams' Medium E media (1x, reconstituted powder without supplements). Aliquots of 30 µL were stored at -20°C until needed. Generally, two treatment schemes were performed for the assessment of mitochondrial toxicity using the Seahorse XF^{e}96 instrument. In this assay, compound exposure was performed *in situ* (i.e. without pre-incubation) or started 24 h prior to measurement. For the 24 h treatment, 180 µL medium was added to each well together with 20 µL of the 10-fold stock solution to result in the concentrations listed in Table 13. The *in situ* treatment is described in section 2.3.9.

2.3 Molecular biological techniques and data analysis

2.3.1 Cell viability

In order to estimate the cytotoxic potential of test compounds, the cell viability was determined after exposing the cells to a range of concentrations of the drug for different durations. The cell viability of PRH was assessed using the ATP assay. Viability was expressed as a percentage of the control values.

The assessment of the cell viability using ATP content is based on the assumption that the amount of ATP is directly relative to the number of living cells. Figure 13 depicts the luciferase reaction within which the *Ultra-Glo™ Recombinant Luciferase* catalyses the transformation of Beetle Luciferin to Oxyluciferin in the presence of ATP, oxygen and magnesium. Adenosine monophosphate, inorganic pyrophosphate, CO_2 and light are generated simultaneously in a proportional manner but the latter is exploited to measure the luminescent signal using a luminometer.

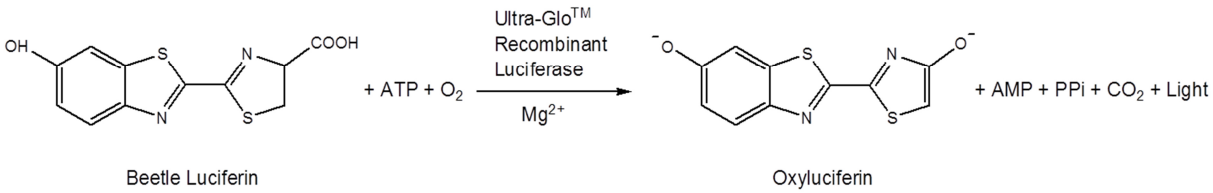

Figure 13. Ultra-Glo™ Recombinant Luciferase reaction for the assessment of the cell viability. The adenosine triphosphate (ATP) level positively correlates with the generation of light which is measured using a luminometer. Since viable cells contain more ATP than dead cells, this reaction can be used to quantify the extent of cytotoxicity.
Abbreviations: O_2 - oxygen; Mg^{2+} - magnesium ion; AMP - adenosine monophosphate; PPi - inorganic pyrophosphate; CO_2 - carbon dioxide.

The cytotoxic potential of the compounds was measured by quantifying the cellular ATP content using the *CellTiter-Glo® Luminescent Cell Viability Assay*, according to a slightly modified

version of the manufacturer's protocol. In brief, after appropriate treatment durations, the medium was replaced with 100 µL, 600 µL or 900 µL *CellTiter-Glo® Reagent*-medium mixture (equal volumes of *CellTiter-Glo® Reagent* and corresponding cell culture medium) per well of a 96-, 24- or 6-well plate, respectively. The plates were placed on an orbital shaker at RT for 2 min, and then incubated at RT for 10 min for stabilisation of the luminescence signal. Finally, the signal was measured with the LUMIstar luminometer.

2.3.2 Transcriptomics

Illumina's gene expression arrays represent a cost-effective, highly robust and reproducible system for the analysis of gene expression. As described by Hrach (Hrach, 2009) the Illumina system compares favourably with the long-term gold-standard Affymetrix microarray technology. In the present work, Illumina's *Expression BeadChips* were used for the whole-genome gene expression analysis of rat and human samples.

An *Expression BeadChip* consists of up to twelve *BeadArrays* allowing a higher throughput of sample processing. Typically, each *BeadArray* contains a high number of different silica beads which are introduced by random self-assembly into the etched microwells (Figure 14). The beads measure 3 µm in diameter and a single bead is covered with approximately 700,000 copies of a particular sequence consisting of (i) a 29-mer address sequence which allows identifying the location of the bead on the array after random distribution and (ii) a 50-mer gene-specific probe to capture the gene of interest. The DNA-based decoding procedure, using dye-labelled oligonucleotides and described by Gunderson et al. (2004), is used for the identification of the exact localisation of each bead type. For a more reliable and precise readout, an average of 30 beads per probe/transcript are present on an array, and the software calculates a mean intensity for all actually existing beads of one type (Kuhn et al., 2004; Gunderson et al., 2004; Illumina, 2011).

The *RatRef-12 v1 Expression BeadChip* contains over 22,000 probes, corresponding to 21,792 rat genes. In addition, the *HumanHT-12 v4 Expression BeadChip* contains over 47,000 transcripts (34,693 human genes). For both *Expression BeadChip* types the probe sequence information was derived from the National Center for Biotechnology Information (NCBI) Reference Sequence (Release 16 for the rat version and Release 38 for the human) and UniGene databases (Illumina, 2011).

Figure 14 depicts the steps used for the amplification and hybridisation process ending with the scan of the *BeadChips*.

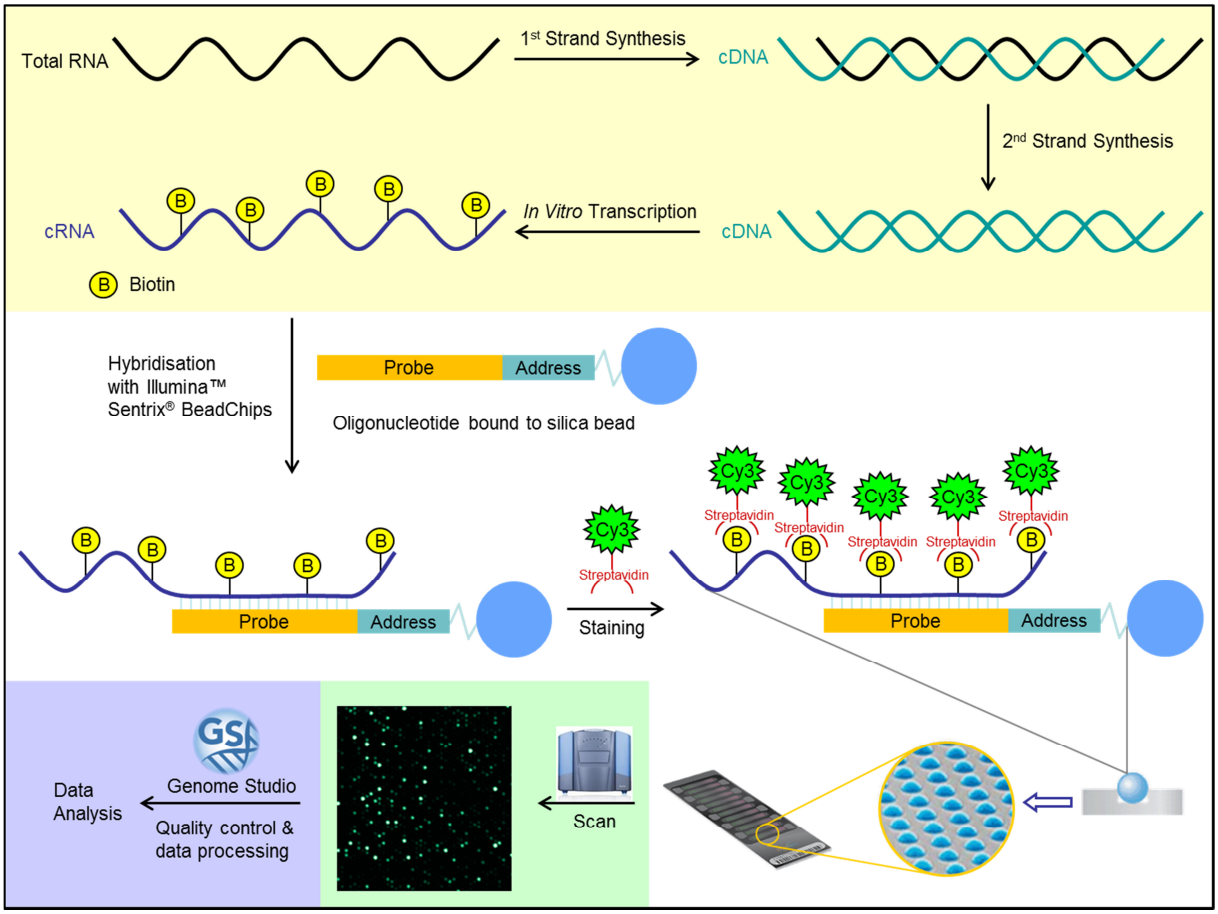

Figure 14. Workflow from total RNA to analysis of gene expression data, including amplification of copy RNA (cRNA), hybridisation of labelled cRNA to Illumina Sentrix® BeadChips, scan and first data processing steps.

Sample homogenates were prepared after 1, 3 and 14 days of treatment for transcriptome analyses, as described below.

2.3.2.1 Isolation of total RNA

Qiagen's RNeasy® Plus Mini kit enables a fast and efficient isolation of total RNA from cultured cells and tissues. Only RNA molecules larger than 200 nucleotides are isolated with this kit, i.e. 5S and 5.8S ribosomal RNAs or transfer RNAs are not recovered (Qiagen, 2010).

The PBS-washed SW cultured PRH were harvested using a cell scraper together with the collagen in 5 mL *RNAprotect™ Cell Reagent* and centrifuged at 5,000 x g and RT for 5 min. *RNAprotect™ Cell Reagent* was added to immediately stabilise RNA and DNA within the cells, thus avoiding changes in gene expression during sample processing. After discarding the supernatant and washing the pellet in fresh *RNAprotect™ Cell Reagent* (3 mL), a second centrifugation step with identical settings was performed and the resulting cell pellet was then lysed in 350 µL 2-mercaptoethanol (2-ME) supplemented *RLT Buffer Plus* (10 µL 2-ME per 1 mL *RLT Buffer Plus*). Important components of the *RLT Buffer Plus* are (i) guanidine isothiocyanate, which optimises the binding of the RNA molecules to the silica membrane of the *RNeasy spin column* and (ii) detergents for an improved elimination of DNA molecules via the

gDNA Eliminator column. Furthermore, 2-ME was added, as it is required for an efficient inactivation of RNases. For full homogenisation of the cell lysate, the total volume was then loaded onto a *QIAshredder™ spin column* placed in a 2 mL collection tube and centrifuged at 16,000 x g and RT for 2 min. The resulting eluate was stored at -80°C until sampling of five biological replicates was completed for the PRH.
The total RNA was isolated according the manufacturer's protocol (*RNeasy® Plus Mini* kit, Qiagen) using the QIAcube™ robotic workstation for fully automated sample preparation. Finally, the total RNA was recovered in 40 µL RNase-free water, which was stored on ice during the performance of quantitative and qualitative analyses (see later) and subsequently at -80°C until further processing.

2.3.2.2 RNA quantification and quality assessment

Prior to further processing of the total RNA, its concentration and quality was assessed using the NanoDrop 2000 and Agilent 2100 Bioanalyzer, respectively.
The nucleic acids were quantified using the NanoDrop 2000 UV/Vis spectrophotometer. The quantification of nucleic acids is based on a modified Lambert-Beer equation:

$$c = \frac{A \cdot \varepsilon}{d}$$

c – concentration of nucleic acid in ng/µL
A – absorbance without unit
ε – extinction coefficient for nucleic acids in ng x cm/µL
d – distance between the optical surfaces / pathlength

The value of the extinction coefficient is dependent on the original material, i.e. RNA (ε = 40 ng x cm/µL), dsDNA (ε = 50 ng x cm/µL) or ssDNA (ε = 33 ng x cm/µL), and these values are used by the software to calculate the concentration of the nucleic acid solution. At the beginning of each measurement a blanking is mandatory and performed with the solution corresponding to the nucleic acid solvent. Figure 15 shows a typical spectrum for nucleic acids (Thermo Fisher Scientific, 2010).

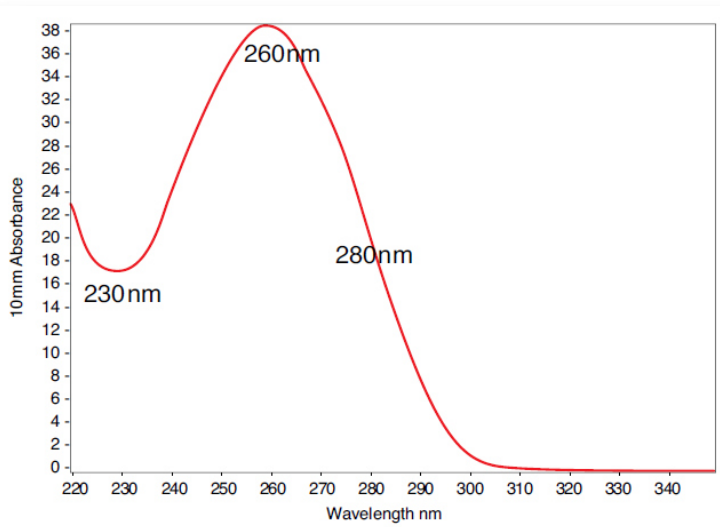

Figure 15. Typical spectrum of good quality RNA.

For the concentration measurement, 1 µL RNA sample was pipetted onto the clean pedestal of the NanoDrop 2000 and the measurement was started by means of the NanoDrop 2000 / 2000c Operating Software. Along with the concentration of RNA, the 260/280 and 260/230 absorbance ratios were obtained, both ratios giving a preliminary indication of the RNA purity. The samples had to fulfil the following quality criteria: a minimum concentration of 50 ng/µL and a value approximately 2.0 for the 260/280 and 260/230 absorbance ratios.

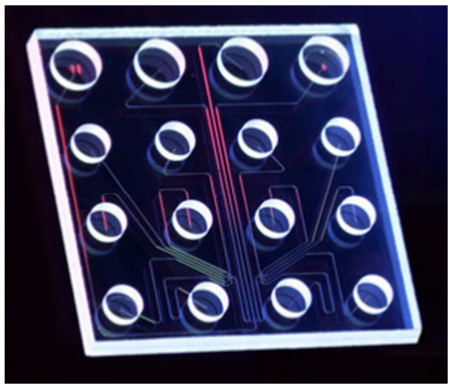

Figure 16. A glass core with micro connections is inside a Nano 6000 RNA Chip.

The Agilent 2100 Bioanalyzer allows rapid quantity and quality assessment of nucleic acids, proteins and whole cells. The applied Lab-on-a-Chip platform is based on microfluidics technology, which enabled the miniaturisation of conventional analytics such as gel electrophoresis and flow cytometry. Here, within a short analysis time and consuming small sample amounts, the RNA quality was determined using a RNA LabChip® kit. Figure 16 shows the glass core of a *LabChip*® with its micro channels which connect the wells to each other. When filled with fluorescent dye-containing polymer (gel-dye mixture), the interconnected micro channel system builds a closed electric circuit. Each *LabChip*® well can be controlled individually through the 16-pin electrode cartridge of the instrument, where a single pin immerses into each well. After the application of a voltage gradient the intrinsically negative charged RNA molecules of the sample are retained by the polymer to different extents based on their size. As a result of the fluorescent dye within the gel-dye mix intercalating into the strands, the RNA molecules can be detected by means of laser-induced fluorescence. The fluorescence intensity versus migration time is then compiled into an electropherogram (Figure 17 A). In order to finally translate the migration time into fragment

size, a standard curve deriving from the electrophoretic trace of the ladder, which holds elements of known sizes, is measured immediately upon the start of each analysis (Agilent Technologies, 2005).

A software algorithm introduced by Agilent Technologies (Schroeder et al., 2006) uses critical features within the entire recorded electrophoretic trace (Figure 17 B) of the sample to calculate the RNA integrity number (RIN). The RIN resembles a system of numeration ranging from 10 for intact RNA to 1 for degraded RNA, and was taken into account for RNA quality assessment.

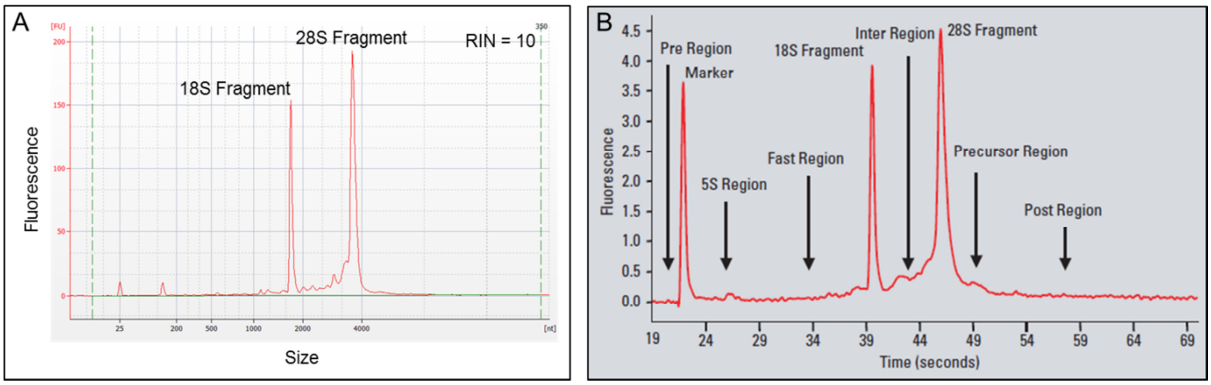

Figure 17. Electropherogram of total RNA after isolation (A) and detailed regions of an electrophoretic trace (B) which are taken into account for the RNA quality.

The RNA quality was evaluated with the Agilent 2100 Bioanalyzer using the Agilent RNA 6000 Nano kit according to the manufacturer's protocol (Agilent Technologies, 2005). Generally, only total RNA sample preparations possessing a RIN greater than 9 were used for further processing.

2.3.2.3 cRNA amplification

The generation of biotin-labelled antisense copy RNA (cRNA) for hybridisation with Illumina™ microarrays was performed with the Illumina® TotalPrep™-96 RNA Amplification kit (Ambion®), which is based on the principles of the Eberwine protocol (Van Gelder et al., 1990). A fully automated process was achieved with the TheOnyx (AVISO) automated liquid handling system. Figure 18 depicts the TheOnyx workspace where all plastic ware and reagents were loaded, as described in the following section, prior to start the program for the 2-day amplification process.

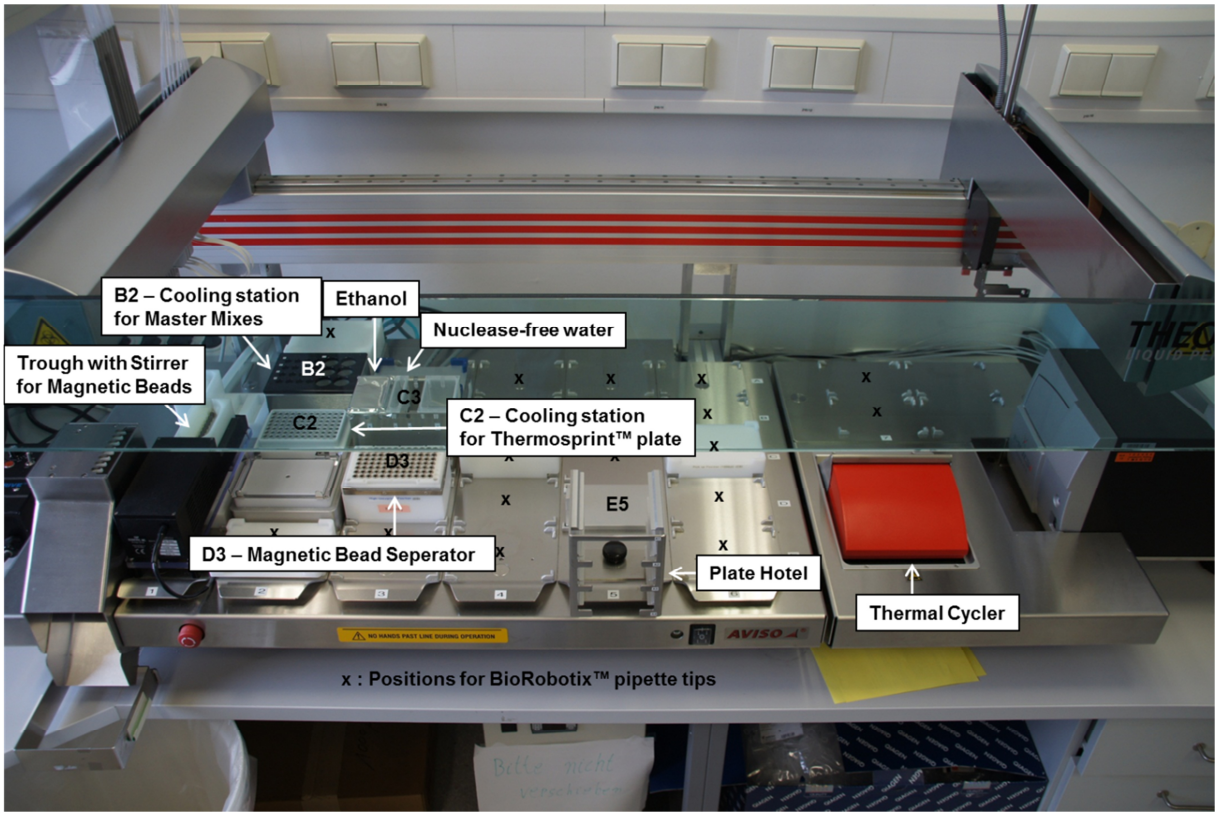

Figure 18. TheOnyx automated liquid handling system with loading positions of equipment needed for the copy RNA (cRNA) amplification process.

On day 1, 500 ng total RNA, adjusted with nuclease-free water to a final volume of 11 µL, was prepared per sample in a *Thermosprint*™ 96-well plate and placed on the chilled sample plate platform (C2- Figure 18) of the robot. The robot was loaded with *BioRobotix*™ pipette tips (10, 50, 175 and 1000 µL), where the number of each pipette tip type and the correct position was dependent on the sample number to be processed and was calculated beforehand with the *Robo Manager THEONYX* software. A round-bottom plate for the complementary DNA (cDNA) purification and a *Thermosprint*™ plate, used later for pooling the *in vitro* transcription (IVT) components, were loaded into the respective positions A1 and A3 of the Plate Hotel (E5 – Figure 18). The Master Mix composites for (i) first strand cDNA synthesis, (ii) second strand cDNA synthesis and (iii) IVT were prepared (for details see Table 14) and placed into the corresponding position on the cooled platform (B2 – position 1, 17 and 3, respectively – Figure 18). Finally, 70% ethanol (C3 – Pos.1, Figure 18), nuclease-free water (C3 – Pos.2, Figure 18) and *Agencourt® RNAclean XP magnetic bead solution* (trough with stirrer), i.e. the reagents needed for purification of the intermediate (cDNA) product were loaded onto the corresponding platforms into clean containers, where the 70% ethanol was sealed with adhesive foil to avoid evaporation of the volatile chemical as this would change its concentration.

Table 14. Master mix compositions for reverse transcription, 2nd strand synthesis and *in vitro* transcription (IVT).

	Component	Volume per sample in µL
Reverse Transcription Master Mix	10x First Strand buffer	2.0
	dNTP Mix	4.0
	T7 Oligo(dT) Primer	1.0
	RNase Inhibitor	1.0
	ArrayScript™ Reverse Transcriptase	1.0
2nd Strand Master Mix	Nuclease-free water	63.0
	10x Second Strand buffer	10.0
	dNTP Mix	4.0
	DNA polymerase	2.0
	RNase H	1.0
IVT Master Mix	Biotin-NTP Mix	2.5
	T7 10x Reaction buffer	2.5
	T7 Enzyme Mix	2.5

After all reagents and consumables were loaded, the protocol for day 1 was started via the *Robo Manager THEONYX* software. In a first step, 9 µL *Reverse Transcription Master Mix* was added per RNA sample and mixed by pipetting up and down several times. For the first strand cDNA synthesis, the plate was incubated in the integrated thermal cycler at 42°C for 2 h. A volume of 80 µL *Second Strand Master Mix* was then added to each sample and mixed by pipetting up and down. The reaction mixture was incubated at 16°C for 2 h to allow the synthesis of the second cDNA strand. Before starting the IVT, the cDNA had to be free from salts, excessive enzymes, primers and other reaction educts/products – this was achieved using magnetic beads. The sample was transferred into a 96-well round bottom plate and 180 µL *Agencourt® RNAclean XP magnetic bead solution* was mixed with each sample and incubated for 5min before placing the plate on the 96-ring magnetic bead separator (D3 – Figure 18). During a 10 min incubation, the cDNA adherent magnetic beads were attracted by the magnet, building a circular deposit at the bottom of the plate, hence allowing removal of the liquid from the middle of the well without loss of bead-bound cDNA. The immobilised cDNA was washed three times with 200 µL 70% ethanol for 25 s. Following the last wash, the ethanol was completely aspirated and residual ethanol evaporated by incubating for an additional 15 min. After the addition of 20 µL nuclease-free water, the plate was transported by the robot to the horizontal shaker where the cDNA was eluted from the magnetic beads by shaking at 1500 rpm for 2 min and resting for 3 min. The plate was reset onto the magnet and incubated for 10 min in order to access the eluted cDNA which was then pipetted into a new *Thermosprint*™ 96-well plate sitting on the chilled sample plate platform (C3 – Figure 18). A volume of 7.5 µL *IVT Master Mix* was added to the cDNA and then the plate was placed into the thermal cycler at 37°C for 13 h. The end of the Day 1 protocol included the storage of the sample plate at 4°C after the completed IVT.

On the following day, new pipette tips (number and position calculated by the software), a *Thermosprint*™ and round bottom plate and fresh reagents, namely 80% ethanol, nuclease-free water and magnetic bead solution, for the purification of the end product (cRNA) were loaded onto the corresponding platforms (see Figure 18), before starting the Day 2 protocol. Initially, 15 µL nuclease-free water was added to each cRNA sample, before adding 88 µL *Agencourt® RNAclean XP magnetic bead solution*. The complete volume was transferred to the round bottom plate and placed on the magnetic bead separator. The cRNA was purified in an analogous manner to the cDNA. Finally, the biotin-labelled cRNA was re-suspended in 40 µL nuclease-free water.

2.3.2.4 cRNA quantitation and quality assessment

The cRNA was quantified with the NanoDrop 2000 system and the quality checked with the Agilent 2100 Bioanalyzer. The electropherogram for cRNA lacks distinct regions compared to RNA (e.g. peaks for 18S and 28S fragments) (see Figure 17). Here, only the empiric cRNA-typical shape of the entire electrophoretic trace (Figure 19) was used for quality assessment. Furthermore a minimum concentration of 150 ng/µL cRNA was a requirement for the next steps.

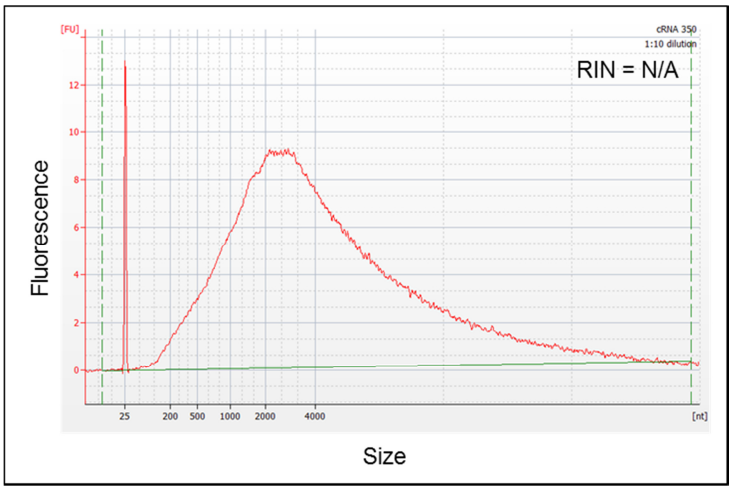

Figure 19. Electropherogram of copy RNA (cRNA).

2.3.2.5 Hybridisation on Illumina™ Sentrix® BeadChips and scan

Before the actual hybridisation of the biotinylated cRNA with the Illumina™ *Sentrix® BeadChips*, the samples were prepared as follows: 750 ng cRNA was adjusted to 5 µL with nuclease-free water in a 96-well PCR plate and re-suspended for 10 min at RT. In parallel, the *GEX-HYB* and *GEX-HCB* buffer were warmed to 58°C for 10 min in order to dissolve the salts completely. Both buffers were allowed to cool down to RT and checked for any residual salt crystals prior to use. After adding 10 µL hybridisation buffer *GEX-HYB* per cRNA sample, the plate was sealed with RNase-free foil and incubated at 65°C for 5 min for denaturation. The plate was then centrifuged (20 x g for 1 min and RT) and 200 µL humidity chamber buffer *GEX-HCB* was filled into the reservoirs of the microarray hybridisation cartridges to maintain a humid atmosphere in the wet chamber during hybridisation. A volume of 15 µL of each sample was

pipetted onto the *BeadChip* and the cartridge, containing a maximum of four *BeadChip*s. The plate was sealed carefully and placed into the hybridisation oven (58°C and rocker speed at 5) for 20 h.

Before the end of the 20 h incubation, the Little Dipper® Processor for Illumina™ *BeadChip*s was prepared for washing and staining the *BeadChip*s. Table 15 lists the required buffer preparations and reagents. The indicated *E1BC Buffer* preparation was prepared twice since this buffer was also needed during the coverseal removal of the *BeadChip*s. All buffers were then poured in baths and placed into the corresponding positions (Table 16) of the Little Dipper®, with pre-heating of the *High Temperature Wash Buffer* to 55°C in the instrument.

The *BeadChip*s were taken out of the hybridisation cartridges and prepared for the wash and staining protocol. First, the *BeadChip*s were submerged in *E1BC Buffer* to remove the coverseal and collected in a 12-position slide rack placed in an *E1BC Buffer*-containing dish, to avoid drying-out of the microarrays, and until all samples had been processed. The 'Bead2' protocol (Table 17) was started and the slide rack holding the *BeadChip*s was loaded on the automated gripper. The protocol included an instrument pause after completion of the 4th step during which the baths at position 2 and 3 were replaced by *Block E1* and *Streptavidin-Cy3 Stain*, respectively. Finally, the protocol ended with the centrifugation of the *BeadChip*s, which were removed from the slide rack and stored in a light-tight storage container until scanned.

Table 15. Buffers and reagents for the washing and staining protocol of the Sentrix® BeadChips.

Buffer / Reagent	Ingredients
High Temperature Wash Buffer	630 mL Nuclease-free water + 70 mL High Temperature Wash Buffer stock (10x)
E1BC Buffer	800 mL Nuclease-free water + 2.4 mL E1BC stock
Absolute Ethanol	-
Block E1 Buffer	-
Streptavidin-Cy3 Stain	200 mL Block E1 Buffer + 200 µL Streptavidin-Cy3 stock (1 mg/mL)

Table 16. List of Little Dipper® positions, temperature and volumes of the corresponding buffers and reagents.

Bath position	Buffer / Reagent	Temperature in °C	Volume in mL
1	High Temperature Wash	55	670
2	E1BC	RT	200
3	Ethanol	RT	200
4	E1BC	RT	200
5	E1BC	RT	200
	Pause		
2	Block E1	RT	200
3	Streptavidin-Cy3 Stain	RT	200

Table 17. Little Dipper® 'Bead2' protocol for Sentrix® BeadChip processing.

Step	Bath position	Buffer / Reagent	Agitation rate	Time in min
1	1	High Temperature Wash	250	10
2	2	E1BC	250	5
3	3	Ethanol	250	10
4	4	E1BC	250	2
		Pause		
5	2	Block E1	50	10
6	3	Streptavidin-Cy3 Stain	50	10
7	5	E1BC	250	5
8	Centrifuge	-	-	5

The scanning of the *BeadChip*s was performed using Illumina's BeadArray Reader (a laser scanning confocal microscope).

2.3.2.6 Transcriptomics data analysis

The *Gene Expression Module* in Illumina's *GenomeStudio® Data Analysis Software* was used to extract the transcriptomics data from the corresponding images scanned by the *BeadArray Reader*. This software was used to carry out a preliminary quality check of the single samples by built-in controls. In the so-called *Control Summary* tab different plots visualise the performance of the conducted experiments. A total of six controls are integrated in the *Illumina Direct Hyb System* that considers quality of the biological material, hybridisation procedure and generation of the read-out signal.

At the level of the biological specimen, its integrity was checked by surveillance of housekeeping genes that should be constitutively expressed due to their task in maintenance of basic cellular functions. To achieve this, a total of six probes were included for rat, with up to two probes per gene, corresponding to four genes, namely *Txn1* (*Thioredoxin 1*), *Eef1a1* (*Eukaryotic translation elongation factor 1 alpha 1*), *Alb* (*Albumin*) and *Rps9* (*Ribosomal protein S9*). Seven probes were allocated on the human arrays pertaining *EEF1A1*, *UBC* (*Ubiquitin C*), *ACTB* (*Actin, beta*), *RSP9*, *GAPDH* (*Glyceraldehyde-3-phosphate dehydrogenase*), *TUBB2A* (*Tubulin, beta 2A*) and *TXN*. The second category of controls is present in the *GEX-HYB* buffer, which is added to the samples prior to their incubation with the arrays, i.e. hybridisation of these probes is independent of sample quality, cRNA amplification success and secondary Cy3 labelling since Cy3 is part of the probes. The hybridisation process is monitored using three different controls:

(i) *Cy3-labelled Hyb Control*, which includes to a total number of six probes. Counterpart oligonucleotides on the array are in present at low, medium and high concentrations, leading to a hybridisation response gradient.

(ii) *Low stringency Hyb Control*, which involves four probes corresponding to those binding to the medium and high concentrated targets on the array, but here mismatch of two bases are built into the target oligonucleotide sequence. A normal stringency leads eventually to a low signal compared to the signal derived from the perfect-match probes (*Cy3-labelled Hyb Control*).
(iii) *High stringency Hyb Control* comprises one probe (included on the rat *BeadChip* only). Both probe and array target sequences possess a high proportion of G and C bases, resulting in a high signal at adequate hybridisation stringency. Furthermore, a biotin-control is introduced into each sample via the *HybE1* buffer which allows examination of the labelling with Streptavidin-Cy3 during the 'staining' process, i.e. signal generation. Here, biotin-tagged probes bind to their corresponding partner sequence on the array. If staining is successful, these probes deliver a positive signal.
Finally, so-called *Negative Controls* are part of the array and comprise a total of 825 or 770 oligonucleotides for rat or human, respectively. Their random sequence is chosen in such a way that it does not have any complementary RNA sequence in the species' genome. The resulting signal gives information on cross reactions during hybridisation and unspecific binding of the dye, overall, its mean is taken to set the imaging system background (Illumina, 2008).
The analysis of the transcriptomics data was computed within Genedata Analyst™ - software for statistical analysis and visualisation of experimental data. A total of five biological replicates (rat) were collected for the transcriptomics endpoint, yielding 150 samples (four compounds, two concentrations, two controls per time point, three time points, five replicates – (4x2+2)x3x5). Correspondingly, for the three human donors a total number of 90 samples were processed.
Initially, all gene expression samples were visualised in a boxplot diagram in order to get an overview of the complete data set. Using this method, it became apparent that the "IBU-high concentration-day 1" sample behaved quite differently compared to the other 149 samples, hence this sample was excluded from further analyses. None of the samples were excluded from analysis of the human data set.

2.3.2.6.1 Filter by Average Signal

Initially, the application of an *Average Signal* filter was necessary to exclude gene expression values from within the systems background. For the transcriptomics data deriving from rat, the background threshold was defined as 100, while it was set to 60 for the PHH data. In practice, the groups of genes were filtered by an *Average Signal* $\geq$100 or 60 (rat or human, respectively) and a new group was built within the software containing genes holding a valid signal intensity.

2.3.2.6.2 Normalisation

The data was normalised for samples with valid signal intensity. This adjusted the values from different samples to a common basis to improve subsequent analyses. It was important to choose

a normalisation approach that aligned the sample values without removing the desired biological effects.

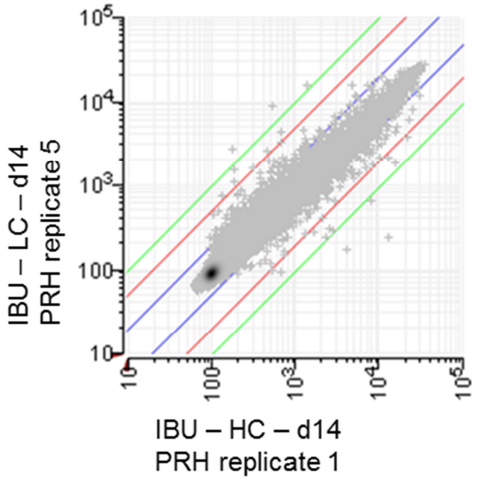

Figure 20. Scatter (Log-Log) plots of all probes (grey crosses) for ibuprofen (IBU) treated primary rat hepatocytes (PRH) samples from two randomly chosen biological replicates (1 and 5). The linear scattering between two pairs reasons the absence of artefacts, whereas the residual data showed very similar distributions. Low concentration (LC), high concentration (HC).

In order to get an overview of the generated gene expression data scatter plots (Log-Log plots) were created which compare the entire probe set between two selected conditions. This analysis was used to identify potential experimental artefacts and on this basis the normalisation method was selected. Figure 20 shows a representative scatter plot from PRH data. The gene expression data followed a linear signal response, hence only a mild normalisation was needed. Here, the *Quantile Normalisation* was applied with data dependent distribution (Bolstad et al., 2003). The aim of this normalisation method was to reduce the variation between different samples, making signal intensities the same for all samples. Rat and human data sets were both subjected to *Quantile Normalisation*.

2.3.2.6.3 Linear Model

The *Linear Model* within Analyst™ was used to reduce the number of genes to those that are significant, using several hypotheses prior to evaluating their deregulation. *Linear Model*s are based on the assumption that there is a linear relationship between the data and known factors. These factors have to be defined prior to implementation of the *Linear Model*, of which there are three different categories, namely, fixed factors, random factors and covariates. Fixed factors are by definition variables which are controlled by the scientist and known to have an influence upon the data (in this case gene expression values). By contrast, random factors are not controllable and potentially influence the data, for example, subjects chosen from a population which serve as replicates but eventually alter the outcome due to different individual characteristics (e.g. enzyme activity). Finally, covariates are concomitant variables which lead to a systematic response within the data, e.g. increasing doses or age groups. The specification and/or combination of factors serve to increase the power of the model (Genedata, 2011).

For the rat transcriptomics data, time points (1, 3 and 14 days) and concentrations (low and high) were set as fixed factors and the replicate number was carried along as random factor, while no covariate was selected. Hence, the following equation was used:

y ~ a + b + c + a:b	a – time point (fixed factor) b – concentration (fixed factor) c – replicate (random factor) a:b – interaction between time point and concentration

The focus was on a single hypothesis, namely concentration (b), since its effect reflected the main interest and consequently Benjamini-Hochberg corrected p-values (BH q-values) were calculated.

For PRH data, the model was applied to low and high concentrations of the compounds, together with the corresponding vehicle control. The genes with a BH q-value ≤ 0.05 were filtered and grouped for further processing (see below). At the end of this analysis, very few genes were identified to be significantly deregulated for the low concentrations of the different compounds. Therefore, the low concentration was excluded from further analyses; the *Linear Model* was applied to the high concentration and appropriate vehicle control group with identical settings and processing, as described above.

The data from PHH required a very different analysis procedure, due to an expected high inter-individual variability in metabolic capacities. Hence, the different donors were processed separately, which made the application of the *Linear Model* for statistical evaluation impossible.

2.3.2.6.4 Effect size

The *Effect Size* (fold change) was calculated for each gene of the PRH and PHH data. The *Effect Size* analysis directly compares the gene expression values from a treatment group against a reference, yielding regulation factors that identify the direction of any deregulation (over- or under-expression) plus its order of magnitude. For the study described here, a comparison of the compound treatment was calculated against the corresponding time-matched vehicle control. The outcome was filtered according to a deregulation threshold of at least 2-fold. Finally, lists were exported containing genes with a BH q-value ≤ 0.05 (for rat only) and a fold change ≥ 2 in both directions (up or down).

2.3.2.7 Biological interpretation

The numbers of deregulated genes for the PRH samples obtained after statistical analysis are summarised in the Appendix 1, Table 39. These data sets were evaluated manually by assignment of gene functions, according to public databases and current publications (NBCI: Gene and PubMed, Medical College of Wisconsin: The Rat Genome Database). The genes were then categorised into arbitrary global functions, e.g. *Carbohydrate Metabolism* or *Inflammation and immune response*.

In contrast to PRH, the gene lists resulting from the PHH (Appendix 1, Table 40) revealed much higher numbers of deregulated genes. Hence, the data of the various donors was analysed by means of the web-based Ingenuity Pathway Analysis® (IPA®) software. Within IPA® the liver specific 'Tox Functions' were used to generate pathway hypotheses; whereas, only those functions were considered further that held a minimum of ten genes in any of the six conditions (low and high concentration: 1, 3 and 14 days). The evaluation and expansion of the hepatotoxic pathway hypotheses was performed by manual curation using public databases and current publications (NCBI: Gene and PubMed, Weizmann Institute of Science: The GeneCards Human Gene Database).

2.3.3 Proteomics

2.3.3.1 Sample preparation for proteomic analyses

Following treatment, cells were washed twice with ice-cold PBS to remove excess medium. A volume of 500 µL ice-cold methanol was added to the well and the cell/collagen layer was scraped off and transferred to a 2 mL Eppendorf tube. The well was rinsed with 250 µL methanol which was also added to the collection tube and an in-probe sonicator was used to homogenise the sample. After centrifugation (18,000 x g for 10 min and 4°C), the supernatant was transferred into a new 2 mL collection tube. The resulting protein pellet was stored at -80°C until shipping for proteomics analyses.

For each compound, sampling from all biological replicates was completed prior to protein analysis. The protein pellets were sent to the Molecular Biology Unit of the Paris-Lodron-University of Salzburg (Austria). On site, the samples were processed as described by Wilmes et al. (2013). The generated proteomics data was sent to the Department of Mathematics and Computer Science at the Freie Universitaet, in Berlin, for comprehensive evaluation and data analysis as described by Wilmes et al. (2013).

2.3.4 Biokinetic measurements

In order to generate information about the biokinetic profile of the compounds in the different cell culture systems, quantitative analysis of the parent test compound was performed. Based on literature and preliminary experiments, the specific kinetic time points were chosen on day 0 and day 13 of treatment.

2.3.4.1 Sample preparation for biokinetic analyses

The primary hepatocyte long-term cultures were treated on day 0 and 13 (see Figure 12) for different times, namely 2 min, 30 min, 1 h, 3 h, and 24 h. The exception to this was the first CsA treated biological replicate for PRH, which were treated for 1, 2, 4, 8 and 24 h.

After treatment, media from each well were transferred into a *LoBind Eppendorf* tube and stored on ice. An aliquot of compound-containing medium (which was not given to the cells – time point 0 min) was also put into a tube and placed on ice. The SW cultured cell layer was washed twice with PBS and scraped and transferred to a new *LoBind* tube placed on ice. The same well was rinsed with 250 µL methanol and the whole volume was added to the tube containing the harvested cells. Following in-probe sonication to homogenise the cell lysate fraction, the volume was adjusted with methanol to 1 mL. In order to measure the adsorption of the compound to plastic, the empty culture wells were rinsed twice with PBS before incubating the Parafilm-sealed culture vessel with 2 mL methanol per well at RT on a horizontal shaker set at 300 rpm. The methanol then was pipetted into another *LoBind* tube. All fractions (i.e. media, supernatants, cell lysate and plastic binding methanol) plus an aliquot of the appropriate stock solution were stored at -80°C until shipment to the respective analytical laboratory – an overview is given in Table 18.

Table 18. Overview on sample volumes and collection time points for biokinetic analysis in primary rat (PRH) and human (PHH) hepatocytes. The values were identical for all compounds. The different sampling times applied only to the 1st biological replicate of PRH treated with cyclosporine A were 1, 2, 4, 8 and 24 h (not included in the table).

Fraction	Vehicle Control	Low concentration	High concentration
Stock solution	-	500 µL	500 µL
Media / Supernatant (PRH: 1.5 mL; PHH: 2 mL)	0 min, 2 min, 30 min, 1 h, 3 h, 24 h	0 min, 2 min, 30 min, 1 h, 3 h, 24 h	0 min, 2 min, 30 min, 1 h, 3 h, 24 h
Cell lysate (PRH and PHH: 1 mL)	2 min, 30 min, 1 h, 3 h, 24 h	2 min, 30 min, 1 h, 3 h, 24 h	2 min, 30 min, 1 h, 3 h, 24 h
Plastic binding (PRH and PHH: 2 mL)	2 min, 30 min, 1 h, 3 h, 24 h	2 min, 30 min, 1 h, 3 h, 24 h	2 min, 30 min, 1 h, 3 h, 24 h

2.3.4.2 Sample preparation for blank experiments

Repeated exposure experiments were conducted in the absence of cells to determine the amount of compound sequestered by the matrix molecules surrounding the sandwich cultured primary hepatocytes. The corresponding volumes of collagen I (PRH) and Geltrex™ (PHH) were exposed to high, low concentrations of the compounds or vehicle control. Sampling was performed as previously described for the cell cultures on day 0 and 13, but only at two specific time points, i.e. 2 min and 24 h.

2.3.4.3 Biokinetics analyses

The collected samples were sent to the corresponding analytical laboratories, and analysed as delineated in Table 19.

Table 19. Summary of sample analysis methods and sites for the four compounds.
Abbreviations: IBU - ibuprofen; CPZ - chlorpromazine; CsA - cyclosporine A; AMI - amiodarone; HPLC - high-performance liquid chromatography; UV - ultraviolet; LC-MS/MS - liquid chromatpgraphy-tandem mass spectrometry.

Compound	Detection method	Analytical laboratory
IBU	HPLC-UV	'Environment and Primary Prevention Department' at the ISS, Rome (Italy)
CPZ	HPLC-UV	'Institute for Risk Assessment Sciences' at Utrecht University, Utrecht (The Netherlands)
CsA	LC-MS/MS	'Department of Toxicology' at the University, Wuerzburg (Germany)
AMI	HPLC-UV	'Environment and Primary Prevention Department' at the ISS, Rome (Italy)

2.3.5 Determination of cell number

The assessment of the cell number is an important factor for normalisation of the kinetics data. Therefore, the number of cells 1 and 14 days after treatment were of interest. A first approach was the measurement of DNA quantity. A volume of 10 µL homogenised cell lysate sample (see section 2.3.4.1) was analysed using the Quant-iT™ PicoGreen® dsDNA Assay according to the manufacturer's instructions. The outcome was inconclusive for the 14 day time point, where a wide discrepancy between the microscopic appearance of the cell layer and the DNA amount was observed. According to the PicoGreen® assay the cell number varied between 17 and 128% when compared to day 1. Therefore, a different strategy was considered which employed the use of high content imaging; however, this meant that a separate plate had to be used, thus not allowing the determination of the cell number in the actual kinetic sample well. The staining of an additional plate on day 1 and 14 of culture was prepared for supportive information only, i.e. for all compounds for a specific biological replicate.

Cells were seeded into 6-well plates as described in section 2.2.2.4. After 24 h of treatment starting on day 1 and 14, PRH cultures were washed with PBS before incubation with DNA-binding Hoechst 33342 dye (5 µg/mL in PBS) for 20 min in the incubator. The cells were washed twice with PBS, 1.5 mL PBS was added per well to avoid desiccation and the plate was imaged within 30 min using the Cellomics ArrayScan® VTI. The preinstalled bioapplication *CellHealthProfiling* was adapted to a cell count protocol to the SW cell culture system. Here, the first channel detected the fluorescent nuclei and the second channel recorded a bright field image, both with the 10-fold magnification microscope objective.

2.3.6 Cytochrome P450 induction

The inducibility of specific CYP enzymes with prototypical inducers was used to characterise the PRH. The simultaneous quantification of different target mRNAs was performed with the QuantiGene® Plex 2.0 Assay from Panomics (Affymetrix®). A customised Plex Set for rat (Panel number 31104) containing a target-specific mixture of *Probe Set* and *Capture beads* was used to detect 17 targets (Appendix 2, Table 41).

The QuantiGene® Plex 2.0 assay is based on the hybridisation of the target sequence to xMAP® Luminex® magnetic beads and the signal which is amplified via the branched DNA technology is detected with the Luminex® 200™ System; the measuring principle is shown in Figure 21.

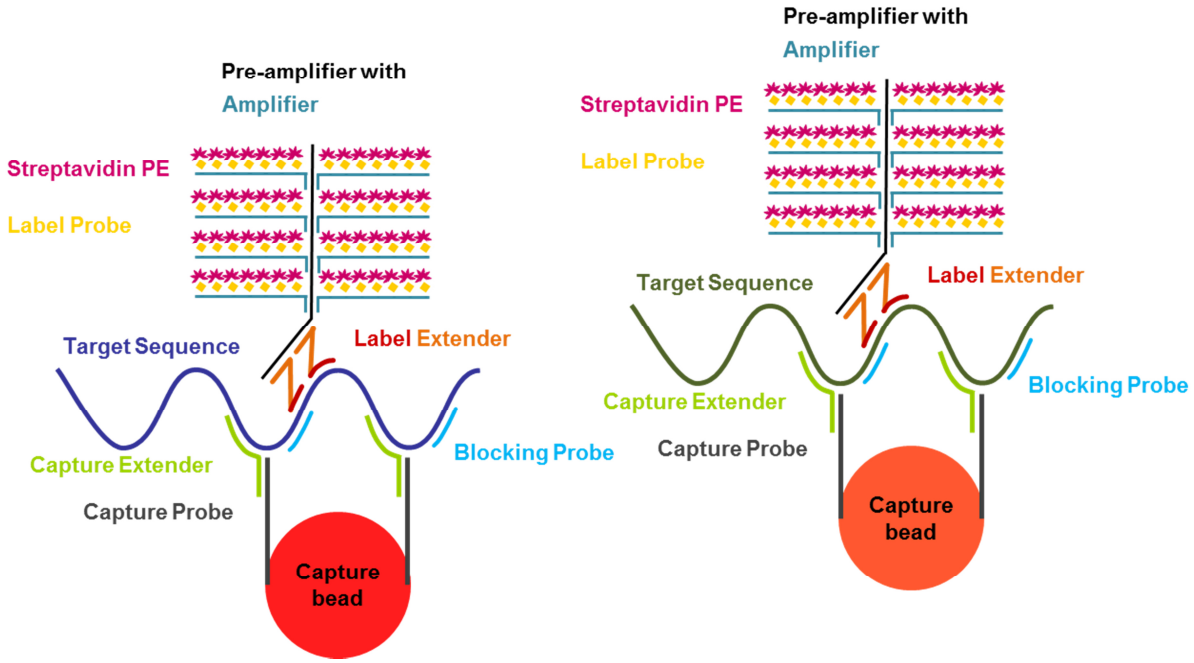

Figure 21. Principle of the measurement of two target genes using the QuantiGene® Plex 2.0 Assay. After sample preparation and hybridisation of the bead-bound capture extender to the target sequence the signal amplification tree is build in sequential hybridisation steps (detailed steps are given in the text). Finally, phycoerythrin (PE) is exploited as fluorescence-based indicator for signal generation which allows the quantification of target RNA present in the sample.

PRH were seeded onto a 96-well plate as described in section 2.2.2.3. The prototypical inducers were 3-methylcholanthren (3-MC), dexamethasone (Dex), phenobarbital (PB) and pregnenolone-16α-carbonitrile (PCN). A total of six wells were incubated per treatment, which included the prototypical inducer, solvent and medium controls. The cells were treated daily for a total duration of 72 h and starting 1 day after seeding. Stock solutions of the inducers (3-MC, Dex, PB and PCN) were stored at -20°C. On the day of treatment, the stock solutions were thawed and, in addition to DMSO, freshly diluted 1:1000 in serum-free culture medium prior to application to the cells. The final concentrations used were: 5 µM 3-MC, 50 µM Dex, 1000 µM PB and 10 µM PCN, while the DMSO vehicle control concentration was 0.1%. After 3 days, the cells were lysed by replacing the media with 75 µL *Working Lysis Mixture* (1:3 dilution of *QGP2.0 Lysis Mixture* in serum-free culture media supplemented with 5 µL proteinase K per mL), followed by

an incubation at 37°C for 1 h in the incubator. All six wells of a treatment condition were pooled in an Eppendorf tube and stored at -80°C until the five biological replicates were completed. All replicates were processed at the same time.

2.3.6.1 Hybridisation (Day 1)

The samples were thawed at RT and stored on ice until needed. The appropriate *Probe Set* was thawed on ice and then transferred to an Eppendorf tube and denaturated by heating at 95°C for 5 min, before storing it on ice. For the hybridisation of the target RNAs to the corresponding *capture beads*, so-called *Working Plex Set*s for (i) samples and (ii) total liver RNA were prepared according to Table 20 and Table 21, respectively. Bead-containing solutions were vortexed thoroughly prior to use. The *total liver RNA* served as an internal quality control to confirm the linearity of the assay. A standard curve of total liver RNA with nuclease-free water, ranging from 0.78 ng/µL to 25 ng/µL (2-fold dilution steps, six concentrations), was included in each measurement. An empirically determined 1:5 dilution of the samples in *Working Lysis Mixture* resulted in an adequate concentration to assay the CYP induction at the mRNA level.

Table 20. Working Plex Set composition for samples.

Order	Reagent	Volume per well in µL
1	Nuclease-free water	5.2
2	Lysis Mixture	6.6
3	Blocking Reagent	2.0
4	Proteinase K	0.2
5	Capture Beads	1.0
6	Probe Set	5.0

Table 21. Working Plex Set composition for total liver RNA.

Order	Reagent	Volume per well in µL
1	Nuclease-free water	38.7
2	Lysis Mixture	33.3
3	Blocking Reagent	2.0
4	Capture Beads	1.0
5	Probe Set	5.0

A volume of (i) 80 µL *Working Plex Set for total liver RNA* and 20 µL corresponding *total liver RNA*, including blank, and (ii) 20 µL 'Working Plex Set for samples' and 80 µL sample, plus blank, were added to each well of a 96-well round bottom plate. The hybridisation plate was then sealed with pressure seals and incubated in a VorTemp™ 56 Shaking Incubator at 600 rpm and 54°C for 16 h.

2.3.6.2 Signal amplification (Day 2)

On the second day, sequential hybridisation steps were performed to amplify the signal, this procedure – allowing the detection of low abundance RNA molecules – is based on the branched DNA technology first introduced by Urdea et al. (1987).

The buffer solution for the washing steps were prepared freshly by combining 114 mL diethylpyrocarbonat (DEPC) treated water with 6 mL wash buffer *Component 1* and 360 µL

Component 2. The HydroFlex™ microplate washer for 96-well format was rinsed with DEPC treated water, primed with air and filled with the prepared wash buffer solution. The *Amplifier Diluent* was pre-warmed at 38°C for 30 min, while the *Label Probe* and *SAPE Diluent* were allowed to equilibrate to RT. After 16 h, the hybridisation plate was taken out of the shaking incubator and centrifuged at 240 x g and RT for 1 min in order to collect evaporated liquid from the cover on the well bottom. The plate was then mixed before transferring the entire sample volume to a 96-well magnetic bead plate. The plate was placed into the HydroFlex™ microplate washer and program "*QGP2*" was started. During the automated washing procedure, the magnetic beads are attracted by the magnet, hence allowing the removal of excess material, i.e. unbound nucleic acids, enzymes and buffer. Immediately after the last suction of the wash buffer, the magnetic bead plate was taken out of the automated washer and 100 µL *Pre-Amplifier working solution* (Table 22) was added to each well. The plate was sealed with adhesive foil and placed on the plate shaker at 800 rpm and RT for 1 min to re-suspend the beads prior to incubating it at 600 rpm and 50°C for 1h in the shaking incubator. The plate then was taken out and washed as previously described. A volume of 100 µL *Amplifier working solution* (Table 22) was added to each well and the plate was processed according to the procedure described for *Pre-Amplifier* hybridisation. Before proceeding with the washing step, 100 µL *Label Probe* (Table 22) working solution was added to each well. For the last step of signal amplification tree construction, 100 µL *SAPE* working solution was added to each well; the plate was sealed, the beads re-suspended and the plate was shaken and incubated at 600 rpm and RT for 30 min. The washing station was primed with air and pre-filled with ready to use *SAPE* wash buffer solution. Following the last incubation period, the plate was washed and 130 µL *SAPE* wash buffer was added to each well. Finally, to re-suspend the beads, the plate was shaken at 800 rpm and RT for 5 min, before measuring the plate using the Luminex® 200™ instrument.

Table 22. List of the working solution preparations for the stepwise construction of the signal amplification tree.

Working solution	Diluent	Stock solution
Pre-Amplifier	12 mL Amplifier Diluent	36 µL Pre-Amplifier
Amplifier	12 mL Amplifier Diluent	36 µL Amplifier
Label Probe	12 mL Label Probe Diluent	36 µL Label Probe
SAPE	12 mL *SAPE* Diluent	36 µL *SAPE*

2.3.6.3 CYP induction data analysis

Due to the fact that each bead carries slightly different amounts of signal reporting phycoerythrin molecules, a certain distribution is detected for one set of beads, i.e. tracking an analyte. The xPonent® software calculates the median from the data range generating so-called "median fluorescence intensity (MFI)" values which were used for evaluation of the results.

The quality of the performed bDNA assay was assessed by evaluating the housekeeping gene expression across the total liver RNA concentration gradient. The blank-corrected averages of the duplicates were plotted against the applied total liver RNA concentrations. The computed correlation coefficient R^2 was 0.9989 for *Ppib*, 0.9924 for *Hmbs* and 0.09889 for *Hprt1*, which represent an acceptable linearity.

The stability of the housekeeping genes (*Ppib*, *Hprt1*, *Hmbs*) was validated for future normalisation purposes. The triplicate mean was taken to calculate the fold change from the treated samples compared to the corresponding DMSO control. A housekeeper gene should be stably expressed independently from the applied treatment, thus the fold changes for these genes should approximate unity. Only housekeeper genes with a fold change of 0.7 to 1.3 were used to normalise the residual gene products. If more housekeeper genes met this requirement, the MFI range of the target gene was taken into account – *Ppib*, *Hprt1*, *Hmbs* for high, mid and low MFI ranges, respectively.

For inducer- and vehicle (DMSO) treated samples, the blank-corrected mean of the target genes was calculated and normalised to the appropriate housekeeping gene. The absolute fold change in inducer treated versus vehicle control treated cells was calculated.

2.3.7 Cytochrome P450 activity

The CYP activity in PRH was measured at the Merck Serono DMPK department in Grafing (Munich, Germany). In order to support the interpretation of the endpoints included in this study and to identify intraspecies differences (i.e. between the different biological replicates), the CYP activity of two important CYPs, namely Cyp3a1 and Cyp1a2, was assessed. Preliminary studies to establish the protocol were performed by Lauer (2012); these included inhibition and induction studies to identify additional CYP isoforms involved in the metabolism of the substrate.

The substrates were midazolam and phenacetin. The benzodiazepine midazolam is mainly metabolised by Cyp3a isoforms to 1'-hydroxy-midazolam (1-hydroxymethylmidazolam or α-hydroxymidazolam) and 4-hydroxy-midazolam (Hoen et al, 2001). Brown et al. (2007) showed that 1'-hydroxy-midazolam is the predominant metabolite in rat hepatocytes.

Phenacetin is an analgesic and is metabolised by Cyp1a2 to acetaminophen. In the preliminary inhibition experiment with the Cyp1a inhibitor, α-naphthoflavone, phenacetin was still converted to APAP, which was possibly due to other CYPs being involved in the phenacetin metabolism (Lauer, 2012). Kobayashi et al. (2002) reported that Cyp1a2 and 2c6 both metabolised low concentrations (10µM) of phenacetin in rat liver micorsomes. At a higher phenacetin concentration (500µM), multiple CYPs were involved in its metabolism, namely Cyp2a2, 2c11, 2c12, 2c13, 2d1, 2d2, 2e1, 3a1 and 3a2 (Kobayashi et al., 2002).

2.3.7.1 CYP activity in PRH

Freshly isolated PRH were seeded in ML configuration at a density of 1.5 x 10^6 cells per well in a 6-well plate (see section 2.2.2.3). On the second day after seeding the ML triplicate cultures were treated with 1.5 mL 10 µM midazolam, 20 µM phenacetin or 0.5% methanol, as the control. The compounds were prepared in serum-free culture medium from 200-fold stock solutions in methanol, stored at -20°C, to keep the solvent concentration at 0.5%. After the incubation of substrates for 1 h in the incubator, the supernatants were transferred into an Eppendorf tube and stored at -80°C. The samples were shipped to the "Drug metabolism and pharmacokinetics" (DMPK) department for quantification of CYP metabolites via liquid chromatpgraphy-tandem mass spectrometry (LC-MS/MS). For normalisation purposes, the protein was quantified via Bradford assay (see next paragraph).

2.3.7.2 Protein quantification using the Bradford Assay

The Bradford protein assay is a colorimetric method that determines the protein content in the microgram range. It is based on an absorption shift of the Coomassie Brilliant Blue G-250 dye upon the formation of complexes with proteins in solutions (Bradford, 1976).
In an acidic environment (aqueous solution of phosphoric acid and ethanol) the dye stays in its cationic and neutral form where it exerts absorption maxima of 470 nm (red) and 620 nm (green), respectively. The formation of protein-dye complexes is mainly driven by the presence of basic amino acids within a protein which stabilise the anionic form of the dye resulting in its blue colour with an absorption maximum at 595 nm (Reisner et al., 1975).
Protein samples were prepared by first removing the culture media and then adding 600 µL 0.1% Triton-PBS (1:1000 dilution of Triton x-100 in PBS) to each well. The cells were lysed by shaking and incubating the plates at 500 rpm and RT for 5 min on a horizontal plate shaker. The complete lysis of the cells was checked under the microscope. Triplicate 1:5 dilutions of lysate from each well were made in 0.1% Triton-PBS (2 µL sample + 8 µL Triton-100) in a transparent 96-well plate. A volume of 200 µL Bradford Reagent was added to each well, including blank wells, and the plates incubated at 500 rpm and RT for 10 min. Subsequently, the absorbance at 595 nm was measured using a microplate spectrophotometer and KC4™ Data analysis software. For each assay, a standard curve was included using the same 0.1% Triton-PBS as that used for the samples.

2.3.7.3 Metabolite quantification

The metabolites 1'- and 4-hydroxymidazolam, as well as acetaminophen were analysed by LC-MS/MS at the DMPK department of Merck Serono in Grafing according to in-house SOPs.

2.3.7.4 CYP activity data analysis

The metabolite concentration was normalised to protein content and the specific activity of the CYPs was expressed as pmol x min^{-1} x mg $protein^{-1}$.

2.3.8 MitoXpress® O_2 assay (LUXCEL®)

This assay uses a phosphorescent probe of proprietary structure (MitoXpress® O_2-sensitive probe) with an excitation wavelength of 340 - 390 nm or 535 nm and an emission wavelength of 630 - 680 nm. In the presence of oxygen the exited state of the probe is quenched, hence diminishing the emitted light. In cell-surrounding culture medium the phosphorescent probe acts as an oxygen sensor. To ensure an accurate analysis of the amount of oxygen the measuring volume is isolated from surrounding air by application of oil which hermetically seals the well, preventing external oxygen diffusion into the reaction chamber. Cell-based assays require the use of *high-sensitivity oil* (provided in the MitoXpress®-Xtra HS) while for isolated mitochondria mineral oil is used. The level of oxygen decreases gradually as the cells respire, resulting in an increase of the emitted signal by decreased quenching. The oxygen metabolism of plated cells is monitored over an arbitrary fixed period of time thus enabling an *in situ* measurement.
In order to prepare the stock solution, 1 mL Millipore water was added to a *MitoXpress® probe* vial, which was kept in the dark. The working solution was prepared by diluting the probe stock 1:15 in appropriate medium and keeping it in the dark at 37°C. Before starting the experiment, (i) Luxcel's *high-sensitivity oil* was warmed to 37°C, (ii) the frozen compound concentration gradient was thawed and vortexed, (iii) the TECAN Infinite F500 instrument was started and (iv), within the Magellan™ software, the adequate "Mitotox" method was initiated, which included heating of the reader chamber to 37°C for the entire measurement. The cell culture medium was carefully aspirated from a black 96-well tissue plate, 150 µL *MitoXpress® working solution* was added to each well and 1 µL compound stock was added in quadruplicate. A volume of 1 µL DMSO was added if the compound stock was prepared in water. The first column of the plate did not contain any cells – *MitoXpress®* containing medium was added to the first upper wells and simple media was added to the four lower wells. Subsequently, warm *high-sensitivity oil* was applied onto each media mixture and the kinetic measurement was started, during which time, the phosphorescent signal of each well was measured every minute for a total of 60 cycles (1 h).

2.3.8.1 MitoXpress® O_2 assay data analysis

The Magellan™ software was used to select only data points within the linear range of the slope. The data selection was performed for every plate, i.e. separate experiments, mean slope plus correlation coefficient per well were exported from the software into the excel software.

All values were blank corrected, using the mean of the signals (relative fluorescence unit) derived from wells without cells but with *MitoXpress*® containing medium plus oil (upper four wells of the first column). Fold changes of each value of the quadruplicate to the geometric mean of the vehicle-control were calculated. The values were logarithmised to the base of e ("Euler's constant", i.e. natural logarithm) and then, the mean of the quadruplicate was calculated. The mean was de-logarithmised again and, finally, the response was expressed as a percentage of the control value. One-way repeated measures analysis of variance (ANOVA) followed by post-hoc Dunnett contrast testing was performed using the statistical analysis software GraphPad Prism® version 5.02 (GraphPad Prism®, 2007) to compare the *Oxygen Consumption Rate* between treatment (different compound concentrations) and vehicle control on a statistical significance level of 5%.

2.3.9 Seahorse XF96^e extracellular flux analysis

The Seahorse XF96^e instrument allows the measurement of oxygen consumption and acidification rate of adherent cells in 96-well plate format by means of optical sensors. Similar to the *MitoXpress*® *O_2-sensitive probe*, this system is also based on the property of oxygen and H^+ to quench the light emission of an excited phosphorescent probe (Gerencser et al., 2009). Distinct fluorophores are used for the two analytes (O_2 and H^+). The sensor cartridge lowers to create a temporary microchamber, which allows the real-time monitoring of oxygen consumption and proton production. Here, only the oxygen consumption rate was considered.
The *XF Cell Mito Stress Test* kit contains a set of four compounds, namely oligomycin, FCCP, antimycin and rotenone. These compounds, with well-described effects on the mitochondrial respiration (Table 23), allow the assessment of a mitochondrial capacity profile when added to the cells. This mitochondrial profile was recorded after compound treatment (*in situ* and after 24 h pre-incubation) to assess the potential of the compound to act as mitochondrial toxicant.

Table 23. Overview of the effects of compounds contained in the *XF Cell Mito Stress Test* kit. Abbreviation: FCCP - carbonyl cyanide 4-(trifluoromethoxy)phenylhydrazone; OXPHOS - oxidative phosphorylation.

Compound	Effect
Oligomycin	F1/F0 ATPase inhibitor
FCCP	OXPHOS uncoupler
Antimycin	Complex III inhibitor
Rotenone	Complex I inhibitor

2.3.9.1 Measurement of oxygen consumption rate

For re-hydration of the fluorophore patches, the disposable *XF96 Sensor Cartridges* were placed into *XF96 Calibration Plates* containing *XF Calibrant Solution* (200 µL per well) over night at

37°C and ambient CO_2. The Seahorse Bioscience XF^{e}96 instrument was connected to the operating software that enabled the equilibration to 37°C overnight.

XF assays generally required non-buffered medium that was obtained by preparation of basal DMEM and Williams' Medium powder without sodium bicarbonate. The different cell systems required distinct *XF* assay media preparations, according to the appropriate cell culture medium composition, which was determined beforehand. Table 24 summarises the applied cell types and concentrations of the essential components for this assay. The *XF* assay medium was prepared freshly every day by addition of eventually lacking components (sugar, sodium pyruvate and /or L-glutamine) up to the appropriate concentration (Table 24) followed by the pH-adjustment (at 37°C) to 7.4. The *XF* assay media was kept at 37°C until needed.

Table 24. Overview of final sugar, sodium pyruvate and L-glutamine concentrations and used basal medium source in the *XF* assay medium for the different cell systems.

	Concentration in mM			
Cell system	**Sugar**	**Sodium pyruvate**	**L-glutamine**	**Basal medium**
PRH	17.51 (Glucose)	1.5	2.5	DMEM
HepG2 – Glucose	17.51 (Glucose)	1.5	2.5	DMEM
HepG2 – Galactose	10 (Galactose)	1	6	DMEM
HepaRG	11.11 (Glucose)	0.227	2 (GlutaMAX™)	Williams' Medium E

The pre-weighed reagent powders within the *XF Cell Mito Stress Test* kit were dissolved in 180 µL DMSO, thus obtaining 2.5 mM stock solutions of each compound. The reagents were aliquoted and stored at -20°C until needed. For the assay, a 10-fold stock solution was prepared freshly in the corresponding *XF* assay media. The concentrations of oligomycin, antimycin and rotenone were consistent for all cell systems (all 1 µM final concentration), whereas, the concentration for FCCP was cell type-dependent, which were determined in preliminary tests.

The cells in the *XF Cell Culture Mircoplate*s were prepared for the measurement as follows. The culture media was aspirated and the cells were washed twice with corresponding *XF* assay media (200 µL per well). After the last wash, 180 µL *XF* assay medium was added to each well and the plate was placed into a plate heater (37°C) for at least 30 min to allow equilibration to ambient CO_2. During this time, the injection ports (four ports, A-D, per well) of the *XF Sensor Cartridge* were loaded with reagent solutions as listed in Table 25.

Table 25. Layout of the injection ports in the two experimental settings.
Abbreviation: FCCP - carbonyl cyanide 4-(trifluoromethoxy)phenylhydrazone.

Injection Port	In situ treatment	24h pre-treatment
A	20 µL Compound	20 µL Oligomycin (1 µM)
B	22 µL Oligomycin (1 µM)	22 µL FCCP (cell type dependent)
C	25 µL FCCP (cell type dependent)	25 µL Antimycin/ rotenone (1 µM/ 1 µM)
D	27 µL Antimycin/ rotenone (1 µM/ 1 µM)	-

The analysis protocol was set up within the XF^e Wave software, and included the plate layout and injection schedule. As shown in Figure 22, three basal rate measurements were conducted before starting the schedule for "*in situ*" or "pre-treated". Overall "3 min mix / 3 min measure" cycles were applied.

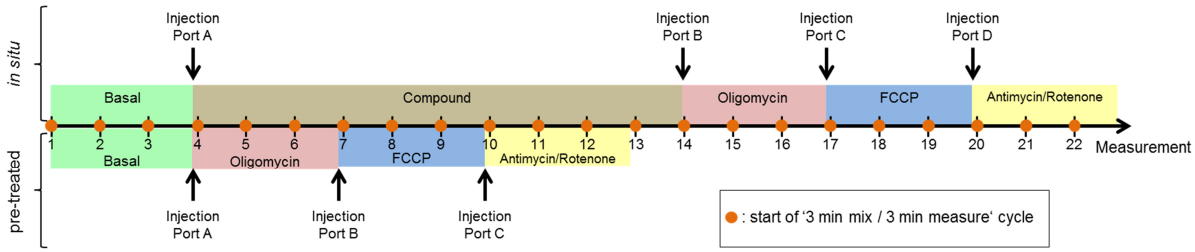

Figure 22. Measurement schedule with the Seahorse XF^{e}96 instrument for the assessment of mitochondrial capacity (i) *in situ* and (ii) after 24 h pre-treatment (upper and lower panel, respectively).

The measurement started with the calibration of the *XF Sensor Cartridge*, which was placed in the *XF Calibrant Solution* containing *XF Calibration Plate* and held the reagents for injection in the ports A to C/D (Table 25). After completion of the calibration, the instrument retained the *XF Sensor Cartridge*, i.e. only the *XF Calibration Plate* was released and thus replaced by the CO_2-equilibrated *XF Cell Culture Microplate*. The measurement started automatically and lasted approximately 140 min for the *in situ* treatment and 75 min when the cells were pre-treated with the compounds.

2.3.9.2 Seahorse XF96^e extracellular flux data analysis

The third measurement was defined as basal *Oxygen Consumption Rate* and as 100%. In relation to this value, all other *Oxygen Consumption Rate* values were used to create response curves. The first *Oxygen Consumption Rate* after FCCP injection was used to calculate the *Spare Respiratory Capacity* (Figure 23), which served as benchmark to reveal concentration-dependent compound effects.

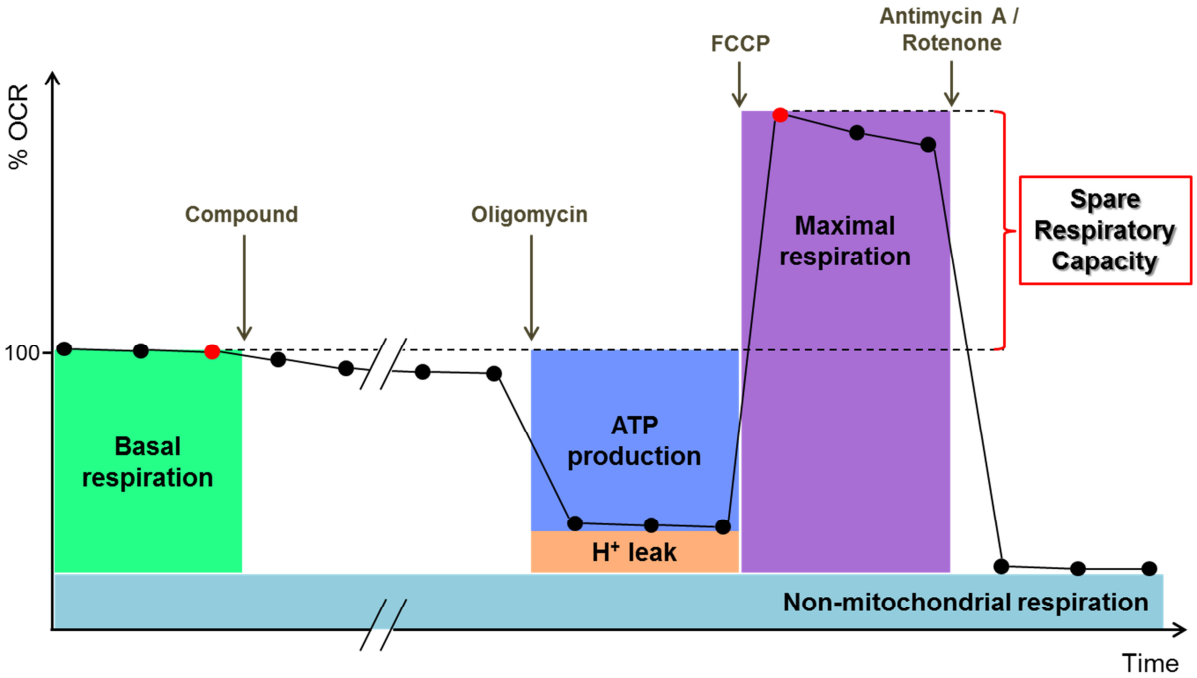

Figure 23. Principle of the measurement using the Seahorse Biosciences XF^{e}96 instrument with the *XF Cell MitoStress Test* kit and considering the *in situ* treatment protocol. The percentage of oxygen consumption rate (OCR) is given over time and refers to the basal (3rd measurement) OCR in pmol/min set to 100%. Each dot represents a measurement ("3 min mix / 3 min measure" cycle). Initially the basal respiration is measured. Subsequently, the compound is injected and OCR determined for a total of ten measurements before addition of oligomycin inhibits adenosine triphosphate (ATP) production thus allowing to determine the OCR due to proton (H^+) leak. After carbonyl cyanide 4-(trifluoromethoxy)phenylhydrazone (FCCP) injection the oxidative phosphorylation is uncoupled, therefore maximal respiration can be determined. Finally, injection of antimycin A/rotenone fully blocks the mitochondrial respiration and reveals how much non-mitochondrial respiration contributes to the OCR. The red dots indicate measurements that were used for calculation of the *Spare Respiratory Capacity*.

One-way repeated measures ANOVA followed by post-hoc Dunnett contrast testing was performed using the statistical analysis software GraphPad Prism® version 5.02 (GraphPad Prism®, 2007) to compare the *Spare Respiratory Capacity* between treatment (different compound concentrations) and vehicle control on a statistical significance level of 5%.

3 Results and Discussion

This thesis dealt with data from primary rat (PRH) and human (PHH) hepatocytes after short- and long-term repeated treatment with four marketed pharmaceuticals. In this section the results from different endpoints, including *in vitro* dose finding studies, biokinetic, transcriptomic and proteomic profiling as well as mitochondrial toxicity are presented and discussed.

As part of the Predict-IV project, the handling of the PHH, including cell isolation, tissue culture, compound exposure and sampling (for dose finding, biokinetic and transcriptomics analysis) was conducted by the Predict-IV project partner KaLy-Cell in Plobsheim (France). The handling of the PRH was performed by me at Merck Serono in Darmstadt (Germany). The measurement of the biokinetics and proteomics samples was conducted by experts from the corresponding fields. While the proteomics samples were send to the Predict-IV partner at the University of Salzburg, the biokinetics samples were distributed to different partners depending on the treatment compound (Table 19).

Data analyses, illustrations and comprehensive biological interpretation of the results represent my own work. A detailed overview on the personal contribution within the Predict-IV project is given in section 1.7 Personal contributions.

3.1 Ibuprofen

Ibuprofen (IBU) is a commonly used over-the-counter analgesic and can be considered among the safest non-steroidal anti-inflammatory drugs (NSAIDs) (NIH - Ibuprofen, 2014). Gastrointestinal side-effects are reported frequently (RxList - Motrin, 2007), while adverse effects to the liver are rare (Bennett et al., 2009). Hence, with respect to hepatotoxicity this compound was included as a negative compound.

3.1.1 *In vitro* dose finding

At the beginning, *in vitro* dose finding studies were performed in order to specify the ibuprofen treatment concentrations for the biokinetic, transcriptomic and proteomics profiling studies. Therefore, the cell viability of primary rat and human hepatocytes after short- and long-term exposure to increasing concentrations of IBU was assessed. The resulting TC_{10} (concentration exerting 10% cytotoxicity) was eventually used as high concentration.

A clear concentration-dependent cytotoxicity was caused by IBU in the different PRH cultures (Figure 24), whereas time-dependence (24-well: 1, 3 and 14 days; Figure 24 B) was less pronounced. A concentration of 10 µM IBU had no obvious effect on the morphology of PRH cultured in 6-well plates (Figure 24 E), compared to the vehicle treated control cells (Figure 24 D). Generally, none of the three IBU concentrations affected the bile canaliculi-like structures or

cuboidal shape and the partly binucleated hepatocytes assembled in cell islands were conserved. A 50-fold higher concentration (500 µM; Figure 24 F) resulted in moderate cell death, apparent as cell debris and the presence of single rounded-up cells. There was an increase of cell debris and the number of rounded-up cells at a higher concentration of 1000 µM IBU (Figure 24 G). The high concentration for the final experiments was therefore set to 100 µM and the low concentration to 10 µM. The high concentration was determined mainly based on the morphological evaluation, such that 10 µM did not affect the culture morphology; whereas, 500 µM IBU resulted in a high cytotoxicity.

IBU is thought to passively enter the cytoplasm, where it can quickly affect cellular metabolism. Furthermore, it is known to inhibit beta-oxidation, which leads to adenosine triphosphate (ATP)-generating oxidative phosphorylation being reduced. Both pathways are essential for energy production and thus cell survival. However, ATP is produced by many pathways, thus giving the cell the opportunity to alter its metabolism in response to adverse constraints on energy homeostasis. *In vitro*, culture medium contains high glucose concentrations, i.e. 315 mg/dL in the PRH media used in these studies, compared to blood levels of ~ 115 mg/dL (male Sprague-Dawley; Kohn and Clifford, 2002). Therefore, it is very likely, that the PRH have increased glycolysis rates for the generation of ATP, thus compensating for the insufficient oxidation of fatty acids after IBU exposure.

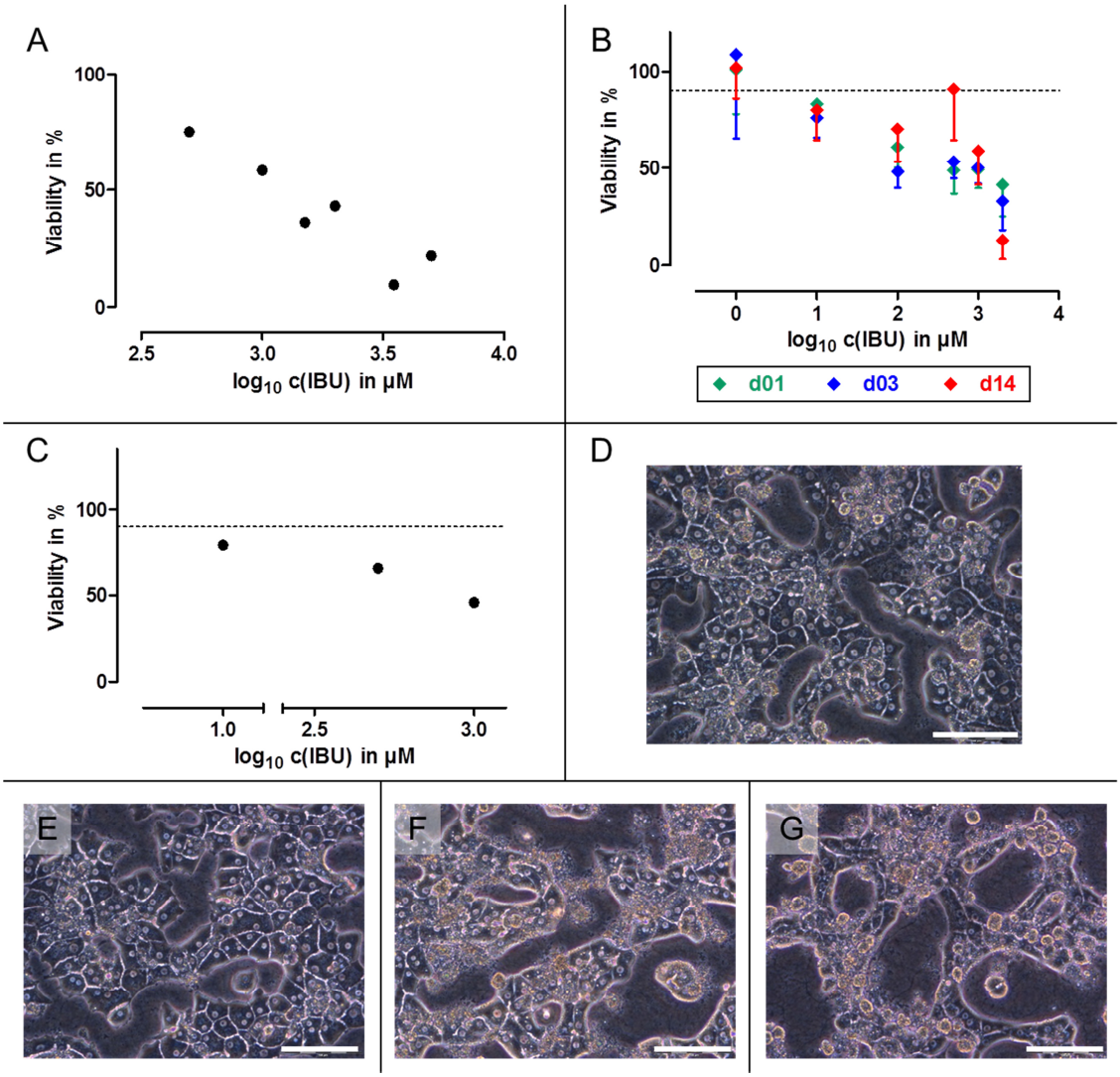

Figure 24. Cell viability results of primary rat hepatocytes (PRH) treated with ibuprofen (IBU) in 96-well mono layer for 24 h (A), 24-well sandwich (SW) for 1 (green), 3 (blue) and 14 days (red) (B) or 6-well SW culture for 14 days (C) at the indicated concentrations. Results of the 24-well SW culture derived from 3 biological replicates and are displayed as mean - standard deviation (B). Viability (measured using ATP content) was expressed as the percent relative to the corresponding time matched DMSO control. The dotted line denotes the 90% viability threshold (B and C). Pictures of PRH in 6-well SW culture on day 14 after daily treatment with DMSO (D) or IBU at 10 µM (E), 500 µM (F) or 1000 µM (G). The white scale bar on the bottom right of each picture corresponds to 100 µm.

IBU was not toxic to PHH up to 1000 µM. However, after treatment with 2000 µM a prolonged exposure for 14 days led to a pronounced decrease in viability. The characterisation of the donor's metabolic capacity was not conducted for the dose finding studies; hence, no conclusion based on specific cytochrome P450-dependent oxygenase (CYP) activities can be made (KaLy-Cell (Parmentier), personal communication).

The treatment concentrations which were set based on these initial studies for the final experiments in PRH and PHH are summarised in Table 26.

Table 26. Treatment concentration of ibuprofen (IBU) for final experiments in primary rat (PRH) and human (PHH) hepatocytes. High (HC) and corresponding low (LC) concentration.

	IBU concentration in µM	
	HC	**LC**
PRH	100	10
PHH	1000	100

The comparison of the two species showed that PRH were more sensitive to IBU treatment than PHH. This observation could either be due to intra-species differences or to the different assays that were used to assess cytotoxicity. As described previously, cytotoxicity in PRH was determined by measuring the amount of ATP. The MTT assay (PHH) is based on the reduction of 3-(4,5-dimethylthiazol-2-yl)-2,5-diphenyl tetrazolium bromide (MTT) to a formazan, occurring to a significant extent in the cytoplasm and not in mitochondria and mainly dependent on nicotinamide adenine dinucleotide (NADH) as a cofactor (Berridge et al., 2005). It seems likely that, with IBU being a beta-oxidation and complex I inhibitor, the quantification of ATP is a more direct and thus sensitive measure. Whereas the MTT assay indirectly (in terms of IBU's adverse effects on ATP synthesis) determines the activity of reducing enzymes and cofactors acting as reducing agents. For both hepatic systems, a time-dependent response was seen only at 2000 µM (24-well screen). Here, an increased cell death is likely due to the accumulation of adverse effects over long-term treatment.

3.1.2 Biokinetics

The bioavailability of a drug *in vitro* is influenced by distinct characteristics of the cell system and the compound itself. Therefore, the biokinetic profile of IBU was assessed in the two hepatic systems through quantification of parent compound in the cell lysates and supernatants over time. The biokinetics data helped to estimate the actual level of compound exposure of the cells and to comment on cellular metabolism of the parent compound.

Initially, the cell number per well was required to normalise the cell lysate concentration measured for biokinetics. A first approach, in which the cell number was correlated to the DNA content, determined with the PicoGreen™ assay, was unsuccessful. Therefore, a cell count protocol was established for PRH using high content imaging, which was measured only for the last two biological replicates since the first replicate was completed prior to full assay establishment. Since the cell numbers were comparable in the different biological replicates (Appendix 5, Table 48) the amount of parent compound was calculated in nmol/well to assure comparability between the different biological replicates and species. Hence, in the following all biokinetic profiles of cell lysate and supernatant fractions were uniformly expressed as nmol/well.

The cell lysate fractions of sandwich cultured hepatocytes contained extracellular matrix proteins because the separation of the hepatocytes from the surrounding collagen I (PRH) or GelTrex™ (PHH) was not feasible. Therefore, so-called "blank experiments" were conducted to determine the amount of compound bound to the extra cellular matrix proteins used in the sandwich cultures. The results of the blank experiments revealed that IBU accumulated in collagen I (PRH) in a time- and concentration-dependent manner (Appendix 6, Table 49). Low and high IBU concentration increased on day 0 after 24 h up to 13.6 - 15.1%. However, on day 13 the percentages levelled around 30% at each time point and concentration, suggesting a saturation of the extracellular matrix. Rates of 15 and 30%, found at 24 h on day 0 and 13, respectively, were subtracted from the measured cell lysate IBU concentrations. Rates < 5% were within the experimental variance and hence were not taken into consideration. In contrast to the PRH sandwich cultures, analyses of Geltrex™ preparations (PHH) showed that binding of IBU to the matrix molecules was negligible (at all time points and concentrations) (data not shown).

The biokinetic profile of IBU within the cell lysate and the supernatant fractions of PRH was the same for the low (Figure 25 A and B) and high (Figure 25 D and E) concentrations. In PRH, a rapid and progressive intracellular uptake of IBU was observed. IBU has a pKa of 4.52 (Ràfols et al., 1997) and a logarithmised octanol/water partition coefficient (log K_{OW}) of 2.48 (Scheytt et al., 2005), is a weak acid and is neither a strong lipophilic nor hydrophilic compound. Thus, based on its physicochemical properties, it is likely that IBU is passively transported through the cell membrane. IBU is a known inhibitor of organic ion transporters, such as OCT-1 (Wang et al., 2012) and OAT-1 (Mulato et al., 2000), but by contrast, Mulato et al. (2000) showed that [H^3]-IBU was not efficiently transported by OAT-1. In the liver, OCT and OAT are involved in hepatic uptake processes of endogenous and exogenous xenobiotics. The biokinetic studies showed that profiles in the cell lysates of IBU treated PRH were similar at both concentrations after short- and long-term exposure. This indicated IBU uptake into the cell was not inhibited; hence, suggesting that transporter-mediated uptake of IBU was, if at all, minor and passive transport could be regarded as the major uptake route for this compound. After a steady state up to 3 h, the amount of IBU decreased in the cell lysates, while at the same time, the amount also decreased disproportionally in the supernatants. This suggested that all IBU entering the cells was quickly metabolised, i.e. assuming minimal or no efflux of IBU parent compound. The calculation of the relative distribution revealed a time-dependent increase in the apparent loss of IBU, which was attributed to an efficient IBU metabolism. The biokinetic profile of IBU in PRH on day 0 was comparable to day 13; hence, the metabolism was neither induced nor inhibited over the course of repeated treatment. This was in accordance with Mills et al. (1973), who reported that after repeated exposures in rats IBU did not induce its own metabolism. Furthermore, the fact that the recovered amount of IBU after 24 h from day 13 was similar to that on day 0 suggested that the drug did not accumulate in the PRH cultures. All of these observations were independent of the applied concentration (10 and 100 µM). Thus, it was

concluded that, at both concentrations, the culture system was not saturated in terms of metabolic capacity and that no accumulation of IBU occurred in any compartment.

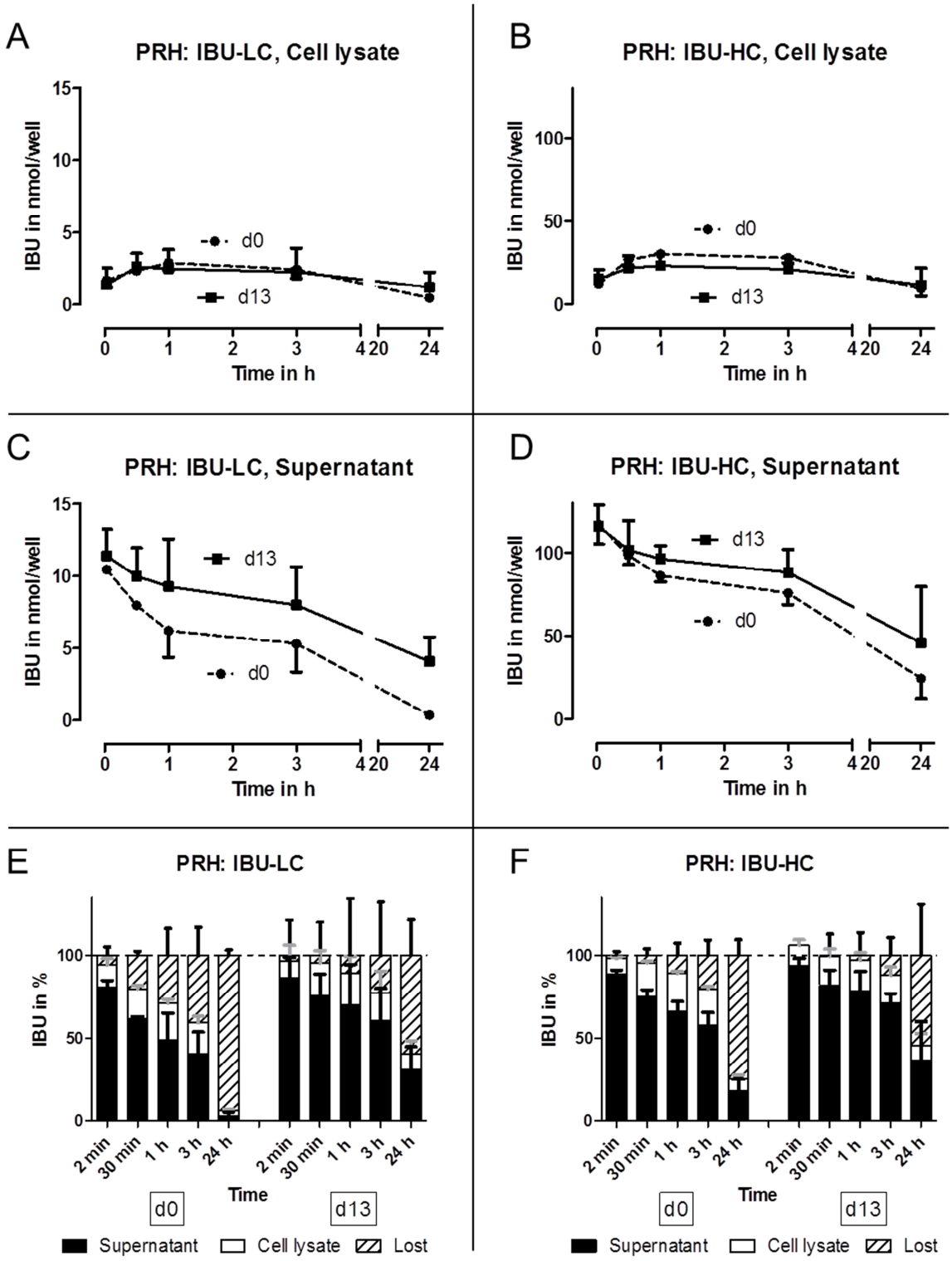

Figure 25. Kinetic profile of ibuprofen (IBU) (nmol/well) in primary rat hepatocytes (PRH) (A, B) and culture supernatants (C, D) after single (day 0 – dashed line) and repeated (day 13 – solid line) treatment with 10 µM (low concentration (LC); A, C) and 100 µM (high concentration (HC); B, D) IBU at the indicated time points. Relative distribution of IBU in percent in the different analysed PRH fractions at the indicated time points on day 0 and 13, supernatant (bold) and cell lysate (blank) as well as the apparent loss (striped) for the LC (E) and HC (F). Values are given as mean of 3 biological replicates +/- standard deviation.

The TC_{10} in PHH, determined in preliminary experiments, was tenfold higher than for the PRH. The biokinetic profiles between the PHH treated with 100 µM (Figure 26 A and B) and 1000 µM (Figure 26 D and E) IBU differed considerably. At the low concentration, a very rapid uptake in the cell lysates with 7.3 ± 6.4 nmol/well (4 ± 3%) at 2 min (day 0) and 7.9 ± 4.6 nmol/well (4 ± 2%) at 30 min (day 13) was observed (Figure 26 A). The amount of IBU reached a plateau already after 2 min. As observed previously in the PRH, the amount of intracellular uptake in PHH did not correlate to the decrease observed in the supernatant fraction (Figure 26 B), suggesting a very efficient metabolism by the PHH cultures. The fact that (i) the biokinetic profile of day 0 was comparable to that on day 13 and (ii) the recovery after 24 h was equally low, indicated an absence of IBU accumulation. By contrast, at the high concentration, a very rapid intracellular uptake was followed by a steady state of IBU at an elevated level, with no drop to a minimum level after 24 h. In the supernatant fractions a similar observation was made, with the relative distribution levelling off between 70 and 80% on both days (0 and 13). These findings were specific for the 1000 µM IBU and could be explained by a saturated metabolism in PHH. The results from the hepatocyte cultures showed a high donor-to-donor variability, leading to a standard deviation of up to 50%. However, since hepatocytes from all donors showed comparable biokinetic profiles, the results were given as mean ± standard deviation and therefore interpreted collectively.

After treatment, increased cytotoxicity was observed microscopically in the PHH from Donor 1 at 1000 µM IBU. Therefore, on day 7 the high and low treatment concentrations were reduced to 500 and 50 µM, respectively. Generally, the metabolism of IBU is considered to be a detoxification of the parent compound and in humans it is well-documented that IBU is metabolised mainly by CYP2C9 (Chang et al., 2008). Therefore, consideration of the CYP2C9 activities in the different donors was important. CYP2C9 activity (Appendix 4, Table 47) revealed a low activity for PHH from Donor 1 compared to the other donors and was a potential explanation for the high cytotoxic effect of IBU in this donor. The cytotoxicity of IBU seems highly dependent on the inherent metabolic capacity, i.e. detoxification efficiency of the cells. Therefore, if the PHH used for this pre-screening study all metabolised (and thus detoxified) IBU extensively, the experimentally determined high treatment concentration could unintentionally have been set too high. The metabolic activity of the donors used for the dose finding studies were not assessed, i.e. it can only be speculated that those donors led to an overestimation of the TC_{10}. On the other hand, the sensitivity of Donor 1 towards 1000 µM IBU could be explained by the metabolism-dependent toxicity, and therefore be considered a link to the reported idiosyncratic nature of IBU-induced liver injury (Bennett et al., 2009; Rodriguez-Gonzalez et al., 2002; Laurent et al., 2000). In order to confirm toxicity is driven by CYP2C9 activity, incubation with IBU in the presence of a CYP2C9 inhibitor (such as sulphafenazole (Baldwin et al., 1995)) should give more insights into the mechanism of cytotoxicity.

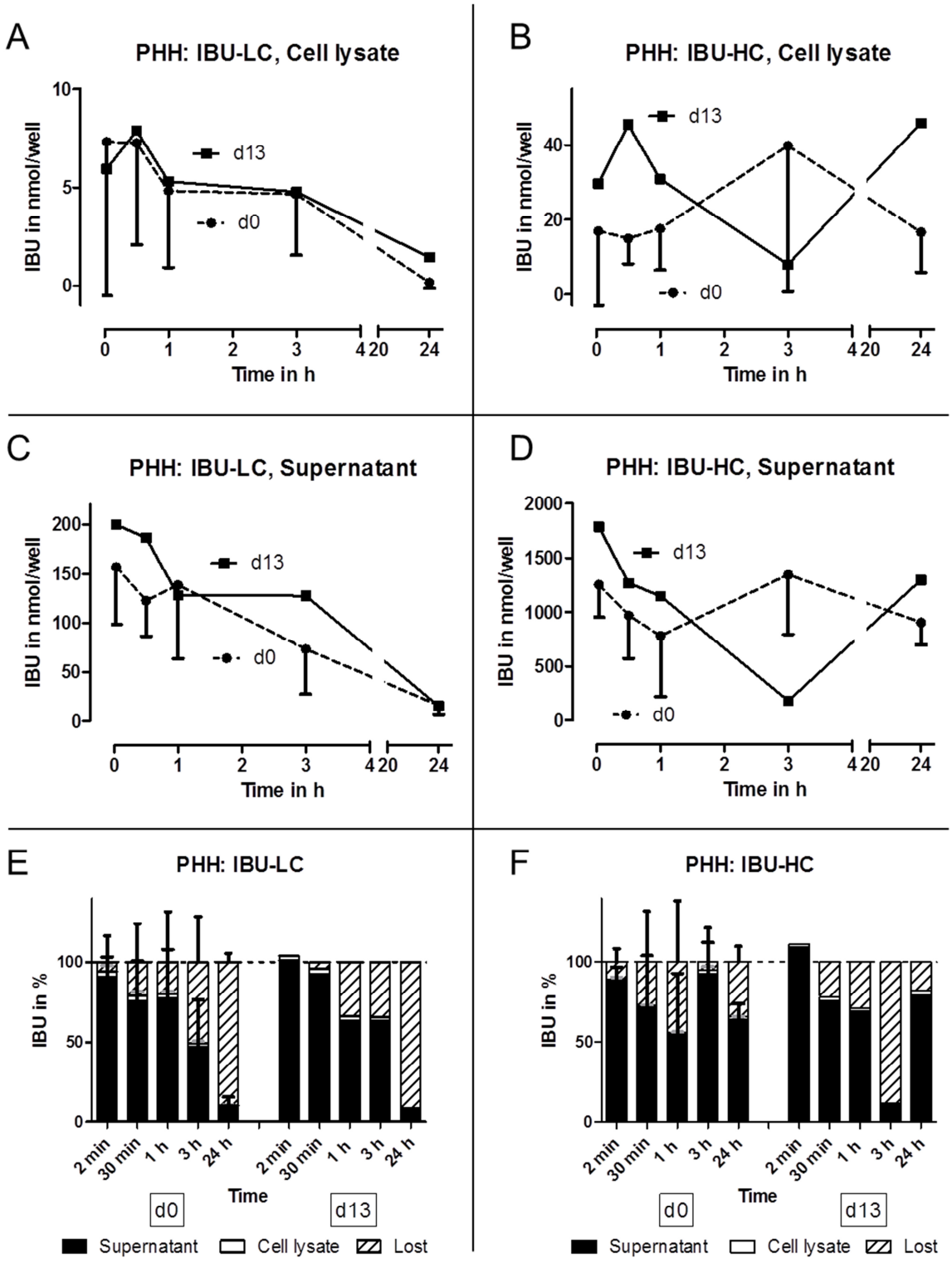

Figure 26. Kinetic profile of ibuprofen (IBU) (nmol/well) in primary human hepatocytes (PHH) (A, B) and culture supernatants (C, D) after single (day 0 – dashed line) and repeated (day 13 – solid line) treatment with 100 µM (low concentration (LC); A, C) and 1000 µM (high concentration (HC); B, D) IBU at the indicated time points. Relative distribution of IBU in percent in the different analysed PHH fractions at the indicated time points on day 0 and 13, supernatant (bold) and cell lysate (blank) as well as the apparent loss (striped) for the LC (E) and HC (F). Values are given as mean of 3 biological replicates +/- standard deviation.

The comparison of the biokinetic profile in the supernatants from PRH and PHH treated with 100 µM IBU, showed no major differences. Thus, no clear conclusions could be made in terms of species-differences, when considering only the biokinetic profile of this single compartment.

Therefore, the simultaneous assessment of the cell lysate concentration was considered essential. The determination of the initial actual IBU concentration at 0 min was crucial, because for both systems the nominal concentration would have resulted in an overestimated concentration (data not shown). Consequently, the concentration at 0 min allowed a more accurate calculation of the relative distribution using mass-balanced values that gave a comprehensive overview on the biokinetic data. There is a consensus on the importance of the intracellular concentration for concentration-response extrapolations as reviewed by Groothuis et al. (2013). When comparing the cell lysate fractions of PRH and PHH treated with 100 µM IBU, the concentration close to human peak plasma concentration (C_{max}), it was observed that the cell lysate level of IBU was higher in the PRH at each time point measured. An explanation for this is very likely a less efficient metabolism in the PRH, which additionally can be considered the major reason for the tenfold lower TC_{10} compared to the PHH.

Future work should include the simultaneous determination of principle and/or important IBU metabolites, e.g. 2-, 3-hydroxy-IBU, carboxy-IBU, IBU-coenzyme A (IBU-CoA) and IBU-acylglucuronide. This knowledge would add valuable additional information and contribute to a more comprehensive understanding of the underlying metabolic mechanisms in the *in vitro* system.

Within the present work, additional experiments were performed with cell lysates from IBU treated cells in order to elucidate the proposed cytotoxic mechanism of the compound *in vitro*. IBU is reported to exert its toxic effect *in vivo* through protein-adducts which arise via unstable, chemically reactive IBU metabolites, namely IBU-1-O-acylglucuronide and IBU-S-acyl-CoA that bind to macromolecules (Castillo et al., 1995; Grillo and Hua, 2008; Dong and Smith, 2009). Analyses of PRH and PHH lysates were performed with beta-glucuronidase, an enzyme which hydrolyses acyl glucuronides to the free carboxylic acid moiety, i.e. in this case IBU. Under these conditions, beta-glucuronidase treatment did not result in higher IBU recovery (data not shown). An explanation for this could be that the IBU-glucuronide, which is considered a reactive metabolite, had already reacted with macromolecules and was consequently not available as a substrate for the beta-glucuronidase.

3.1.3 Transcriptomics

The transcriptomic profiling was performed to elucidate underlying mechanisms of altered cellular processes after exposure to the analgesic IBU. In PRH, changes at the gene expression level were observed only after treatment with the high concentration (100 µM), while in PHH changes were seen at both concentrations (100 and 1000 µM).

Many genes involved in fatty acid and lipid metabolism were significantly up-regulated (compared to the time-matched vehicle treated control) after IBU treatment of PRH (Figure 27).

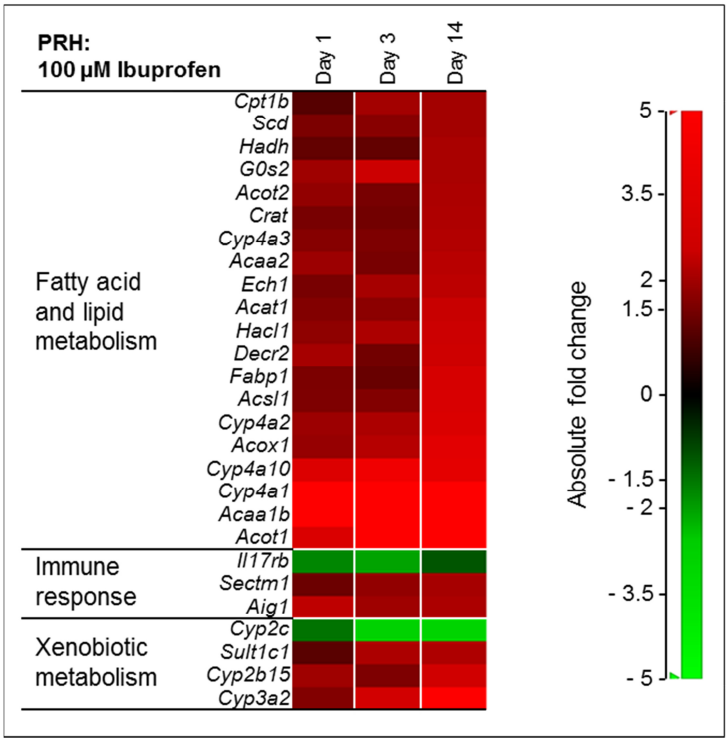

Figure 27. Gene function profile display of significantly deregulated genes in primary rat hepatocytes (PRH) after treatment with 100 µM ibuprofen for 1, 3 or 14 days. The heatmap shows 27 genes involved in fatty acid and lipid metabolism, immune response and xenobiotic metabolism identified to be deregulated by at least 2-fold compared to the time-matched vehicle treated control. The statistical significance (BH q-value ≤ 0.05) by a linear model and absolute fold changes were calculated using the statistical analysis software Genedata Analyst™ version 7.5, the detailed data analysis is given in the Materials and Methods section. The colour scale shows increased fold changes in red and decreased fold changes in green. Genes are sorted according to their fold change value on day 14 (from decreased to increased fold changes) within the corresponding pathway. Absolute fold change values and gene acronyms are given in the appendix.

IBU is known to inhibit mitochondrial beta-oxidation, leading to the accumulation of fatty acids. For example, the cytoplasmic *Fabp1*[9] and *Pdk4*, both reported to be induced by long-chain fatty acids (Landrier et al., 2004; Huang et al., 2002), were up-regulated by IBU (100 µM, day 1/14 and day 14, respectively). Interestingly, the expression of many genes involved in the peroxisomal degradation of fatty acids was increased. For example, *Acaa1b*, *Acox1* and *Hacl1*, which are known to be involved in catalysis reactions in peroxisomal beta- and alpha-oxidation. The strongest induction was seen for *Acot1* (20.5-fold on day 3), an acyl-CoA-thioesterase catalysing the hydrolysis of acyl-CoA to free fatty acids and CoA. An up-regulation of *Acot1*, *Acox* and *Cyp4a1* is reported to be an indication of peroxisome proliferation (Bjork and Wallace, 2009). IBU is known to activate peroxisome proliferator-activated receptor (PPAR)-alpha and -gamma, similar to fibrates (Lehmann et al., 1997); hence, it is not surprising that some genes up-regulated in the experiments are also reported to be induced by fibrates (well-known peroxisome proliferators). Evidence for the impairment of the beta-oxidation by IBU was the up-

[9] Corresponding gene names are provided in the appendix.

regulation of Cyp4a enzymes (*Cyp4a1*, *4a2* and *4a3*), which catalyse the omega-oxidation of fatty acids (as an alternative to the normal fatty acid oxidation pathway). The omega-oxidation of fatty acids results in toxic dicarboxylic acids that subsequently enter the mitochondrial or peroxisomal beta-oxidation pathways. Severe inhibition of fatty acid oxidation leads to the accumulation of fatty acids and their esterification to triglycerides that are stored in very small lipid droplets within the hepatocyte cytoplasm, termed microvesicular steatosis. By contrast, prolonged and less severe inhibition of fatty acid oxidation leads to the development of large lipid vacuoles (macrovacuolar steatosis) and represents a less harmful pathology to the patient (Labbe et al., 2008). In rats, mild microvesicular steatosis was described after treatment with both IBU enantiomers (Freneaux et al., 1990). The microscopic observations of treated hepatocytes did not reveal an obvious accumulation of lipid droplets or vacuoles when comparing treatment (10 and 100 µM IBU) to vehicle control. Therefore, it seems likely that higher concentrations are required to cause the previously described morphological changes. However, in the 14 days dose finding study PRH treated with 500 and 1000 µM IBU appeared grainy with minor inclusion bodies. An objective quantification of lipid inclusion bodies (e.g. via high content imaging and neutral lipid stain, e.g. nile red) would help to confirm if IBU causes microvesicular or macrovacuolar steatosis *in vitro*.

Peroxisome proliferators are classical non-genotoxic carcinogens in rodents (Green, 1995; Reddy and Lalwai, 1983). However, it is well-known that PPAR-dependent adverse effects in rodents do not translate into humans. The underlying mechanisms of this species-specific response are probably due to a lower abundance of PPAR-alpha mRNA in human liver and its deficiency in DNA binding activity compared to mice (Palmer et al., 1998). Furthermore, differential down-stream targets upon receptor activation in the different species have been identified (Yang et al., 2008). Carcinogenicity studies with IBU did not reveal an increased incidence of tumours in rat (Adams, 1970). Interestingly, no clear cell proliferation pattern was observed in the gene expression data of the PRH, therefore confirming the *in vivo* findings.

Reactive metabolites, such as the formation of IBU-acylglucuronides, are able to bind macromolecules and potentially induce immune responses by acting as haptens. Here, only few genes involved in the immune response were deregulated after IBU treatment (Figure 27). This was either an artefact or due to only very few immune cells being present in the cell culture (which is not a pure hepatocyte culture and my contain Kupffer cells).

Impairment of oxidative phosphorylation is always linked to the generation of reactive oxygen species (ROS) due to an increased risk of electrons leaking from the electron transport chain. A further source of ROS is the hydrogen peroxide-generating peroxisomal beta-oxidation. Even though both ROS-generating pathways can be triggered by IBU, only a single gene, reported as being protective during oxidative stress (Stoelting et al., 2009), was found (*Abhd1*) and which was not up-regulated ≥ 2-fold before day 14.

There was a time-dependent decrease of *Cyp2c* expression in PRH. This observation could explain the more pronounced effect after repeated treatment, assuming that the parent compound is responsible for the toxicity of IBU. At the same time, other genes involved in xenobiotic metabolism were up-regulated (*Sult1c1*, *Cyp2b15*, *Cyp3a2*; Figure 27) which also participate in fatty acid and cholesterol metabolism.

The number of deregulated genes increased with the exposure time to IBU. Furthermore, gene deregulation was more pronounced after long-term treatment. The low number of deregulated genes on day 1 (10 genes) did not reflect the mechanisms affected by IBU. Here, a less stringent threshold, e.g. 1.5-fold, would have certainly allowed a more comprehensive interpretation. In summary, the three time points revealed adverse effects in a time-dependent manner, with the long-term treatment delivering the most valuable information. This is an important finding when considering the fact that IBU is given repeatedly to patients with chronic diseases, such as rheumatoid arthritis and osteoarthritis.

Taken together, the gene expression data from rat hepatocytes confirmed IBU's potential to disrupt the fatty acid and lipid metabolism, thus potentially leading to pathology as hepatic steatosis.

The transcriptomic data from PHH were analysed using the Ingenuity Pathway Analysis® (IPA®) software which classified the genes into so-called "tox functions". This classification was used to generate hypotheses on the adverse effects of the compound. Subsequently, manual evaluation of the function of classified genes was essential to confirm the conclusions from IPA® derived tox functions. Here, the comparison of the global gene expression profiles in PHH after treatment with IBU revealed marked donor differences. In PHH from Donor 1, a time-dependent increase of deregulated genes was observed at both concentrations, despite the fact that both IBU concentrations were halved on day 7 due to enhanced cytotoxicity in the high concentration treatment. Therefore, any interpretation of day 14 in PHH from Donor 1 should be taken with caution. However, the response to the low concentration treatment was most pronounced in PHH from Donor 1. This observation could also be linked to the low CYP2C9 activity of PHH from Donor 1, as previously described with the biokinetics data. On the level of mRNA expression, *CYP2C9* and *CYP2C8* were also deregulated, while *CYP2C19* was not affected by IBU treatment (Table 27).

Table 27. Fold change values of *CYP2C9*, *CYP2C8* and *CYP2C19* (gene expression changes compared to time-matched vehicle treated control). Results derive from primary human hepatocytes (PHH from Donor 1) treated with low (LC: 100 µM) or high (HC: 1000 µM) concentration of ibuprofen (IBU) at the indicated time points. Bold numbers highlight values ≤ -2-fold (green) or ≥ 2-fold (red).

PHH from		IBU LC			IBU HC		
		day 1	day 3	day 14	day 1	day 3	day 14
Donor 1	***CYP2C9***	1.1	-1.4	1.7	-1.1	**-2.6**	1.6
	CYP2C8	1.7	1.3	**2.1**	1.2	**-3.9**	**3.1**
	CYP2C19	1.1	1.0	1.1	1.3	1.0	1.0

In summary, the reduced expression of IBU-metabolising enzymes observed on day 3 could help explain the increased toxicity seen in PHH from Donor 1. By contrast, there was a different pattern in IBU-metabolising CYPs in PHH from the other two donors (Table 28).

Table 28. Fold change values of *CYP2C9*, *CYP2C8* and *CYP2C19* (gene expression changes compared to time-matched vehicle treated control). Results derive from primary human hepatocytes (PHH from Donors 2 and 3) treated with low (LC: 100 µM) or high (HC: 1000 µM) concentration of ibuprofen (IBU) at the indicated time points. Bold numbers highlight values ≤ -2-fold (green) or ≥ 2-fold (red).

PHH from		IBU LC			IBU HC		
		day 1	day 3	day 14	day 1	day 3	day 14
Donor 2	*CYP2C9*	-1.2	1.5	1.2	**-3.1**	-1.1	1.9
	CYP2C8	1.3	1.1	1.9	**-2.5**	1.1	1.0
	CYP2C19	-1.5	-1.2	1.3	-1.3	-1.2	1.4
Donor 3	*CYP2C9*	1.1	1.3	**2.2**	1.7	-1.2	**3.5**
	CYP2C8	1.1	1.3	**2.2**	**2.4**	-1.2	**11.1**
	CYP2C19	-1.2	**3.0**	1.3	**2.4**	**-2.1**	1.7

A down-regulation of *CYP2C9* and *CYP2C8* on day 1 (1000 µM) was seen for PHH from Donor 2, without observing an increased cytotoxicity. This finding suggested that the basal enzyme activity of CYP2C in PHH from different donors plays a principal role; and thus was more predictive for observed IBU-mediated cytotoxicity compared to changes at the gene expression level which were variable over time. In fact, gene polymorphisms of *CYP2C9* and *CYP2C8* are linked to stereoselective transformation of IBU and more importantly, impaired metabolic activity of this specific isoenzyme (Hao et al., 2005). The most common allele frequencies in the Caucasian population are CYP2C9*2 ($Arg^{144} \rightarrow Cys^{144}$) and CYP2C9*3 ($Ile^{359} \rightarrow Leu^{359}$), and show reduced activities relative to the wild type (CYP2C9*1) (Zhou et al., 2010). Here, SNP profiling would deliver valuable information on the underlying genotype and further contribute to data interpretation. In practice, the selection of donors with polymorphic enzymes is an important aspect during the decision making process of new drug candidates. When assessing the toxicity of a new drug candidate, it is essential not to select candidates that are selectively metabolised by the polymorphic enzymes which reflect only a small percentage in population. Furthermore, no induction of *CYP2C9* or *CYP2C8* mRNA was observed in hepatocytes from Donor 2, who was the only patient reported to be taking medications. A more detailed analysis of the drugs taken by this donor helped explain at least some of the donor differences. *Atenolol* is a known substrate and inhibitor of the transporter ABCB1, while acetylsalicylic acid (pharmacologic active component of *kardegic*) inhibits prostaglandin synthases (PTGS1 and 2), AKR1C1 and SLC22A6 and induces CYP2C19. In PHH from Donor 2, PTGS2 was not deregulated, whereas in PHH from Donors 1 and 3, it was down-regulated on day 14. Here, it seems likely that acetylsalicylic acid derived inhibition persisted in cell culture, in such a way that IBU, also a PTGS2 inhibitor, did not exert further inhibition. *Ramipril* (ACE and chonlinesterase BCHE inhibitor), *inspra* (generic name: eplerenone: CYP11B2 inhibitor) and

rasilez (aliskiren: Renin inhibitor) are reported to not affect enzymes involved in IBU transformation or transport. Taken together, the NSAID acetylsalicylic acid was considered as the only medication taken by Donor 2 that potentially influenced the gene expression profile after treatment with IBU. However, other intra-donor differences may be more prominent and thus potentially masked concomitant drug effects.

In order to reveal inter-donor differences, the human gene expression data was analysed per individual donor, i.e. calculation of fold changes compared to the time-matched vehicle treated control. The lack of statistical threshold resulted in a complex transcriptomic dataset for each of the four compounds. Therefore, Ingenuity® Pathway Analysis (IPA®) software was used to analyse the relatively large transcriptomics datasets of the PHH compared to those of PRH. IPA® uses a proprietary, manually curated knowledge base by which the genes are categorised in different pathways. Here, the so-called "tox functions" were used as starting point for hypotheses generation which subsequently were verified manually. After IBU treatment of PHH the majority of the genes within IPA®'s *Liver Steatosis* cluster included those involved in the fatty acid and lipid metabolism (Appendix 10, Table 59). This suggests that IBU exerted the same adverse mechanisms as previously reported for the PRH. As a result of the idiosyncratic nature of IBU-induced hepatotoxicity, only little human *in vivo* data is available. However, microvesicular steatosis has been reported after IBU overdose, although the patient had a previous record of alcohol abuse (Laurent et al., 2000), which is known to cause the same pathology.

Many genes in the IPA® *Liver Hyperplasia/Hyperproliferation* signature were assigned to cancer, inflammation and xenobiotic metabolism, and a near-complete overlap was observed with the tox function *Hepatocellular Carcinoma*. Generally, the occurrence of *Hepatocellular Carcinoma* should be considered with reservation. This tox function comprises many genes involved in stress responses and recovery; thus, genes which are not directly linked to cancer and can be affected by multiple perturbations of the cellular homeostasis. Here, mechanistic information on the carcinogenic mode of action would be required to decide on the validity of this hypothesis. However, genes involved in cell cycle regulation were mostly down-regulated, e.g. *CCND1* (regulatory subunit of the cyclin dependent kinases), *ESR1* (cell cycle G1/S transition), *ERBB2* (cell cycle G1 phase progression) and *KIT* (catalytic subunit of the cyclin dependent kinases). This finding was in accordance with the literature, where IBU is described as an inhibitor of cell proliferation (Palayoor et al., 2012) and was even considered for anti-tumour therapy (Milas, 2003).

Interestingly, within the different tox functions only a small overlap of commonly deregulated genes among the PHH from the three donors was seen, i.e. groups of transcripts contributing to a tox function were distinct in the different donors. This supports the basic assumption that there was a high variation between human individuals.

The comparison of the two species revealed that very few genes involved in cell proliferation were deregulated by IBU in PRH, a function that was highly affected by IBU in PHH. Changes in fatty acid and lipid metabolism was the predominating effect of IBU in rat but not in human, which was explained by species differences in response to peroxisome proliferators. Furthermore, the inhibition of cell proliferation, which can be regarded as IBU's secondary pharmacological effect, was more pronounced in the PHH. In summary, the findings from the transcriptomics data were species-specific and most importantly reflected the corresponding *in vivo* situation.

3.1.4 Proteomics

The profiling at the level of protein abundance provided an additional level of information on the altered molecular mechanisms in PRH after short- and long-term exposure to IBU.

At the protein level, six proteins involved in fatty acid and lipid metabolism were altered by IBU compared to the time-matched vehicle treated control (Figure 28). Of these, four overlapped with genes of the transcriptomics dataset: namely Acyl-coenzyme A oxidase (mitochondrial and peroxisomal; corresponding gene: *Acot1*), 2-hydroxyacyl-CoA lyase 1 (gene: *Hacl*) and Cytochrome P450 4A14 (gene: *Cyp3a4*). Interestingly, changes were seen only after high concentration treatment, which resulted in the increase of the proteins and thus, was in accordance with the gene expression results. In addition, Peroxisomal bifunctional enzyme (peroxisomal beta-oxidation; gene *Ehhadh*) and Apolipoprotein A-IV (lipid transport and lipoprotein metabolism; gene *Apoa4*) were increased in PRH upon exposure to IBU. Apolipoprotein A-IV responds to triglycerides, which corroborated to the hypothesis that accumulation of free fatty acids results in formation of triglycerides within the cells. At the gene level, *Apoa4* was not deregulated in the IBU dataset because this gene did not fulfil the BH q-value requirement of ≤ 0.05. Furthermore, proteins involved in carbohydrate metabolism were changed. This finding can be explained by the strong interconnection of the carbohydrate and the fatty acid metabolism pathways, very likely via acetyl-CoA feedback regulation. Two proteins playing a role in xenobiotic metabolism, Glutathione S-transferase Yb-3 and Cytochrome P450 2B6 (gene: *Cyp2b3*) showed both a decreased abundance in the IBU high concentration group. By contrast, on the gene level, an up-regulation was recorded for *Cyp2b3*. Many proteins involved in transcription regulation, i.e. regulating cell proliferation, were decreased in the proteomics dataset of the PRH. Interestingly, this finding was not seen in the gene expression data of PRH, but of PHH.

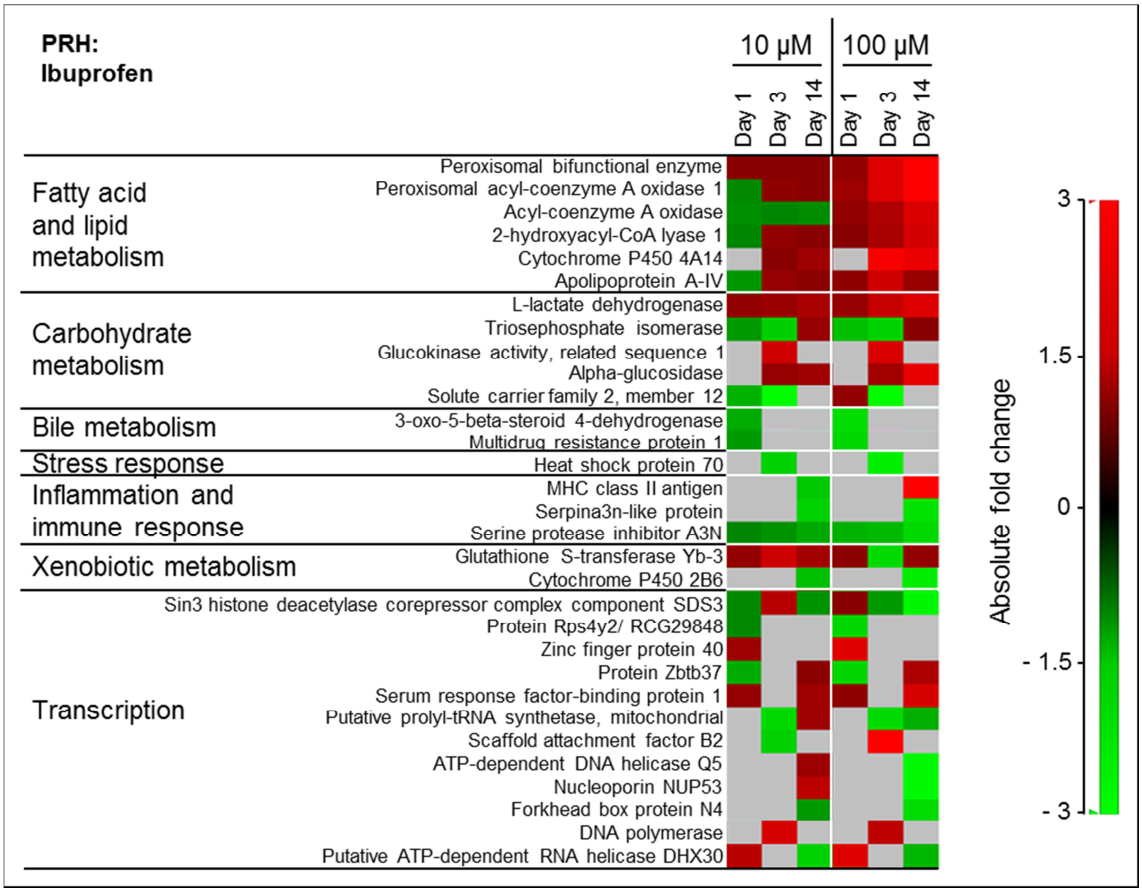

Figure 28. Protein function profile display of significantly changed proteins in primary rat hepatocytes (PRH) after treatment with 10 and 100 µM ibuprofen for 1, 3 or 14 days. The heatmap shows 36 proteins involved in fatty acid and lipid metabolism, carbohydrate metabolism, bile metabolism, stress response, inflammation and immune response, xenobiotic metabolism and transcription identified to be changed by at least 1.5-fold compared to the time-matched vehicle treated control. The statistical significance (p-value ≤ 0.05) and absolute fold changes were calculated as described by Wilmes et al., (2013). The colour scale shows increased fold changes in red and decreased fold changes in green. Absolute fold change values and UniProt accessions are given in the appendix.

The small overlap of commonly deregulated genes and their corresponding proteins confirms that an induction on the mRNA level did not automatically result in an increased protein expression. However, the direction of the commonly deregulated genes/proteins was confirmed and the extent comparable; hence, for these individual genes/proteins, gene expression did not seem to act as precursor. Nevertheless, from a global perspective, the gene expression delivered more deregulated entities and thus giving a more comprehensive insight into IBU-dependent molecular mechanisms. In contrast to the homogeneity of the nucleic acids used for transcriptome analysis, cellular proteins resemble an extremely heterogeneous group, ranging in weight, form and lipophilicity. Therefore, it is very likely that isolation efficiency differed between different types of proteins. Furthermore, the applied detection method (isobaric tags for relative and absolute quantification (iTRAQ)) did not comprehensively capture the whole proteome, due to analytical thresholds (limit of detection (LOD), limit of quantification (LOQ)) and restriction to certain peptide mass-to-charge (m/z) ratios. Altogether, these limitations led to a rather distorted proteomic dataset, which needed to be considered during data interpretation.

3.1.5 Mitochondrial toxicity

In literature, IBU is reported to inhibit complex I of the electron transport chain and thus impair oxidative phosphorylation. Hence, functional assays for the assessment of IBU-mediated adverse effects on mitochondrial respiration were performed. Here, different assays for the assessment of mitochondrial toxicity were implemented and evaluated in four different hepatic systems (PRH, HepaRG, HepG2 cells cultured in either glucose or galactose medium). The aim was to identify the most valuable model system for this endpoint. IBU is known to inhibit mitochondrial beta-oxidation and complex I, which leads to the accumulation of fatty acids and the impairment of mitochondrial function. Furthermore, four positive control substances, namely carbonyl cyanide 4-(trifluoromethoxy)phenylhydrazone (FCCP), oligomycin, antimycin and rotenone, were used in addition to the four test compounds. These substances are known to act on mitochondria by uncoupling (FCCP) or inhibition of oxidative phosphorylation via distinct complexes of the respiratory chain (oligomycin, antimycin, rotenone). The alkyl halide, n-butyl chloride, and the sugar, D-mannitol, served as negative controls. These compounds were not cytotoxic up to the maximum applied concentration of 1000 µM and are not reported to exert any (adverse) effects in mitochondria. In preliminary experiments, the suitability of these positive and negative controls was successfully tested.

3.1.5.1 ATP level for detection of mitochondrial toxicity

The measurement of ATP levels is frequently used to assess cytotoxicity because it is a sensitive marker of cell function and is also correlated to the number of viable cells. ATP generation occurs largely via oxidative phosphorylation in the mitochondria; hence, impairment of this organelle's function in turn affects ATP levels. The ATP test served primarily as an exclusion criterion of compound concentrations, which could lead to misinterpretation of the *MitoXpress O_2-sensitive probe respiration assay* data (see following section 3.1.5.2), by exerting too high levels of cytotoxicity (arbitrary set to > 50%). For this purpose, the incubation with test compound was 1 h, corresponding to the measurement time of the respiration assay. Preliminary experiments revealed that this short treatment time correlated very well with prolonged incubations of 24 and 48 h (data not shown).

After treatment with IBU (concentration range 1 to 1000 µM) the cytotoxicity curves (Figure 29, A) revealed minor differences in the four hepatocyte systems. A close to identical curve progression was seen for HepaRG and HepG2-galactose (HepG2-Gal) cells, showing a constant decrease from 107 ± 12 and 107 ± 16% (100 µM), respectively, to 48 ± 3 and 45 ± 9% (1000 µM), respectively. This observation seems to be linked to the underlying mechanism of IBU acting on the mitochondria. IBU's inhibitory effect on complex I is considered weak compared to other NSAIDs (Sandoval-Acuna et al., 2012), thus, suggesting a reduced activity rather than a full inhibition. More importantly, oxidative phosphorylation is thought to be still

functional via flavin adenine dinucleotide ($FADH_2$), which donates electrons to the electron transport chain via complex II, i.e. complex I is not involved. Thus, detrimental effects on the cellular viability might require a prolonged and/or stronger (increased concentration) exposure. This explanation is in line with observations made in the dose finding and transcriptomics studies. Here, marked cytotoxicity and gene expression changes were observed only after long-term exposure to 100 µM IBU. HepG2-glucose (HepG2-Glu) cells appeared to be more sensitive compared to the other cell systems, exceeding the 50% cytotoxicity (TC_{50}) at 500 µM and dropping to 31 ± 10% viability at 1000 µM. IBU was reported to inhibit glycolysis in *Streptococcus mutans* GS-5, presumably via acidification of the cytoplasm that results in enzyme inhibition (Belli et al., 1995). In theory, glycolytic HepG2 cells need an adaptation phase in order to reactivate alternative energy sources, e.g. mitochondrial oxidative phosphorylation. A rapid switch is not likely, which makes the cells dependent on glycolysis to cover their ATP need. This dependence might be an explanation for the higher sensitivity of HepG2-Glu cells towards IBU-mediated cytotoxicity.

The variation between replicates was highest for HepG2-Gal cells. In PRH, a constant decrease throughout the concentration range, from 102 ± 7% at 1 µM to 55 ± 12% at 1000 µM, was observed. The CYP activities were not determined in the different hepatic systems; however, a similar rate of IBU biotransformation can be inferred from the data. The biokinetics studies in PHH indicated an inverse correlation between CYP2C9 activity and IBU-induced cytotoxicity.

The effects of the positive (FCCP, antimycin, oligomycin) and negative (n-butyl chloride, D-mannitol) control substances on the different systems are shown in Figure 29 B-D and E-F, respectively. After treatment with the uncoupler FCCP, only weak cytotoxicity was observed in HepG2-Glu cells. In HepaRG cells, the viability decreased to ~ 57% at 30, 60 and 125 µM FCCP, while in HepG2-Gal cells it dropped to 41 ± 5, 42 ± 6 and 32 ± 9%, respectively. PRH were most sensitive to FCCP, showing nearly complete loss of viability (~ 10%) at ≥ 3 µM. Exposure to antimycin resulted in weak cytotoxicity in HepG2-Glu cells, which plateaued at ~ 80% at concentrations ≥ 0.03 µM. PRH and HepaRG cells showed a similar sensitivity to antimycin, with a TC_{50} at > 0.3 µM. HepG2-Gal cells were very sensitive to antimycin, with a TC_{50} already reached at 0.03 µM. Treatment with the ATP synthase inhibitor, oligomycin, caused only weak cytotoxicity in PRH, HepaRG and HepG2-Glu cells. By contrast, the TC_{50} in HepG2-Gal cells was 0.03 µM and the toxic effect plateaued at 44% at ≥ 0.3 µM oligomycin. In summary, the positive compounds revealed the following sensitivities in the different hepatic systems:

- FCCP: PRH > HepG2-Gal > HepaRG > HepG2-Glu.
- Antimycin: HepG2-Gal > PRH = HepaRG > HepG2-Glu.
- Oligomycin: HepG2-Gal > PRH = HepaRG = HepG2-Glu.

This is in accordance with the knowledge that ATP production in PRH and HepG2-Gal depends on mitochondrial oxidative phosphorylation; hence, these systems were expected to be more

sensitive to mitochondrial toxicants. By contrast, HepG2-Glu cells, which generate most ATP via glycolysis, were less susceptible to compounds that impair the cellular respiratory chain. Interestingly, for antimycin and oligomycin the human HepaRG cell line was comparable to the PRH and was almost always more sensitive than the human HepG2 cell line, although both were cultured in glucose-containing media.

As expected, the negative control substances n-butyl chloride and D-mannitol were non-toxic (Figure 29 E and F, respectively). Notably, there was a high variability among the biological replicates for HepG2-Glu cells in these studies, despite being handled in the same manner as the other test systems.

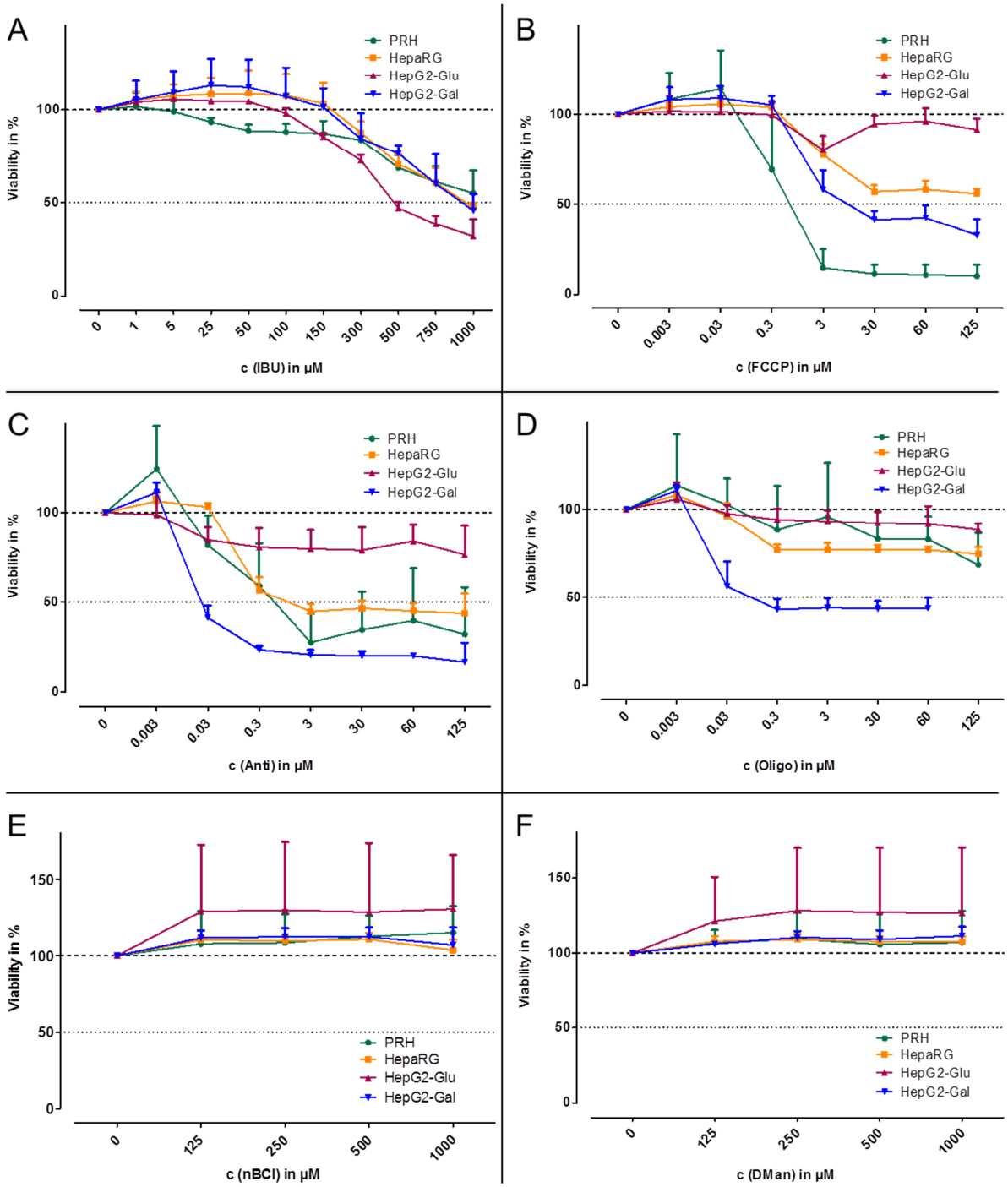

Figure 29. A comparison of cell viability results (measured using ATP content) in percent using the four hepatocyte systems (primary rat hepatocytes (PRH), HepaRG, HepG2 cultured in regular glucose-containing medium (HepG2-Glu) and HepG2 adapted to galactose-containing medium (HepG2-Gal)) after treatment for 1 h with the indicated concentrations of ibuprofen (IBU) (A), carbonyl cyanide 4-(trifluoromethoxy)phenylhydrazone (FCCP) (B), antimycin (Anti) (C), oligomycin (Oligo), n-butyl chloride (nBCl) (E) or D-mannitol (DMan) (F). The percentages refer to the vehicle treated control, in relative light units, set to 100%. The values given represent the mean of 3 - 4 biological replicates + standard deviation.

3.1.5.2 MitoXpress O_2-sensitive probe respiration assay

The results generated from the MitoXpress O_2-sensitive probes are given as oxygen consumption rates. Figure 30 shows the results for IBU treated cells in the 4 different hepatic systems. In PRH (A) and HepaRG cells (B) a significant decrease in oxygen consumption was seen at

concentrations ≥ 300 µM. Respiration dropped to 64 ± 8 and 32 ± 6% in PRH and 63 ± 19 and 30 ± 11% in HepaRG cells at 300 and 500 µM, respectively. The decrease of the oxygen consumption rate was greater than expected based on the loss of cell viability. This indicated a drug-induced inhibition of the cellular oxygen consumption. Freshly isolated primary hepatocytes are thought to maintain functional mitochondria *in vitro*. The oxygen consumption rate reduction at 500 µM IBU was comparable between PRH and HepaRG cells. The CYP2C9 mRNA in HepaRG cells is reported to be ~ 80% lower than in freshly isolated primary human hepatocytes (DMSO-free culture; Aninat et al., 2006). As observed previously, the IBU-induced cytotoxicity was similar in PRH and HepaRG cells. This indicated a comparable biotransformation rate of the parent compound in these hepatic systems. PRH and HepaRG cells appeared to detect impairment of the cellular respiration mediated by IBU. By contrast, the oxygen consumption rate in HepG2 cells (with (C) and without (D) glucose) change significantly after treatment with any concentration of IBU. No values are shown for HepG2 cells treated with higher IBU concentrations, due to a poor correlation of the linear fit to the raw data curve (HepG2-Glu: 300 µM), increased (i.e. ≥ 50%) cytotoxicity (HepG2-Glu: ≥ 500 µM) or due to lack of biological replicates based on the previously stated reasons (HepG2-Gal: ≥ 500 µM). Although lacking statistical significance, a downward trend was inferred in the HepG2 cells. It was assumed that more biological replicates, potentially narrowing the standard deviation, would lead to a significant reduction in oxygen consumption rate. Taken together, the HepG2-Glu and -Gal system were considered inappropriate in capturing IBU-induced mitochondrial toxicity.

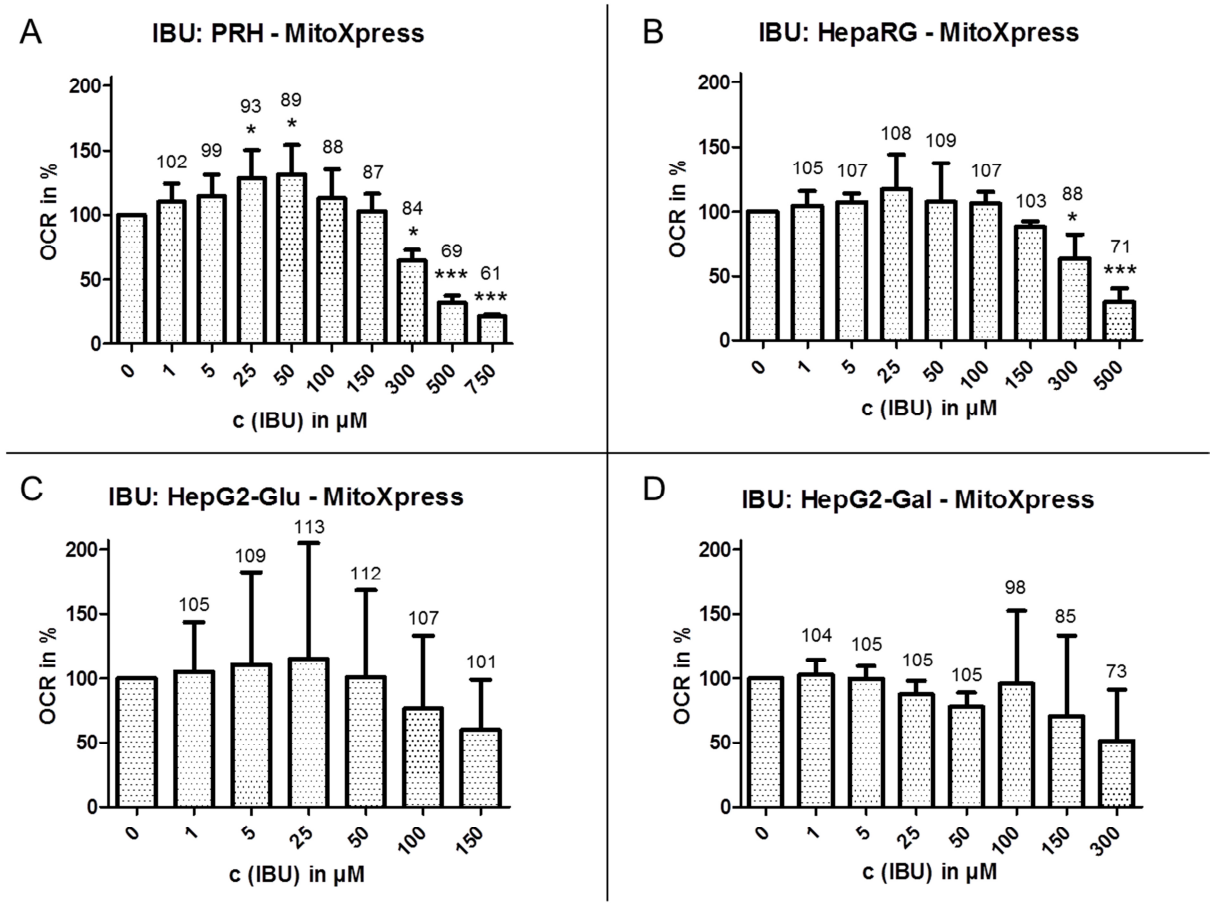

Figure 30. Oxygen consumption rate (OCR) in percent in the different hepatic systems (primary rat hepatocytes (PRH) (A), HepaRG (B), HepG2 cultured in regular glucose-containing medium (HepG2-Glu) (C) and HepG2 adapted to galactose-containing medium (HepG2-Gal) (D)) after treatment with different concentrations of ibuprofen (IBU). The percentages refer to the mean slope of the vehicle treated control, in relative fluorescence units per minute (RFU/min), set to 100%; corresponding to ~ 570 RFU/min in PRH, ~ 150 RFU/min in HepaRG, ~ 80 RFU/min in HepG2-Glu and ~ 140 RFU/min in HepG2-Gal. Values are given as mean of 3 biological replicates + standard deviation. Numbers above columns represent viabilities in percent taken from the 1 h ATP test. Statistical significance is expressed in p-value ≤ 0.05 (*), ≤ 0.01 (**) and ≤ 0.001 (***) and was calculated by one-way repeated-measures analysis of variance (ANOVA) of a treatment towards the vehicle control and application of the Dunnett's post test.

Figure 31 shows the oxygen consumption rate in PRH treated with the positive (FCCP (A), antimycin (B), oligomycin (C)) and negative (n-butyl chloride (D), D-mannitol (E)) controls. Results from the other three hepatic systems are given in Appendix 11 (Figure 59 - Figure 61). FCCP, a well-known uncoupling agent, led to an increased respiration in PRH. Statistical analysis was not possible due to the low number of samples and FCCP concentrations exceeding 0.03 µM were not analysed due to cytotoxicity (≥ threshold of 50%). In all other systems, FCCP uncoupled the cell's mitochondrial respiration and a significant increase was observed. The maximum uncoupling occurred at 3 µM in the different systems, but to various degrees:

- HepaRG: 846 ± 197%.
- HepG2-Glu: 261 ± 45%.
- HepG2-Gal: 409 ± 149%.

Following these high increases, a reduction of oxygen consumption was seen at the higher concentrations (30 and 60 µM) in HepaRG and HepG2-Glu cells, while the HepG2-Gal cells were not sensitive to FCCP at concentrations ≥ 30 µM.

Antimycin and oligomycin (Figure 31 B and C, respectively) resemble typical inhibitors of complex III and ATP-synthase, respectively, resulting in reduced respiratory capacity. In this study, these inhibitors reduced oxygen consumption in PRH: antimycin to 40 ± 29 and 15 ± 10% at 0.03 and 0.3 µM, respectively, and oligomycin to 71 ± 25% at 0.03 µM and ~ 34% at ≥ 0.3 µM. Furthermore, antimycin inhibited respiration in HepG2-Glu; whereas, no effect was observed in HepaRG or HepG2-Gal cells. Oligomycin also decreased oxygen consumption in HepaRG, HepG2-Glu and HepG2-Gal cells, although compared to PRH, the concentration-dependence was less pronounced. In all hepatic systems, antimycin was more cytotoxic than oligomycin.

The negative controls n-butyl chloride and D-mannitol (Figure 31 D and E, respectively) did not show any effect in PRH, up to 1000 µM. Analogous findings were observed in HepG2-Glu and -Gal cells. The HepaRG cells revealed a slight increase in oxygen consumption at all concentrations of n-butyl chloride (151 ± 31, 152 ± 38, 165 ± 10, 154 ± 34%) and at ≥ 500 µM D-mannitol (137 ± 33, 139 ± 15%). These increases were not concentration-dependent and thus considered biologically irrelevant.

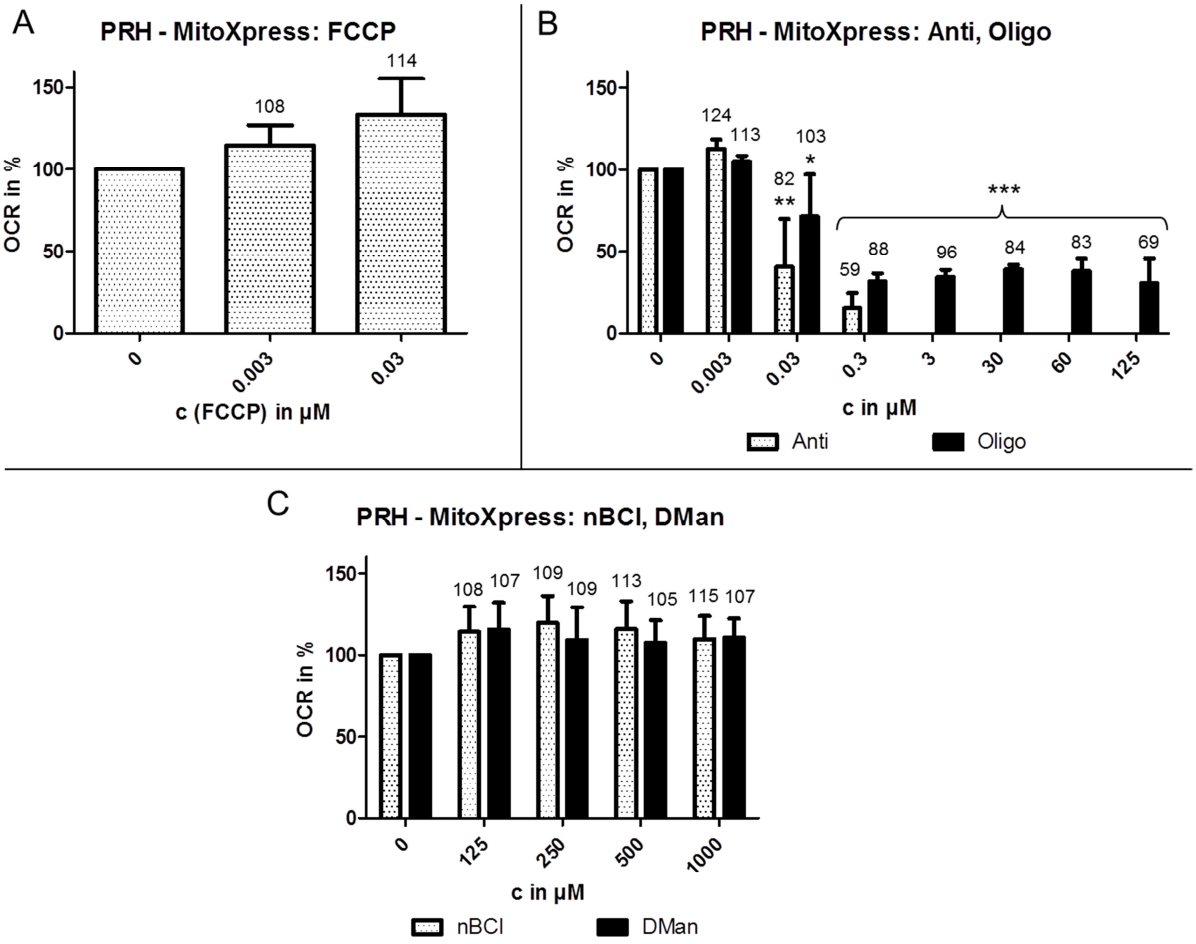

Figure 31. Oxygen consumption rate (OCR) in percent in primary rat hepatocytes (PRH) after treatment with different concentrations of the applied positive (A: carbonyl cyanide 4-(trifluoromethoxy)phenylhydrazone (FCCP), B: antimycin (Anti), oligomycin (Oligo)) and negative (C: n-butyl chloride (nBCl), D-mannitol (DMan)) controls. The percentages refer to the slope of the vehicle treated control, in relative fluorescence units per minute (RFU/min), set to 100%; corresponding to ~ 470 RFU/min. Values are given as mean of 3 biological replicates + standard deviation. Numbers above columns represent viabilities in percent taken from the 1 h ATP test. Statistical significance is expressed in p-value ≤ 0.05 (*), ≤ 0.01 (**) and ≤ 0.001 (***) and was calculated by one-way repeated-measures analysis of variance (ANOVA) of a treatment towards the vehicle control and application of the Dunnett's post test.

3.1.5.3 Seahorse MitoStress assay

In preliminary experiments, the optimal FCCP concentration was determined in the four different hepatic systems. Finally, the FCCP was applied as follows:

- PRH: 0.6 µM
- HepaRG: 0.9 µM
- HepG2-Glu: 0.3 µM
- HepG2-Gal: 0.6 µM

As an example, Figure 32 shows the complete kinetic profile of the cellular respiration measured using the *Seahorse MitoStress assay* in PRH treated with IBU. It was clear that treatment with the lowest concentration (1 µM) did not change the respiratory profile compared to the vehicle

treatment. By contrast, the highest concentration (1000 µM) continuously reduced the oxygen consumption rate up to measurement 13. Thus, the kinetic profile in PRH revealed a concentration-dependent inhibitory effect of IBU on the cellular respiration. IBU inhibits beta-oxidation that eventually impairs mitochondrial functions. Whereas, this adverse effect on the respiration is expected after prolonged treatment, the observed inhibition occurred immediately after exposure to IBU. Hence, this was very likely attributed to the inhibition of complex I (Sandoval-Acuna et al., 2012). Furthermore, oxidative phosphorylation uncoupling by FCCP was reduced after treatment with 1000 µM IBU (Figure 32). The maximum respiratory capacity can be determined by uncoupling the oxidative phosphorylation with FCCP. In addition, this helps to reveal a disruption of the electron transport chain and is thus considered as stress response marker (Beeson et al., 2010). After treatment with 1000 µM IBU, the maximum respiratory capacity was reduced by ~ 80% compared to the vehicle control. Consequently, IBU apparently disrupted the electron transport chain. Finally, after addition of the antimycin/rotenone mixture, which is supposed to fully inhibit mitochondrial respiration, the oxygen consumption rate was not changed by pre-treatment with the test compound. This finding suggests that short-term treatment with IBU did not affect non-mitochondrial respiration. The non-mitochondrial respiration accounts for a certain level of cellular oxygen consumption that is independent of ATP generating oxidative phosphorylation. The specification on the extent of non-mitochondrial oxygen consumption of the liver varies in current literature: 9% (Rolfe et al., 1999), 13% (Porter et al., 1995), up to 35% (De Duve and Baudhuin, 1966). However, the majority might be accounted for by peroxisomal oxidation processes (De Duve and Baudhuin, 1966). The discrepancy is supposedly attributed to different culture conditions, analytical methods and chemicals used to block mitochondrial oxygen consumption. Here, the non-mitochondrial oxygen consumption rate was ~ 35%. The gene expression profiles in PRH confirmed that repeated exposure to IBU resulted in peroxisome proliferation. Hence, it was hypothesised that prolonged treatment with IBU would result in an elevation of the non-mitochondrial respiration activity.

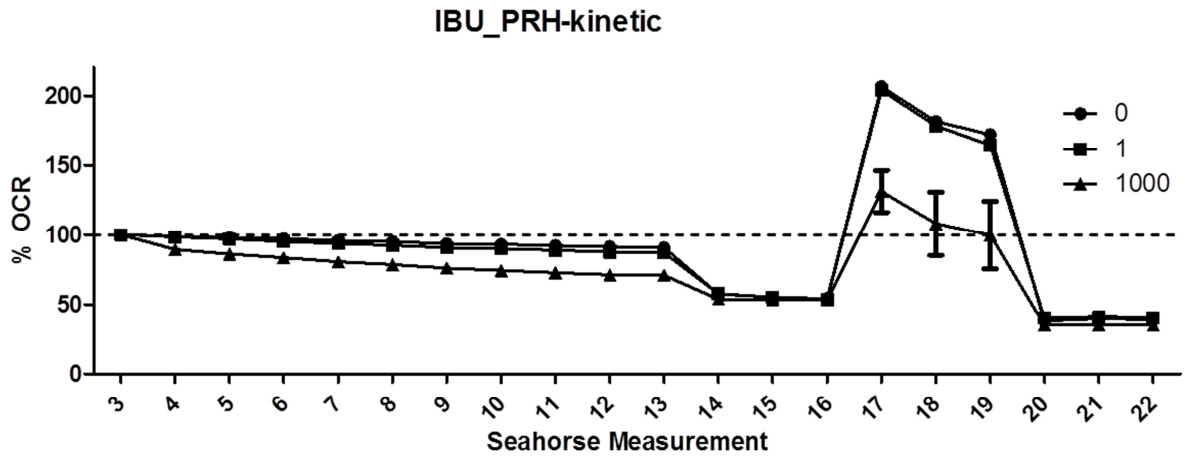

Figure 32. Oxygen consumption rate (OCR) in percent measured in primary rat hepatocytes (PRH) treated with ibuprofen (IBU) (1 and 1000 µM) or DMSO vehicle control (0 µM) at the indicated Seahorse measurements ("3 min mix/3 min measure" cycles). The percentages refer to the basal (3rd measurement) OCR in pmol/min set to 100%; corresponding to ~ 140 pmol/min. Compound or DMSO was injected after the 3rd measurement, while 1 µM oligomycin, 0.6 µM carbonyl cyanide 4-(trifluoromethoxy)phenylhydrazone (FCCP) and 1 µM antimycin/ 1 µM rotenone were injected after measurement 13, 16 and 19, respectively. Values are given as mean of 3 biological replicates ± standard deviation.

As described in the Materials and Methods (section 2.3.9.2), the spare respiratory capacity was chosen as a benchmark by which a compound's effect upon the mitochondrial respiration was compared. The results from the different hepatic systems treated *in situ* with the compound IBU are illustrated in Figure 33. In PRH (A) a concentration-dependent decrease of the spare respiratory capacity was observed, down to 31 ± 15% at 1000 µM. By contrast, the HepaRG (B) and HepG2-Glu (C) cells were not affected by IBU-treatment. Although some values from the HepG2-Gal (D) cells were statistically significant, this appeared randomly and did not correlate to the compound treatment. Thus the significant increases in spare respiratory capacity in HepG2-Gal cells were designated as biologically irrelevant. These findings were almost all in accordance with those obtained with the *MitoXpress O_2-sensitive probe respiration assay*. IBU apparently inhibited the cellular respiration only in PRH, whereas a significant reduction was seen at much lower concentrations (25 and 300 µM in *Seahorse MitoStress assay* and *MitoXpress O_2-sensitive probe respiration assay*, respectively). Here, IBU did not cause any inhibition in the HepaRG cells, although it was possible to evaluate higher compound concentrations compared to the *MitoXpress O_2-sensitive probe respiration assay*. This could be due to the different seeding densities used in the two assays. In preliminary experiments, the optimal seeding density in the Seahorse *XF Cell Culture Microplates* was tested experimentally (data not shown). Here, the seeding density of 9 x 10^4 cells/cm² was almost 2-fold lower than in the standard 96-well plates used for the MitoXpress assay (1.6 x 10^4 cells/cm²). The expression of several CYP enzymes and nuclear receptors was shown to be reduced in low density cultured HepaRG cells (Aninat et al., 2006; Merck Millipore (Ranade), personal communication). As a consequence, response to adverse effects can be altered and even absent. For both HepG2 cell systems, the vehicle treated control seemed to have an abnormally low spare respiratory capacity

(32 ± 4% and 10 ± 29% for HepG2-Glu and -Gal, respectively). This potentially led to inaccurate data evaluation and thus an interpretation was not possible.

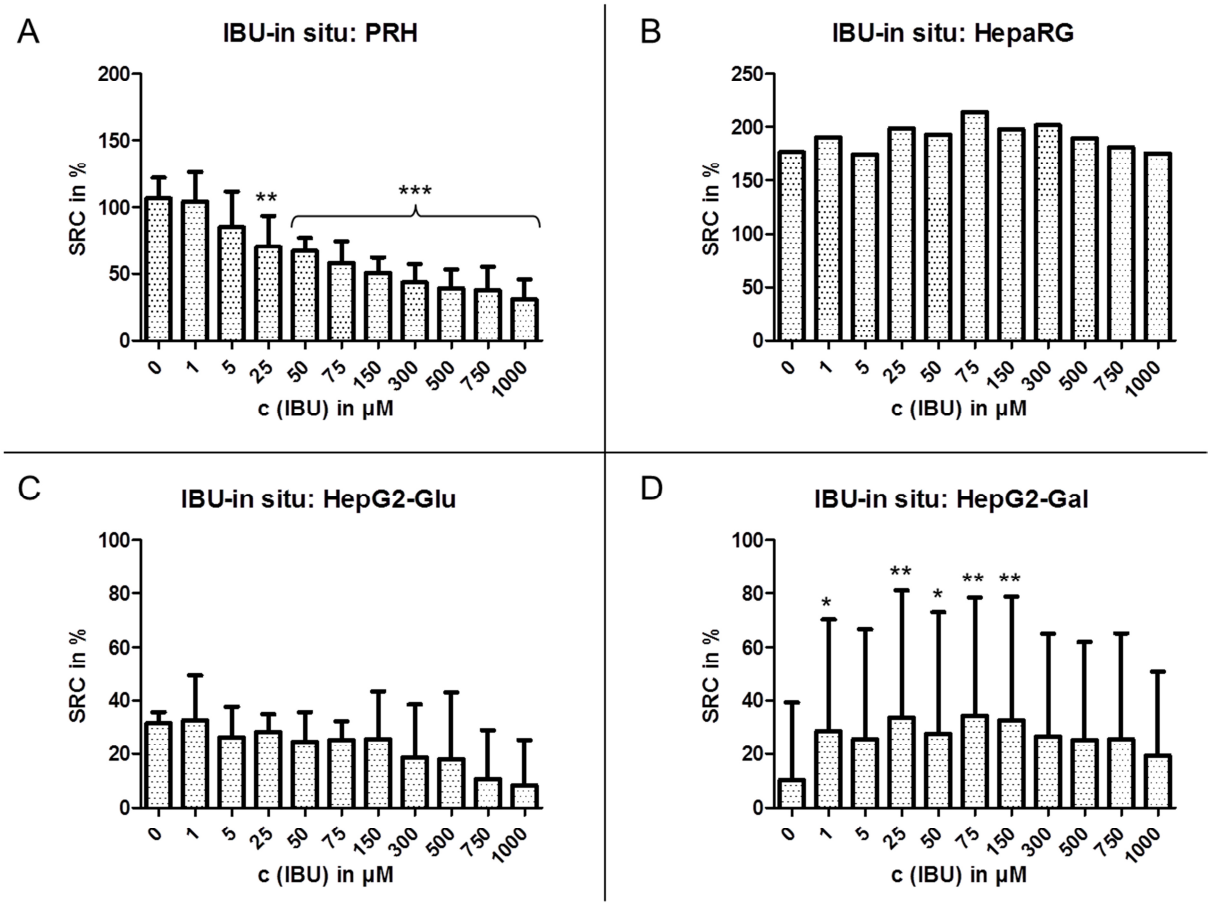

Figure 33. Spare respiratory capacity (SRC) in percent in the different hepatic systems (primary rat hepatocytes (PRH) (A), HepaRG (B), HepG2 cultured in regular glucose-containing medium (HepG2-Glu) (C) and HepG2 adapted to galactose-containing medium (HepG2-Gal) (D)) after *in situ* treatment with the indicated concentrations of ibuprofen (IBU). The raw data curves of the single biological replicates were normalised to the corresponding basal (3rd measurement) oxygen consumption rate in pmol/min set to 100%; corresponding to ~ 140 pmol/min in PRH, ~ 130 pmol/min in HepaRG, ~ 140 pmol/min in HepG2-Glu, ~ 110 pmol/min in HepG2-Gal. The percentages refer to the difference between basal (100%) and maximum (1st measurement after carbonyl cyanide 4-(trifluoromethoxy)phenylhydrazone (FCCP) injection) respiration. Values are given as mean of 2 (HepaRG) or 3 biological replicates + standard deviation. Statistical significance is expressed in p-value ≤ 0.05 (*), ≤ 0.01 (**) and ≤ 0.001 (***) and was calculated by one-way repeated-measures analysis of variance (ANOVA) of a treatment towards the vehicle control and application of the Dunnett's post test. A detailed description of the compound treatment and SRC calculation is given in the Materials and Methods.

In sum, all analysed endpoints (biokinetics, transcriptomics, proteomics and mitochondrial toxicity) provided comprehensive information of species differences and underlying mechanisms of IBU-induced adverse effects. Although IBU was included as negative compound in terms of hepatotoxicity, the affected functions identified in this work did not allow declaring IBU as such. The observations made were likely due to the applied *in vitro* concentrations, which were intentionally chosen in such a manner as to exert some degree of cytotoxicity (high concentration set to TC_{10} or screening of a concentration range in the mitochondrial toxicity experiments).

3.2 Chlorpromazine

In the early years, the antipsychotic drug, chlorpromazine (CPZ), was commonly prescribed for the treatment of psychotic disorders. The known adverse effects include those to the central nervous and cardiovascular system; whereas, hepatotoxicity was always associated with CPZ. CPZ-mediated hepatotoxicity primarily manifests in serum enzyme elevations and clinically apparent cholestatic liver injury (NIH - Chlorpromazine, 2014).

3.2.1 *In vitro* dose finding

The *in vitro* dose finding studies were performed to assess the cytotoxic potential of chlorpromazine in the two hepatic systems and thus determine the corresponding TC_{10}. The TC_{10} was used as high concentration and one-tenth of the TC_{10} as low concentration in the subsequent biokinetics, transcriptomics and proteomics studies.

The dose finding studies in PRH treated with CPZ revealed a time- and concentration-dependent cytotoxicity. The PRH treated with a total of 12 CPZ concentrations for 24 h showed a typical sigmoidal dose-response curve (Figure 34 A). Complete cell death was observed at concentrations ≥ 60 µM. However, a marked difference in response was observed at 50 µM CPZ, which resulted in 33 and 73% viability after 24 h in the 96-well monolayer (ML) (Figure 34 A) and 24-well sandwich (SW) (Figure 34 B) culture, respectively. This discrepancy is likely due to the fact that either the only replicate for the preliminary screen delivered a distorted TC_{50} or that the different culture conditions result in diverging vulnerability of the cells. The compound is thought to passively enter the cell (Roberts and Hammersley, 1985), where it inhibits various efflux transporters (Antherieu et al., 2013; Feng et al., 2008; Wang et al. 2008) and mitochondrial proteins (Furuno et al., 2001; Lores-Arnaiz et al., 2004; Modica-Napolitano et al., 2003). There was little or no cytotoxicity (measured using ATP content) after long-term treatment with 15, 20 and 25 µM CPZ, but microscopic inspection revealed considerable morphological changes, which were concentration-dependent. The cuboidal shape of the cells and the bile canaliculi-like structures were scarcely visible and in some areas of the culture, the clear borders of the cytoplasm had disappeared completely (data not shown). The physicochemical properties of CPZ (log K_{ow} = 5.41; pKa = 9.3) indicate that the compound is lipophilic and basic. In fact, CPZ accumulates in the cell lipid bilayer (Martins et al., 2012) and acidic lysosomes, due to its basic nature (Heikkinen et al., 2009). At physiological pH CPZ is protonated, forming a cationic amphiphilic molecule, which are well-known to induce phospholipidosis (Brosnan et al., 1970). These effects are suggested to cause the observed morphological changes, at concentrations that do not primarily affect ATP levels. Hence, after taking the cell morphological appearance into account, the high concentration of CPZ was set at 20 µM and the low concentration at 2 µM. While the viability of cultures treated with 20 µM was approximately 100% in both long-term cultures (24-well and 6-well SW culture formats) it

clearly affected the cell's morphology, but very importantly, without highly disrupting the cellular network.

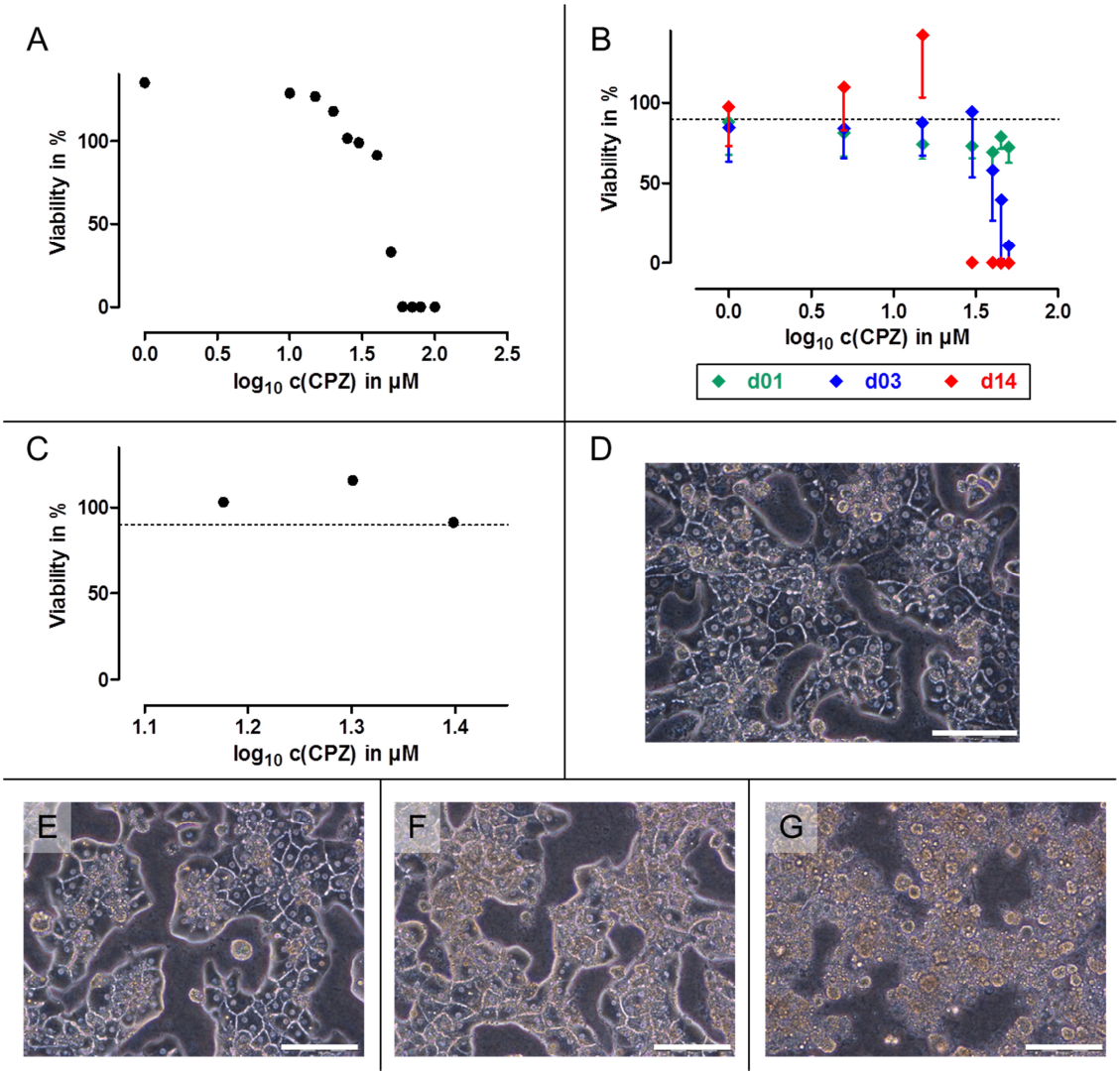

Figure 34. Cell viability results of primary rat hepatocytes (PRH) treated with chlorpromazine (CPZ) in 96-well mono layer for 24h (A), 24-well sandwich (SW) for 1 (green), 3 (blue) and 14 days (red) (B) or 6-well SW culture for 14 days (C) at the indicated concentrations. Results of the 24-well SW culture derived from 3 biological replicates and are displayed as mean - standard deviation (B). Viability (measured using ATP content) was expressed as the percent relative the corresponding time matched DMSO control. The dotted line shows the 90% viability threshold (B and C). Pictures of PRH in 6-well SW culture on day 14 after daily treatment with DMSO (D) or CPZ at 15 µM (E), 20 µM (F) or 25 µM (G). The white scale bar on the bottom right of each picture corresponds to 100 µm.

There was a time- and concentration-dependent increase in cytotoxicity of CPZ in PHH, the effects being most pronounced after long-term (day 14) exposure. Here, maximum cell death was recorded after treatment with 20 µM CPZ for 14 days (KaLy-Cell (Parmentier), personal communication).

The CPZ high concentration for the PHH was set to 1 µM, with the result that the corresponding low concentration is close to the human C_{max} (0.14 µM, Borges et al., 2011). The treatment concentrations for the final experiments in PRH and PHH are given in Table 29.

Table 29. Treatment concentration of chlorpromazine (CPZ) for final experiments in primary rat (PRH) and human (PHH) hepatocytes. High (HC) and corresponding low (LC) concentration.

	CPZ concentration in µM	
	HC	**LC**
PRH	20	2
PHH	1	0.1

The observed species-specific sensitivity towards CPZ was in accordance with the literature, where the reported TC_{50} after short-term cultures was 46 ± 17 µM in PRH (Wang et al., 2002) and 9 ± 7 µM in PHH (Gerets et al., 2012). In the final experiments, long-term exposure to 20 µM CPZ (high concentration) resulted in changed morphological appearance of PRH, as described in the dose finding section above. By contrast, PHH treated with 1 µM (high concentration) did not show any morphological changes compared to the time matched control (KaLy-Cell (Parmentier), personal communication). This observation was very likely due to the different concentrations applied, since the incorporation of CPZ into the cell membrane and accumulation in lysosomes was based on the compound's inherent physicochemical properties, i.e. it cannot be attributed to species-specific differences. Furthermore, only minimal changes in morphology of the PRH were seen after treatment with 2 µM CPZ.

3.2.2 Biokinetics

After determination of the high and low treatment concentrations in the two hepatic systems, the biokinetic profiles revealed how CPZ distributed in the cell lysates and supernatants.

In PRH, there was a rapid and progressive uptake of CPZ, which is thought to enter the cytoplasm via passive transport. Following a steady state from 1 - 3 h, either a decrease was observed after exposure to 2 µM or the amount of CPZ stayed elevated up to 24 h for the 20 µM treated PRH (Figure 35 A and D, respectively). This concentration-dependent response was likely to be linked to a saturated metabolism after high concentration treatment. However, a non-proportional decrease in the supernatant fraction was recorded that was independent from the applied concentration and time point (Figure 35 B and E). Here, the saturated metabolism proposed for 20 µM CPZ did not justify the disappearance of CPZ from the supernatant fraction, which could only be explained by further accumulation of CPZ in the plasma membrane and lysosomes. Overall, higher amounts were recovered from the cell lysates after repeated exposure (14 days) and were more pronounced after high concentration treatment. The cell lysate amount of CPZ after 14 days was 3 - 5 times higher at 2 µM and 6 - 30 times higher at 20 µM compared to the corresponding time points on day 0/1. Intracellular inclusion bodies were observed only in the high concentration treated PRH. CPZ is known to induce the formation of lamellar bodies, a pathophysiological hallmark for phospholipidosis (Anderson and Borlak, 2006). These inclusion bodies sequester CPZ further. After 2 µM CPZ treatment, the relative amount in the cells and

medium showed an apparent loss of CPZ (Figure 35 C), indicating an efficient biotransformation of the parent compound. Furthermore, a drop to 0 and 6% CPZ was observed for the low concentration on day 0 and 13, respectively, indicating that compound accumulation over time was negligible. This was different for the samples treated with 20 µM (high concentration) CPZ (Figure 35 F), where an apparent loss of the parent compound was observed exclusively on day 0. The loss of CPZ increased from 30 ± 21% at 2 min to 96 ± 4% after 24 h. For day 13, the cell lysate fraction itself exceeded 100% of the added CPZ amount. This indicated an apparent CPZ accumulation upon repeated exposures. The recovery of CPZ from the supernatant compartment decreased over time, which was likely due to metabolism.

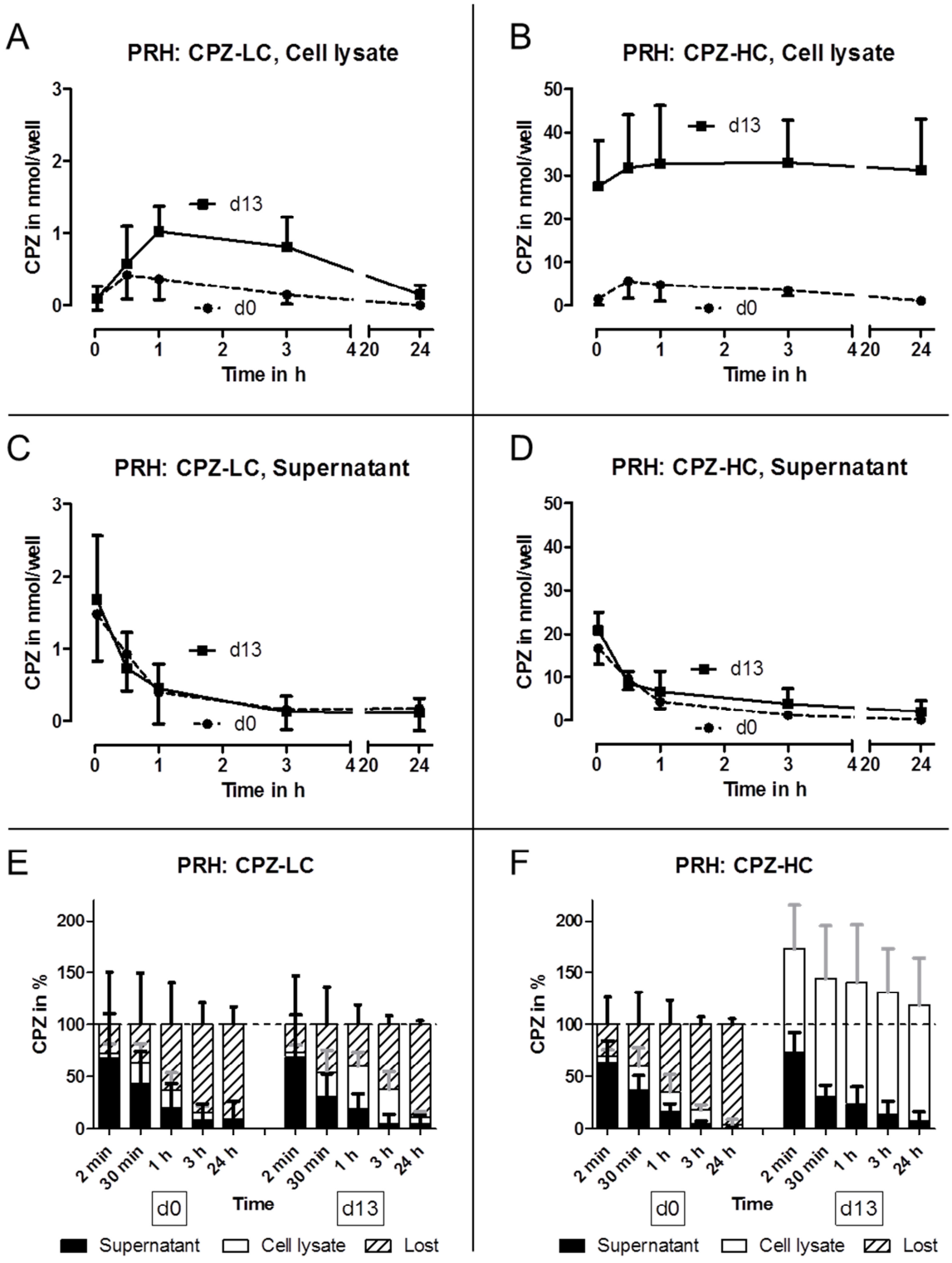

Figure 35. Kinetic profile of chlorpromazine (CPZ) (nmol/well) in primary rat hepatocytes (PRH) (A, C) and culture supernatants (B, D) after single (day 0 – dashed line) and repeated (day 13 – solid line) treatment with 2 µM (low concentration (LC); A, C) and 20 µM (high concentration (HC); B, D) CPZ at the indicated time points. Relative distribution of CPZ in percent in the different analysed PRH fractions at the indicated time points on day 0 and 13, supernatant (bold) and cell lysate (blank) as well as the apparent loss (striped) for the LC (E) and HC (F). Values are given as mean of 3 biological replicates +/- standard deviation.

As determined in the dose finding studies, the treatment concentrations for the PHH were 20-fold lower compared to the PRH. The lysates and supernatants collected after treatment with the CPZ low concentration (0.1 µM) of the PHH system resulted in compound concentrations that fell

below or were around the analytical LOD. For this reason the low concentration treated samples (Figure 36 A-C) were excluded from further analysis.

CPZ was rapidly taken up by PHH treated with the high concentration (1 µM), which was concomitant with a non-proportional decrease of this compound in the supernatants (Figure 36 D and E, respectively). This was concluded to be due to an efficient metabolism. In addition, the same biokinetic profile was observed on day 0 and 13, which indicated the absence of intracellular accumulation. The latter was in line with the lack of intracellular vacuoles observed microscopically. The relative distribution of the high concentration (Figure 36 F) showed a gradual decrease of CPZ in the supernatant fraction over time and on both treatment days. In the cell lysate fraction an increase was noted on both days up to 3 h, exceeding the CPZ originally applied to the cells at 30 min, 1 and 3 h. This increase was followed by an extreme drop at 24 h. A close to complete loss of CPZ in the analysed fractions was observed after 24 h incubation on both days (86 ± 2% on day 0 and 98 ± 2% on day 13).

CYP1A and CYP2D6 are known to be involved in the biotransformation of CPZ (Yoshii et al., 2000; Shin et al., 1999). The CYP characterisation of PHH revealed a low basal CYP1A activity in the PHH from all three donors (Appendix 4, Table 47). CYP1A1 and CYP1A2 remained inducible after 14 days (data not shown). Furthermore, PHH from Donors 1 and 3 had low basal CYP2D6 activities, while PHH from Donor 2 exhibited higher CYP2D6 activity. CYP2D6 is known to be highly polymorphic and non-inducible. Taken together, the CYP characterisation, especially CYP2D6, correlated with the high inter-donor variation in PHH shown in the biokinetics profiles. PHH from all donors efficiently metabolised CPZ, although to different extents.

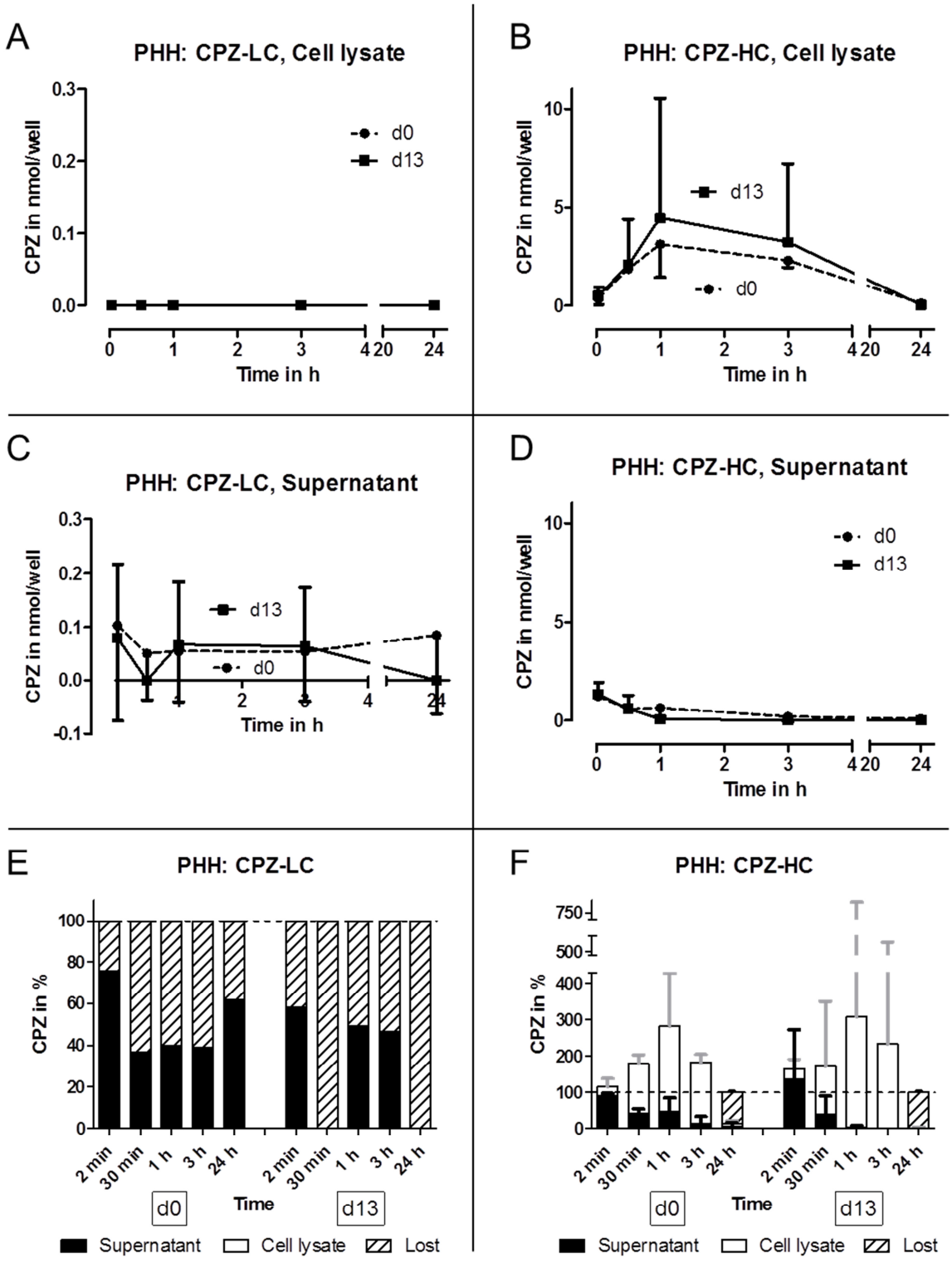

Figure 36. Kinetic profile of chlorpromazine (CPZ) (nmol/well) in primary human hepatocytes (PHH) (A, B) and culture supernatants (C, D) after single (day 0 – dashed line) and repeated (day 13 – solid line) treatment with 0.1 µM (low concentration (LC); A, C) and 1 µM (high concentration (HC); B, D) CPZ at the indicated time points. Relative distribution of CPZ in percent in the different analysed PHH fractions at the indicated time points on day 0 and 13, supernatant (bold) and cell lysate (blank) as well as the apparent loss (striped) for the LC (E) and HC (F). Values are given as 1 biological replicate (LC; A, C, E) and as mean of 3 biological replicates +/- standard deviation (HC; B, D, F).

The biokinetic profiles of the supernatants from the different species were very similar. By contrast, comparison of the biokinetic profile of the cell lysates treated with similar

concentrations of CPZ, i.e. 2 µM in PRH and 1 µM in PHH, revealed important differences. At steady state, the amount of CPZ was higher in PHH compared to PRH (~ 11- and 4-fold on day 0 and 13, respectively), although the concentration used in PHH was 2-fold lower. A potential explanation could be the sequestration of CPZ in the PRH cultures by (i) albumin which was a component of the culture medium of PRH and/or (ii) collagen, which was contained in the cell lysate fraction, because a separation of cells from collagen was not feasible. Comparison of the CPZ biokinetics between serum-containing and serum-free culture medium in the HepaRG cell line revealed a faster and higher intracellular uptake of CPZ in the serum-free cultures (Broeders et al., manuscript in preparation). In addition, the blank studies revealed that collagen I (PRH; Appendix 6, Table 50), but not Geltrex™ (PHH) sequestered CPZ. However, the amount of CPZ extracted from the collagen I exceeded the amount found in the PRH lysates of the regular experiments. This finding led to the assumption that sequestration of CPZ by collagen might be lower in the presence of cells. Therefore, in contrast to IBU, a correction for collagen binding was not performed. Finally, a higher metabolic capacity of PRH could also explain the lower cell lysate amount of CPZ. Although plastic binding of basic drugs is reported to be substantial (Palmgren et al., 2006), no plastic binding of the basic drug CPZ (pKa = 9.3) was recorded in these experiments. The apparent loss of the CPZ parent was concluded to be due to its metabolism. In addition to CYP1A, CYP2C and CYP2D6, CYP3A is also known to metabolise CPZ (Wójcikowski et al., 2010; Yoshii et al., 2000; Shin et al., 1999). Preliminary characterisation of the PRH culture system showed that Cyp1a1/1a2 and 3a1 were still inducible after 10 days in culture (Tuschl et al., 2009). The individual characterisation of PHH from different donors revealed the metabolic capacity of the cells, as described above. As previously described for IBU, the simultaneous determination of major CPZ metabolites would be an advantage for a more in-depth data interpretation, potentially unveiling the reasons for the observed species differences. On the basis of these results, it cannot be excluded that the observed phospholipidosis is a rat-specific effect. Hypothetically treatment of PHH with a higher concentration would have resulted in the same pathology. Overall, the biokinetic profiles in the two primary hepatic cell systems were shown to be influenced by inherent species-differences, but also by the specific culture conditions.

3.2.3 Transcriptomics

Transcriptional alterations after exposure to the antipsychotic drug, CPZ, were analysed in order to gain insight into adversely affected cellular mechanisms.

In the global gene expression profile of PRH, various pathways were affected after short- and long-term treatment with 20 µM CPZ (some altered functions are included in Figure 37). CPZ treatment deregulated many genes involved in the cholesterol metabolism. Three genes (*Ces3*, *Lcat* and *Es22*), involved in the esterification of cholesterol, were down-regulated. Accordingly,

CPZ was reported to inhibit *Lcat* in human and rat *in vivo* (Bell and Hubert, 1981). *Cyp3a18*, which catalyses the hydroxylation of testosterone, was also down-regulated. As a steroid hormone, testosterone is derived from cholesterol. *Apom*, an apolipoprotein associated with high density lipoprotein (HDL), was down-regulated by 2.9-fold on day 14. Taken together, these decreased expressions could be attributed to a reduced cholesterol level in the CPZ treated PRH. The up-regulation of genes involved in cholesterol synthesis (*Cyp2b15*) and uptake (*Vldlr*, *Pltp*) could be the response of the cells to the reduced cholesterol level. Cyp2b15, a typically skin-specific CYP (Keeney et al., 1998), is known to take part in cholesterol biosynthesis. The increased expression of lipoprotein receptor, *Vldlr*, could be attributed to the cell's attempt to import cholesterol from the extracellular space. In line with this hypothesis, *Pltp* was also up-regulated. Pltp is a protein bound to HDL and thus, involved in the reverse cholesterol transport, i.e. cholesterol and phospholipid transport to the liver.

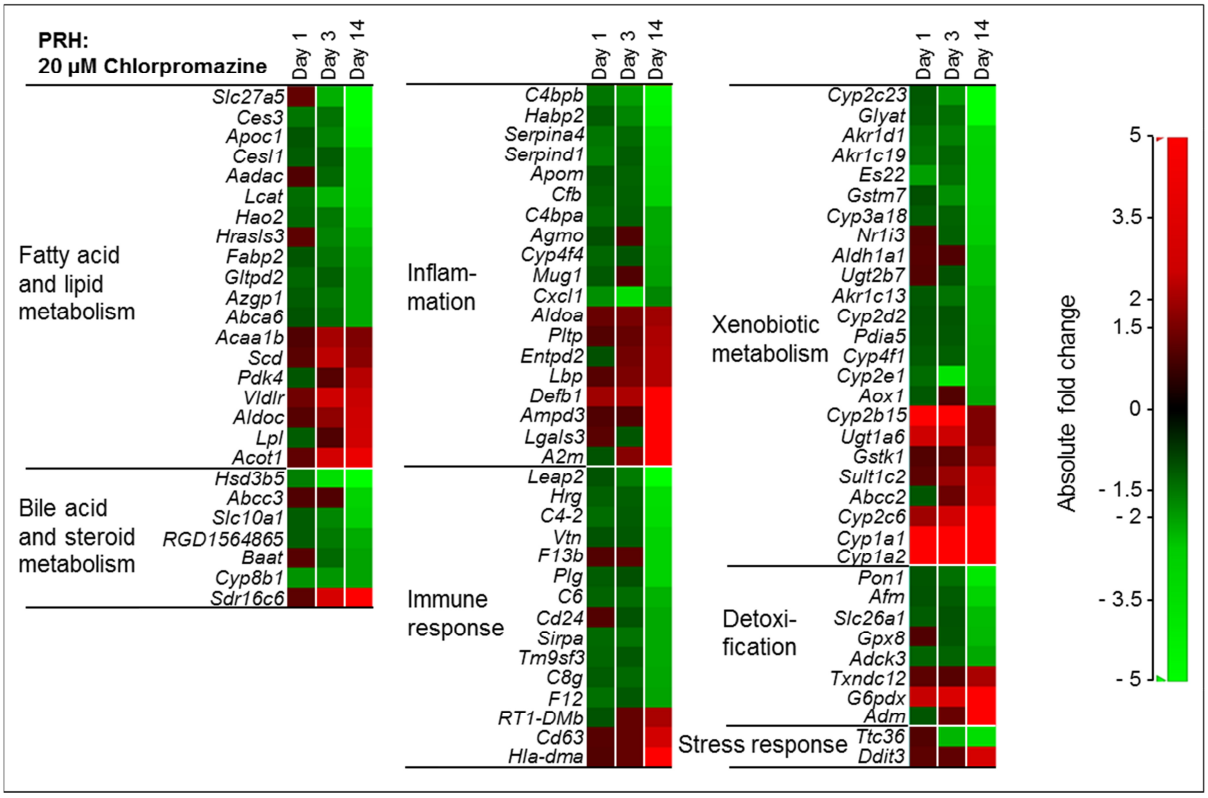

Figure 37. Gene function profile display of significantly deregulated genes in primary rat hepatocytes (PRH) after treatment with 20 µM chlorpromazine for 1, 3 or 14 days. The heatmap shows 94 genes involved in fatty acid and lipid metabolism, bile acid and steroid metabolism, inflammation, immune response, xenobiotic metabolism, detoxification and stress response identified to be deregulated by at least 2-fold compared to the time-matched vehicle treated control. The statistical significance (BH q-value ≤ 0.05) by a linear model and absolute fold changes were calculated using the statistical analysis software Genedata Analyst™ version 7.5, the detailed data analysis is given in the Materials and Methods section. The colour scale shows increased fold changes in red and decreased fold changes in green. Genes are sorted according to their fold change value on day 14 (from decreased to increased fold changes) within the corresponding pathway. Absolute fold change values and gene acronyms are given in the appendix.

The biliary secreted conjugated bile salts are needed for dietary lipid solubilisation and fat-soluble vitamin E uptake. Two enzymes, *Slc27a5* and *Baat*, involved in the conjugation of bile acids to glycin or taurine were down-regulated after CPZ treatment. Inherited dysfunction of

these enzymes was reported to be linked to vitamin E deficiency and cholestasis (Setchell et al., 2013). The biliary transporters, situated at the canalicular pole of hepatocytes, transport conjugated bile salts more efficiently than unconjugated salts. An accumulation of unconjugated bile salts induces apoptosis and necrosis and is implicated in cholestatic liver disease. The bile salt transporters, *Slc10a1* and *Abcc3*, responsible for uptake and efflux of unconjugated bile salts, respectively, were both down-regulated. Furthermore, *Cyp8b1*, involved in bile acid synthesis was down-regulated. The decreased expression of *Slc10a1* (aka *Ntcp*) and *Cyp8b1* is in agreement with Antherieu et al. (2013) who treated human HepaRG cells with CPZ. These authors also reported canalicular bile salt transporters to be down-regulated (Antherieu et al., 2013). In the data presented here, no canalicular transporters were in the dataset (even without considering a fold change cutoff), suggesting that the corresponding genes did not fulfil the statistical threshold (BH q-value ≤ 0.05).

The proposed increased bile salt concentration could only be assumed; however, the affected genes involved in fatty acid and lipid metabolism, suggested a disruption of cholesterol catabolism, and consequently bile salt metabolism. In fact, CPZ is reported to have hypercholesterolemic activity (Clark et al, 1967).

Interestingly, *Cyp1a1* and *Cyp1a2* were highly up-regulated (Figure 37, Table 30). These CYPs are known to metabolise CPZ, generating metabolites that mediate CPZ-induced toxicity. This indicated that CPZ accelerates its own metabolism.

Table 30. Fold change values of *Cyp1a1* and *Cyp1a2* (gene expression). Results derive from primary rat hepatocytes treated with a high concentration (20 µM) of chlorpromazine at the indicated time points. Bold numbers highlight values ≥ 2-fold (red).

	day 1	day 3	day 14
Cyp1a1	**27.7**	**31.4**	**17.5**
Cyp1a2	**14.6**	**6.6**	**19.0**

Furthermore, *Gstk1* and *G6pdx* were up-regulated; these genes are involved in the glutathione (GSH) transfer and the recovery of $NADP^+$ for its reduction, respectively. Conjugation with GSH is an important pathway for CPZ detoxification (MacAllister et al., 2013). An up-regulation of the phase II enzymes, *Ugt1a6* and *Sult1c2*, indicated that further pathways were activated for CPZ detoxification. *Adm* expression was increased 7.3-fold only on day 14. This gene codes for the protein adrenomedullin, which is reported to possess significant antioxidant properties. The up-regulation of genes with antioxidant capacities (*Txndc12*, *Adm*) suggested the activation of rescuing pathways against oxidative stress. In fact, oxidative stress was reported to aggravate CPZ-mediated cholestasis (Antherieu et al., 2013). With the exception of Cyp1a1/2 the majority of the genes involved in phase I and II drug metabolising enzymes (DMEs) and detoxification were down-regulated, but mostly not before day 14. Interestingly, *in vivo* a decrease of hepatic DMEs was observed in rats after acute exposure to CPZ (Senda et al., 1989). However, many of the down-regulated genes are reported to be also involved in other pathways, e.g. fatty acid and

lipid metabolism (*Cyp2c23*, *Cesl1*, *Es22*, *Cyp3a18*, *Aldh1a1*, *Ces3*, *Apom*), bile acid synthesis (*Akr1d1*) and steroid metabolism (*Akr1d1*, *Akr1c13*). As discussed above, the effects of CPZ on these pathways could help explain the down-regulation of the specific genes.

Many genes involved in inflammation and immune response pathways were deregulated. The expression of *C4bpb*, *C4bpa* and *Cyp4f4*, reported to be down-regulated during inflammation, was decreased on day 14 by 4.5, 2.1 and 2.0-fold, respectively. The up-regulated genes included those promoting inflammation (*Entpd2*, *Lbp*) as well as genes reported to reduce inflammation (*Pltp*, *Ampd3*). The latter can be regarded as cellular response to the evolving inflammation. *A2m*, a typical inflammatory marker in rats (Kuribayashi et al., 2011), was up-regulated by 14.2-fold on day 14. Approximately 80% of the immune response genes were down-regulated on day 14. It can be assumed that CPZ-mediated adverse effects were not restricted to hepatocytes. Hence, immune cells comprised in the PRH cultures, and responsible for the immune response, may have lost their function after repeated exposure. *In vivo* findings indicate that CPZ-mediated adverse effects include liver inflammation (Buchweitz et al., 2002).

A direct comparison of IBU and CPZ effects revealed an overlap of 16 genes. The direction of deregulation for most of these genes was the same, and were scattered over multiple pathways. With an overlap of only 5 genes (*Acaa1b*, *Scd*, *Acot1*, *Vldlr* and *Pdk4*), the fatty acid and lipid metabolism pathway of CPZ differed considerably from the one after exposure to IBU. For CPZ, *Acot1* was the only gene up-regulated of the classical PPAR activation genes (*Acot1*, *Acox* and *Cyp4a1*). In addition, after 14 days, *Acot1* expression was increased by only 4-fold, compared to 19-fold for IBU. In contrast to IBU, which is reported a peroxisome proliferator, CPZ is reported to be a peroxisome inhibitor (Leighton et al., 1984), which explained the different manifestations on molecular level. The mechanisms by which CPZ inhibits peroxisomes are still unknown; however, several genes known to be activated through PPAR were identified, namely *Pdk4*, *Vldlr*, *Lpl* and *Acot1*. This finding could be explained by the accumulation of long-chain fatty acids, which activate PPAR and subsequently, the target genes. Genes involved in free fatty acid generation, such as *Scd*, *Vldlr*, *Lpl* and *Acot1*, were up-regulated. However, the inducing potential of the accumulating fatty acids did not seem to exceed the inhibitory effect of CPZ. Only 5 peroxisomal genes were deregulated in this dataset (*Acaa1b*, *Hao2*, *Pxmp2*, *Pipox* and *Baat*) and of these, a total of 2 genes were involved in the peroxisomal fatty acid oxidation: *Acaa1b* and *Hao2*. *Acaa1b* is an acetyl-CoA acyltransferase that was up-regulated > 2-fold only on day 3. By contrast, *Hao2*, a hydroxyacid oxidase, was down-regulated (by 1.5- and 2.8-fold on day 3 and 14, respectively). Other genes associated with peroxisomes, namely *Pxmp2*, *Pipox* and *Baat*, were also down-regulated. Taken together, these findings indicate that CPZ impairs the fatty acid and lipid metabolism (Figure 37) and decreases the general activity in peroxisomes, which is in line with CPZ being a peroxisome inhibitor.

There was a large variation in the gene expression results using PHH from three different donors. The number of deregulated genes increased with time only for PHH from Donors 1 (at 1 µM)

and 2 (at 0.1 µM). There was a drop in the number of genes involved in the different functions on day 3 for PHH from Donors 1 and 3, which was also independent of the treatment concentration. This observation could be attributed to a cellular adaptation phase in response to drug exposure that was donor-dependent. In accordance with this, it is reported that genes deregulated on day 1 are not automatically detected on day 3 (Richert et al., 2009). A detailed analysis of the transcriptomic profiles derived from PHH was performed using the gene expression analysis software IPA®. As previously described for IBU, the software was used for hypothesis generation, whereas genes that were classified into different tox functions were reviewed manually for interpretation. IPA® revealed *Liver Hyperplasia/Hyperproliferation* as the most affected tox function in PHH from all donors. In this function, the genes were mainly attributed to inflammation, immune response (Figure 38) and cancer. The genes, *LTB*, *ADAMTS1*, *CCL2* and *IL6*, which mediate inflammation and the immune response, were up-regulated only in PHH from Donor 2 at the low concentration (0.1 µM), which is close to the human C_{max} (0.16 µM; Borges et al., 2011). By contrast, these genes were down-regulated in PHH from Donor 3 but not Donor 1. Inflammatory mediators are often linked to tissue regeneration. In fact, *TNF*, a cytokine involved in the regulation of cell proliferation, showed an identical expression pattern in PHH from the corresponding donors. In accordance with the results in PRH, immune response genes (here: *C3*, *CD44*, *ICAM1*, *OSMR*, *IL8*) were down-regulated in PHH from Donor 3 but not deregulated in PHH from the other two donors. This inter-donor variability is suggested to be an important factor contributing to the low predictive value of frequently used animal models.

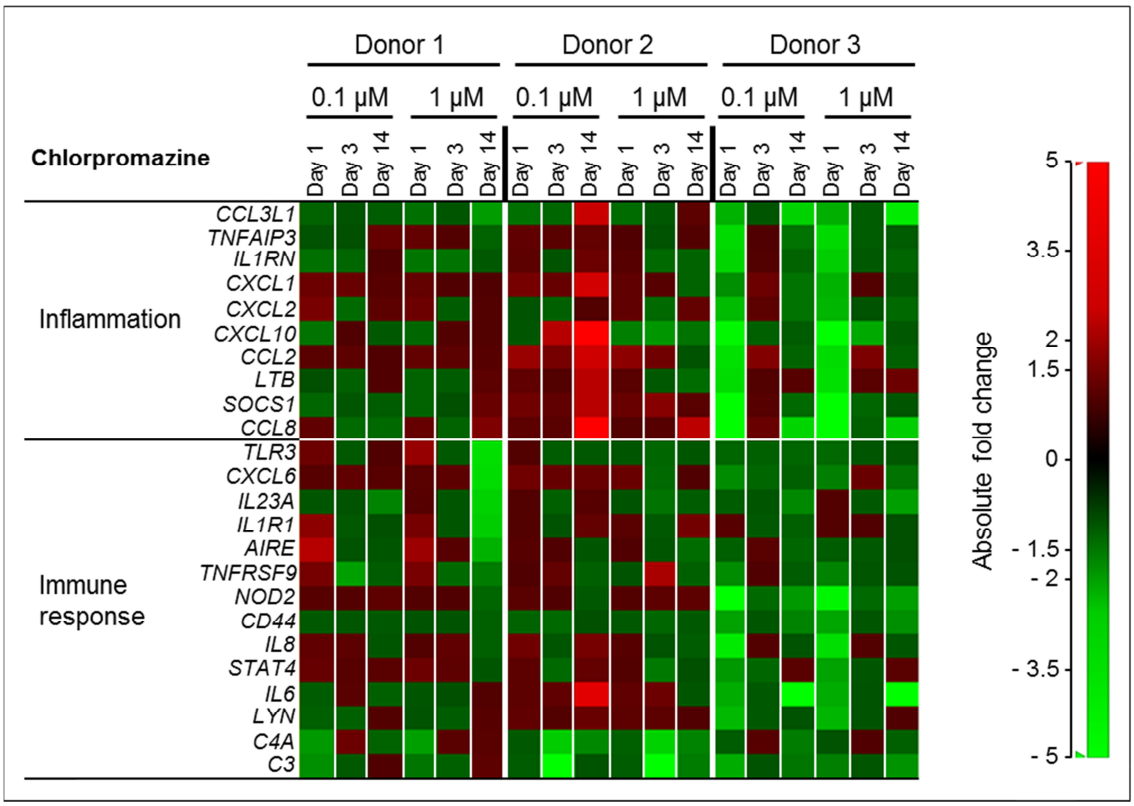

Figure 38. Gene function profile display of significantly deregulated genes in primary human hepatocytes from different donors after treatment with 0.1 µM and 1 µM chlorpromazine for 1, 3 or 14 days. The heatmap shows 24 genes involved in inflammation and immune response identified to be deregulated by at least 2-fold compared to the time-matched vehicle treated control. The absolute fold change was calculated using the statistical analysis software Genedata Analyst™ version 7.5, the detailed data analysis is given in the Materials and Methods section. The colour scale shows increased fold changes in red and decreased fold changes in green. Absolute fold change values and gene acronyms are given in the appendix.

The consideration of the basal CYP1A activities did not contribute to a better understanding of the observed inter-donor variations. The basal activities were very low and comparable between PHH from the three donors (Appendix 4, Table 47).

At the gene expression level, the CPZ-metabolising *CYP1A1* and *CYP1A2* (Wojcikowski et al., 2010) were up-regulated in PHH from all donors (Table 31).

Table 31. Fold change values of *CYP1A1* and *CYP1A2* (gene expression). Results are given for primary human hepatocytes (Donor 1, 2 and 3) treated with low (LC: 0.1 µM) or high (HC: 1 µM) concentration of chlorpromazine (CPZ) at the indicated time points. Bold numbers highlight values ≥ 2-fold (red).

		CPZ LC			CPZ HC		
		day 1	**day 3**	**day 14**	**day 1**	**day 3**	**day 14**
CYP1A1	**Donor 1**	1.2	**3.1**	1.8	1.2	**3.0**	**2.1**
	Donor 2	**4.4**	1.9	1.0	**5.1**	1.5	**3.9**
	Donor 3	**3.2**	**3.0**	**4.5**	**3.4**	**3.6**	**2.1**
CYP1A2	**Donor 1**	**2.5**	1.2	**2.4**	**2.6**	1.4	1.9
	Donor 2	**2.8**	**2.6**	-1.4	**3.6**	1.1	1.9
	Donor 3	**2.8**	1.5	1.9	**3.2**	1.5	1.7

As previously observed for PRH, these studies also indicated that CPZ induces its own metabolism in PHH. The up-regulation in PHH was not as pronounced as in PRH, which might be due to the lower treatment concentration. The other CYP enzyme known to metabolise CPZ is CYP2D6 (Yoshii et al., 2000), a non-inducible CYP isoform that was consequently not deregulated on mRNA level. The basal activities of CYP2D6 differed considerably between the donors (Appendix 4, Table 47), such that activities were low in PHH from Donors 1 and 3 but comparably high in PHH from Donor 2. However, the basal CYP2D6 activity could not be directly linked to the adverse effects seen in the gene expression data.

The genes relating to *Liver Cholestasis* and *Liver Steatosis* were present in PHH from all donors, although these appeared most relevant for PHH from Donor 2. Many genes in PHH from Donor 1 and 2 were down-regulated, including those involved in beta-oxidation (*ACOX1*, *ACADM*, *EHHADH*), cholesterol metabolism (*INSIG1/2*, *HMGCR*) and fatty acid metabolism (*ACOX2*, *PHYH*, *CYP4A11*, *FASN*). By contrast, PHH from Donor 3 had only one gene that was up-regulated: *EHHADH*. This gene participates in the peroxisomal beta-oxidation pathway. As a peroxisome inhibitor, CPZ is thought to reduce the expression of peroxisomal genes. The single gene induced in PHH from Donor 3 was therefore considered non-essential and not contradictory to the other findings. As previously described, genes in the inflammation pathway were up-regulated in PHH from Donor 2. In the rat, LPS-induced inflammation promoted CPZ-induced cholestasis (Buchweitz et al., 2002); hence, inflammation was suggested to play an important role in CPZ-mediated cholestasis, making PHH from Donor 2 the most susceptible individual for this pathology. We have recently shown that the donor-dependent response of PHH cultures from five donors to inflammation was positively correlated with the strength of various hepatotoxic pathways at the gene expression level (Parmentier et al., 2013); thus, supporting the hypothesis that inflammation renders patients more susceptible towards drug-induced toxicity and can be linked to idiosyncratic effects (Roth et al., 2003).

At therapeutic concentrations, CPZ-induced hepatotoxicity mainly manifests in form of intrahepatic cholestasis (Boelsterli et al., 1987; de Abajo et al., 2004; NIH - Chlorpromazine, 2014). Drug-induced intrahepatic cholestasis often includes impairment of hepatobiliary transporters, resulting in the accumulation of cytotoxic bile acids. Here, PHH from Donor 2 had a decreased expression of *NTCP* (*SLC10A1*) and *CYP8B1*, involved in bile acid uptake and synthesis, respectively. This can be interpreted as protective mechanism of the cell, aiming to react to the accumulation of bile acids. *NTCP* was reported to be down-regulated during cholestasis (Zollner et al., 2001). By contrast, there was an increased expression of *NTCP* in PHH from Donor 3, which is probably due to the lacking accumulation of NTCP-inhibiting bile acids. Taken together, this observation contributes further to the hypothesis that PHH from Donor 2 demonstrate overt signs of cholestasis after treatment with CPZ. The canalicular transporters, *BSEP* and *MDR3*, reported to be decreased in HepaRG cells (Antherieu et al., 2013) were not deregulated in PHH from any of the donors tested here.

Overall, the PHH data showed that CPZ treatment impaired genes involved in fatty acid and lipid metabolism and bile acid metabolism. The degree of the effect was donor-dependent, potentially being attributed to different susceptibilities of human patients (proposed order for the susceptibility of CPZ-induced cholestasis: PHH from Donor 2 > Donor 1 > Donor 3). Furthermore, underlying mechanisms and inherent donor features that contribute to the idiosyncratic nature of CPZ-mediated hepatotoxicity could be suggested.

A direct comparison of the two species demonstrated similar pathways affected after CPZ treatment. PRH seemed to provide a comprehensive insight into the underlying mechanisms of the CPZ-mediated hepatotoxicity pathways found *in vivo*. These included the impairment of fatty acid and lipid metabolism, bile acid metabolism, cholesterol metabolism, as well as the involvement of the immune response, inflammation and oxidative stress. However, some difficulties of translating the results from PRH to PHH were seen. The rat data, although reproducible, appeared not useful for predicting the susceptibility of individual donors, which may not be reproducible from one donor to another. Along with genetic factors which influence the ADME processes in humans, environmental factors play an essential role in altering the susceptibility to drug-induced adverse effects. Environmental factors may include concomitant drugs (resulting in drug-drug interactions), age, nutritional status and pre-existing morbidities. These factors, which additionally influence the activity of DMEs are multiple, may vary in intensity and are mostly not controllable or identifiable. By contrast, reports on genetic variations in rats are less common compared to humans; thus, intra-species differences in rats from one strain are not expected. Furthermore, rats for the laboratory use are grown isolated from most sources of contamination. Most importantly, a total of five biological replicates were processed for the transcriptomic profiling and initial check of the dataset (visualisation using principal component analysis) did not reveal any difference between the hepatocytes from different rats. Taken together, these intra-individual variations are likely contributing to the finding that PRH fail to predict donor-specific hepatotoxicity mediated by CPZ.

3.2.4 Proteomics

It is known that changes at the mRNA level do not automatically translate into changed protein abundance. Therefore, proteomics was included as additional endpoint.

In the proteomics dataset, only 2 proteins relating to fatty acid and lipid metabolism were increased compared to the time-matched vehicle control: 5'-AMP-activated protein kinase subunit beta-1 and Apolipoprotein A-IV. The hypothesis that CPZ treatment led to the accumulation of long-chain fatty acids, which further form triglycerides could explain the higher level of Apolipoprotein A-IV. However, the effect of CPZ on this pathway was considered minor in the proteomics data. Oxidative stress plays a major role in CPZ-mediated cholestasis (Antherieu et al., 2013). CPZ is known to act as complex I inhibitor and impairment of the

oxidative phosphorylation always represents a source of ROS. Proteins involved in stress responses were increased, suggesting the onset of protective pathways. Further detoxifying mechanisms showed a higher abundance at the protein level, including phase II xenobiotic metabolism (UDP-glucuronosyltransferase 2B1) and glutathione disulfide reduction (Glutaredoxin-1). Interestingly, the CYP1A enzymes with highly induced mRNA were not increased at the protein level. This was possibly due to technical aspects such as a reduced efficacy of extraction of membrane proteins or the low focus on the corresponding m/z ratio. Furthermore, it was possible that the elevated mRNA was not translated into protein. Most importantly, protein abundance is known to correlate poorly with the enzyme activity of the corresponding CYP; whereas, there is a good correlation between the CYP induction activities and mRNA expression (Richert et al., 2009). Hence, the lack of increases at the protein level does not contradict the hypothesis that CPZ induced its own metabolism.

Inflammatory proteins were changed, which was in accordance with the gene expression data. Here, the acute inflammatory marker, alpha-2-macroglobulin was decreased at the protein level while the deregulation was opposed to the gene expression results. The up-regulation at the mRNA level could be attributed to the actual low abundance of the protein, i.e. a response or feedback mechanism. The product, alpha-2-macroglobulin, was the only overlap between the two datasets. The proteins involved in cellular proliferation were mostly decreased, which corresponded to the findings in the transcriptome of the PRH. This suggested that CPZ does not primarily induce liver cancer and occurrences of this pathology can be regarded as a secondary effect. Other proteins playing roles in cell adhesion, signalling and homeostasis could not be linked to any specific CPZ-mediated adverse effect. It was likely that accumulating impairments led to changes of proteins involved in these general cellular functions.

3.2.5 Mitochondrial toxicity

CPZ affects mitochondrial function by inhibition of complex I and impairment of the mitochondrial membrane potential. In order to determine the potential of CPZ to act as mitochondrial toxicant, different experimental approaches were considered.

3.2.5.1 ATP level for detection of mitochondrial toxicity

A pronounced cytotoxicity was seen after treatment of cells with higher concentrations of CPZ (Figure 39). Two distinct response profiles were observed. First, PRH and HepG2-Gal exhibited a similar sensitivity, reaching the TC_{50} at ~ 40 µM and complete loss of viability at 80 µM CPZ. By contrast, HepaRG and HepG2-Glu cells were less sensitive to CPZ, with a TC_{50} at ~ 60 µM and complete cytotoxicity at concentrations only above 200 µM. Overall, the cytotoxicity curves were clustered into aerobic (PRH and HepG2-Gal) and poorly aerobic metabolising hepatic cell

systems (HepaRG and HepG2-Glu). This finding was in accordance with the hypothesis that PRH and galactose-adapted HepG2 cells are more susceptible to mitochondrial toxicants. CPZ is reported to inhibit complex I (Modica-Napolitano et al., 2003) as well as the mitochondrial membrane potential that is required for ATP synthesis (MacAllister et al., 2013).

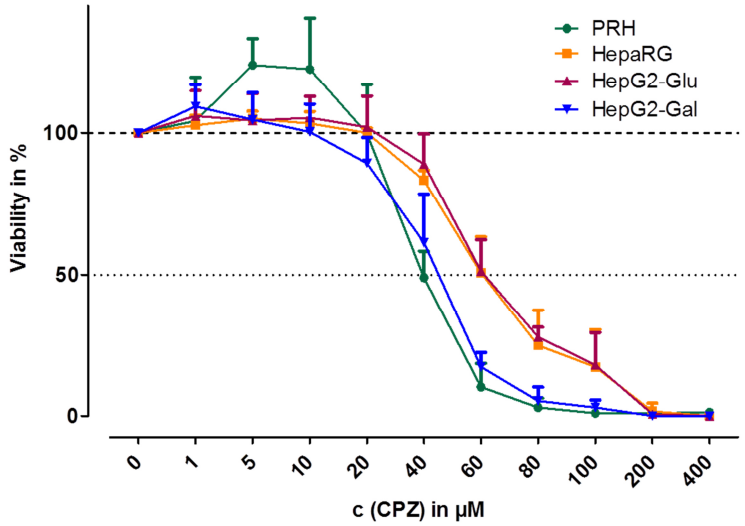

Figure 39. Cell viability results (measured using ATP content) in percent using the four hepatocyte systems (primary rat hepatocytes (PRH), HepaRG, HepG2 cultured in regular glucose-containing medium (HepG2-Glu) and HepG2 adapted to galactose-containing medium (HepG2-Gal)) after treatment for 1 h with the indicated concentrations of chlorpromazine (CPZ). The percentages refer to the vehicle treated control, in relative light units, set to 100%. The values given represent the mean of 3 - 4 biological replicates + standard deviation.

3.2.5.2 MitoXpress O_2-sensitive probe respiration assay

After treatment of PRH with CPZ, the oxygen consumption rate increased from 142 ± 17% at 10 µM to 153 ± 35% at 20 µM. CPZ is reported to be an inhibitor of mitochondrial nitric oxide synthase (Lores-Arnaiz et al., 2004). Nitric oxide acts as competitive inhibitor of cytochrome c oxidase and thus is able to modulate mitochondrial oxygen consumption (Brown , 1995; Cleeter et al., 1994). The inhibition of nitric oxide synthase by CPZ results in a reduced production of nitric oxide, and consequently to increased respiration (Haynes et al., 2003). By contrast, in all the other hepatic systems the respiration rate was reduced at concentrations ≥ 20 µM (HepG2-Gal: 67 ± 5%) or 40 µM (HepaRG: 73 ± 15% and HepG2-Glu: 44 ± 12%). Here, the CPZ-mediated inhibition of complex I seemed to predominate since this effect of CPZ was most pronounced in HepG2-Gal cells.

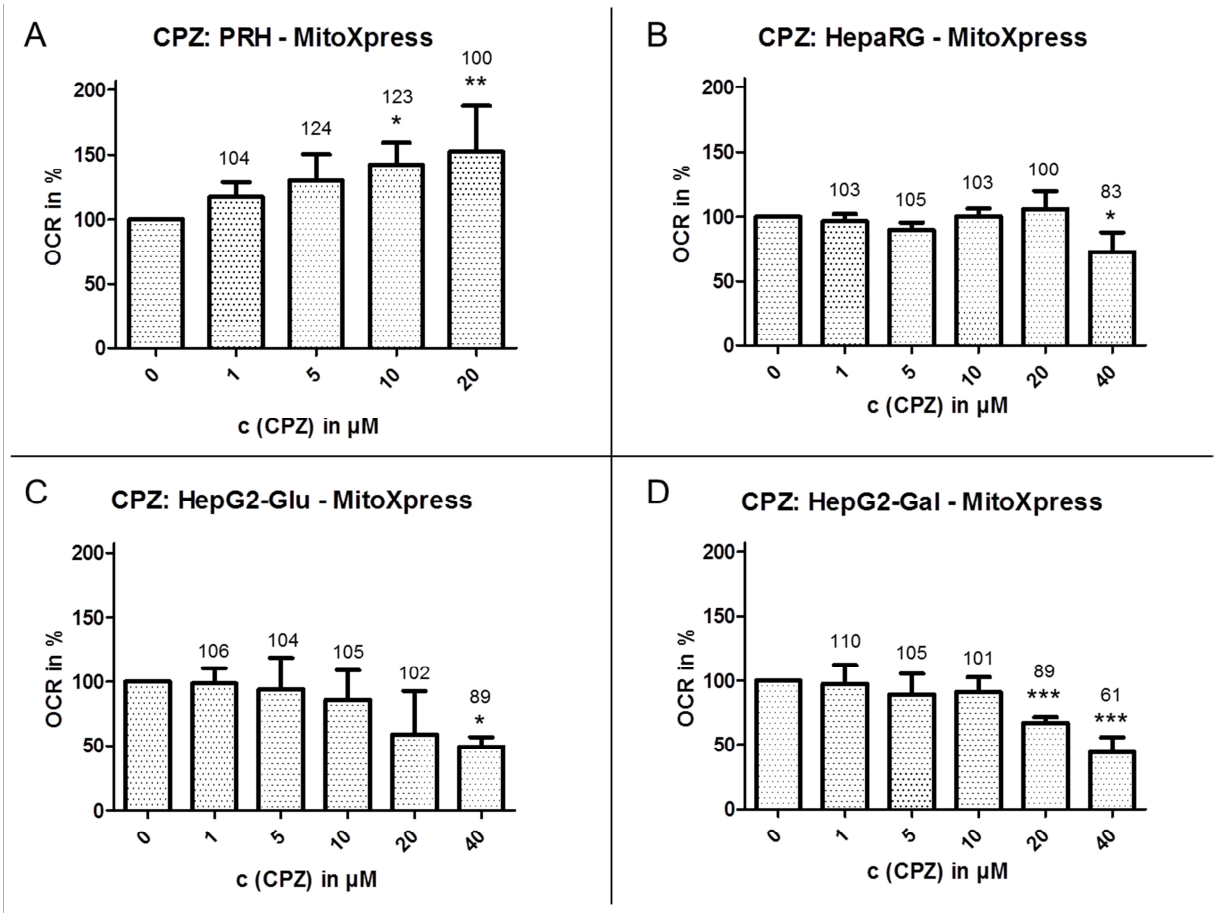

Figure 40. Oxygen consumption rate (OCR) in percent in the different hepatic systems (primary rat hepatocytes (PRH) (A), HepaRG (B), HepG2 cultured in regular glucose-containing medium (HepG2-Glu) (C) and HepG2 adapted to galactose-containing medium (HepG2-Gal) (D)) after treatment with different concentrations of chlorpromazine (CPZ). The percentages refer to the slope of the vehicle treated control, in relative fluorescence units per minute (RFU/min), set to 100%; corresponding to ~ 440 RFU/min in PRH, ~ 160 RFU/min in HepaRG, ~ 80 RFU/min in HepG2-Glu and ~ 140 RFU/min in HepG2-Gal. Values are given as mean of 3 biological replicates + standard deviation. Numbers above columns represent viabilities in percent taken from the 1 h ATP test. Statistical significance is expressed in p-value ≤ 0.05 (*), ≤ 0.01 (**) and ≤ 0.001 (***) and was calculated by one-way repeated-measures analysis of variance (ANOVA) of a treatment towards the vehicle control and application of the Dunnett's post test.

3.2.5.3 Seahorse MitoStress assay

The complete oxygen consumption rate profile of CPZ treated PRH is shown in Figure 41. As previously described for IBU, the lowest concentration (1 µM CPZ) did not change the respiratory profile compared to the vehicle treatment. After treatment with 100 µM CPZ, the oxygen consumption rate increased up to measurement 13. This observation was in accordance with the results of the *MitoXpress O_2-sensitive probe respiration assay* (Figure 40 A), where an increase in respiration was also observed in PRH. Furthermore, after addition of oligomycin, the inhibition of oxygen consumption via ATP synthesis was clearly affected. Here, the oxygen consumption rate was reduced to 100%, compared to ~ 60%. This finding indicated increased oxygen consumption via proton leak. However, a drug-induced elevation of proton leak was not reported in literature so far. The uncoupling with FCCP revealed a markedly reduced maximum respiratory capacity and thus the disruption of the electron transport chain by 100 µM CPZ. A

disrupted electron transport chain further helps explain the previously described elevated proton leak. Considering the oxygen consumption rate in the uncoupled state and the applied compound concentration, CPZ was the most potent drug.

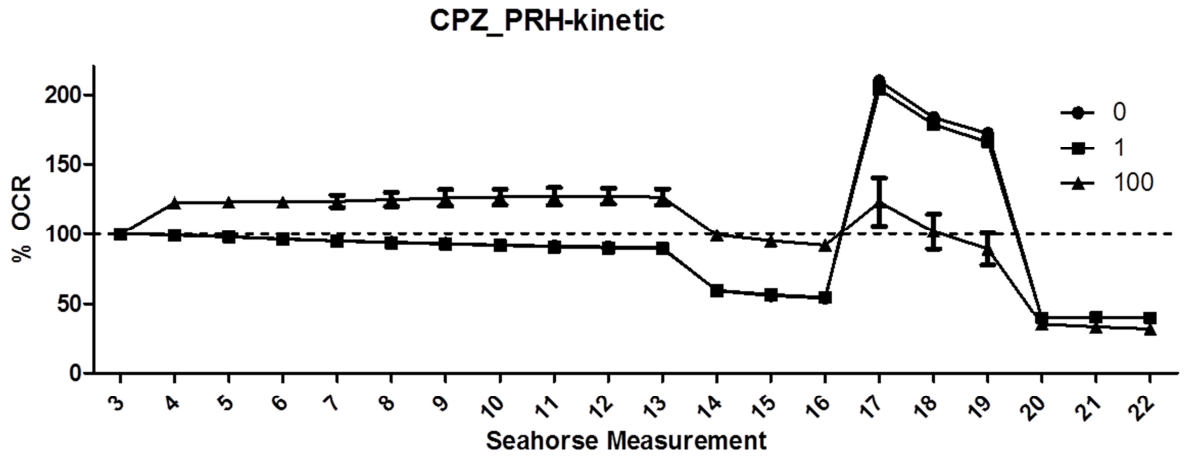

Figure 41. Oxygen consumption rate (OCR) in percent measured in primary rat hepatocytes (PRH) treated with chlorpromazine (CPZ) (1 and 100 µM) or DMSO vehicle control (0 µM) at the indicated Seahorse measurements ("3 min mix/3 min measure" cycles). The percentages refer to the basal (3rd measurement) OCR in pmol/min set to 100%; corresponding to ~ 150 pmol/min. Compound or DMSO was injected after the 3rd measurement, while 1 µM oligomycin, 0.6 µM carbonyl cyanide 4-(trifluoromethoxy)phenylhydrazone (FCCP) and 1 µM antimycin/ 1 µM rotenone were injected after measurement 13, 16 and 19, respectively. Values are given as mean of 3 biological replicates ± standard deviation.

The spare respiratory capacities after CPZ treatment in the different hepatic systems are shown in Figure 42. In summary, CPZ caused a significant reduction of the spare respiratory capacity in PRH at 80 µM to 53 ± 20% ($p \leq 0.05$) and 100 µM to 26 ± 14% ($p \leq 0.001$). As observed in the kinetic profile of the oxygen consumption rate (Figure 41), this reduction was attributed to an increased oxygen consumption rate in response to CPZ and a decreased maximum respiratory capacity, thus, confirming the adverse effect of CPZ on the mitochondrial function. A concentration-dependent decrease in spare respiratory capacity was also observed in HepaRG cells (138 ± 6% at 0 µM to 20 ± 23% at 100 µM), which, although not statistically significant, was considered biologically relevant. Generally, the statistical analysis for the HepaRG cells was not performable because only two biological replicates were valid. No relevant effects of CPZ were observed in HepG2-Glu or -Gal cells. This was very likely due to (i) the low spare respiratory capacity (low uncoupling rate) and (ii) the high variability between the biological replicates.

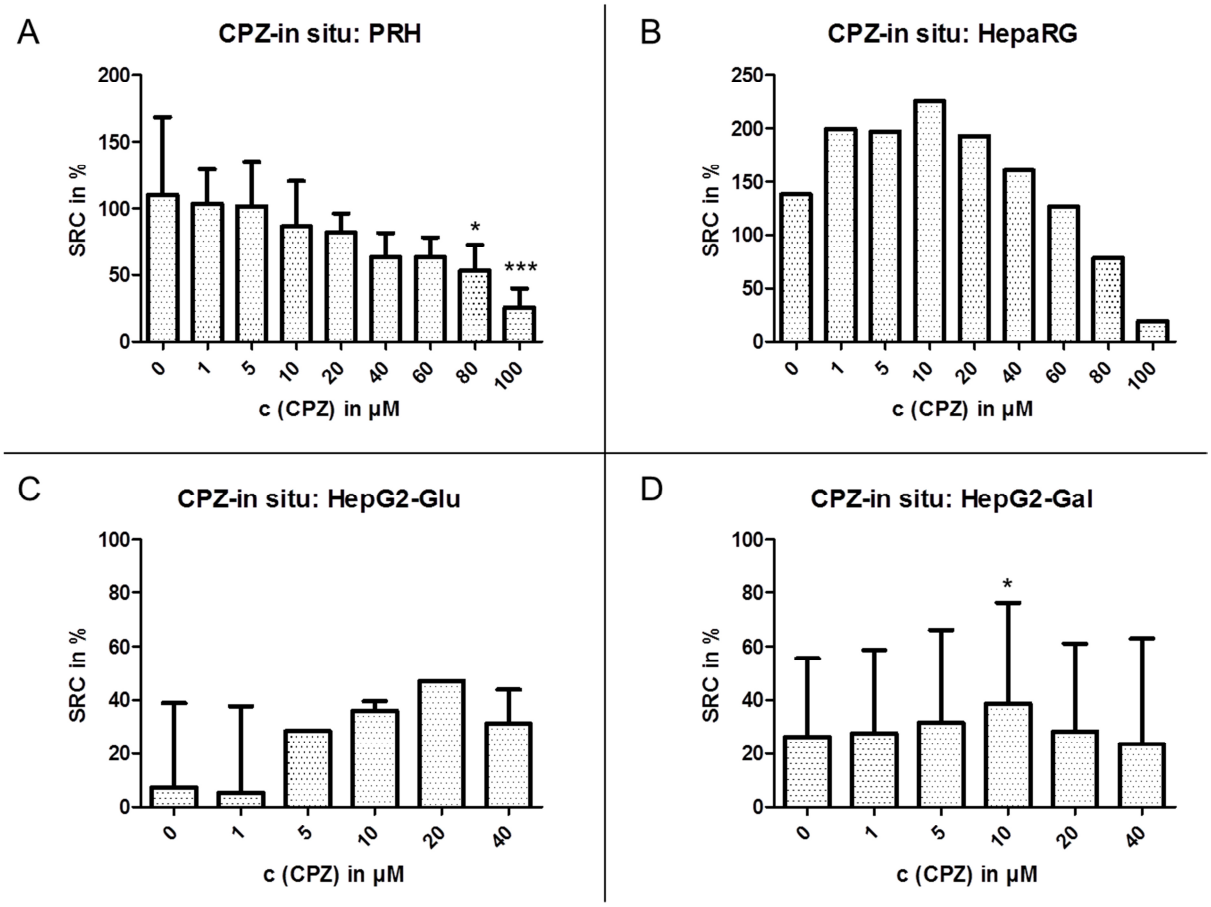

Figure 42. Spare respiratory capacity (SRC) in percent in the different hepatic systems (primary rat hepatocytes (PRH) (A), HepaRG (B), HepG2 cultured in regular glucose-containing medium (HepG2-Glu) (C) and HepG2 adapted to galactose-containing medium (HepG2-Gal) (D)) after *in situ* treatment with the indicated concentrations of chlorpromazine (CPZ). The raw data curves of the single biological replicates were normalised to the corresponding basal (3rd measurement) oxygen consumption rate in pmol/min set to 100%; corresponding to ~ 150 pmol/min in PRH, ~ 130 pmol/min in HepaRG, ~ 130 pmol/min in HepG2-Glu, ~ 100 pmol/min in HepG2-Gal. The percentages refer to the difference between basal (100%) and maximum (1st measurement after carbonyl cyanide 4-(trifluoromethoxy)phenylhydrazone (FCCP) injection) respiration. Values are given as mean of 2 (HepaRG) or 3 biological replicates + standard deviation. Statistical significance is expressed in p-value ≤ 0.05 (*), ≤ 0.01 (**) and ≤ 0.001 (***) and was calculated by one-way repeated-measures analysis of variance (ANOVA) of a treatment towards the vehicle control and application of the Dunnett's post test. A detailed description of the compound treatment and SRC calculation is given in the Materials and Methods.

3.3 Cyclosporine A

The immunosuppressant cyclosporine A (CsA) is one of the leading drugs in clinical use to prevent graft rejection after organ transplantation. The occurrences of toxic effects, associated with CsA, were recognised early on and include nephrotoxicity, hepatotoxicity, neuro- and cardiotoxicity (Rezzani et al., 2006). CsA-induced hepatotoxicity has been noted in 4 - 7% of cases of kidney, heart and liver transplantations (LTKB, 2014).

3.3.1 *In vitro* dose finding

The dose finding studies *in vitro* aimed to determine the TC_{10} which was used as the high treatment concentration for the biokinetics, transcriptomics and proteomics experiments in primary rat and human hepatocytes. Therefore cytotoxicity experiments were conducted at Merck Serono with PRH and at KaLy Cell with PHH.

There was a concentration- and time-dependent toxicity of CsA in PRH (Figure 43). Repeated exposure up to 14 days resulted in marked vacuole accumulation in the PRH at CsA concentrations as low as 1 µM. Thus 0.1 µM CsA was included in the third replicate (24-well plate screen). The dose finding in 6-well plates for 14 days was carried out with 0.1, 1 and 10 µM CsA. The lack of effect on cell viability can be explained by varying cell densities which result in higher ATP content in some wells (Figure 43 C). CsA is known to induce lipid accumulation *in vitro* at concentrations lower than cytotoxic concentrations (McMillian et al., 2001). In fact, after 14 days treatment with up to 10 µM the viability was not affected, although detrimental morphological changes were observed. Here, a treatment concentration lower than the envisaged TC_{10} was selected based on the consideration of the morphology. When taking the long-term cytotoxicity results and the morphological findings into account, the high concentration for the final experiment with CsA was set at 2.5 µM and the low concentration was set at 0.25 µM. The cytotoxicity of CsA is linked to the generation of ROS, since antioxidants were shown to reduce its cytotoxic potential (deArriba et al., 2013; Jennings et al., 2007; Rezzani, 2006). This hypothesis appears plausible since CsA is known to impair mitochondrial function. The time-dependent cytotoxicity can also be linked to the accumulation of the compound within the cells. With a log K_{OW} of 4.3 (Lucangioli et al., 2003), the cyclic undecapeptide can be considered lipophilic and able to associate with cellular lipids; hence, increasing the concentration the cells were exposed to (see CsA biokinetics section 3.3.2).

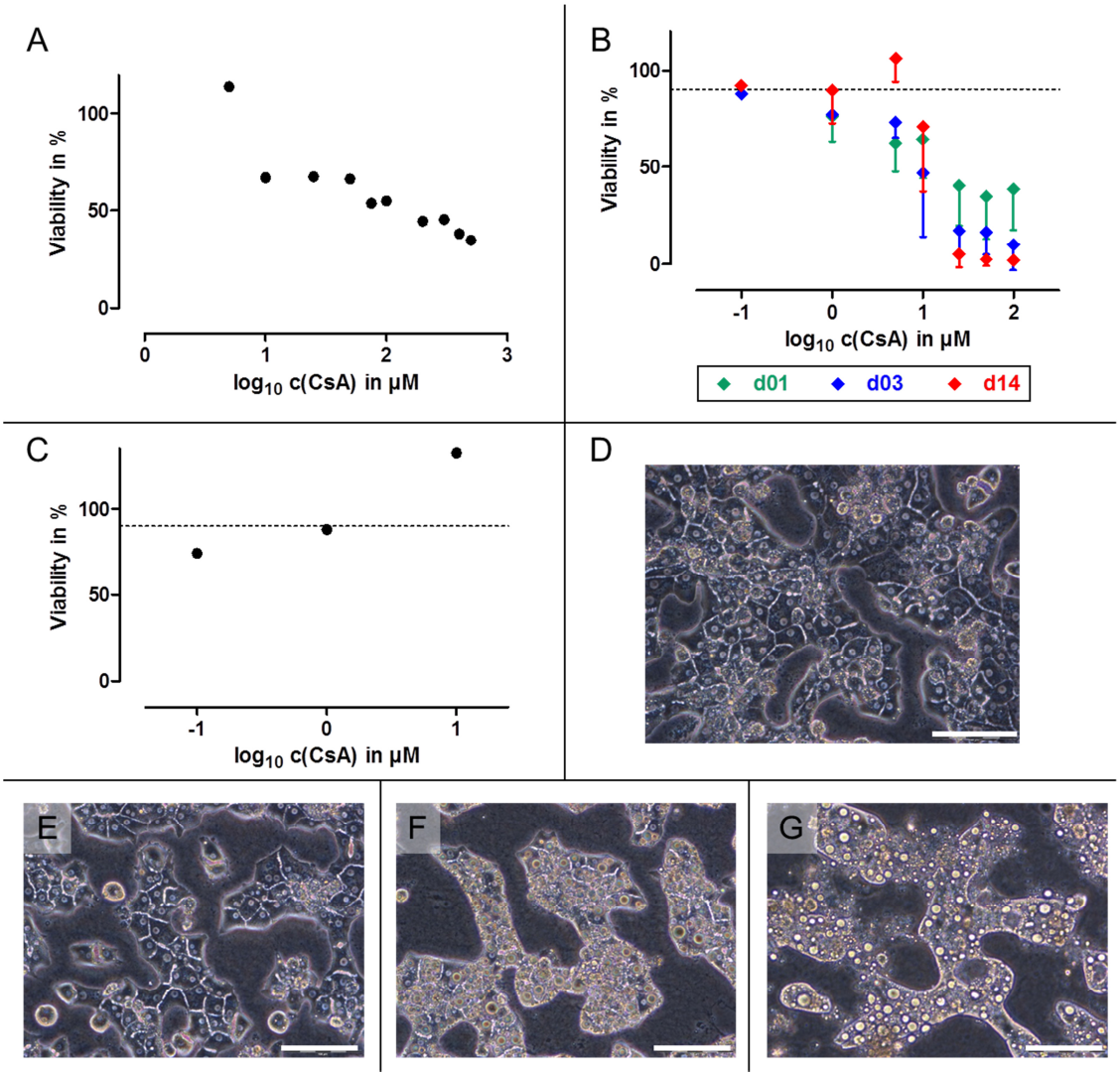

Figure 43. Cell viability results of primary rat hepatocytes (PRH) treated with cyclosporine A (CsA) in 96-well mono layer for 24 h (A), 24-well sandwich (SW) for 1 (green), 3 (blue) and 14 days (red) (B) or 6-well SW culture for 14 days (C) at the indicated concentrations. Results of the 24-well SW culture derived from 3 biological replicates, except for the lowest concentration (1 replicate), and are displayed as mean - standard deviation (B). Viability (measured using ATP content) was expressed as the percent relative the corresponding time matched DMSO control. The dotted line shows the 90% viability threshold (B and C). Pictures of PRH in 6-well SW culture on day 14 after daily treatment with DMSO (D) or CsA at 0.1 µM (E), 1 µM (F) or 10 µM (G). The white scale bar on the bottom right of each picture corresponds to 100 µm.

In PHH, CsA-induced cytotoxicity was most pronounced after repeated treatment for up to 14 days. The long-term exposure to 10 µM decreased the viability to 73% (KaLy-Cell (Parmentier), personal communication).

For the final experiments the TC_{10} (high concentration) was set to 7 µM. The human C_{max} is reported to be between 0.4 and 0.9 µM (Ducharme et al., 1995; Grant et al., 1999; Mueller et al., 1994). Table 32 summarises the treatment concentration of CsA applied in the final experiments.

Table 32. Treatment concentration of cyclosporine A (CsA) for final experiments in primary rat (PRH) and human hepatocytes (PHH). High (HC) and corresponding low concentration (LC).

	CsA concentration in µM	
	HC	**LC**
PRH	2.5	0.25
PHH	7	0.7

The PHH were less sensitive compared to PRH, when treated for short periods (1 and 3 days) with identical CsA concentrations. This finding can be attributed to a more efficient CsA biotransformation in PHH. The rat does not represent a good model for the human situation with respect to CYP3A, especially considering the high variation in response to inducers and substrate specificity between these species (Martignoni et al., 2006; Zuber et al., 2002). CsA is reported as substrate of human CYP3A, while inhibiting isoforms of CYP2C, CYP2D6 and CYP3A4 (Drugbank - Cyclosporine, 2013). The biotransformation of CsA is considered to be a detoxifying process because inhibition of CsA metabolism results in an increased toxicity (Rezzani, 2004). Furthermore, the ability to increase protective GSH levels needs to be considered. For example, long-term (4 weeks) treatment with high dose CsA resulted in the adaptive elevation of GSH in rat livers (Mueller et al., 1992).

3.3.2 Biokinetics

After assessment of the treatment concentrations, it was worth monitoring the bioavailability of CsA in the experimental setup. The concentration of the compound was determined in cell lysates and supernatants as a function of time. Based on existing literature (Schmelzer et al., 2006), the specific sampling time points of the first biological replicate for CsA biokinetic profiling were set to 1, 2, 4, 8 and 24 h. However, these time points showed only weak effects in the biokinetic profile (Appendix 7, Figure 58). The deviation from the reported time points was mainly attributed to the different culture conditions. In comparison to a nominal cell seeding density of 1559 cells/mm², Schmelzer et al. (2006) applied much lower cell densities (707 cells/mm²). We have shown previously that subconfluent PRH cultures sustain a loss in metabolic activity of important DMEs (own unpublished data). In addition, the use of PRH from female rats and a different rat strain could further contribute to the observed variations.

For the second and third biological replicates, the time points were adjusted to 2 min, 30 min, 1 h, 3 h and 24 h. In Figure 44, results of the overlapping time points from the first biological replicate, namely 1 h and 24 h were considered in the calculation of the mean.

The biokinetic profiling of CsA treated PRH cultures showed that this compound was very rapidly taken up by cells, independent of the concentration applied (Figure 44 A and D). This finding suggested that the compound enters the cell mainly via passive transport. After repeated exposure, accumulation of CsA in the cell lysates was observed, which was more pronounced

with high concentration treatment. The microscopic observations revealed a marked accumulation of vacuoles, especially after long-term exposure of the PRH. McMillian et al. (2001) showed that vacuoles, accumulating after CsA treatment, contain neutral lipids. These biokinetic studies supported the hypothesis that these vacuoles contained parent compound. In the calculations of the relative distribution (Figure 44 C and F), the sum of the extracted CsA amount (cell lysate plus supernatant) always exceeded the actual CsA added. This observation was most striking after repeated treatment with 2.5 µM CsA, indicating an intracellular accumulation of the parent compound. By contrast, PHH did not show a disturbed morphology after CsA treatment, despite higher concentrations being used. With respect to this finding, vacuole formation in PRH was very likely due to an inefficient biotransformation in these cells compared to that in PHH. In addition, the sequestration of CsA in intracellular vacuoles further impeded the metabolism of CsA by preventing it from contact with CYPs. CsA is metabolised by rat Cyp3a1/2 (Brunner et al., 1998) which was inducible and functional in these cells (Appendix 2, Table 43 - Table 45 and Appendix 3, Table 46, respectively). The presence of basal enzyme functions did not explain the observed accumulation. However, it is reported that CsA impairs its own metabolism in the rat by suppression of hepatic Cyp3a in a time- and dose-dependent manner (Brunner et al., 2000). Thus, the *in vitro* data confirmed the observation made *in vivo*. A hepatocellular fat accumulation *in vitro* often serves as surrogate marker for steatosis-inducing agents (Gomez-Lechon et al., 2007; McMillian et al., 2001). However, this observation can be misleading. Here, CsA-mediated steatosis was suggested to be an *in vitro* artefact, as it is not observed *in vivo*. A potential explanation for this *in vitro-in vivo* discrepancy was the lack of extra-hepatic metabolism in this *in vitro* setting. Especially when taken orally, the expression and activity pattern of enzymes in the small intestine should be considered. For example, CYP3A activity and ABCB1 (P-glycoprotein) efflux has been shown to play an important role for CsA. In intestinal enterocytes, CsA is repeatedly pumped into the intestinal lumen by P-glycoprotein (Hebert, 1997) and consequently, this results in the multiple exposure of CsA to CYP3A, which metabolises it.

In sum, the biokinetic analysis revealed the CsA amount the cells were actually exposed to. The low concentration resulted in a mean exposure of PRH lysates to ~ 0.3 nmol (60% of added CsA amount) on day 0 or ~ 0.5 nmol (100%) on day 13. After high concentration treatment PRH were exposed to ~ 1.9 nmol (50%) or ~ 10 nmol (320%), respectively. The binding of CsA to collagen I in the PRH cultures was negligible, although increased after long-term exposure (Appendix 6, Table 51). Therefore, concentration- and time-dependent increase of CsA recovered in the cell lysate fraction could be attributed to the intracellular accumulation as described above.

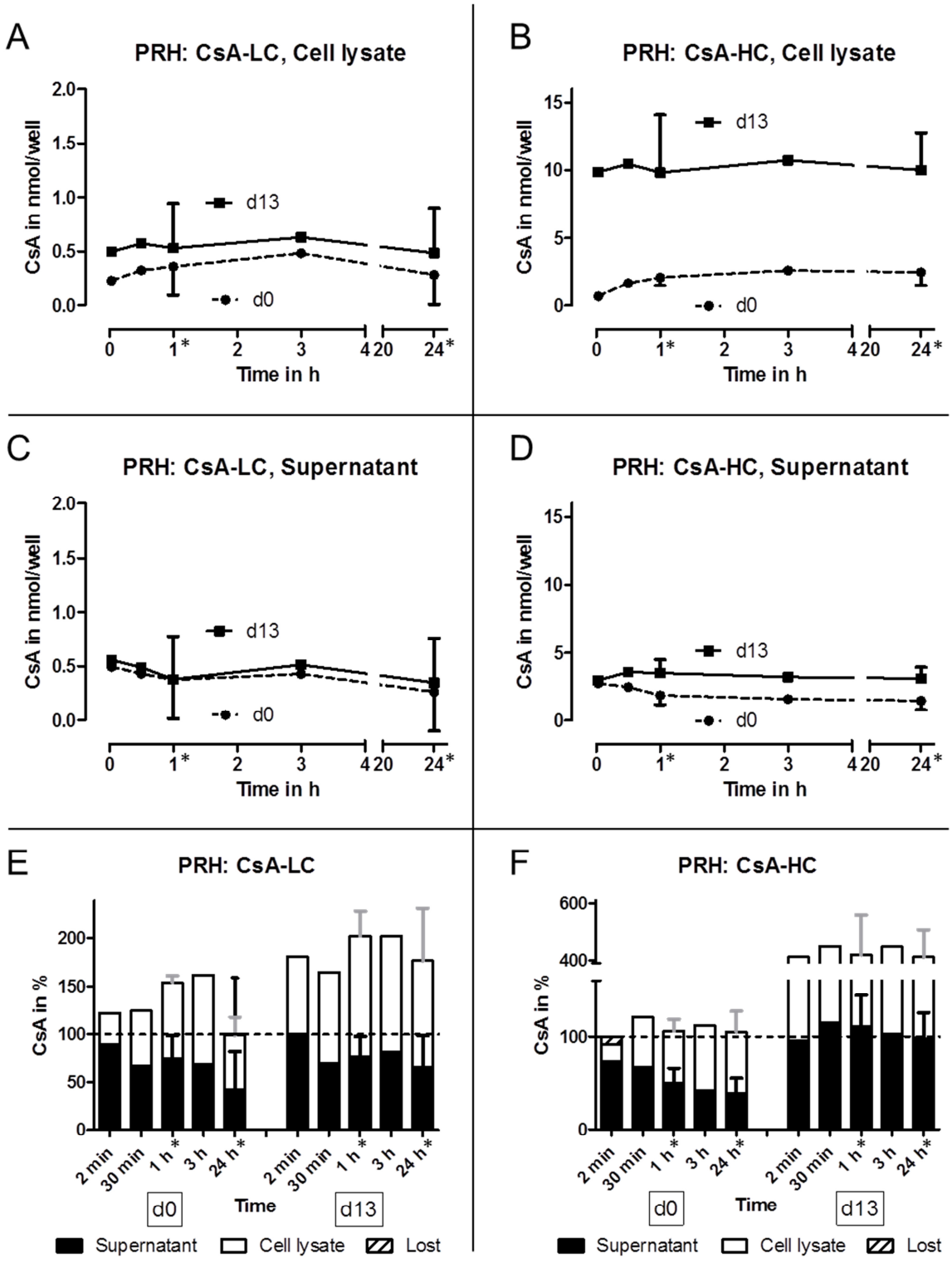

Figure 44. Kinetic profile of cyclosporine A (CsA) (nmol/well) in primary rat hepatocytes (PRH) (A, B) and culture supernatants (C, D) after single (day 0 – dashed line) and repeated (day 13 – solid line) treatment with 0.25 µM (low concentration (LC); A, C) and 2.5 µM (high concentration (HC); B, D) CsA at the indicated time points. Relative distribution of CsA in percent in the different analysed PRH fractions at the indicated time points on day 0 and 13, supernatant (squared) and cell lysate (blank) as well as the apparent loss (striped) for the LC (E) and HC (F). Values are given as mean of 2 or 3 (*) biological replicates +/- standard deviation.

A rapid and progressive CsA uptake in the PHH was followed by a drop at 24 h on day 0 at both concentrations. This indicated an efficient biotransformation of the parent compound. CYP3A4 and CYP3A5 are the most abundant CYP isoforms in human liver (Martignoni et al., 2006) and

both are known to metabolise CsA. Basal CYP3A4/5 activities varied between PHH from the 3 donors (Donor 1: low activity, Donor 2: high activity, Donor 3: no peak; see Appendix 4, Table 47). In fact, PHH from Donor 2 had the lowest amount of CsA in cell lysates and supernatants after 24 h (both concentrations, day 0; data not shown). This effect was not observed after repeated treatment, which was very likely due to the inhibitory effect of CsA on CYP3A protein levels and activity (Amundsen et al., 2012; deJonge et al., 2011). Interestingly, CYP3A4/5 activity did not seem to affect the biokinetic profile of the different donors. The continuous decrease in the supernatant fractions suggested an efficient metabolism of CsA. In contrast to the cell lysates, the decrease in amount of CsA in the supernatants was evident also after repeated treatment for 14 days. The apparent steady-state in the cell lysate fractions was apparently due to enrichment in the Geltrex™ (extra cellular matrix). In order to determine the amount of compound bound to the extra cellular matrix molecules, so-called “blank studies” were conducted. In these studies, Geltrex™ in the absence of PHH was treated in the same way as the PHH cultures. After repeated treatment, an accumulation of CsA in the extra cellular matrix fraction was observed. Despite this non-specific effect of the matrix, a high inter-donor variation was observed in the decrease of CsA concentrations, which were also not fully attributable to the CYP3A activities in these cells. A higher number of human donors is therefore required for a more comprehensive understanding of CsA’s biokinetic profile in PHH. Finally, the relative distribution of the low concentration samples (Figure 45 C) showed a very high fluctuation, which could not entirely be attributed to inter-donor variability. A further explanation for this observation could be due to the handling procedure, e.g. pipetting errors. Furthermore, contact to plastic materials should be kept to a minimum because CsA is known to bind to plastic. Consequently, any variation in the sampling process (e.g. frequency of transferring solutions from one vessel to the other) might influence the CsA recovery during the analytical process.

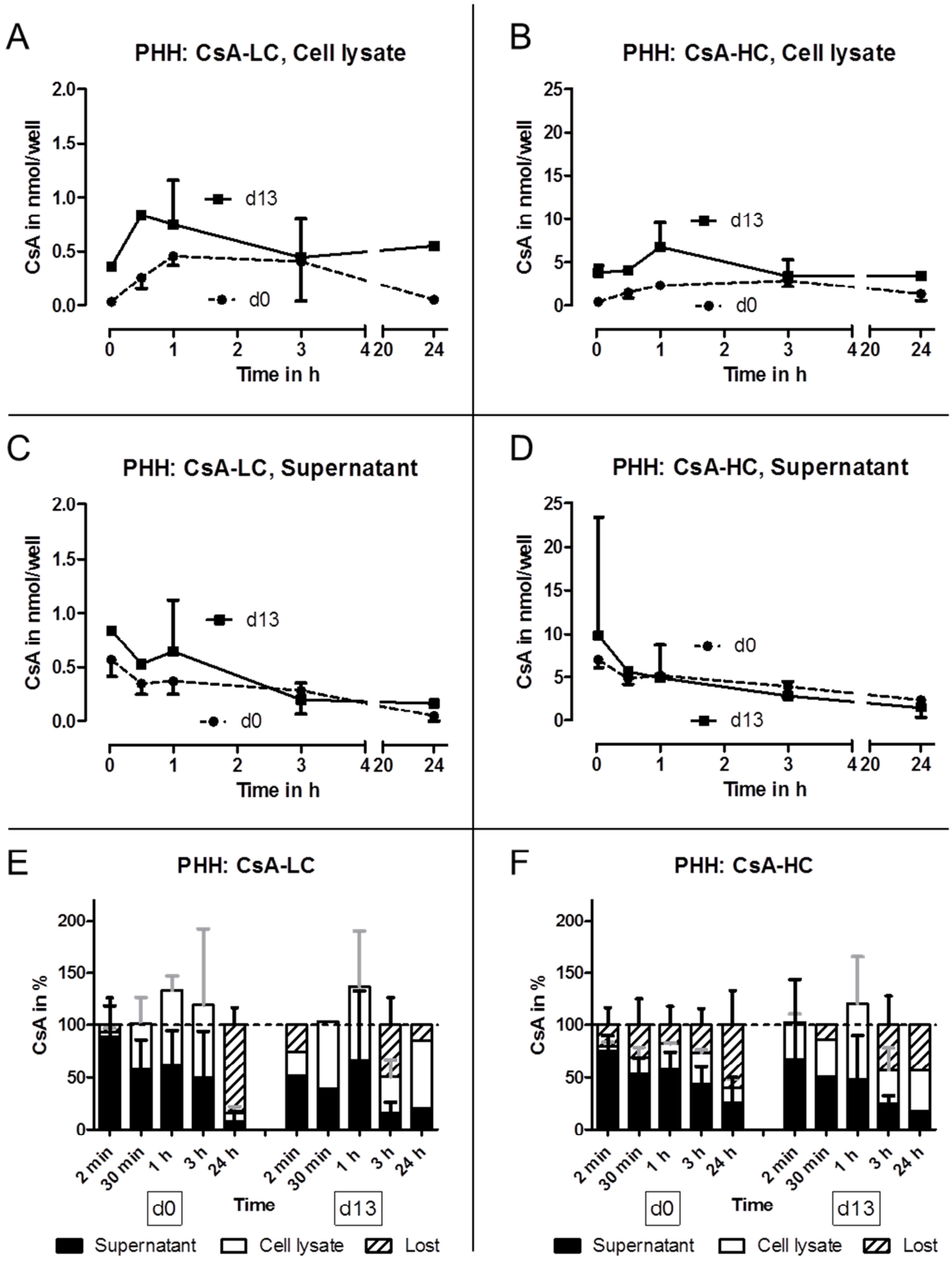

Figure 45. Kinetic profile of cyclosporine A (CsA) (nmol/well) in primary human hepatocytes (PHH) (A, B) and culture supernatants (C, D) after single (day 0 – dashed line) and repeated (day 13 – solid line) treatment with 0.7 µM (low concentration (LC); A, C) and 7 µM (high concentration (HC); B, D) CsA at the indicated time points. Relative distribution of CsA in percent in the different analysed PHH fractions at the indicated time points on day 0 and 13, supernatant (bold) and cell lysate (blank) as well as the apparent loss (striped) for the LC (E) and HC (F). Values are given as mean of 3 biological replicates +/- standard deviation.

A comparison of the two species revealed a more efficient metabolism of CsA in PHH. This is in line with *in vivo* studies, in which the rat is reported to be a poor model for drugs that are metabolised by human CYP3A4 (Martignoni et al., 2006; Zuber et al., 2002). In both hepatic

systems the basal activities of the corresponding CYPs could not be linked to the biokinetic profiles. It was assumed that the weak metabolism of CsA in PRH and thus its accumulation, led to a higher concentration in the cell lysates. This observation was most pronounced after long-term treatment with 2.5 µM CsA (high concentration). Here, recovered CsA in PRH exceeded that in PHH, although the PHH were treated with a 3-fold higher concentration. An accumulation of CsA, i.e. increased exposure, can be linked to an elevated cytotoxicity, since CsA metabolism is considered to be detoxifying. In line with this, as reported previously, a higher cytotoxicity was observed in PRH. The analytical verification of the CsA treatment concentrations in the applied medium at 0 min was considered important. Here, the low concentration for PRH and PHH were determined to be 0.3 and 0.5 µM (nominally 0.25 and 0.7 µM), respectively. Notably, both concentrations were close to or within the human C_{max} range (0.4 and 0.9 µM), reported in literature (Ducharme et al., 1995; Grant et al., 1999; Mueller et al., 1994). The high concentration treatment media at 0 min for PRH and PHH was 2.3 and 5.2 µM, respectively; hence, close to the nominal concentrations (TC_{10}) of 2.5 and 7 µM. Considering the therapeutic target trough CsA level of 0.29 µM (Grant et al., 1999) almost all incubation media exceeded the target therapeutic plasma concentration.

3.3.3 Transcriptomics

The analysis of the gene expression profiles derived from CsA treated primary rat and human hepatocytes aimed the discovery of information on underlying mechanisms of toxicity. Based on the CsA data, in PRH a total of 23 and 65 significantly deregulated genes overlapped with genes from IBU and CPZ, respectively. Notably, a greater accordance in the direction of the CsA-related gene deregulation was observed with CPZ. After CsA treatment, the genes involved in fatty acid and lipid metabolism again showed a different pattern compared to the other two compounds and were mainly down-regulated (29 out of 34 genes). This is in accordance with the literature, where CsA is reported to inhibit enzymes of the fatty acid oxidation (Illsinger et al., 2011). Most of the up-regulated genes play a role in lipid metabolism, including PPAR responsive genes (*Vldlr*, *G0s1* and *Acot1*). *Acot1* was up-regulated by 8.1-fold, but not before day 14. The typical genes, indicating the onset of peroxisome proliferation (*Acot1*, *Acox*, *Cyp4a1*) were not all up-regulated, as previously seen for CPZ. All genes involved in bile acid metabolism were down-regulated. In fact, CsA is known to induce cholestasis (Chan and Shaffer, 1997). This pathology mainly develops as a result of a decrease in bile salt secretion via competitive inhibition of bile salt export pump (BSEP). The endogenous BSEP substrates (conjugated bile salts) accumulate and induce adverse effects within the cell. The genes involved in bile acid synthesis (*Cyp7a1*, *Cyp8b1*, *Akr1d1*) and bile salt uptake transporter *Slc10a1* were down-regulated. This observation resembles a hepatoprotective response to accumulating cytotoxic bile salts. Nearly all genes playing a role in xenobiotic metabolism were down-

regulated after exposure to CsA. A possible explanation for this finding could be an impaired bile homeostasis. It is reported that bile acid and drug metabolism are closely linked (Li and Chiang, 2013; Wagner et al., 2009). Oxidative stress is thought to be the main mechanism of CsA-induced cytotoxicity (deArriba et al., 2013; Mostafavi-Pour et al., 2013). The ROS and lipid peroxidation products lower the concentration of protective GSH. Here, *G6pdx*, which is involved in the regeneration of intracellular GSH levels, was up-regulated at all time points (Figure 46). Interestingly, this gene was highest up-regulated (an increase of 8.2-fold) on day 3, suggesting an acute response.

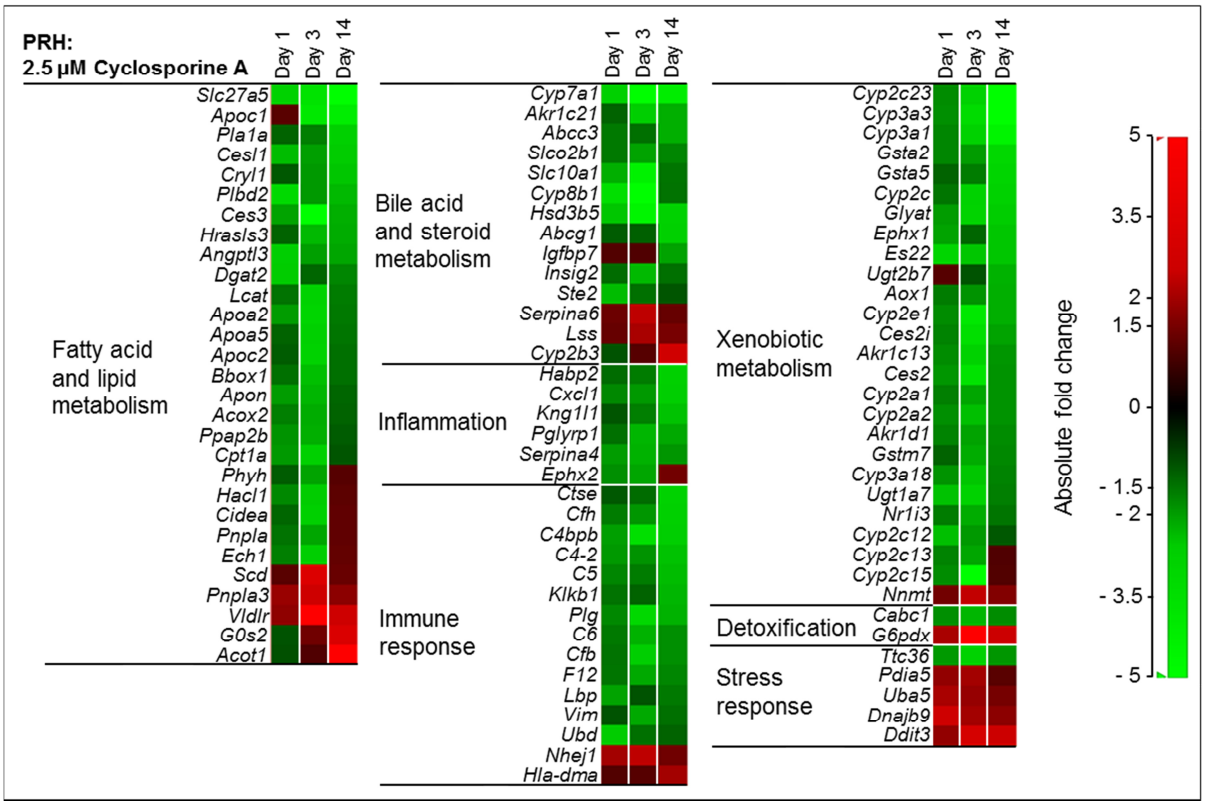

Figure 46. Gene function profile display of significantly deregulated genes in primary rat hepatocytes (PRH) after treatment with 2.5 µM cyclosporine A for 1, 3 or 14 days. The heatmap shows 98 genes involved in fatty acid and lipid metabolism, bile acid and steroid metabolism, inflammation, immune response, xenobiotic metabolism, detoxification and stress response identified to be deregulated by at least 2-fold compared to the time-matched vehicle treated control. The statistical significance (BH q-value ≤ 0.05) by a linear model and absolute fold changes were calculated using the statistical analysis software Genedata Analyst™ version 7.5, the detailed data analysis is given in the Materials and Methods section. The colour scale shows increased fold changes in red and decreased fold changes in green. Genes are sorted according to their fold change value on day 14 (from decreased to increased fold changes) within the corresponding pathway. Absolute fold change values and gene acronyms are given in the appendix.

The pharmacological effect of CsA is to down-regulate the immune system via inhibition of T-cell activation (Reynolds and Al-Daraji, 2002; Schreiber and Crabtree, 1992). Here, the expression of the majority of the genes involved in inflammation and immune response were decreased (Figure 46). Carcinogenicity studies in mice revealed a carcinogenic potential for CsA (Beems, 2002; NTP - 12th RoC, 2011). In the PRH dataset, many genes involved in the regulation of apoptosis, proliferation and transcription were deregulated. Only a few genes could

be directly attributed to cancer and the deregulation of the tumour suppressor genes was inconsistent. *Txnip*, *Egr1* and *Rarres1* were down-regulated, while *Prkcdbp* and *Armcx3* were up-regulated. Taken together, the transcriptomics results in PRH indicate the onset of pathways linked to cell regeneration and stress responses which were likely due to regular, treatment-induced cell damage; hence, suggesting that CsA cannot be considered as a primary carcinogen.

The IPA® software was used for hypotheses generation using transcriptomics results derived from PHH treated with AMI. In PHH from Donors 1 and 2, there was a time- and concentration-dependent amount of deregulated genes in the various pathways in IPA®. By contrast, PHH from Donor 3 had the highest number of deregulated genes on day 1 after treatment with 0.7 µM CsA (low concentration). This high variation could be associated to the basal CYP activities in the PHH from the different donors. CYP3A4 is the dominant CYP3A isoform responsible for CsA metabolism, with minor and donor-specific contribution from CYP3A5. The expression of *CYP3A5* varies between individuals and only some express significantly high levels (Staatz et al., 2010). In the PHH from the different donors, *CYP3A5* was expressed at marginally higher levels in PHH from Donor 2 than in PHH from the Donors 1 and 3 (only vehicle treated controls were considered). Hence, the consideration of the *CYP3A5* expression in PHH from the different donors did not help explain the observed transcriptomics results. *Liver Hyperplasia/Hyperproliferation* and *Hepatocellular Carcinoma* were the top tox functions, suggesting a carcinogenic potential for CsA. However, any conclusion on this pathology should be drawn with caution and the caveats of the applied IPA® software need to be considered. Many genes in the *Liver Hyperplasia/Hyperproliferation* and *Hepatocellular Carcinoma* classification cluster are not directly linked to cancer. In fact, a detailed analysis of the genes in both tox functions revealed that the majority were attributed to pathways that indicate general perturbations of cellular functions (namely, fatty acid and lipid metabolism, bile salt metabolism, carbohydrate metabolism, inflammation and immune response, xenobiotic metabolism and stress response). Furthermore, genes that could be linked to cancer were also involved in apoptosis and regeneration. CsA is considered to be a non-genotoxic human carcinogen (NTP - 12th RoC, 2011), but tumour development in patients is reported only after long-term treatment with CsA and is most likely linked to the immunosuppressive effect (Ryffel et al., 1992). This secondary carcinogenic effect was very unlikely picked up by the applied hepatic model; thus, supporting the approach to manually evaluate the genes classified via IPA®. In accordance with the pharmacological action of CsA, genes involved in inflammation and the immune response were down-regulated (Figure 47). The inhibition of calcineurin by CsA results in the transcriptional down-regulation of several cytokines (Staatz et al., 2010). In PHH from all donors, chemokine (chemotactic cytokines) expression was decreased (e.g. *CXCL6*, *CXCL10*, *CCL2*). After exposure to CsA, the mRNA expression of *CCL5* and *CCL8* was decreased in human primary bronchoalveolar cells (Sekerova et al., 2003) and graft-versus-host disease mouse model (Hori et al., 2008), respectively. Whereas *CCL5* was down-regulated only in PHH from Donor 1, the

expression of *CCL8* was decreased in PHH from Donors 1 and 3. This finding ultimately reflects the susceptibility of the different donors.

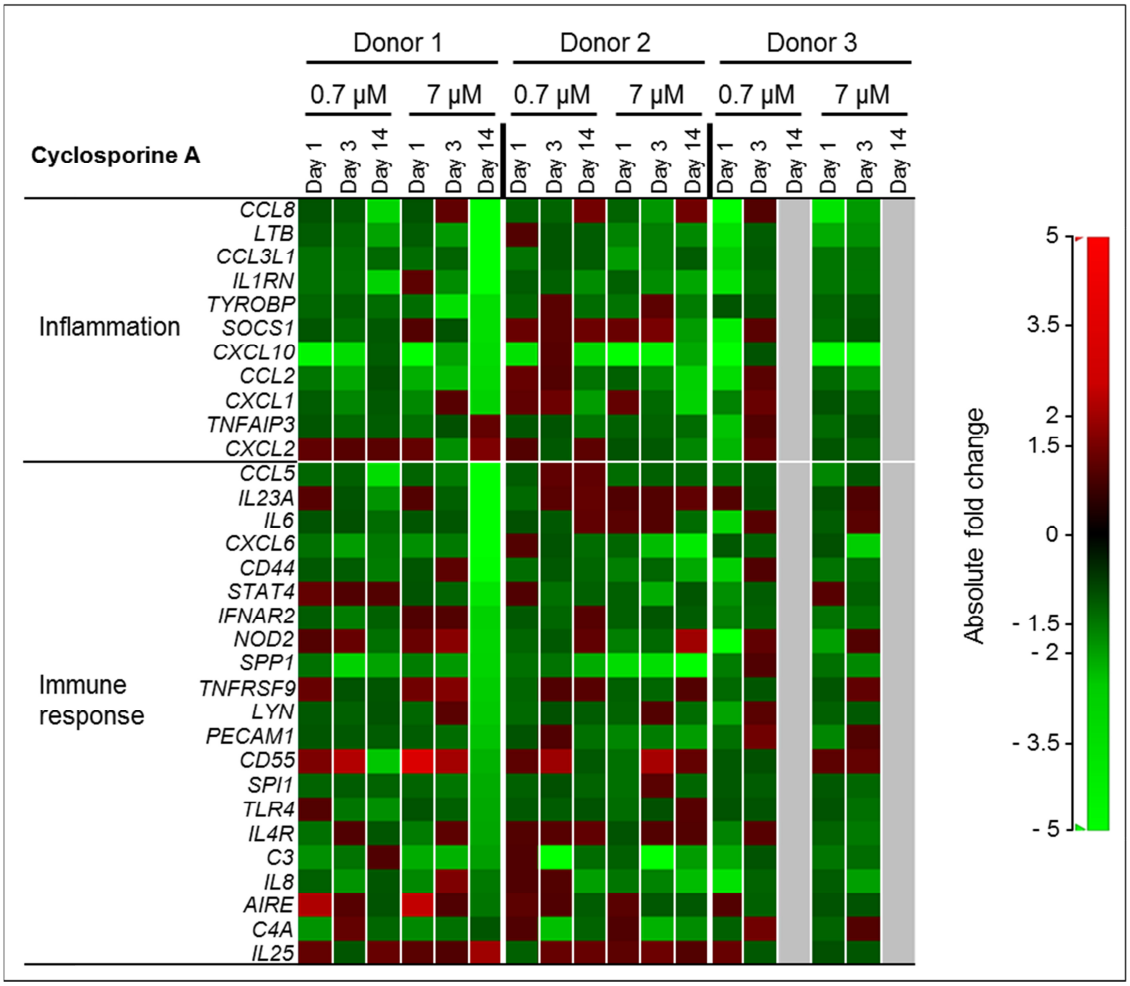

Figure 47. Gene function profile display of significantly deregulated genes in primary human hepatocytes from different donors after treatment with 0.7 µM and 7 µM cyclosporine A for 1, 3 or 14 days. The heatmap shows 32 genes involved in inflammation and immune response identified to be deregulated by at least 2-fold compared to the time-matched vehicle treated control. The absolute fold change was calculated using the statistical analysis software Genedata Analyst™ version 7.5, the detailed data analysis is given in the Materials and Methods section. The colour scale shows increased fold changes in red and decreased fold changes in green. Absolute fold change values and gene acronyms are given in the appendix.

Overall, PHH from Donor 2 appeared to be the least sensitive to CsA-mediated adverse gene expression changes. Since Donor 2 was the only donor with reported medications, the decreased susceptibility of the PHH from this donor could be linked to the medications taken by this donor, namely *atenolol*, *kardegic*, *inspra*, *rasilez* and *ramipril*. CsA is transported out of the cell via the canalicular bile salt transporter, ABCB1, and is reported to competitively inhibit this transporter (Broccatelli et al., 2011; Watkins, 1997). The drugs *atenolol* and *kardegic* (acetylsalicylic acid) are substrates of ABCB1 and thus competitive inhibitors. A sustained inhibition of ABCB1 in PHHs would result in an augmented intracellular CsA concentration and hence higher cytotoxicity. However, it can be assumed that inhibition of the transporter did not persist in absence of the drugs, i.e. in culture. Furthermore, the mineralocorticoid receptor antagonist

inspra (eplerenone) and renin inhibitor *rasilez (*aliskiren) are both CYP3A substrates and both reported to induce the corresponding CYP3A isoforms (including CsA-metabolising 3A4 and 5). Consequently, considering a sustained induction, CsA was more efficiently metabolised in the PHH from Donor 2. This more rapid detoxification of the drug could help explain the decreased sensitivity of PHH from Donor 2. Cook et al. (2002) concluded that eplerenone does not inhibit the metabolism of other CYP3A substrates. Furthermore, a single dose of aliskiren did not alter the pharmacokinetics of CsA *in vivo* (Rebello et al., 2011), whereas mRNA induction might require repeated exposure. Unfortunately, the treatment duration of the various medications was not reported. Finally, the effects of *ramipril* on cellular metabolism were not considered relevant for CsA biotransformation.

A comparison of the gene expression profiles of the two species revealed very similar adverse effects after CsA treatment. For example, the genes involved in the inflammation and immune response pathways were down-regulated in both hepatic systems. This effect reflects the primary pharmacology of CsA. Furthermore, many deregulated genes in PRH and PHH cultures were linked to regeneration and stress response. With a concentration of 2.3 µM in PRH and 5.2 µM in PHH, the real (as determined in the biokinetics experiment) high concentration exceeded by far the reported human C_{max} (~ 0.41 - 0.75 µM) (Grant et al., 1999). The biokinetics studies revealed that repeated treatment increased the exposure further. However, the intracellular accumulation of neutral lipids and thus of the drug is thought to be an *in vitro* artefact, since no signs of steatosis are reported *in vivo*. From a toxicological point of view, these findings suggest a large safety margin between the applied *in vitro* and the reported *in vivo* concentrations, even without consideration of the elevated intracellular concentration after repeated exposure.

3.3.4 Proteomics

Next, proteomic profiling was included to complement the transcriptomics data and facilitate the identification of potential biomarkers. On the basis of the proteomics data, not many proteins were changed in PRH after treatment with CsA (35 distinct proteins in total). The lipid metabolism pathway comprised of 5 proteins and none overlapped with the gene expression dataset. However, these proteins were mainly decreased (compared to the time-matched vehicle control), which was in accordance with the gene deregulations. The protein acyl-CoA-binding domain-containing protein 5 was increased. It functions in transport and distribution of long-chain acyl-CoA and thus in lipid catabolism. There was a lower level of the fatty acid synthase and, taken together, these findings contribute to the impaired fatty acid oxidation after CsA treatment. Proteins involved in the organisation of the extra cellular matrix were mainly increased. CsA has been linked to accumulation of extra cellular matrix components, resulting in gingival overgrowth (Vertemati et al., 2009). The abundance pattern of proteins involved in transcription regulation and apoptosis was incomplete over the time- and concentration-scale.

Hence, no clear conclusion could be drawn from the few proteins that were changed. Here, only 1 protein overlapped with the gene expression data, namely aldehyde oxidase (gene symbol: *Aox1*). This was the only protein related to xenobiotic metabolism which was decreased by 5-fold after 14 days of treatment with 2.5 µM CsA. This was in accordance with the down-regulation at the mRNA level, whereas the gene was down-regulated by only 2.2-fold (on day 14). Unfortunately, data on protein abundance for day 1 and 3 were lacking; hence, it cannot be concluded if aldehyde oxidase alteration was quicker at the protein level compared to the gene expression. To summarise, it was not possible to obtain a comprehensive picture of the CsA-derived adverse effects in PRH due to (i) the low number of changed proteins, (ii) inconsistent protein production levels over the various time points and (iii) lacking values over the entire dataset.

3.3.5 Mitochondrial toxicity

Finally, the potential of CsA to induce mitochondrial toxicity was assessed in functional assays. Cellular injury upon mitochondria-derived ROS generation is proposed to play a central role in CsA-mediated cytotoxicity.

3.3.5.1 ATP level for detection of mitochondrial toxicity

CsA was not cytotoxic to any of the hepatic cell systems tested (Figure 48) and the viabilities ranged from 83 - 110%, over the concentration range. CsA is known to affect mitochondrial respiration via a number of ways. Illsinger et al. (2011) showed that respiratory complex I, III, IV and V were impaired after 48 h treatment of endothelial cells. Furthermore, CsA is a known inhibitor of stress induced mitochondrial permeability transition, leading to cell death (Kim et al., 2003). In renal tubular cells, deArriba et al. (2013) reported that CsA induced mitochondrial fission. An indirect effect on mitochondrial respiration is the ability of CsA to competitively inhibit the transporter, BSEP. This results in the intracellular accumulation of toxic bile salts that deplete the mitochondrial membrane potential and induce cell death via mitochondrial permeability transition (Schulz et al., 2013). As become evident in the dose finding studies, CsA exerts its cytotoxic action after prolonged treatment. Taken together, CsA's effects on mitochondria seem secondary to other effects. Hence, it was concluded that the 1 h treatment with CsA was not sufficient to bring about any alteration of cellular ATP levels.

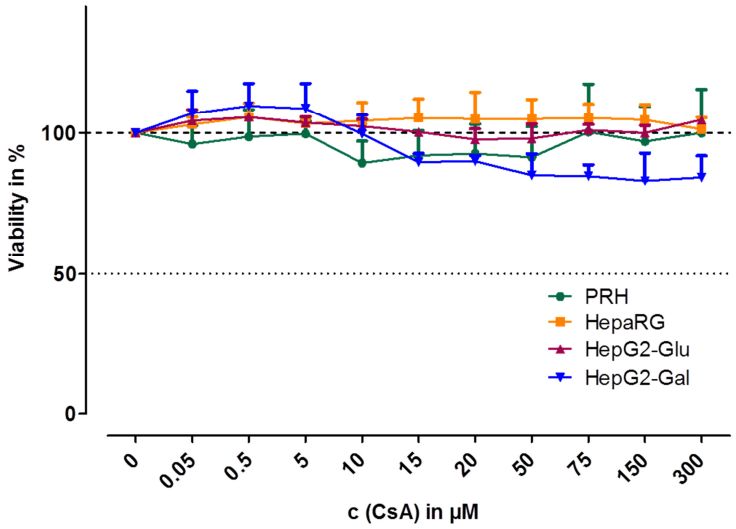

Figure 48. Cell viability results (measured using ATP content) in percent using the four hepatocyte systems (primary rat hepatocytes (PRH), HepaRG, HepG2 cultured in regular glucose-containing medium (HepG2-Glu) and HepG2 adapted to galactose-containing medium (HepG2-Gal)) after treatment for 1 h with the indicated concentrations of cyclosporine A (CsA). The percentages refer to the vehicle treated control, in relative light units, set to 100%. The values given represent the mean of 3 - 4 biological replicates + standard deviation.

3.3.5.2 MitoXpress O_2-sensitive probe respiration assay

In PRH, HepaRG and HepG2-Glu cells, CsA caused no significant change of the respiratory rate compared to the corresponding vehicle treated control. One exception was PRH treated with 150 µM CsA, which showed a statistically significant (p-Value ≥ 0.05) increased oxygen consumption to 132 ± 44%. However, this was not deemed to be biologically relevant due to the weak effect and the lack of concentration-dependence. These results confirmed the hypothesis that short-term exposure to CsA did not cause any adverse effects to mitochondrial respiration. By contrast, HepG2-Gal cells were clearly more susceptible to CsA treatment. Here, a marked reduction of the oxygen consumption rate ($\leq 49\%$) was evident already at ≥ 10 µM CsA. This was attributed to the combination of the low CYP3A4 activity in HepG2 cells (Boehme et al., 2010) and the adaptation to aerobic metabolism. CsA-induced cytotoxicity is reported to be primarily attributed to ROS generation (deArriba et al., 2013; Jennings et al., 2007; Rezzani, 2006). Thus, a reduced CYP3A metabolism is expected to result in elevated ROS levels. Additionally, the HepG2-Gal cells are thought to have an increased rate of oxidative phosphorylation compared to the glycolytic counterpart HepG2-Glu and consequently, they have a larger capacity for ROS generation.

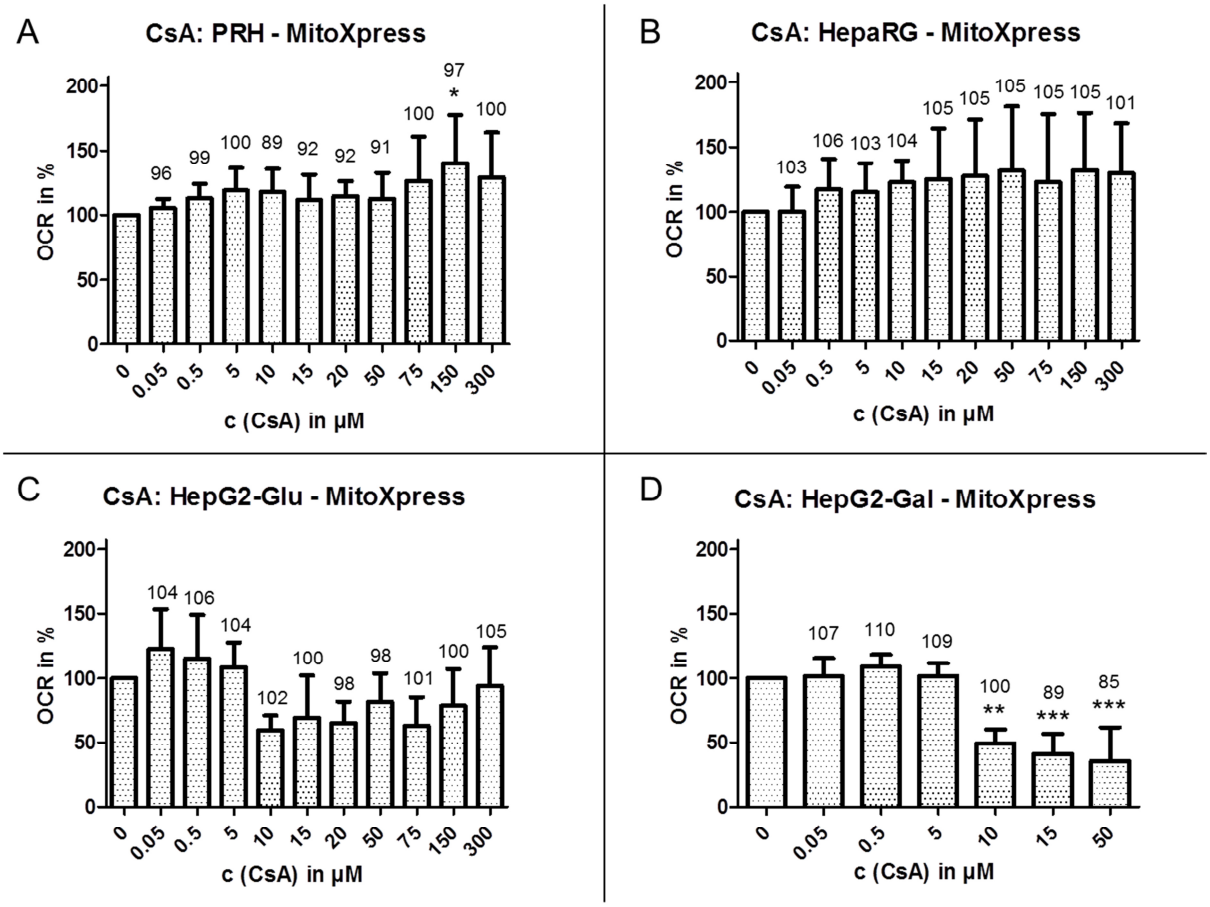

Figure 49. Oxygen consumption rate (OCR) in percent in the different hepatic systems (primary rat hepatocytes (PRH) (A), HepaRG (B), HepG2 cultured in regular glucose-containing medium (HepG2-Glu) (C) and HepG2 adapted to galactose-containing medium (HepG2-Gal) (D)) after treatment with different concentrations of cyclosporine A (CsA). The percentages refer to the slope of the vehicle treated control, in relative fluorescence units per minute (RFU/min), set to 100%; corresponding to ~ 560 RFU/min in PRH, ~ 150 RFU/min in HepaRG, ~ 80 RFU/min in HepG2-Glu and ~ 120 RFU/min in HepG2-Gal. Values are given as mean of 3 biological replicates + standard deviation. Numbers above columns represent viabilities in percent taken from the 1 h ATP test. Statistical significance is expressed in p-value ≤ 0.05 (*), ≤ 0.01 (**) and ≤ 0.001 (***) and was calculated by one-way repeated-measures analysis of variance (ANOVA) of a treatment towards the vehicle control and application of the Dunnett's post test.

3.3.5.3 Seahorse MitoStress assay

The complete kinetic profile in PRH revealed a slight reduction of the oxygen consumption rate only after treatment with 300 µM CsA (Appendix 12, Figure 62 A). Whereas inhibitory potency of oligomycin was not affected, oxidative phosphorylation uncoupling with FCCP was reduced at 300 µM CsA.

CsA reduced the spare respiratory capacity in PRH in a concentration-dependent manner (Figure 50 A). The value dropped from 106 ± 15% at the vehicle control to ~ 71% at concentrations ≥ 20 µM CsA. By contrast, no effect on the oxygen consumption rate was measured with the *MitoXpress O_2-sensitive probe respiration assay* described above (Figure 49 A). This difference was attributed to the different approach of the *Seahorse MitoStress assay*. The consideration of the responsiveness to different stimuli (inhibition or uncoupling) might result in a more sensitive readout compared to the isolated consideration of oxygen consumption. HepaRG and HepG2-

Glu cells did not respond to CsA treatment; whereas HepG2-Gal cells showed an apparent spare respiratory capacity increase. The latter effect was attributed to an extremely low spare respiratory capacity at the vehicle control (0 µM) and was therefore classified as an artefact. Furthermore, the highest CsA concentration did reduce the spare respiratory capacity; but this was not statistically significant.

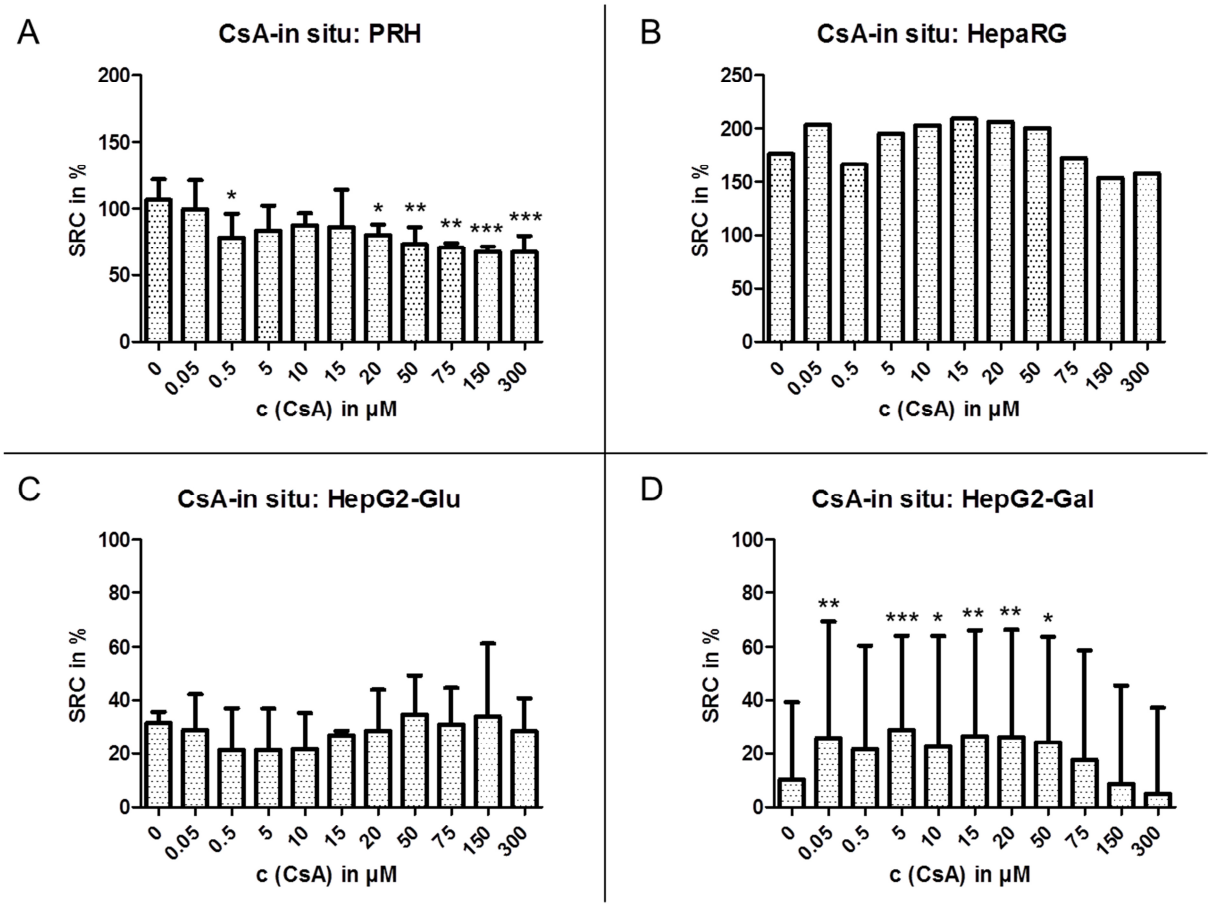

Figure 50. Spare respiratory capacity (SRC) in percent in the different hepatic systems (primary rat hepatocytes (PRH) (A), HepaRG (B), HepG2 cultured in regular glucose-containing medium (HepG2-Glu) (C) and HepG2 adapted to galactose-containing medium (HepG2-Gal) (D)) after *in situ* treatment with the indicated concentrations of cyclosporine A (CsA). The raw data curves of the single biological replicates were normalised to the corresponding basal (3rd measurement) oxygen consumption rate in pmol/min set to 100%; corresponding to ~ 140 pmol/min in PRH, ~ 130 pmol/min in HepaRG, ~ 140 pmol/min in HepG2-Glu, ~ 110 pmol/min in HepG2-Gal. The percentages refer to the difference between basal (100%) and maximum (1st measurement after carbonyl cyanide 4-(trifluoromethoxy)phenylhydrazone (FCCP) injection) respiration. Values are given as mean of 2 (HepaRG) or 3 biological replicates + standard deviation. Statistical significance is expressed in p-value ≤ 0.05 (*), ≤ 0.01 (**) and ≤ 0.001 (***) and was calculated by one-way repeated-measures analysis of variance (ANOVA) of a treatment towards the vehicle control and application of the Dunnett's post test. A detailed description of the compound treatment and SRC calculation is given in the Materials and Methods.

3.4 Amiodarone

The antiarrhythmic amiodarone (AMI) is known to cause side effects to the lung, liver, eyes and skin. Liver injury is a common adverse effect with AMI. After long-term therapy with AMI, 15 - 50% of patients show abnormal serum enzymes. Although elevated serum levels might resolve themselves, severe liver injuries are reported with AMI (NIH - Amiodarone, 2014).

3.4.1 *In vitro* dose finding

In order to estimate the cytotoxic potential of AMI in the two hepatic systems (PRH and PHH) the viability in response to increasing compound concentrations was determined after short- and long-term treatment. The *in vitro* dose finding studies described hereafter aimed the determination of the TC_{10} serving as the corresponding high concentration in the final experiments.

AMI treatment of PRH resulted in a time- and concentration-dependent cytotoxicity (Figure 51 A and B). In the 24-well plate format, a large variability was observed between the different biological replicates, resulting in high standard deviation (Figure 51 B). This could be due to actual inter-replicate differences in terms of cell quality or number that might differ between different preparations and thus picked up by the highly sensitive ATP assay. Due to the large difference in the viability (~ 70 - 140%) at 10 µM in the first two biological replicates (data not shown), 1 µM was included in the third replicate as the lowest concentration. In the 6-well plate culture format, all concentrations of AMI (1, 10 and 25 µM) resulted in culture viabilities of approximately 90%. However, treatment with 10 or 25 µM AMI resulted in a massive accumulation of intracellular vesicles in PRH. Hence, taking the adverse effects on cell morphology into account, 1 µM was chosen as TC_{10}. AMI is a cationic amphiphilic drug (pKa = 8.47), a property which is known to be linked to drugs causing phospholipidosis (Choi et al., 2013), and indeed was shown to occur in rats and humans given AMI (Reasor and Kacew, 2001). AMI metabolism mediated by Cyp3a2 in the rat (Shayeganpour et al., 2006), results in the formation of active desethylamiodarone metabolites (mono-N-desethylamiodarone and di-N-desethylamiodarone). This is a distinctive feature of this drug, since not only the parent compound, but also active metabolites are responsible for the pharmacological action and toxicity. AMI's biphasic effect in the mitochondrial respiration starts with oxidative phosphorylation uncoupling and progresses into inhibition of complex I and II. The inhibition is reported only for *in vitro* concentrations > 200 µM (Fromenty et al., 1990b). However, it seems very likely that repeated treatment over 14 days with 1 µM resulted in the accumulation of lipophilic AMI in the mitochondrial matrix. Furthermore, the inhibitory effect on the respiratory chain is reported to be more potent for AMI metabolites than for the parent compound (Zahno et al., 2011). Taken together, a cumulative and hence marked effect on the mitochondrial respiration was expected, which consequently decreased ATP concentrations, measured as a

marker for toxicity. AMI-induced phospholipidosis was observed at lower concentrations than those which markedly affected ATP levels.

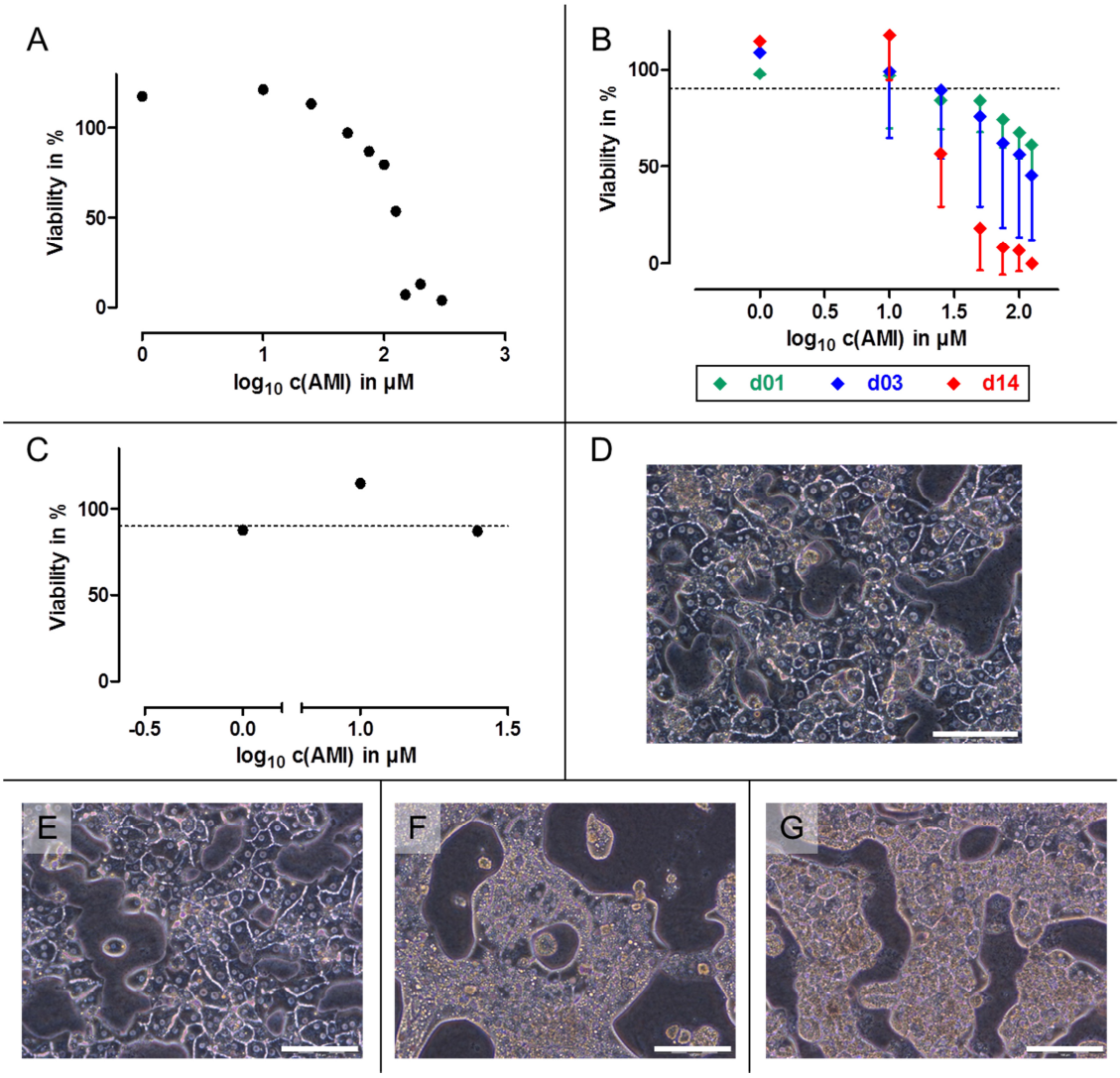

Figure 51. Cell viability results of primary rat hepatocytes (PRH) treated with amiodarone (AMI) in 96-well mono layer for 24 h (A), 24-well sandwich (SW) for 1 (green), 3 (blue) and 14 days (red) (B) or 6-well SW culture for 14 days (C) at the indicated concentrations. Results of the 24-well SW culture derived from 3 biological replicates, except for the lowest concentration, and are displayed as mean - standard deviation (B). Viability (measured using ATP content) was expressed as the percent relative the corresponding time matched methanol (MeOH) control. The dotted line shows the 90% viability threshold (B and C). Pictures of PRH in 6-well SW culture on day 14 after daily treatment with MeOH (D) or AMI at 1 µM (E), 10 µM (F) or 25 µM (G). The white scale bar on the bottom right of each picture corresponds to 100 µm.

As with PRH, AMI-induced cytotoxicity in PHH was time- and concentration-dependent. Long-term exposure to 10 µM for 14 days resulted in complete cell death (KaLy-Cell (Parmentier), personal communication).

The concentrations for the final experiments with AMI are given in Table 33.

Table 33. Treatment concentration of amiodarone (AMI) for final experiments in primary rat (PRH) and human (PHH) hepatocytes. High (HC) and corresponding low (LC) concentration.

	AMI concentration in µM	
	HC	**LC**
PRH	1	0.1
PHH	5	0.5

The complete cytotoxicity at 10 µM (14 days) in PHH was in contrast to the finding in PRH, which were ≥ 90% viable even at higher concentrations. In humans, AMI is metabolised by CYP3A4 and CYP2C8 (Fabre et al., 1993; Ohyama et al., 2000). Induction of CYP-mediated biotransformation was shown to increase the cytotoxicity of AMI in PHH (Zahno et al., 2011). Thus, it can be assumed that PHH metabolised AMI more efficiently than PRH. As described previously, pronounced species differences have been reported for human CYP3A4 substrates. These results comparing PRH and PHH confirmed the *in vivo* findings.

3.4.2 Biokinetics

In order to elucidate the characteristics that influence the bioavailability of AMI *in vitro*, biokinetic studies were performed using the high and low concentrations determined in the dose finding experiments. Therefore, at five specific time points on the first (day 0) and last (day 14) treatment day the amount of AMI was assessed in the cell lysates and supernatants.

The samples for the first biological replicate for the PRH were conducted soon after sampling and produced reasonable results. However, samples from the last two replicates were stored for a longer period of time at -80°C and this resulted in a much poorer recovery of AMI. Very low or no AMI was recovered from the supernatant at 0 min and supernatant samples of the second and third biological replicates (data not shown). Furthermore, the amount of AMI in the cell lysates was low throughout and, most importantly, did not provide interpretable results. This observation was very likely due to the plastic binding of AMI, despite *Eppendorf LoBind* tubes being used for sample storage. AMI is a basic (pKa = 8.47) and highly lipophilic (log K_{OW} ~ 7.5) compound (Drugbank - Amiodarone, 2013) and substantial plastic binding is reported for basic drugs (Palmgren et al., 2006). Here, this effect appeared relevant during long-term storage, although samples were stored at very low temperatures. By contrast, no plastic binding to cell culture vessels was observed during treatment in culture. Therefore, interpretation of the results from the first biological replicate was considered with reservation. Furthermore, the low concentration of AMI (0.1 µM) fell below the analytical LOD, hence only samples from the PRH cultures treated with 1 µM AMI were measured.

The cellular uptake of AMI is reported to be mediated by OATP2B1 (Seki et al., 2009), although its physicochemical properties suggest that passive diffusion may also contribute to some degree. An increased expression at the mRNA and protein levels of OATP2B1 after AMI treatment

indicates that the drug induces its own uptake (Segawa et al., 2013). This was supported in these studies in which the biokinetic profiles revealed a higher uptake rate in PRH, after repeated treatment (day 13) (Figure 52 A). After short-term treatment (day 0), the relative distribution indicated a loss of AMI (Figure 52 C), which suggested an efficient metabolism of the parent compound. After long-term exposure, the continuous decrease in the cell lysates was paralleled by a non-proportional decrease in the supernatant fraction. This confirmed that the metabolic capacity of the PRH was maintained over 14 days. AMI is reported to inhibit its own metabolism (Drugbank - Amiodarone, 2013), whereas no inhibition was observed in the PRH. However, this lack of inhibition may be due to the low cell lysate concentration of maximal 0.4 µM AMI which was insufficient to fully inhibit Cyp3a2. Furthermore, there was a trend of AMI accumulation in PRH after long-term exposure evident from the calculation of the relative distribution on day 13 (Figure 52 C). This correlates with the findings of the dose finding studies (Figure 51 E), in which a small amount of intracellular vesicles were observed after treatment with 1 µM AMI.

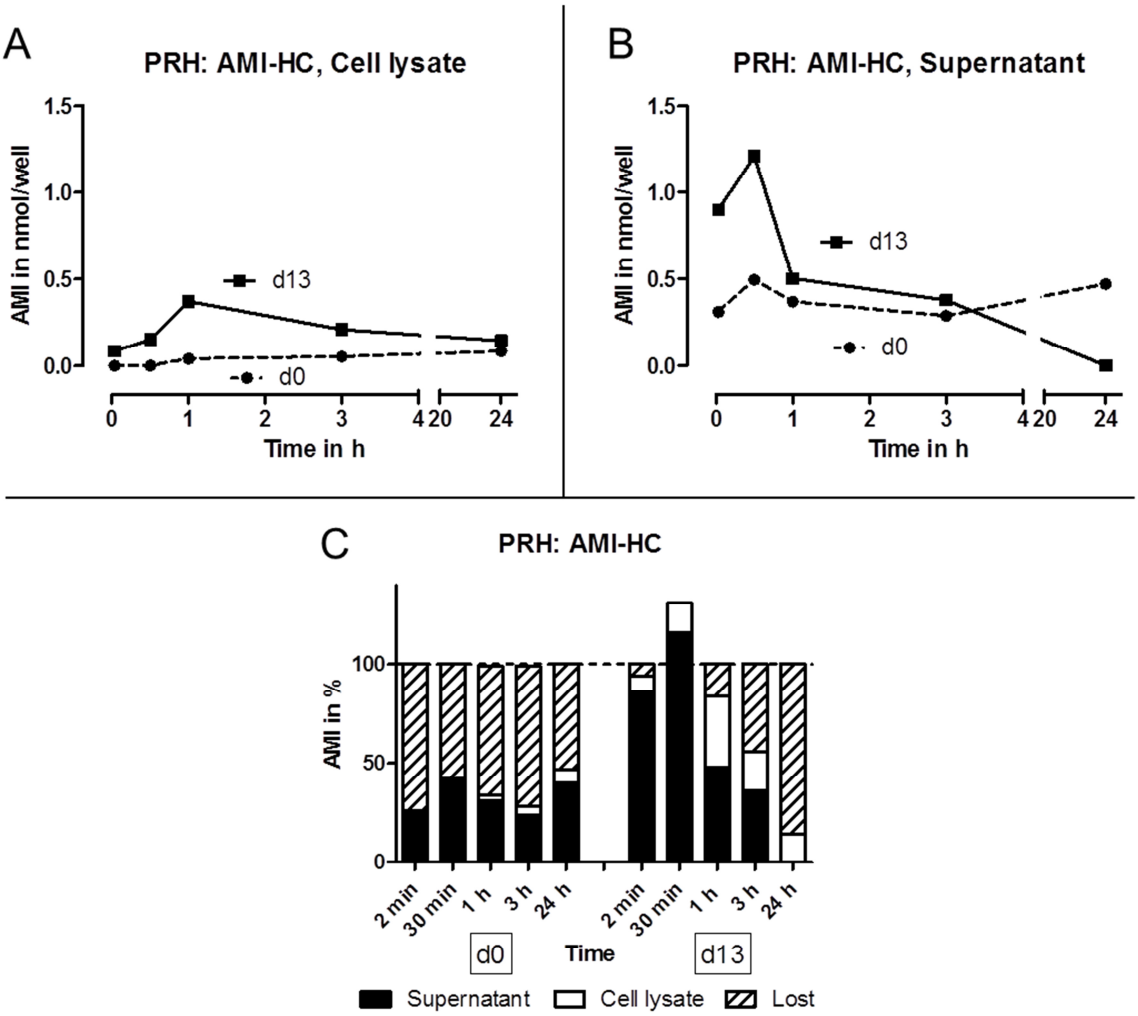

Figure 52. Kinetic profile of amiodarone (AMI) (nmol/well) in primary rat hepatocytes (PRH) (A, D) and culture supernatants (B, E) after single (day 0 – dashed line) and repeated (day 13 – solid line) treatment with 1 µM (high concentration (HC); A, B) AMI at the indicated time points. Relative distribution of AMI in percent in the different analysed PRH fractions at the indicated time points on day 0 and 13, supernatant (bold) and cell lysate (blank) as well as the apparent loss (striped) for the HC (C). Values derive from 1 biological replicate.

AMI uptake was slow in PHH on day 0 and was independent of the treatment concentration (Figure 53 A and C). By contrast, a rapid uptake was observed after repeated treatment. This finding could be explained by an induction of the uptake transporter, OATP2B1, in PHH, which was in accordance with the observations in PRH. Furthermore, the capacity of PHH to metabolise AMI after long-term exposure depended on the treatment concentration. In the samples treated with 0.5 µM AMI (low concentration), the amount of parent compound in the cell lysates dropped to a minimum after 24 h (day 13), which indicated an efficient metabolism of this drug at this concentration. By contrast, in the PHH treated with 5 µM, there was no decline of AMI in the cell lysates. However, there was a continuous decrease in the corresponding supernatant fraction, possibly due to uptake (Figure 53 D). The relative distributions were calculated for the AMI high concentration only, since no AMI was recovered from the supernatants at 0 min for the low concentration samples (day 0 and day 13). As Figure 53 E shows, there was no loss of AMI in the incubations since the sum of supernatant and cell lysate fractions always reached 100%. The amount of AMI in the supernatants decreased gradually over time on both treatment days, due to uptake into the cells. This was concomitant with an increase in the amount of AMI in the cell lysates: on day 0 from 6 ± 3% at 2 min to 96 ± 19% at 24 h, and on day 13 from 299 ± 100% at 2 min to 305 ± 11% at 24 h. The lack of metabolism in these cultures is in accordance with literature findings in which AMI inhibits CYP3A4 (Drugbank - Amiodarone, 2013). These data suggest that there is a concentration threshold for inhibition of CYP3A4 since there was still some metabolism over 24 h in low concentration cultures but not in high concentration cultures at day 13. The cell lysate concentration after repeated treatment with 5 µM was > 13-fold higher compared to the 0.5 µM treated samples (14.8 versus 1.1 µM, respectively). Therefore, impaired metabolism increased the cell lysate concentration and consequently increased the inhibitory effect. These observations emphasised the importance of determining the biokinetic profiles in different compartments simultaneously. As previously seen with PRH, an accumulation of AMI in PHH was observed after repeated exposure to the high concentration. The data suggests that AMI induced phospholipidosis might be linked to the formation of non-degradable drug-phospholipid complexes. Generally, this pathology is not restricted to distinct cell types. Honegger et al. (1993) showed the accumulation of AMI and its metabolite, DEA in human skin fibroblasts treated with 5 µM AMI. Overall, this data is in accordance with the *in vivo* situation, where phospholipidosis in both species is reported to occur (Reasor and Kacew, 2001).

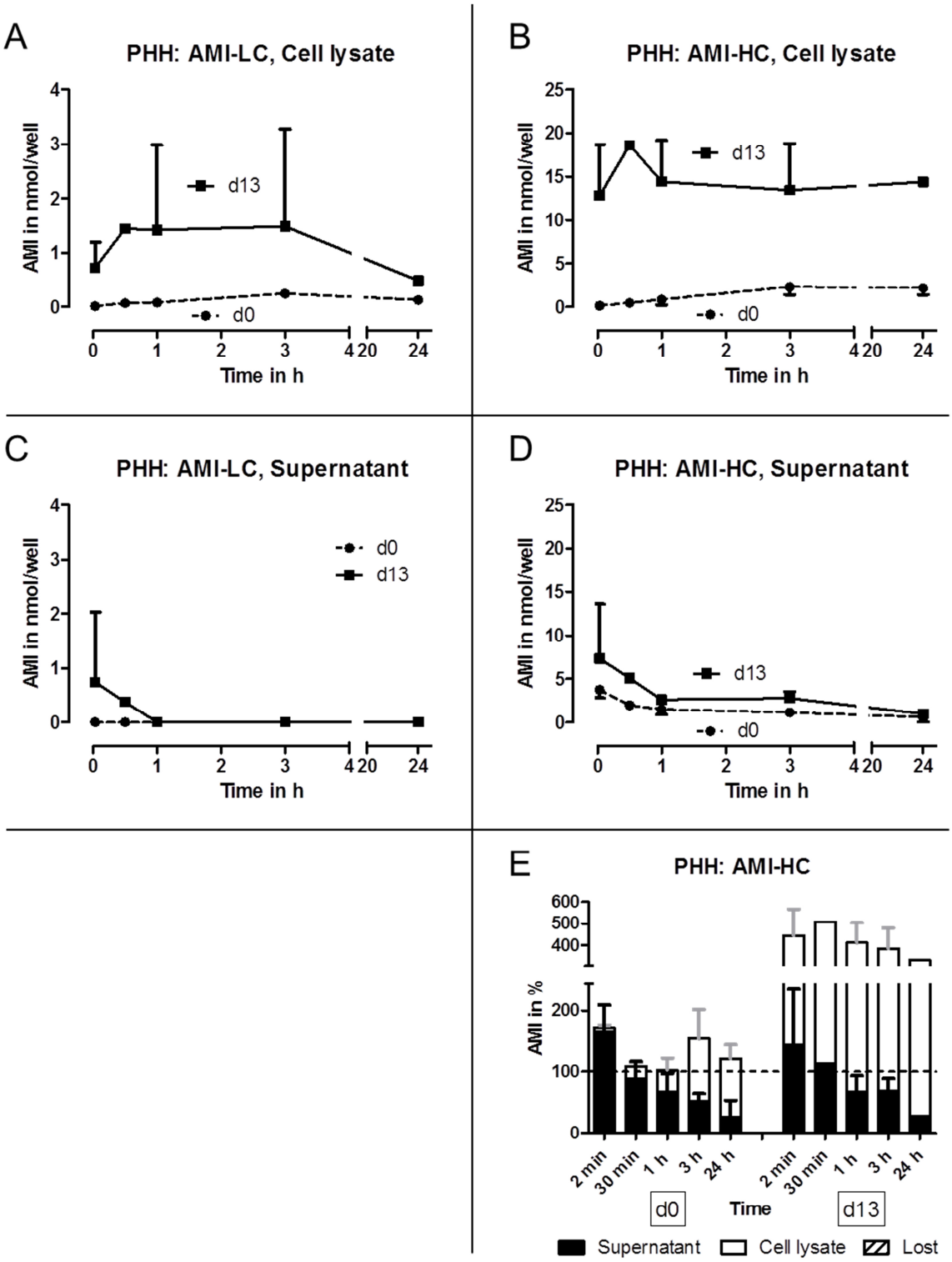

Figure 53. Kinetic profile of amiodarone (AMI) (nmol/well) in primary human hepatocytes (PHH) (A, B) and culture supernatants (C, D) after single (day 0 – dashed line) and repeated (day 13 – solid line) treatment with 0.5 µM (low concentration (LC); A, C) and 5 µM (high concentration (HC); B, D) AMI at the indicated time points. Relative distribution of AMI in percent in the different analysed PHH fractions at the indicated time points on day 0 and 13, supernatant (bold) and cell lysate (blank) as well as the apparent loss (striped) for the HC (E). Values are given as mean of 3 biological replicates +/- standard deviation.

The bioavailability of orally administered AMI is substantially affected by concomitant food intake. Meng et al. (2001) demonstrated that AMI release is more rapid and complete under fed conditions, leading to wide discrepancies (> 3.5-fold) in C_{max}. This observation can be explained

by an increased bile production after food intake, which helps solubilise the highly lipophilic AMI. It was assumed that the conducted *in vitro* experiments reflected the fasting condition; hence, relevant C_{max} being 0.6 ± 0.3 µM (Meng et al., 2001). However, the therapeutic levels for AMI are reported to range between 2.2 - 3.7 µM (Goldschlager et al., 2000). Therefore, the treatment concentration (TC_{10} = 5 µM, but supernatant concentration at time 0 min being ~ 1.7 µM) used in these studies for PHH thus was very representative of *in vivo* plasma concentrations.

3.4.3 Transcriptomics

In order to elucidate adverse effects of AMI on molecular level, transcriptomics studies were performed. In the following paragraphs only the results of PHH from the different donors are presented and discussed, since no significantly deregulated genes were found for the AMI treated PRH. A potential explanation for the lack of deregulated genes in the PRH treated with AMI was the treatment concentration which was selected too low. During the *in vitro* dose finding studies, the compound's effect on the cell morphology played a role. AMI exerted a detrimental effect on the cells' morphology (section 3.4.1 *In vitro* dose finding), which resulted in a selected concentration which deceeded the TC_{10}.

After AMI treatment, marked differences between the three donors were observed in the gene expression pattern of PHH. The total number of deregulated genes varied between 3 and 68 (Appendix 1, Table 40) for PHH from Donor 1. Consequently, only a very low number of deregulated genes (1 - 4) were classified in IPA®'s tox functions. For PHH from Donor 3, the majority of deregulated genes were found after low concentration treatment on day 1. Day 14 samples were missing for this donor due to contamination of the culture (KaLy-Cell (Parmentier), personal communication). By contrast, there was a time- and concentration-dependent number of deregulated genes in the different tox functions for PHH from Donor 2.

The top two functions within IPA® were *Liver Hyperplasia/Hyperproliferation* and *Hepatocellular Carcinoma*. Here, a detailed analysis of the genes involved in these pathways revealed that the majority were assigned to inflammation, immune response and cancer. AMI and its metabolites are considered potent oxidative phosphorylation uncouplers and inhibitors of the respiratory chain (Zahno et al., 2011). Furthermore, AMI blocks beta-oxidation which leads to the accumulation of free fatty acids (Spaniol et al., 2003; Kennedy et al., 1996). The impairment of the cellular respiration and accumulation of fatty acids results in the generation of ROS via electron leakage and lipid peroxidation, respectively. The induced oxidative stress is suggested to induce apoptosis and necrosis; whereas, the latter potentially leads to inflammatory and immune responses. There are no reports that AMI is linked to liver cancer. Indeed, Uehara et al. (2008) used AMI, amongst other negative compounds, as non-carcinogenic compound to develop a microarray-based prediction tool to categorise non-genotoxic hepatocarcinogens. This

result demonstrated nicely that IPA® should be used primarily for hypothesis generation and that manual investigation of the genes involved was essential. The tox function *Liver Inflammation/Hepatitis* was flagged up after AMI treatment. In fact, acute hepatitis is frequently reported with AMI (Nasser et al., 2013). The authors reviewed the current literature and found that many case reports of AMI-induced hepatitis are connected to intravenous application of the drug (Nasser et al., 2013). Thus, indicating that the route of administration plays a major role in AMI-induced toxicity. When taken orally, AMI has a low bioavailability and undergoes marked pre-systemic metabolism (first pass effect); hence, these may be the main causes for the observed differences. The experimental set-up of the primary hepatocyte cultures reflected an intravenous bolus injection. However, the gene expression responses varied considerably between PHH from different donors. Here, genes involved in inflammation and immune response were primarily down-regulated in PHH from Donor 2; whereas, they were up-regulated in PHH from Donor 3 (Figure 54). This implied a high inter-individual variation in the effects of this drug. Consideration of the basal CYP3A4 activities revealed pronounced differences between the donors. In relation to PHH from Donor 1, which had a low activity, PHH from Donor 2 exhibited a high CYP3A4 activity (Appendix 4, Table 47). CYP3A4 was not detected in PHH from Donor 3, which was due to technical reasons. The CYP-derived major metabolite, desethylamiodarone, is known to be pharmacologically active and a more potent mediator of adverse effects than the parent compound. The C_{max} of desethylamiodarone was lower or equal to AMI after oral dosing (Meng et al., 2001; Holt et al., 1983) but nearly 3-fold higher after intravenous administration (Cushing et al., 2009). This finding correlates with the observations made by Nasser et al. (2013). The relevance of CYP3A4, which generates the active AMI metabolite was important in the toxic effects of AMI, such that the activities in PHH studied here correlated directly with the extent of deregulated genes, i.e. a high activity resulted in a more pronounced adverse effect. From this correlation, it is likely that PHH from Donor 3 exhibited a medium CYP3A4 activity (between that of PHH from Donors 1 and 2). Taken together, this hypothesis provided an explanation for the inter-individual susceptibility observed in the different PHH donors. Interestingly, at the mRNA level, *CYP3A4* deregulation was inconsistent (Figure 54); *CYP3A4* was up-regulated in PHH from Donor 1, not deregulated in PHH from Donor 2, and down-regulated (> 3.2-fold) in PHH from Donor 3. AMI is reported to be a substrate and inhibitor of CYP3A4 (Drugbank - Amiodarone, 2013) but this cannot be linked to down-regulation at the mRNA level in PHH from Donor 3. Genes involved in the response to oxidative stress were almost all up-regulated in PHH from Donors 2 and 3 (Figure 54). This finding also correlated to the different basal CYP3A4 activities in these cells, since a higher concentration of the metabolite, desethylamiodarone, is assumed to mediate oxidative stress (Nasser et al., 2013). Since the mRNA expression is a good surrogate marker for CYP enzyme activity (Richert et al., 2009), it was concluded that the *CYP3A4* gene expressions data was not biologically relevant.

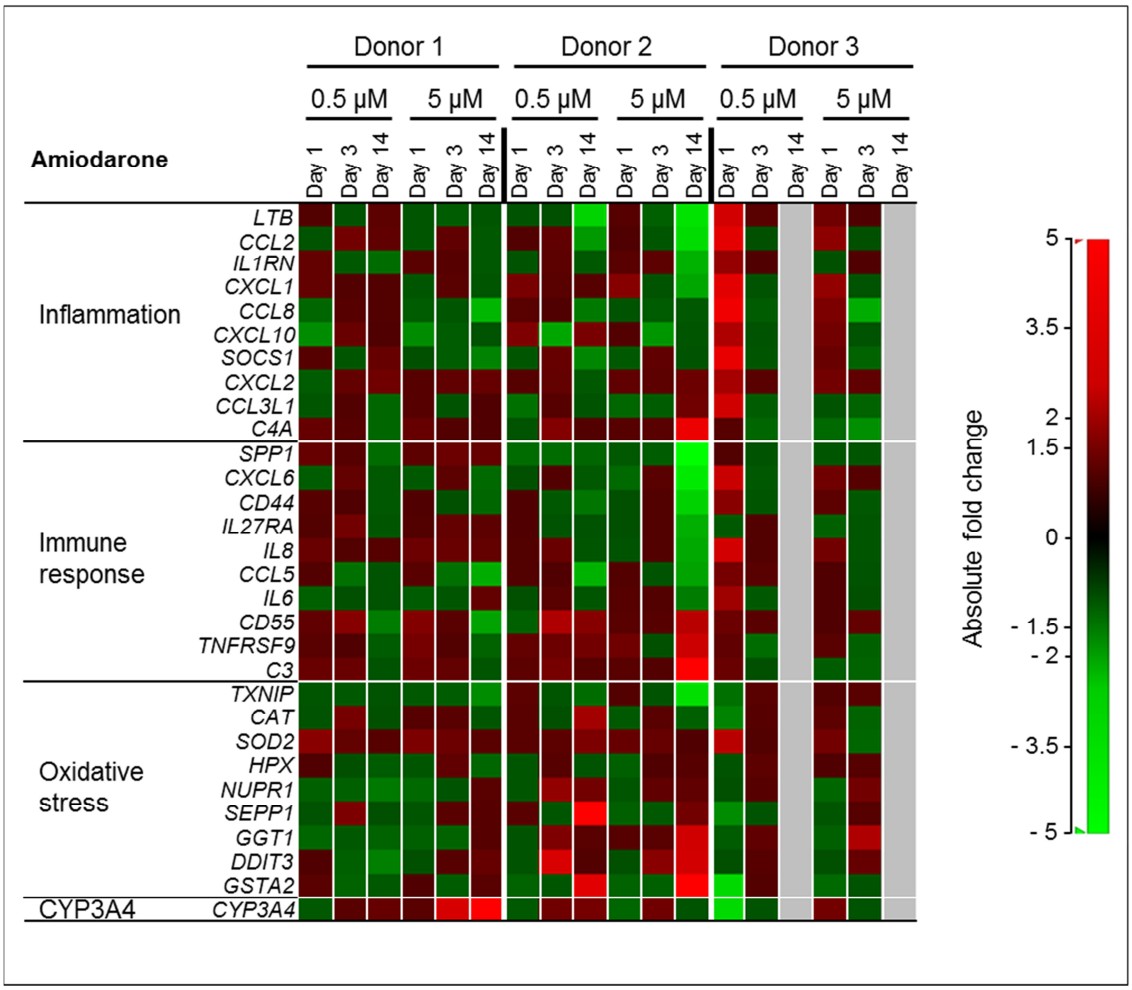

Figure 54. Gene function profile display of significantly deregulated genes in primary human hepatocytes from different donors after treatment with 0.5 µM and 5 µM amiodarone for 1, 3 or 14 days. The heatmap shows 30 genes involved in inflammation, immune response, oxidative stress and CYP3A4 identified to be deregulated by at least 2-fold compared to the time-matched vehicle treated control. The absolute fold change was calculated using the statistical analysis software Genedata Analyst™ version 7.5, the detailed data analysis is given in the Materials and Methods section. The colour scale shows increased fold changes in red and decreased fold changes in green. Absolute fold change values and gene acronyms are given in the appendix.

AMI-induced liver pathologies commonly include lesions of non-alcoholic fatty liver disease (Lewis et al., 1990; Babany et al., 1986), including hepatitis, steatosis, Mallory bodies[10] and fibrosis or even cirrhosis. In addition, AMI was specifically associated with micro- and macrovesicular steatosis (Puli et al., 2005; Lewis et al., 1990). Along with the previously discussed *Liver Inflammation/Hepatitis*, the tox function *Liver Steatosis* appeared in IPA® after AMI treatment. The genes involved in *Liver Steatosis* included those of the fatty acid and lipid metabolism, which were mainly down-regulated. This finding was in line with the knowledge that AMI inhibits mitochondrial beta-oxidation (Massart et al., 2013). However, AMI's potential to stimulate de novo lipogenesis (Massart et al., 2013) could not be confirmed in this dataset analysed with IPA®. Here, the gene coding for the fatty acid synthase (*FASN*) was the only one

[10] Mallory bodies are cytoplasmic inclusion bodies that have been associated with a variety of liver diseases including non-alcoholic liver disease. These intracytoplasmic bodies are mainly made up of keratins, ubiquitin and p62 (Zatloukal et al., 2007).

relatable to lipogenesis and it was up-regulated only in PHH from Donor 1. By contrast, *FASN* was down-regulated in PHH from Donors 2 and 3. Furthermore, genes attributed to inflammation and immune response were included in the *Liver Steatosis* function. In accordance with the liver pathologies reported *in vivo*, *Liver Fibrosis and Cirrhosis* function was flagged up with genes mainly involved in inflammation and immune response and extra cellular matrix organisation. AMI is further reported to induce the biosynthesis of cholesterol (Sawada et al., 2005). *Liver Cholestasis* was one of the minor affected tox functions and revealed deregulated genes in various pathways (fatty acid and lipid metabolism, bile salt metabolism, inflammation, immune response, xenobiotic metabolism and response to oxidative stress). Sawada et al. (2005) analysed the induction mechanism of AMI-induced phospholipidosis at the gene level. The group selected an arbitrary set of marker genes (Table 34), which correlated with the occurrence of lamellar bodies in AMI treated HepG2 cells. The consideration of this marker gene set in PHH from the different donors revealed a deregulation of some genes only in PHH from Donor 2. A low concordance (down-regulation of *TAGLN* in both cell systems) was given only when a less stringent fold change cutoff of 1.5-fold was considered (Table 34).

Table 34. Phospholipidosis marker genes according to Sawada et al. (2005). Absolute fold changes (FC) stated by the authors were compared to the FC of Donor 2 treated with amiodarone high concentration (5 µM) for 14 days. Some genes of the marker set were not found in the primary human hepatocytes (PHH) dataset (N/A). The acronyms are provided in the appendix for the genes found in the PHH dataset only.

Gene symbol	Gene function according to Sawada et al. (2005)	Fold change (Sawada et al., 2005)	Fold change Donor 2, high concentration, day 14
ASAH1	Phospholipid degradation	**1.7**	-1.4
MGC4171	Phospholipid degradation	1.3	N/A
LSS	Cholesterol biosynthesis	**1.8**	-1.2
NR0B2	Regulation of cholesterol metabolism	1.4	**-2.5**
PHYH	Fatty acid alpha-oxidation	-1.1	**-2.0**
FABP1	Fatty acid transport	**2.0**	-1.1
INHBE	Cell cycle, proliferation, death	**1.9**	1.4
P8	Cell cycle, proliferation, death	**1.9**	1.2
HPN	Proteolysis and peptidolysis	**2.2**	1.1
SERPINA3	Endopeptidase inhibition	1.2	1.0
ASNS	Miscellaneous	1.2	1.7
C10orf10	Unknown/EST	1.1	**-2.9**
FLJ10055	Unknown/EST	**1.6**	N/A
FRCP1	Unknown/EST	1.1	N/A
AP1S1	Transport	**-1.6**	1.0
SLC2A3	Transport	**-2.9**	1.1
TAGLN	Miscellaneous	**-1.8**	**-10.3**

This discrepancy can be attributed to diverse reasons. First of all, HepG2 cells are known to have low-level of CYP expression and activity. The most relevant CYP for AMI is CYP3A4 which

evidences a lower expression at the mRNA level compared to PHH (Boehme et al., 2010). Although CYP3A activities are reported to be similar in HepG2 cells and human hepatocytes (Hewitt and Hewitt, 2004), HepG2 cells are expected to produce a lower amount of active metabolites. For gene expression analysis, HepG2 cells were exposed to 8.3 µM AMI for a maximum of 24 h. Interestingly, none of these genes were deregulated in PHH from any of the donors on day 1 (low and high concentration). This indicates that long-term exposure was essential in PHH. The set of marker genes was identified using the DNA microarray platform Affymetrix™. Real-time PCR is generally considered more sensitive than global transcriptomics, therefore, this was also performed to confirm the genes and calculate the relative fold change values stated in. Taken together, these results demonstrate that marker genes are non-transferable from one cell system to the other. However, the detailed analysis of the global gene expression data revealed underlying mechanisms of toxicity, which are in accordance with the current literature and, most importantly, confirmed the *in vivo* situation.

3.4.4 Mitochondrial toxicity

AMI is known to exert a biphasic effect on mitochondrial function, comprising uncoupling and inhibition of the mitochondrial oxidative phosphorylation. Consequently, the potential of AMI to impair mitochondrial functions was assessed via different approaches.

3.4.4.1 ATP level for detection of mitochondrial toxicity

There was a similar concentration-dependent toxicity of AMI in the different cell systems (Figure 55). At concentrations > 10 µM, the viability decreased continuously and AMI was 100% cytotoxic at 200 µM (PRH, HepaRG) or 400 - 600 µM (HepG2-Glu, HepG2-Gal). Overall, PRH and HepaRG cells appeared slightly more sensitive to AMI cytotoxicity than the other two systems. This could be due to a more efficient biotransformation of the parent compound, since AMI metabolites are known to be more potent. Inducible *CYP3A4* expression was detected in the HepG2 cell line, however, lower compared to human hepatocytes (Boehme et al., 2010). The CYP3A activity was reported to be similar to human hepatocytes (Hewitt and Hewitt, 2004); nevertheless, the data suggested that the metabolic rate was lower compared to that in PRH and HepaRG cells.

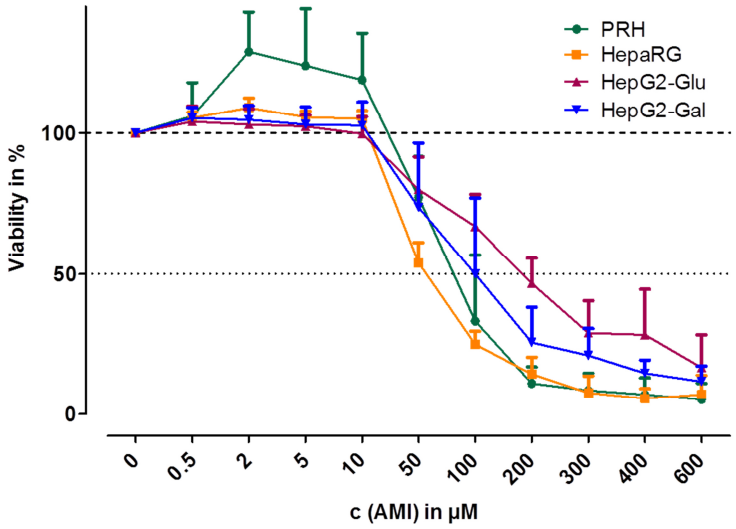

Figure 55. Cell viability results (measured using ATP content) in percent using the four hepatocyte systems (primary rat hepatocytes (PRH), HepaRG, HepG2 cultured in regular glucose-containing medium (HepG2-Glu) and HepG2 adapted to galactose-containing medium (HepG2-Gal)) after treatment for 1 h with the indicated concentrations of amiodarone (AMI). The percentages refer to the vehicle treated control, in relative light units, set to 100%. The values given represent the mean of 3 - 4 biological replicates + standard deviation.

3.4.4.2 MitoXpress O_2-sensitive probe respiration assay

Diverging outcomes were found in the different cell systems treated with AMI. A significant increase in oxygen consumption was observed in PRH at 10 (147 ± 21%) and 50 µM (168 ± 18%) AMI. The respiration of HepaRG cells was not affected by AMI, although concentrations ≥ 50 µM could not be evaluated in these cells due to cytotoxicity exceeding the arbitrary set threshold of 50%. In HepG2 cells cultured in both glucose- and galactose-containing media, oxygen consumption was reduced at concentrations ≥ 50 µM. The decrease at 50 µM was more pronounced in HepG2-Glu cells, in which oxygen consumption was reduced to 40 ± 13% compared to 69 ± 29% in HepG2-Gal cells.

Both findings, i.e. increased and decreased respiration, are in accordance with the underlying molecular action reported for AMI. AMI is reported to be an uncoupler and inhibitor of the mitochondrial respiratory chain (Felser et al., 2013; Fromenty et al., 1990b). Inhibition of complex I and II are reported to occur at concentrations of ≥ 200 µM (Fromenty et al., 1990b). The biokinetics results showed that AMI was accumulated intracellularly after repeated exposure to PHH. Although intracellular accumulation occurs, it is unlikely that the concentration threshold that causes an inhibition of complex I and II was reached within 1 h (exposure time for this assay). If higher concentrations were reached, the same effect would also have been observed in HepG2-Gal cells. Thus, there was no explanation for the observed inhibition of the oxygen consumption, which manifested only in the HepG2-Glu cells.

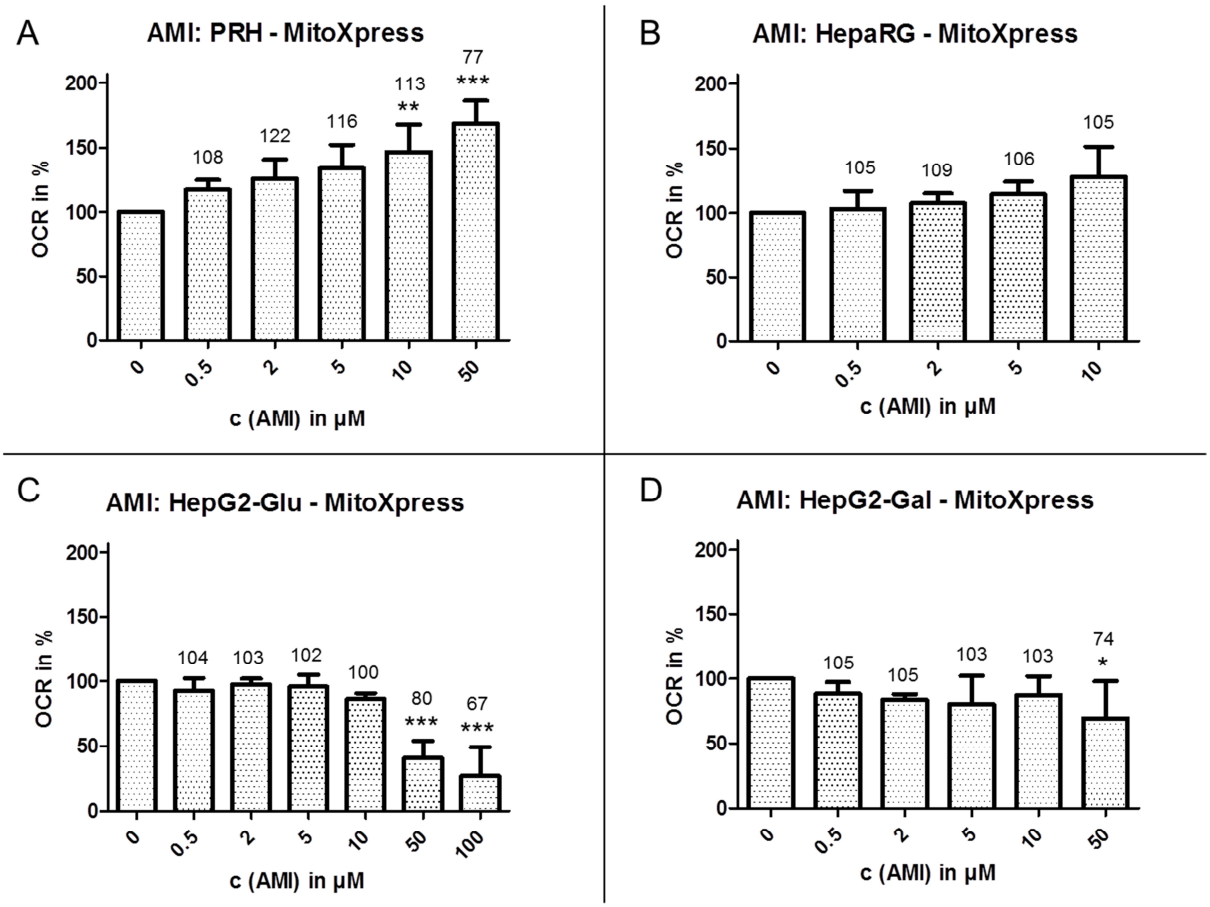

Figure 56. Oxygen consumption rate (OCR) in percent in the different hepatic systems (primary rat hepatocytes (PRH) (A), HepaRG (B), HepG2 cultured in regular glucose-containing medium (HepG2-Glu) (C) and HepG2 adapted to galactose-containing medium (HepG2-Gal) (D)) after treatment with different concentrations of amiodarone (AMI). The percentages refer to the slope of the vehicle treated control, in relative fluorescence units per minute (RFU/min), set to 100%; corresponding to ~ 440 RFU/min in PRH, ~ 150 RFU/min in HepaRG, ~ 80 RFU/min in HepG2-Glu and ~ 120 RFU/min in HepG2-Gal. Values are given as mean of 3 biological replicates + standard deviation. Numbers above columns represent viabilities in percent taken from the 1 h ATP test. Statistical significance is expressed in p-value ≤ 0.05 (*), ≤ 0.01 (**) and ≤ 0.001 (***) and was calculated by one-way repeated-measures analysis of variance (ANOVA) of a treatment towards the vehicle control and application of the Dunnett's post test.

3.4.4.3 Seahorse MitoStress assay

The complete kinetic profile of AMI treated PRH (Appendix 12, Figure 62 B) showed a marginal increase of the oxygen consumption rate at 300 µM. This observation correlated with the increased oxygen consumption measured with the *MitoXpress O_2-sensitive probe respiration assay* (Figure 56 A). As previously seen for CPZ, treatment with 300 µM AMI resulted in an elevated proton leak. Here, also the maximum respiratory capacity (uncoupled state after addition of FCCP) was reduced, which indicated a disruption of the electron transport chain. Again, this could help explain the increased oxygen consumption via proton leak.

The spare respiratory capacity in PRH treated with AMI was significantly ($p \leq 0.001$) reduced at 300 µM, a concentration that was cytotoxic in all the other cell systems tested. In the ATP test (which lasted 1 h, as described in section 3.4.4.1), 300 µM AMI was also categorised as very cytotoxic in PRH (the viability was 7 ± 7%). Nevertheless, the cells in this setup were responsive

to the chemicals of the *XF Cell MitoStress Test* kit, which would not be the case if cytotoxicity was too high. The reduction of spare respiratory capacity in PRH resulted from the uncoupling effect by AMI and the reduced maximum respiratory capacity. This finding was in line with the outcome of the *MitoXpress O_2-sensitive probe respiration assay* and the literature, where AMI is reported to impair the mitochondrial respiration (Zahno et al., 2011). In the other cell systems, AMI treatment did not cause any biologically relevant changes in the spare respiratory capacity. Assuming accordance with the *MitoXpress O_2-sensitive probe respiration assay*, this result indicates that the inhibition in HepG2-Glu by AMI seen in the other assay (Figure 56 C) was potentially an artefact.

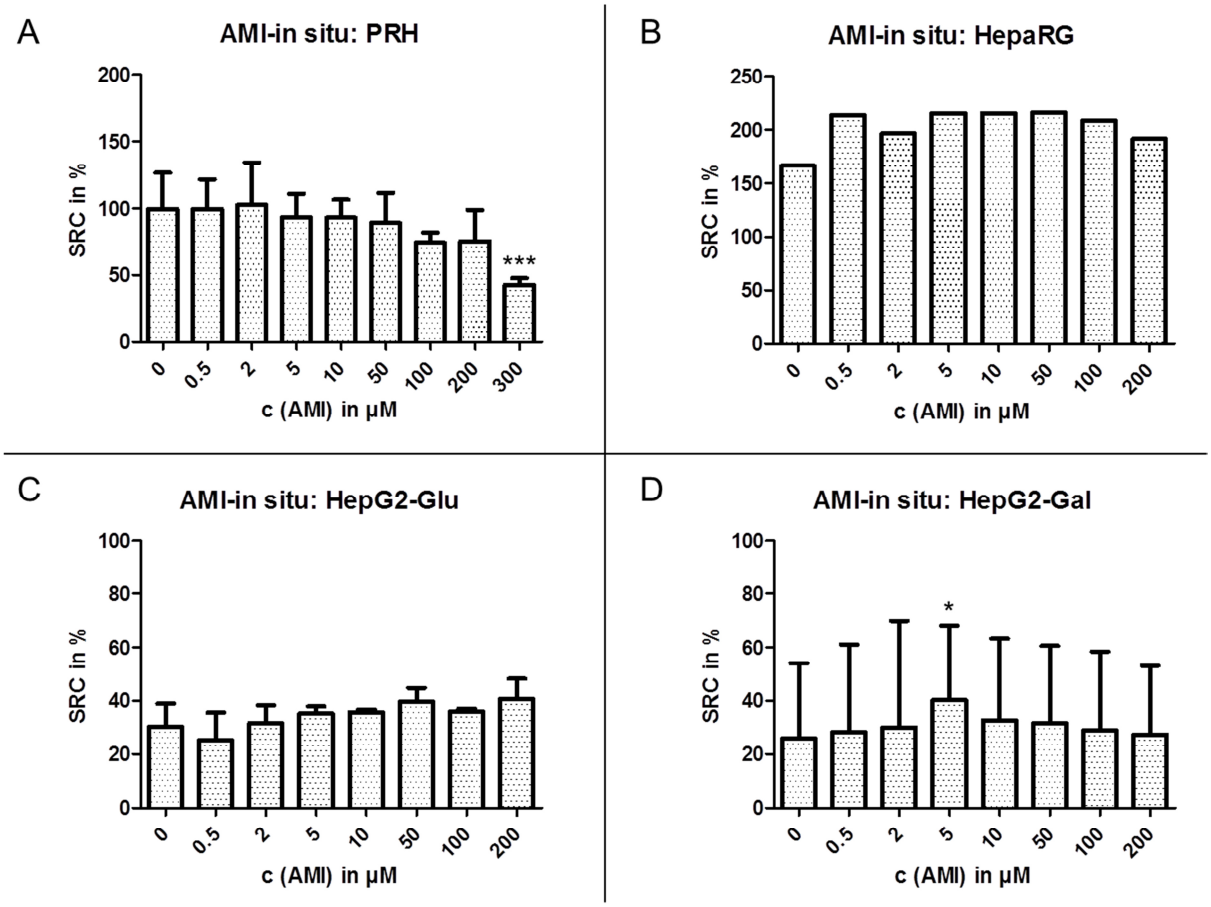

Figure 57. Spare respiratory capacity (SRC) in percent in the different hepatic systems (primary rat hepatocytes (PRH) (A), HepaRG (B), HepG2 cultured in regular glucose-containing medium (HepG2-Glu) (C) and HepG2 adapted to galactose-containing medium (HepG2-Gal) (D)) after *in situ* treatment with the indicated concentrations of amiodarone (AMI). The raw data curves of the single biological replicates were normalised to the corresponding basal (3rd measurement) oxygen consumption rate in pmol/min set to 100%; corresponding to ~ 150 pmol/min in PRH, ~ 130 pmol/min in HepaRG, ~ 130 pmol/min in HepG2-Glu, ~ 100 pmol/min in HepG2-Gal. The percentages refer to the difference between basal (100%) and maximum (1st measurement after carbonyl cyanide 4-(trifluoromethoxy)phenylhydrazone (FCCP) injection) respiration. Values are given as mean of 2 (HepaRG) or 3 biological replicates + standard deviation. Statistical significance is expressed in p-value ≤ 0.05 (*), ≤ 0.01 (**) and ≤ 0.001 (***) and was calculated by one-way repeated-measures analysis of variance (ANOVA) of a treatment towards the vehicle control and application of the Dunnett's post test. A detailed description of the compound treatment and SRC calculation is given in the Materials and Methods.

4 Conclusions and future perspectives

Currently, drug-induced hepatotoxicity is still one of the main reasons for drug attrition; therefore, there is an urgent need for more predictive models to identify the toxic potential of new drug candidates. The liver plays a central role because it is the first organ to encounter orally applied drugs and the main drug-metabolising organ in the body. Drug-induced liver injury can manifest in multiple liver pathologies and with varying degrees of severity, mainly depending on the cellular process altered by the drug. *Omics* technologies have proven to be powerful tools providing information on such altered cellular processes. They can help elucidate the mode-of-action of a compound and the underlying mechanisms potentially leading to adverse effects. To date, promising *in vitro* systems lack full acceptance, mainly because they deliver only discrete information on single endpoints.

In this thesis, multiple endpoints to predict the hepatotoxic potential of pharmaceuticals were evaluated. In order to make a conclusive evaluation, marketed pharmaceuticals with well described toxicities and kinetic profiles in animals and humans were applied, namely ibuprofen (IBU), chlorpromazine (CPZ), cyclosporine A (CsA) and amiodarone (AMI). Advanced analytical tools to gain biokinetic, transcriptomic and proteomic information were used. In addition, functional experiments were performed to provide insight as to whether the compounds acted as mitochondrial toxicants.

4.1 Value of applied *in vitro* models

For the studies reported here different well-established *in vitro* models were employed, namely primary rat (PRH) and human (PHH) hepatocyte cultures for biokinetic, transcriptomic and proteomic profiling, as well as PRH and human hepatoma cell lines (HepaRG and HepG2) for the functional assessment of mitochondrial toxicity.

For drug metabolism studies, primary hepatocytes are the so-called “gold standard” culture model because they maintain metabolic competence in culture (Castell et al., 2006). The limitation of primary hepatocyte cultures is the reduction of metabolic capacity over an extended time in culture. However, when cultured in a collagen sandwich configuration with defined serum-free medium, primary hepatocytes maintain characteristics of differentiated hepatocytes over a long-term (Tuschl et al., 2006). The long-term culture of primary hepatocytes was used in this work to enable repeated compound treatment; thus, mimicking, as far as possible *in vitro*, long-term exposures *in vivo*. A time-dependent response was seen for most endpoints measured in both primary hepatic systems, confirming the benefit of repeated treatment. The PRH and PHH were employed to reveal any species differences, for example, species-specific metabolism of compounds. As an example, CsA was metabolised less efficiently by PRH compared to PHH. Since the biotransformation of CsA is considered detoxifying, this finding helped explain the

higher sensitivity of the PRH towards CsA-induced cytotoxicity (lower TC_{10} in PRH compared to PHH). By contrast, the affected pathways revealed at the gene expression level were similar in both species; as was shown for CsA, where genes involved in inflammation and immune response were down-regulated and genes of the cholesterol and fatty acid and lipid metabolism were affected in primary hepatocytes from both species. This showed that PRH can predict general mechanisms of toxicity that also occur in PHH; although this PRH model was not sufficient to predict important inter-donor variations that are known to occur in humans. For example, the donor-dependent gene expression changes for CPZ, where induced inflammation pathways were correlated to an increased hepatotoxicity. PRH short-term cultures also provided valuable information regarding mitochondrial toxicity; whereas, the metabolic capacity of the cells was an essential feature. In fact, compounds that were metabolically bioactivated and caused mitochondrial toxicity in PRH, e.g. AMI, did not alter mitochondrial respiration in the cell lines, HepaRG and HepG2. To conclude, if the selected cell system lacks relevant metabolic competence there is a risk of not picking all compounds that act toxic on the mitochondria.

One goal of this work was to use established cell lines that do not require the sacrifice of animals or are limited by the supply (e.g. PHH). The cryopreserved HepaRG cells employed for the assessment of mitochondrial toxicity resemble terminally differentiated hepatocyte-like cells and are available in large quantities; therefore, representing a relevant alternative model to PHH. HepaRG cells were used to detect changes in mitochondrial functions but did not identify all four drugs as being toxic to mitochondria; therefore PRH were the most predictive cell system used for this endpoint. Furthermore, in the *Seahorse MitoStress assay*, uncoupling of the respiratory chain with FCCP was achieved only in the first two HepaRG replicates, while cells of the third and fourth replicate were not affected by FCCP. The reason for this observation could not be established because (i) FCCP injection did not fail due to instrument malfunction (the injection was checked visually), (ii) the same FCCP stock solution was effective with other cells and, most importantly, (iii) uncoupling of the oxidative phosphorylation with the third and fourth HepaRG replicate was observed in the separate *MitoXress O_2-sensitive probe respiration assay*. Finally, the human hepatoma cell line, HepG2, was used to assess adverse effects of the drugs on mitochondria. The HepG2 cells grown in standard, glucose-containing media predominantly rely on glycolytic ATP generation and are thus less susceptible to mitochondrial toxicity which impairs ATP production via oxidative phosphorylation. The culture in glucose-free, galactose-containing medium forces the cells to generate ATP via oxidative phosphorylation because oxidation of galactose to pyruvate via glycolysis yields no net ATP (Marroquin et al., 2007; Rossignol et al., 2004). Therefore, HepG2 cells were additionally adapted to galactose-containing medium. However, HepG2 cells grown in glucose- as well as galactose-containing medium performed poorly which was due to a lack of robustness and the described reduced metabolic capacity of these cells. The latter may be improved using an external source of drug-

metabolising enzymes, e.g. liver S9 fraction[11]. This so-called "external metabolic activation system" is added to the compound-containing medium in order to metabolise the compound outside the cell's cytoplasm; thus, picking up metabolite-induced toxic effects.

Taken together primary hepatocytes proved valuable for the applied endpoints. As described above, the use of these cells from different species helped explain inter-species differences between rat and human as well as intra-donor variations in PHH from the different donors. Their inherent metabolic capacity, for which primary hepatocytes are valued, was an important characteristic allowing the application for metabolite-mediated hepatotoxicity and mitochondrial toxicity. By contrast, the cell line HepG2 did not pick up mitochondrial toxicity of AMI that required metabolic activation for this effect. Overall, it can be concluded that the applied primary hepatocyte systems were suitable for the study of biokinetics, *Omics* and mitochondrial toxicity.

4.2 Value of applied endpoints

The primary hepatocyte models were suitable for the applied endpoints - but were the selected endpoints helpful to elucidate modes of action? This question was a key element of the presented work. Since, beside the value of an adequate cell system, the used endpoints are essential for the biological interpretation of the generated results. The so-called initial "dose finding" experiments are an important step for both *in vitro*, as well as *in vivo* studies. If the selected concentration is too low, no adverse effects may be observed compared to the vehicle control, which is especially important in resource-consuming animal studies. If the selected treatment concentration is too high, cytotoxicity is the prevailing effect *in vitro*, including induction of cell death mechanisms at the molecular level (seen at the gene and protein level). *In vivo*, dosing at excessively high levels may result in low survival rates and false positive results; the latter being frequently reported for rodent carcinogenicity studies, which are usually carried out at the maximum tolerated dose. To study adverse effects *in vitro*, TC_{10} and TC_{20} are frequently used as the high treatment concentration, theoretically exerting only minor cytotoxicity but high enough to initiate compound-induced and thus specific adverse effects at the molecular level. The corresponding low treatment concentration is either extrapolated from the high concentration (e.g. one-fifth of TC_{20}) or also experimentally determined (e.g. concentration at which no significant cytotoxicity is observed) (Barros and Martin, 2008).

In this thesis, the high concentration was set to the TC_{10}, measured using standard cytotoxicity assays in the corresponding cell system; and the low concentration was one-tenth of the TC_{10}. The dose finding studies revealed valuable information, especially in terms of metabolic differences between the primary hepatocytes from the two species. As described above, the cytotoxicity data can be used to (i) rank the compounds according to their *in vitro* cytotoxic potential, (ii) help interpret reported human toxicity data and (iii) generate metabolism-related

[11] The post-mitochondrial supernatant fraction from homogenised liver. The liver S9 fraction contains phase I and II drug metabolising enzymes.

hypothesis to species-differences. For the data presented here, compound-induced morphological changes played a role during dose selection in PRH. Although assessment of morphology is an essential parameter of the toxicity of a compound, this was not the optimal strategy in these studies with these compounds. For some compounds consideration of the morphology led to the selection of lower concentrations than the aimed TC_{10}. This was the case for CPZ, CsA and AMI, which all changed the cellular appearance microscopically, especially after long-term exposure, without affecting ATP levels. While for CPZ and CsA, the chosen concentration induced significant changes at the gene expression level of PRH, this was not observed with the high concentration selected for AMI.

Taken together, selection criteria for the treatment concentration (here, TC_{10}) should have been chosen differentially. For a sound concentration selection, human therapeutic exposures and toxic dose levels in animals and humans should be considered if available. Alternatively, pharmacologic effective concentrations *in vitro* which are available in early stages of drug discovery can be considered. Nevertheless, confirming dose-finding studies in the *in vitro* system that is used for the final studies are pivotal due to a limited transferability of concentrations from different systems (e.g. *in vivo*) to the applied cell model. For the purpose of confirmation, (i) the assessment of the cell viability to identify exaggerated cytotoxicity (e.g. $> 50\%$), (ii) CYP induction assay or (iii) gene expression screening of a relevant gene set (using real-time PCR analysis) are time- and cost-effective and biologically relevant endpoints. Furthermore, the consideration of more than two compound concentrations should help to determine no-observed-effect-concentration (NOECs) *in vitro* which was an aim of the EU-project Predict-IV that was not achieved.

The measurement of biokinetic information in *in vitro* systems has been mainly ignored; thus far, there are no reports on long-term *in vitro* models considering the biokinetic behaviour of the investigated compound. It is assumed that 100% of the nominal concentration of a compound reaches the cellular target without any limitations due to drug metabolism or the plasma membrane barrier. However, the bioavailability of a drug may be altered by physicochemical factors such as binding to medium or matrix components, plastic vessels, evaporation or chemical instability. In addition, biological factors such as transport processes (uptake and efflux) and biotransformation can be altered by the investigated drug. The biokinetic profiling proved to be a very important factor in this work as distinct compound characteristics were revealed, e.g. induction of uptake (CPZ, AMI), inhibition of the drug's own metabolism (CsA) or intracellular accumulation (CPZ, CsA, AMI). Furthermore, the biokinetic data revealed species differences that were in accordance with the literature. The determination of the compound concentration in the different fractions (i.e. supernatant and cell lysate) was essential. For example, the cell lysates of PHH treated with CsA at a high concentration suggested that metabolism of this drug was saturated after long-term exposure; whereas, the supernatant fractions revealed an efficient CsA biotransformation even after repeated treatment. However, an

accurate determination of intracellular concentrations was not possible without the exact cell number, cell volume or cell mass for normalisation. The consideration of a normalisation factor would be further important to compare across biological replicates or donors, as well as across the different species. The corresponding measurements for the assessment of such normalisation factors failed mainly due to technical issues. In a first approach the cell number was correlated to the DNA quantity measured using the Quant-iT™ PicoGreen® dsDNA assay. This approach was unsuccessful because the results revealed repeatedly wide discrepancies between the microscopic appearance of the cell layer and the DNA content. The second approach used the high content imaging, where a separate plate was processed for the determination of the cell number per well. This approach had several limitations. Firstly, the determination of the cell number in the actual kinetic sample well was not feasible because a separate plate had to be processed for high content imaging. Secondly, the cell number was determined only for the last two biological replicates since the first replicate was completed prior to full assay establishment. Thirdly, it was established only for the rat hepatocyte model because the high content imaging technology was available only at Merck Serono. The alternative normalisation factors, such as cell volume or cell mass were not approached due to technological limitations. Consequently, the biokinetic data was uniformly expressed in nmol/well. Nevertheless, biokinetics profiling helped to characterise further the hepatocyte systems (including the matrix effects), as well as the compounds under investigation (e.g. potential for bioaccumulation).

Another important characteristic of any *in vitro* model is its metabolic capacity. CYP enzymes play a central role in drug metabolism and are thus potentially important in the cause of adverse drug reactions (Ingelman-Sundberg, 2002). There is extensive inter-individual variation in human drug metabolism that can be attributed to the CYP family. Genetic polymorphisms and concomitant drug use, foodstuffs or environmental factors leading to an induction or inhibition of the CYPs are the main causes for this variation (Ingelman-Sundberg, 1999).

In these studies, the basal CYP activities in the primary hepatocyte systems were determined. The results demonstrated that CYP characterisation was especially important for the different human donors of the PHH cultures where marked differences in basal activity were seen. By contrast, CYP activities and mRNA expressions were similar in the PRH from the different animals. For all four test compounds, the biokinetic and/or transcriptomic results of PHH could be correlated to the corresponding CYP activity. For example, after treatment with AMI the PHH from Donor 2 which had the highest CYP3A4 activity, showed the highest number of deregulated genes compared to the other two donors. This finding could be explained with the CYP-mediated metabolism that in case of AMI generated the toxic metabolite, desethylamiodarone, which evoked an increased adverse effect.

As described for CYP2C9 (main IBU-metabolising CYP), varying susceptibility is due to differences in the metabolic capacity in the different polymorphic isoforms of DMEs. Therefore, it could be suggested that when starting to assess the toxicity of a new drug candidate, it is

essential not to use cells taken from donors with a rare polymorphism. However, at later stages during drug development, cells with known polymorphisms (e.g. known to be from extensive and poor metabolisers of the investigational drug) should be used. This procedure will identify the patients at higher risk and support further decision-making via a risk/benefit calculation or exclusion criteria for high-risk patients.

A basic assumption that justifies the use of transcriptome analysis in toxicology is that mRNA expression changes in response to compound-induced adverse effects. These gene expression changes aim to maintain cellular homeostasis and are expected to occur (i) much earlier than pathologic manifestations and (ii) at lower compound concentrations. The microarray technology enables the analysis of the entire transcriptome, i.e. thousands of genes at the mRNA level, and transcriptomic profiling is well established and frequently applied in *in vitro* and *in vivo* studies (Barros and Martin, 2008; Roth et al., 2011). In the presented work, transcriptomic profiling was used for the elucidation of compound-specific toxic mechanisms. In PRH, there were marked differences between the three compounds, IBU, CPZ and CsA, when comparing the gene expression profiles. This finding could be linked to different underlying mechanisms of adverse effects. Therefore, a comprehensive analysis of the generated gene expression profiles was essential. Furthermore, care must be taken when looking for published sets of marker genes potentially deriving from different *in vitro* systems. For example, the published marker gene set for phospholipidosis (from gene expression studies performed in AMI treated HepG2 cells; Sawada et al., 2005) was not confirmed in the present work for PHH treated with AMI. In PHH, the gene expression data revealed a high variation between cells from different donors, which may explain varying susceptibilities that could be translated to donor-dependent toxicities observed *in vivo*. At the same time, statistical analysis was not applicable because of the variation, which was a clear disadvantage in terms of throughput. Taken together, transcriptomics was considered indispensable for the elucidation of mechanisms for the toxic effect of the four compounds tested. Although providing valuable information on toxic mechanisms, it needs to be considered that a comprehensive analysis of the gene expression profiles is time consuming and expensive. Therefore, this approach appears more suited for the application in the stages of drug development where only a low number of drug candidates need to be tested.

Since mRNA analysis does not automatically reflect protein abundance, proteomics on PRH samples was included as additional endpoint. Proteomics analysis was not performed for PRH treated with AMI because these cells lacked changes at the gene expression level. The samples of PHH posed a problem for the proteomic profiling and were not analysed. The proteomic profiling identified only a very low number of altered proteins (compared to the corresponding time-matched vehicle treated control). For all compounds, the protein data often mirrored partly the transcriptomic data and added some information on affected cellular events that were not marked in the transcriptomic analysis. After IBU treatment, for example, the proteomics dataset

revealed proteins involved in carbohydrate and transcription regulation pathways, both pathways were not pronounced in the transcriptomics data. A slight overlap between genes and proteins was found. The opposing findings observed for some of the overlapping genes and proteins were attributed to feedback regulatory mechanisms. The small overlap was linked to the main limitations of the proteomic profiling conducted here, including the low number of significantly altered proteins and incomplete datasets for detected proteins at all time points (data was lacking randomly for discrete days, Appendix 9). These drawbacks could partly be attributed to the sandwich culture configuration used for the PRH. The high levels of extracellular matrix protein, collagen-I, posed a problem during protein quantification and thus, further processing via iTRAQ™. Apart from the sample-derived issues, this technology faces major challenges and limitations. Firstly, the wide dynamic range of protein abundance makes it difficult to quantify proteins in a comprehensive and specific manner (high abundant proteins will superimpose low abundant proteins). Secondly, the heterogenic nature of proteins makes a complete isolation in a single approach impossible, especially hydrophobic membrane proteins are difficult to extract and solubilise (Cho, 2007). Thirdly, high-throughput protocols result in a limited dynamic range of measurements (Qian et al., 2006). The latter limitation could be resolved by fine tuning the protocols which consequently would deliver a more complete protein dataset. Nevertheless, generally, the monitoring of changes at the protein level is considered important because changes on mRNA level do not always translate into altered protein amounts. However, the proteomics dataset had only a limited informative content compared to the gene expression signatures which allowed a comprehensive interpretation of compound-specific mechanisms of toxicity. Therefore, in the present work it was concluded that proteomics was less meaningful compared to the transcriptomics data.

Mitochondrial toxicity is becoming recognised as a major contributing factor to drug-induced organ toxicities (Dykens and Will, 2007; Pessayre et al., 2012), whereby highly energetic cells, i.e., with a large proportion of mitochondria, show increased susceptibilities (e.g. hepatocytes, cardiomyocytes and renal tubular cells) (Wilmes et al., 2013). A prominent example of a drug causing mitochondrial toxicity is the anti-diabetic, troglitazone, which was withdrawn from the market in 1997 - 2000 due to severe idiosyncratic liver toxicity. Here, mitochondrial dysfunction was shown to play a role in mediating the manifested hepatotoxicity (Okuda et al., 2008). Studies using isolated mitochondria (from organ tissue or cells) are considered to be the gold standard to detect mitochondrial toxicity (Picard et al., 2011). Recent advances in oxygen-sensitive probes (quenched phosphorescence measurement of oxygen) have improved assays such that they are sensitive enough to allow measurement of oxygen consumption in whole cells. The functional studies on mitochondrial toxicity included in this work showed that oxygen consumption was a suitable measure for the assessment of mitochondrial toxicity; and metabolically and respiratory competent cells, such as PRH, gave the most predictive results. The compound AMI is a representative example because it was the only compound for which

CYP-mediated biotransformation was toxifying. Here, reasonable results were obtained only with the metabolically competent PRH. Furthermore, the oxygen consumption assays used in these studies provided valuable information on the underlying mechanism of mitochondrial impairment (i.e. uncoupling or inhibition of oxidative phosphorylation). For example, IBU, a known inhibitor of complex I of the respiratory chain was shown to inhibit cellular respiration in both oxygen consumption assays (*MitoXpress O_2-sensitive probe respiration assay* and *Seahorse MitoStress assay*). In contrast to the oxygen consumption assays, the determination of the ATP level was less sensitive and mitochondrial impairment could only be assumed if galactose-grown cells were more susceptible compared to glucose-grown cells.

In conclusion, all endpoints provided some level of information about the cell systems itself and the compounds tested. As shown for IBU, the biokinetics data revealed that PRH metabolised the compound less efficient than PHH. Furthermore, the biokinetic analysis showed that a low activity of the IBU metabolising CYP2C9 correlated with an increased cytotoxicity (Donor 1). This donor-specific effect was also seen in the gene expression signatures which were more pronounced in Donor 1 compared to the other two donors. The transcriptomics dataset of primary hepatocytes from rat and human further revealed altered cellular processes after IBU treatment which could be linked to findings *in vivo*, e.g. fatty acid and lipid metabolism. The proteomics data, which was analysed for PRH only, supplemented additional pathways to the set identified on the mRNA level after exposure to IBU, e.g. carbohydrate metabolism. Finally, the oxygen consumption assays showed that IBU inhibited the oxidative phosphorylation, however, at concentrations exceeding human therapeutic plasma levels by far. Of the endpoints used, the most information was gained from biokinetics and transcriptomics which helped elucidate species-differences and underlying mechanisms of toxicity.

4.3 Cross-compound comparison

Pharmaceuticals from different therapeutic classes were studied to evaluate the different endpoints used in this work. The different chemical properties of drugs lead to diverse modes of action and are thus expected to cause distinct adverse effects at the molecular level. Indeed, the four compounds selected resulted in different patterns of *in vivo* hepatic pathologies, varying in severity and occurrence.

The drugs, IBU and AMI, are both reported to cause liver steatosis. In line with this common pathology, the data reported in this thesis clearly showed that both compounds impaired fatty acid and lipid metabolism by impairment of mitochondrial beta-oxidation. By contrast, a different pattern of alterations of genes involved in fatty acid and lipid metabolism was observed after treatment of hepatocytes with CPZ and CsA. CPZ and CsA are known to induce cholestatic liver disease and these studies revealed that both compounds could impair bile salt transporters. Another common adverse *in vitro* effect was phospholipidosis which was observed for AMI and

CPZ. AMI induced marked phospholipidosis in PRH at concentrations much lower than CPZ. In contrast to CPZ, AMI is reported to induce phospholipidosis in humans. In fact, AMI received a *Boxed Warning*[12] (LTKB, 2014) from the FDA and, out of the four test compounds, is the drug causing the severest hepatotoxicity *in vivo*. Taken together, the endpoints employed provided comprehensive information on the distinct molecular mechanisms of action of the compounds with a high predictive value (Table 35).

[12] The most serious alert for drugs carrying an increased risk of serious adverse effects. The FDA is responsible to assign the warning, whereupon it must be added to the drug label.

Table 35. Predictive value of the main *in vitro* findings to the reported *in vivo* situation. The listed *in vitro* findings were obtained mainly from the transcriptomics dataset, while the proteomics data for PRH contributed only little information due to the limitations described in section 4.2 Value of applied endpoints.

Compound	Main *in vitro* findings (PRH/PHH)	Proposed *in vivo* pathology	Validity of prediction
Ibuprofen	Impaired fatty acid and lipid metabolism (PRH and PHH)	Liver steatosis	Valid
	Down-regulation of genes in cell cycle regulation (PHH)	Inhibition of cell proliferation	Valid
	Impaired carbohydrate metabolism (PRH)	Impaired energy homeostasis	Valid (cautious: inhibition seen in bacteria)
	Inter-individual differences attributed to CYP activity (PHH)	Inter-individual susceptibility	Valid (idiosyncrasy)
Chlorpromazine	Impaired cholesterol metabolism (PRH)	Hypercholesterolemia	Valid
	Impaired bile metabolism (PRH)	Liver cholestasis	Valid
	Oxidative stress (PRH)	Oxidative stress	Partially valid (seen *in vitro*)
	Intracellular vacuolisation (PRH)	Phospholipidosis	Partially valid (seen in rat)
	Down-regulation of genes in inflammation and immune response (PRH and PHH)	Hepatitis	Valid
	Inter-individual differences in response to inflammation (PHH)	Inter-individual susceptibility	Not reported
Cyclosporine A	Impaired bile metabolism (PRH)	Liver cholestasis	Valid
	Oxidative stress (PRH)	Oxidative stress	Valid
	Intracellular lipid accumulation (PRH)	Liver steatosis	Not seen *in vivo*
	Dysbalance of apoptosis, proliferation and transcription (PRH and PHH)	Carcinogenic potential	Invalid (cancer attributed to immune-suppression)
	Down-regulation of genes in inflammation and immune response (PHH)	Decreased immune response	Valid
Amiodarone	Intracellular vacuolisation (PRH)	Phospholipidosis	Valid
	Inflammation (PHH)	Hepatitis	Valid
	Inter-individual differences in response to inflammation (PHH)	Inter-individual susceptibility	Not reported
	Oxidative stress (PHH)	Oxidative stress	Valid
	Impaired fatty acid and lipid metabolism (PHH)	Liver steatosis	Valid
	Deregulation of genes involved in cancer (PHH)	Hepatocellular carcinoma	Not seen *in vivo*

The comprehensive analysis of global gene expression data is time and cost consuming. Therefore, it would be beneficial to consider only a reduced set of genes which reflect the early onset of drug-induced toxicity, i.e. use so-called “biomarkers”. The approach of the Predict-IV project foresaw the identification of early biomarkers of toxicity for pharmaceuticals. Hence, the gene expression data from PRH was used to investigate genes which could serve as potential

early biomarkers for hepatotoxicity. The transcriptomics datasets from PRH treated with IBU, CPZ and CsA were compared to identify genes that were deregulated ≥ 2-fold compared to the time-matched vehicle control, at any time point. A total of ten genes were identified (Table 36). All genes involved in fatty acid and lipid metabolism were up-regulated across all compounds. This finding could be attributed to the fact that all compounds impair mitochondrial function, thus resembling rather a compound-specific effect. Overall, the suitability of this potential gene biomarker set needs to be re-considered with a larger dataset including a higher number of compounds covering various modes of action. In addition, more concentrations are needed to reveal a dose-dependent response of the biomarkers; if possible the concentrations include benchmark values (therapeutic concentrations, toxic dose levels, pharmacologic effective concentrations *in vitro*), as described above (section 4.2 Value of applied endpoints).

The deregulation of the proposed gene biomarker set in the human gene expression dataset showed only a small overlap. Whereas *VLDLR* was the only gene deregulated across all compounds (IBU, CPZ, CsA, AMI) in PHH from all donors, the direction of its deregulation (up- or down-regulated) was inconsistent (data not shown). The marginal concordance indicated either that the biomarker genes are non-transferable across species or that the defined gene biomarkers are invalid.

Table 36. Potential biomarker gene set derived from the primary rat hepatocyte transcriptomics dataset. Included were genes deregulated ≥ 2-fold compared to the time-matched vehicle control at any time point (day 1, 3 or 14) across all compounds.

Function	Gene symbol	Ibuprofen			Chlorpromazine			Cyclosporine A		
		d01	d03	d14	d01	d03	d14	d01	d03	d14
Fatty acid and lipid metabolism	*Acot1*	3.2	20.5	18.8	1.2	2.9	4.1	-1.0	1.0	8.1
	Scd	1.1	2.0	2.0	1.1	2.3	1.7	1.1	3.3	1.3
	Vldlr	1.1	2.6	1.7	1.4	2.7	2.5	1.8	5.5	2.7
Xenobiotic metabolism, Cholesterol biosynthesis	*Cyp2b15*	2.0	1.6	2.8	7.5	5.6	1.6	-1.7	-5.5	1.0
Inflammation, fibrosis	*Habp2*	-1.2	-1.3	-2.0	-1.2	-1.7	-4.3	-1.4	-1.5	-2.7
Proliferation	*Spink1*	1.2	1.8	2.7	1.2	-1.1	-2.1	-1.4	-3.0	-1.4
Transport	*A2ug*	1.6	4.1	3.2	1.2	2.4	2.2	-1.2	-3.1	1.2
Unknown function	*Flna*	-1.3	-1.1	-2.2	-1.1	-1.1	-2.0	-1.2	-1.3	-2.5
Signalling	*Rgs2*	-1.0	-2.0	-2.1	1.0	-1.4	-2.0	1.0	-2.1	-1.9
ECM organisation	*Lox*	-1.2	-1.1	-2.8	-1.2	-1.0	-5.1	-1.6	-1.5	-4.8

The second focus of this thesis was on mitochondrial toxicity. All four compounds tested have the potential to cause mitochondrial toxicity although the modes of action are different. For example, CPZ inhibits complex I and impairs the mitochondrial membrane potential, while AMI acts in a concentration-dependent manner as uncoupler or inhibitor of the oxidative phosphorylation. The functional assays applied revealed the specific mechanisms of each compound and showed that perturbation of cellular respiration occurred at compound

concentrations exceeding the human C_{max}. The latter finding either suggests that repeated exposure is required to cause toxicity at a low concentration or that additional factors increasing the susceptibility of human patients contribute to the drug-induced toxicity.

With reference to the statement by Paracelsus "the dose makes the poison", consideration of the drug concentration is essential during the analysis and interpretation of compound-induced adverse effects. Therefore, the high treatment concentration (TC_{10}) determined and employed in the two hepatic cell systems was compared to the reported human C_{max} (Table 37). The selected high concentrations used in the *in vitro* assays were all higher than the corresponding therapeutic level in humans. This finding was not surprising because the high concentration selection aimed to identify the TC_{10}, a concentration that exerts some degree of cytotoxicity. In addition, higher concentrations can be achieved *in vitro*, where systemic absorption/distribution and pre-hepatic metabolism of orally applied drugs are lacking.

Table 37. Comparison of the applied treatment concentrations to the corresponding human peak plasma concentration (C_{max}). The high concentration (HC; determined TC_{10}) and low concentration (LC; one-tenth of TC_{10}) used to treat primary rat (PRH, HC only) and human (PHH) hepatocyte cultures is given as measured (real) concentration in the culture supernatants at 0 min.

		Ibuprofen	Chlorpromazine	Cyclosporine	Amiodarone
Concentration in µM	HC in PRH	85	18	2.3	0.7
	HC in PHH	750	0.7	5.2	1.7
	Reported human C_{max}	0.3	0.14	0.4 - 0.8	0.6

However, a comparison of *in vitro* with *in vivo* concentrations and the corresponding adverse effects is not straightforward and thus, several assumptions have to be made. The difference between TC_{10} and C_{max} (*in vitro-in vivo* ratio) was used as an indication of the safety margin; but this margin applies only in terms of concentration and only with the model used. Since the most valuable endpoint in these studies was transcriptomics, alterations at the gene expression level were included as a measure of compound-induced adverse effect. For this purpose all genes deregulated at each time point were included. This approach was valid, since the TC_{10} was derived under the same treatment conditions as the genomics analysis i.e. after long-term treatment with the compounds, thus it could be assumed that changes were relevant over the entire incubation period. In order to have comparable values, the percentage of deregulated genes in relation to the corresponding statistical population was calculated (Table 38) (e.g. out of a statistical population of 1439 genes with a BH q-value ≤ 0.05, 62 were deregulated > 2-fold after treatment of PRH with IBU). Deregulated genes occurred for PRH only at the TC_{10} and for PHH at both concentrations tested (TC_{10} and one-tenth of TC_{10}).

Table 38. Percentage of genes deregulated at each time point (1, 3 and 14 days) after treatment with ibuprofen (IBU), chlorpromazine (CPZ), cyclosporine A (CsA) or amiodarone (AMI) in primary rat hepatocytes (PRH) or primary human hepatocytes (PHH) from the different donors. The percentages refer to the corresponding universe (for PRH the universe was dependent on the compound, i.e. 1439 for IBU, 1887 for CPZ, 4595 for CsA and not applicable (N/A) for AMI; for PHH the universe was 27,378). While for PRH gene changes after treatment with the TC_{10} were considered, both concentrations were considered for PHH.

		IBU	CPZ	CsA	AMI
	PRH	4.3	9.2	4.3	N/A
PHH from	**Donor 1**	17.5	9.8	14.6	0.4
	Donor 2	10.7	2.1	2.1	3.7
	Donor 3	7.0	2.3	1.8	1.0

The TC_{10} of IBU in PHH and the human C_{max} were compared to determine an *in vitro-in vivo* ratio, which was > 1000-fold (Table 37), i.e. indicating a large safety margin. Intriguingly, the number of genes changed in PHH after IBU treatment was the highest compared to the other compounds, i.e. suggesting the assumption of the highest adverse effect (Table 38). However, the larger number of genes and proteins altered at the TC_{10} *in vitro* does not necessarily imply that they will be changed at C_{max} *in vivo*; especially since the gene changes were observed at an *in vitro* concentration that was > 1000-fold higher than the C_{max}. For CPZ, CsA and AMI, the *in vitro-in vivo* ratios were 5-, 9- and 3-fold the C_{max}, respectively; however, the relevance of the percentage of changes at the gene level was not known due to a lack of a positive control. For example, the changes may be due to an adaptive response of the cells to the drug, rather than indicating a non-reversible toxic event. Here, a positive control compound which shows toxicity *in vitro* at C_{max} concentrations would help interpret whether the percentage of deregulated genes is biologically relevant. These examples illustrate the difficulty of interpreting findings using direct *in vitro-in vivo* concentration comparisons and corresponding adverse effects from *in vitro* studies with those reported *in vivo*. Taken together, these findings emphasise the use of transcriptomics to identify pathway alterations rather than extrapolations based on numerical gene changes. Hence, the key aspect was to identify which genes are affected at the TC_{10} (exceeding the C_{max}) to identify possible mechanisms of toxicity and/or adaptive responses.

Finally, it should be noted that all four pharmaceuticals are still marketed drugs. Although cases of liver injury are reported for these drugs, the overall positive benefit-risk profile justifies the continued use of these pharmaceuticals.

4.4 Future perspectives

The endeavour of the pharmaceutical industry is the improvement of candidate selection in early stages of the drug discovery process. The overall aim is the development of a testing strategy relying on non-animal based *in vitro* systems which will be supportive of the decision-making in early phases of drug discovery. This issue was addressed by the EU-project Predict-IV, aiming to derive such a testing strategy. The thesis in hand, which was embedded in the Predict-IV project, aimed the evaluation of multiple endpoints to predict the hepatotoxicity of pharmaceuticals.

During the course of these investigations, it became apparent that some endpoints should have been approached differentially.

For the dose finding study *in vitro*, more than one cytotoxicity test should be used in order to have a clearer and more accurate overview of the toxicity of a compound. The determination of cellular ATP levels alone was insufficient because it is too sensitive to drugs which may affect ATP synthesis. Additional assays for cellular toxicity which could be considered include (i) lactate dehydrogenase leakage due to damaged cell membrane integrity, (ii) the MTT assay (Mosmann, 1983) which considers the cellular reduction capacity and/or (iii) lactate production as a temporal measure of cell stress over time (Limonciel et al., 2011). In addition to the cytotoxicity screening, biologically relevant endpoints should be considered during dose finding studies, e.g. CYP induction capacity or drug-induced gene expression changes of a selection of phase I and II DMEs, nuclear receptors and transporters (real-time PCR analysis using Applied Biosystem's TaqMan Low Density Array cards) (Richert et al., 2009).

If possible, knowledge on CYPs involved in the metabolism of the compound must be taken into account since information on basal CYP activities may help interpret the data. For this purpose, the use of cryopreserved PHH (with pre-characterised basal CYP activities) would allow the selection of poor and extensive metaboliser donors with respect of the relevant CYPs. Advances in cryopreservation processes and culture conditions helped improve the quality of cryopreserved PHH to keep the same properties as freshly isolated cells (Alexandre et al., 2012; Bi et al., 2006; De Bruyn et al., 2011; Li, 2007; Richert et al., 2006). A further advantage of cryopreserved PHH is their availability which, by contrast, is limited for fresh human hepatocytes. However, when using fresh PHH, the basal activities of CYPs need also to be assessed. In this work, the basal CYP activity of PHH from the different donors was not assessed for those used in the *in vitro* dose finding studies. As discussed for IBU (section 3.1 Ibuprofen, 3.1.1 *In vitro* dose finding) this could result in a distorted concentration selection when cells from extensive or poor metabolising donors are used unknowingly. Therefore, the inherent CYP activity should be considered early on, i.e. during dose finding *in vitro*, as well as for the subsequent dynamic (e.g. transcriptomics) and biokinetic endpoints.

In order to keep track on the metabolic fate of the compound it would have been beneficial to quantify the arising metabolites; while knowledge on metabolite quantities in the hepatic models from rat and human could further help elucidate species-specific metabolism. The HPLC method was applied in these studies for the assessment of the biokinetic profiles in the different compartments of the hepatic *in vitro* models (supernatant, cell lysate). However, this method is hardly suited to the identification of unknown compounds (Levsen et al., 2003), including metabolites. Thus, liquid chromatography in combination with mass spectrometry should be the analytical method of choice because it allows quantification and identification of unknowns.

In analogy with transcriptomics and proteomics, metabolomics is expected to provide valuable knowledge on compound-induced toxic mechanisms. This technology is based on the fact that

xenobiotics can easily perturb the fragile balance of endogenous metabolites which help the cells to maintain homeostasis. In response to altered cellular functions and processes the intra- and extracellular biofluid composition changes and these can be detected using metabolomics. Multiple cell and supernatant samples were collected throughout the 14 days repeated compound treatment for metabolomic profiling. However, preliminary experiments showed that the metabolomic analysis of the cell lysate fraction was not feasible because of the contamination by collagen which co-eluted with the cellular fraction. More specifically, the presence of collagen resulted in a large peak which superimposed cellular metabolites. However, metabolites were detected in the supernatant fraction, thus providing so-called "metabolic footprints"[13]. Due to the need for optimisation of the data extraction process and the large number of samples from different partners of the project, the analysis of the primary hepatocyte samples was deprioritised (mainly due to the inability to use the cell fraction). Metabolomics could be helpful to identify endogenous metabolites serving as relevant biomarkers that would be measurable in a non-invasive manner. Hence, once generated, the metabolic profiles would be of great importance and could be correlated with the transcriptomic and proteomic profiles, also adding to the overall mechanistic picture. As we were able to show for the human-derived renal epithelial cells (RPTEC/TERT1) treated with the nephrotoxin CsA, metabolomics added an additional level of information. The identified metabolite alterations pointed to an inhibition of the mitochondrial oxidative phosphorylation. Furthermore, an increased abundance of glutathione precursor (gamma-glutamylcysteine) and oxidation products (glutathione disulphide, cysteine glutathione disulfide) indicated the onset of cellular response mechanisms (Wilmes et al., 2013). However, there exist also limitations of this emerging methodology, including data extraction from the complex and large datasets and metabolite identification (Scalbert et al., 2009).

Some adverse effects reported *in vivo* are known to resolve after discontinuation of drug therapy, e.g. elevated serum enzymes with NSAIDs. It would be interesting to see if this recovery can be mirrored *in vitro* by including a recovery phase (e.g. 7 days repeated treatment and 2 - 7 days recovery) after which the biokinetic and transcriptomic profiling should reveal a return to control levels.

An important next step will be the use of the *in vitro* data in a physiologically-based pharmacokinetic (PBPK) model to predict human *in vivo* concentrations. PBPK models use differential equations to simulate adsorption, distribution, metabolism and excretion (ADME) processes of a drug (Jones et al., 2013). These ADME processes influence the drug concentration at the target organ and are not reflected by the *in vitro* systems used in these studies. A drug concentration at which a predictive endpoint caused no adverse effects will be used as the input for the transformation using PBPK modelling. In PRH, almost no changes at the gene expression level were seen after treatment with the low concentration for IBU (10 µM), CPZ (2 µM) and CsA (0.25 µM), or with the high concentration for AMI (1 µM); therefore the 1/10 TC_{10}

[13] The metabolic profile of the cell fraction is called "fingerprint".

concentrations used in these incubations could be considered as suitable NOECs. The results from the PBPK modelling of the PRH data will be extrapolated to human (with appropriate consideration of safety factors) to predict human NOAELs. The difference between these predicted NOAELs and the reported human C_{max} (or predicted values for novel compounds) will be used to calculate margins-of-safety that can be used as a benchmark for candidate selection. For PHH, applied treatment concentrations resulted in significant gene expression changes that were attributed to adverse outcome pathways; therefore, it was not possible to derive a NOEC in PHH. Follow-up experiments using lower compound concentrations are required to establish this value. Once the NOEC for PHH is known, this can be used in PBPK modelling to predict a NOAEL in humans (according to the procedure explained for rat).

The study in hand provided a basis to the overall aim of the Predict-IV project, which was the derivation of a new testing strategy to improve the assessment of drug safety in the early phases of drug development. However, before actually being able to provide such a new testing strategy further studies are needed to validate the most valuable endpoints in the primary hepatocyte systems presented. In such a validation approach biokinetics and transcriptomics analyses should be conducted with more reference compounds (comprising positive and negative controls with respect to hepatotoxicity). Although hypotheses can be generated on the basis of the transcriptomics results, the performance of functional assays to determine compound-induced mitochondrial toxicity was considered essential. While, because of its limited value proteomics profiling was considered not yet suitable to be included in a strategy (reasons for its limitations are provided above in section 4.2 Value of applied endpoints). Especially for the mitochondrial toxicity assays, the additional data will enable the calculation of benchmark values such as sensitivity and specificity which help estimate the performance of the proposed assays. Finally, the validation studies will generate comprehensive datasets which may identify early, relevant biomarkers of drug-induced hepatotoxicity. As was shown previously (section 4.3 Cross-compound comparison), a total of ten genes were identified across all compounds for the PRH, these potential biomarkers could be further validated with the data deriving from the screening of the new compounds. After successful validation the new *in vitro* system strategy will be a promising tool for candidate selection, eventually being applied before *in vivo* experiments are performed.

Taken together, the applied endpoints delivered valuable information which will be supportive of the decision-making in the early phases of drug discovery. Although a full picture will be obtained only by including all endpoints, the selection of single endpoints on a case-by-case basis, is conceivable. Overall, the presented data provides a sound basis for future efforts in this area.

The data presented here demonstrated the benefit of an integrated approach for the delineation of drug-induced hepatotoxicity. However, the development of new alternative methods and testing strategies continues. To date, new interdisciplinary projects are running, for example the

IMI/EFPIA[14] funded MIP-DILI project, which aims to develop innovative preclinical test systems to predict drug-induced human liver injury (MIP-DILI, 2014) or the FP7 funded DETECTIVE project that focusses on the biomarker development for target organs of repeated dose toxicity (liver, heart and kidney) (Detect-iv-e, 2014). Furthermore, continuous efforts are being made by the European Union Reference Laboratory for alternatives to animal testing (EURL ECVAM) which have a long tradition in the validation of alternative testing methods, contributing to the *3 R* principle (JRC, 2014a). Constant advances are also made in the development of new cell models, including (i) co-cultures aiming to mimic the cell to cell cross-talk and improve function and viability (Bhandari et al., 2001), (ii) 3D models that mirror the native hepatic microenvironment and (iii) induced pluripotent stem cells-derived hepatocytes as improved alternatives to traditional hepatic cell culture systems (Godoy and Hewitt et al., 2013).

[14] Abbreviations:
IMI: Innovative Medicines Initiative
EFPIA: European Federation of Pharmaceutical Industries and Associations

"Although hepatocytes have been isolated for decades,
the hunt for relevant alternative systems has only just begun."
(Godoy and Hewitt et al., 2013)

5 References

Anonymous [no authors listed] (1967). Central action of chlorpromazine. Lancet *1*, 553-554.

Abernathy, C.O., Lukacs, L., and Zimmerman, H.J. (1977). Adverse effects of chlorpromazine metabolites on isolated hepatocytes. Proceedings of the Society for Experimental Biology and Medicine Society for Experimental Biology and Medicine (New York, NY) *155*, 474-478.

Adam-Vizi, V., and Chinopoulos, C. (2006). Bioenergetics and the formation of mitochondrial reactive oxygen species. Trends in pharmacological sciences *27*, 639-645.

Adams, S.S., Bough, R.G., Cliffe, E.E., Dickinson, W., Lessel, B., McCullough, K.F., Mills, R.F., Nicholson, J.S., and Williams, G.A. (1970). Some aspects of the pharmacology, metabolism, and toxicology of ibuprofen. I. Pharmacology and metabolism. Rheumatology and physical medicine *10*, Suppl 10:19-26.

Adams, S.S., Bresloff, P., and Mason, C.G. (1976). Pharmacological differences between the optical isomers of ibuprofen: evidence for metabolic inversion of the (-)-isomer. The Journal of pharmacy and pharmacology *28*, 256-257.

Adams, S.S., Cliffe, E.E., Lessel, B., and Nicholson, J.S. (1967). Some biological properties of 2-(4-isoburylphenyl)-propionic acid. Journal of pharmaceutical sciences *56*, 1686.

Agilent Technologies (2005). Agilent 2100 Bioanalyzer – 2100 Expert User's Guide, G2946-90004, Agilent Technologies, May 2005.

Alexandre, E., Baze, A., Parmentier, C., Desbans, C., Pekthong, D., Gerin, B., Wack, C., Bachellier, P., Heyd, B., Weber, J.C., *et al.* (2012). Plateable cryopreserved human hepatocytes for the assessment of cytochrome P450 inducibility: experimental condition-related variables affecting their response to inducers. Xenobiotica; the fate of foreign compounds in biological systems *42*, 968-979.

Amundsen, R., Asberg, A., Ohm, I.K., and Christensen, H. (2012). Cyclosporine A- and tacrolimus-mediated inhibition of CYP3A4 and CYP3A5 in vitro. Drug metabolism and disposition: the biological fate of chemicals *40*, 655-661.

Anderson, L., and Seilhamer, J. (1997). A comparison of selected mRNA and protein abundances in human liver. Electrophoresis *18*, 533-537.

Anderson, N., and Borlak, J. (2006). Drug-induced phospholipidosis. FEBS letters *580*, 5533-5540.

Aninat, C., Piton, A., Glaise, D., Le Charpentier, T., Langouët, S., Morel, F., Guguen-Guillouzo, C., and Guillouzo, A. (2006). Expression of cytochromes P450, conjugating enzymes and nuclear receptors in human hepatoma HepaRG cells. Drug Metabolism and Disposition *34*, 75-83.

Antherieu, S., Azzi, P.B.-E., Dumont, J., Abdel-Razzak, Z., Guguen-Guillouzo, C., Fromenty, B., Robin, M.-A., and Guillouzo, A. (2013). Oxidative stress plays a major role in chlorpromazine-induced cholestasis in human HepaRG cells. Hepatology *57*, 1518-1529.

Antherieu, S., Chesne, C., Li, R., Guguen-Guillouzo, C., and Guillouzo, A. (2012). Optimization of the HepaRG cell model for drug metabolism and toxicity studies. Toxicology in vitro *26*, 1278-1285.

Arrowsmith, J. (2011a). Trial watch: Phase II failures: 2008-2010. Nature reviews Drug discovery *10*, 328-329.

Arrowsmith, J. (2011b). Trial watch: phase III and submission failures: 2007-2010. Nature reviews Drug discovery *10*, 87.

Assis, D.N., and Navarro, V.J. (2009). Human drug hepatotoxicity: a contemporary clinical perspective. Expert opinion on drug metabolism & toxicology *5*, 463-473.

Babany, G., Mallat, A., Zafrani, E.S., Saint-Marc Girardin, M.F., Carcone, B., and Dhumeaux, D. (1986). Chronic liver disease after low daily doses of amiodarone. Report of three cases. Journal of hepatology *3*, 228-232.

Baldwin, S.J., Bloomer, J.C., Smith, G.J., Ayrton, A.D., Clarke, S.E., and Chenery, R.J. (1995). Ketoconazole and sulphaphenazole as the respective selective inhibitors of P4503A and 2C9. Xenobiotica; the fate of foreign compounds in biological systems *25*, 261-270.

Ban, T.A. (2007). Fifty years chlorpromazine: a historical perspective. Neuropsychiatric disease and treatment *3*, 495-500.

Barros, S.A., and Martin, R.B. (2008). Predictive toxicogenomics in preclinical discovery. Methods in molecular biology (Clifton, NJ) *460*, 89-112.

Beems, R., van Kreijl, C., and van Steeg, H. (2002). 39-week carcinogenicity study with cyclosporin A in XPA-/-mice, wild type mice and XPA-/-. P53+/-double transgenic mice. Part of the ILSI/HESI Program on Alternative Methods for Carcinogenicity Testing.

Beeson, C.C., Beeson, G.C., and Schnellmann, R.G. (2010). A high-throughput respirometric assay for mitochondrial biogenesis and toxicity. Analytical biochemistry *404*, 75-81.

Begriche, K., Massart, J., Robin, M.A., Borgne-Sanchez, A., and Fromenty, B. (2011). Drug-induced toxicity on mitochondria and lipid metabolism: mechanistic diversity and deleterious consequences for the liver. Journal of hepatology *54*, 773-794.

Bell, F.P., and Hubert, E.V. (1981). Inhibition of LCAT in plasma from man and experimental animals by chlorpromazine. Lipids *16*, 815-819.

Belli, W.A., Buckley, D.H., and Marquis, R.E. (1995). Weak acid effects and fluoride inhibition of glycolysis by Streptococcus mutans GS-5. Canadian journal of microbiology *41*, 785-791.

Bennett, W.E., Jr., Turmelle, Y.P., and Shepherd, R.W. (2009). Ibuprofen-induced liver injury in an adolescent athlete. Clinical pediatrics *48*, 84-86.

Berridge, M.V., Herst, P.M., and Tan, A.S. (2005). Tetrazolium dyes as tools in cell biology: new insights into their cellular reduction. Biotechnology annual review *11*, 127-152.

Bhandari, R.N., Riccalton, L.A., Lewis, A.L., Fry, J.R., Hammond, A.H., Tendler, S.J., and Shakesheff, K.M. (2001). Liver tissue engineering: a role for co-culture systems in modifying hepatocyte function and viability. Tissue engineering *7*, 345-357.

Bi, Y.A., Kazolias, D., and Duignan, D.B. (2006). Use of cryopreserved human hepatocytes in sandwich culture to measure hepatobiliary transport. Drug metabolism and disposition: the biological fate of chemicals *34*, 1658-1665.

Bissell, D.M., Gores, G.J., Laskin, D.L., and Hoofnagle, J.H. (2001). Drug-induced liver injury: mechanisms and test systems. Hepatology *33*, 1009-1013.

Bjork, J.A., and Wallace, K.B. (2009). Structure-activity relationships and human relevance for perfluoroalkyl acid-induced transcriptional activation of peroxisome proliferation in liver cell cultures. Toxicological sciences: an official journal of the Society of Toxicology *111*, 89-99.

BMEL, Bundesministerium für Ernährung und Landwirtschaft (2013). http://bmel.de/SharedDocs/Downloads/Landwirtschaft/Tier/Tierschutz/2011-TierversuchszahlenGesamt.html [updated 13/11/2012] (accessed on 02/02/2014).

Boehme, K., Dietz, Y., Hewitt, P., and Mueller, S.O. (2010). Activation of P53 in HepG2 cells as surrogate to detect mutagens and promutagens in vitro. Toxicology letters *198*, 272-281.

Boelsterli, U.A., Bouis, P., and Donatsch, P. (1987). Relative cytotoxicity of psychotropic drugs in cultured rat hepatocytes. Cell biology and toxicology *3*, 231-250.

Boess, F., Kamber, M., Romer, S., Gasser, R., Muller, D., Albertini, S., and Suter, L. (2003). Gene expression in two hepatic cell lines, cultured primary hepatocytes, and liver slices compared to the in vivo liver gene expression in rats: possible implications for toxicogenomics use of in vitro systems. Toxicological Sciences *73*, 386-402.

Bolstad, B.M., Irizarry, R.A., Astrand, M., and Speed, T.P. (2003). A comparison of normalization methods for high density oligonucleotide array data based on variance and bias. Bioinformatics (Oxford, England) *19*, 185-193.

Borges, N.C., Rezende, V.M., Santana, J.M., Moreira, R.P., Moreira, R.F., Moreno, P., Borges, D.C., Donato, J.L., and Moreno, R.A. (2011). Chlorpromazine quantification in human plasma by UPLC-electrospray ionization tandem mass spectrometry. Application to a comparative pharmacokinetic study. Journal of chromatography B, Analytical technologies in the biomedical and life sciences *879*, 3728-3734.

Borzelleca, J.F. (2000). Paracelsus: Herald of Modern Toxicology. Toxicological Sciences *53*, 2-4.

Bradford, M.M. (1976). A rapid and sensitive method for the quantitation of microgram quantities of protein utilizing the principle of protein-dye binding. Analytical biochemistry *72*, 248-254.

Brenner, C., and Moulin, M. (2012). Physiological roles of the permeability transition pore. Circulation research *111*, 1237-1247.

Broccatelli, F., Carosati, E., Neri, A., Frosini, M., Goracci, L., Oprea, T.I., and Cruciani, G. (2011). A novel approach for predicting P-glycoprotein (ABCB1) inhibition using molecular interaction fields. Journal of medicinal chemistry *54*, 1740-1751.

Brosnan, C.F., Bunge, M.B., and Murray, M.R. (1970). The response of lysosomes in cultured neurons to chlorpromazine. Journal of neuropathology and experimental neurology *29*, 337-353.

Brown, G.C. (1995). Nitric oxide regulates mitochondrial respiration and cell functions by inhibiting cytochrome oxidase. FEBS letters *369*, 136-139.

Brown, H.S., Chadwick, A., and Houston, J.B. (2007). Use of isolated hepatocyte preparations for cytochrome P450 inhibition studies: comparison with microsomes for Ki determination. Drug metabolism and disposition: the biological fate of chemicals *35*, 2119-2126.

Brunner, L.J., Bennett, W.M., and Koop, D.R. (1998). Cyclosporine suppresses rat hepatic cytochrome P450 in a time-dependent manner. Kidney Int *54*, 216-223.

Brunner, L.J., Werner, U., and Gravenall, C.E. (2000). Effect of dose on cyclosporine-induced suppression of hepatic cytochrome P450 3A2 and 2C11. European journal of pharmaceutics and biopharmaceutics: official journal of Arbeitsgemeinschaft fuer Pharmazeutische Verfahrenstechnik eV *49*, 129-135.

Buchweitz, J.P., Ganey, P.E., Bursian, S.J., and Roth, R.A. (2002). Underlying endotoxemia augments toxic responses to chlorpromazine: is there a relationship to drug idiosyncrasy? The Journal of pharmacology and experimental therapeutics *300*, 460-467.

Cabezas, R., El-Bacha, R.S., Gonzalez, J., and Barreto, G.E. (2012). Mitochondrial functions in astrocytes: neuroprotective implications from oxidative damage by rotenone. Neuroscience research *74*, 80-90.

Canales, R.D., Luo, Y., Willey, J.C., Austermiller, B., Barbacioru, C.C., Boysen, C., Hunkapiller, K., Jensen, R.V., Knight, C.R., Lee, K.Y.*, et al.* (2006). Evaluation of DNA microarray results with quantitative gene expression platforms. Nature biotechnology *24*, 1115-1122.

Castell, J.V., Jover, R., Martinez-Jimenez, C.P., and Gomez-Lechon, M.J. (2006). Hepatocyte cell lines: their use, scope and limitations in drug metabolism studies. Expert opinion on drug metabolism & toxicology *2*, 183-212.

Castillo, M., Lam, Y.W., Dooley, M.A., Stahl, E., and Smith, P.C. (1995). Disposition and covalent binding of ibuprofen and its acyl glucuronide in the elderly. Clinical pharmacology and therapeutics *57*, 636-644.

Chan, F.K., and Shaffer, E.A. (1997). Cholestatic effects of cyclosporine in the rat. Transplantation *63*, 1574-1578.

Chang, S.Y., Li, W., Traeger, S.C., Wang, B., Cui, D., Zhang, H., Wen, B., and Rodrigues, A.D. (2008). Confirmation that cytochrome P450 2C8 (CYP2C8) plays a minor role in (S)-(+)- and (R)-(-)-ibuprofen hydroxylation in vitro. Drug metabolism and disposition: the biological fate of chemicals *36*, 2513-2522.

Chen, M., Bisgin, H., Tong, L., Hong, H., Fang, H., Borlak, J., and Tong, W. (2014). Toward predictive models for drug-induced liver injury in humans: are we there yet? Biomarkers in medicine *8*, 201-213.

Chitturi, S., and George, J. (2002). Hepatotoxicity of Commonly Used Drugs: Nonsteroidal Anti-Inflammatory Drugs, Antihypertensives, Antidiabetic Agents, Anticonvulsants, Lipid-Lowering Agents, Psychotropic Drugs. Semin Liver Dis *22*, 169-184.

Cho, W.C. (2007). Proteomics technologies and challenges. Genomics, proteomics & bioinformatics *5*, 77-85.

Choi, S.S., Kim, J.S., Valerio, L.G., Jr., and Sadrieh, N. (2013). In silico modeling to predict drug-induced phospholipidosis. Toxicology and applied pharmacology *269*, 195-204.

Christians, U., Strohmeyer, S., Kownatzki, R., Schiebel, H.M., Bleck, J., Greipel, J., Kohlhaw, K., Schottmann, R., and Sewing, K.F. (1991). Investigations on the metabolic pathways of cyclosporine: I. Excretion of cyclosporine and its metabolites in human bile--isolation of 12 new cyclosporine metabolites. Xenobiotica; the fate of foreign compounds in biological systems *21*, 1185-1198.

Clark, M.L., Ray, T.S., Paredes, A., Ragland, R.E., Costiloe, J.P., Smith, C.W., and Wolf, S. (1967). Chlorpromazine in women with chronic schizophrenia: the effect on cholesterol levels and cholesterol-behavior relationships. Psychosomatic medicine *29*, 634-642.

Cleeter, M.W., Cooper, J.M., Darley-Usmar, V.M., Moncada, S., and Schapira, A.H. (1994). Reversible inhibition of cytochrome c oxidase, the terminal enzyme of the mitochondrial respiratory chain, by nitric oxide. Implications for neurodegenerative diseases. FEBS letters *345*, 50-54.

Coccia, P.F., and Westerfeld, W.W. (1967). The metabolism of chlorpromazine by liver microsomal enzyme systems. The Journal of pharmacology and experimental therapeutics *157*, 446-458.

Cook, C.S., Berry, L.M., Kim, D.H., Burton, E.G., Hribar, J.D., and Zhang, L. (2002). Involvement of CYP3A in the metabolism of eplerenone in humans and dogs: differential metabolism by CYP3A4 and CYP3A5. Drug metabolism and disposition: the biological fate of chemicals *30*, 1344-1351.

Cushing, D.J., Adams, M.P., Cooper, W.D., Kowey, P.R., and Lipicky, R.J. (2009). Bioequivalence of 2 intravenous amiodarone formulations in healthy participants. Journal of clinical pharmacology *49*, 407-415.

Dambach, D.M., Andrews, B.A., and Moulin, F. (2005). New technologies and screening strategies for hepatotoxicity: use of in vitro models. Toxicologic pathology *33*, 17-26.

Daniel, W.A., Haduch, A., Syrek, M., and Boksa, J. (2006). Direct and indirect interactions between antidepressant drugs and CYP2C6 in the rat liver during long-term treatment. European neuropsychopharmacology: the journal of the European College of Neuropsychopharmacology *16*, 580-587.

de Abajo, F.J., Montero, D., Madurga, M., and Garcia Rodriguez, L.A. (2004). Acute and clinically relevant drug-induced liver injury: a population based case-control study. British journal of clinical pharmacology *58*, 71-80.

de Arriba, G., Calvino, M., Benito, S., and Parra, T. (2013). Cyclosporine A-induced apoptosis in renal tubular cells is related to oxidative damage and mitochondrial fission. Toxicology letters *218*, 30-38.

De Bruyn, T., Ye, Z.W., Peeters, A., Sahi, J., Baes, M., Augustijns, P.F., and Annaert, P.P. (2011). Determination of OATP-, NTCP- and OCT-mediated substrate uptake activities in individual and pooled batches of cryopreserved human hepatocytes. European journal of pharmaceutical sciences: official journal of the European Federation for Pharmaceutical Sciences *43*, 297-307.

De Duve, C., and Baudhuin, P. (1966). Peroxisomes (microbodies and related particles). Physiological reviews *46*, 323-357.

de Jonge, H., de Loor, H., Verbeke, K., Vanrenterghem, Y., and Kuypers, D.R. (2011). In vivo CYP3A activity is significantly lower in cyclosporine-treated as compared with tacrolimus-treated renal allograft recipients. Clinical pharmacology and therapeutics *90*, 414-422.

Detect-iv-e (2014). http://www.detect-iv-e.eu/ (accessed on 08/03/2014).

DIDB, Metabolism and Transport Drug Interaction Database™ - Amiodarone (2014). http://didb.druginteractioninfo.org/Results/DrugListing.aspx?oid=75 (accessed on 18/02/2014).

Dixit, R., and Boelsterli, U.A. (2007). Healthy animals and animal models of human disease(s) in safety assessment of human pharmaceuticals, including therapeutic antibodies. Drug discovery today *12*, 336-342.

Dong, J.Q., and Smith, P.C. (2009). Glucuronidation and covalent protein binding of benoxaprofen and flunoxaprofen in sandwich-cultured rat and human hepatocytes. Drug metabolism and disposition: the biological fate of chemicals *37*, 2314-2322.

Drugbank - Amiodarone (2013). http://www.drugbank.ca/drugs/DB01118 [updated 08/10/2013] (accessed on 14/01/2014).

Drugbank - Cyclosporine (2013). http://www.drugbank.ca/drugs/DB00091 [updated 16/09/2013] (accessed on 29/12/2013).

Ducharme, M.P., Warbasse, L.H., and Edwards, D.J. (1995). Disposition of intravenous and oral cyclosporine after administration with grapefruit juice. Clinical pharmacology and therapeutics *57*, 485-491.

Dykens, J.A., and Will, Y. (2007). The significance of mitochondrial toxicity testing in drug development. Drug discovery today *12*, 777-785.

EFPIA, European Federation of Pharmaceutical Industries and Associations (2014). http://efpia.eu/facts-figures (accessed on 02/02/2014).

Eichelbaum, M., and Schwab, M. (2009). Wirkungen des Organismus auf Pharmaka: allgemeine Pharmakokinetik. Allgemeine und spezielle Pharmakologie und Toxikologie, 10th edn Urban & Fischer, München, 36-64.

Elferink, M. G. L., Olinga, P., Draaisma, A. L., Merema, M. T., Bauerschmidt, S., Polman, J., Schoonen, W.G., and Groothuis, G. M. M. (2008). Microarray analysis in rat liver slices correctly predicts in vivo hepatotoxicity. Toxicology and applied pharmacology *229*, 300-309.

Elkrief, L., Chryssostalis, A., Moachon, L., Franck, N., Terris, B., Chaussade, S., and Sogni, P. (2007). [Severe cholestatic hepatitis associated with Stevens-Johnson syndrome after taking ibuprofen]. Gastroenterologie clinique et biologique *31*, 1043-1045.

EMA, European Medicines Agency (2008). Non-Clinical Guideline on Drug-induced hepatotoxicity. http://www.ema.europa.eu/ema/pages/includes/document/open_document.jsp?webContentId=WC500003355 [updated 21/07/2013] (accessed on 23/03/2014).

Fabre, G., Julian, B., Saint-Aubert, B., Joyeux, H., and Berger, Y. (1993). Evidence for CYP3A-mediated N-deethylation of amiodarone in human liver microsomal fractions. Drug metabolism and disposition: the biological fate of chemicals *21*, 978-985.

FDA, Food and Drug Administration (2009). Guidance for Industry Drug-Induced Liver Injury: Premarketing Clinical Evaluation. http://www.fda.gov/downloads/Drugs/.../Guidances/UCM174090.pdf (accessed on 21/03/2014).

FDA - Food and Drug Administration (2011). http://www.fda.gov/ScienceResearch/BioinformaticsTools/MicroarrayQualityControlProject/#MAQC-IIIalsoknownasSEQC [updated 07/03/2014] (accessed on 08/03/2014).

FDA, Food and Drug Administration (2012). Guidance for Industry: Drug Interaction Studies - Study Design, Data Analysis, Implications for Dosing, and Labeling Recommendations. http://www.fda.gov/downloads/Drugs/GuidanceComplianceRegulatoryInformation/Guidances/ucm292362.pdf (accessed on 25/02/2014).

Felser, A., Blum, K., Lindinger, P.W., Bouitbir, J., and Krahenbuhl, S. (2013). Mechanisms of hepatocellular toxicity associated with dronedarone--a comparison to amiodarone. Toxicological sciences: an official journal of the Society of Toxicology *131*, 480-490.

Feng, B., Mills, J.B., Davidson, R.E., Mireles, R.J., Janiszewski, J.S., Troutman, M.D., and de Morais, S.M. (2008). In vitro P-glycoprotein assays to predict the in vivo interactions of P-glycoprotein with drugs in the central nervous system. Drug metabolism and disposition: the biological fate of chemicals *36*, 268-275.

Flynn, T.J., and Ferguson, M.S. (2010). An in vitro system for studying potential biological mechanisms of human sex differences in susceptibility to acute liver injury. Toxicology letters *198*, 232-236.

Francavilla, A., Ove, P., Polimeno, L., Sciascia, C., Coetzee, M.L., and Starzl, T.E. (1986). Epidermal growth factor and proliferation in rat hepatocytes in primary culture isolated at different times after partial hepatectomy. Cancer research *46*, 1318-1323.

Freneaux, E., Fromenty, B., Berson, A., Labbe, G., Degott, C., Letteron, P., Larrey, D., and Pessayre, D. (1990). Stereoselective and nonstereoselective effects of ibuprofen enantiomers on mitochondrial beta-oxidation of fatty acids. The Journal of pharmacology and experimental therapeutics *255*, 529-535.

Friedman, M.A., Fleming, L.E., Fernandez, M., Bienfang, P., Schrank, K., Dickey, R., Bottein, M.Y., Backer, L., Ayyar, R., Weisman, R.*, et al.* (2008). Ciguatera fish poisoning: treatment, prevention and management. Marine drugs *6*, 456-479.

Fromenty, B., Fisch, C., Berson, A., Letteron, P., Larrey, D., and Pessayre, D. (1990a). Dual effect of amiodarone on mitochondrial respiration. Initial protonophoric uncoupling effect followed by inhibition of the respiratory chain at the levels of complex I and complex II. Journal of Pharmacology and Experimental Therapeutics *255*, 1377-1384.

Fromenty, B., Fisch, C., Labbe, G., Degott, C., Deschamps, D., Berson, A., Letteron, P., and Pessayre, D. (1990b). Amiodarone inhibits the mitochondrial beta-oxidation of fatty acids and produces microvesicular steatosis of the liver in mice. The Journal of pharmacology and experimental therapeutics *255*, 1371-1376.

Fromenty, B., and Pessayre, D. (1995). Inhibition of mitochondrial beta-oxidation as a mechanism of hepatotoxicity. Pharmacology & therapeutics *67*, 101-154.

Furuno, T., Kanno, T., Arita, K., Asami, M., Utsumi, T., Doi, Y., Inoue, M., and Utsumi, K. (2001). Roles of long chain fatty acids and carnitine in mitochondrial membrane permeability transition. Biochemical pharmacology *62*, 1037-1046.

Genedata (2011). Analyst Application Note, Data analysis using Linear Models.

Gerencser, A.A., Neilson, A., Choi, S.W., Edman, U., Yadava, N., Oh, R.J., Ferrick, D.A., Nicholls, D.G., and Brand, M.D. (2009). Quantitative microplate-based respirometry with correction for oxygen diffusion. Analytical chemistry *81*, 6868-6878.

Gerets, H.H., Tilmant, K., Gerin, B., Chanteux, H., Depelchin, B.O., Dhalluin, S., and Atienzar, F.A. (2012). Characterization of primary human hepatocytes, HepG2 cells, and HepaRG cells at the mRNA level and CYP activity in response to inducers and their predictivity for the detection of human hepatotoxins. Cell biology and toxicology *28*, 69-87.

Godoy, P., Hewitt, N., Albrecht, U., Andersen, M., Ansari, N., Bhattacharya, S., Bode, J., Bolleyn, J., Borner, C., Boettger, J.*, et al.* (2013). Recent advances in 2D and 3D in vitro systems using primary hepatocytes, alternative hepatocyte sources and non-parenchymal liver cells and their use in investigating mechanisms of hepatotoxicity, cell signaling and ADME. Arch Toxicol *87*, 1315-1530.

Goldschlager, N., Epstein, A.E., Naccarelli, G., Olshansky, B., and Singh, B. (2000). Practical guidelines for clinicians who treat patients with amiodarone. Practice Guidelines

Subcommittee, North American Society of Pacing and Electrophysiology. Archives of internal medicine *160*, 1741-1748.

Golli-Bennour, E.E., Bouslimi, A., Zouaoui, O., Nouira, S., Achour, A., and Bacha, H. (2012). Cytotoxicity effects of amiodarone on cultured cells. Experimental and toxicologic pathology: official journal of the Gesellschaft fur Toxikologische Pathologie *64*, 425-430.

Gomez-Lechon, M.J., Castell, J.V., and Donato, M.T. (2010). The use of hepatocytes to investigate drug toxicity. Methods in molecular biology (Clifton, NJ) *640*, 389-415.

Gomez-Lechon, M.J., Donato, M.T., Martinez-Romero, A., Jimenez, N., Castell, J.V., and O'Connor, J.E. (2007). A human hepatocellular in vitro model to investigate steatosis. Chemico-biological interactions *165*, 106-116.

Grant, D., Kneteman, N., Tchervenkov, J., Roy, A., Murphy, G., Tan, A., Hendricks, L., Guilbault, N., and Levy, G. (1999). Peak cyclosporine levels (Cmax) correlate with freedom from liver graft rejection: results of a prospective, randomized comparison of neoral and sandimmune for liver transplantation (NOF-8). Transplantation *67*, 1133-1137.

Grant, M.H., Melvin, M.A., Shaw, P., Melvin, W.T., and Burke, M.D. (1985). Studies on the maintenance of cytochromes P-450 and b5, monooxygenases and cytochrome reductases in primary cultures of rat hepatocytes. FEBS letters *190*, 99-103.

GraphPad Prism® (2007). GraphPad Prism® Statistics Guide. http://graphpad.com/downloads/docs/Prism5Stats.pdf (accessed on 05/10/2013).

Grapin-Botton, A. (2008). Endoderm specification. In StemBook (Cambridge MA: 2008 Anne Grapin-Botton.).

Green, D.R., and Reed, J.C. (1998). Mitochondria and apoptosis. Science (New York, NY) *281*, 1309-1312.

Green, S. (1995). PPAR: a mediator of peroxisome proliferator action. Mutation research *333*, 101-109.

Grillo, M.P., and Hua, F. (2008). Enantioselective formation of ibuprofen-S-acyl-glutathione in vitro in incubations of ibuprofen with rat hepatocytes. Chemical research in toxicology *21*, 1749-1759.

Groothuis, F.A., Heringa, M.B., Nicol, B., Hermens, J.L., Blaauboer, B.J., and Kramer, N.I. (2013). Dose metric considerations in in vitro assays to improve quantitative in vitro-in vivo dose extrapolations. Toxicology.

Gunderson, K.L., Kruglyak, S., Graige, M.S., Garcia, F., Kermani, B.G., Zhao, C., Che, D., Dickinson, T., Wickham, E., Bierle, J., *et al.* (2004). Decoding randomly ordered DNA arrays. Genome research *14*, 870-877.

Gygi, S.P., Rochon, Y., Franza, B.R., and Aebersold, R. (1999). Correlation between protein and mRNA abundance in yeast. Molecular and cellular biology *19*, 1720-1730.

Hamman, M.A., Thompson, G.A., and Hall, S.D. (1997). Regioselective and stereoselective metabolism of ibuprofen by human cytochrome P450 2C. Biochemical pharmacology *54*, 33-41.

Hao, H., Wang, G., and Sun, J. (2005). Enantioselective pharmacokinetics of ibuprofen and involved mechanisms. Drug metabolism reviews *37*, 215-234.

Hartmann, F., Gruenke, L.D., Craig, J.C., and Bissell, D.M. (1983). Chlorpromazine metabolism in extracts of liver and small intestine from guinea pig and from man. Drug metabolism and disposition: the biological fate of chemicals *11*, 244-248.

Haynes, V., Elfering, S.L., Squires, R.J., Traaseth, N., Solien, J., Ettl, A., and Giulivi, C. (2003). Mitochondrial nitric-oxide synthase: role in pathophysiology. IUBMB life *55*, 599-603.

Hebert, M.F. (1997). Contributions of hepatic and intestinal metabolism and P-glycoprotein to cyclosporine and tacrolimus oral drug delivery. Advanced drug delivery reviews *27*, 201-214.

Heidebrecht, F., Schulz, I., Keller, M., Behrens, S.E., and Bader, A. (2009). Improved protocols for protein and RNA isolation from three-dimensional collagen sandwich cultures of primary hepatocytes. Analytical biochemistry *393*, 141-144.

Heikkinen, A.T., Monkkonen, J., and Korjamo, T. (2009). Kinetics of cellular retention during Caco-2 permeation experiments: role of lysosomal sequestration and impact on permeability estimates. The Journal of pharmacology and experimental therapeutics *328*, 882-892.

Hellerbrand, C. (2013). Hepatic stellate cells--the pericytes in the liver. Pflugers Archiv: European journal of physiology *465*, 775-778.

Hewitt, N.J., and Hewitt, P. (2004). Phase I and II enzyme characterization of two sources of HepG2 cell lines. Xenobiotica; the fate of foreign compounds in biological systems *34*, 243-256.

HGNC, HUGO Gene Nomenclature Committee (2014). http://www.genenames.org/guidelines.html [updated 02/2014] (accessed on 16/03/2014).

Hoen, P.A., Bijsterbosch, M.K., van Berkel, T.J., Vermeulen, N.P., and Commandeur, J.N. (2001). Midazolam is a phenobarbital-like cytochrome p450 inducer in rats. The Journal of pharmacology and experimental therapeutics *299*, 921-927.

Holt, D.W., Tucker, G.T., Jackson, P.R., and Storey, G.C. (1983). Amiodarone pharmacokinetics. American heart journal *106*, 840-847.

Honegger, U.E., Zuehlke, R.D., Scuntaro, I., Schaefer, M.H., Toplak, H., and Wiesmann, U.N. (1993). Cellular accumulation of amiodarone and desethylamiodarone in cultured human cells. Consequences of drug accumulation on cellular lipid metabolism and plasma membrane properties of chronically exposed cells. Biochemical pharmacology *45*, 349-356.

Horgan, D.J., Singer, T.P., and Casida, J.E. (1968). Studies on the respiratory chain-linked reduced nicotinamide adenine dinucleotide dehydrogenase. 13. Binding sites of rotenone, piericidin A, and amytal in the respiratory chain. The Journal of biological chemistry *243*, 834-843.

Hori, T., Naishiro, Y., Sohma, H., Suzuki, N., Hatakeyama, N., Yamamoto, M., Sonoda, T., Mizue, Y., Imai, K., Tsutsumi, H., *et al.* (2008). CCL8 is a potential molecular candidate for the diagnosis of graft-versus-host disease. Blood *111*, 4403-4412.

Hrach, J. (2009). Toxicogenomic approaches for the prediction of hepatotoxicity in vitro.

HSDB, Hazardous Substances Data Bank - n-butyl chloride (2003). http://toxnet.nlm.nih.gov/cgi-bin/sis/htmlgen?HSDB, searched for n-butyl chloride (CAS 109-69-3) [updated 27/04/2010] (accessed on 22/02/2014).

Huang, B., Wu, P., Bowker-Kinley, M.M., and Harris, R.A. (2002). Regulation of pyruvate dehydrogenase kinase expression by peroxisome proliferator-activated receptor-alpha ligands, glucocorticoids, and insulin. Diabetes *51*, 276-283.

ICH, International Conference on Harmonisation of Technical Requirements for Registration of Pharmaceuticals for Human Use (2009). http://ich.org/products/guidelines/multidisciplinary/article/multidisciplinary-guidelines.html (accessed on 03/02/2014).

ICH, International Conference on Harmonisation of Technical Requirements for Registration of Pharmaceuticals for Human Use (2011). ICH guideline S2(R1): Guidance on genotoxicity testing and data interpretation for pharmaceuticals intended for human use. http://www.ich.org/fileadmin/Public_Web_Site/ICH_Products/Guidelines/Safety/S2_R1/Step4/S2R1_Step4.pdf (accessed on 03/02/2014).

Illsinger, S., Janzen, N., Lucke, T., Bednarczyk, J., Schmidt, K.H., Hoy, L., Sander, J., and Das, A.M. (2011). Cyclosporine A: impact on mitochondrial function in endothelial cells. Clinical transplantation *25*, 584-593.

Illumina (2008). Gene Expression on Sentrix® Arrays – Direct Hybridisation System Manual; Document number 11162460, Revision C 2008.

Illumina (2011). Data Sheet: Gene Expression. Array-Based Gene Expression Analysis. Expression profiling products tailored for a variety of genetic research applications. Illumina Inc. 2011. http://www.illumina.com/documents/products/datasheets/datasheet_gene_exp_analysis.pdf (accessed on 29/10/2012).

Ingelman-Sundberg, M. (2002). Polymorphism of cytochrome P450 and xenobiotic toxicity. Toxicology *181-182*, 447-452.

Ingelman-Sundberg, M., Oscarson, M., and McLellan, R.A. (1999). Polymorphic human cytochrome P450 enzymes: an opportunity for individualized drug treatment. Trends in pharmacological sciences *20*, 342-349.

Iwakiri, Y., and Groszmann, R.J. (2007). Vascular endothelial dysfunction in cirrhosis. Journal of hepatology *46*, 927-934.

Jennings, P., Koppelstaetter, C., Aydin, S., Abberger, T., Wolf, A.M., Mayer, G., and Pfaller, W. (2007). Cyclosporine A induces senescence in renal tubular epithelial cells. American journal of physiology Renal physiology *293*, F831-838.

Jones, H.M., Mayawala, K., and Poulin, P. (2013). Dose selection based on physiologically based pharmacokinetic (PBPK) approaches. The AAPS journal *15*, 377-387.

JRC, Joint Research Centre (2014a). http://ihcp.jrc.ec.europa.eu/our_labs/eurl-ecvam [updated 12/03/2014] (accessed 13/03/2014).

JRC, Joint Research Centre (2014b). http://tsar.jrc.ec.europa.eu/ (accessed 05/02/2014).

Kadenbach, B. (2003). Intrinsic and extrinsic uncoupling of oxidative phosphorylation. Biochimica et biophysica acta *1604*, 77-94.

Kahan, B.D., Shaw, L.M., Holt, D., Grevel, J., and Johnston, A. (1990). Consensus document: Hawk's Cay meeting on therapeutic drug monitoring of cyclosporine. Clinical chemistry *36*, 1510-1516.

Kaplowitz, N. (2004). Drug-induced liver injury. Clinical infectious diseases: an official publication of the Infectious Diseases Society of America *38 Suppl 2*, S44-48.

Katz, N.R. (1992). Metabolic heterogeneity of hepatocytes across the liver acinus. The Journal of nutrition *122*, 843-849.

Kaufmann, P., Torok, M., Hanni, A., Roberts, P., Gasser, R., and Krahenbuhl, S. (2005). Mechanisms of benzarone and benzbromarone-induced hepatic toxicity. Hepatology *41*, 925-935.

Keeney, D.S., Skinner, C., Wei, S., Friedberg, T., and Waterman, M.R. (1998). A keratinocyte-specific epoxygenase, CYP2B12, metabolizes arachidonic acid with unusual selectivity, producing a single major epoxyeicosatrienoic acid. The Journal of biological chemistry *273*, 9279-9284.

Kennedy, J.A., Unger, S.A., and Horowitz, J.D. (1996). Inhibition of carnitine palmitoyltransferase-1 in rat heart and liver by perhexiline and amiodarone. Biochemical pharmacology *52*, 273-280.

Kim, J.S., He, L., and Lemasters, J.J. (2003). Mitochondrial permeability transition: a common pathway to necrosis and apoptosis. Biochemical and biophysical research communications *304*, 463-470.

Kirkland, D., Aardema, M., Henderson, L., and Muller, L. (2005). Evaluation of the ability of a battery of three in vitro genotoxicity tests to discriminate rodent carcinogens and non-carcinogens I. Sensitivity, specificity and relative predictivity. Mutation research *584*, 1-256.

Knadler, M.P., and Hall, S.D. (1990). Stereoselective arylpropionyl-CoA thioester formation in vitro. Chirality *2*, 67-73.

Knights, K.M., Drew, R., and Meffin, P.J. (1988). Enantiospecific formation of fenoprofen coenzyme A thioester in vitro. Biochemical pharmacology *37*, 3539-3542.

Knihinicki, R.D., Day, R.O., Graham, G.G., and Williams, K.M. (1990). Stereoselective disposition of ibuprofen and flurbiprofen in rats. Chirality *2*, 134-140.

Knihinicki, R.D., Williams, K.M., and Day, R.O. (1989). Chiral inversion of 2-arylpropionic acid non-steroidal anti-inflammatory drugs--1. In vitro studies of ibuprofen and flurbiprofen. Biochemical pharmacology *38*, 4389-4395.

Kobayashi, K., Urashima, K., Shimada, N., and Chiba, K. (2002). Substrate specificity for rat cytochrome P450 (CYP) isoforms: screening with cDNA-expressed systems of the rat. Biochemical pharmacology *63*, 889-896.

Kohn, D.F., and Clifford, C. (2002). Biology and diseases of rats. Laboratory animal medicine *2*, 128-131.

Kola, I., and Landis, J. (2004). Can the pharmaceutical industry reduce attrition rates? Nature reviews Drug discovery *3*, 711-715.

Kopera, J., and Armitage, A.K. (1954). Comparison of some pharmacological properties of chlorpromazine, promethazine, and pethidine. British journal of pharmacology and chemotherapy *9*, 392-401.

Kuehl, G.E., Lampe, J.W., Potter, J.D., and Bigler, J. (2005). Glucuronidation of nonsteroidal anti-inflammatory drugs: identifying the enzymes responsible in human liver microsomes. Drug metabolism and disposition: the biological fate of chemicals *33*, 1027-1035.

Kuhn, K., Baker, S.C., Chudin, E., Lieu, M.H., Oeser, S., Bennett, H., Rigault, P., Barker, D., McDaniel, T.K., and Chee, M.S. (2004). A novel, high-performance random array platform for quantitative gene expression profiling. Genome research *14*, 2347-2356.

Kukidome, D., Nishikawa, T., Sonoda, K., Imoto, K., Fujisawa, K., Yano, M., Motoshima, H., Taguchi, T., Matsumura, T., and Araki, E. (2006). Activation of AMP-activated protein kinase reduces hyperglycemia-induced mitochondrial reactive oxygen species production and promotes mitochondrial biogenesis in human umbilical vein endothelial cells. Diabetes *55*, 120-127.

Kuribayashi, T., Tomizawa, M., Seita, T., Tagata, K., and Yamamoto, S. (2011). Relationship between production of acute-phase proteins and strength of inflammatory stimulation in rats. Laboratory animals *45*, 215-218.

Labbe, G., Pessayre, D., and Fromenty, B. (2008). Drug-induced liver injury through mitochondrial dysfunction: mechanisms and detection during preclinical safety studies. Fundamental & clinical pharmacology *22*, 335-353.

Lamb, D.C., Waterman, M.R., Kelly, S.L., and Guengerich, F.P. (2007). Cytochromes P450 and drug discovery. Current opinion in biotechnology *18*, 504-512.

Landrier, J.F., Thomas, C., Grober, J., Duez, H., Percevault, F., Souidi, M., Linard, C., Staels, B., and Besnard, P. (2004). Statin induction of liver fatty acid-binding protein (L-FABP) gene expression is peroxisome proliferator-activated receptor-alpha-dependent. The Journal of biological chemistry *279*, 45512-45518.

Lauer, B. (2012). Gene expression profiling in primary rat hepatocytes for the prediction of hepatotoxicity.

Laurent, S., Rahier, J., Geubel, A.P., Lerut, J., and Horsmans, Y. (2000). Subfulminant hepatitis requiring liver transplantation following ibuprofen overdose. Liver *20*, 93-94.

Lee, E.J., Williams, K., Day, R., Graham, G., and Champion, D. (1985). Stereoselective disposition of ibuprofen enantiomers in man. British journal of clinical pharmacology *19*, 669-674.

Lee, W.M. (2003). Drug-induced hepatotoxicity. The New England journal of medicine *349*, 474-485.

Lehmann, J.M., Lenhard, J.M., Oliver, B.B., Ringold, G.M., and Kliewer, S.A. (1997). Peroxisome proliferator-activated receptors alpha and gamma are activated by indomethacin and other non-steroidal anti-inflammatory drugs. The Journal of biological chemistry *272*, 3406-3410.

Leighton, F., Persico, R., and Necochea, C. (1984). Peroxisomal fatty acid oxidation is selectively inhibited by phenothiazines in isolated hepatocytes. Biochemical and biophysical research communications *120*, 505-511.

Levsen, K., Preiss, A., and Spraul, M. (2003). Structure Elucidation of Unknown Pollutants in Environmental Samples by Coupling of HPLC to NMR and MS. In New horizons and challenges in environmental analysis and monitoring, Workshop, Gdansk (PL), August (pp. 18-29).

Lewis, D.F., and Lake, B.G. (2002). Species differences in coumarin metabolism: a molecular modelling evaluation of CYP2A interactions. Xenobiotica; the fate of foreign compounds in biological systems *32*, 547-561.

Lewis, J.H., Mullick, F., Ishak, K.G., Ranard, R.C., Ragsdale, B., Perse, R.M., Rusnock, E.J., Wolke, A., Benjamin, S.B., Seeff, L.B.*, et al.* (1990). Histopathologic analysis of suspected amiodarone hepatotoxicity. Human pathology *21*, 59-67.

Li, A.P. (2007). Human hepatocytes: isolation, cryopreservation and applications in drug development. Chemico-biological interactions *168*, 16-29.

Li, T., and Chiang, J.Y. (2013). Nuclear receptors in bile acid metabolism. Drug metabolism reviews *45*, 145-155.

Lichtenstein, D.R., Syngal, S., and Wolfe, M.M. (1995). Nonsteroidal antiinflammatory drugs and the gastrointestinal tract. The double-edged sword. Arthritis and rheumatism *38*, 5-18.

Limonciel, A., Aschauer, L., Wilmes, A., Prajczer, S., Leonard, M.O., Pfaller, W., and Jennings, P. (2011). Lactate is an ideal non-invasive marker for evaluating temporal alterations in cell stress and toxicity in repeat dose testing regimes. Toxicology in vitro: an international journal published in association with BIBRA *25*, 1855-1862.

Liu, X., and De Haan, S. (2009). Chlorpromazine dose for people with schizophrenia. The Cochrane database of systematic reviews, CD007778.

Livesey, G. (2003). Health potential of polyols as sugar replacers, with emphasis on low glycaemic properties. Nutrition research reviews *16*, 163-191.

Lores-Arnaiz, S., D'Amico, G., Czerniczyniec, A., Bustamante, J., and Boveris, A. (2004). Brain mitochondrial nitric oxide synthase: in vitro and in vivo inhibition by chlorpromazine. Archives of biochemistry and biophysics *430*, 170-177.

Lovric, J. (2011). Introducing Proteomics: From concepts to sample separation, mass spectrometry and data analysis (John Wiley & Sons).

LTKB, Liver Toxicity Knowledge Base (2014). http://www.fda.gov/ScienceResearch/BioinformaticsTools/LiverToxicityKnowledgeBase/ucm226811.htm [updated 04/01/2014] (accessed on 02/03/2014).

Lucangioli, S.E., Kenndler, E., Carlucci, A., Tripodi, V.P., Scioscia, S.L., and Carducci, C.N. (2003). Relation between retention factors of immunosuppressive drugs in microemulsion electrokinetic chromatography with biosurfactants and octanol-water partition coefficients. Journal of pharmaceutical and biomedical analysis *33*, 871-878.

MacAllister, S.L., Young, C., Guzdek, A., Zhidkov, N., and O'Brien, P.J. (2013). Molecular cytotoxic mechanisms of chlorpromazine in isolated rat hepatocytes. Canadian journal of physiology and pharmacology *91*, 56-63.

Mandenius, C.F., Andersson, T.B., Alves, P.M., Batzl-Hartmann, C., Bjorquist, P., Carrondo, M.J., Chesne, C., Coecke, S., Edsbagge, J., Fredriksson, J.M., *et al.* (2011). Toward preclinical predictive drug testing for metabolism and hepatotoxicity by using in vitro models derived from human embryonic stem cells and human cell lines - a report on the Vitrocellomics EU-project. Alternatives to laboratory animals: ATLA *39*, 147-171.

Marroquin, L.D., Hynes, J., Dykens, J.A., Jamieson, J.D., and Will, Y. (2007). Circumventing the Crabtree effect: replacing media glucose with galactose increases susceptibility of HepG2 cells to mitochondrial toxicants. Toxicological sciences: an official journal of the Society of Toxicology *97*, 539-547.

Martignoni, M., Groothuis, G.M., and de Kanter, R. (2006). Species differences between mouse, rat, dog, monkey and human CYP-mediated drug metabolism, inhibition and induction. Expert opinion on drug metabolism & toxicology *2*, 875-894.

Martins, P.T., Velazquez-Campoy, A., Vaz, W.L., Cardoso, R.M., Valerio, J., and Moreno, M.J. (2012). Kinetics and thermodynamics of chlorpromazine interaction with lipid bilayers: effect of charge and cholesterol. Journal of the American Chemical Society *134*, 4184-4195.

Massart, J., Begriche, K., Buron, N., Porceddu, M., Borgne-Sanchez, A., and Fromenty, B. (2013). Drug-Induced Inhibition of Mitochondrial Fatty Acid Oxidation and Steatosis. Current Pathobiology Reports *1*, 147-157.

McMillian, M.K., Grant, E.R., Zhong, Z., Parker, J.B., Li, L., Zivin, R.A., Burczynski, M.E., and Johnson, M.D. (2001). Nile Red binding to HepG2 cells: an improved assay for in vitro studies of hepatosteatosis. In vitro & molecular toxicology *14*, 177-190.

Mefferd, R.B., Jr., Labrosse, E.H., Gawienowski, A.M., and Williams, R.J. (1958). Influence of chlorpromazine on certain biochemical variables of chronic male schizophrenics. The Journal of nervous and mental disease *127*, 167-179.

Meng, X., Mojaverian, P., Doedee, M., Lin, E., Weinryb, I., Chiang, S.T., and Kowey, P.R. (2001). Bioavailability of amiodarone tablets administered with and without food in healthy subjects. The American journal of cardiology *87*, 432-435.

MGI, Mouse Genome Informatics (2014). http://www.informatics.jax.org/mgihome/nomen/gene.shtml [updated 04/01/2014] (accessed on 16/03/2014).

Milas, L. (2003). Cyclooxygenase-2 (COX-2) enzyme inhibitors and radiotherapy: preclinical basis. American journal of clinical oncology *26*, S66-69.

Milles, D. (1999). History of toxicology. Toxicology California Academic Press, San Diego, 11-23.

Mills, R.F., Adams, S.S., Cliffe, E.E., Dickinson, W., and Nicholson, J.S. (1973). The metabolism of ibuprofen. Xenobiotica; the fate of foreign compounds in biological systems *3*, 589-598.

MIP-DILI (2014). http://mip-dili.eu/index.php#2 (accessed on 08/03/2014).

Modica-Napolitano, J.S., Lagace, C.J., Brennan, W.A., and Aprille, J.R. (2003). Differential effects of typical and atypical neuroleptics on mitochondrial function in vitro. Archives of pharmacal research *26*, 951-959.

Morgan, K.P., Buie, L.W., and Savage, S.W. (2012). The role of mannitol as a nephroprotectant in patients receiving cisplatin therapy. The Annals of pharmacotherapy *46*, 276-281.

Mosmann, T. (1983). Rapid colorimetric assay for cellular growth and survival: application to proliferation and cytotoxicity assays. Journal of immunological methods *65*, 55-63.

Mostafavi-Pour, Z., Khademi, F., Zal, F., Sardarian, A.R., and Amini, F. (2013). In Vitro Analysis of CsA-Induced Hepatotoxicity in HepG2 Cell Line: Oxidative Stress and alpha2 and beta1 Integrin Subunits Expression. Hepatitis monthly *13*, e11447.

Mueller, E.A., Kovarik, J.M., van Bree, J.B., Tetzloff, W., Grevel, J., and Kutz, K. (1994). Improved dose linearity of cyclosporine pharmacokinetics from a microemulsion formulation. Pharmaceutical research *11*, 301-304.

Mulato, A.S., Ho, E.S., and Cihlar, T. (2000). Nonsteroidal anti-inflammatory drugs efficiently reduce the transport and cytotoxicity of adefovir mediated by the human renal organic anion transporter 1. The Journal of pharmacology and experimental therapeutics *295*, 10-15.

Mueller, K., Siems, W.G., Grune, T., David, H., Henke, W., and Jung, K. (1992). Adaptational increase of liver glutathione content during long-term application of cyclosporine A may attenuate toxic side effects. Cellular and molecular biology (Noisy-le-Grand, France) *38*, 729-738.

Mutschler, E., Geisslinger, G., Kroemer, H., and Schaefer-Korting, M. (2013). Mutschler Arzneimittelwirkungen, Lehrbuch der Pharmakologie und Toxikologie. 10. Auflage. Stuttgart: Wissenschaftliche Verlagsgesellschaft mbH.

Nadanaciva, S., and Will, Y. (2009). Current concepts in drug-induced mitochondrial toxicity. Current protocols in toxicology / editorial board, Mahin D Maines (editor-in-chief) [et al] *Chapter 2*, Unit 2 15.

Nasser, M., Larsen, T.R., Waanbah, B., Sidiqi, I., and McCullough, P.A. (2013). Hyperacute drug-induced hepatitis with intravenous amiodarone: case report and review of the literature. Drug, healthcare and patient safety *5*, 191-198.

NIH, National Institutes of Health - Amiodarone (2014). http://livertox.nlm.nih.gov/Amiodarone.htm [updated 03/04/2014] (accessed on 04/04/2014).

NIH, National Institutes of Health - Chlorpromazine (2014). http://livertox.nih.gov/Chlorpromazine.htm [updated 03/04/2014] (accessed on 04/04/2014).

NIH, National Institutes of Health - Cyclosporine (2014). http://livertox.nih.gov/Cyclosporine.htm [updated 03/04/2014] (accessed on 04/04/2014).

NIH, National Institutes of Health - Ibuprofen (2014). http://livertox.nlm.nih.gov/Ibuprofen.htm [updated 03/04/2014] (accessed on 04/04/2014).

Novak, R.F., and Woodcroft, K.J. (2000). The alcohol-inducible form of cytochrome P450 (CYP 2E1): role in toxicology and regulation of expression. Archives of pharmacal research *23*, 267-282.

NTP, National Toxicology Program - 12th Report on Carcinogens (2011). http://ntp.niehs.nih.gov/ntp/roc/twelfth/roc12.pdf (accessed on 19/02/2014).

Oesch, F., and Arand, M. (1999). Xenobiotic metabolism. In Toxicology, H. Marquardt, ed. (New York: Academic Press), pp. 83-109.

Ohyama, K., Nakajima, M., Nakamura, S., Shimada, N., Yamazaki, H., and Yokoi, T. (2000). A significant role of human cytochrome P450 2C8 in amiodarone N-deethylation: an approach to predict the contribution with relative activity factor. Drug metabolism and disposition: the biological fate of chemicals *28*, 1303-1310.

Okuda, T., Norioka, M., Shitara, Y., and Horie, T. (2010). Multiple mechanisms underlying troglitazone-induced mitochondrial permeability transition. Toxicology and applied pharmacology *248*, 242-248.

Ostapowicz, G., Fontana, R.J., Schiodt, F.V., Larson, A., Davern, T.J., Han, S.H., McCashland, T.M., Shakil, A.O., Hay, J.E., Hynan, L.*, et al.* (2002). Results of a prospective study of acute liver failure at 17 tertiary care centers in the United States. Annals of internal medicine *137*, 947-954.

Padda, M.S., Sanchez, M., Akhtar, A.J., and Boyer, J.L. (2011). Drug-induced cholestasis. Hepatology *53*, 1377-1387.

Pagliarani, A., Nesci, S., and Ventrella, V. (2013). Modifiers of the oligomycin sensitivity of the mitochondrial F1F0-ATPase. Mitochondrion *13*, 312-319.

Palayoor, S.T., M, J.A., Makinde, A.Y., Cerna, D., Falduto, M.T., Magnuson, S.R., and Coleman, C.N. (2012). Gene expression profile of coronary artery cells treated with nonsteroidal anti-inflammatory drugs reveals off-target effects. Journal of cardiovascular pharmacology *59*, 487-499.

Palmer, C.N., Hsu, M.H., Griffin, K.J., Raucy, J.L., and Johnson, E.F. (1998). Peroxisome proliferator activated receptor-alpha expression in human liver. Molecular pharmacology *53*, 14-22.

Palmgren, J.J., Monkkonen, J., Korjamo, T., Hassinen, A., and Auriola, S. (2006). Drug adsorption to plastic containers and retention of drugs in cultured cells under in vitro conditions. European journal of pharmaceutics and biopharmaceutics: official journal of Arbeitsgemeinschaft fur Pharmazeutische Verfahrenstechnik eV *64*, 369-378.

Parmentier, C., Truisi, G.L., Moenks, K., Stanzel, S., Lukas, A., Kopp-Schneider, A., Alexandre, E., Hewitt, P.G., Mueller, S.O., and Richert, L. (2013). Transcriptomic hepatotoxicity signature of chlorpromazine after short- and long-term exposure in primary human sandwich cultures. Drug metabolism and disposition: the biological fate of chemicals *41*, 1835-1842.

Pessayre, D., Fromenty, B., Berson, A., Robin, M.A., Letteron, P., Moreau, R., and Mansouri, A. (2012). Central role of mitochondria in drug-induced liver injury. Drug metabolism reviews *44*, 34-87.

PhRMA, Pharmaceutical Research and Manufacturers of America (2014). http://www.phrma.org/research-development-process (accessed on 02/02/2014).

Picard, M., Taivassalo, T., Gouspillou, G., and Hepple, R.T. (2011). Mitochondria: isolation, structure and function. The Journal of physiology *589*, 4413-4421.

Porter, R.K., and Brand, M.D. (1995). Causes of differences in respiration rate of hepatocytes from mammals of different body mass. The American journal of physiology *269*, R1213-1224.

Puli, S.R., Fraley, M.A., Puli, V., Kuperman, A.B., and Alpert, M.A. (2005). Hepatic cirrhosis caused by low-dose oral amiodarone therapy. The American journal of the medical sciences *330*, 257-261.

Qiagen (2010). RNeasy Plus Mini Handbook.

Qian, W.J., Jacobs, J.M., Liu, T., Camp, D.G., 2nd, and Smith, R.D. (2006). Advances and challenges in liquid chromatography-mass spectrometry-based proteomics profiling for clinical applications. Molecular & cellular proteomics: MCP *5*, 1727-1744.

Ràfols, C., Rosés, M., and Bosch, E. (1997). A comparison between different approaches to estimate the aqueous pK_a values of several non-steroidal anti-inflammatory drugs. Analytica chimica acta *338*, 127-134.

Rainsford, K. (1999). History and development of ibuprofen (London: Taylor & Francis, 1999).

Rana, P., Naven, R., Narayanan, A., Will, Y., and Jones, L.H. (2013). Chemical motifs that redox cycle and their associated toxicity. MedChemComm *4*, 1175-1180.

Reasor, M.J., and Kacew, S. (2001). Drug-induced phospholipidosis: are there functional consequences? Experimental biology and medicine (Maywood, NJ) *226*, 825-830.

Rebello, S., Compain, S., Feng, A., Hariry, S., Dieterich, H.A., and Jarugula, V. (2011). Effect of cyclosporine on the pharmacokinetics of aliskiren in healthy subjects. Journal of clinical pharmacology *51*, 1549-1560.

Reddy, J.K., and Lalwai, N.D. (1983). Carcinogenesis by hepatic peroxisome proliferators: evaluation of the risk of hypolipidemic drugs and industrial plasticizers to humans. Critical reviews in toxicology *12*, 1-58.

Regan, S.L., Maggs, J.L., Hammond, T.G., Lambert, C., Williams, D.P., and Park, B.K. (2010). Acyl glucuronides: the good, the bad and the ugly. Biopharmaceutics & drug disposition *31*, 367-395.

Reisner, A.H., Nemes, P., and Bucholtz, C. (1975). The use of Coomassie Brilliant Blue G250 perchloric acid solution for staining in electrophoresis and isoelectric focusing on polyacrylamide gels. Analytical biochemistry *64*, 509-516.

Reynolds, N.J., and Al-Daraji, W.I. (2002). Calcineurin inhibitors and sirolimus: mechanisms of action and applications in dermatology. Clinical and experimental dermatology *27*, 555-561.

Rezzani, R. (2004). Cyclosporine A and adverse effects on organs: histochemical studies. Progress in histochemistry and cytochemistry *39*, 85-128.

Rezzani, R. (2006). Exploring cyclosporine A-side effects and the protective role-played by antioxidants: the morphological and immunohistochemical studies. Histology and histopathology *21*, 301-316.

Richert, L., Liguori, M.J., Abadie, C., Heyd, B., Mantion, G., Halkic, N., and Waring, J.F. (2006). Gene expression in human hepatocytes in suspension after isolation is similar to the liver of origin, is not affected by hepatocyte cold storage and cryopreservation, but is strongly changed after hepatocyte plating. Drug metabolism and disposition: the biological fate of chemicals *34*, 870-879.

Richert, L., Tuschl, G., Abadie, C., Blanchard, N., Pekthong, D., Mantion, G., Weber, J.C., and Mueller, S.O. (2009). Use of mRNA expression to detect the induction of drug metabolising enzymes in rat and human hepatocytes. Toxicology and applied pharmacology *235*, 86-96.

Roberts, K.R., and Hammersley, P.A. (1985). In vitro uptake of gallium and chlorpromazine by mouse tumour cells. European journal of nuclear medicine *10*, 366-368.

Rodriguez-Gonzalez, F.J., Montero, J.L., Puente, J., Fraga, E., Costan, G., Barrera, P., Muntane, J., De la Mata, M., and Zambrana, J.L. (2002). Orthotopic liver transplantation after subacute liver failure induced by therapeutic doses of ibuprofen. The American journal of gastroenterology *97*, 2476-2477.

Rolfe, D.F., Newman, J.M., Buckingham, J.A., Clark, M.G., and Brand, M.D. (1999). Contribution of mitochondrial proton leak to respiration rate in working skeletal muscle and liver and to SMR. The American journal of physiology *276*, C692-699.

Roth, A., Boess, F., Landes, C., Steiner, G., Freichel, C., Plancher, J.M., Raab, S., de Vera Mudry, C., Weiser, T., and Suter, L. (2011). Gene expression-based in vivo and in vitro prediction of liver toxicity allows compound selection at an early stage of drug development. Journal of biochemical and molecular toxicology *25*, 183-194.

Roth, R.A., Luyendyk, J.P., Maddox, J.F., and Ganey, P.E. (2003). Inflammation and drug idiosyncrasy--is there a connection? The Journal of pharmacology and experimental therapeutics *307*, 1-8.

Russell, W.M.S., Burch, R.L., and Hume, C.W. (1959). The principles of humane experimental technique.

Ryffel, B., Mihatsch, M.J., and Fisher, G.L. (1992). Immunosuppression and cancer: the ciclosporin case. Drug and chemical toxicology *15*, 95-115.

RxList - Cordarone (2014). http://www.rxlist.com/cordarone-drug/side-effects-interactions.htm [last reviewed 06/02/2014] (accessed on 18/02/2014).

RxList - Motrin (2007). http://www.rxlist.com/ibuprofen-drug/side-effects-interactions.htm [last reviewed 18/09/2007] (accessed on 18/02/2014).

RxList - Sandimmune (2013). http://www.rxlist.com/sandimmune-drug/side-effects-interactions.htm [17/05/2013] (accessed on 19/02/2014).

RxList - Thorazine (2008). http://www.rxlist.com/thorazine-drug/side-effects-interactions.htm [last reviewed 02/06/2008] (accessed on 20/02/2014).

Sandoval-Acuna, C., Lopez-Alarcon, C., Aliaga, M.E., and Speisky, H. (2012). Inhibition of mitochondrial complex I by various non-steroidal anti-inflammatory drugs and its protection by quercetin via a coenzyme Q-like action. Chemico-biological interactions *199*, 18-28.

Sanoh, S., Horiguchi, A., Sugihara, K., Kotake, Y., Tayama, Y., Ohshita, H., Tateno, C., Horie, T., Kitamura, S., and Ohta, S. (2012). Prediction of in vivo hepatic clearance and half-life of drug candidates in human using chimeric mice with humanized liver. Drug metabolism and disposition: the biological fate of chemicals *40*, 322-328.

Sava, I.G., Battaglia, V., Rossi, C.A., Salvi, M., and Toninello, A. (2006). Free radical scavenging action of the natural polyamine spermine in rat liver mitochondria. Free radical biology & medicine *41*, 1272-1281.

Sawada, H., Takami, K., and Asahi, S. (2005). A toxicogenomic approach to drug-induced phospholipidosis: analysis of its induction mechanism and establishment of a novel in vitro screening system. Toxicological sciences: an official journal of the Society of Toxicology *83*, 282-292.

Scalbert, A., Brennan, L., Fiehn, O., Hankemeier, T., Kristal, B. S., van Ommen, B., Pujos-Guillot, E., Verheij, E., Wishart, D., Wopereis. S. (2009). Mass-spectrometry-based

metabolomics: limitations and recommendations for future progress with particular focus on nutrition research. *Metabolomics*, *5*(4), 435-458.

Schaegger, H., Brandt, U., Gencic, S., and von Jagow, G. (1995). Ubiquinol-cytochrome-c reductase from human and bovine mitochondria. Methods in enzymology *260*, 82-96.

Schena, M., Shalon, D., Davis, R.W., and Brown, P.O. (1995). Quantitative monitoring of gene expression patterns with a complementary DNA microarray. Science (New York, NY) *270*, 467-470.

Scheytt, T., Mersmann, P., Lindstaedt, R., and Heberer, T. (2005). 1-Octanol/water partition coefficients of 5 pharmaceuticals from human medical care: carbamazepine, clofibric acid, diclofenac, ibuprofen, and propyphenazone. Water, air, and soil pollution *165*, 3-11.

Schmelzer, E., Acikgoez, A., Fruhauf, N.R., Crome, O., Klempnauer, J., Christians, U., and Bader, A. (2006). Biotransformation of cyclosporin in primary rat, porcine and human liver cell co-cultures. Xenobiotica; the fate of foreign compounds in biological systems *36*, 693-708.

Schreiber, S.L., and Crabtree, G.R. (1992). The mechanism of action of cyclosporin A and FK506. Immunology today *13*, 136-142.

Schroeder, A., Mueller, O., Stocker, S., Salowsky, R., Leiber, M., Gassmann, M., Lightfoot, S., Menzel, W., Granzow, M., and Ragg, T. (2006). The RIN: an RNA integrity number for assigning integrity values to RNA measurements. BMC molecular biology *7*, 3.

Schulz, S., Schmitt, S., Wimmer, R., Aichler, M., Eisenhofer, S., Lichtmannegger, J., Eberhagen, C., Artmann, R., Tookos, F., Walch, A.*, et al.* (2013). Progressive stages of mitochondrial destruction caused by cell toxic bile salts. Biochimica et biophysica acta *1828*, 2121-2133.

Segawa, M., Ogura, J., Seki, S., Itagaki, S., Takahashi, N., Kobayashi, M., Hirano, T., Yamaguchi, H., and Iseki, K. (2013). Rapid stimulating effect of the antiarrhythmic agent amiodarone on absorption of organic anion compounds. Drug metabolism and pharmacokinetics *28*, 178-186.

Seglen, P. O. (1976). Preparation of isolated rat liver cells. Methods in cell biology *13*, 29-83.

Seipke, R.F., and Hutchings, M.I. (2013). The regulation and biosynthesis of antimycins. Beilstein journal of organic chemistry *9*, 2556-2563.

Sekerova, V., Subrtova, D., Mrazek, F., Gibejova, A., Kolek, V., du Bois, R.M., and Petrek, M. (2003). In vitro pharmacoregulation of CC chemokine ligand 5 and its receptor CCR5 in diffuse lung diseases. Mediators of inflammation *12*, 215-220.

Seki, S., Kobayashi, M., Itagaki, S., Hirano, T., and Iseki, K. (2009). Contribution of organic anion transporting polypeptide OATP2B1 to amiodarone accumulation in lung epithelial cells. Biochimica et biophysica acta *1788*, 911-917.

Senda, N., Hoshi, K., and Fujino, S. (1989). Effects of perphenazine, chlorpromazine or CoCl2 on the activities of delta-aminolevulinic acid synthetase and heme oxygenase and on the

content of hemoprotein in rat liver. Research communications in chemical pathology and pharmacology *65*, 57-64.

Senoo, H., Kojima, N., and Sato, M. (2007). Vitamin A-storing cells (stellate cells). Vitamins and hormones *75*, 131-159.

Setchell, K.D., Heubi, J.E., Shah, S., Lavine, J.E., Suskind, D., Al-Edreesi, M., Potter, C., Russell, D.W., O'Connell, N.C., Wolfe, B.*, et al.* (2013). Genetic defects in bile acid conjugation cause fat-soluble vitamin deficiency. Gastroenterology *144*, 945-955.

Shayeganpour, A., El-Kadi, A.O., and Brocks, D.R. (2006). Determination of the enzyme(s) involved in the metabolism of amiodarone in liver and intestine of rat: the contribution of cytochrome P450 3A isoforms. Drug metabolism and disposition: the biological fate of chemicals *34*, 43-50.

Shi, L., Reid, L.H., Jones, W.D., Shippy, R., Warrington, J.A., Baker, S.C., Collins, P.J., de Longueville, F., Kawasaki, E.S., Lee, K.Y.*, et al.* (2006). The MicroArray Quality Control (MAQC) project shows inter- and intraplatform reproducibility of gene expression measurements. Nature biotechnology *24*, 1151-1161.

Shin, J.G., Soukhova, N., and Flockhart, D.A. (1999). Effect of antipsychotic drugs on human liver cytochrome P-450 (CYP) isoforms in vitro: preferential inhibition of CYP2D6. Drug metabolism and disposition: the biological fate of chemicals *27*, 1078-1084.

Shin, K.J., Lee, D.G., Park, H.M., Choi, M.Y., Bae, J.H., and Lee, E.T. (2013). The merits of mannitol in the repair of orbital blowout fracture. Archives of plastic surgery *40*, 721-727.

Shorrock, C.J., and Rees, W.D. (1988). Overview of gastroduodenal mucosal protection. The American journal of medicine *84*, 25-34.

Simon-Hettich, B., Rothfuss, A., and Steger-Hartmann, T. (2006). Use of computer-assisted prediction of toxic effects of chemical substances. Toxicology *224*, 156-162.

Slikker, W., Jr., Andersen, M.E., Bogdanffy, M.S., Bus, J.S., Cohen, S.D., Conolly, R.B., David, R.M., Doerrer, N.G., Dorman, D.C., Gaylor, D.W.*, et al.* (2004). Dose-dependent transitions in mechanisms of toxicity: case studies. Toxicology and applied pharmacology *201*, 226-294.

Smedsrod, B., De Bleser, P.J., Braet, F., Lovisetti, P., Vanderkerken, K., Wisse, E., and Geerts, A. (1994). Cell biology of liver endothelial and Kupffer cells. Gut *35*, 1509-1516.

Sohns, C., and Zabel, M. (2010). [Current role of amiodarone in antiarrhythmic therapy]. Herzschrittmachertherapie & Elektrophysiologie *21*, 239-243.

Solvobiotech (2014). http://www.solvobiotech.com/barriers/hepatic-barrier (accessed on 09/03/2014).

Spaniol, M., Bracher, R., Ha, H.R., Follath, F., and Krahenbuhl, S. (2001). Toxicity of amiodarone and amiodarone analogues on isolated rat liver mitochondria. Journal of hepatology *35*, 628-636.

Spaniol, M., Kaufmann, P., Beier, K., Wuthrich, J., Torok, M., Scharnagl, H., Marz, W., and Krahenbuhl, S. (2003). Mechanisms of liver steatosis in rats with systemic carnitine

deficiency due to treatment with trimethylhydraziniumpropionate. Journal of lipid research *44*, 144-153.

Staatz, C.E., Goodman, L.K., and Tett, S.E. (2010). Effect of CYP3A and ABCB1 single nucleotide polymorphisms on the pharmacokinetics and pharmacodynamics of calcineurin inhibitors: Part I. Clinical pharmacokinetics *49*, 141-175.

Staehelin, H. (1996). The history of cyclosporin A (Sandimmune®) revisited: Another point of view. Experientia *52*, 5-13.

Stoelting, M., Geyer, M., Reuter, S., Reichelt, R., Bek, M.J., and Pavenstadt, H. (2009). Alpha/beta hydrolase 1 is upregulated in D5 dopamine receptor knockout mice and reduces O2- production of NADPH oxidase. Biochemical and biophysical research communications *379*, 81-85.

Su, Z., Li, Z., Chen, T., Li, Q.Z., Fang, H., Ding, D., Ge, W., Ning, B., Hong, H., Perkins, R.G., *et al.* (2011). Comparing next-generation sequencing and microarray technologies in a toxicological study of the effects of aristolochic acid on rat kidneys. Chemical research in toxicology *24*, 1486-1493.

Taghian, M., Tran, T.A., Bresson-Hadni, S., Menget, A., Felix, S., and Jacquemin, E. (2004). Acute vanishing bile duct syndrome after ibuprofen therapy in a child. The Journal of pediatrics *145*, 273-276.

Tee, L.B., Davies, D.S., Seddon, C.E., and Boobis, A.R. (1987). Species differences in the hepatotoxicity of paracetamol are due to differences in the rate of conversion to its cytotoxic metabolite. Biochemical pharmacology *36*, 1041-1052.

Thermo Fisher Scientific (2010). Thermo Scientific NanoDrop Spectrophotometers – Nucleic Acid, Booklet 2010.

Tracy, T.S., and Hall, S.D. (1991). Determination of the epimeric composition of ibuprofenyl-CoA. Analytical biochemistry *195*, 24-29.

Tracy, T.S., Wirthwein, D.P., and Hall, S.D. (1993). Metabolic inversion of (R)-ibuprofen. Formation of ibuprofenyl-coenzyme A. Drug metabolism and disposition: the biological fate of chemicals *21*, 114-120.

Turrens, J.F. (2003). Mitochondrial formation of reactive oxygen species. The Journal of physiology *552*, 335-344.

Tuschl, G., Hrach, J., Walter, Y., Hewitt, P.G., and Mueller, S.O. (2009). Serum-free collagen sandwich cultures of adult rat hepatocytes maintain liver-like properties long term: a valuable model for in vitro toxicity and drug-drug interaction studies. Chemico-biological interactions *181*, 124-137.

Tuschl, G., Lauer, B., and Mueller, S.O. (2008). Primary hepatocytes as a model to analyze species-specific toxicity and drug metabolism. Expert opinion on drug metabolism & toxicology *4*, 855-870.

Tuschl, G., and Mueller, S.O. (2006). Effects of cell culture conditions on primary rat hepatocytes-cell morphology and differential gene expression. Toxicology *218*, 205-215.

Uehara, T., Kiyosawa, N., Shimizu, T., Omura, K., Hirode, M., Imazawa, T., Mizukawa, Y., Ono, A., Miyagishima, T., Nagao, T., *et al.* (2008). Species-specific differences in coumarin-induced hepatotoxicity as an example toxicogenomics-based approach to assessing risk of toxicity to humans. Human & experimental toxicology *27*, 23-35.

Urdea, M.S., Running, J.A., Horn, T., Clyne, J., Ku, L.L., and Warner, B.D. (1987). A novel method for the rapid detection of specific nucleotide sequences in crude biological samples without blotting or radioactivity; application to the analysis of hepatitis B virus in human serum. Gene *61*, 253-264.

Vamecq, J. (1987). Chlorpromazine and carnitine-dependency of rat liver peroxisomal beta-oxidation of long-chain fatty acids. The Biochemical journal *241*, 783-791.

Van Gelder, R.N., von Zastrow, M.E., Yool, A., Dement, W.C., Barchas, J.D., and Eberwine, J.H. (1990). Amplified RNA synthesized from limited quantities of heterogeneous cDNA. Proceedings of the National Academy of Sciences of the United States of America *87*, 1663-1667.

Vaughan Williams, E.M. (1975). Classification of antidysrhythmic drugs. Pharmacology & therapeutics. Part B: General & systematic pharmacology *1*, 115-138.

Vecera, R., Zacharova, A., Orolin, J., Strojil, J., Skottova, N., and Anzenbacher, P. (2011). Fenofibrate-induced decrease of expression of CYP2C11 and CYP2C6 in rat. Biopharmaceutics & drug disposition *32*, 482-487.

Vertemati, M., Minola, E., Dolci, C., Stabellini, G., Pezzetti, F., Moscheni, C., Calastrini, C., Bramerio, M., Palmieri, A., and Vizzotto, L. (2009). Gene expression, cytoskeletal changes and extracellular matrix synthesis in human osteoblasts treated with cyclosporin A. Biomedicine & pharmacotherapy = Biomedecine & pharmacotherapie *63*, 619-626.

Vickers, A.E., Fischer, V., Connors, S., Fisher, R.L., Baldeck, J.P., Maurer, G., and Brendel, K. (1992). Cyclosporin A metabolism in human liver, kidney, and intestine slices. Comparison to rat and dog slices and human cell lines. Drug metabolism and disposition: the biological fate of chemicals *20*, 802-809.

Wagner, M., Zollner, G., and Trauner, M. (2009). New molecular insights into the mechanisms of cholestasis. Journal of hepatology *51*, 565-580.

Waldhauser, K.M., Torok, M., Ha, H.R., Thomet, U., Konrad, D., Brecht, K., Follath, F., and Krahenbuhl, S. (2006). Hepatocellular toxicity and pharmacological effect of amiodarone and amiodarone derivatives. The Journal of pharmacology and experimental therapeutics *319*, 1413-1423.

Wang, J., Hughes, T.P., Kok, C.H., Saunders, V.A., Frede, A., Groot-Obbink, K., Osborn, M., Somogyi, A.A., D'Andrea, R.J., and White, D.L. (2012). Contrasting effects of diclofenac and

ibuprofen on active imatinib uptake into leukaemic cells. British journal of cancer *106*, 1772-1778.

Wang, J.S., Zhu, H.J., Markowitz, J.S., Donovan, J.L., Yuan, H.J., and Devane, C.L. (2008). Antipsychotic drugs inhibit the function of breast cancer resistance protein. Basic & clinical pharmacology & toxicology *103*, 336-341.

Wang, K., Shindoh, H., Inoue, T., and Horii, I. (2002). Advantages of in vitro cytotoxicity testing by using primary rat hepatocytes in comparison with established cell lines. The Journal of toxicological sciences *27*, 229-237.

Watkins, P.B. (1997). The barrier function of CYP3A4 and P-glycoprotein in the small bowel. Advanced drug delivery reviews *27*, 161-170.

Werther, J.L., and Korelitz, B.I. (1957). Chlorpromazine jaundice; analysis of twenty-two cases. The American journal of medicine *22*, 351-366.

Williamson, J.R., and Corkey, B.E. (1979). Assay of citric acid cycle intermediates and related compounds--update with tissue metabolite levels and intracellular distribution. Methods in enzymology *55*, 200-222.

Wilmes, A., Limonciel, A., Aschauer, L., Moenks, K., Bielow, C., Leonard, M.O., Hamon, J., Carpi, D., Ruzek, S., Handler, A.*, et al.* (2013). Application of integrated transcriptomic, proteomic and metabolomic profiling for the delineation of mechanisms of drug induced cell stress. Journal of proteomics *79*, 180-194.

Wisse, E., Luo, D., Vermijlen, D., Kanellopoulou, C., De Zanger, R., and Braet, F. (1997). On the function of pit cells, the liver-specific natural killer cells. Semin Liver Dis *17*, 265-286.

Wissen (2014). http://www.wissen.de/medizin/leberlaeppchen (accessed on 10/02/2014).

Wojcikowski, J., Boksa, J., and Daniel, W.A. (2010). Main contribution of the cytochrome P450 isoenzyme 1A2 (CYP1A2) to N-demethylation and 5-sulfoxidation of the phenothiazine neuroleptic chlorpromazine in human liver--A comparison with other phenothiazines. Biochemical pharmacology *80*, 1252-1259.

Wu, E.Y., Smith, M.T., Bellomo, G., and Di Monte, D. (1990). Relationships between the mitochondrial transmembrane potential, ATP concentration, and cytotoxicity in isolated rat hepatocytes. Archives of biochemistry and biophysics *282*, 358-362.

Xiao, Z., Shan, J., Li, C., Luo, L., Lu, J., Li, S., Long, D., and Li, Y. (2013). Mechanisms of cyclosporine-induced renal cell apoptosis: a systematic review. American journal of nephrology *37*, 30-40.

Yang, Q., Nagano, T., Shah, Y., Cheung, C., Ito, S., and Gonzalez, F.J. (2008). The PPAR alpha-humanized mouse: a model to investigate species differences in liver toxicity mediated by PPAR alpha. Toxicological sciences: an official journal of the Society of Toxicology *101*, 132-139.

Yoshii, K., Kobayashi, K., Tsumuji, M., Tani, M., Shimada, N., and Chiba, K. (2000). Identification of human cytochrome P450 isoforms involved in the 7-hydroxylation of chlorpromazine by human liver microsomes. Life sciences *67*, 175-184.

Zahno, A., Brecht, K., Morand, R., Maseneni, S., Torok, M., Lindinger, P.W., and Krahenbuhl, S. (2011). The role of CYP3A4 in amiodarone-associated toxicity on HepG2 cells. Biochemical pharmacology *81*, 432-441.

Zatloukal, K., French, S.W., Stumptner, C., Strnad, P., Harada, M., Toivola, D.M., Cadrin, M., and Omary, M.B. (2007). From Mallory to Mallory-Denk bodies: what, how and why? Experimental cell research *313*, 2033-2049.

Zhou, S.F., Zhou, Z.W., and Huang, M. (2010). Polymorphisms of human cytochrome P450 2C9 and the functional relevance. Toxicology *278*, 165-188.

Zieske, L.R. (2006). A perspective on the use of iTRAQ reagent technology for protein complex and profiling studies. Journal of experimental botany *57*, 1501-1508.

Zochowska, D., Wyzgał, J., and Paczek, L. (2011). Impact of CYP3A4* 1B and CYP3A5* 3 polymorphisms on the pharmacokinetics of cyclosporine and sirolimus in renal transplant recipients. Annals of transplantation: quarterly of the Polish Transplantation Society *17*, 36-44.

Zollner, G., Fickert, P., Zenz, R., Fuchsbichler, A., Stumptner, C., Kenner, L., Ferenci, P., Stauber, R.E., Krejs, G.J., Denk, H.*, et al.* (2001). Hepatobiliary transporter expression in percutaneous liver biopsies of patients with cholestatic liver diseases. Hepatology *33*, 633-646.

Zorn, A.M. (2008). Liver development. In StemBook [Internet]. Cambridge (MA) Harvard Stem Cell Institute. http://www.ncbi.nlm.nih.gov/books/NBK27068/ (accessed on 09/02/2014).

Zuber, R., Anzenbacherova, E., and Anzenbacher, P. (2002). Cytochromes P450 and experimental models of drug metabolism. Journal of cellular and molecular medicine *6*, 189-198.

6 Appendix

Appendix 1: Total numbers of deregulated genes in primary rat and human hepatocytes.

Table 39. Number of deregulated genes (BH q-Value ≤ 0.05 and fold change ≥ 2) in primary rat hepatocytes after treatment with the corresponding high concentration of selected compounds for 1, 3 or 14 days (d).

Compound	d1	d3	d14
Ibuprofen	13	36	56
Chlorpromazine	7	24	178
Cyclosporine A	45	155	78
Amiodarone	0	0	0

Table 40. Number of deregulated genes (fold change ≥ 2) in primary human hepatocytes from the different donors after treatment with the corresponding low and high concentration of selected compounds for 1, 3 or 14 days (d).

		Low concentration			High concentration		
Compound	Donor	d1	d3	d14	d1	d3	d14
Ibuprofen	1	1254	85	2048	1684	1357	1719
	2	24	85	162	762	977	2104
	3	912	220	113	401	1037	294
Chlorpromazine	1	1336	6	20	1348	11	1630
	2	7	63	135	10	356	12
	3	367	16	65	367	17	73
Cyclosporine A	1	1101	173	156	1624	667	2104
	2	10	55	34	143	166	315
	3	317	10	-	88	127	-
Amiodarone	1	8	34	8	3	15	68
	2	6	37	173	28	4	840
	3	212	7	-	7	62	-

Appendix 2: CYP induction in primary rat hepatocytes.

Table 41. Target genes included in the 17-plex set for rat (customised panel, number 31104).

Target Symbol	Target Name
Ahr	Aryl hydrocarbon receptor
Nr1i3	Nuclear receptor subfamily 1, group I, member 3
Nr1i2	Nuclear receptor subfamily 1, group I, member 2
Cyp1a1	Cytochrome P450, family 1, subfamily a, polypeptide 1
Cyp1a2	Cytochrome P450, family 1, subfamily a, polypeptide 2
Cyp2b2	Cytochrome P450, family 1, subfamily b, polypeptide 1
Cyp2c	Cytochrome P450, family 1, subfamily IIc (Mephenytoin 4-hydroxylase)
Cyp3a1	Cytochrome P450-PCN (PNCN inducible)
Cyp4a1	Cytochrome P450, family 4, subfamily a, polypeptide 22
Abcb1a	ATP-binding cassette, sub-family B (MDR/TAP), member 1A
Abcb1b	ATP-binding cassette, sub-family B (MDR/TAP), member 1
Abcb11	ATP-binding cassette, sub-family B (MDR/TAP), member 11
Abcc2	ATP-binding cassette, sub-family C (CFTR/MRP), member 2
Ugt1a6	UDP glycosyltransferase 1 family, polypeptide A6
Ppib	Cyclophilin B
Hprt1	Hypoxanthine guanine phosphoribosyl transferase
Hmbs	Hydroxymethylbilane synthase

Table 42. Results of the cytochrome P450 induction study of the primary rat hepatocytes from the five replicates treated with 3-methylcholanthren for 72 h. Values are normalised to the gene expression of a housekeeper and given as fold changes towards the vehicle treated control.

	Replicate 1	Replicate 2	Replicate 3	Replicate 4	Replicate 5
Ahr	1.3	1.2	1.4	1.3	1.4
Nr1i3	3.0	32.6	5.7	1.6	1.2
Nr1i2	0.6	0.7	1.2	0.6	0.7
CYP1a1	38.6	127.1	199.0	147.6	86.4
CYP1a2	125.6	278.1	323.2	259.9	431.1
CYP2b2	1.4	0.8	1.4	0.9	0.5
CYP2c	0.2	0.3	0.9	0.3	0.4
CYP3a1	1.5	1.5	1.9	0.6	0.7
CYP4a1	1.1	1.5	1.9	0.5	0.3

Table 43. Results of the cytochrome P450 induction study of the primary rat hepatocytes from the five replicates treated with pregnenolone-16α-carbonitrile for 72 h. Values are normalised to the gene expression of a housekeeper and given as fold changes towards the vehicle treated control.

	Replicate 1	Replicate 2	Replicate 3	Replicate 4	Replicate 5
Ahr	1.0	1.1	1.2	1.3	1.1
Nr1i3	0.5	10.5	3.2	2.1	1.6
Nr1i2	0.5	0.8	1.2	1.3	1.3
CYP1a1	0.8	2.3	1.7	2.4	3.8
CYP1a2	0.7	1.0	0.8	0.6	2.0
CYP2b2	1.1	1.1	1.2	1.0	1.0
CYP2c	3.2	3.6	3.3	2.3	2.5
CYP3a1	162.4	324.3	63.9	22.7	26.6
CYP4a1	0.2	0.1	0.4	0.3	0.2

Table 44. Results of the cytochrome P450 induction study of the primary rat hepatocytes from the five replicates treated with dexamethasone for 72 h. Values are normalised to the gene expression of a housekeeper and given as fold changes towards the vehicle treated control.

	Replicate 1	Replicate 2	Replicate 3	Replicate 4	Replicate 5
Ahr	1.4	1.3	1.6	1.4	1.4
Nr1i3	1.1	3.5	5.6	0.9	0.7
Nr1i2	0.9	0.2	1.3	1.0	1.2
CYP1a1	0.8	0.2	2.2	1.6	6.2
CYP1a2	1.2	0.1	1.1	0.5	1.7
CYP2b2	1.8	0.1	1.2	0.5	0.6
CYP2c	4.4	4.5	2.2	0.9	1.3
CYP3a1	241.8	382.7	67.4	14.8	17.9
CYP4a1	0.4	0.0	0.5	0.2	0.2

Table 45. Results of the cytochrome P450 induction study of the primary rat hepatocytes from the five replicates treated with phenobarbital for 72 h. Values are normalised to the gene expression of a housekeeper and given as fold changes towards the vehicle treated control.

	Replicate 1	Replicate 2	Replicate 3	Replicate 4	Replicate 5
Ahr	1.3	1.3	1.5	1.4	1.7
Nr1i3	2.7	13.9	1.8	1.5	2.9
Nr1i2	1.3	1.4	1.7	1.1	1.5
CYP1a1	1.0	3.5	7.6	24.0	7.1
CYP1a2	2.8	3.6	3.5	5.3	4.5
CYP2b2	12.8	3.3	2.8	5.0	36.0
CYP2c	3.7	3.4	3.1	1.6	2.8
CYP3a1	176.3	123.8	25.9	8.7	16.7
CYP4a1	1.1	0.8	1.6	0.6	0.7

Appendix 3: CYP activities in primary rat hepatocytes.

The quantification of the rat CYP metabolites was performed at the DMPK department in Grafing. Several preliminary experiments were conducted for method evaluation. The method was not fully established by the time the first biological replicate was processed, thus these results are missing in Table 46.

Table 46. Cytochrome P450 activities in the primary rat hepatocytes from the four replicates.

	Metabolite in nM/min x mg protein			
	Replicate 2	**Replicate 3**	**Replicate 4**	**Replicate 5**
1-OH-Midazolam (CYP3A1)	2.9	3.1	2.9	3.6
4-OH-Midazolam (CYP3A1)	0.8	0.9	1.3	1.2
Acetaminophen (CYP2A1)	1.7	2.1	3.1	3.9

Appendix 4: CYP activities in primary human hepatocytes from different donors.

Table 47. Cytochrome P450 activities in the primary human hepatocytes from the three donors (personal communication).

	Activity in pmol/min/mg protein		
	Donor 1	**Donor 2**	**Donor 3**
CYP1A2	0.0	0.2	0.1
CYP2B6	5.3	23.1	22.1
CYP3A4	0.1	33.4	No peak
CYP2C9	3.8	29.9	15.1
CYP2D6	0.3	3.4	0.8

Appendix 5: High-content imaging cell count.

Table 48. Mean primary rat hepatocyte number per well of a 6-well plate from the different biological replicates after 1 and 14 days (d) in culture.

	Replicate 3	Replicate 5
d 1	520,386	789,254
d 14	616,580	625,620

Appendix 6: Biokinetic blank experiments

For the biokinetics studies so-called "blank experiments" were performed in order to evaluate the amount of compound potentially sequestered by the collagen I (PRH). The blank experiments were processed in the same manner as the cell culture experiment but just without cells. The blank experiments in PHH are therefore not included here because the media at 0 min was not collected; thus, the relative amount sequestered by the GelTrex™ could not be calculated.

Table 49. Percentage of ibuprofen (IBU) in collagen I treated with 10 and 100 µM IBU, corresponding to the treatment concentrations for primary rat hepatocytes (PRH) on day (d) 0 and 13. The results are given in percent of the total added amount measured in the medium at 0 min.

PRH		10 µM IBU	100 µM IBU
		% of IBU	
d 0	2 min	1.6	3.4
	24 h	13.6	15.1
d 13	2 min	29.3	28.5
	24 h	31.4	26.4

Table 50. Percentage of chlorpromazine (CPZ) in collagen I treated with 2 and 20 µM CPZ, corresponding to the treatment concentrations for primary rat hepatocytes (PRH) on day (d) 0 and 13. The results are given in percent of the total added amount measured in the medium at 0 min.

PRH		2 µM CPZ	20 µM CPZ
		% of CPZ	
d 0	2 min	9.8	0.6
	24 h	9.7	2.0
d 13	2 min	35.9	33.0
	24 h	25.9	26.1

Table 51. Percentage of cyclosporine A (CsA) in collagen I treated with 0.25 and 2.5 µM CsA, corresponding to the treatment concentrations for primary rat hepatocytes (PRH) on day (d) 0 and 13. The results are given in percent of the total added amount measured in the medium at 0 min.

PRH		0.25 µM CsA	2.5 µM CsA
		% of CsA	
d 0	2 min	2.8	3.6
	24 h	11.9	7.9
d 13	2 min	29.5	36.5
	24 h	19.9	28.4

Table 52. Percentage of amiodarone (AMI) in collagen I treated with 0.1 and 1 µM AMI, corresponding to the treatment concentrations for primary rat hepatocytes (PRH) on day (d) 0 and 13. The results are given in percent of the total added amount measured in the medium at 0 min.
Abbreviation: LOD - limit of detection.

PRH		0.1 µM AMI	1 µM AMI
		% of AMI	
d 0	2 min	< LOD	5.4
	24 h	< LOD	81.6
d 13	2 min	< LOD	384.8
	24 h	< LOD	356.7

Appendix 7: Biokinetic profile of 1st biological PRH replicate.

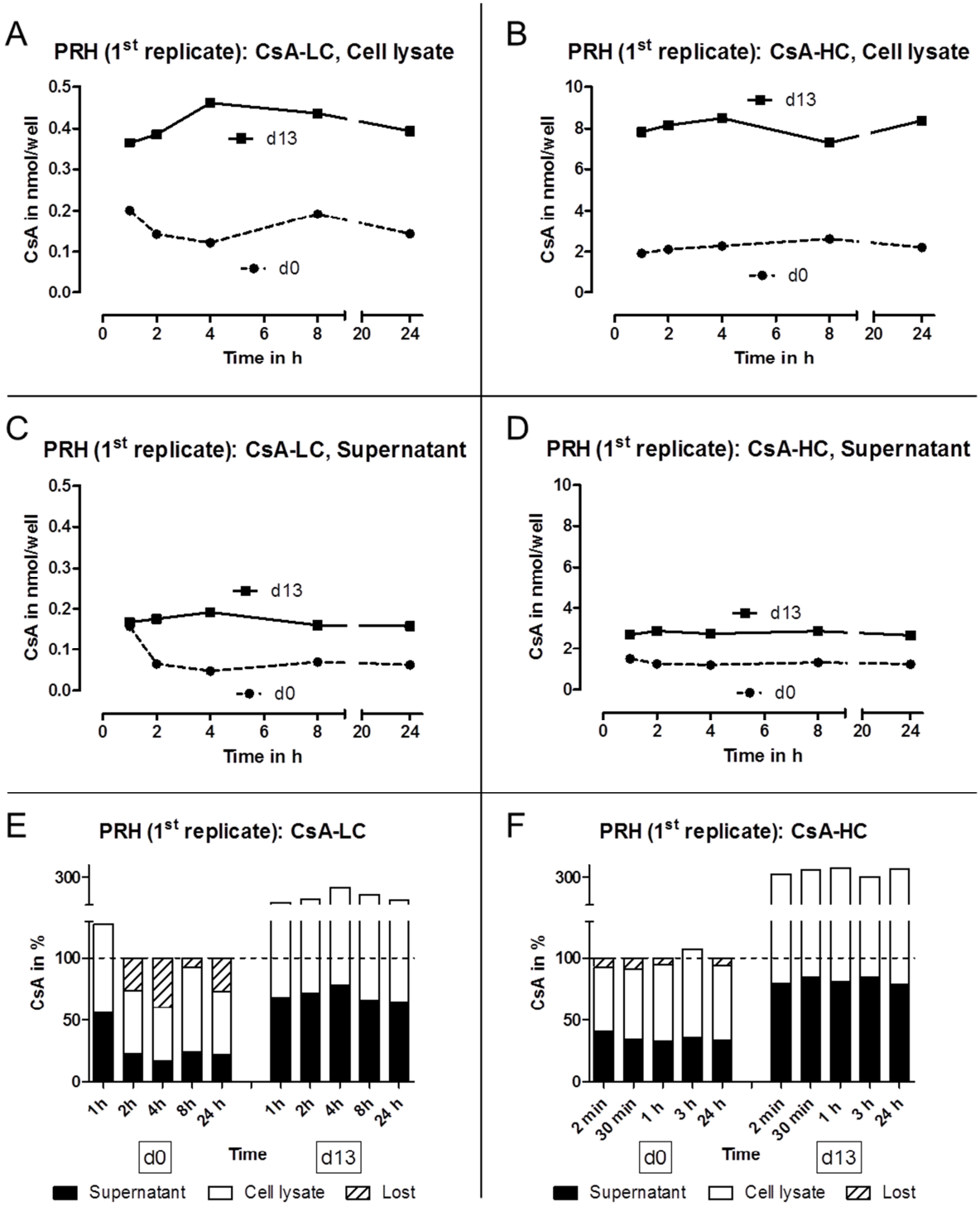

Figure 58. Kinetic profile of cyclosporine A (CsA) (nmol/well) in primary rat hepatocytes (PRH) (A, B) and culture supernatants (B, E) after single (day 0 – dashed line) and repeated (day 13 – solid line) treatment with 0.25 µM (low concentration (LC); A, C) and 2.5 µM (high concentration (HC); B, D) CsA at the indicated time points. Relative distribution (%) of CsA in the different analysed PRH fractions at the indicated time points on day 0 and 13, supernatant (bold) and cell lysate (blank) as well as the apparent loss (striped) for the LC (E) and HC (F). Values derive from 1 biological replicate (1st biological replicate).

Appendix 8: Gene deregulations in primary rat hepatocytes.

Table 53. Absolute fold changes of genes deregulated at least 2-fold (BH q-value ≤ 0.05) compared to the time matched vehicle treated control in primary rat hepatocytes treated with 100 µM ibuprofen for 1, 3 or 14 days. The genes are in alphabetic order within each function.

RefSeq	Symbol	Function	Gene name	d01	d03	d14
XM_001062085.1	*Acaa1b*		acetyl-Coenzyme A acyltransferase 1B (RGD1562373_predicted)	7.2	7.7	8.6
NM_130433.1	*Acaa2*		acetyl-Coenzyme A acyltransferase 2 (Acaa2), nuclear gene encoding mitochondrial protein	1.7	1.6	2.2
NM_017075.1	*Acat1*		acetyl-coenzyme A acetyltransferase 1 (Acat1), nuclear gene encoding mitochondrial protein	1.5	2.1	2.3
NM_031315.1	*Acot1*		acyl-CoA thioesterase 1 (Acot1)	3.2	20.5	18.8
NM_138907.2	*Acot2*		acyl-CoA thioesterase 2 (Acot2), nuclear gene encoding mitochondrial protein	2.0	2.6	2.1
NM_017340.1	*Acox1*		acyl-Coenzyme A oxidase 1, palmitoyl (Acox1)	1.9	2.3	3.6
NM_012820.1	*Acsl1*		acyl-CoA synthetase long-chain family member 1 (Acsl1)	1.6	1.6	3.1
NM_013200.1	*Cpt1b*		carnitine palmitoyltransferase 1b, muscle (Cpt1b), nuclear gene encoding mitochondrial protein	1.6	2.3	1.7
NM_001004085.2	*Crat*		carnitine acetyltransferase (Crat), nuclear gene encoding mitochondrial protein	1.8	1.5	2.1
NM_175837.1	*Cyp4a1*	Fatty acid and lipid metabolism	cytochrome P450, family 4, subfamily a, polypeptide 1 (Cyp4a1)	5.6	5.0	5.4
NM_153307.1	*Cyp4a10*		cytochrome P450, family 4, subfamily a, polypeptide 10 (Cyp4a10)	3.3	4.3	3.7
XM_001072959.1	*Cyp4a2*		cytochrome P450, family 4, subfamily a, polypeptide 2 (CYPIVA2) (LOC690021)	1.9	2.2	3.3
NM_175760.2	*Cyp4a3*		cytochrome P450, family 4, subfamily a, polypeptide 3 (Cyp4a3)	1.5	1.5	2.2
NM_171996.2	*Decr2*		2,4-dienoyl CoA reductase 2, peroxisomal (Decr2)	1.8	2.2	2.5
NM_022594.1	*Ech1*		enoyl coenzyme A hydratase 1, peroxisomal (Ech1)	2.0	1.5	2.3
NM_012556.1	*Fabp1*		fatty acid binding protein 1, liver (Fabp1)	2.1	1.4	2.6
NM_001009632.1	*G0s2*		G0/G1switch 2 (G0s2)	1.2	1.2	2.1
NM_053493.1	*Hacl1*		2-hydroxyacyl-CoA lyase 1 (Hacl1)	1.6	1.7	2.5
NM_057186.1	*Hadh*		hydroxyacyl-Coenzyme A dehydrogenase (Hadh), nuclear gene encoding mitochondrial protein	1.5	1.7	2.0
NM_053551.1	*Pdk4*		pyruvate dehydrogenase kinase, isozyme 4 (Pdk4)	1.6	1.3	3.0
NM_031841.1	*Scd*		stearoyl-CoA desaturase (delta-9-desaturase) (Scd)	1.1	2.0	2.0
NM_013155.1	*Vldlr*		very low density lipoprotein receptor (Vldlr)	1.1	2.6	1.7

Table 53 (continued)

RefSeq	Symbol	Function	Gene name	d01	d03	d14
NM_012753.1	*Cyp17a1*	Steroid metabolism	cytochrome P450, family 17, subfamily a, polypeptide 1 (Cyp17a1)	2.1	2.3	2.0
NM_173294.1	*Cyp2b3*		cytochrome P450IIB3 (Cyp2b3)	1.2	-1.2	2.1
XM_001069696.1	*Sdr16c6*		short chain dehydrogenase/reductase family 16C, member 6 (RGD1562060_predicted)	1.0	1.8	6.8
XM_001074217.1	*ste2*		estrogen sulfotransferase (ste2)	1.4	4.8	3.2
NM_022936.1	*Ephx2*	Inflammation	epoxide hydrolase 2, cytoplasmic (Ephx2)	1.8	1.8	2.5
NM_001001505.1	*Habp2*		hyaluronan binding protein 2 (Habp2)	-1.2	-1.3	-2.0
NM_053373.1	*Pglyrp1*		peptidoglycan recognition protein 1 (Pglyrp1)	-1.6	-2.1	-1.7
XM_001071113.1	*Aig1*	Immune response	androgen-induced 1 (RGD1562920_predicted)	2.4	2.0	2.2
XM_001063391.1	*Il17rb*		interleukin 17 receptor B (predicted) (Il17rb_predicted)	-1.7	-2.0	-1.1
NM_199082.1	*Sectm1*		secreted and transmembrane 1 (Sectm1)	1.4	1.8	2.1
XM_001070818.1	*Cyp2b15*	Xenobiotic metabolism	cytochrome P450, family 2, subfamily b, polypeptide 15, transcript variant 2 (Cyp2b15)	2.0	1.6	2.8
NM_019184.1	*Cyp2c*		Cytochrome P450, subfamily IIC (mephenytoin 4-hydroxylase) (Cyp2c)	-1.4	-2.8	-2.9
NM_153312.2	*Cyp3a2*		cytochrome P450, family 3, subfamily a, polypeptide 2 (Cyp3a2)	1.6	2.8	7.6
NM_031732.1	*Sult1c1*		sulfotransferase family, cytosolic, 1C, member 1 (Sult1c1)	1.1	2.2	2.2
XM_001062962.1	*A2ug*	Other and unknown functions	alpha 2U globulin (LOC366380)	1.6	4.1	3.2
NM_001008520.1	*Abhd1*		abhydrolase domain containing 1 (Abhd1)	1.8	1.8	2.2
NM_012498.1	*Akr1b1*		aldo-keto reductase family 1, member B1 (aldose reductase) (Akr1b1)	-1.0	-1.2	-2.2
NM_019157.2	*Aqp7*		aquaporin 7 (Aqp7)	1.1	3.0	3.9
NM_053995.3	*Bdh1*		3-hydroxybutyrate dehydrogenase, type 1 (Bdh1), nuclear gene encoding mitochondrial protein	1.2	1.9	2.3
NM_019274.1	*Colq*		collagen-like tail subunit (single strand of homotrimer) of asymmetric acetylcholinesterase (Colq)	2.0	2.3	2.0
NM_021750.1	*Csad*		cysteine sulfinic acid decarboxylase (Csad)	1.2	1.6	2.4
NM_022266.2	*Ctgf*		connective tissue growth factor (Ctgf)	-2.6	-1.7	-1.5
XM_001077664.1	*Cyp4f37*		cytochrome P450, family 4, subfamily f, polypeptide 37	1.1	2.0	1.3

Table 53 (continued)

RefSeq	Symbol	Function	Gene name	d01	d03	d14
XM_001060919.1	*Dapk1*	Other and unknown functions	death associated protein kinase 1 (predicted) (Dapk1_predicted)	1.3	2.0	1.7
XM_001056685.1	*Flna*		filamin, alpha (predicted) (Flna_predicted)	-1.3	-1.1	-2.2
XM_219785.4	*Gldc*		glycine decarboxylase (predicted) (Gldc_predicted)	1.4	2.5	1.8
NM_017061.1	*Lox*		lysyl oxidase (Lox)	-1.2	-1.1	-2.8
NM_203325.1	*Mup5*		major urinary protein 5 (Mup5)	1.0	1.8	2.2
NM_022521.2	*Oat*		ornithine aminotransferase (gyrate atrophy) (Oat), nuclear gene encoding mitochondrial protein	1.0	2.1	1.7
XM_001073225.1	*Rcn1*		reticulocalbin 1 (predicted) (Rcn1_predicted)	-2.1	-1.5	-1.6
NM_145084.1	*Retsat*		retinol saturase (all trans retinol 13,14 reductase) (Retsat)	1.5	2.4	3.1
NM_053453.1	*Rgs2*		regulator of G-protein signaling 2 (Rgs2)	-1.0	-2.0	-2.1
XM_343823.2	*Serpina7*		serine (or cysteine) peptidase inhibitor, clade A (alpha-1 antipeptidase, antitrypsin), member 7 (Serpina7)	1.4	1.4	2.9
XM_343604.3	*Serpine2*		serine (or cysteine) proteinase inhibitor, clade E, member 2 (Serpine2)	1.2	2.5	3.9
NM_053424.1	*Slc4a4*		solute carrier family 4 (anion exchanger), member 4 (Slc4a4)	1.0	2.4	1.9
NM_133623.1	*Slc6a13*		solute carrier family 6 (neurotransmitter transporter, GABA), member 13 (Slc6a13)	1.6	2.2	2.2
NM_152936.1	*Spink1*		serine peptidase inhibitor, Kazal type 1 (Spink1)	1.2	1.8	2.7
NM_022298.1	*Tuba1a*		tubulin, alpha 1A (Tuba1a)	-1.3	-1.4	-2.3
XM_574282.2	*Vnn3*		vanin 3 (RGD1560609_predicted)	1.1	1.4	2.2
NM_052798.1	*Zfp354a*		zinc finger protein 354A (Zfp354a)	1.1	1.2	2.1

Table 54. Absolute fold changes of genes deregulated at least 2-fold (BH q-value ≤ 0.05) compared to the vehicle treated control in primary rat hepatocytes treated with 20 µM chlorpromazine for 1, 3 or 14 days. The genes are in alphabetic order within each function.

RefSeq	Symbol	Function	Gene name	d01	d03	d14
NM_020538.1	*Aadac*	Fatty acid and lipid metabolism	arylacetamide deacetylase (esterase) (Aadac)	1.0	-1.3	-3.4
XM_001081607.1	*Abca6*		ATP-binding cassette, sub-family A (ABC1), member 6 (Abca6_predicted)	-1.0	-1.3	-2.1
XM_001062085.1	*Acaa1b*		acetyl-Coenzyme A acyltransferase 1B (RGD1562373_predicted)	1.0	2.1	1.6
NM_031315.1	*Acot1*		acyl-CoA thioesterase 1 (Acot1)	1.2	2.9	4.1
NM_012497.1	*Aldoc*		aldolase C, fructose-bisphosphate (Aldoc)	1.1	1.8	2.6
NM_012824.1	*Apoc1*		apolipoprotein C-I (Apoc1)	-1.1	-1.6	-4.7
NM_012826.1	*Azgp1*		alpha-2-glycoprotein 1, zinc-binding (Azgp1)	-1.2	-1.5	-2.1
NM_133295.2	*Ces3*		carboxylesterase 3 (Ces3)	-1.5	-1.4	-8.2
NM_001024365.1	*Cesl1*		carboxylesterase-like 1 (Cesl1)	-1.1	-1.2	-3.4
NM_013068.1	*Fabp2*		fatty acid binding protein 2, intestinal (Fabp2)	-1.1	-1.5	-2.2
XM_573131.2	*Gltpd2*		glycolipid transfer protein domain containing 2 (RGD1560459_predicted)	-1.3	-1.2	-2.1
NM_032082.1	*Hao2*		hydroxyacid oxidase 2 (long chain) (Hao2)	-1.3	-1.5	-2.8
NM_017060.1	*Hrasls3*		HRAS like suppressor 3 (Hrasls3)	1.2	-1.6	-2.4
NM_017024.1	*Lcat*		lecithin cholesterol acyltransferase (Lcat)	-1.4	-2.2	-3.3
NM_012598.1	*Lpl*		lipoprotein lipase (Lpl)	-1.2	1.0	2.7
NM_053551.1	*Pdk4*		pyruvate dehydrogenase kinase, isozyme 4 (Pdk4)	-1.1	1.1	2.3
NM_031841.1	*Scd*		stearoyl-CoA desaturase (delta-9-desaturase) (Scd)	1.1	2.3	1.7
NM_024143.1	*Slc27a5*		solute carrier family 27 (fatty acid transporter), member 5 (Slc27a5)	1.2	-2.2	-30.2
NM_013155.1	*Vldlr*		very low density lipoprotein receptor (Vldlr)	1.4	2.7	2.5
NM_080581.1	*Abcc3*	Bile acid and steroid metabolism	ATP-binding cassette, sub-family C (CFTR/MRP), member 3 (Abcc3)	1.0	1.0	-2.9
NM_017300.1	*Baat*		bile acid-Coenzyme A: amino acid N-acyltransferase (Baat)	1.1	-1.3	-2.0
NM_031241.1	*Cyp8b1*		cytochrome P450, family 8, subfamily b, polypeptide 1 (Cyp8b1)	-1.8	-1.9	-2.0
NM_012584.1	*Hsd3b5*		hydroxy-delta-5-steroid dehydrogenase, 3 beta- and steroid delta-isomerase 5 (Hsd3b5)	-1.6	-3.3	-6.5
XM_001068218.1	*RGD1564865*		similar to 20-alpha-hydroxysteroid dehydrogenase (RGD1564865_predicted)	-1.2	-1.5	-2.1

Table 54 (continued)

RefSeq	Symbol	Function	Gene name	d01	d03	d14
XM_001069696.1	*Sdr16c6*	Bile acid and steroid metabolism	short chain dehydrogenase/reductase family 16C, member 6 (RGD1562060_predicted)	1.2	3.0	6.4
NM_017047.1	Slc10a1		solute carrier family 10 (sodium/bile acid cotransporter family), member 1 (Slc10a1)	-1.2	-1.7	-2.6
NM_012488.1	*A2m*		alpha-2-macroglobulin (A2m)	-1.0	1.7	14.2
XM_343054.2	*Agmo*		alkylglycerol monooxygenase (LOC362732)	-1.0	1.0	-2.1
NM_012495.1	*Aldoa*		aldolase A, fructose-bisphosphate (Aldoa)	1.3	1.5	2.0
NM_031544.1	*Ampd3*		adenosine monophosphate deaminase 3 (Ampd3)	1.0	1.0	6.5
NM_019373.1	*Apom*		apolipoprotein M (Apom)	-1.1	-1.2	-2.9
NM_012516.1	*C4bpa*		complement component 4 binding protein, alpha (C4bpa)	-1.3	-1.2	-2.1
NM_016995.2	*C4bpb*		complement component 4 binding protein, beta (C4bpb)	-1.5	-1.9	-4.5
NM_212466.2	*Cfb*		complement factor B (Cfb)	-1.2	-1.2	-2.7
NM_030845.1	*Cxcl1*		chemokine (C-X-C motif) ligand 1 (melanoma growth stimulating activity, alpha) (Cxcl1)	-1.8	-3.2	-1.7
NM_173123.1	*Cyp4f4*	Inflammation	cytochrome P450, family 4, subfamily f, polypeptide 4 (Cyp4f4)	-1.3	-1.1	-2.0
NM_031810.1	*Defb1*		defensin beta 1 (Defb1)	2.0	2.1	5.4
NM_172030.1	*Entpd2*		ectonucleoside triphosphate diphosphohydrolase 2 (Entpd2)	-1.0	1.4	2.2
NM_001001505.1	*Habp2*		hyaluronan binding protein 2 (Habp2)	-1.2	-1.7	-4.3
NM_017208.1	*Lbp*		lipopolysaccharide binding protein (Lbp)	1.1	1.5	2.2
NM_031832.1	*Lgals3*		lectin, galactose binding, soluble 3 (Lgals3)	1.1	-1.1	7.8
XM_579477.1	*Mug1*		murinoglobulin 1 (LOC497794)	-1.1	1.0	-2.0
XM_215939.4	*Pltp*		phospholipid transfer protein (Pltp_predicted)	1.0	1.3	2.2
NM_145097.2	*Serpina4*		serine (or cysteine) proteinase inhibitor, clade A (alpha-1 antiproteinase, antitrypsin), member 4 (Serpina4)	-1.5	-1.3	-3.3
NM_024382.1	*Serpind1*		serine (or cysteine) peptidase inhibitor, clade D, member 1 (Serpind1)	-1.5	-1.1	-3.1
NM_001002805.1	*C4-2*	Immune response	complement component 4, gene 2 (C4-2)	-1.3	-1.2	-3.3
NM_176074.2	*C6*		complement component 6 (C6)	-1.3	-1.3	-2.2
XM_001073643.1	*C8g*		complement component 8, gamma polypeptide (C8g_predicted)	-1.1	-1.3	-2.1

Table 54 (continued)

RefSeq	Symbol	Function	Gene name	d01	d03	d14
NM_012752.2	*Cd24*	Immune response	CD24 antigen (Cd24)	1.0	-1.1	-2.1
NM_017125.2	*Cd63*		CD63 antigen (Cd63)	1.1	1.3	2.9
NM_001014006.1	*F12*		coagulation factor XII (Hageman factor) (F12)	-1.4	-1.1	-2.0
XM_222693.3	*F13b*		coagulation factor XIII, beta subunit (F13b_predicted)	1.0	1.1	-2.8
NM_198741.1	*Hla-dma*		major histocompatibility complex, class II, DM alpha (Hla-dma)	1.0	1.3	5.2
NM_133428.1	*Hrg*		histidine-rich glycoprotein (Hrg)	-1.2	-1.2	-3.4
XM_573087.2	*Leap2*		liver-expressed antimicrobial peptide 2 (LOC497901)	-1.0	-1.6	-4.9
XM_574314.2	*Plg*		plasminogen (Plg)	-1.1	-1.0	-2.8
NM_198740.1	*RT1-DMb*		major histocompatibility complex, class II, DM beta (Hla-dmb)	-1.0	1.2	2.1
NM_013016.2	*Sirpa*		signal-regulatory protein alpha (Sirpa)	-1.3	-1.4	-2.1
XM_220013.3	*Tm9sf3*		transmembrane protein TM9SF3 (LOC309475)	-1.3	-1.1	-2.1
NM_019156.1	*Vtn*		vitronectin (Vtn)	-1.1	-1.1	-2.8
XM_577883.2	*Abcc2*	Xenobiotic metabolism	ATP-binding cassette, sub-family C (CFTR/MRP), member 2 (Abcc2)	-1.1	1.3	3.1
NM_001014240.2	*Akr1c13*		aldo-keto reductase family 1, member C13 (LOC364773)	-1.1	-1.4	-2.2
XM_001062695.1	*Akr1c19*		aldo-keto reductase family 1, member C19 (RGD1562954_predicted)	-1.5	-1.3	-2.9
NM_138884.1	*Akr1d1*		aldo-keto reductase family 1, member D1 (delta 4-3-ketosteroid-5-beta-reductase) (Akr1d1)	-1.3	-1.6	-2.9
NM_022407.3	*Aldh1a1*		aldehyde dehydrogenase 1 family, member A1 (Aldh1a1)	1.1	1.0	-2.4
NM_019363.2	*Aox1*		aldehyde oxidase 1 (Aox1)	-1.1	1.0	-2.1
NM_012540.2	*Cyp1a1*		cytochrome P450, family 1, subfamily a, polypeptide 1 (Cyp1a1)	27.7	31.4	17.5
NM_012541.2	*Cyp1a2*		cytochrome P450, family 1, subfamily a, polypeptide 2 (Cyp1a2)	14.6	6.6	19.0
XM_001070818.1	*Cyp2b15*		cytochrome P450, family 2, subfamily b, polypeptide 15, transcript variant 2 (Cyp2b15)	7.5	5.6	1.6
NM_031839.2	*Cyp2c23*		cytochrome P450, family 2, subfamily c, polypeptide 23 (Cyp2c23)	-1.1	-1.9	-9.8
XM_574666.1	*Cyp2c6*		Cytochrome P450, subfamily IIC6 (Cyp2c6)	2.0	2.9	5.3
NM_012730.1	*Cyp2d2*		cytochrome P450, family 2, subfamily d, polypeptide 2 (Cyp2d2)	-1.0	-1.1	-2.2
NM_031543.1	*Cyp2e1*		cytochrome P450, family 2, subfamily e, polypeptide 1 (Cyp2e1)	-1.3	-3.7	-2.1

Table 54 (continued)

RefSeq	Symbol	Function	Gene name	d01	d03	d14
NM_145782.1	*Cyp3a18*	Xenobiotic metabolism	cytochrome P450, 3a18 (Cyp3a18)	-1.2	-1.2	-2.6
NM_019623.2	*Cyp4f1*		cytochrome P450, family 4, subfamily f, polypeptide 1 (Cyp4f1)	-1.2	-1.2	-2.2
NM_031565.1	*Es22*		esterase 22 (Es22)	-2.0	-1.4	-2.8
NM_001009648.1	*Glyat*		glycine-N-acyltransferase (Glyat)	-1.2	-1.4	-5.2
NM_181371.2	*Gstk1*		glutathione S-transferase kappa 1 (Gstk1)	1.0	1.2	2.0
NM_031154.1	*Gstm7*		glutathione S-transferase, mu 7 (Gstm7)	-1.0	-1.8	-2.8
NM_022941.2	*Nr1i3*		nuclear receptor subfamily 1, group I, member 3 (Nr1i3)	1.0	-1.2	-2.6
NM_001014125.1	*Pdia5*		protein disulfide isomerase family A, member 5 (Pdia5)	-1.1	-1.1	-2.2
NM_133547.2	*Sult1c2*		sulfotransferase family, cytosolic, 1C, member 2 (Sult1c2)	1.2	1.9	2.8
NM_001039691.1	*Ugt1a6*		UDP glucuronosyltransferase 1 family, polypeptide A6 (Ugt1a6), transcript variant 1	2.7	2.5	1.6
NM_173323.1	*Ugt2b7*		UDP-glucuronosyltransferase (LOC286989)	1.0	-1.0	-2.4
NM_001013185.1	*Adck3*	Detoxification	aarF domain containing kinase 3 (Cabc1)	-1.2	-1.3	-2.1
NM_012715.1	*Adm*		adrenomedullin (Adm)	-1.1	1.3	7.3
NM_172320.1	*Afm*		afamin (Afm)	-1.0	-1.1	-2.9
NM_017006.1	*G6pdx*		glucose-6-phosphate dehydrogenase X-linked (G6pdx)	2.5	3.2	5.0
XM_001067684.1	*Gpx8*		glutathione peroxidase 8 (RGD1307506_predicted)	1.0	-1.1	-2.3
NM_032077.1	*Pon1*		paraoxonase 1 (Pon1)	-1.1	-1.4	-3.9
NM_022287.1	*Slc26a1*		solute carrier family 26 (sulfate transporter), member 1 (Slc26a1)	-1.2	-1.1	-2.4
XM_001067457.1	*Txndc12*		thioredoxin domain containing 12 (endoplasmic reticulum) (Txndc12)	1.1	1.1	2.1
NM_024134.1	*Ddit3*	Stress response	DNA-damage inducible transcript 3 (Ddit3)	1.2	1.2	3.0
NM_001005546.1	*Ttc36*		tetratricopeptide repeat domain 36 (Ttc36)	1.0	-2.3	-3.4
XM_001062962.1	*A2ug*	Transport	alpha 2U globulin (LOC366380)	1.2	2.4	2.2
NM_001024338.1	*Bcl2l14*		Bcl2-like 14 (apoptosis facilitator) (Bcl2l14)	-1.1	1.2	2.9
XM_001067944.1	*Cd320*		CD320 antigen (Cd320)	-1.1	1.3	2.1
NM_031648.1	*Fxyd1*		FXYD domain-containing ion transport regulator 1 (Fxyd1)	-1.1	-1.1	-3.2
NM_030834.1	*Slc16a3*		solute carrier family 16, member 3 (monocarboxylic acid transporter 4) (Slc16a3)	1.0	1.3	2.1

Table 54 (continued)

RefSeq	Symbol	Function	Gene name	d01	d03	d14
NM_053424.1	*Slc4a4*	Transport	solute carrier family 4 (anion exchanger), member 4 (Slc4a4)	1.1	2.2	1.3
NM_053715.2	*Slc5a3*		solute carrier family 5 (inositol transporters), member 3 (Slc5a3)	-1.0	1.0	2.1
XM_001054180.1	*Cldn2*	ECM organisation	claudin 2 (Cldn2_predicted)	1.1	1.2	2.2
NM_022501.1	*Crip2*		cysteine-rich protein 2 (Crip2)	-1.2	-1.6	-2.5
XM_213925.3	*Dpt*		dermatopontin (Dpt_predicted)	-1.2	-1.3	-2.1
XM_243637.4	*Fbln1*		fibulin 1 (Fbln1_predicted)	-1.0	-1.2	-2.0
XM_001063663.1	*Lad1*		ladinin (Lad1_predicted)	-1.0	1.7	3.7
NM_017061.1	*Lox*		lysyl oxidase (Lox)	-1.2	-1.0	-5.1
XM_001077795.1	*Ltbp4*		latent transforming growth factor beta binding protein 4 (Ltbp4)	-1.4	-1.5	-2.4
NM_001006993.1	*Sgcg*		sarcoglycan, gamma (dystrophin-associated glycoprotein) (Sgcg)	-1.2	-1.4	-2.4
NM_001004265.2	*Spint1*		serine peptidase inhibitor, Kunitz type 1 (Spint1)	1.0	1.2	2.2
XM_001060919.1	*Dapk1*	Apoptosis	death associated protein kinase 1 (Dapk1_predicted)	1.1	1.8	2.1
NM_133599.1	*Lgals2*		lectin, galactoside-binding, soluble 2 (Lgals2)	1.1	1.1	-2.2
NM_001009646.1	*Qprt*		quinolinate phosphoribosyltransferase (Qprt)	-1.3	-1.3	-2.3
XM_343479.3	*Sema3b*		sema domain, immunoglobulin domain (Ig), short basic domain, secreted, (semaphorin) 3B (Sema3b_predicted)	1.1	1.1	2.1
XM_001068302.1	*Sox4*		SRY-box containing gene 4 (Sox4_predicted)	-1.0	-1.0	-2.1
NM_001015008.1	*Tcea3*		transcription elongation factor A (SII), 3 (Tcea3)	-1.5	-1.4	-2.3
NM_080582.1	*Abcb6*	Proliferation	ATP-binding cassette, sub-family B (MDR/TAP), member 6 (Abcb6), nuclear gene encoding mitochondrial protein	-1.0	-1.1	-2.1
NM_175757.2	*Cryl1*		crystallin, lambda 1 (Cryl1)	-1.0	-1.2	-2.5
NM_001013098.1	*Dhrs7*		dehydrogenase/reductase (SDR family) member 7 (Dhrs7)	-1.1	-1.3	-7.6
NM_017113.1	*Grn*		granulin (Grn)	1.1	1.1	2.1
XM_341957.2	*Ifitm3*		interferon induced transmembrane protein 3 (Ifitm3)	-1.2	-1.6	-2.8
XM_001070215.1	*Prg4*		proteoglycan 4, (Prg4_predicted)	-1.3	-1.6	-4.9
NM_001015012.1	*Rab30*		RAB30, member RAS oncogene family (Rab30)	1.2	1.0	2.7
NM_001004096.1	*Reg4*		regenerating islet-derived family, member 4 (Reg4)	1.0	-1.3	-2.5

Table 54 (continued)

RefSeq	Symbol	Function	Gene name	d01	d03	d14
NM_152936.1	*Spink1*	Proliferation	serine peptidase inhibitor, Kazal type 1 (Spink1)	1.2	-1.1	-2.1
NM_053785.1	*Tm4sf4*		transmembrane 4 L six family member 4 (Tm4sf4)	-1.1	-1.3	-2.1
NM_012789.1	*Dpp4*	Signalling	dipeptidylpeptidase 4 (Dpp4)	-1.3	-1.2	-2.1
NM_031973.1	*Dpp7*		dipeptidylpeptidase 7 (Dpp7)	1.0	2.1	5.3
NM_012843.2	*Emp1*		epithelial membrane protein 1 (Emp1)	-1.2	1.4	2.2
NM_022962.1	*Lphn1*		latrophilin 1 (Lphn1)	-1.2	-1.2	-2.6
XM_001080468.1	*Ppapdc1a*		phosphatidic acid phosphatase type 2 domain containing 1A (RGD1306289_predicted)	1.1	-1.0	-2.6
NM_053453.1	*Rgs2*		regulator of G-protein signaling 2 (Rgs2)	1.0	-1.4	-2.0
XM_001077578.1	*Uap1l1*		UDP-N-acteylglucosamine pyrophosphorylase 1-like 1 (Uap1l1_predicted)	1.2	2.2	3.8
NM_031003.1	*Abat*	Other and unknown functions	4-aminobutyrate aminotransferase (Abat), nuclear gene encoding mitochondrial protein	-1.4	-1.5	-2.1
NM_175754.1	*Agrn*		agrin (Agrn)	-1.1	1.0	-2.1
NM_001024990.1	*Amdhd2*		amidohydrolase domain containing 2 (RGD1304601)	1.1	1.3	2.2
NM_001010970.1	*Amy1a*		amylase, alpha 1A (salivary) (Amy1a)	-1.5	-1.3	-2.1
XM_343245.3	*Anxa13*		annexin A13 (Anxa13_predicted)	-1.0	-1.0	-2.7
NM_001009643.1	*Aspdh*		aspartate dehydrogenase domain containing (RGD1310111)	-1.1	-1.4	-3.7
NM_001011972.1	*Atp6v0d2*		ATPase, H+ transporting, lysosomal 38kDa, V0 subunit d2 (Atp6v0d2)	1.1	1.3	2.0
NM_199386.1	*Atp6v1d*		ATPase, H+ transporting, lysosomal V1 subunit D (Atp6v1d)	-1.0	1.3	2.1
XM_001077768.1	*Cisd2*		CDGSH iron sulfur domain 2 (RGD1566242_predicted)	1.0	1.3	2.1
NM_012812.1	*Cox6a2*		cytochrome c oxidase, subunit VIa, polypeptide 2 (Cox6a2)	-1.0	1.4	11.7
NM_212532.1	*Ddah2*		dimethylarginine dimethylaminohydrolase 2 (Ddah2)	-1.3	-1.4	-3.3
NM_021664.1	*Dnase2b*		deoxyribonuclease II beta (Dnase2b)	1.1	1.1	2.6
NM_031705.1	*Dpys*		dihydropyrimidinase (Dpys)	-1.3	-1.2	-3.0
NM_001024791.1	*Epn3*		epsin 3 (Epn3)	1.1	1.2	2.0
NM_017004.1	*Es1*		esterase 1 (Es1)	-1.3	-1.5	-2.1
NM_199390.2	*Flcn*		folliculin (Flcn)	-1.1	1.2	2.4

Table 54 (continued)

RefSeq	Symbol	Function	Gene name	d01	d03	d14
XM_001056685.1	*Flna*		filamin, alpha (Flna_predicted)	-1.1	-1.1	-2.0
NM_031776.1	*Gda*		guanine deaminase (Gda)	-1.1	-1.4	-2.0
NM_133298.1	*Gpnmb*		glycoprotein (transmembrane) nmb (Gpnmb)	1.0	1.2	2.2
NM_021593.1	*Kmo*		kynurenine 3-monooxygenase (kynurenine 3-hydroxylase) (Kmo)	-1.1	-1.2	-2.4
NM_001002826.1	*Mug2*		murinoglobulin 2 (Mug2)	-1.1	-1.2	-2.4
NM_031817.1	*Omd*		osteomodulin (Omd)	-1.9	-1.7	-2.3
NM_013078.1	*Otc*		ornithine carbamoyltransferase (Otc), nuclear gene encoding mitochondrial protein	1.0	-1.2	-4.8
NM_206847.1	*Pfkp*		phosphofructokinase, platelet (Pfkp)	1.1	1.6	6.7
XM_573147.1	*Pipox*		pipecolic acid oxidase (Pipox_predicted)	-1.1	-1.2	-2.0
NM_001008323.1	*Pmm1*		phosphomannomutase 1 (Pmm1)	-1.0	1.1	2.1
NM_199113.1	*Popdc2*		popeye domain containing 2 (Popdc2)	-1.2	-1.6	-2.2
NM_031587.1	*Pxmp2*	Other and unknown functions	peroxisomal membrane protein 2 (Pxmp2)	-1.3	-1.3	-2.2
NM_031095.1	*Renbp*		renin binding protein (Renbp)	1.0	1.4	7.3
XM_001063809.1	*Rragd*		Ras-related GTP binding D (Rragd_predicted)	1.2	1.4	3.7
NM_001008776.1	*Serpina11*		serine (or cysteine) peptidase inhibitor, clade A (alpha-1 antiproteinase, antitrypsin), member 11 (Serpina11)	-1.3	-1.3	-2.4
XM_001067511.1	*Serpina3m*		serine (or cysteine) proteinase inhibitor, clade A, member 3M (Serpina3m)	-1.0	-1.2	-2.1
XM_343604.3	*Serpine2*		serine (or cysteine) proteinase inhibitor, clade E, member 2 (Serpine2)	1.1	1.3	2.6
XM_340825.3	*Slc38a2*		solute carrier family 38, member 2 (Sat2_predicted)	1.1	1.6	3.3
NM_001009283.1	*Syne4*		spectrin repeat containing, nuclear envelope family member 4 (RGD1304580)	-1.0	-1.2	-3.5
NM_031807.1	*Tpbg*		trophoblast glycoprotein (Tpbg)	-1.1	-1.3	-2.4
NM_001011903.1	*Tpst1*		tyrosylprotein sulfotransferase 1 (Tpst1)	-1.1	-1.1	-2.3
NM_001009965.2	*Tsku*		tsukushin (Tsku)	1.8	2.6	1.1
NM_053845.1	*Upb1*		ureidopropionase, beta (Upb1)	-1.2	-1.5	-3.0
XM_237288.4	*Vil1*		villin 1 (Vil1_predicted)	-1.0	1.0	-2.4

Table 55. Absolute fold changes of genes deregulated at least 2-fold (BH q-value ≤ 0.05) compared to the vehicle treated control in primary rat hepatocytes treated with 2.5 µM cyclosporine A for 1, 3 or 14 days. The genes are in alphabetic order within each function.

RefSeq	Symbol	Function	Gene name	d01	d03	d14
NM_031315.1	*Acot1*	Fatty acid and lipid metabolism	acyl-CoA thioesterase 1 (Acot1)	-1.0	1.0	8.1
NM_145770.1	*Acox2*		acyl-Coenzyme A oxidase 2, branched chain (Acox2)	-1.6	-2.1	-1.2
XM_578476.1	*Angptl3*		angiopoietin-like 3 (LOC502970)	-2.6	-2.0	-2.1
NM_013112.1	*Apoa2*		apolipoprotein A-II (Apoa2)	-1.9	-3.0	-1.5
NM_080576.1	*Apoa5*		apolipoprotein A-V (Apoa5)	-1.2	-2.8	-1.5
NM_012824.1	*Apoc1*		apolipoprotein C-I (Apoc1)	1.1	-3.9	-4.1
XM_001076000.1	*Apoc2*		apolipoprotein C-II (Apoc2_predicted)	-1.2	-2.9	-1.4
NM_001009385.1	*Apon*		apolipoprotein N (Apon)	-1.9	-2.3	-1.3
NM_022629.1	*Bbox1*		butyrobetaine (gamma), 2-oxoglutarate dioxygenase (gamma-butyrobetaine hydroxylase) 1 (Bbox1)	-1.4	-2.4	-1.4
NM_133295.2	*Ces3*		carboxylesterase 3 (Ces3)	-2.0	-6.1	-2.2
NM_001024365.1	*Cesl1*		carboxylesterase-like 1 (Cesl1)	-2.3	-2.0	-2.6
XM_214551.4	*Cidea*		cell death-inducing DNA fragmentation factor, alpha subunit-like effector A (Cidea_predicted)	-1.3	-2.7	1.2
NM_031559.1	*Cpt1a*		carnitine palmitoyltransferase 1a, liver (Cpt1a)	-1.9	-2.7	-1.1
NM_175757.2	*Cryl1*		crystallin, lambda 1 (Cryl1)	-1.1	-1.9	-2.5
NM_001012345.1	*Dgat2*		diacylglycerol O-acyltransferase homolog 2 (mouse) (Dgat2)	-2.5	-1.3	-1.7
NM_022594.1	*Ech1*		enoyl coenzyme A hydratase 1, peroxisomal (Ech1)	-1.6	-2.6	1.3
NM_001009632.1	*G0s2*		G0/G1switch 2 (G0s2)	-1.0	1.4	3.2
NM_053493.1	*Hacl1*		2-hydroxyacyl-CoA lyase 1 (Hacl1)	-1.7	-2.5	1.1
NM_017060.1	*Hrasls3*		HRAS like suppressor 3 (Hrasls3)	-1.2	-2.3	-2.1
NM_017024.1	*Lcat*		lecithin cholesterol acyltransferase (Lcat)	-1.4	-2.8	-1.6
NM_053674.1	*Phyh*		phytanoyl-CoA hydroxylase (Phyh)	-1.2	-2.0	1.1
NM_138882.1	*Pla1a*		phospholipase A1 member A (Pla1a)	-1.2	-1.6	-2.7
NM_139255.2	*Plbd2*		phospholipase B domain containing 2 (LOC246120)	-3.2	-1.9	-2.3
XM_341960.3	*Pnpla2*		patatin-like phospholipase domain containing 2 (Pnpla2_predicted)	-1.4	-2.1	1.2

Table 55 (continued)

RefSeq	Symbol	Function	Gene name	d01	d03	d14
XM_001078083.1	*Pnpla3*	Fatty acid and lipid metabolism	patatin-like phospholipase domain containing 3 (LOC362972)	1.9	2.7	1.7
NM_138905.2	*Ppap2b*		phosphatidic acid phosphatase type 2B (Ppap2b)	-1.8	-2.2	-1.2
NM_031841.1	*Scd*		stearoyl-CoA desaturase (delta-9-desaturase) (Scd)	1.1	3.3	1.3
NM_024143.1	*Slc27a5*		solute carrier family 27 (fatty acid transporter), member 5 (Slc27a5)	-2.8	-3.6	-5.3
NM_013155.1	*Vldlr*		very low density lipoprotein receptor (Vldlr)	1.8	5.5	2.7
NM_080581.1	*Abcc3*	Bile acid and steroid metabolism	ATP-binding cassette, sub-family C (CFTR/MRP), member 3 (Abcc3)	-1.5	-1.4	-2.2
NM_053502.1	*Abcg1*		ATP-binding cassette, sub-family G (WHITE), member 1 (Abcg1)	-1.2	-1.2	-2.7
NM_001013057.1	*Akr1c21*		aldo-keto reductase family 1, member C21 (Akr1c21)	-1.2	-2.6	-2.2
NM_173294.1	*Cyp2b3*		cytochrome P450IIB3 (Cyp2b3)	-1.0	1.1	2.8
NM_012942.1	*Cyp7a1*		cytochrome P450, family 7, subfamily a, polypeptide 1 (Cyp7a1)	-2.8	-7.9	-4.1
NM_031241.1	*Cyp8b1*		cytochrome P450, family 8, subfamily b, polypeptide 1 (Cyp8b1)	-3.4	-6.2	-1.4
NM_012584.1	*Hsd3b5*		hydroxy-delta-5-steroid dehydrogenase, 3 beta- and steroid delta-isomerase 5 (Hsd3b5)	-2.5	-4.5	-2.9
NM_001013048.1	*Igfbp7*		insulin-like growth factor binding protein 7 (Igfbp7)	1.0	1.0	-2.0
NM_178091.3	*Insig2*		insulin induced gene 2 (Insig2)	-1.4	-2.3	-1.4
XM_579502.1	*Lss*		lanosterol synthase (2,3-oxidosqualene-lanosterol cyclase) (LOC497745)	1.3	2.1	1.5
NM_001009663.1	*Serpina6*		serine (or cysteine) peptidase inhibitor, clade A, member 6 (Serpina6)	1.4	2.4	1.3
NM_017047.1	*Slc10a1*		solute carrier family 10 (sodium/bile acid cotransporter family), member 1 (Slc10a1)	-2.2	-4.4	-1.5
NM_080786.1	*Slco2b1*		solute carrier organic anion transporter family, member 2b1 (Slco2b1)	-1.5	-2.0	-1.7
XM_001074217.1	*ste2*		estrogen sulfotransferase (ste2)	-2.3	-1.4	-1.1
NM_030845.1	*Cxcl1*	Inflammation	chemokine (C-X-C motif) ligand 1 (melanoma growth stimulating activity, alpha) (Cxcl1)	-1.7	-1.9	-2.6
NM_022936.1	*Ephx2*		epoxide hydrolase 2, cytoplasmic (Ephx2)	-1.8	-2.1	1.4
NM_001001505.1	*Habp2*		hyaluronan binding protein 2 (Habp2)	-1.4	-1.5	-2.7
NM_001009628.1	*Kng1l1*		kininogen 1-like 1 (Kng1l1)	-1.1	-1.6	-2.4
NM_053373.1	*Pglyrp1*		peptidoglycan recognition protein 1 (Pglyrp1)	-1.4	-2.2	-2.1

Table 55 (continued)

RefSeq	Symbol	Function	Gene name	d01	d03	d14
NM_145097.2	*Serpina4*	Inflammation	serine (or cysteine) proteinase inhibitor, clade A (alpha-1 antiproteinase, antitrypsin), member 4 (Serpina4)	-1.9	-2.2	-1.9
NM_001002805.1	*C4-2*	Immune response	complement component 4, gene 2 (C4-2)	-1.9	-1.8	-2.4
NM_016995.2	*C4bpb*		complement component 4 binding protein, beta (C4bpb)	-2.0	-3.5	-2.7
XM_345342.3	*C5*		complement component 5 (C5)	-1.7	-1.6	-2.3
NM_176074.2	*C6*		complement component 6 (C6)	-1.5	-2.2	-1.8
NM_212466.2	*Cfb*		complement factor B (Cfb)	-1.4	-2.7	-1.8
NM_130409.1	*Cfh*		complement component factor H (Cfh)	-1.5	-1.9	-2.7
NM_012938.1	*Ctse*		cathepsin E (Ctse)	-1.1	-1.3	-2.8
NM_001014006.1	*F12*		coagulation factor XII (Hageman factor) (F12)	-1.5	-2.1	-1.7
NM_198741.1	*Hla-dma*		major histocompatibility complex, class II, DM alpha (Hla-dma)	1.1	1.1	2.0
NM_012725.1	*Klkb1*		kallikrein B, plasma 1 (Klkb1)	-1.4	-1.2	-2.3
NM_017208.1	*Lbp*		lipopolysaccharide binding protein (Lbp)	-2.0	-1.0	-1.5
NM_001014217.1	*Nhej1*		nonhomologous end-joining factor 1 (Nhej1)	2.0	2.4	1.4
XM_574314.2	*Plg*		plasminogen (Plg)	-1.7	-3.1	-2.2
NM_053299.1	*Ubd*		ubiquitin D (Ubd)	-2.5	-1.4	-1.3
NM_031140.1	*Vim*		vimentin (Vim)	-1.0	-2.1	-1.4
NM_001014240.2	*Akr1c13*	Xenobiotic metabolism	aldo-keto reductase family 1, member C13 (LOC364773)	-1.7	-2.8	-1.9
NM_138884.1	*Akr1d1*		aldo-keto reductase family 1, member D1 (delta 4-3-ketosteroid-5-beta-reductase) (Akr1d1)	-1.6	-2.0	-1.7
NM_019363.2	*Aox1*		aldehyde oxidase 1 (Aox1)	-1.6	-1.8	-2.2
NM_133586.1	*Ces2*		carboxylesterase 2 (intestine, liver) (Ces2)	-1.9	-3.7	-1.8
XM_212849.3	*Ces2i*		carboxylesterase isoenzyme gene (RGD1565045_predicted)	-1.6	-3.5	-2.0
NM_012692.1	*Cyp2a1*		cytochrome P450 IIA1 (hepatic steroid hydroxylase IIA1) gene (Cyp2a1)	-1.6	-2.1	-1.8
NM_012693.1	*Cyp2a2*		cytochrome P450, subfamily 2A, polypeptide 1 (Cyp2a2)	-1.8	-2.4	-1.8
XM_001070818.1	*Cyp2b15*		cytochrome P450, family 2, subfamily b, polypeptide 15, transcript variant 2 (Cyp2b15)	-1.7	-5.5	1.0

Table 55 (continued)

RefSeq	Symbol	Function	Gene name	d01	d03	d14
NM_019184.1	*Cyp2c*	Xenobiotic metabolism	Cytochrome P450, subfamily IIC (mephenytoin 4-hydroxylase) (Cyp2c)	-1.5	-2.8	-2.9
NM_031572.1	*Cyp2c12*		cytochrome P450, family 2, subfamily c, polypeptide 12 (Cyp2c12)	-2.4	-1.9	-1.1
NM_138514.1	*Cyp2c13*		cytochrome P450 2c13 (Cyp2c13)	-1.6	-2.1	1.0
NM_031839.2	*Cyp2c23*		cytochrome P450, family 2, subfamily c, polypeptide 23 (Cyp2c23)	-1.8	-2.8	-6.1
NM_031543.1	*Cyp2e1*		cytochrome P450, family 2, subfamily e, polypeptide 1 (Cyp2e1)	-1.8	-3.9	-2.2
NM_173144.1	*Cyp3a1*		cytochrome P450, family 3, subfamily a, polypeptide 1 (Cyp3a1)	-1.7	-2.8	-4.5
NM_145782.1	*Cyp3a18*		cytochrome P450, 3a18 (Cyp3a18)	-1.8	-2.5	-1.6
NM_013105.1	*Cyp3a3*		cytochrome P450, subfamily 3A, polypeptide 3 (Cyp3a3)	-1.8	-3.3	-5.9
NM_001034090.1	*Ephx1*		epoxide hydrolase 1, microsomal (Ephx1), transcript variant 1	-2.0	-1.3	-2.5
NM_031565.1	*Es22*		esterase 22 (Es22)	-3.0	-2.4	-2.5
NM_001009648.1	*Glyat*		glycine-N-acyltransferase (Glyat)	-2.0	-2.9	-2.6
NM_017013.4	*Gsta2*		glutathione S-transferase A2 (Gsta2)	-1.7	-1.9	-3.1
NM_001010921.1	*Gsta5*		glutathione S-transferase alpha 5 (LOC494499)	-1.3	-1.6	-3.0
NM_031154.1	*Gstm7*		glutathione S-transferase, mu 7 (Gstm7)	-1.2	-2.2	-1.7
XM_001066533.1	*Nnmt*		nicotinamide N-methyltransferase (Nnmt_predicted)	1.4	2.4	1.6
NM_022941.2	*Nr1i3*		nuclear receptor subfamily 1, group I, member 3 (Nr1i3)	-1.5	-2.2	-1.5
NM_130407.1	*Ugt1a7*		UDP glycosyltransferase 1 family, polypeptide A7 (Ugt1a7)	-2.4	-2.8	-1.6
NM_173323.1	*Ugt2b7*		UDP glucuronosyltransferase 2 family, polypeptide B7 (LOC286989)	1.1	-1.0	-2.2
NM_001013185.1	*Cabc1*	Detoxification	chaperone, ABC1 activity of bc1 complex homolog (S. pombe) (Cabc1), nuclear gene encoding mitochondrial protein	-1.8	-2.3	-1.7
NM_017006.1	*G6pdx*		glucose-6-phosphate dehydrogenase X-linked (G6pdx)	2.1	8.2	2.5
NM_019184.1	*Cyp2c*	Stress response	Cytochrome P450, subfamily IIC (mephenytoin 4-hydroxylase) (Cyp2c)	-1.5	-2.8	-2.9
NM_024134.1	*Ddit3*		DNA-damage inducible transcript 3 (Ddit3)	1.8	3.0	2.6
NM_012699.2	*Dnajb9*		DnaJ (Hsp40) homolog, subfamily B, member 9 (Dnajb9)	2.7	2.0	1.7
NM_001014125.1	*Pdia5*		protein disulfide isomerase family A, member 5 (Pdia5)	1.8	2.0	1.1
NM_001005546.1	*Ttc36*		tetratricopeptide repeat domain 36 (Ttc36)	-1.9	-2.8	-1.9
NM_001009669.1	*Uba5*		ubiquitin-like modifier activating enzyme 5 (Uba5)	2.1	1.9	1.5

Table 55 (continued)

RefSeq	Symbol	Function	Gene name	d01	d03	d14
XM_001062962.1	*A2ug*		alpha 2U globulin (LOC366380)	-1.2	-3.1	1.2
XM_001062704.1	*Efcab4a*		EF-hand calcium binding domain 4A (RGD1560911_predicted)	-1.4	-2.3	-1.2
NM_031648.1	*Fxyd1*		FXYD domain-containing ion transport regulator 1 (Fxyd1)	-1.4	-2.1	-1.8
XM_235558.4	*Mlc1*		megalencephalic leukoencephalopathy with subcortical cysts 1 homolog (human) (Mlc1_predicted)	-1.7	-2.2	1.0
NM_023950.3	*Rab7a*		RAB7A, member RAS oncogene family (Rab7a)	-1.6	-2.5	-1.5
XM_215285.4	*Rbp4*		retinol binding protein 4, plasma (Rbp4)	-1.5	-2.4	-1.0
XM_001059811.1	*Slc17a9*	Transport	solute carrier family 17 (vesicular nucleotide transporter), member 9 (RGD1311940_predicted)	2.1	1.4	1.6
NM_053515.1	*Slc25a4*		solute carrier family 25 (mitochondrial carrier; adenine nucleotide translocator), member 4 (Slc25a4), nuclear gene encoding mitochondrial protein	-1.5	-2.6	1.0
NM_019283.1	*Slc3a2*		solute carrier family 3 (activators of dibasic and neutral amino acid transport), member 2 (Slc3a2)	1.1	2.1	1.5
NM_017353.1	*Slc7a5*		solute carrier family 7 (cationic amino acid transporter, y+ system), member 5 (Slc7a5)	1.1	2.2	2.1
NM_017199.1	*Ssr4*		signal sequence receptor, delta (Ssr4)	2.0	2.0	1.7
NM_001004249.1	*Tmed3*		transmembrane emp24 protein transport domain containing 3 (Tmed3)	2.9	2.1	1.9
NM_022501.1	*Crip2*		cysteine-rich protein 2 (Crip2)	-1.0	-2.8	-2.3
NM_022266.2	*Ctgf*	ECM organisation	connective tissue growth factor (Ctgf)	-2.0	-1.4	-1.6
XM_213925.3	*Dpt*		dermatopontin (Dpt_predicted)	-2.1	-1.9	-1.8
NM_017061.1	*Lox*		lysyl oxidase (Lox)	-1.6	-1.5	-4.8
NM_001006993.1	*Sgcg*		sarcoglycan, gamma (dystrophin-associated glycoprotein) (Sgcg)	-1.2	-2.1	-1.5
NM_053736.1	*Casp11*		caspase 11 (Casp11)	2.0	4.1	2.5
NM_130422.1	*Casp12*		caspase 12 (Casp12)	1.1	2.4	1.6
XM_573834.1	*Commd6*		COMM domain containing 6 (LOC498559)	2.1	2.0	1.3
NM_031970.1	*Hspb1*	Apoptosis	heat shock 27kDa protein 1 (Hspb1)	-1.0	-2.0	-1.2
NM_212505.1	*Ier3*		immediate early response 3 (Ier3)	-1.2	-1.3	-2.2
NM_139259.1	*Nradd*		neurotrophin receptor associated death domain (Nradd)	-1.0	1.1	-2.2
NM_001009646.1	*Qprt*		quinolinate phosphoribosyltransferase (Qprt)	-1.8	-2.1	-1.3

Table 55 (continued)

RefSeq	Symbol	Function	Gene name	d01	d03	d14
NM_001015008.1	*Tcea3*	Apoptosis	transcription elongation factor A (SII), 3 (Tcea3)	-1.9	-2.2	-1.4
NM_144755.1	*Trib3*		tribbles homolog 3 (Drosophila) (Trib3)	1.6	2.7	1.9
NM_001008767.1	*Txnip*		thioredoxin interacting protein (Txnip)	-1.3	-2.1	-1.0
XM_579997.2	*Cks1b*	Proliferation	CDC28 protein kinase regulatory subunit 1B (RGD1561797_predicted)	2.8	1.9	1.9
XM_001070215.1	*Prg4*		proteoglycan 4 (Prg4_predicted)	-1.1	1.0	-3.1
NM_134449.1	*Prkcdbp*		protein kinase C, delta binding protein (Prkcdbp)	1.1	2.2	1.3
NM_001014790.1	*Rarres1*		retinoic acid receptor responder (tazarotene induced) 1 (Rarres1)	-1.5	-2.1	-2.2
XM_343823.2	*Serpina7*		serine (or cysteine) peptidase inhibitor, clade A (alpha-1 antipeptidase, antitrypsin), member 7 (Serpina7)	-1.4	-2.2	-1.0
NM_152936.1	*Spink1*		serine peptidase inhibitor, Kazal type 1 (Spink1)	-1.4	-3.0	-1.4
NM_019288.1	*App*	Transcription	amyloid beta (A4) precursor protein (App)	-1.0	2.1	1.1
NM_001014273.1	*Armcx3*		armadillo repeat containing, X-linked 3 (Armcx3)	2.0	2.3	1.7
XM_342632.3	*Cdk14*		cyclin-dependent kinase 14 (Pftk1_predicted)	1.3	2.3	1.3
NM_012551.1	*Egr1*		early growth response 1 (Egr1)	-1.1	-2.1	-2.3
NM_013060.2	*Id2*		inhibitor of DNA binding 2 (Id2)	-1.1	-1.2	-2.0
NM_053713.1	*Klf4*		Kruppel-like factor 4 (gut) (Klf4)	1.4	2.0	1.6
XM_579353.1	*Mist1*		muscle, intestine and stomach expression 1 (Mist1)	2.2	1.8	1.6
NM_052798.1	*Zfp354a*		zinc finger protein 354A (Zfp354a)	-1.1	-1.3	2.0
XM_342965.3	*Arhgef19*	Signalling	Rho guanine nucleotide exchange factor (GEF) 19 (Arhgef19_predicted)	-1.4	-2.4	-1.3
NM_053883.2	*Dusp6*		dual specificity phosphatase 6 (Dusp6)	-1.2	-1.3	-2.6
NM_012843.2	*Emp1*		epithelial membrane protein 1 (Emp1)	-1.2	-2.3	1.0
NM_133583.1	*Ndrg2*		NDRG family member 2 (Ndrg2)	-1.7	-2.6	-1.5
XM_001080468.1	*Ppapdc1a*		phosphatidic acid phosphatase type 2 domain containing 1A (RGD1306289_predicted)	1.0	-1.1	-2.3
NM_053453.1	*Rgs2*		regulator of G-protein signaling 2 (Rgs2)	1.0	-2.1	-1.9

Table 55 (continued)

RefSeq	Symbol	Function	Gene name	d01	d03	d14
NM_019212.2	*Acta1*		actin, alpha 1, skeletal muscle (Acta1)	-1.0	-1.1	-3.7
NM_175754.1	*Agrn*		agrin (Agrn)	-1.3	-1.0	-2.3
NM_001006992.1	*Ang1*		angiogenin, ribonuclease A family, member 1 (Ang1)	-1.4	-2.6	-1.6
NM_001012079.1	*Arhgef2*		rho/rac guanine nucleotide exchange factor (GEF) 2 (Arhgef2)	1.1	3.2	2.2
NM_001009643.1	*Aspdh*		aspartate dehydrogenase domain containing (RGD1310111)	-1.2	-2.3	-1.7
NM_030850.1	*Bhmt*		betaine-homocysteine methyltransferase (Bhmt)	-2.3	-2.5	-1.2
NM_012812.1	*Cox6a2*		cytochrome c oxidase, subunit VIa, polypeptide 2 (Cox6a2)	1.4	6.9	11.6
NM_017072.1	*Cps1*		carbamoyl-phosphate synthetase 1, mitochondrial (Cps1), nuclear gene encoding mitochondrial protein	-1.9	-4.1	-1.6
NM_001037208.1	*Creld2*		cysteine-rich with EGF-like domains 2 (Creld2)	2.0	1.6	1.3
XM_574665.2	*Cyp2c24*		cytochrome P450, family 2, subfamily c, polypeptide 24 (RGD1563697_predicted)	-1.9	-1.8	-2.4
NM_175766.2	*Cyp2j3*		cytochrome P450, family 2, subfamily j, polypeptide 3 (Cyp2j3)	-1.6	-2.7	-1.2
NM_001013098.1	*Dhrs7*	Other and unknown functions	dehydrogenase/reductase (SDR family) member 7 (Dhrs7)	-1.4	-2.3	-2.3
NM_031705.1	*Dpys*		dihydropyrimidinase (Dpys)	-1.7	-2.0	-1.8
NM_017004.1	*Es1*		esterase 1 (Es1)	-4.9	-2.0	-3.0
XM_340907.3	*Fam134c*		family with sequence similarity 134, member C (RGD1561189_predicted)	-3.0	-2.1	-2.4
XM_001056685.1	*Flna*		filamin, alpha (Flna_predicted)	-1.2	-1.3	-2.5
NM_053567.1	*Ftcd*		formiminotransferase cyclodeaminase (Ftcd)	-1.5	-2.7	-1.4
NM_013098.1	*G6pc*		glucose-6-phosphatase, catalytic (G6pc)	-1.8	-3.3	-1.0
NM_031802.1	*Gabbr2*		gamma-aminobutyric acid (GABA) B receptor 2 (Gabbr2)	1.3	2.1	1.1
NM_017084.1	*Gnmt*		glycine N-methyltransferase (Gnmt)	-1.9	-3.2	-1.5
NM_031039.1	*Gpt*		glutamic-pyruvate transaminase (alanine aminotransferase) (Gpt)	-1.3	-2.6	-1.5
XM_343535.3	*Gtpbp2*		GTP binding protein 2 (Gtpbp2)	1.7	2.3	1.7
XM_001062255.1	*Hm13*		histocompatibility 13 (RGD1563595_predicted; H13_predicted)	1.7	2.1	1.6
NM_030844.1	*Ica1*		islet cell autoantigen 1 (Ica1)	2.2	1.8	1.8
NM_001024334.2	*LOC500300*		similar to hypothetical protein MGC6835 (LOC500300)	-1.6	-2.0	-1.1

Table 55 (continued)

RefSeq	Symbol	Function	Gene name	d01	d03	d14
XM_001077558.1	*Man1b1*		mannosidase, alpha, class 1B, member 1 (RGD1563595_predicted)	1.6	2.1	1.6
NM_199404.1	*Man2b1*		mannosidase 2, alpha B1 (Man2b1)	-1.6	-2.0	-1.5
XM_001067912.1	*Mthfd2*		methylenetetrahydrofolate dehydrogenase (NADP+ dependent) 2, methenyltetrahydrofolate cyclohydrolase (LOC684490)	1.1	2.4	1.5
NM_001013975.1	*Notum*		notum pectinacetylesterase homolog (Drosophila) (RGD1307119)	-1.6	-2.2	-1.5
NM_138530.2	*Pbld1*		phenazine biosynthesis-like protein domain containing (Pbld)	-1.2	-2.3	-1.8
NM_012744.2	*Pc*		pyruvate carboxylase (Pc), nuclear gene encoding mitochondrial protein	-1.7	-2.3	-1.0
NM_198780.3	*Pck1*		phosphoenolpyruvate carboxykinase 1, cytosolic (Pck1)	-1.1	-2.4	1.1
XM_001055522.1	*Pck2*		phosphoenolpyruvate carboxykinase 2 (mitochondrial) (Pck2_predicted)	1.4	2.6	2.2
NM_199113.1	*Popdc2*		popeye domain containing 2 (Popdc2)	-1.4	-2.6	-2.7
XM_001062694.1	*Ppapdc1b*		phosphatidic acid phosphatase type 2 domain containing 1B (LOC683534)	2.1	1.9	1.5
NM_001012072.1	*Ppp1r3c*	Other and unknown functions	protein phosphatase 1, regulatory (inhibitor) subunit 3C (Ppp1r3c)	-1.5	-2.7	1.2
NM_001007691.1	*Prss23*		protease, serine, 23 (Prss23)	-1.1	-1.0	-2.1
NM_080580.2	*Rab3d*		RAB3D, member RAS oncogene family (Rab3d)	2.8	2.4	1.8
NM_173120.1	*Ratsg2*		Ratsg2 (Ratsg2)	2.2	2.2	1.7
XM_001063211.1	*Rbm3*		RNA binding motif protein 3 (Rbm3)	1.4	2.7	1.6
XM_001073225.1	*Rcn1*		reticulocalbin 1 (Rcn1_predicted)	1.2	2.9	1.3
NM_199208.1	*Rdh2*		retinol dehydrogenase 2 (Rdh2)	-1.5	-2.6	1.0
NM_145084.1	*Retsat*		retinol saturase (all trans retinol 13,14 reductase) (Retsat)	-1.7	-2.0	-1.1
NM_001014206.1	*RGD1309534*		similar to RIKEN cDNA 4931406C07 (RGD1309534)	-1.4	-2.2	-1.3
XM_001069921.1	*RGD1564804*		similar to chromosome 1 open reading frame 50 (RGD1564804_predicted)	-1.2	-2.1	-1.0
NM_031741.1	*Slc2a5*		solute carrier family 2 (facilitated glucose/fructose transporter), member 5 (Slc2a5)	-1.8	-2.3	-1.1
NM_053464.1	*Srm*		spermidine synthase (Srm)	1.9	2.6	1.7
XM_341010.3	*Tango2*		transport and golgi organization 2 homolog (Drosophila) (RGD1310348_predicted)	-1.5	-2.4	-1.4
NM_134390.2	*Tmem176b*		transmembrane protein 176B (Tmem176b)	-1.5	-2.0	-1.7

Table 55 (continued)

RefSeq	Symbol	Function	Gene name	d01	d03	d14
XM_233431.4	*Tmem53*	Other and unknown functions	transmembrane protein 53 (Tmem53_predicted)	-1.4	-2.1	-1.2
NM_001004213.1	*Tmem66*		transmembrane protein 66 (Tmem66)	2.6	2.2	1.7
NM_013044.2	*Tmod1*		tropomodulin 1 (Tmod1)	-1.4	-2.0	-1.3
NM_031807.1	*Tpbg*		trophoblast glycoprotein (Tpbg)	-1.1	-1.4	-2.6
XM_237288.4	*Vil1*		villin 1 (Vil1_predicted)	-1.0	-1.1	-2.6

Appendix 9: Protein abundance in primary rat hepatocytes.

Table 56. Absolute fold changes of proteins with at least 1.5-fold changed abundance compared to the vehicle treated control (q-value ≤ 0.05) in primary rat hepatocytes treated with 10 µM (low concentration) or 100 µM (high concentration) ibuprofen for 1, 3 or 14 days.

UniProt accession	Function	Protein name	Low concentration			High concentration		
			d01	d03	d14	d01	d03	d14
Q8CHM7	Fatty acid and lipid metabolism	2-hydroxyacyl-CoA lyase 1	-1.0	1.1	1.0	1.0	1.3	1.7
F1M609		Acyl-coenzyme A oxidase	-1.1	-1.0	-1.0	1.1	1.3	2.0
P02651		Apolipoprotein A-IV	-1.1	1.1	1.1	1.1	1.6	1.1
P20817		Cytochrome P450 4A14	-	1.0	1.2	-	2.8	2.5
P07872		Peroxisomal acyl-coenzyme A oxidase 1	-1.0	1.1	1.0	1.2	2.0	3.2
P07896		Peroxisomal bifunctional enzyme	1.0	1.0	1.0	1.1	2.0	3.6
G2IHE7	Carbohydrate metabolism	Alpha-glucosidase	-	1.1	1.2	-	1.2	2.3
D3Z8F7		Glucokinase activity, related sequence 1 (Predicted) / Protein Gykl1	-	1.6	-	-	1.9	-
Q7TNA8		L-lactate dehydrogenase	1.1	1.1	1.3	1.1	1.5	2.0
D3ZNG4		Solute carrier family 2 (Facilitated glucose transporter), member 12 (Predicted)	-1.3	-3.2	-	1.1	-4.0	-
P48500		Triosephosphate isomerase	-1.1	-1.6	1.1	-1.4	-1.7	1.0
P31210	Bile metabolism	3-oxo-5-beta-steroid 4-dehydrogenase	-1.3	-	-	-2.0	-	-
G5C4X3		Multidrug resistance protein 1	-1.1	-	-	-1.9	-	-
Q63718	Stress response	Heat shock protein 70	-	-1.7	-	-	-2.5	-
Q9XRS1	Immune response	MHC class II antigen	-	-	-1.5	-	-	5.9
P09006	Inflammation	Serine protease inhibitor A3N	-1.0	-1.1	-1.3	-1.3	-1.4	-1.9
E0A3N4		Serpina3n-like protein	-	-	-1.7	-	-	-2.2
G5AVD3	Xenobiotic metabolism	Cytochrome P450 2B6	-	-	-1.4	-	-	-2.4
P08009		Glutathione S-transferase Yb-3	1.1	1.6	1.2	1.1	-1.9	1.1
G5B5P1	Cell development	Alpha-fetoprotein	1.4	-	-	2.3	-	-

Table 56 (continued)

UniProt accession	Function	Protein name	Low concentration			High concentration		
			d01	d03	d14	d01	d03	d14
G5BNA8	Transcription	ATP-dependent DNA helicase Q5	-	-	1.2	-	-	-2.8
G5ANV9		DNA polymerase	-	1.8	-	-	1.4	
G5BL20		Forkhead box protein N4	-	-	-1.2	-	-	-2.0
G5C492		Nucleoporin NUP53	-	-	1.4	-	-	-2.8
D3ZX01		Protein Rps4y2/ RCG29848	-1.0	-	-	-1.8	-	-
D3ZGJ3		Protein Zbtb37/Zinc finger and BTB domain containing 37 (Predicted)	-1.3	-	1.1	-1.8	-	1.3
G5BTG2		Putative ATP-dependent RNA helicase DHX30	1.4	-	-1.7	2.0	-	-1.4
G5BXH3		Putative prolyl-tRNA synthetase, mitochondrial	-	-1.9	1.2	-	-1.9	-1.3
G5C0Q9		Scaffold attachment factor B2	-	-1.6	-	-	3.7	-
Q66H19		Serum response factor-binding protein 1	1.1	-	1.2	1.1	-	1.8
G5BJC8		Sin3 histone deacetylase corepressor complex component SDS3	-1.0	1.3	-1.1	1.0	-1.1	-2.7
G5BN53		Zinc finger protein 40	1.2	-	-	2.1	-	-
G5APK6	Cytoskeleton organisation	Dynein heavy chain 7, axonemal	-1.2	-	-	-1.7	-	-
G5AKC5		Laminin subunit alpha-4	-	1.3	-	-	1.9	-
F1M9P7		Protein Mamdc2	1.3	-	-	2.4	-	-
G5C7R0		Thrombospondin-2	7.1	-	-	-	-	-
G5ATL4		Villin-like protein	-	-2.1	-	-	-1.1	-
G5BPJ6	Other and unknown functions	Ankyrin repeat and SOCS box protein 13	-1.2	1.4	1.3	-1.5	-1.1	-2.6
G5C776		Arginase-1	1.0	-	1.1	-2.1	-	1.0
G5C8S5		Cytochrome P450 19A1	-	1.4	-	-	1.6	-
G5BV95		Dynein heavy chain 3, axonemal	1.6	-	-	1.1	-	-
D3ZXS6		Elongation factor 1-alpha	1.5	1.2	-	1.4	1.8	-
G5BSX2		Fc receptor-like protein 2	1.0	-	-1.3	1.7	-	-1.7

Table 56 (continued)

UniProt accession	Function	Protein name	Low concentration			High concentration		
			d01	d03	d14	d01	d03	d14
D3ZPI7		Glyceraldehyde-3-phosphate dehydrogenase	-1.0	-1.4	-	-1.1	-1.8	-
Q920R4		G-protein coupled receptor-associated sorting protein 1	1.0	1.2	-	1.1	1.6	-
G5C6Z6		Guanine nucleotide exchange factor VAV3	-1.8	-	1.3	-1.1	-	1.1
P70712		Kynureninase	1.9	-	-	2.0	-	-
Q5EBC3		Methylenetetrahydrofolate dehydrogenase (NADP+ dependent) 1, methenyltetrahydrofolate cyclohydrolase, formyltetrahydrofolate synthetase	1.6	-1.8	-	1.0	-1.6	-
G5BYU9		Methylthioribose-1-phosphate isomerase	2.1	1.1	-1.3	1.2	-1.2	-1.2
G2IF84		Negative regulator of genetic competence ClpC/mecB	-1.1	1.0	1.2	1.1	1.1	2.8
Q5USB8		Olfactory receptor 1108 (Predicted)/ Olfactory receptor MOR160-5 like protein/Protein Olr1108	-1.7	-	-	-1.5	-	-
G5B1G3		Olfactory receptor 2T4	1.2	-	-	2.8	-	-
G5C478	Other and unknown functions	Phosphatidylserine synthase 2	-	-	-1.0	-	-	2.3
D3ZMI0		Protein Gm6484	1.0	-1.1	1.3	1.1	1.4	3.4
D3ZLM2		Protein LOC100910350	1.3	-1.2	-1.1	2.5	-1.2	-1.2
Q5BK77		Protein Rarres2/ Retinoic acid receptor responder (Tazarotene induced) 2 / Retinoic acid receptor responder (Tazarotene induced) 2, isoform CRA_a	-	-	-1.0	-	-	2.2
D3ZAH0		Protein Trcg1	-1.0	-	-	2.0	-	-
G5B7Z6		RUN and FYVE domain-containing protein 2	1.2	1.2	1.1	1.1	-1.6	-1.2
G2IH46		Signal recognition particle receptor FtsY	-	1.6	-	-	1.7	-
G5BY42		Target of rapamycin complex subunit LST8	1.7	1.1	1.3	2.7	1.1	3.5
G5CB15		Transcription factor BTF3	-1.6	-	-	-2.0	-	-
Q68FT1		Ubiquinone biosynthesis protein COQ9, mitochondrial	-1.0	1.3	-1.1	-1.0	1.8	1.4
G5ANL4		UDP-glucuronosyltransferase 1-5	-1.7	-	-1.2	-1.1	-	1.8
G5AU68		Xaa-Pro aminopeptidase 2	-1.5	-	-	1.7	-	-

Table 57. Absolute fold changes of proteins with at least 1.5-fold changed abundance compared to the vehicle treated control (q-value ≤ 0.05) in primary rat hepatocytes treated with 2 µM (low concentration) or 20 µM (high concentration) chlorpromazine for 1, 3 or 14 days.

UniProt accession	Function	Protein name	Low concentration			High concentration		
			d01	d03	d14	d01	d03	d14
P80386	Fatty acid and lipid metabolism	5'-AMP-activated protein kinase subunit beta-1	-	1.9	-	-	2.8	-
P02651		Apolipoprotein A-IV	1.1	1.1	1.3	-1.1	1.4	2.2
P15943	Carbohydrate metabolism	Amyloid-like protein 2	-1.9	-	-	-1.1	-	-
Q7TNA8		L-lactate dehydrogenase	-1.1	1.1	1.4	-1.2	1.2	1.7
G5AXR5		N-acetyllactosaminide alpha-1,3-galactosyltransferase	1.9	-	-	1.6	-	-
P82995	Stress response	Heat shock protein HSP 90-alpha	1.2	1.6	1.5	1.1	1.4	1.3
Q63716		Peroxiredoxin-1	-1.4	1.0	1.2	-1.3	1.2	1.7
P09006	Inflammation	Serine protease inhibitor A3N	-1.0	1.1	1.1	-1.2	-1.3	-3.6
P24090	Immune response	Alpha-2-HS-glycoprotein	-1.3	1.3	-	-1.1	2.8	-
E3VX33		Alpha-2-macroglobulin	1.1	-1.1	-1.1	-1.0	1.0	-1.5
Q9ESH6	Xenobiotic metabolism	Glutaredoxin-1	-	-	1.2	-	-	1.8
P09875		UDP-glucuronosyltransferase 2B1	1.1	1.2	1.6	1.3	1.4	1.4
G5AP16	Detoxification	Gastric intrinsic factor	-	1.1	1.4	-	1.8	2.4
G5BE83		Retinol-binding protein 4	-	2.1	1.1	-	1.7	-1.1
Q7TQ16	Respiratory chain	Cytochrome b-c1 complex subunit 8	1.1	-1.1	1.2	1.1	-1.0	2.0
Q06QA1		NADH-ubiquinone oxidoreductase chain 5	1.7	-	-	1.5	-	-
G5C657	Protein metabolism	BTB/POZ domain-containing protein KCTD19	-	1.9	-	-	1.3	-
P07154		Cathepsin L1	-	1.3	-1.2	-	1.5	2.7
G5C053		Clathrin heavy chain 2	-	1.0	-1.1	-	1.9	-2.7
Q3T1J4		Protein Galnt3	-	-1.1	-	-	-1.9	-
Q7TNJ4	Apoptosis	Amphoterin-induced protein 2	-2.1	-	-	-1.6	-	-
G5BX56		Protein FAM72A	1.9	-	-	2.5	-	-

Table 57 (continued)

UniProt accession	Function	Protein name	Low concentration			High concentration		
			d01	d03	d14	d01	d03	d14
D3J0V7	Cell proliferation	Growth hormone receptor	-	-	2.3	-	-	2.0
G5BI09		Rap1 GTPase-activating protein 1	-1.9	-	-	-1.7	-	-
G5B2S6	Transcription/ Translation	AT-rich interactive domain-containing protein 1B	-	1.0	-1.5	-	-1.2	-2.7
G5AY05		Gem-associated protein 5	-1.3	-	-1.3	-1.7	-	-1.0
G5BU47		Protein archease	-11.0	-	-	-	-	-
D3ZHQ9		Protein Asxl1	-	-	1.3	-	-	2.0
G5AKW1		Protein deltex-1	-1.0	1.1	-1.1	-1.1	-1.1	-2.2
G5BXS3	ECM organisation	Ankyrin-3	-	1.7	-	-	1.4	-
G5C4J0		Collagen alpha-1(I) chain	-1.5	1.1	1.1	-2.4	1.1	1.1
G5B5V9		Protocadherin Fat 4	-	2.4	-	-	1.7	-
O35817	Signalling	A-kinase anchor protein 14	-1.2	-1.4	-1.5	-1.3	-1.4	-1.6
Q5XI73		Rho GDP-dissociation inhibitor 1	-	1.3	-	-	2.4	-
Q3KR78		Similar to speedy B isoform	-1.1	-	1.8	-1.0	-	2.3
Q7TP91	Other and unknown functions	Ab1-205	1.7	-	-	1.6	-	-
G5AKU7		Aldehyde dehydrogenase, mitochondrial	-	-1.7	1.1	-	-1.8	1.5
G5C776		Arginase-1	-2.1	1.2	1.1	-1.5	1.1	-1.1
G5AXD5		Calcyphosin-2	1.2	-	-	1.7	-	-
G5B009		Early endosome antigen 1	-	-	-1.2	-	-	-2.5
G5C6Z6		Guanine nucleotide exchange factor VAV3	1.2	-	-	2.6	-	-
G5BUQ4		Kelch-like protein 28	-	2.5	-	-	1.8	-
G5ALS8		Keratin, type II cytoskeletal 1	-	-2.9	-	-	-2.2	-
G2IF84		Negative regulator of genetic competence ClpC/mecB	-2.3	-1.1	-	-1.1	1.1	-
G5B1G3		Olfactory receptor 2T4	1.7	-	-	1.4	-	-
F1M1E7		Protein E030019B06Rik	-	-1.3	-	-	-2.2	-
D4A5P3		Protein Fam73a	-2.7	-	-	-1.4	-	-
D3ZJI0		Protein Olr1600	1.3	1.4	-1.7	1.3	1.2	-2.2

Table 57 (continued)

UniProt accession	Function	Protein name	Low concentration			High concentration		
			d01	d03	d14	d01	d03	d14
D4A466	Other and unknown functions	Protein RGD1563307	2.0	-	-	1.2	-	-
G5BFV0		TOX high mobility group box family member 4	-1.5	-	-	-3.6	-	-
G5ATV8		Vomeronasal type-2 receptor 26	-	2.1	-	-	1.1	-

Table 58. Absolute fold changes of proteins with at least 1.5-fold changed abundance compared to the vehicle treated control (q-value ≤ 0.05) in primary rat hepatocytes treated with 0.25 µM (low concentration) or 2.5 µM (high concentration) cyclosporine A for 1, 3 or 14 days.

UniProt accession	Function	Protein name	Low concentration			High concentration		
			d01	d03	d14	d01	d03	d14
G5AXY3	Fatty acid and lipid metabolism	Acyl-CoA-binding domain-containing protein 5	-	-	1.3	-	-	4.6
G5BJ97		Fatty acid synthase	-	-1.4	-1.3	-	-3.5	-1.1
P17425		Hydroxymethylglutaryl-CoA synthase, cytoplasmic	-	-1.0	1.1	-	-2.3	-1.2
G5AUQ1		Platelet-activating factor acetylhydrolase 2, cytoplasmic	-	-1.1	1.0	-	1.2	-2.8
D4A1Y9		Protein Tecrl	1.0	-1.0	-1.2	-1.8	-1.0	1.0
Q07071	Carbohydrate metabolism	Glucokinase regulatory protein	-	1.1	1.1	-	-1.5	-1.4
G5BHD5		L-lactate dehydrogenase	-	-1.2	-1.2	-	1.2	1.5
P49432		Pyruvate dehydrogenase E1 component subunit beta, mitochondrial	-3.2	1.0	-1.0	-	-1.1	1.1
Q9Z0U5	Xenobiotic metabolism	Aldehyde oxidase	-	-	1.0	-	-	-5.0
G5ATW8	Oxidative stress	Carbonic anhydrase 3	-2.6	1.0	-1.3	-3.4	1.0	-1.1
G5C6A9	Transcription	General transcription factor II-I repeat domain-containing protein 1	-	-	3.2	-	-	1.2
C7BVN5		Putative Mediator of RNA polymerase II transcription subunit 6	-	-	1.3	-	-	2.5
G5BJC8		Sin3 histone deacetylase corepressor complex component SDS3	-	1.0	-	-	-2.2	-
G5C4J0	ECM organisation	Collagen alpha-1(I) chain	-	1.2	-1.1	2.7	1.1	1.1
P02466		Collagen alpha-2(I) chain	1.2	1.4	-1.0	2.6	1.1	-1.0
G5ANN1		CUB domain-containing protein 1	1.3	-	-	4.5	-	-
F1M5B8		Protein Astn1	-1.4	-	-	-2.1	1.0	-
F1LZF4		Protein Col6a5	1.5	-	-1.3	1.3	-	1.0
D4A536		Protein Cpxm2	-	1.8	-	-	1.2	-
G5ARS0		Tenascin-N	-	-	1.7	-	-	3.2
G5B9E8	cytoskeleton	Tubulin alpha-1C chain	-	-2.7	1.5	-	-2.2	1.1

Table 58 (continued)

UniProt accession	Function	Protein name	Low concentration			High concentration		
			d01	d03	d14	d01	d03	d14
G5CAC9	Apoptosis	26S proteasome non-ATPase regulatory subunit 10	-	2.1	-	-	1.3	-
O35821		Myb-binding protein 1A	-1.7	1.2	1.1	-	2.1	-1.0
G5B921		Myb-binding protein 1A	-	-	3.4	-	-	3.6
G5BPJ6	Amino acid and protein metabolism	Ankyrin repeat and SOCS box protein 13	-	-	-	-3.5	-	-
Q4V8H5		Aspartyl aminopeptidase	-1.1	1.0	1.2	2.7	1.0	1.3
G5BQ90		Alanine--glyoxylate aminotransferase 2, mitochondrial	-	-	1.3	-	-	2.5
G5AXZ3	Other functions	2-oxoglutarate dehydrogenase E1 component-like, mitochondrial	-	-1.2	1.3	-	-1.8	2.0
G5ARV3		Bestrophin-4	-	-	1.5	-	-	5.2
B5DF65		Biliverdin reductase B (Flavin reductase (NADPH))	-3.4	1.0	-1.1	-4.3	-1.0	-1.4
Q5HZB2		Cytosolic 10-formyltetrahydrofolate dehydrogenase	4.5	-1.0	-1.3	2.6	-1.1	-1.3
B0BNF6		Membrane-associated ring finger (C3HC4) 5	-	-	1.1	-	-	1.8
D4A9A3		Protein Cenpv	-2.4	-	-1.0	-1.7	-	-1.2
Q9JLA3		UDP-glucose:glycoprotein glucosyltransferase 1	-1.9	1.2	-1.0	-1.8	1.3	-1.0
G5CBF3		Voltage-dependent calcium channel gamma-6 subunit	-	1.6	2.4	-	1.3	2.5
G5BCV2		WD repeat-containing protein 81	-	-	2.9	-	-	-
D4A929		WD repeat-containing protein 81	-	-	2.0	-	-	2.6

Appendix 10: Gene deregulations in primary human hepatocytes

The complete gene expression dataset of PHH from the different donors was not included here, due to the high number of deregulated genes. Therefore, the following tables (Table 59 - Table 62) include only genes of IPA® tox functions that were discussed in this thesis.

The genes of PHH that were deregulated ≥ 2-fold compared to the corresponding time-matched vehicle control were uploaded into a public database (ArrayExpress). The microarray data of PHH are available in the ArrayExpress database (**www.ebi.ac.uk/arrayexpress**) under accession number **E-MTAB-2473**.

Table 59. Absolute fold changes of genes deregulated at least 2-fold compared to the time matched vehicle treated control in primary human hepatocytes from three different donors treated with 100 or 1000 µM ibuprofen for 1, 3 or 14 days. The categorisation of the genes into IPA® tox functions was evaluated manually which is indicated as the additional "function" category. The genes are in alphabetic order within each IPA® tox function and full gene names are given in Table 63.

RefSeq	Symbol	IPA® Tox function	Function	Donor 1						Donor 2						Donor 3					
				100 µM IBU			1000 µM IBU			100 µM IBU			1000 µM IBU			100 µM IBU			1000 µM IBU		
				d01	d03	d14	d01	d03	d14	d01	d03	d14	d01	d03	d14	d01	d03	d14	d01	d03	d14
NM_005502.2	*ABCA1*	Liver Steatosis	Fatty acid and lipid metabolism	-1.0	1.1	-1.4	1.1	-1.4	1.1	-1.0	1.1	-1.0	-1.2	1.0	-1.1	-3.1	1.3	-1.0	-1.7	-1.3	1.0
NM_016818.2	*ABCG1*			-1.4	1.2	-1.2	-1.7	-1.3	-4.3	1.1	-1.0	-1.2	-1.3	-1.4	1.3	-1.5	-1.0	-1.7	-1.3	-1.4	-1.3
NM_016006.3	*ABHD5*			1.5	1.2	-1.2	1.8	1.8	1.5	-1.3	1.0	1.3	1.5	1.5	3.1	1.9	1.1	1.1	1.1	1.2	-1.1
NM_198836.1	*ACACA*			1.0	-1.1	-1.3	1.1	-1.3	-2.3	-1.2	-1.1	-1.2	-1.5	-2.0	-2.5	1.1	-1.3	-1.0	1.2	-1.2	1.0
NM_000016.2	*ACADM*			2.6	1.6	1.1	2.8	1.1	2.0	1.0	1.0	1.2	1.2	1.9	-1.5	1.5	1.6	1.6	1.6	1.4	2.0
NM_001033859.1	*ACADVL*			-1.0	2.2	1.8	1.1	2.2	1.4	1.6	1.5	1.4	2.4	3.4	1.8	1.3	2.5	1.3	1.1	2.6	1.7
NM_018473.2	*ACOT13*			-1.2	-1.0	1.8	-1.5	-1.3	1.0	-1.4	-1.1	1.1	-1.5	-1.0	-2.5	-1.1	1.1	1.1	1.3	-1.3	-1.2
NM_007292.4	*ACOX1*			1.2	1.7	1.1	1.6	1.2	2.1	1.1	1.2	1.4	1.6	1.9	1.4	2.2	1.3	1.0	2.1	1.7	1.3
NM_003500.2	*ACOX2*			-1.1	-1.1	1.6	-1.5	-2.0	2.0	1.0	-1.2	1.2	-1.4	-1.5	-4.6	1.1	1.1	1.7	1.7	1.2	1.8
NM_001012727.1	*AGPAT2*			-1.0	1.7	2.1	1.4	2.7	5.3	1.1	1.1	1.5	1.7	1.7	2.3	3.6	2.0	1.0	1.7	3.0	1.2
NM_006412.3	*AGPAT2*			-1.3	1.8	2.4	1.2	2.9	5.0	1.0	1.6	1.6	1.5	2.0	2.3	2.8	1.6	-1.1	1.8	2.2	1.1
NM_000041.2	*APOE*			-1.5	-1.2	1.1	-1.5	-1.9	-7.4	-1.2	-1.2	1.0	-1.4	-2.1	1.0	-1.3	-1.1	1.0	-1.1	-1.5	-1.2
NM_001031847.1	*CPT1A*			1.5	2.8	1.4	2.9	3.6	2.6	1.6	1.2	1.8	4.8	4.9	2.0	4.2	1.8	1.1	1.7	4.4	1.1
NM_001966.2	*EHHADH*			1.4	1.0	1.5	1.1	-2.3	2.2	1.3	1.3	1.7	-1.1	1.4	-2.4	1.6	1.4	1.5	2.7	1.0	2.1
NM_001442.1	*FABP4*			1.6	1.5	-1.3	3.9	1.3	1.3	1.5	-1.1	-1.3	6.0	5.1	1.6	3.8	-2.5	-1.9	1.8	1.2	-1.6
NM_004104.4	*FASN*			-1.4	-1.2	1.0	-1.1	-2.4	-2.4	-1.6	-1.8	-1.6	-1.3	-6.0	-1.5	1.4	-1.6	-1.9	1.3	-2.2	-1.5
NM_000167.3	*GK*			1.6	2.3	-1.5	3.0	6.6	1.0	1.4	1.3	1.6	4.8	4.9	2.3	2.5	2.4	-1.1	-1.1	7.5	1.1

Table 59 (continued)

RefSeq	Symbol	IPA® Tox function	Function	Donor 1						Donor 2						Donor 3					
				100 µM IBU			1000 µM IBU			100 µM IBU			1000 µM IBU			100 µM IBU			1000 µM IBU		
				d01	d03	d14	d01	d03	d14	d01	d03	d14	d01	d03	d14	d01	d03	d14	d01	d03	d14
NM_203391.1	*GK*			1.8	2.4	-1.6	3.6	6.6	1.1	1.5	1.5	1.6	5.1	4.9	2.1	2.2	2.7	-1.1	-1.4	7.9	-1.1
NM_005276.2	*GPD1*			1.3	1.4	1.1	1.3	-1.4	1.1	1.4	-1.1	1.4	-1.4	-1.2	-2.3	-1.1	1.1	1.6	1.6	-1.8	1.4
NM_000182.4	*HADHA*			-1.1	2.3	2.4	1.5	2.6	3.3	1.3	1.4	1.6	2.7	2.9	1.2	2.5	2.2	-1.2	1.4	3.6	1.3
NM_000859.1	*HMGCR*			-1.2	-1.8	1.3	1.1	-1.2	-2.2	-1.3	-1.2	-1.6	1.2	-4.8	-1.1	2.2	-1.8	-1.5	1.7	-2.5	1.0
NM_198336.1	*INSIG1*			1.4	-1.4	-1.3	2.2	-1.3	-1.5	1.0	-1.1	1.0	1.7	-2.0	1.0	3.0	-1.3	-1.2	1.7	1.0	1.7
NM_000527.2	*LDLR*			-1.1	-2.0	1.2	1.3	1.5	-2.1	-1.1	1.1	-1.3	2.1	-1.9	1.8	1.6	-1.6	-1.4	-1.3	-1.2	-1.1
NM_005577.2	*LPA*			-1.8	-1.4	-1.0	-2.4	-6.3	-3.1	1.1	1.3	1.1	-2.6	-3.2	-1.6	-2.3	1.3	-1.6	1.4	-4.0	1.1
NM_145693.1	*LPIN1*			1.2	-1.8	-1.3	1.7	-1.4	1.1	-1.3	1.0	-1.2	1.3	-2.1	1.1	2.0	-1.9	-1.2	1.1	-1.3	1.1
NM_000237.2	*LPL*			-1.3	-1.2	1.2	-1.2	-1.2	-1.1	-1.2	1.1	-1.5	-1.4	-1.3	-3.2	-1.1	-1.7	1.0	1.1	-1.9	1.2
NM_000253.2	*MTTP*			1.8	1.0	-1.4	1.5	-1.4	1.6	-1.2	-1.1	1.2	-2.0	-1.0	-4.1	-1.1	-1.0	1.3	1.4	-1.3	1.4
NM_000255.1	*MUT*		Fatty acid and lipid metabolism	-1.3	1.1	1.5	-2.1	-2.1	1.1	1.1	1.1	1.2	-1.6	-1.3	-2.2	-1.2	1.2	1.2	1.8	-1.5	1.7
NM_005693.1	*NR1H3*			-1.2	-1.2	1.5	-1.3	1.1	1.3	1.1	1.0	-1.4	-1.1	-1.4	-2.0	-1.3	1.0	-1.1	-1.1	-1.3	1.1
NM_148978.1	*PANK1*			-1.0	1.2	1.5	1.6	1.3	2.8	1.0	1.0	1.3	1.4	1.5	-2.0	3.1	1.3	1.3	2.5	2.3	1.8
NM_000922.2	*PDE3B*			1.2	-1.1	-2.5	1.4	-1.3	-1.7	1.2	-1.1	1.2	1.1	-1.0	-2.0	1.4	1.1	1.3	1.4	1.4	1.5
NM_001122.2	*PLIN2*			1.3	4.0	2.0	5.5	16.9	2.3	-1.2	1.3	1.8	3.0	5.5	1.9	5.5	2.7	1.2	2.3	4.7	-1.1
NM_020376.2	*PNPLA2*	Liver Steatosis		-1.1	2.2	2.1	1.2	2.3	2.7	-1.0	1.3	1.2	1.9	2.1	3.5	3.6	1.5	1.1	1.7	1.9	-1.3
NM_001001928.2	*PPARA*			1.1	1.1	1.5	1.4	1.2	4.1	1.1	1.3	1.9	1.3	1.4	-1.0	1.2	1.3	1.1	1.2	1.3	1.2
NM_015869.4	*PPARG*			-1.0	-1.0	1.3	1.1	1.7	2.0	1.1	1.1	1.2	1.1	1.1	1.3	1.4	1.5	-1.1	1.0	2.1	1.4
NM_003060.2	*SLC22A5*			-1.1	1.1	-1.0	1.0	1.4	1.0	1.2	1.1	1.3	1.5	1.4	2.1	1.5	1.0	-1.0	-1.0	1.4	1.1
NM_012254.1	*SLC27A5*			-1.3	1.0	1.6	-1.5	-2.0	1.4	-1.0	1.0	-1.1	-2.4	-2.1	-1.2	-1.4	1.2	-1.0	1.7	-4.0	1.2
NM_004176.3	*SREBF1*			-1.6	-1.1	1.9	-1.6	-2.0	-2.0	1.3	1.1	-1.4	-1.5	-2.2	-4.0	-2.1	-1.2	-1.0	1.1	-2.1	-1.1
NM_001005291.1	*SREBF1*			-1.6	1.1	1.5	-1.5	-3.5	-2.0	-1.1	-1.0	-1.4	-2.3	-2.2	-5.0	-1.7	-1.6	1.0	1.1	-2.3	1.2
NM_000594.2	*TNF*			-1.0	1.1	1.2	-1.1	-1.2	-3.4	1.3	-1.3	-1.1	-1.0	-1.6	-1.2	-1.9	-1.0	-3.8	-1.6	-1.1	-2.3
NM_000151.2	*G6PC*			1.8	1.7	-1.4	1.9	3.2	2.7	1.2	-1.1	1.1	4.9	1.5	5.9	2.5	-1.4	1.6	2.9	-1.5	-1.5
NM_005309.1	*GPT*			-1.7	-1.4	3.3	-2.2	-1.7	3.7	1.1	2.0	1.7	-2.5	-1.2	-1.9	-1.4	2.3	1.1	1.4	-1.2	3.0
NM_003749.2	*IRS2*		Carbo-hydrate metabolism	-1.5	1.3	1.6	-1.2	2.5	3.0	-1.4	1.1	-1.1	1.1	1.1	3.9	-1.5	-1.1	1.3	-1.3	1.3	1.5
NM_002591.2	*PCK1*			3.4	1.8	1.4	5.5	4.1	19.6	-1.1	1.2	1.1	1.3	1.7	-1.0	2.1	3.6	1.6	2.7	2.9	1.6
NM_002591.2	*PCK1*			1.1	2.1	7.7	2.0	4.3	15.1	1.7	-1.0	2.8	5.8	5.1	-1.5	2.6	8.0	1.1	3.3	4.7	1.2
NM_017761.2	*PNRC2*			1.1	-1.1	-2.2	1.0	-1.1	-2.4	1.1	1.2	-1.0	1.2	1.2	1.9	-1.2	-1.0	-1.1	-1.2	-1.0	-1.0
NM_013261.3	*PPARGC1A*			1.0	-1.0	-1.0	-1.2	1.3	14.3	1.1	-1.1	1.5	-1.4	-1.4	-2.4	1.3	1.3	1.4	1.9	-1.0	1.5

Table 59 (continued)

RefSeq	Symbol	IPA® Tox function	Function	Donor 1						Donor 2						Donor 3					
				100 µM IBU			1000 µM IBU			100 µM IBU			1000 µM IBU			100 µM IBU			1000 µM IBU		
				d01	d03	d14	d01	d03	d14	d01	d03	d14	d01	d03	d14	d01	d03	d14	d01	d03	d14
NM_002982.3	*CCL2*		In-flammation	-1.4	-2.0	-1.6	-1.6	-3.4	-11.4	1.6	1.1	-1.9	1.6	-2.2	-5.1	-6.8	-1.8	-1.5	-5.2	-1.8	-2.1
NM_001099856.1	*IKBKG*			-1.0	1.2	1.6	1.1	1.5	1.1	1.2	1.3	1.0	2.6	1.5	2.8	1.6	-1.3	1.0	-1.1	1.5	-1.2
NM_000958.2	*PTGER4*			1.1	-1.1	-1.3	1.2	-1.3	-2.5	1.2	-1.1	-1.1	-1.0	-1.4	-1.8	-1.7	-1.1	-2.2	-1.7	-1.1	-1.5
NM_000064.1	*C3*		Immune response	-2.1	-1.4	1.1	-2.5	-2.8	-4.7	-1.1	-1.1	-1.1	-1.4	-2.2	-1.6	-2.5	-1.2	-1.0	-1.2	-2.4	-1.1
NM_000064.2	*C3*			-1.5	-1.2	1.2	-1.5	-2.0	-3.0	-1.0	-8.2	-1.7	-1.4	-12.1	-3.0	-2.3	1.1	-1.5	-1.4	-1.9	-1.2
NM_001753.3	*CAV1*			-1.0	-1.3	-1.1	-1.8	-3.3	-1.5	-1.0	-1.1	-1.5	-1.6	-3.4	1.1	-1.2	-1.6	1.4	1.1	-2.8	2.0
NM_000591.2	*CD14*			-1.4	-1.1	1.7	-1.0	1.1	-1.4	1.2	-1.3	-2.5	3.5	-1.1	1.0	1.4	-1.1	-1.1	-1.3	-2.0	-2.3
NM_001001392.1	*CD44*			-1.1	1.2	-1.3	1.0	1.4	-1.3	1.0	-1.0	-1.1	1.4	-1.0	4.1	-1.3	1.0	-1.3	-1.6	1.3	-1.3
NM_000576.2	*IL1B*			-1.1	-1.2	-1.2	1.1	-1.2	-3.6	1.6	1.2	1.4	1.4	-1.3	1.7	-3.8	1.1	-2.8	-4.6	1.1	-2.6
NM_000600.1	*IL6*			-1.2	-1.3	-1.7	-1.1	-1.2	-4.1	1.2	1.1	-1.3	1.1	-1.1	-1.5	-2.9	-1.0	-4.9	-2.9	-1.1	-3.2
NM_000582.2	*SPP1*			-1.1	-1.1	1.2	-1.2	-3.0	-1.1	1.1	-1.0	-2.2	-1.4	-4.0	-11.8	-2.6	-1.3	-1.8	-1.3	-1.8	1.0
NM_001040058.1	*SPP1*			-1.1	-1.2	1.2	-1.2	-2.8	-1.4	1.1	1.2	-1.7	-1.4	-3.7	-11.3	-2.9	-1.1	-2.2	-1.3	-1.7	1.0
NM_138554.2	*TLR4*			-1.1	-1.2	-1.5	-1.1	-1.5	-2.0	1.2	-1.2	1.1	1.1	-1.3	1.3	-1.0	-1.3	-1.3	1.3	-1.5	-1.1
NM_031917.2	*ANGPTL6*		Cancer	-1.2	-1.2	2.1	-1.3	1.1	1.6	-1.1	-1.0	1.2	-1.5	-1.4	-2.0	-1.4	1.4	1.1	1.0	-1.0	1.3
NM_053056.2	*CCND1*			1.1	-1.1	-1.9	1.1	-2.1	-3.0	-1.0	-1.2	-1.4	-1.5	-2.4	1.3	-1.1	-1.5	-1.0	-1.2	-2.2	-1.3
NM_078467.1	*CDKN1A*			-1.2	-1.1	-1.1	1.0	1.3	-1.1	-1.1	-1.1	1.0	1.9	-1.0	5.6	1.4	-1.3	-1.3	1.3	1.1	-1.1
NM_022094.2	*CIDEC*			2.3	3.5	2.2	7.5	21.6	5.5	2.1	2.5	1.4	10.9	3.2	1.0	8.4	2.8	1.3	1.7	14.7	1.6
NM_000125.2	*ESR1*			-1.2	-1.7	-1.0	-1.6	-3.9	1.1	-1.3	-1.7	1.1	-1.7	-3.1	-1.7	-1.6	-1.2	-1.1	1.5	-3.0	-1.2
NM_000545.4	*HNF1A*			-1.7	1.2	2.2	-1.7	1.1	1.6	1.0	-1.1	-1.1	-1.4	1.1	-2.1	-1.0	-1.0	1.1	-1.1	-1.2	1.0
NM_005957.2	*MTHFR*			-1.5	-1.1	-2.2	-1.1	1.4	-2.1	-1.0	-1.2	-1.3	1.2	-1.6	-1.0	1.0	-1.4	-1.3	-1.5	1.1	-1.2
NM_139276.2	*STAT3*			-1.4	-1.7	-1.1	-1.3	-1.9	-2.4	1.1	-1.0	1.1	1.1	-1.7	-1.4	-1.8	-1.1	-1.1	-1.4	-1.3	1.0
NM_000773.3	*CYP2E1*		Xenobiotic metabolism	-1.0	1.2	1.9	-2.1	-2.3	1.3	1.1	1.9	-1.1	-1.3	2.5	1.0	-2.2	2.0	1.5	-1.1	1.0	1.9
NM_001077469.1	*NR1I3*			-1.4	-1.2	2.4	-1.7	-3.2	1.4	-1.1	1.2	1.5	-2.2	-1.4	-2.9	-2.8	1.8	1.4	1.3	-2.2	1.4
NM_001752.2	*CAT*		Stress response	4.9	1.1	-1.8	4.7	-1.4	2.6	-1.1	1.0	1.1	-1.4	2.0	-2.3	1.3	1.0	2.1	2.0	-1.5	2.7
NM_000636.2	*SOD2*			1.5	-1.7	-2.1	1.0	-1.5	-1.3	1.1	1.2	-1.7	-1.2	-1.5	-1.9	-3.1	-1.4	1.1	-2.6	-1.8	1.8
NM_138455.2	*CTHRC1*		ECM organisation	1.1	-1.4	-1.8	-1.3	-3.5	-1.3	-1.0	-1.0	-1.3	-1.4	-1.6	-3.2	-1.4	-1.2	1.0	-1.1	-1.3	1.9
NM_003742.2	*ABCB11*		Other and unknown functions	-1.2	-1.1	-1.3	-1.2	-1.8	-1.3	1.0	1.2	1.2	-1.6	-2.8	-1.8	-2.1	-1.8	1.2	1.2	-6.3	1.1

Table 59 (continued)

RefSeq	Symbol	IPA® Tox function	Function	Donor 1						Donor 2						Donor 3					
				100 µM IBU			1000 µM IBU			100 µM IBU			1000 µM IBU			100 µM IBU			1000 µM IBU		
				d01	d03	d14	d01	d03	d14	d01	d03	d14	d01	d03	d14	d01	d03	d14	d01	d03	d14
NM_001123.2	*ADK*			-1.2	-1.5	1.3	-1.5	-2.1	2.0	-1.1	-1.1	1.3	-1.2	-1.2	-1.0	-1.1	1.1	-1.0	1.1	-1.6	-1.3
NM_000675.3	*ADORA2A*			-1.1	-1.1	-1.3	-1.0	1.0	-2.5	-1.1	-1.1	-1.1	1.1	-1.0	-1.0	1.1	-1.2	1.2	-1.1	1.1	-1.1
NM_001011645.1	*AR*			-1.3	-1.3	1.1	-1.4	-2.7	-1.4	1.1	-1.2	1.2	-1.9	-1.6	-2.1	-1.5	1.4	1.2	1.6	-1.3	1.1
NM_004281.3	*BAG3*			-1.3	1.1	1.4	-1.1	1.1	1.1	-1.0	1.1	1.2	1.8	1.4	2.3	1.5	1.1	-1.3	-1.3	1.2	-1.2
NM_001713.1	*BHMT*			-1.7	-1.3	2.8	-3.1	-7.9	6.9	1.1	1.4	3.3	-2.8	1.3	-2.1	-1.5	2.0	1.9	4.8	-2.4	2.7
NM_000071.1	*CBS*			-1.1	-1.4	1.3	-1.1	-1.2	-1.0	1.1	1.2	-1.1	-1.4	1.0	-2.5	-1.1	1.3	1.2	1.0	1.1	1.2
NM_000790.2	*DDC*			-1.3	1.0	2.8	-2.2	-2.4	2.5	-1.1	1.5	1.6	-3.6	-1.5	-2.7	-3.0	1.9	1.3	1.4	-2.4	1.8
NM_004417.2	*DUSP1*			-1.1	-1.2	1.5	1.1	2.8	-1.0	-1.0	-1.2	-1.0	2.3	-1.1	3.1	1.4	1.3	-1.0	-1.1	2.1	-1.1
NM_033632.2	*FBXW7*			1.6	-1.0	-1.8	1.5	1.0	-1.3	-1.1	-1.3	1.2	1.1	1.1	2.0	-1.1	-1.1	1.2	-1.0	-1.1	1.2
NM_019113.2	*FGF21*			1.2	1.4	7.4	2.5	16.8	12.9	-1.1	-1.1	-1.0	2.5	-1.1	1.6	1.7	-2.3	1.2	-1.0	2.2	-2.2
NM_005860.2	*FSTL3*			-1.6	1.4	1.7	-2.1	1.1	-1.6	-1.2	-1.1	-1.3	1.4	-1.8	4.5	-1.8	-1.0	-1.4	-2.2	1.1	-1.2
NM_001482.2	*GATM*			1.2	1.0	-1.4	-1.1	-2.8	-1.6	1.1	1.2	1.3	-1.3	-1.5	-3.0	-1.4	1.1	-1.0	1.5	-1.4	-1.1
NM_000163.2	*GHR*			1.6	-1.2	-1.5	1.1	-2.3	-1.7	1.0	-1.4	-1.1	-1.5	-2.0	-4.5	-1.6	-1.8	-1.1	1.2	-2.7	-1.8
NM_018960.4	*GNMT*			-2.0	-2.7	1.3	-3.0	-6.5	1.1	-1.8	1.3	-1.1	-3.7	-2.1	-2.9	-2.3	1.2	1.1	1.2	-2.3	1.6
NM_004489.4	*GPS2*	Liver Steatosis	Other and unknown functions	-1.3	1.5	1.5	-1.2	1.7	1.6	1.0	1.3	1.1	1.4	1.4	2.1	1.1	1.3	1.0	-1.0	2.0	-1.3
NM_001945.1	*HBEGF*			-1.1	1.0	3.1	-1.2	-1.1	-2.9	-1.0	1.2	-1.1	1.1	-1.5	3.7	1.0	-1.4	1.1	-1.2	-1.2	1.0
NM_004972.2	*JAK2*			1.3	1.2	-3.8	1.3	1.3	-4.7	1.0	-1.1	1.3	1.3	-1.1	2.3	1.2	-1.1	-1.4	1.1	1.1	1.4
NM_018433.3	*KDM3A*			1.7	1.1	-1.3	1.8	1.0	3.1	-1.6	-1.1	1.0	-1.9	-1.1	1.2	1.2	1.4	1.1	1.1	-1.1	-1.0
NM_000429.2	*MAT1A*			-1.8	1.4	5.4	-2.5	-1.4	3.9	-1.1	-1.1	1.2	-1.8	-1.1	-5.1	-1.5	1.5	2.0	1.6	-1.0	1.5
NM_001618.2	*PARP1*			-1.3	-1.0	-1.1	-1.9	-1.3	-2.2	1.1	-1.3	-1.0	-1.1	-1.2	-1.4	-2.6	-1.2	-1.1	-2.0	-1.2	1.1
NM_002600.3	*PDE4B*			1.1	-1.2	-2.8	-1.1	-1.6	-3.7	1.0	-1.0	-1.0	-1.4	-1.7	-1.1	-1.6	-1.5	-1.9	-1.3	-1.4	-2.3
NM_001083.3	*PDE5A*			1.3	1.0	-1.1	1.3	1.6	1.4	-1.0	-1.2	1.2	-1.2	-1.4	2.2	1.9	-1.1	1.1	1.2	-1.1	1.1
NM_007169.2	*PEMT*			1.2	1.4	3.1	1.2	-2.1	4.2	2.1	1.9	3.2	1.7	2.0	-1.9	-1.5	3.0	1.2	2.0	-1.5	2.5
NM_000941.2	*POR*			-1.1	1.8	2.3	2.1	4.1	3.5	-1.0	-1.0	1.0	2.3	2.2	2.4	3.7	1.2	-1.1	1.4	1.5	-1.6
NM_005789.2	*PSME3*			1.0	1.1	1.1	1.3	1.1	-2.1	1.1	-1.1	1.0	1.1	-1.8	-1.2	1.1	-1.7	-1.1	-1.3	1.0	-1.2
NM_152869.2	*RGN*			-1.1	-1.0	1.2	-1.8	-2.5	1.1	-1.1	1.3	1.2	-2.9	-1.1	-2.7	-1.4	1.7	1.6	1.6	-1.7	1.9
NM_152869.2	*RGN*			-1.3	-1.0	1.8	-1.9	-2.3	1.3	-1.1	1.3	1.7	-3.1	-1.2	-1.7	-1.3	1.4	1.1	2.1	-2.7	2.0
NM_001002236.1	*SERPINA1*			-1.1	-1.0	-1.3	-1.2	-1.3	-2.2	-1.4	1.1	1.4	-1.1	1.2	-1.2	-2.0	1.2	-1.1	-1.7	-1.0	1.1
NM_012238.3	*SIRT1*			1.8	1.0	-2.6	2.4	1.3	1.7	-1.7	1.1	1.1	-1.3	-1.3	2.5	1.2	-1.1	1.0	1.0	1.2	-1.1
NM_006472.2	*TXNIP*			-1.1	1.0	-2.1	1.9	1.9	-1.5	1.1	-1.4	-1.1	3.4	1.4	3.6	1.7	-2.2	-1.1	-1.1	2.1	1.2

Table 59 (continued)

RefSeq	Symbol	IPA® Tox function	Function	Donor 1						Donor 2						Donor 3					
				100 µM IBU			1000 µM IBU			100 µM IBU			1000 µM IBU			100 µM IBU			1000 µM IBU		
				d01	d03	d14	d01	d03	d14	d01	d03	d14	d01	d03	d14	d01	d03	d14	d01	d03	d14
NM_001134.1	*AFP*			1.1	-1.4	1.5	-1.3	-3.2	3.9	1.2	1.2	2.1	-1.5	1.1	-1.5	1.1	2.0	1.2	3.2	-1.6	1.6
NM_001002857.1	*ANXA2*			1.0	-1.2	-1.0	1.1	-1.3	-1.1	1.3	1.1	1.4	1.4	-1.3	3.1	1.1	-1.8	-1.3	-1.3	-1.0	-1.3
NM_198434.1	*AURKA*			-1.0	1.2	1.0	1.1	1.3	1.8	1.2	1.0	1.7	1.8	1.2	2.6	1.4	1.3	1.2	1.2	1.4	1.2
NM_181050.1	*AXIN1*			-1.3	1.0	1.6	-1.2	1.8	1.7	-1.2	1.1	1.1	-1.1	1.2	2.8	1.6	-1.0	-1.2	1.1	1.4	-1.0
NM_001216.1	*CA9*			-1.0	-1.3	1.6	-1.0	-1.3	1.3	-1.3	-1.4	1.4	-3.3	-1.8	-2.8	-1.7	1.6	-1.1	1.2	-1.0	1.6
NM_053056.2	*CCND1*			1.1	-1.1	-1.9	1.1	-2.1	-3.0	-1.0	-1.2	-1.4	-1.5	-2.4	1.3	-1.1	-1.5	-1.0	-1.2	-2.2	-1.3
NM_001238.1	*CCNE1*			-1.2	1.2	1.0	-1.2	2.2	-1.2	1.3	1.0	-1.0	1.5	1.1	1.4	1.3	1.0	-1.1	-1.1	1.3	1.0
NM_004358.3	*CDC25B*			-1.5	1.3	1.3	-1.5	1.2	-2.7	1.0	-1.0	-1.2	1.2	-1.1	-1.0	-1.8	1.1	1.1	-1.9	-1.0	1.3
NM_004360.2	*CDH1*			-1.1	-1.2	1.2	-1.1	-1.3	1.9	1.1	1.0	-1.1	-1.1	-1.3	-1.2	-1.3	-1.1	1.5	1.3	-2.0	1.5
NM_000075.2	*CDK4*			1.0	1.3	-1.0	1.1	2.0	1.3	-1.1	-1.0	1.1	-1.0	1.0	1.1	-1.1	1.1	1.0	-1.3	1.3	-1.0
NM_078467.1	*CDKN1A*			-1.2	-1.1	-1.1	1.0	1.3	-1.1	-1.1	-1.1	1.0	1.9	-1.0	5.6	1.4	-1.3	-1.3	1.3	1.1	-1.1
NM_078487.2	*CDKN2B*			-1.1	-1.5	-1.6	-1.2	-1.4	-2.2	-1.0	1.2	-1.3	2.2	-1.5	2.1	1.6	-1.4	-1.4	1.1	1.0	-1.0
NM_001826.1	*CKS1B*	Liver Hyper-plasia/ Hyper-proliferation	Cancer	-1.1	1.2	1.2	1.1	2.1	1.1	1.2	1.1	-1.0	2.0	1.5	1.7	1.9	1.1	-1.3	-1.1	2.0	-1.1
NM_012242.2	*DKK1*			-1.0	1.0	1.0	-1.0	-1.3	-1.1	-1.1	1.0	-1.4	-1.2	-1.2	-2.1	-1.1	-1.1	-1.2	-1.1	1.0	-1.2
NM_013352.2	*DSE*			1.2	-1.1	-1.5	-1.1	-1.8	-2.5	-1.1	-1.3	-1.3	-1.6	-1.7	-1.2	-1.9	-1.3	-1.3	-1.3	-1.8	1.1
NM_018098.4	*ECT2*			2.7	1.1	-3.7	3.0	2.1	-2.2	-1.0	-1.4	-1.3	2.2	1.3	1.3	-1.0	-1.3	-1.1	-2.4	1.7	-1.1
NM_001040092.1	*ENPP2*			1.0	-1.3	-1.1	-1.4	-2.4	-1.2	1.0	-1.2	1.4	-2.4	-2.9	-2.6	-1.7	-1.1	-1.1	1.7	-3.3	1.2
NM_004448.2	*ERBB2*			-1.5	-1.0	1.3	-2.1	-2.3	1.2	1.1	-1.7	-1.3	1.0	-4.0	-1.8	-1.4	-1.8	-1.2	1.3	-5.3	-1.8
NM_001005915.1	*ERBB3*			-1.4	1.2	1.7	-1.6	1.1	2.7	1.0	-1.0	1.2	-1.2	1.1	-1.6	-1.0	-1.0	-1.4	1.1	-1.1	-1.2
NM_000125.2	*ESR1*			-1.2	-1.7	-1.0	-1.6	-3.9	1.1	-1.3	-1.7	1.1	-1.7	-3.1	-1.7	-1.6	-1.2	-1.1	1.5	-3.0	-1.2
NM_002006.3	*FGF2*			1.2	-1.0	-2.4	1.1	1.8	-1.2	-1.0	1.1	1.1	1.6	-1.2	3.1	1.5	-1.3	-1.2	-1.2	-1.3	-1.0
NM_004467.3	*FGL1*			4.2	-1.7	-4.7	3.8	-2.1	-1.4	-1.3	1.1	-1.2	-2.1	-1.0	-3.3	-1.3	-1.2	1.1	-1.1	-1.7	-1.5
NM_005252.2	*FOS*			-1.2	-1.0	3.2	1.3	1.4	-2.8	-1.1	-1.3	-1.5	2.3	-1.0	-1.0	-3.5	-1.4	1.2	-2.0	1.1	1.2
NM_033260.3	*FOXQ1*			-1.2	-1.3	1.4	1.2	3.1	-1.8	-1.0	1.0	1.1	-1.1	-1.9	5.6	2.6	1.4	1.2	1.9	1.1	1.6
NM_001924.2	*GADD45A*			1.1	1.2	8.1	1.3	1.3	4.4	-1.1	1.3	1.0	1.4	1.4	1.8	1.3	1.3	1.0	1.2	1.2	-1.6
NM_000545.4	*HNF1A*			-1.7	1.2	2.2	-1.7	1.1	1.6	1.0	-1.1	-1.1	-1.4	1.1	-2.1	-1.0	-1.0	1.1	-1.1	-1.2	1.0
NM_000597.2	*IGFBP2*			-1.8	-1.2	2.1	-2.0	-1.5	-2.2	-1.1	1.2	-1.3	-1.6	-1.4	-2.4	-1.7	-1.3	1.4	-1.1	-2.5	-1.4
NM_000598.4	*IGFBP3*			-1.1	1.2	1.3	1.0	3.9	1.2	-1.3	1.3	-1.2	-1.7	1.2	-1.1	1.2	1.1	1.6	1.0	-1.0	1.3

Table 59 (continued)

RefSeq	Symbol	IPA® Tox function	Function	Donor 1						Donor 2						Donor 3					
				100 µM IBU			1000 µM IBU			100 µM IBU			1000 µM IBU			100 µM IBU			1000 µM IBU		
				d01	d03	d14	d01	d03	d14	d01	d03	d14	d01	d03	d14	d01	d03	d14	d01	d03	d14
NM_001093772.1	*KIT*			1.1	1.1	1.6	-1.0	-2.1	-1.4	-1.2	-1.3	-1.1	-1.8	-2.8	-1.6	-1.4	-1.0	1.0	-1.2	-1.5	-1.2
NM_057159.2	*LPAR1*			1.2	1.1	-1.5	1.2	-1.1	-2.8	-1.1	-1.1	-1.1	1.1	1.0	-1.2	1.0	-1.0	-1.4	-1.0	-1.1	-1.2
NM_002392.2	*MDM2*			1.3	-1.2	1.4	1.4	-1.1	2.8	1.0	1.0	1.2	1.6	1.1	2.1	1.2	-1.0	-1.2	-1.2	1.3	-1.1
NM_000245.2	*MET*			2.0	1.1	-2.8	2.7	1.9	-1.3	-1.3	-1.1	-1.1	1.3	1.2	3.2	1.6	-1.8	1.5	1.1	-1.2	1.2
NM_004994.2	*MMP9*			-1.4	-1.9	1.4	-1.7	-2.8	-5.9	1.0	1.1	-2.3	-2.0	-5.9	-7.5	-5.2	-2.1	-2.2	-2.0	-4.5	-2.5
NM_002467.3	*MYC*			-1.2	-1.1	1.8	-1.1	2.7	-1.4	-1.1	1.1	-2.0	-1.1	-1.1	-1.2	-1.8	-1.4	-1.1	-1.5	1.5	-1.1
NM_198175.1	*NME1*			-1.2	1.3	1.2	1.0	2.0	1.5	1.3	1.0	-1.0	2.3	1.6	1.1	1.5	-1.1	-1.1	-1.2	2.0	-1.4
NM_153292.1	*NOS2*			1.2	1.4	-2.0	1.1	1.6	-26.4	-1.2	-1.2	-1.0	-1.1	-1.3	1.0	-1.3	-1.0	-3.3	-1.4	1.1	-1.3
NM_000903.2	*NQO1*			-1.0	1.7	1.7	1.1	-1.1	2.2	1.2	1.3	1.4	2.1	1.5	1.5	-1.2	1.1	-1.1	-1.1	1.0	-1.1
NM_002524.2	*NRAS*			1.5	1.1	-1.4	1.4	1.4	1.1	1.0	1.1	1.2	1.4	1.2	2.2	1.3	-1.2	1.0	1.1	1.4	1.2
NM_006206.3	*PDGFRA*			1.8	-1.4	-3.2	1.7	-1.6	-2.4	1.1	-1.1	-1.1	1.0	-1.1	-1.4	-2.9	-1.4	-1.0	-2.1	-1.3	-1.0
NM_002609.3	*PDGFRB*			-1.5	-1.0	1.1	-1.5	-1.3	-3.1	-1.2	1.1	-2.1	1.3	-1.3	-2.7	1.2	-1.3	1.2	-1.4	1.4	-1.1
NM_052880.3	*PIK3IP1*	Liver Hyper-plasia/ Hyper-proliferation	Cancer	-1.3	-1.6	2.0	-2.0	-3.4	-1.7	-1.3	-1.2	-1.5	-1.3	-2.4	-1.2	-2.1	-2.0	-1.2	1.0	-4.1	-1.1
NM_001005376.1	*PLAUR*			1.0	-1.0	-1.1	-1.0	-1.0	-4.1	1.0	1.0	-1.3	-1.2	-1.3	2.0	-1.3	1.0	-2.3	-1.3	1.1	-2.5
NM_000301.1	*PLG*			-1.7	-1.5	1.1	-2.7	-10.9	-3.2	-1.3	-1.0	1.2	-3.0	-3.4	-1.3	-2.3	1.1	-1.1	1.4	-6.0	1.1
NM_004156.2	*PPP2CB*			5.0	1.0	-4.7	5.3	1.3	1.1	-1.7	-1.1	1.5	-1.4	-1.1	3.2	1.9	-1.7	1.7	1.5	-1.5	1.3
NM_002763.3	*PROX1*			1.6	-1.2	-2.0	1.5	-2.4	-1.6	1.0	-1.2	-1.1	-1.7	-1.6	-3.5	-1.6	1.0	1.3	-1.0	-1.5	1.4
NM_000964.2	*RARA*			-1.1	1.2	1.2	-1.0	-1.7	-1.5	-1.3	-1.2	1.1	-1.7	-3.0	-1.3	-1.6	-1.4	1.5	-1.1	-3.0	-1.1
NM_007182.4	*RASSF1*			1.1	1.2	1.0	1.3	1.8	-1.1	1.3	1.1	1.1	1.5	-1.2	2.4	1.4	-1.1	1.0	1.1	-1.0	-1.1
NM_182664.2	*RASSF5*			-1.4	1.1	1.0	-1.3	1.0	-2.7	-1.3	-1.0	1.0	-1.6	-1.3	-1.2	-2.0	1.1	-1.1	-1.7	-1.5	1.5
NM_020630.4	*RET*			1.1	1.4	-1.3	1.0	1.2	-1.2	-1.1	1.3	-2.1	-1.5	-2.5	-2.5	1.0	-1.1	1.1	-1.1	-1.1	-1.1
NM_019554.2	*S100A4*			-1.4	-1.3	1.3	-1.3	-1.6	-2.2	1.1	1.1	-1.2	-1.2	-1.5	-2.4	-1.3	-1.2	-1.4	-1.1	-1.3	-1.4
NM_003107.2	*SOX4*			-1.1	-1.5	1.0	-2.0	-2.8	-2.5	-1.5	-1.3	-1.3	-1.7	-2.2	1.1	1.0	-2.1	1.2	1.8	-3.5	-1.1
NM_003118.2	*SPARC*			-1.3	-1.3	1.3	-2.0	-4.6	-2.4	-1.2	-1.2	-1.3	-2.1	-3.4	-3.0	-1.5	-1.5	-1.7	-1.1	-1.8	-2.3
NM_139276.2	*STAT3*			-1.4	-1.7	-1.1	-1.3	-1.9	-2.4	1.1	-1.0	1.1	1.1	-1.7	-1.4	-1.8	-1.1	-1.1	-1.4	-1.3	1.0
NM_002353.1	*TACSTD2*			-1.2	-1.1	-1.2	1.1	2.4	-1.1	1.2	-1.1	-1.1	3.4	1.3	2.3	-1.2	-1.5	-1.0	-1.5	-1.5	-1.1
NM_005651.1	*TDO2*			-1.3	1.1	1.4	-1.6	-1.4	-1.4	1.0	1.0	1.3	-2.0	1.0	-4.6	-1.7	1.4	1.2	1.2	2.0	1.5
NM_003236.1	*TGFA*			1.5	1.3	-1.3	1.7	1.7	2.4	1.0	-1.1	1.1	1.3	1.5	2.5	2.8	-1.1	1.3	1.3	1.4	1.3

Table 59 (continued)

RefSeq	Symbol	IPA® Tox function	Function	Donor 1						Donor 2						Donor 3					
				100 µM IBU			1000 µM IBU			100 µM IBU			1000 µM IBU			100 µM IBU			1000 µM IBU		
				d01	d03	d14	d01	d03	d14	d01	d03	d14	d01	d03	d14	d01	d03	d14	d01	d03	d14
NM_014220.2	*TM4SF1*	Liver Hyper-plasia/ Hyper-proliferation	Cancer	-1.2	-1.4	1.1	-1.6	-3.2	-2.5	-1.1	-1.3	-1.6	1.4	-2.5	2.3	-2.4	-1.5	-1.2	-1.1	-3.6	-1.1
NM_000594.2	*TNF*			-1.0	1.1	1.2	-1.1	-1.2	-3.4	1.3	-1.3	-1.1	-1.0	-1.6	-1.2	-1.9	-1.0	-3.8	-1.6	-1.1	-2.3
NM_003810.2	*TNFSF10*			-1.2	-1.6	-2.2	-2.1	-8.8	-10.2	1.3	-1.5	1.3	-1.8	-1.9	-2.6	-12.5	-1.7	-1.0	-1.7	-5.6	1.2
NM_015905.2	*TRIM24*			-1.1	1.7	1.2	1.6	2.0	1.7	-1.1	1.2	1.5	1.1	1.8	1.2	1.6	1.4	1.2	1.1	2.0	1.2
NM_030912.2	*TRIM8*			-1.6	-1.3	-1.2	-1.8	-1.1	-2.3	-1.0	-1.1	-1.3	-1.5	-1.8	-1.2	-2.2	-1.1	-1.2	-1.9	-1.3	-1.1
NM_003376.4	*VEGFA*			-1.2	-1.4	2.7	-1.1	1.3	2.3	1.5	-1.1	-1.1	-1.6	-1.3	-1.4	-1.9	3.2	-1.6	-1.6	1.1	-1.1
NM_005429.2	*VEGFC*			1.1	-1.2	-1.1	-1.1	-1.4	-2.0	-1.4	-1.2	-1.1	-1.5	-1.9	-1.8	-1.1	-1.1	-1.2	-1.1	-1.0	-1.0
NM_152415.1	*VPS37A*			2.2	1.1	-1.8	2.6	1.6	2.2	-1.0	-1.1	1.2	1.0	1.3	-1.0	2.1	1.2	1.2	1.3	1.8	1.2
NM_001614.2	*ACTG1*		ECM organisation	-1.5	-1.6	1.2	-1.5	-1.1	-1.0	-1.1	2.1	1.1	1.0	1.6	2.3	1.4	-1.1	-1.3	1.4	-1.2	-1.1
NM_014800.9	*ELMO1*			-1.3	-1.2	1.2	-1.8	-2.7	1.1	1.0	-1.3	-1.1	-1.5	-2.1	-2.2	-1.6	-1.4	-1.1	1.4	-1.7	1.2
NM_004132.2	*HABP2*			-1.9	1.0	1.9	-1.9	-2.7	-1.1	-1.4	-1.3	1.3	-3.4	-2.3	-4.3	-2.4	-1.1	1.0	1.2	-2.8	1.1
NM_006633.2	*IQGAP2*			-1.5	1.1	1.5	-1.7	-1.1	1.1	-1.2	-1.1	-1.3	-2.0	1.0	-4.4	-1.2	1.1	1.5	1.5	-1.4	1.5
NM_052972.2	*LRG1*			-1.3	-1.4	1.4	-1.9	-2.1	-1.3	1.1	1.2	-1.1	-1.1	1.2	-4.5	-5.2	1.7	1.1	-3.1	2.0	1.4
NM_012325.1	*MAPRE1*			1.1	1.1	1.0	1.2	1.5	-1.3	1.1	1.2	1.2	1.7	1.2	2.6	1.3	-1.5	-1.1	-1.3	1.3	-1.3
NM_003255.4	*TIMP2*			-1.8	-1.1	1.2	-2.2	-2.2	-1.5	-1.1	-1.1	-1.5	-1.5	-2.1	-2.0	-1.1	-1.3	-1.6	1.3	-1.7	-1.6
NM_000666.1	*HPX*		Stress response	-1.3	-1.1	1.0	-1.5	-2.1	-4.3	-1.0	1.0	-1.2	-1.2	-1.2	-1.3	-1.2	-1.0	-1.1	1.1	-1.6	-1.5
NM_004958.2	*MGMT*			1.3	-1.2	1.0	1.1	-1.3	1.5	-1.0	-1.1	-1.0	-2.0	-1.5	-2.4	-1.6	-1.0	1.2	1.3	-1.9	1.2
NM_006623.2	*MTOR*			-1.4	1.2	1.2	-1.7	-1.3	-2.4	-1.0	-1.2	-1.1	-1.1	-1.1	-1.7	-1.3	-1.3	1.1	-1.1	-1.4	-1.2
NM_000613.1	*NUPR1*			-1.1	1.1	2.1	-1.2	1.7	3.6	-1.1	1.3	-1.3	-1.3	-1.2	-1.9	-1.1	1.5	-1.1	1.4	1.3	1.3
NM_030593.1	*PARG*			-1.2	1.2	1.2	-1.1	1.6	1.3	-1.1	-1.1	1.1	1.0	1.2	2.5	1.4	1.1	-1.1	1.4	1.4	-1.2
NM_012385.1	*SIRT1*			1.8	1.0	-2.6	2.4	1.3	1.7	-1.7	1.1	1.1	-1.3	-1.3	2.5	1.2	-1.1	1.0	1.0	1.2	-1.1
NM_002150.2	*SIRT2*			-1.4	1.3	1.7	-1.2	1.3	2.0	-1.2	-1.0	1.2	1.3	1.5	-1.0	1.3	1.1	1.1	1.3	1.3	1.2
NM_002412.2	*TXNIP*			-1.1	1.0	-2.1	1.9	1.9	-1.5	1.1	-1.4	-1.1	3.4	1.4	3.6	1.7	-2.2	-1.1	-1.1	2.1	1.2
XM_001124642.1	*ACY1*		Other and unknown functions	-1.4	1.2	1.4	-1.6	-1.8	-1.1	1.2	1.4	1.6	-1.5	1.1	-2.3	-1.6	1.3	1.4	1.4	-1.5	-1.1
NM_000478.3	*ALPL*			-1.5	-1.7	-1.4	-1.7	-2.0	-3.4	1.1	1.0	-1.9	-2.7	-3.2	-3.2	-9.3	1.2	-1.1	-3.6	-2.7	-1.3
NM_001011645.1	*AR*			-1.3	-1.3	1.1	-1.4	-2.7	-1.4	1.1	-1.2	1.2	-1.9	-1.6	-2.1	-1.5	1.4	1.2	1.6	-1.3	1.1
NM_000047.1	*ARSE*			-1.3	1.3	1.6	-1.7	-1.3	-1.2	-1.3	-1.3	-1.1	-2.2	-1.8	-2.7	-1.3	-1.1	1.1	1.1	-1.7	-1.1
NM_001713.1	*BHMT*			-1.7	-1.3	2.8	-3.1	-7.9	6.9	1.1	1.4	3.3	-2.8	1.3	-2.1	-1.5	2.0	1.9	4.8	-2.4	2.7

Table 59 (continued)

RefSeq	Symbol	IPA® Tox function	Function	Donor 1						Donor 2						Donor 3					
				100 µM IBU			1000 µM IBU			100 µM IBU			1000 µM IBU			100 µM IBU			1000 µM IBU		
				d01	d03	d14	d01	d03	d14	d01	d03	d14	d01	d03	d14	d01	d03	d14	d01	d03	d14
NM_000096.1	*CP*			1.3	-1.7	-2.5	1.1	-3.0	-2.9	-1.0	-1.1	1.1	-1.4	-1.8	-2.3	-2.5	1.3	1.4	-1.1	-2.5	1.6
NM_004431.2	*EPHA2*			-1.6	-1.3	2.4	-1.5	1.1	-2.0	-1.0	1.0	1.0	1.2	-1.2	2.1	-1.1	-1.3	-1.5	-1.4	-1.2	-1.3
NM_000137.1	*FAH*			-1.3	1.4	2.2	-1.4	-1.3	1.9	1.3	1.1	2.0	-1.2	1.5	-3.0	1.2	2.1	1.5	1.8	1.7	1.2
NM_001033030.1	*FAIM*			1.4	1.0	-1.2	1.1	-1.2	-1.3	-1.2	-1.2	-1.2	1.2	-1.1	2.3	1.5	-1.6	1.2	1.1	-1.2	1.1
NM_030919.2	*FAM83D*			1.1	-1.4	-1.1	-1.2	-2.8	-2.6	1.4	-1.1	1.3	-1.1	-1.6	-1.5	-2.1	1.2	-1.1	-1.2	-1.2	-1.0
NM_000508.3	*FGA*			-1.9	-2.1	1.3	-3.1	-6.8	-2.8	1.0	-1.5	-1.1	1.1	-2.3	-5.0	-7.4	1.1	1.0	-2.0	-4.8	-1.4
NM_000166.4	*GJB1*			-1.9	1.1	3.9	-2.7	-2.1	1.7	-1.7	-1.3	-1.2	-3.1	-1.8	-6.2	-1.9	-1.1	1.7	1.3	-2.2	1.4
NM_018960.4	*GNMT*			-2.0	-2.7	1.3	-3.0	-6.5	1.1	-1.8	1.3	-1.1	-3.7	-2.1	-2.9	-2.3	1.2	1.1	1.2	-2.3	1.6
NM_177937.1	*GOLM1*			1.1	1.1	-1.0	1.1	1.3	1.8	-1.0	1.4	1.2	1.1	1.7	1.1	1.1	1.7	1.1	1.1	2.2	1.4
NM_003801.3	*GPAA1*			-1.7	1.1	1.7	-2.3	-1.1	-1.6	-1.0	1.1	1.1	-1.3	1.2	-2.1	-1.2	1.3	-1.0	-1.0	-1.1	1.0
NM_021175.2	*HAMP*			-1.3	-1.5	1.2	-2.3	-10.6	-1.5	1.5	1.4	-2.1	2.5	2.3	-2.1	-4.0	-1.3	-1.2	-5.7	-1.4	-2.0
NM_004712.3	*HGS*			-1.3	1.2	1.3	-1.3	1.4	1.2	-1.0	1.4	-1.3	1.2	1.2	2.1	-1.2	-1.0	-1.5	-1.7	1.1	-1.3
NM_001530.2	*HIF1A*	Liver Hyper-plasia/ Hyper-proliferation	Other and unknown functions	3.6	-1.5	-4.8	2.8	-1.7	-3.1	1.0	-1.1	1.0	1.2	-1.0	-1.3	-1.6	-1.3	-1.2	-1.6	-1.2	-1.2
NR_003249.1	*HNRPDL*			-1.3	-1.1	-1.1	-1.3	1.3	1.4	-1.0	-1.5	1.0	-1.2	-2.3	2.8	-1.7	-1.2	-1.3	-1.6	-1.1	-2.1
NM_006472.2	*HPD*			-1.4	-1.1	2.3	-1.8	-2.5	1.6	-1.0	1.3	1.3	-2.3	-1.6	-2.0	-2.0	-1.0	-1.1	1.1	-1.8	-1.1
NM_005347.2	*HSPA5*			-1.5	1.1	1.2	-5.7	-4.3	-1.4	1.0	1.0	-1.3	-1.2	1.5	1.1	-2.1	-1.5	-1.5	-1.1	-3.1	-1.8
NM_000867.3	*HTR2B*			1.1	-1.1	-1.2	-1.2	-2.1	-1.6	1.0	-1.1	1.1	-1.2	-1.2	-1.5	-1.6	1.5	1.2	1.7	-2.0	2.0
NM_002302.2	*LECT2*			-1.1	-1.1	-1.6	-2.3	-14.7	-6.3	-1.2	-1.2	1.2	-7.1	-12.1	-3.1	-1.9	-2.0	-1.9	1.5	-13.6	-3.8
NM_000240.2	*MAOA*			-1.3	1.1	1.8	-1.5	-1.1	2.4	1.0	-1.1	-1.1	-1.6	-1.4	-4.9	-1.6	1.2	1.5	1.4	-1.3	2.2
NM_005911.4	*MAT2A*			-1.2	1.3	1.3	-1.4	1.6	-2.6	1.4	1.1	-1.0	1.0	-1.4	1.2	-1.2	-1.5	-1.3	-1.2	-1.8	-1.5
NM_002447.2	*MST1R*			-1.3	1.3	-1.1	-1.0	1.2	-2.1	1.2	-1.1	-1.1	1.9	-1.3	2.4	1.4	-1.3	-1.1	-1.1	1.1	-1.1
NM_198055.1	*MZF1*			-1.3	-1.1	1.0	-1.0	1.5	-1.5	1.4	-1.1	-1.1	2.3	1.3	2.7	1.0	1.3	-1.4	-1.5	1.7	-1.4
NM_152341.2	*PAQR4*			-1.7	1.0	1.2	-1.7	-1.4	-2.3	-1.2	1.2	-1.4	-2.3	-2.7	-1.9	-1.3	1.2	1.3	1.1	-1.8	1.7
NM_001083.3	*PDE5A*			1.3	1.0	-1.1	1.3	1.6	1.4	-1.0	-1.2	1.2	-1.2	-1.4	2.2	1.9	-1.1	1.1	1.2	-1.1	1.1
NM_052890.3	*PGLYRP2*			-1.2	-2.1	1.2	-1.6	-8.9	-8.3	-1.6	1.1	-2.1	-5.1	-11.0	-5.7	-4.3	-1.5	-1.0	-1.4	-10.6	-1.4
NM_012238.3	*PHGDH*			-1.1	1.0	1.4	1.0	2.4	1.5	1.0	1.3	-1.2	1.1	1.2	-1.3	1.5	1.7	-1.1	1.3	2.4	-1.7
NM_006813.1	*PNRC1*			-1.2	-1.1	-1.5	-1.1	-1.2	-2.4	-1.2	1.2	-1.1	-1.3	-1.5	1.4	-2.3	-1.2	1.1	-1.8	-1.5	1.3
NM_000941.2	*POR*			-1.1	1.8	2.3	2.1	4.1	3.5	-1.0	-1.0	1.0	2.3	2.2	2.4	3.7	1.2	-1.1	1.4	1.5	-1.6

Table 59 (continued)

RefSeq	Symbol	IPA® Tox function	Function	Donor 1						Donor 2						Donor 3					
				100 µM IBU			1000 µM IBU			100 µM IBU			1000 µM IBU			100 µM IBU			1000 µM IBU		
				d01	d03	d14	d01	d03	d14	d01	d03	d14	d01	d03	d14	d01	d03	d14	d01	d03	d14
NM_000021.2	*PSEN1*	Liver Hyper-plasia/ Hyper-proliferation	Other and unknown functions	1.3	-1.3	-3.0	1.5	1.1	-1.6	1.0	1.1	1.2	1.1	1.1	2.0	1.1	-1.1	-1.6	1.1	1.1	-1.4
NM_002800.4	*PSMB9*			-1.7	-1.1	1.1	-1.8	-1.2	-3.3	1.0	1.2	-1.2	1.0	1.1	-1.1	-3.8	1.2	-1.4	-2.6	-1.2	-1.0
NM_005789.2	*PSME3*			1.0	1.1	1.1	1.3	1.1	-2.1	1.1	-1.1	1.0	1.1	-1.8	-1.2	1.1	-1.7	-1.1	-1.3	1.0	-1.2
NM_152703.2	*SAMD9L*			1.3	-1.0	-1.8	1.1	-1.4	-4.3	-1.0	-1.0	-1.1	-1.6	-1.8	-1.3	-1.6	-1.1	-1.2	-1.5	-1.4	1.1
NM_001002236.1	*SERPINA1*			-1.1	-1.0	-1.3	-1.2	-1.3	-2.2	-1.4	1.1	1.4	-1.1	1.2	-1.2	-2.0	1.2	-1.1	-1.7	-1.0	1.1
NM_001756.3	*SERPINA6*			-1.2	-1.0	1.7	-1.9	-3.0	-1.2	-1.0	1.1	-1.2	-1.5	-1.7	-3.3	-1.4	1.1	1.3	1.3	-2.3	1.4
NM_000602.1	*SERPINE1*			-1.7	-1.2	1.5	-1.6	1.9	-1.2	-1.1	-1.2	-1.0	-1.2	-2.3	4.2	-1.3	1.6	-1.1	-1.2	1.1	-1.4
NM_032637.2	*SKP2*			-1.1	1.1	1.0	-1.2	-2.3	-1.1	-1.1	-1.3	1.1	-1.1	-1.3	-1.1	-1.4	1.1	1.4	1.3	-1.2	1.3
NM_080866.2	*SLC22A9*			1.2	1.1	2.1	-1.4	-2.2	1.1	1.3	1.1	1.2	-1.2	-1.2	-6.3	-1.5	1.3	1.7	1.6	-1.2	2.1
NM_000346.2	*SOX9*			-1.3	-1.0	-1.3	-1.6	-1.1	-3.8	-1.1	-1.1	-1.3	-1.0	-1.7	-1.2	-1.1	-1.3	-1.5	-1.3	-1.0	-1.1
NM_006288.2	*THY1*			-1.3	1.0	1.8	-2.0	-3.7	-1.7	-1.2	-1.2	-1.7	-1.6	-2.6	-4.6	1.0	-1.1	1.0	-1.0	-1.2	-1.2
NM_006088.5	*TUBB4B*			-2.1	1.1	-1.1	-1.5	-1.0	-3.0	-1.1	1.2	-1.0	-1.1	-1.0	1.0	-1.3	1.0	-1.2	-1.1	-1.1	-1.5
NM_001113756.1	*TYMP*			-1.9	1.2	-1.2	-2.0	-1.3	-3.9	-1.2	1.4	-1.4	-1.9	-1.5	1.6	-1.7	-1.3	-1.0	-1.5	-1.4	-1.0
NM_004181.3	*UCHL1*			-1.0	1.4	1.8	1.1	3.8	3.6	1.4	1.1	1.1	2.2	2.1	2.1	1.5	1.1	-1.2	1.0	2.3	-1.1
NM_018850.2	*ABCB4*	Hepato-cellular Carcinoma	Fatty acid and lipid metabolism	1.1	1.8	1.3	2.0	2.0	1.1	-1.2	-1.1	1.3	1.3	-1.8	1.3	1.1	-1.4	1.0	1.3	-2.1	-1.7
NM_007292.4	*ACOX1*			1.2	1.7	1.1	1.6	1.2	2.1	1.1	1.2	1.4	1.6	1.9	1.4	2.2	1.3	1.0	2.1	1.7	1.3
NM_000668.3	*ADH1B*			-1.2	-1.5	1.2	-2.5	-1.5	-1.8	-1.3	-1.5	1.4	-1.4	-1.1	-4.4	-2.0	1.1	3.2	2.7	-3.2	2.4
NM_000669.3	*ADH1C*			-1.5	-2.6	-1.3	-2.7	-4.5	-2.5	1.0	-1.3	1.4	-1.5	1.2	-5.9	-2.2	-2.0	2.0	1.9	-21.5	-1.1
NM_000859.1	*HMGCR*			-1.2	-1.8	1.3	1.1	-1.2	-2.2	-1.3	-1.2	-1.6	1.2	-4.8	-1.1	2.2	-1.8	-1.5	1.7	-2.5	1.0
NM_001003679.1	*LEPR*			3.0	-1.2	-1.5	1.9	-1.2	2.7	-1.1	1.1	-1.0	-1.8	-1.1	-1.6	-1.3	1.2	1.8	1.3	-1.8	1.7
NM_001001928.2	*PPARA*			1.1	1.1	1.5	1.4	1.2	4.1	1.1	1.3	1.9	1.3	1.4	-1.0	1.2	1.3	1.1	1.2	1.3	1.2
NM_015869.4	*PPARG*			-1.0	-1.0	1.3	1.1	1.7	2.0	1.1	1.1	1.2	1.1	1.1	1.3	1.4	1.5	-1.1	1.0	2.1	1.4
NM_003742.2	*ABCB11*		Bile acid metabolism	-1.2	-1.1	-1.3	-1.2	-1.8	-1.3	1.0	1.2	1.2	-1.6	-2.8	-1.8	-2.1	-1.8	1.2	1.2	-6.3	1.1
NM_005989.2	*AKR1D1*			1.3	-1.2	1.5	-1.1	-6.1	-1.1	1.2	1.5	1.8	-3.2	-3.3	1.1	-2.9	2.2	1.0	1.2	-2.9	-1.3
NM_003049.2	*SLC10A1*			-1.6	-1.3	2.4	-6.3	-20.3	-1.9	-1.5	-1.2	1.2	-9.5	-8.9	-2.2	-3.7	-1.2	1.3	2.1	-14.4	-1.1
NM_006446.3	*SLCO1B1*			1.6	-1.1	1.0	1.2	-1.5	1.3	-1.3	-1.1	1.6	-2.4	-1.5	-2.7	-1.1	1.0	1.4	2.1	-1.7	2.0
NM_019844.2	*SLCO1B3*			2.7	-1.4	-4.2	1.9	-1.4	-2.3	1.1	-1.4	1.2	-1.0	-2.6	-1.0	1.4	-1.6	1.2	1.8	-3.2	1.2

Table 59 (continued)

RefSeq	Symbol	IPA® Tox function	Function	Donor 1						Donor 2						Donor 3					
				100 µM IBU			1000 µM IBU			100 µM IBU			1000 µM IBU			100 µM IBU			1000 µM IBU		
				d01	d03	d14	d01	d03	d14	d01	d03	d14	d01	d03	d14	d01	d03	d14	d01	d03	d14
NM_001249.1	*ENTPD5*		Carbo-hydrate metabolism	1.2	1.1	2.3	1.3	-1.2	2.3	1.1	1.3	1.5	1.1	1.8	-1.7	2.0	1.1	1.0	2.0	1.2	1.2
NM_002612.3	*PDK4*			1.5	3.0	1.2	4.5	2.2	24.3	-1.0	-1.1	1.3	10.2	11.2	5.8	21.7	-1.2	1.3	5.8	1.5	-1.5
NM_181523.1	*PIK3R1*			-1.1	-1.4	-1.2	-1.5	-2.7	-2.4	-1.2	-1.4	-1.2	-2.5	-2.2	-3.2	-1.6	1.1	1.4	1.7	-2.8	1.9
NM_001134.1	*AFP*			1.1	-1.4	1.5	-1.3	-3.2	3.9	1.2	1.2	2.1	-1.5	1.1	-1.5	1.1	2.0	1.2	3.2	-1.6	1.6
NM_001002857.1	*ANXA2*			1.0	-1.2	-1.0	1.1	-1.3	-1.1	1.3	1.1	1.4	1.4	-1.3	3.1	1.1	-1.8	-1.3	-1.3	-1.0	-1.3
NM_198434.1	*AURKA*			-1.0	1.2	1.0	1.1	1.3	1.8	1.2	1.0	1.7	1.8	1.2	2.6	1.4	1.3	1.2	1.2	1.4	1.2
NM_181050.1	*AXIN1*			-1.3	1.0	1.6	-1.2	1.8	1.7	-1.2	1.1	1.1	-1.1	1.2	2.8	1.6	-1.0	-1.2	1.1	1.4	-1.0
NM_053056.2	*CCND1*			1.1	-1.1	-1.9	1.1	-2.1	-3.0	-1.0	-1.2	-1.4	-1.5	-2.4	1.3	-1.1	-1.5	-1.0	-1.2	-2.2	-1.3
NM_004358.3	*CDC25B*			-1.5	1.3	1.3	-1.5	1.2	-2.7	1.0	-1.0	-1.2	1.2	-1.1	-1.0	-1.8	1.1	1.1	-1.9	-1.0	1.3
NM_004360.2	*CDH1*			-1.1	-1.2	1.2	-1.1	-1.3	1.9	1.1	1.0	-1.1	-1.1	-1.3	-1.2	-1.3	-1.1	1.5	1.3	-2.0	1.5
NM_078467.1	*CDKN1A*			-1.2	-1.1	-1.1	1.0	1.3	-1.1	-1.1	-1.1	1.0	1.9	-1.0	5.6	1.4	-1.3	-1.3	1.3	1.1	-1.1
NM_001826.1	*CKS1B*			-1.1	1.2	1.2	1.1	2.1	1.1	1.2	1.1	-1.0	2.0	1.5	1.7	1.9	1.1	-1.3	-1.1	2.0	-1.1
NM_012242.2	*DKK1*			-1.0	1.0	1.0	-1.0	-1.3	-1.1	-1.1	1.0	-1.4	-1.2	-1.2	-2.1	-1.1	-1.1	-1.2	-1.1	1.0	-1.2
NM_013352.2	*DSE*	Hepato-cellular Carcinoma		1.2	-1.1	-1.5	-1.1	-1.8	-2.5	-1.1	-1.3	-1.3	-1.6	-1.7	-1.2	-1.9	-1.3	-1.3	-1.3	-1.8	1.1
NM_018098.4	*ECT2*			2.7	1.1	-3.7	3.0	2.1	-2.2	-1.0	-1.4	-1.3	2.2	1.3	1.3	-1.0	-1.3	-1.1	-2.4	1.7	-1.1
NM_001040092.1	*ENPP2*		Cancer	1.0	-1.3	-1.1	-1.4	-2.4	-1.2	1.0	-1.2	1.4	-2.4	-2.9	-2.6	-1.7	-1.1	-1.1	1.7	-3.3	1.2
NM_004448.2	*ERBB2*			-1.5	-1.0	1.3	-2.1	-2.3	1.2	1.1	-1.7	-1.3	1.0	-4.0	-1.8	-1.4	-1.8	-1.2	1.3	-5.3	-1.8
NM_001005915.1	*ERBB3*			-1.4	1.2	1.7	-1.6	1.1	2.7	1.0	-1.0	1.2	-1.2	1.1	-1.6	-1.0	-1.0	-1.4	1.1	-1.1	-1.2
NM_000125.2	*ESR1*			-1.2	-1.7	-1.0	-1.6	-3.9	1.1	-1.3	-1.7	1.1	-1.7	-3.1	-1.7	-1.6	-1.2	-1.1	1.5	-3.0	-1.2
NM_002006.3	*FGF2*			1.2	-1.0	-2.4	1.1	1.8	-1.2	-1.0	1.1	1.1	1.6	-1.2	3.1	1.5	-1.3	-1.2	-1.2	-1.3	-1.0
NM_004467.3	*FGL1*			4.2	-1.7	-4.7	3.8	-2.1	-1.4	-1.3	1.1	-1.2	-2.1	-1.0	-3.3	-1.3	-1.2	1.1	-1.1	-1.7	-1.5
NM_033260.3	*FOXQ1*			-1.2	-1.3	1.4	1.2	3.1	-1.8	-1.0	1.0	1.1	-1.1	-1.9	5.6	2.6	1.4	1.2	1.9	1.1	1.6
NM_000545.4	*HNF1A*			-1.7	1.2	2.2	-1.7	1.1	1.6	1.0	-1.1	-1.1	-1.4	1.1	-2.1	-1.0	-1.0	1.1	-1.1	-1.2	1.0
NM_057159.2	*LPAR1*			1.2	1.1	-1.5	1.2	-1.1	-2.8	-1.1	-1.1	-1.1	1.1	1.0	-1.2	1.0	-1.0	-1.4	-1.0	-1.1	-1.2
NM_002392.2	*MDM2*			1.3	-1.2	1.4	1.4	-1.1	2.8	1.0	1.0	1.2	1.6	1.1	2.1	1.2	-1.0	-1.2	-1.2	1.3	-1.1
NM_004994.2	*MMP9*			-1.4	-1.9	1.4	-1.7	-2.8	-5.9	1.0	1.1	-2.3	-2.0	-5.9	-7.5	-5.2	-2.1	-2.2	-2.0	-4.5	-2.5
NM_198175.1	*NME1*			-1.2	1.3	1.2	1.0	2.0	1.5	1.3	1.0	-1.0	2.3	1.6	1.1	1.5	-1.1	-1.1	-1.2	2.0	-1.4
NM_153292.1	*NOS2*			1.2	1.4	-2.0	1.1	1.6	-26.4	-1.2	-1.2	-1.0	-1.1	-1.3	1.0	-1.3	-1.0	-3.3	-1.4	1.1	-1.3

Table 59 (continued)

RefSeq	Symbol	IPA® Tox function	Function	Donor 1						Donor 2						Donor 3					
				100 µM IBU			1000 µM IBU			100 µM IBU			1000 µM IBU			100 µM IBU			1000 µM IBU		
				d01	d03	d14	d01	d03	d14	d01	d03	d14	d01	d03	d14	d01	d03	d14	d01	d03	d14
NM_000903.2	*NQO1*			-1.0	1.7	1.7	1.1	-1.1	2.2	1.2	1.3	1.4	2.1	1.5	1.5	-1.2	1.1	-1.1	-1.1	1.0	-1.1
NM_002524.2	*NRAS*			1.5	1.1	-1.4	1.4	1.4	1.1	1.0	1.1	1.2	1.4	1.2	2.2	1.3	-1.2	1.0	1.1	1.4	1.2
NM_006206.3	*PDGFRA*			1.8	-1.4	-3.2	1.7	-1.6	-2.4	1.1	-1.1	-1.1	1.0	-1.1	-1.4	-2.9	-1.4	-1.0	-2.1	-1.3	-1.0
NM_002609.3	*PDGFRB*			-1.5	-1.0	1.1	-1.5	-1.3	-3.1	-1.2	1.1	-2.1	1.3	-1.3	-2.7	1.2	-1.3	1.2	-1.4	1.4	-1.1
NM_001005376.1	*PLAUR*			-1.1	1.1	1.1	1.2	1.1	-1.9	-1.0	1.2	1.1	-1.1	-1.4	3.1	-1.4	-1.1	-1.8	-1.4	1.2	-1.7
NM_001005376.1	*PLAUR*			1.0	-1.0	-1.1	-1.0	-1.0	-4.1	1.0	1.0	-1.3	-1.2	-1.3	2.0	-1.3	1.0	-2.3	-1.3	1.1	-2.5
NM_002763.3	*PROX1*			1.6	-1.2	-2.0	1.5	-2.4	-1.6	1.0	-1.2	-1.1	-1.7	-1.6	-3.5	-1.6	1.0	1.3	-1.0	-1.5	1.4
NM_000964.2	*RARA*			-1.1	1.2	1.2	-1.0	-1.7	-1.5	-1.3	-1.2	1.1	-1.7	-3.0	-1.3	-1.6	-1.4	1.5	-1.1	-3.0	-1.1
NM_007182.4	*RASSF1*			1.1	1.2	1.0	1.3	1.8	-1.1	1.3	1.1	1.1	1.5	-1.2	2.4	1.4	-1.1	1.0	1.1	-1.0	-1.1
NM_182664.2	*RASSF5*			-1.4	1.1	1.0	-1.3	1.0	-2.7	-1.3	-1.0	1.0	-1.6	-1.3	-1.2	-2.0	1.1	-1.1	-1.7	-1.5	1.5
NM_020630.4	*RET*		Cancer	1.1	1.4	-1.3	1.0	1.2	-1.2	-1.1	1.3	-2.1	-1.5	-2.5	-2.5	1.0	-1.1	1.1	-1.1	-1.1	-1.1
NM_019554.2	*S100A4*			-1.4	-1.3	1.3	-1.3	-1.6	-2.2	1.1	1.1	-1.2	-1.2	-1.5	-2.4	-1.3	-1.2	-1.4	-1.1	-1.3	-1.4
NM_003107.2	*SOX4*			-1.1	-1.5	1.0	-2.0	-2.8	-2.5	-1.5	-1.3	-1.3	-1.7	-2.2	1.1	1.0	-2.1	1.2	1.8	-3.5	-1.1
NM_139276.2	*STAT3*	Hepato-cellular Carcinoma		-1.4	-1.7	-1.1	-1.3	-1.9	-2.4	1.1	-1.0	1.1	1.1	-1.7	-1.4	-1.8	-1.1	-1.1	-1.4	-1.3	1.0
NM_003236.1	*TGFA*			1.5	1.3	-1.3	1.7	1.7	2.4	1.0	-1.1	1.1	1.3	1.5	2.5	2.8	-1.1	1.3	1.3	1.4	1.3
NM_014220.2	*TM4SF1*			-1.2	-1.4	1.1	-1.6	-3.2	-2.5	-1.1	-1.3	-1.6	1.4	-2.5	2.3	-2.4	-1.5	-1.2	-1.1	-3.6	-1.1
NM_000594.2	*TNF*			-1.0	1.1	1.2	-1.1	-1.2	-3.4	1.3	-1.3	-1.1	-1.0	-1.6	-1.2	-1.9	-1.0	-3.8	-1.6	-1.1	-2.3
NM_003810.2	*TNFSF10*			-1.2	-1.6	-2.2	-2.1	-8.8	-10.2	1.3	-1.5	1.3	-1.8	-1.9	-2.6	-12.5	-1.7	-1.0	-1.7	-5.6	1.2
NM_015905.2	*TRIM24*			-1.1	1.7	1.2	1.6	2.0	1.7	-1.1	1.2	1.5	1.1	1.8	1.2	1.6	1.4	1.2	1.1	2.0	1.2
NM_030912.2	*TRIM8*			-1.6	-1.3	-1.2	-1.8	-1.1	-2.3	-1.0	-1.1	-1.3	-1.5	-1.8	-1.2	-2.2	-1.1	-1.2	-1.9	-1.3	-1.1
NM_003376.4	*VEGFA*			-1.2	-1.4	2.7	-1.1	1.3	2.3	1.5	-1.1	-1.1	-1.6	-1.3	-1.4	-1.9	3.2	-1.6	-1.6	1.1	-1.1
NM_000613.1	*HPX*			-1.3	-1.1	1.0	-1.5	-2.1	-4.3	-1.0	1.0	-1.2	-1.2	-1.2	-1.3	-1.2	-1.0	-1.1	1.1	-1.6	-1.5
NM_002412.2	*MGMT*			1.3	-1.2	1.0	1.1	-1.3	1.5	-1.0	-1.1	-1.0	-2.0	-1.5	-2.4	-1.6	-1.0	1.2	1.3	-1.9	1.2
NM_004958.2	*MTOR*			-1.4	1.2	1.2	-1.7	-1.3	-2.4	-1.0	-1.2	-1.1	-1.1	-1.1	-1.7	-1.3	-1.3	1.1	-1.1	-1.4	-1.2
NM_012385.1	*NUPR1*		Stress response	-1.1	1.1	2.1	-1.2	1.7	3.6	-1.1	1.3	-1.3	-1.3	-1.2	-1.9	-1.1	1.5	-1.1	1.4	1.3	1.3
XM_001124642.1	*PARG*			-1.2	1.2	1.2	-1.1	1.6	1.3	-1.1	-1.1	1.1	1.0	1.2	2.5	1.4	1.1	-1.1	1.4	1.4	-1.2
NM_012238.3	*SIRT1*			1.8	1.0	-2.6	2.4	1.3	1.7	-1.7	1.1	1.1	-1.3	-1.3	2.5	1.2	-1.1	1.0	1.0	1.2	-1.1
NM_030593.1	*SIRT2*			-1.4	1.3	1.7	-1.2	1.3	2.0	-1.2	-1.0	1.2	1.3	1.5	-1.0	1.3	1.1	1.1	1.3	1.3	1.2

Table 59 (continued)

RefSeq	Symbol	IPA® Tox function	Function	Donor 1						Donor 2						Donor 3					
				100 µM IBU			1000 µM IBU			100 µM IBU			1000 µM IBU			100 µM IBU			1000 µM IBU		
				d01	d03	d14	d01	d03	d14	d01	d03	d14	d01	d03	d14	d01	d03	d14	d01	d03	d14
NM_006988.3	*ADAMTS1*			1.1	-1.0	-1.7	-1.0	-1.1	-3.6	1.0	1.2	-1.5	-1.1	-1.0	-3.6	-1.8	-1.3	-1.4	-2.1	1.1	-1.0
NM_001633.2	*AMBP*			-1.2	-1.2	1.1	-1.3	-2.9	-3.3	-1.3	-1.2	-1.6	-1.7	-2.5	-2.0	-1.9	1.0	-1.1	-1.2	-2.0	-1.4
NM_000700.1	*ANXA1*			1.1	1.1	-1.2	1.2	1.1	2.1	-1.2	-1.0	-1.1	1.1	-1.3	1.4	1.2	-1.8	-1.2	-1.1	-1.4	-1.2
NM_001679.2	*ATP1B3*			-1.1	1.1	-1.2	1.2	1.9	1.2	1.0	1.2	-1.1	1.5	1.5	-1.1	1.4	1.2	-1.3	-1.0	2.3	-1.2
NM_032607.1	*CREB3L3*			2.0	3.4	1.3	3.6	5.7	1.2	1.3	1.3	-1.0	2.1	2.1	-2.1	-1.5	1.8	-1.2	-4.0	3.4	-1.2
NM_005211.2	*CSF1R*		In-flammation	-1.5	-1.4	1.4	-2.4	-3.0	-1.0	-1.1	1.1	-1.5	-1.5	-2.0	-4.7	-1.3	1.1	-1.5	-1.2	-1.7	-1.2
NM_001099856.1	*IKBKG*			-1.0	1.2	1.6	1.1	1.5	1.1	1.2	1.3	1.0	2.6	1.5	2.8	1.6	-1.3	1.0	-1.1	1.5	-1.2
NM_000893.2	*KNG1*			-1.6	-1.3	-1.0	-2.4	-4.4	-4.0	-1.1	1.0	-1.3	-2.2	-1.5	-1.3	-1.6	-1.1	-1.0	-1.0	-2.4	-1.0
NM_002341.1	*LTB*			-1.2	-1.3	-1.4	-1.3	-1.7	-4.8	1.6	1.1	-1.9	1.9	-1.5	-3.1	-4.5	-1.3	-1.3	-5.2	-1.8	-1.6
NM_000963.1	*PTGS2*			1.0	1.1	-2.3	1.3	1.1	-2.3	1.0	1.0	-1.1	1.2	1.1	-1.2	-1.1	-1.1	-1.5	-1.0	-1.0	-1.2
NM_003745.1	*SOCS1*			-1.3	-1.2	-1.9	1.2	1.2	-8.4	1.4	1.2	-1.2	1.3	1.0	-1.2	-5.7	1.0	-1.2	-4.9	-1.1	-1.2
NM_003955.3	*SOCS3*			-1.3	1.2	-1.0	-1.2	1.0	-2.3	1.0	1.3	1.2	-1.2	-1.2	-1.3	-6.1	1.1	-1.1	-5.2	-1.1	1.0
NM_201442.1	*C1S*	Hepato-cellular Carcinoma		-1.2	-1.7	-1.4	-1.4	-3.0	-2.7	-1.0	-1.0	-1.0	-1.3	-2.0	-2.1	-1.9	1.1	-1.5	-1.1	-2.0	-1.2
NM_001734.2	*C1S*			-1.6	-1.1	1.1	-1.7	-2.2	-2.6	-1.1	-1.0	-1.1	-1.1	-1.4	-1.3	-1.2	1.0	1.1	1.4	-2.3	-1.0
NM_001737.2	*C9*			3.1	-1.8	-6.3	2.3	-11.3	-3.7	-1.6	-1.1	-1.1	-6.1	-3.3	-4.1	-2.3	1.1	1.4	-1.3	-2.7	1.3
NM_000591.2	*CD14*			-1.4	-1.1	1.7	-1.0	1.1	-1.4	1.2	-1.3	-2.5	3.5	-1.1	1.0	1.4	-1.1	-1.1	-1.3	-2.0	-2.3
NM_021023.3	*CFHR3*			1.1	-2.8	-3.9	-1.4	-9.3	-4.1	-1.1	-1.1	1.3	-2.6	-2.1	-3.6	-2.3	1.5	1.9	1.1	-4.1	2.1
NM_021023.4	*CFHR3*			1.5	-2.0	-5.4	1.3	-4.5	-5.7	-1.4	-1.4	1.8	-2.3	-1.6	-1.6	-1.6	1.3	1.3	-1.0	-1.6	1.2
NM_006684.2	*CFHR4*		Immune response	1.3	-1.7	-1.7	1.0	-3.1	-2.0	1.3	-1.6	1.8	-2.4	-3.4	-3.1	-2.0	1.9	1.1	-1.1	-1.2	1.4
NM_003665.2	*FCN3*			-1.3	-1.5	1.4	-2.9	-3.5	-1.3	1.0	-1.5	-4.6	-2.2	-4.3	-10.0	-1.8	-1.5	-1.7	-1.8	-1.7	-2.5
NM_000201.1	*ICAM1*			-1.6	1.1	1.2	-1.6	1.5	-2.8	-1.2	1.6	-1.5	-1.1	-1.5	-2.2	-5.2	-1.3	-1.7	-4.2	-1.6	-1.9
NM_000600.1	*IL6*			-1.2	-1.3	-1.7	-1.1	-1.2	-4.1	1.2	1.1	-1.3	1.1	-1.1	-1.5	-2.9	-1.0	-4.9	-2.9	-1.1	-3.2
NM_000584.2	*IL8*			-1.2	-1.6	1.1	-1.3	2.5	-2.2	1.4	1.1	-2.0	2.9	-2.2	-1.6	-4.4	-1.5	1.1	-4.4	-1.4	-1.2
NM_003999.1	*OSMR*			1.2	-1.3	-1.3	1.6	1.0	-2.0	1.1	1.2	1.5	1.6	1.5	1.2	-1.8	1.1	-1.1	-1.6	1.5	1.2
NM_000582.2	*SPP1*			-1.1	-1.1	1.2	-1.2	-3.0	-1.1	1.1	-1.0	-2.2	-1.4	-4.0	-11.8	-2.6	-1.3	-1.8	-1.3	-1.8	1.0
NM_003380.2	*VIM*			1.0	-1.2	-1.4	-1.2	-2.1	-1.2	-1.2	-1.1	-1.1	-1.2	-2.0	3.6	1.2	-1.1	-1.5	-1.1	1.0	1.1
NM_001614.2	*ACTG1*		ECM organisation	-1.5	-1.6	1.2	-1.5	-1.1	-1.0	-1.1	2.1	1.1	1.0	1.6	2.3	1.4	-1.1	-1.3	1.4	-1.2	-1.1
NM_014800.9	*ELMO1*			-1.3	-1.2	1.2	-1.8	-2.7	1.1	1.0	-1.3	-1.1	-1.5	-2.1	-2.2	-1.6	-1.4	-1.1	1.4	-1.7	1.2

Table 59 (continued)

RefSeq	Symbol	IPA® Tox function	Function	Donor 1						Donor 2						Donor 3					
				100 µM IBU			1000 µM IBU			100 µM IBU			1000 µM IBU			100 µM IBU			1000 µM IBU		
				d01	d03	d14	d01	d03	d14	d01	d03	d14	d01	d03	d14	d01	d03	d14	d01	d03	d14
NM_006633.2	*IQGAP2*		ECM organisation	-1.5	1.1	1.5	-1.7	-1.1	1.1	-1.2	-1.1	-1.3	-2.0	1.0	-4.4	-1.2	1.1	1.5	1.5	-1.4	1.5
NM_012325.1	*MAPRE1*			1.1	1.1	1.0	1.2	1.5	-1.3	1.1	1.2	1.2	1.7	1.2	2.6	1.3	-1.5	-1.1	-1.3	1.3	-1.3
NM_003255.4	*TIMP2*			-1.8	-1.1	1.2	-2.2	-2.2	-1.5	-1.1	-1.1	-1.5	-1.5	-2.1	-2.0	-1.1	-1.3	-1.6	1.3	-1.7	-1.6
NM_000499.2	*CYP1A1*		Xenobiotic metabolism	-1.1	3.6	12.5	2.1	2.7	24.7	2.1	1.3	1.5	3.3	3.7	1.4	1.7	13.7	2.7	1.6	2.4	1.3
NM_006169.2	*NNMT*			-1.3	-1.4	-1.0	-1.3	1.4	-2.4	-1.0	1.4	-1.2	1.2	1.4	-1.3	-3.9	-1.0	-1.1	-2.9	1.3	1.1
NM_000463.2	*UGT1A1*			1.2	1.3	3.0	1.1	1.0	3.8	1.6	1.8	2.4	2.2	3.3	1.5	1.3	7.5	1.8	1.6	4.7	2.2
NM_019093.2	*UGT1A3*			1.0	-1.0	1.5	1.1	-1.3	1.6	1.4	1.3	1.6	1.9	2.8	1.6	1.6	2.6	1.4	1.5	2.5	1.2
NM_007120.2	*UGT1A4*			1.7	-1.2	1.4	1.6	-2.3	1.7	1.2	1.4	2.6	1.8	3.7	1.8	1.5	3.1	1.7	1.7	2.5	2.8
NM_001072.3	*UGT1A6*			1.5	-1.1	1.3	1.4	-1.8	2.4	1.2	1.1	2.0	1.4	2.1	-2.1	1.4	1.7	-1.0	1.5	1.9	1.4
NM_001072.3	*UGT1A6*			1.0	-1.0	1.5	1.0	-1.5	2.3	1.2	1.1	1.8	1.5	2.0	-2.1	1.3	1.7	-1.5	1.2	2.2	1.0
NM_019075.2	*UGT1A9*			1.5	-1.6	-1.5	-1.1	-6.9	-1.3	1.1	1.3	3.4	-1.2	-1.2	-1.4	-2.0	1.2	-1.0	2.1	-3.5	1.6
NM_000666.1	*ACY1*	Hepato-cellular Carcinoma	Other and unknown functions	-1.4	1.2	1.4	-1.6	-1.8	-1.1	1.2	1.4	1.6	-1.5	1.1	-2.3	-1.6	1.3	1.4	1.4	-1.5	-1.1
NM_000478.3	*ALPL*			-1.5	-1.7	-1.4	-1.7	-2.0	-3.4	1.1	1.0	-1.9	-2.7	-3.2	-3.2	-9.3	1.2	-1.1	-3.6	-2.7	-1.3
NM_001011645.1	*AR*			-1.3	-1.3	1.1	-1.4	-2.7	-1.4	1.1	-1.2	1.2	-1.9	-1.6	-2.1	-1.5	1.4	1.2	1.6	-1.3	1.1
NM_001713.1	*BHMT*			-1.7	-1.3	2.8	-3.1	-7.9	6.9	1.1	1.4	3.3	-2.8	1.3	-2.1	-1.5	2.0	1.9	4.8	-2.4	2.7
NM_004431.2	*EPHA2*			-1.6	-1.3	2.4	-1.5	1.1	-2.0	-1.0	1.0	1.0	1.2	-1.2	2.1	-1.1	-1.3	-1.5	-1.4	-1.2	-1.3
NM_000137.1	*FAH*			-1.3	1.4	2.2	-1.4	-1.3	1.9	1.3	1.1	2.0	-1.2	1.5	-3.0	1.2	2.1	1.5	1.8	1.7	1.2
NM_001033030.1	*FAIM*			1.4	1.0	-1.2	1.1	-1.2	-1.3	-1.2	-1.2	-1.2	1.2	-1.1	2.3	1.5	-1.6	1.2	1.1	-1.2	1.1
NM_030919.2	*FAM83D*			1.1	-1.4	-1.1	-1.2	-2.8	-2.6	1.4	-1.1	1.3	-1.1	-1.6	-1.5	-2.1	1.2	-1.1	-1.2	-1.2	-1.0
NM_000508.3	*FGA*			-1.9	-2.1	1.3	-3.1	-6.8	-2.8	1.0	-1.5	-1.1	1.1	-2.3	-5.0	-7.4	1.1	1.0	-2.0	-4.8	-1.4
NM_000508.3	*FGA*			2.8	-2.1	-4.2	1.9	-6.5	-2.5	-1.4	-1.3	1.2	-2.3	-1.4	-3.3	-3.5	-1.5	1.7	-1.5	-5.1	-1.0
NM_000166.4	*GJB1*			-1.9	1.1	3.9	-2.7	-2.1	1.7	-1.7	-1.3	-1.2	-3.1	-1.8	-6.2	-1.9	-1.1	1.7	1.3	-2.2	1.4
NM_018960.4	*GNMT*			-2.0	-2.7	1.3	-3.0	-6.5	1.1	-1.8	1.3	-1.1	-3.7	-2.1	-2.9	-2.3	1.2	1.1	1.2	-2.3	1.6
NM_021175.2	*HAMP*			-1.3	-1.5	1.2	-2.3	-10.6	-1.5	1.5	1.4	-2.1	2.5	2.3	-2.1	-4.0	-1.3	-1.2	-5.7	-1.4	-2.0
NM_001530.2	*HIF1A*			3.6	-1.5	-4.8	2.8	-1.7	-3.1	1.0	-1.1	1.0	1.2	-1.0	-1.3	-1.6	-1.3	-1.2	-1.6	-1.2	-1.2
NM_005347.2	*HSPA5*			-1.5	1.1	1.2	-5.7	-4.3	-1.4	1.0	1.0	-1.3	-1.2	1.5	1.1	-2.1	-1.5	-1.5	-1.1	-3.1	-1.8
NM_000240.2	*MAOA*			-1.3	1.1	1.8	-1.5	-1.1	2.4	1.0	-1.1	-1.1	-1.6	-1.4	-4.9	-1.6	1.2	1.5	1.4	-1.3	2.2
NM_198055.1	*MZF1*			-1.3	-1.1	1.0	-1.0	1.5	-1.5	1.4	-1.1	-1.1	2.3	1.3	2.7	1.0	1.3	-1.4	-1.5	1.7	-1.4

Table 59 (continued)

RefSeq	Symbol	IPA® Tox function	Function	Donor 1						Donor 2						Donor 3					
				100 µM IBU			1000 µM IBU			100 µM IBU			1000 µM IBU			100 µM IBU			1000 µM IBU		
				d01	d03	d14	d01	d03	d14	d01	d03	d14	d01	d03	d14	d01	d03	d14	d01	d03	d14
NM_152341.2	*PAQR4*			-1.7	1.0	1.2	-1.7	-1.4	-2.3	-1.2	1.2	-1.4	-2.3	-2.7	-1.9	-1.3	1.2	1.3	1.1	-1.8	1.7
NM_000941.2	*POR*			-1.1	1.8	2.3	2.1	4.1	3.5	-1.0	-1.0	1.0	2.3	2.2	2.4	3.7	1.2	-1.1	1.4	1.5	-1.6
NM_000021.2	*PSEN1*			1.3	-1.3	-3.0	1.5	1.1	-1.6	1.0	1.1	1.2	1.1	1.1	2.0	1.1	-1.1	-1.6	1.1	1.1	-1.4
NM_002800.4	*PSMB9*			-1.7	-1.1	1.1	-1.8	-1.2	-3.3	1.0	1.2	-1.2	1.0	1.1	-1.1	-3.8	1.2	-1.4	-2.6	-1.2	-1.0
NM_005789.2	*PSME3*	Hepato-cellular Carcinoma	Other and unknown functions	1.0	1.1	1.1	1.3	1.1	-2.1	1.1	-1.1	1.0	1.1	-1.8	-1.2	1.1	-1.7	-1.1	-1.3	1.0	-1.2
NM_152703.2	*SAMD9L*			1.3	-1.0	-1.8	1.1	-1.4	-4.3	-1.0	-1.0	-1.1	-1.6	-1.8	-1.3	-1.6	-1.1	-1.2	-1.5	-1.4	1.1
NM_001756.3	*SERPINA6*			-1.2	-1.0	1.7	-1.9	-3.0	-1.2	-1.0	1.1	-1.2	-1.5	-1.7	-3.3	-1.4	1.1	1.3	1.3	-2.3	1.4
NM_000602.1	*SERPINE1*			-1.7	-1.2	1.5	-1.6	1.9	-1.2	-1.1	-1.2	-1.0	-1.2	-2.3	4.2	-1.3	1.6	-1.1	-1.2	1.1	-1.4
NM_000346.2	*SOX9*			-1.3	-1.0	-1.3	-1.6	-1.1	-3.8	-1.1	-1.1	-1.3	-1.0	-1.7	-1.2	-1.1	-1.3	-1.5	-1.3	-1.0	-1.1
NM_006088.5	*TUBB4B*			-2.1	1.1	-1.1	-1.5	-1.0	-3.0	-1.1	1.2	-1.0	-1.1	-1.0	1.0	-1.3	1.0	-1.2	-1.1	-1.1	-1.5
NM_001113756.1	*TYMP*			-1.9	1.2	-1.2	-2.0	-1.3	-3.9	-1.2	1.4	-1.4	-1.9	-1.5	1.6	-1.7	-1.3	-1.0	-1.5	-1.4	-1.0

Table 60. Absolute fold changes of genes deregulated at least 2-fold compared to the time matched vehicle treated control in primary human hepatocytes from three different donors treated with 0.1 or 1 µM chlorpromazine for 1, 3 or 14 days. The categorisation of the genes into IPA® tox functions was evaluated manually which is indicated as the additional "function" category. The genes are in alphabetic order within each IPA® tox function and full gene names are given in Table 63.

RefSeq	Symbol	IPA® Tox function	Function	Donor 1						Donor 2						Donor 3					
				0.1 µM CPZ			1 µM CPZ			0.1 µM CPZ			1 µM CPZ			0.1 µM CPZ			1 µM CPZ		
				d01	d03	d14	d01	d03	d14	d01	d03	d14	d01	d03	d14	d01	d03	d14	d01	d03	d14
NM_007292.4	*ACOX1*	Liver Hyperplasia/ Hyperproliferation	Fatty acid and lipid metabolism	1.1	-1.1	1.1	1.2	-1.4	-2.5	1.2	-1.1	-1.4	1.2	-1.2	-1.5	-1.0	-1.1	-1.1	1.2	-1.2	-1.0
NM_000668.3	*ADH1B*			-1.1	-1.1	1.2	-1.0	-1.2	-1.2	-1.1	-1.4	-1.6	-1.1	-3.3	-1.0	2.6	-1.0	-1.3	2.7	1.2	1.1
NM_000669.3	*ADH1C*			1.1	-1.2	-1.1	1.1	-1.3	-1.2	-1.1	1.1	-1.6	1.1	-1.2	1.2	2.3	-1.0	1.1	2.7	1.0	2.0
NM_052968.3	*APOA5*			-1.6	-1.1	-1.0	-1.2	-1.0	-1.0	-1.2	1.1	1.1	-1.3	-2.7	-1.1	3.0	1.1	1.7	2.8	1.2	1.4
NM_006684.2	*CFHR4*			1.3	-1.0	1.0	1.5	-1.2	-1.3	1.4	-1.4	-1.0	1.7	-2.4	-1.3	-1.1	1.1	-1.3	1.1	1.0	1.1
NM_032564.2	*DGAT2*			-1.2	1.2	1.1	-1.4	-1.1	1.3	-1.3	-1.3	-1.5	-1.3	-1.4	-1.1	2.3	-1.1	-1.0	1.8	-1.2	1.3
NM_000859.1	*HMGCR*			-1.5	-1.0	1.2	-1.6	1.0	1.2	-1.1	-1.4	-1.1	-1.0	-2.4	-1.2	1.7	1.1	-1.1	1.6	-1.1	1.2
NM_001003679.1	*LEPR*			-1.1	-1.4	-1.1	-1.1	-1.4	-3.4	-1.2	-1.3	1.2	-1.1	-1.5	-1.1	-1.1	-1.3	-1.3	1.1	-1.2	-1.0
NM_002979.3	*SCP2*			1.3	-1.1	1.0	1.4	-1.4	-2.4	1.2	-1.4	-1.1	1.1	-2.0	-1.2	1.1	1.3	-1.6	1.3	1.2	-1.5
NM_002612.3	*PDK4*		Carbohydrate metabolism	-1.0	-1.1	1.0	1.1	-1.2	-1.0	1.3	-1.2	-1.4	1.3	-1.4	-1.3	3.9	1.1	1.1	4.3	1.2	-1.0
NM_005398.4	*PPP1R3C*			1.0	1.1	1.4	1.1	1.0	-2.5	1.1	-1.0	-1.6	-1.1	-1.5	1.1	2.1	1.2	-1.0	2.1	1.2	1.4
NM_002734.3	*PRKAR1A*			1.1	-1.1	-1.1	1.3	1.0	-2.6	-1.2	-1.1	-1.1	-1.0	-1.1	-1.0	-1.1	-1.2	-1.4	-1.1	-1.0	-1.3
NM_006516.1	*SLC2A1*			-1.3	1.2	1.2	-1.4	1.1	-2.2	1.1	1.1	1.0	-1.2	1.5	1.1	1.1	1.1	-1.0	1.2	-1.0	-1.2
XM_943415.1	*AKR1C2*		Bile acid metabolism	1.2	-1.1	1.1	1.1	-1.1	-1.3	-1.1	-2.1	-1.2	-1.1	-2.4	-1.3	-1.1	-1.2	-1.1	-1.1	-1.2	-1.1
NM_005989.2	*AKR1D1*			1.1	-1.1	1.0	1.1	1.0	-1.2	-1.0	1.1	-1.2	-1.0	-2.7	-1.2	-1.0	1.1	-1.1	-1.1	-1.0	-1.0
NM_003049.2	*SLC10A1*			-1.3	1.0	-1.2	-1.2	1.0	-1.2	-1.5	-1.6	-3.4	-1.4	-7.1	-1.3	2.4	1.1	1.1	2.5	1.1	1.6
NM_019844.2	*SLCO1B3*			2.7	1.1	-1.4	2.9	1.1	-3.6	1.0	-1.1	-1.3	1.0	-1.4	1.2	1.6	-1.3	-1.2	1.7	1.0	-1.1
NM_001171.3	*ABCC6*		Xenobiotic metabolism	-2.0	-1.3	-1.2	-2.0	-1.3	-1.4	-1.1	-1.7	-1.4	-1.2	-1.7	-1.3	1.0	-1.2	-1.2	1.1	-1.2	-1.2
NM_004364.2	*CEBPA*			-1.7	-1.0	-1.5	-1.7	-1.0	1.2	-1.2	-1.3	-1.0	-1.1	-1.2	-1.0	2.3	-1.2	1.1	2.1	-1.2	1.2
NM_001266.4	*CES1*			-1.7	-1.4	-1.1	-1.5	-1.6	-2.9	-1.1	1.0	-1.1	-1.1	-1.1	-1.0	-1.2	-1.2	-1.8	-1.2	-1.2	-1.5
NM_000499.2	*CYP1A1*			1.2	3.1	1.8	1.2	3.0	2.1	4.4	1.9	1.0	5.1	1.5	3.9	3.2	3.0	4.5	3.4	3.6	2.1
NM_000771.2	*CYP2C9*			1.1	1.4	-1.5	1.0	1.6	-1.0	-1.2	-1.1	-2.2	-1.3	-1.3	1.1	1.8	1.4	1.2	1.9	1.8	2.4
NM_000561.2	*GSTM1*			-1.1	-1.1	-1.3	-1.2	-1.3	-1.4	-1.4	-1.5	-1.6	-1.4	-2.2	-1.3	1.5	-1.0	-1.4	1.7	1.2	-1.0
NM_006169.2	*NNMT*			-1.2	1.1	1.2	-1.2	1.1	1.1	1.1	1.2	1.2	-1.0	1.2	1.0	-2.9	1.1	-1.0	-3.0	-1.4	-1.1
NM_001077475.1	*NR1I3*			-1.5	-1.0	1.2	-1.4	-1.1	1.3	-1.0	1.0	-2.1	-1.2	-2.3	-1.4	1.3	1.3	-1.1	1.4	1.1	-1.0
NM_003057.2	*SLC22A1*			-1.6	-1.1	-1.2	-1.5	-1.1	1.3	-1.3	-1.8	-2.2	-1.4	-2.3	1.0	1.4	-1.1	-1.3	1.3	1.1	1.0

Table 60 (continued)

RefSeq	Symbol	IPA® Tox function	Function	Donor 1						Donor 2						Donor 3					
				0.1 µM CPZ			1 µM CPZ			0.1 µM CPZ			1 µM CPZ			0.1 µM CPZ			1 µM CPZ		
				d01	d03	d14	d01	d03	d14	d01	d03	d14	d01	d03	d14	d01	d03	d14	d01	d03	d14
NM_007120.2	*UGT1A4*		Xenobiotic metabolism	1.7	-1.1	2.0	2.6	-1.3	-1.2	1.2	1.1	-1.0	1.6	1.3	-1.0	1.0	1.3	1.4	1.3	1.8	1.3
NM_019075.2	*UGT1A9*			1.3	-1.3	-1.0	1.5	-1.6	-2.1	-1.1	-1.1	-1.3	1.1	-1.1	-1.2	1.2	1.2	-1.4	1.3	1.0	-1.3
NM_019075.2	*UGT1A9*			1.3	-1.3	-1.0	1.5	-1.6	-2.1	-1.1	-1.1	-1.3	1.1	-1.1	-1.2	1.2	1.2	-1.4	1.3	1.0	-1.3
NM_006988.3	*ADAMTS1*		Inflammation	1.1	1.1	-1.3	-1.0	1.1	1.2	1.7	1.4	2.5	1.7	1.4	1.1	-2.2	-1.2	-1.5	-2.1	-1.3	-1.6
NM_001679.2	*ATP1B3*			-1.0	-1.2	-1.1	1.1	-1.1	-2.6	-1.1	-1.0	-1.0	-1.0	1.2	-1.1	-1.2	-1.4	-1.3	-1.2	-1.0	-1.3
NM_002982.3	*CCL2*			1.1	1.2	1.0	1.2	1.2	1.1	1.9	1.5	2.6	1.8	1.4	-1.0	-3.6	1.6	-1.3	-3.3	1.6	-1.2
NM_032607.1	*CREB3L3*			-1.4	1.2	-1.1	-1.6	1.2	1.5	1.1	1.2	1.7	-1.1	1.0	-1.1	-3.5	1.0	1.2	-3.9	-1.0	-1.0
NM_000567.2	*CRP*			-1.2	1.2	-1.0	-1.6	1.3	1.0	-1.0	1.2	-1.1	-1.1	1.0	-1.2	-1.8	1.2	-1.0	-2.2	-1.4	-1.2
NM_002341.1	*LTB*			-1.0	-1.2	1.0	-1.2	-1.2	1.2	1.2	1.1	2.3	1.1	-1.1	-1.4	-3.3	1.0	1.1	-3.5	1.1	1.4
NM_000963.1	*PTGS2*			1.2	1.0	-1.1	1.3	1.1	-3.7	1.3	-1.1	-1.1	1.3	-1.2	-1.1	-1.2	-1.1	-4.9	-1.1	1.0	-4.8
NM_003745.1	*SOCS1*			-1.3	-1.1	-1.2	-1.2	-1.0	1.3	1.4	1.2	2.3	1.3	1.7	1.1	-5.0	1.1	-1.3	-5.2	-1.3	-1.1
NM_003955.3	*SOCS3*			-1.5	1.1	-1.2	-1.4	-1.1	1.1	-1.0	1.0	1.5	1.0	-1.1	-1.0	-5.2	-1.1	-1.1	-5.0	-1.1	1.1
NM_000064.2	*C3*	Liver Hyperplasia/ Hyperproliferation	Immune response	-1.8	-1.1	1.0	-1.5	-1.2	1.1	-1.1	-9.8	-1.0	-1.2	-8.6	-1.5	-2.1	-1.0	-1.5	-1.6	-1.1	-1.8
NM_001737.2	*C9*			4.2	-1.1	-1.1	3.6	-1.2	-4.1	1.2	1.3	-1.3	1.1	-1.6	1.0	-1.0	1.0	-2.3	-1.1	-1.1	-1.6
NM_001001392.1	*CD44*			-1.1	-1.1	-1.1	-1.0	-1.0	-1.2	-1.3	-1.3	-1.0	-1.1	-1.3	-1.1	-2.0	-1.1	-1.6	-2.1	-1.1	-1.8
NM_021023.3	*CFHR3*			1.3	1.0	-1.3	1.4	-1.3	-2.1	-1.3	-1.0	-1.3	-1.3	-2.5	-1.1	-1.2	-1.1	-1.6	-1.0	-1.1	-1.3
NM_000201.1	*ICAM1*			-1.5	1.1	-1.2	-1.6	-1.1	-1.3	-1.2	1.9	1.2	-1.2	1.8	-1.2	-3.1	-1.1	-1.8	-2.8	-1.3	-1.9
NM_000600.1	*IL6*			-1.2	1.1	-1.2	-1.1	-1.0	1.0	1.2	1.2	3.7	1.2	1.4	-1.1	-2.2	-1.1	-5.5	-2.2	-1.1	-5.0
NM_000584.2	*IL8*			1.2	1.2	-1.1	1.0	1.2	-1.2	1.4	-1.1	1.5	1.1	-1.0	-1.1	-4.0	1.0	-1.1	-3.4	1.0	-1.1
NM_001879.4	*MASP1*			-1.4	-1.2	-1.0	-1.4	-1.2	-1.4	-1.2	-1.6	-2.6	-1.3	-2.5	-1.3	-1.3	-1.0	-1.3	-1.1	-1.1	-1.1
NM_003999.1	*OSMR*			1.2	1.1	1.3	1.3	-1.0	-1.3	1.1	1.3	1.3	1.2	1.4	-1.1	-2.1	1.1	-1.0	-2.0	1.0	-1.1
NM_001134.1	*AFP*		Cancer	1.2	-1.2	1.0	1.2	-1.1	1.4	1.1	1.1	-1.2	1.0	-1.6	-1.1	3.2	1.2	1.1	3.3	1.0	1.1
NM_001166.3	*BIRC2*			1.3	1.0	-1.2	1.4	1.0	-2.2	-1.0	-1.7	-1.1	1.1	-1.6	-1.2	-1.4	-1.2	-1.4	-1.2	-1.1	-1.4
NM_198590.1	*BSG*			-2.1	1.5	1.0	-2.4	1.4	2.2	-1.1	-1.2	-1.3	1.0	-1.2	-1.1	1.2	-1.1	1.3	1.2	1.2	1.1
NM_001216.1	*CA9*			1.1	-1.3	1.3	1.1	-1.3	1.0	-1.3	1.1	-2.5	-1.4	-2.2	1.2	-1.0	-1.1	-1.1	1.0	1.2	-1.1
NM_001080125.1	*CASP8*			1.9	-1.1	1.1	2.4	-1.2	-2.7	1.0	1.0	1.1	1.0	1.3	-1.2	-1.6	-1.1	-1.2	-1.4	1.0	-1.2
NM_004064.2	*CDKN1B*			-1.2	-1.2	-1.2	-1.1	1.0	-4.8	-1.1	1.1	1.1	-1.1	-1.0	1.1	-1.0	-1.0	-1.5	-1.1	-1.1	-1.4
NM_018098.4	*ECT2*			2.4	1.0	-1.2	2.3	1.1	-1.9	1.3	-1.0	1.8	1.0	1.0	2.1	-2.0	-1.2	-1.5	-2.2	1.1	-1.2

Table 60 (continued)

RefSeq	Symbol	IPA® Tox function	Function	Donor 1						Donor 2						Donor 3					
				0.1 µM CPZ			1 µM CPZ			0.1 µM CPZ			1 µM CPZ			0.1 µM CPZ			1 µM CPZ		
				d01	d03	d14	d01	d03	d14	d01	d03	d14	d01	d03	d14	d01	d03	d14	d01	d03	d14
NM_001040092.1	*ENPP2*			-1.0	-1.1	1.0	-1.0	-1.2	1.0	-1.0	-1.6	-1.4	1.0	-2.4	-1.4	2.2	-1.0	-1.0	2.2	1.0	-1.1
NM_000125.2	*ESR1*			1.0	1.1	-1.2	1.0	1.0	-1.2	1.0	-1.5	-1.1	1.0	-3.1	1.1	2.1	1.1	1.0	1.9	1.5	-1.0
NM_004467.3	*FGL1*			-1.1	-1.1	-1.1	-1.1	-1.2	-4.7	-1.2	-1.0	-1.2	-1.1	-1.1	-1.3	-1.4	-1.1	-1.9	-1.5	-1.1	-1.7
NM_005252.2	*FOS*			-1.1	-1.0	1.8	-1.1	1.1	2.3	1.1	-1.2	1.0	1.1	-1.1	-1.4	-2.4	-1.2	-1.3	-1.8	-1.1	-1.3
NM_033260.3	*FOXQ1*			1.1	1.0	2.0	1.0	-1.1	-1.3	-1.0	1.0	-1.3	-1.1	1.0	1.7	1.4	1.1	-1.1	1.7	-1.0	-1.0
NM_000545.4	*HNF1A*			-2.0	1.1	-1.6	-2.1	1.3	1.9	-1.1	-1.0	1.1	-1.1	-1.0	1.1	1.4	-1.2	1.0	1.3	1.0	-1.0
NM_002342.1	*LTBR*			-1.8	1.0	-1.1	-1.8	1.0	2.1	-1.1	-1.1	1.1	-1.1	-1.1	1.0	-1.2	-1.1	1.0	-1.3	-1.2	1.1
NM_000245.2	*MET*			2.3	1.0	-1.2	1.9	1.0	-2.3	1.1	-1.0	-1.1	1.0	-1.2	-1.2	-1.0	-1.5	-1.6	-1.0	-1.2	-1.6
NM_002467.3	*MYC*		Cancer	-1.1	-1.1	-1.1	-1.1	-1.0	-2.2	-1.1	-1.0	1.0	-1.1	1.3	-1.0	-1.4	-1.2	-1.3	-1.7	1.0	-1.2
NM_006096.2	*NDRG1*			-1.3	1.0	1.2	-1.2	1.1	-2.0	-1.4	1.1	-2.0	-1.6	-1.6	-1.4	1.5	1.0	-1.2	2.1	1.2	-1.3
NM_153292.1	*NOS2*			-1.0	-1.0	-1.4	1.1	1.0	-1.0	1.0	-1.1	1.3	1.1	1.0	1.1	-1.3	1.1	-2.6	-1.2	-1.0	-2.6
NM_006218.2	*PIK3CA*			2.7	-1.2	-1.2	2.4	-1.2	-2.5	-1.1	-1.1	1.2	-1.1	-1.1	1.3	1.0	-1.5	-1.1	1.0	-1.0	-1.3
NM_052880.3	*PIK3IP1*	Liver Hyper-plasia/ Hyper-proliferation		-1.5	-1.1	-1.0	-1.3	-1.2	-1.6	-1.2	-1.0	-1.1	-1.2	-2.0	-1.2	1.0	1.1	-1.2	1.0	-1.1	-1.1
NM_004156.2	*PPP2CB*			-1.1	-1.2	-1.1	-1.0	-1.1	-5.1	-1.1	-1.1	-1.1	1.0	1.1	-1.2	-1.2	-1.3	-1.9	1.0	-1.3	-1.6
NM_005651.1	*TDO2*			-1.0	-1.1	1.3	1.1	-1.0	-2.7	1.1	-1.0	1.1	1.0	-2.6	1.0	1.1	1.2	-1.7	1.1	1.0	-1.4
NM_000594.2	*TNF*			-1.1	1.1	-1.3	1.1	1.0	1.5	1.1	-1.2	4.1	1.1	-1.1	1.1	-1.7	1.2	-5.6	-1.8	-1.1	-5.0
NM_152415.1	*VPS37A*			1.7	-1.0	-1.1	1.5	-1.1	-3.0	1.1	1.1	-1.2	-1.1	1.1	-1.1	1.0	-1.3	-1.5	-1.2	-1.1	-1.5
NM_000478.3	*ALPL*			-1.4	1.0	-1.3	-1.6	1.1	1.1	1.2	1.4	-1.1	1.1	1.1	1.0	-2.3	1.6	-1.1	-2.3	1.0	-1.4
NM_001011645.1	*AR*			-1.1	-1.3	-1.1	1.0	-1.3	1.4	1.1	-1.3	1.0	1.3	-2.1	-1.1	1.8	1.2	-1.0	1.7	1.2	1.2
NM_001713.1	*BHMT*			-1.3	-1.0	1.9	-1.3	-1.0	-1.1	-1.4	-1.0	-2.9	-1.4	-4.1	-1.5	5.0	1.5	1.2	5.7	1.2	1.3
NM_014670.2	*BZW1*			2.5	-1.6	1.0	3.6	-2.1	-5.6	-1.0	-1.0	-1.2	1.1	-1.0	-1.2	-1.3	-1.3	-1.4	-1.2	-1.1	-1.4
NM_000096.1	*CP*			1.6	-1.4	1.3	2.3	-1.5	-2.9	1.2	-1.0	1.0	1.3	-2.7	-1.0	-2.0	1.1	-1.1	-1.7	1.1	-1.2
NM_001412.3	*EIF1AX*		Other and unknown functions	2.4	-1.1	-1.1	1.8	-1.3	-3.2	-1.1	-1.0	-1.1	-1.1	1.2	-1.1	-1.1	-1.3	-1.2	-1.0	1.1	-1.1
NM_001968.2	*EIF4E*			1.4	-1.1	-1.2	1.4	-1.1	-3.0	1.0	1.0	-1.1	1.1	1.1	1.1	-1.1	-1.1	-1.4	-1.2	1.1	-1.4
NM_001098175.1	*ENTPD1*			-1.7	1.1	1.0	-1.7	-1.0	2.8	-1.1	1.0	-1.1	1.0	-1.1	1.0	1.1	1.0	-1.1	-1.0	1.0	1.0
NM_001993.2	*F3*			1.1	-1.1	1.1	1.0	-1.3	-2.5	-1.0	1.0	1.1	-1.0	-1.0	-1.3	-1.1	-1.0	-1.5	-1.0	1.0	-1.2
NM_001033030.1	*FAIM*			1.2	-1.0	-1.3	1.4	-1.2	-2.1	-1.1	-1.1	-1.0	-1.1	-1.0	-1.0	-1.0	-1.2	-1.2	1.0	-1.1	-1.4
NM_000508.3	*FGA*			-1.5	-1.1	-1.1	-1.5	-1.2	-5.3	-1.3	-1.3	-1.1	-1.1	-1.6	-1.1	-1.8	-1.1	-1.8	-1.5	-1.1	-1.9

Table 60 (continued)

RefSeq	Symbol	IPA® Tox function	Function	Donor 1						Donor 2						Donor 3					
				0.1 µM CPZ			1 µM CPZ			0.1 µM CPZ			1 µM CPZ			0.1 µM CPZ			1 µM CPZ		
				d01	d03	d14	d01	d03	d14	d01	d03	d14	d01	d03	d14	d01	d03	d14	d01	d03	d14
NM_000166.4	*GJB1*			-1.5	1.1	-1.1	-1.6	-1.0	2.1	-1.5	-1.2	-1.2	-1.3	-1.8	-1.2	1.6	-1.2	1.1	1.5	-1.2	1.5
NM_003801.3	*GPAA1*			-1.6	1.3	-1.1	-1.6	1.2	2.0	-1.0	1.2	-1.1	1.1	1.1	1.1	1.0	-1.2	1.4	1.2	1.4	1.1
NM_021175.2	*HAMP*			-1.2	1.3	1.4	-1.3	1.4	1.2	1.7	1.8	5.0	1.8	-1.9	-1.0	-3.7	1.2	1.2	-4.2	-1.1	1.2
NM_001530.2	*HIF1A*			3.4	-1.0	-1.0	3.6	-1.2	-3.8	1.4	-1.1	1.4	1.3	-1.1	1.1	-2.6	-1.3	-1.4	-2.3	-1.1	-1.5
NM_002128.4	*HMGB1*			2.1	-1.1	-1.0	1.8	-1.0	-2.1	-1.1	-1.0	-1.1	-1.0	-1.1	1.1	1.1	-1.3	-1.3	1.0	-1.0	-1.3
NR_003249.1	*HNRPDL*			-1.2	1.1	-1.0	-1.1	1.2	-2.0	-1.0	-1.5	1.0	1.2	-1.3	1.0	-1.2	-1.2	-1.1	-1.4	-1.2	-1.1
NM_006531.3	*IFT88*			1.0	-1.2	-1.1	1.1	-1.2	-2.2	-1.0	-1.2	-1.4	1.1	-1.1	-1.4	-1.1	-1.1	-1.4	-1.2	-1.1	-1.2
NM_006391.1	*IPO7*			1.7	-1.0	1.3	2.0	-1.1	-2.5	1.1	-1.3	1.1	1.1	1.2	-1.2	-1.7	1.1	1.1	-1.5	1.0	-1.1
NM_052972.2	*LRG1*			-1.3	-1.1	1.2	-1.3	1.0	1.6	1.1	1.3	1.2	1.0	-1.1	-1.1	-2.0	1.4	-1.0	-2.2	-1.0	-1.0
NM_005911.4	*MAT2A*	Liver Hyper-plasia/ Hyper-proliferation	Other and unknown functions	-1.3	1.7	2.2	-1.2	1.6	4.4	1.3	-1.1	1.7	1.6	1.1	-1.1	1.2	1.2	1.2	1.2	1.0	1.1
NM_018454.5	*NUSAP1*			1.1	-1.0	-1.1	1.1	-1.0	-1.6	1.1	-1.1	-1.1	1.0	-1.8	-1.1	-2.1	1.1	-1.2	-2.0	-1.1	-1.0
NM_152341.2	*PAQR4*			-1.7	1.2	1.0	-1.6	1.3	-1.1	-1.3	1.3	-2.1	-1.5	-1.5	-1.1	1.2	1.1	1.0	1.2	1.0	1.2
NM_052890.3	*PGLYRP2*			-1.0	1.1	1.0	-1.1	1.2	1.5	-1.7	1.2	-1.9	-1.7	-2.0	-1.5	1.5	1.1	1.2	1.4	-1.1	1.2
NM_006813.1	*PNRC1*			1.0	1.0	-1.1	-1.1	1.0	1.3	-1.2	1.0	-1.0	-1.1	1.3	-1.0	-2.0	1.0	1.0	-2.1	-1.1	-1.2
NM_002800.4	*PSMB9*			-1.6	1.0	-1.2	-1.7	1.0	-1.0	-1.1	-1.1	1.4	-1.2	1.0	-1.1	-2.9	-1.1	-1.2	-3.0	-1.2	-1.3
NM_001024921.2	*RPL9*			1.0	-1.2	-1.4	1.0	-1.4	-4.1	-1.1	-1.0	1.0	-1.1	-1.1	1.0	-1.4	-1.4	-1.4	-1.4	-1.2	-1.3
NM_012238.3	*SIRT1*			2.1	1.1	-1.2	1.9	1.0	-2.6	1.1	-1.1	-1.1	-1.1	1.1	1.1	1.1	-1.2	-1.4	1.1	1.0	-1.4
NM_080866.2	*SLC22A9*			-1.2	-1.2	-1.1	-1.1	-1.3	1.1	1.1	-1.0	-1.3	1.0	-2.4	1.1	1.6	-1.1	1.1	1.6	-1.0	1.2
NM_018389.3	*SLC35C1*			-1.8	1.2	-1.2	-1.8	1.2	1.7	1.0	-1.2	1.3	1.1	-1.1	1.2	-2.1	-1.1	-1.1	-2.1	-1.3	1.0
NM_006288.2	*THY1*			-1.4	1.2	1.1	-1.4	1.4	2.3	-1.1	-1.0	-1.1	-1.0	1.1	1.1	1.0	-1.1	-1.0	-1.0	1.0	-1.1
NM_012479.2	*YWHAG*			1.8	-1.0	-1.3	1.6	-1.2	-3.1	-1.1	1.2	1.1	-1.1	1.4	1.1	1.0	-1.5	-1.4	-1.1	-1.1	-1.2
NM_001995.2	*ACSL1*			2.5	-1.1	-1.2	2.4	-1.1	-2.5	-1.2	1.1	-1.2	1.0	-1.3	-1.2	1.4	1.1	-1.8	1.6	1.0	-1.6
NM_000668.3	*ADH1B*			-1.1	-1.1	1.2	-1.0	-1.2	-1.2	-1.1	-1.4	-1.6	-1.1	-3.3	-1.0	2.6	-1.0	-1.3	2.7	1.2	1.1
NM_000669.3	*ADH1C*			1.1	-1.2	-1.1	1.1	-1.3	-1.2	-1.1	1.1	-1.6	1.1	-1.2	1.2	2.3	-1.0	1.1	2.7	1.0	2.0
NM_052968.3	*APOA5*	Liver Cholestasis	Fatty acid and lipid metabolism	-1.6	-1.1	-1.0	-1.2	-1.0	-1.0	-1.2	1.1	1.1	-1.3	-2.7	-1.1	3.0	1.1	1.7	2.8	1.2	1.4
NM_000859.1	*HMGCR*			-1.5	-1.0	1.2	-1.6	1.0	1.2	-1.1	-1.4	-1.1	-1.0	-2.4	-1.2	1.7	1.1	-1.1	1.6	-1.1	1.2
NM_002979.3	*SCP2*			1.3	-1.1	1.0	1.4	-1.4	-2.4	1.2	-1.4	-1.1	1.1	-2.0	-1.2	1.1	1.3	-1.6	1.3	1.2	-1.5
NM_002979.3	*SCP2*			1.3	-1.1	1.0	1.4	-1.4	-2.4	1.2	-1.4	-1.1	1.1	-2.0	-1.2	1.1	1.3	-1.6	1.3	1.2	-1.5

Table 60 (continued)

RefSeq	Symbol	IPA® Tox function	Function	Donor 1						Donor 2						Donor 3					
				0.1 µM CPZ			1 µM CPZ			0.1 µM CPZ			1 µM CPZ			0.1 µM CPZ			1 µM CPZ		
				d01	d03	d14	d01	d03	d14	d01	d03	d14	d01	d03	d14	d01	d03	d14	d01	d03	d14
NM_006759.3	*UGP2*	Liver Cholestasis	Carbo-hydrate metabolism	-1.1	-1.8	-1.4	-1.4	-1.6	-5.3	-1.2	-1.7	-1.5	-1.1	-2.2	-1.4	-1.0	-1.4	-1.9	-1.1	-1.1	-1.3
XM_943415.1	*AKR1C2*		Bile acid metabolism	1.2	-1.1	1.1	1.1	-1.1	-1.3	-1.1	-2.1	-1.2	-1.1	-2.4	-1.3	-1.1	-1.2	-1.1	-1.1	-1.2	-1.1
NM_005989.2	*AKR1D1*			1.1	-1.1	1.0	1.1	1.0	-1.2	-1.0	1.1	-1.2	-1.0	-2.7	-1.2	-1.0	1.1	-1.1	-1.1	-1.0	-1.0
NM_004820.2	*CYP7B1*			1.2	1.1	1.1	1.0	1.1	-2.0	-1.3	1.1	-1.2	-1.1	1.1	1.1	-1.1	1.0	1.0	-1.0	1.1	1.1
NM_003049.2	*SLC10A1*			-1.3	1.0	-1.2	-1.2	1.0	-1.2	-1.5	-1.6	-3.4	-1.4	-7.1	-1.3	2.4	1.1	1.1	2.5	1.1	1.6
NM_019844.2	*SLCO1B3*			2.7	1.1	-1.4	2.9	1.1	-3.6	1.0	-1.1	-1.3	1.0	-1.4	1.2	1.6	-1.3	-1.2	1.7	1.0	-1.1
NM_001752.2	*CAT*		Stress response	-1.0	-1.2	-1.2	1.2	-1.2	-3.2	-1.2	-1.2	-1.5	-1.2	-2.0	-1.2	1.5	-1.3	-1.5	1.8	1.0	-1.4
NM_001216.1	*CA9*		Cancer	1.1	-1.3	1.3	1.1	-1.3	1.0	-1.3	1.1	-2.5	-1.4	-2.2	1.2	-1.0	-1.1	-1.1	1.0	1.2	-1.1
NM_001040092.1	*ENPP2*			-1.0	-1.1	1.0	-1.0	-1.2	1.0	-1.0	-1.6	-1.4	1.0	-2.4	-1.4	2.2	-1.0	-1.0	2.2	1.0	-1.1
NM_000125.2	*ESR1*			1.0	1.1	-1.2	1.0	1.0	-1.2	1.0	-1.5	-1.1	1.0	-3.1	1.1	2.1	1.1	1.0	1.9	1.5	-1.0
NM_152877.1	*FAS*			-1.3	-1.1	-1.3	-1.3	-1.1	-2.9	-1.4	1.0	-1.3	-1.3	-1.1	-1.3	-1.1	1.0	-1.4	-1.1	-1.1	-1.1
NM_052880.3	*PIK3IP1*			-1.5	-1.1	-1.0	-1.3	-1.2	-1.6	-1.2	-1.0	-1.1	-1.2	-2.0	-1.2	1.0	1.1	-1.2	1.0	-1.1	-1.1
NM_005651.1	*TDO2*			-1.0	-1.1	1.3	1.1	-1.0	-2.7	1.1	-1.0	1.1	1.0	-2.6	1.0	1.1	1.2	-1.7	1.1	1.0	-1.4
NM_000064.2	*C3*		Immune response	-1.8	-1.1	1.0	-1.5	-1.2	1.1	-1.1	-9.8	-1.0	-1.2	-8.6	-1.5	-2.1	-1.0	-1.5	-1.6	-1.1	-1.8
NM_021023.3	*CFHR3*			1.3	1.0	-1.3	1.4	-1.3	-2.1	-1.3	-1.0	-1.3	-1.3	-2.5	-1.1	-1.2	-1.1	-1.6	-1.0	-1.1	-1.3
NM_006684.2	*CFHR4*			1.3	-1.0	1.0	1.5	-1.2	-1.3	1.4	-1.4	-1.0	1.7	-2.4	-1.3	-1.1	1.1	-1.3	1.1	1.0	1.1
NM_000600.1	*IL6*			-1.2	1.1	-1.2	-1.1	-1.0	1.0	1.2	1.2	3.7	1.2	1.4	-1.1	-2.2	-1.1	-5.5	-2.2	-1.1	-5.0
NM_000584.2	*IL8*			1.2	1.2	-1.1	1.0	1.2	-1.2	1.4	-1.1	1.5	1.1	-1.0	-1.1	-4.0	1.0	-1.1	-3.4	1.0	-1.1
NM_139125.2	*MASP1*			-1.4	-1.2	-1.0	-1.4	-1.2	-1.4	-1.2	-1.6	-2.6	-1.3	-2.5	-1.3	-1.3	-1.0	-1.3	-1.1	-1.1	-1.1
NM_000561.2	*GSTM1*		Xenobiotic metabolism	-1.1	-1.1	-1.3	-1.2	-1.3	-1.4	-1.4	-1.5	-1.6	-1.4	-2.2	-1.3	1.5	-1.0	-1.4	1.7	1.2	-1.0
NM_001077475.1	*NR1I3*			-1.5	-1.0	1.2	-1.4	-1.1	1.3	-1.0	1.0	-2.1	-1.2	-2.3	-1.4	1.3	1.3	-1.1	1.4	1.1	-1.0
NM_153187.1	*SLC22A1*			-1.6	-1.1	-1.2	-1.5	-1.1	1.3	-1.3	-1.8	-2.2	-1.4	-2.3	1.0	1.4	-1.1	-1.3	1.3	1.1	1.0
NM_001075.3	*UGT2B10*			2.5	-1.0	-1.2	2.4	-1.0	-2.3	1.1	-1.6	-2.7	1.1	-3.6	-1.5	2.1	1.3	1.4	2.3	1.2	1.6
XM_001127829.1	*UGT2B15*			2.0	-1.5	1.1	2.4	-1.4	-2.5	-1.1	-1.5	-1.4	-1.1	-3.4	-1.2	1.6	-1.2	-1.0	1.8	1.1	1.1

Table 60 (continued)

RefSeq	Symbol	IPA® Tox function	Function	Donor 1						Donor 2						Donor 3					
				0.1 µM CPZ			1 µM CPZ			0.1 µM CPZ			1 µM CPZ			0.1 µM CPZ			1 µM CPZ		
				d01	d03	d14	d01	d03	d14	d01	d03	d14	d01	d03	d14	d01	d03	d14	d01	d03	d14
NM_000670.3	*ADH4*			-1.2	1.0	-1.1	-1.1	-1.1	-1.4	-1.5	-1.6	-2.6	-1.3	-4.8	-1.1	4.1	-1.1	-1.2	4.0	1.1	1.0
NM_000672.2	*ADH6*			-1.3	-1.1	1.3	1.1	-1.3	1.5	-1.2	-1.4	-1.8	-1.1	-2.3	-1.0	2.2	1.2	-1.2	2.3	1.1	-1.2
NM_001011645.1	*AR*			-1.1	-1.3	-1.1	1.0	-1.3	1.4	1.1	-1.3	1.0	1.3	-2.1	-1.1	1.8	1.2	-1.0	1.7	1.2	1.2
NM_001713.1	*BHMT*			-1.3	-1.0	1.9	-1.3	-1.0	-1.1	-1.4	-1.0	-2.9	-1.4	-4.1	-1.5	5.0	1.5	1.2	5.7	1.2	1.3
NM_000096.1	*CP*			1.6	-1.4	1.3	2.3	-1.5	-2.9	1.2	-1.0	1.0	1.3	-2.7	-1.0	-2.0	1.1	-1.1	-1.7	1.1	-1.2
NM_000166.4	*GJB1*			-1.5	1.1	-1.1	-1.6	-1.0	2.1	-1.5	-1.2	-1.2	-1.3	-1.8	-1.2	1.6	-1.2	1.1	1.5	-1.2	1.5
NM_002083.2	*GPX2*	Liver Cholestasis	Other and unknown functions	-1.2	1.2	1.2	-1.1	1.1	1.4	1.4	-1.0	1.4	1.2	1.1	1.1	-1.8	1.3	1.2	-2.2	1.2	1.1
NM_000277.1	*PAH*			1.3	-1.2	-1.1	1.6	-1.2	-3.3	1.0	-1.2	-1.2	1.1	-1.5	-1.2	2.0	-1.4	-1.3	2.1	-1.0	-1.1
NM_000277.1	*PAH*			1.3	-1.2	-1.1	1.6	-1.2	-3.3	1.0	-1.2	-1.2	1.1	-1.5	-1.2	2.0	-1.4	-1.3	2.1	-1.0	-1.1
NM_052890.3	*PGLYRP2*			-1.0	1.1	1.0	-1.1	1.2	1.5	-1.7	1.2	-1.9	-1.7	-2.0	-1.5	1.5	1.1	1.2	1.4	-1.1	1.2
NM_001046.2	*SLC12A2*			1.4	-1.1	1.3	1.7	-1.4	-2.5	-1.0	-1.2	1.1	-1.1	-1.0	1.0	-1.2	-1.1	-1.2	-1.2	1.0	-1.3
NM_080866.2	*SLC22A9*			-1.2	-1.2	-1.1	-1.1	-1.3	1.1	1.1	-1.0	-1.3	1.0	-2.4	1.1	1.6	-1.1	1.1	1.6	-1.0	1.2
NM_000544.3	*TAP2*			-1.3	-1.0	-1.1	-1.1	-1.0	1.0	-1.1	-1.2	1.6	-1.0	1.0	-1.3	-2.7	-1.1	-1.4	-2.7	-1.2	-1.4
NM_001075.3	*UGT2B10*			2.5	-1.0	-1.2	2.4	-1.0	-2.3	1.1	-1.6	-2.7	1.1	-3.6	-1.5	2.1	1.3	1.4	2.3	1.2	1.6
NM_000016.2	*ACADM*			1.4	-1.1	1.0	1.7	-1.6	-2.1	-1.1	1.0	-1.3	1.0	-1.3	-1.3	1.3	-1.0	-1.2	1.4	1.1	-1.2
NM_007292.3	*ACOX1*			1.1	-1.1	1.1	1.2	-1.4	-2.5	1.2	-1.1	-1.4	1.2	-1.2	-1.5	-1.0	-1.1	-1.1	1.2	-1.2	-1.0
NM_003500.2	*ACOX2*			-1.2	-1.1	1.0	-1.2	-1.0	1.5	1.1	-1.0	-1.3	1.2	-2.4	-1.1	1.8	1.1	1.1	1.8	-1.1	1.4
NM_004458.1	*ACSL4*			-1.0	-1.2	1.2	1.1	-1.4	-2.0	-1.0	-1.2	1.1	-1.4	-1.4	-1.2	1.0	-1.1	-1.6	1.0	-1.2	-1.6
NM_000778.2	*CYP4A11*			1.3	-1.0	1.1	1.3	-1.1	-1.1	1.0	1.3	-1.7	-1.1	-2.2	-1.2	1.4	-1.1	1.1	1.4	1.0	1.2
NM_001966.2	*EHHADH*		Fatty acid and lipid metabolism	1.3	1.0	1.2	1.8	-1.2	-1.2	1.1	-1.2	-1.7	1.2	-2.0	-1.2	1.8	1.1	-1.1	2.0	1.1	1.0
NM_021814.3	*ELOVL5*	Liver Steatosis		2.4	-1.2	-1.0	2.6	-1.2	-2.2	-1.1	-1.6	1.1	-1.0	-1.3	1.2	1.2	-1.3	-1.3	1.2	-1.1	-1.5
NM_004104.4	*FASN*			-1.7	-1.1	-1.5	-1.5	-1.2	2.3	-1.8	-1.7	-1.2	-1.5	-2.5	-1.5	1.7	-1.1	1.1	1.9	-1.2	-1.0
NM_000859.1	*HMGCR*			-1.5	-1.0	1.2	-1.6	1.0	1.2	-1.1	-1.4	-1.1	-1.0	-2.4	-1.2	1.7	1.1	-1.1	1.6	-1.1	1.2
NM_198336.1	*INSIG1*			-1.2	-1.3	-1.0	-1.1	-1.3	-1.2	-1.0	-1.3	1.1	1.0	-2.4	-1.1	1.0	-1.0	-1.1	1.2	-1.0	-1.2
NM_016133.2	*INSIG2*			1.0	-1.1	1.2	-1.1	-1.1	-2.1	-1.1	-1.1	1.2	-1.3	-1.1	-1.1	-1.1	-1.1	1.0	1.1	-1.1	-1.1
NM_001037537.1	*PHYH*			-1.1	-1.2	-1.1	-1.1	-1.3	-2.1	-1.1	-1.2	-1.4	-1.1	-1.5	-1.2	1.2	-1.1	-1.4	1.3	-1.1	-1.2
NM_002982.3	*CCL2*		In-flammation	1.1	1.2	1.0	1.2	1.2	1.1	1.9	1.5	2.6	1.8	1.4	-1.0	-3.6	1.6	-1.3	-3.3	1.6	-1.2

Table 60 (continued)

RefSeq	Symbol	IPA® Tox function	Function	Donor 1						Donor 2						Donor 3					
				0.1 µM CPZ			1 µM CPZ			0.1 µM CPZ			1 µM CPZ			0.1 µM CPZ			1 µM CPZ		
				d01	d03	d14	d01	d03	d14	d01	d03	d14	d01	d03	d14	d01	d03	d14	d01	d03	d14
NM_000064.2	*C3*	Liver Steatosis	Immune response	-1.8	-1.1	1.0	-1.5	-1.2	1.1	-1.1	-9.8	-1.0	-1.2	-8.6	-1.5	-2.1	-1.0	-1.5	-1.6	-1.1	-1.8
NM_001001391.1	*CD44*			-1.1	-1.1	-1.1	-1.0	-1.0	-1.2	-1.3	-1.3	-1.0	-1.1	-1.3	-1.1	-2.0	-1.1	-1.6	-2.1	-1.1	-1.8
NM_000576.2	*IL1B*			-1.2	-1.1	-1.1	-1.0	1.2	1.0	1.4	1.1	10.7	1.3	1.2	1.2	-3.2	1.2	-1.5	-3.7	-1.1	-2.4
NM_000600.1	*IL6*			-1.2	1.1	-1.2	-1.1	-1.0	1.0	1.2	1.2	3.7	1.2	1.4	-1.1	-2.2	-1.1	-5.5	-2.2	-1.1	-5.0
NM_002184.2	*IL6ST*			2.1	-1.3	1.2	2.8	-1.5	-3.0	1.2	-1.0	1.1	1.2	1.1	-1.0	-1.5	-1.3	-1.1	-1.4	-1.2	-1.0
NM_000151.2	*G6PC*		Carbo-hydrate metabolism	-1.1	-1.1	-1.2	-1.0	-1.1	-1.4	-1.1	-1.3	-1.4	-1.1	-1.6	-1.7	2.3	-1.3	1.0	2.4	-1.5	1.1
NM_001083112.1	*GPD2*			1.7	-1.1	1.2	1.6	-1.1	-2.5	1.1	-1.0	1.2	1.2	-1.0	1.2	-1.0	-1.0	-1.1	-1.0	1.1	-1.3
NM_002591.2	*PCK1*			-1.2	1.0	2.0	-1.0	-1.3	-2.2	-1.1	-1.1	1.0	-1.4	-1.3	-1.1	1.8	-1.2	1.4	1.5	1.1	1.1
NM_017761.2	*PNRC2*			1.1	-1.1	-1.0	-1.0	-1.1	-2.6	1.1	-1.0	1.1	1.0	-1.0	1.0	-1.4	-1.0	-1.3	-1.3	-1.0	-1.5
NM_013261.3	*PPARGC1A*			-1.1	1.0	1.2	-1.0	1.1	1.1	-1.0	-1.1	-1.2	-1.0	-1.2	-1.1	2.3	1.0	-1.1	2.1	-1.0	1.1
NM_001752.2	*CAT*		Stress response	-1.0	-1.2	-1.2	1.2	-1.2	-3.2	-1.2	-1.2	-1.5	-1.2	-2.0	-1.2	1.5	-1.3	-1.5	1.8	1.0	-1.4
NM_000636.2	*SOD2*			-1.5	-1.5	-1.1	-1.4	-1.4	-2.4	1.0	-1.2	1.2	-1.2	1.2	-1.2	-5.4	-1.3	-1.1	-4.2	-1.4	-1.0
NM_000125.2	*ESR1*		Cancer	1.0	1.1	-1.2	1.0	1.0	-1.2	1.0	-1.5	-1.1	1.0	-3.1	1.1	2.1	1.1	1.0	1.9	1.5	-1.0
NM_001077475.1	*NR1I3*		Xenobiotic metabolism	-1.5	-1.0	1.2	-1.4	-1.1	1.3	-1.0	1.0	-2.1	-1.2	-2.3	-1.4	1.3	1.3	-1.1	1.4	1.1	-1.0
NM_173454.1	*AR*		Other and unknown functions	-1.1	-1.3	-1.1	1.0	-1.3	1.4	1.1	-1.3	1.0	1.3	-2.1	-1.1	1.8	1.2	-1.0	1.7	1.2	1.2
NM_001011645.1	*BHMT*			-1.3	-1.0	1.9	-1.3	-1.0	-1.1	-1.4	-1.0	-2.9	-1.4	-4.1	-1.5	5.0	1.5	1.2	5.7	1.2	1.3
NM_004064.2	*CDKN1B*			-1.2	-1.2	-1.2	-1.1	1.0	-4.8	-1.1	1.1	1.1	-1.1	-1.0	1.1	-1.0	-1.0	-1.5	-1.1	-1.1	-1.4
NM_138455.2	*CTHRC1*			1.1	1.0	1.2	1.1	-1.2	-3.0	-1.2	-1.0	1.3	-1.1	-1.3	1.0	-1.1	1.1	-1.3	-1.1	1.1	-1.2
NM_198156.1	*EGLN3*			1.1	1.0	1.1	1.1	-1.2	-2.2	-1.1	1.0	-1.1	-1.1	-1.2	1.0	1.1	-1.4	-1.7	1.0	1.0	-1.3
NM_001482.2	*GATM*			1.1	1.1	-1.5	1.3	-1.1	-2.4	-1.2	-1.1	-1.3	1.0	-1.6	-1.3	1.3	1.0	1.2	1.3	-1.0	1.2
NM_022073.3	*OMA1*			-1.0	-1.2	1.0	-1.0	-1.1	-2.2	1.1	-1.0	1.0	1.1	-1.0	1.1	1.1	-1.2	-1.1	1.2	-1.1	1.0
NM_152869.2	*PARP1*			-1.0	1.3	-1.3	1.0	1.2	1.1	1.1	1.1	1.3	1.1	-1.1	1.2	-1.8	1.1	-1.1	-2.1	1.2	-1.2
NM_145243.3	*PDE8A*			-1.2	-1.4	-1.1	-1.0	-1.3	-2.4	-1.1	-1.1	-1.1	-1.2	-1.2	-1.3	1.0	-1.5	-1.3	-1.1	-1.1	-1.7
NM_001713.1	*RGN*			-1.4	-1.1	-1.0	-1.3	-1.4	-1.3	-1.3	-1.2	-1.7	-1.1	-2.1	-1.4	1.1	1.1	-1.2	1.2	-1.0	-1.2
NM_018433.3	*SIRT1*			2.1	1.1	-1.2	1.9	1.0	-2.6	1.1	-1.1	-1.1	-1.1	1.1	1.1	1.1	-1.2	-1.4	1.1	1.0	-1.4
NM_012238.3	*VHL*			1.1	-1.2	-1.1	1.4	-1.4	-2.4	-1.0	-1.1	-1.0	1.0	-1.0	-1.2	-1.7	-1.1	-1.2	-1.3	-1.0	-1.0

Table 61. Absolute fold changes of genes deregulated at least 2-fold compared to the time matched vehicle treated control in primary human hepatocytes from three different donors treated with 0.7 or 7 µM cyclosporine A (CsA) for 1, 3 or 14 days. The categorisation of the genes into IPA® tox functions was evaluated manually which is indicated as the additional "function" category. The genes are in alphabetic order within each IPA® tox function and full gene names are given in Table 63.

RefSeq	Symbol	IPA® Tox function	Function	Donor 1						Donor 2						Donor 3					
				0.7 µM CsA			7 µM CsA			0.7 µM CsA			7 µM CsA			0.7 µM CsA			7 µM CsA		
				d01	d03	d14	d01	d03	d14	d01	d03	d14	d01	d03	d14	d01	d03	d14	d01	d03	d14
NM_018850.2	*ABCB4*	Liver Hyperplasia/ Hyperproliferation	Fatty acid and lipid metabolism	1.0	-1.2	-1.4	-1.0	-1.8	-1.0	1.0	-1.4	1.3	-1.2	-1.9	1.1	1.1	-1.3	-	-1.8	-2.2	-
NM_000668.3	*ADH1B*			-1.1	1.5	1.7	1.0	-5.9	10.4	-1.6	1.0	1.3	-1.4	1.2	2.7	1.5	-1.2	-	-1.2	1.2	-
NM_000669.3	*ADH1C*			1.1	1.2	1.7	-1.1	-4.3	9.7	-1.0	-1.2	1.0	-1.3	-1.2	1.9	1.8	1.2	-	1.1	1.1	-
NM_052968.3	*APOA5*			1.5	2.5	-1.3	2.5	1.9	4.7	1.0	1.3	1.6	1.6	-1.2	1.7	3.1	-1.2	-	1.3	-1.2	-
NM_006684.2	*CFHR4*			1.3	-1.5	1.1	1.3	-2.5	1.4	1.4	-1.1	1.5	1.4	1.0	1.2	-1.3	1.0	-	-1.0	1.2	-
NM_000271.3	*NPC1*			-1.2	-1.2	-1.4	-1.0	1.3	-3.1	-1.4	-1.4	1.0	-1.7	1.1	-1.1	-1.2	-1.0	-	1.0	-1.1	-
NM_002979.3	*SCP2*			1.0	-2.4	1.4	-1.1	-4.2	1.4	-1.0	-1.1	-1.0	-1.1	1.0	1.0	-1.0	-1.3	-	-1.4	1.0	-
NM_000035.2	*ALDOB*		Carbohydrate metabolism	-1.3	1.2	1.2	-1.4	-1.0	2.5	1.0	1.1	-1.0	-1.1	-1.2	-1.0	1.1	1.0	-	-1.2	1.2	-
NM_001249.1	*ENTPD5*			-1.0	-1.4	1.1	-1.4	-1.6	3.3	1.1	1.4	-1.3	-1.4	1.2	-1.0	1.7	-1.1	-	-1.1	-1.1	-
NM_002612.3	*PDK4*			1.4	1.6	-1.7	3.0	-1.8	3.2	1.1	1.1	-1.7	-1.0	1.0	-1.1	2.8	-1.8	-	1.2	-1.8	-
NM_000291.2	*PGK1*			-1.2	-1.2	-1.5	-1.2	-1.2	-2.5	-1.2	1.1	1.0	-1.0	-1.1	-1.2	-1.5	-1.2	-	-1.1	-1.1	-
NM_005398.4	*PPP1R3C*			-1.2	-1.1	-1.3	-1.4	-1.2	3.1	1.0	1.2	1.4	-1.2	1.1	1.7	2.1	1.4	-	1.2	1.7	-
NM_003742.2	*ABCB11*		Bile acid metabolism	-1.0	1.1	1.0	-1.0	-1.3	2.5	1.3	1.4	1.5	1.5	1.4	3.3	-1.0	-1.0	-	-1.4	1.2	-
XM_943415.1	*AKR1C2*			1.1	-1.3	1.0	1.1	-1.0	-1.0	-1.3	-2.5	-1.2	-1.2	-3.3	-1.3	-1.1	-1.1	-	-1.2	-1.2	-
NM_005989.2	*AKR1D1*			1.2	-1.1	-1.3	-1.3	-2.6	-1.0	1.2	1.1	-1.4	-1.3	-1.0	1.0	-1.3	1.0	-	-1.1	1.3	-
NM_003049.2	*SLC10A1*			-2.0	-1.4	1.5	-5.2	-2.6	10.3	-1.0	1.1	-1.4	-1.7	-1.3	1.3	2.6	-1.1	-	-1.7	-1.3	-
NM_006446.3	*SLCO1B1*			1.2	-1.1	1.1	1.3	-1.3	3.0	-1.2	1.2	-1.8	-1.5	1.4	1.0	1.6	-1.2	-	1.4	1.0	-
NM_019844.2	*SLCO1B3*			2.8	1.3	1.1	3.0	1.6	1.1	-1.1	1.0	1.3	-1.4	1.3	2.8	1.5	1.0	-	1.1	1.3	-
NM_001171.3	*ABCC6*		Xenobiotic metabolism	-2.0	-2.2	-1.2	-2.3	-2.1	-1.4	-1.1	-1.4	-1.1	-1.3	-1.3	-1.2	-1.0	-1.1	-	-1.6	-1.4	-
NM_004364.2	*CEBPA*			-1.4	1.0	1.3	-1.0	-1.2	4.4	1.1	-1.1	-1.1	-1.3	-1.1	1.4	1.9	1.1	-	1.1	-1.1	-
NM_000499.2	*CYP1A1*			1.2	2.2	1.2	-1.1	-1.0	6.6	6.8	2.6	2.8	5.0	3.3	3.3	2.8	1.8	-	1.5	6.0	-
NM_000771.2	*CYP2C9*			-1.5	-1.1	1.4	-2.1	-1.7	2.4	1.1	1.2	1.2	-1.1	1.8	1.1	1.4	-1.2	-	1.1	1.2	-
NM_000561.2	*GSTM1*			-1.5	-2.2	1.6	-2.2	-4.7	5.2	-1.1	-1.0	1.1	-1.6	-1.0	1.3	1.2	-1.5	-	-1.8	-1.1	-
NM_003725.2	*HSD17B6*			-1.4	1.1	2.0	-1.3	-1.4	2.4	1.1	1.1	1.2	1.3	1.5	1.8	1.5	1.0	-	1.4	1.3	-
NM_006169.2	*NNMT*			-1.1	1.2	-1.0	-1.0	-1.4	-2.1	1.1	1.3	1.0	1.1	1.4	-1.8	-2.4	1.7	-	-1.1	1.1	-
NM_001077475.1	*NR1I3*			-1.4	-1.1	1.3	-2.2	-1.6	7.4	-1.1	1.3	1.1	-1.2	1.1	2.1	1.1	-1.3	-	-1.7	1.1	-

Table 61 (continued)

RefSeq	Symbol	IPA® Tox function	Function	Donor 1						Donor 2						Donor 3					
				0.7 µM CsA			7 µM CsA			0.7 µM CsA			7 µM CsA			0.7 µM CsA			7 µM CsA		
				d01	d03	d14	d01	d03	d14	d01	d03	d14	d01	d03	d14	d01	d03	d14	d01	d03	d14
NM_003708.3	*RDH16*			-1.2	1.3	1.9	-1.4	-1.9	11.8	1.4	1.0	1.5	1.5	1.8	2.0	1.4	-1.0	-	1.5	1.5	-
NM_003057.2	*SLC22A1*			-2.1	-1.2	1.3	-3.4	-1.6	2.1	-1.0	-1.2	-1.2	-1.5	-1.2	1.8	1.4	1.0	-	-1.9	1.3	-
NM_018242.2	*SLC47A1*			-1.6	1.1	1.2	-1.8	-1.8	1.7	-1.1	1.1	1.7	-1.3	1.3	2.2	1.2	-1.0	-	-1.2	1.2	-
NM_000463.2	*UGT1A1*		Xenobiotic metabolsim	-1.1	-1.5	1.5	-1.9	-1.4	2.8	1.2	1.5	1.3	1.0	1.5	1.9	1.4	1.2	-	-1.2	1.4	-
NM_007120.2	*UGT1A4*			1.6	-1.7	1.5	1.1	-1.1	4.0	1.2	1.2	-1.0	1.1	1.5	1.8	1.1	1.0	-	1.1	1.9	-
NM_001072.3	*UGT1A6*			1.0	-1.9	-1.1	-1.4	-1.1	1.7	-1.2	-1.1	-1.1	1.0	-1.1	2.0	1.1	-1.0	-	1.0	-1.0	-
NM_019075.2	*UGT1A9*			1.1	-2.6	1.7	-1.3	-1.3	6.6	1.0	1.3	-1.2	-1.0	1.8	2.6	1.5	1.1	-	-1.0	1.7	-
NM_019075.2	*UGT1A9*			1.1	-2.6	1.7	-1.3	-1.3	6.6	1.0	1.3	-1.2	-1.0	1.8	2.6	1.5	1.1	-	-1.0	1.7	-
NM_006988.3	*ADAMTS1*			-1.2	-1.0	-1.5	-1.3	-1.3	-3.0	1.1	-1.5	1.1	-1.2	1.0	-3.3	-2.3	-1.1	-	-1.5	-1.2	-
NM_001679.2	*ATP1B3*			-1.0	-1.5	-1.2	-1.2	-1.2	-2.0	-1.3	-1.2	-1.2	-1.6	-1.1	-1.9	-1.1	-1.2	-	1.0	-1.6	-
NM_002982.3	*CCL2*			-1.5	-2.1	-1.0	-2.2	-2.3	-3.1	1.3	1.0	-1.4	-1.2	-1.7	-2.7	-3.3	1.1	-	-1.3	-1.8	-
NM_032607.1	*CREB3L3*			1.6	1.7	-1.2	2.5	-1.1	-2.8	1.1	-1.1	1.1	1.7	-1.6	-2.6	-3.9	1.1	-	-1.4	1.1	-
NM_000567.2	*CRP*	Liver Hyper-plasia/ Hyper-proliferation		-1.2	-1.1	1.0	-1.0	-3.4	-1.7	1.0	-1.2	-1.2	1.1	1.1	-1.8	-1.9	2.0	-	-1.0	1.2	-
NM_005211.2	*CSF1R*			-1.3	-1.3	-1.4	-1.7	-4.6	-1.4	1.1	1.1	-1.1	-1.0	-1.3	-1.5	-1.1	1.1	-	-1.1	-1.1	-
NM_002218.3	*ITIH4*		In-flammation	-1.3	-1.2	-1.4	-1.6	-2.3	-1.7	-1.0	1.1	1.1	-1.6	-1.4	-1.6	-1.2	1.0	-	-1.3	-1.3	-
NM_000893.2	*KNG1*			-1.6	-1.0	1.3	-2.3	-2.2	1.2	1.0	-1.1	-1.1	-1.1	-1.0	-1.1	1.1	-1.1	-	-1.1	-1.1	-
NM_002341.1	*LTB*			-1.2	-1.3	-2.0	-1.2	-1.9	-8.3	1.0	-1.1	-1.1	-1.7	-1.6	-1.7	-3.5	-1.1	-	-2.1	-1.8	-
NM_000963.1	*PTGS2*			1.0	1.0	-1.7	1.2	-1.1	-9.7	-1.1	-1.2	-1.0	-1.2	-1.2	-1.0	-1.2	-1.2	-	1.0	-1.3	-
NM_003745.1	*SOCS1*			-1.1	-1.4	-1.1	1.0	-1.0	-3.5	1.3	1.1	1.3	1.3	1.5	-1.9	-4.2	1.1	-	-1.3	-1.1	-
NM_003955.3	*SOCS3*			-1.2	1.0	-1.1	-1.3	-1.0	-1.8	1.0	-1.2	-1.2	1.1	-1.0	-1.3	-4.9	1.0	-	-1.0	-1.1	-
NM_004684.2	*SPARCL1*			-1.1	-1.1	-1.4	-1.6	-2.5	1.6	-1.0	1.0	-1.2	-1.3	-1.2	1.5	-1.2	-1.2	-	-1.5	1.1	-
NM_201442.1	*C1S*			-1.3	-1.9	-1.1	-1.6	-2.0	-1.4	-1.1	-1.1	-1.1	-1.2	-1.3	-1.2	-1.2	-1.2	-	-1.4	-1.0	-
NM_000064.2	*C3*			-1.8	-1.5	1.0	-2.1	-2.2	-2.0	1.0	-10.0	-1.4	-1.2	-8.1	-2.0	-2.1	-1.1	-	-1.5	-1.4	-
NM_001737.2	*C9*			2.6	-1.6	1.1	2.7	-4.2	-2.1	-1.1	1.4	-1.1	-1.3	1.6	-1.4	-1.3	1.1	-	1.1	-1.3	-
NM_001001392.1	*CD44*		Immune response	-1.1	-1.2	-1.6	-1.1	1.2	-4.8	-1.4	-1.1	-1.3	-1.6	-1.3	-2.1	-2.6	1.0	-	-1.4	-1.3	-
NM_021023.3	*CFHR3*			-1.0	-2.7	1.2	1.0	-7.3	1.4	-1.1	1.2	1.3	1.1	1.9	-1.0	-1.7	-1.3	-	-1.3	-1.4	-
NM_003665.2	*FCN3*			-1.6	-1.7	-1.1	-2.2	-3.0	-1.5	1.1	-1.3	-2.7	-1.5	-2.8	-10.1	-1.1	1.1	-	-1.7	-1.6	-
NM_000201.1	*ICAM1*			-1.7	-1.4	-1.6	-1.8	1.1	-2.1	-1.0	2.2	-1.2	-1.2	1.5	-1.5	-3.9	1.2	-	-1.8	-1.4	-

Table 61 (continued)

RefSeq	Symbol	IPA® Tox function	Function	Donor 1						Donor 2						Donor 3					
				0.7 µM CsA			7 µM CsA			0.7 µM CsA			7 µM CsA			0.7 µM CsA			7 µM CsA		
				d01	d03	d14	d01	d03	d14	d01	d03	d14	d01	d03	d14	d01	d03	d14	d01	d03	d14
NM_207585.1	*IFNAR2*			-1.2	-1.6	-1.2	1.0	1.0	-2.8	-1.1	-1.3	1.1	-1.2	-1.1	-1.2	-1.6	-1.2	-	-1.4	-1.4	-
NM_000600.1	*IL6*			-1.1	-1.0	-1.4	-1.1	-1.1	-6.6	-1.0	-1.1	1.2	1.1	1.1	-1.4	-2.8	1.1	-	-1.2	1.1	-
NM_000584.2	*IL8*			-1.2	-1.8	-1.1	-1.7	1.6	-1.5	1.0	1.0	-2.0	-1.5	-1.6	-2.3	-3.6	-1.2	-	-1.2	-2.0	-
NM_003999.1	*OSMR*		Immune response	1.3	-1.1	-1.4	1.3	1.1	-3.1	-1.0	1.1	1.1	1.4	1.1	-1.4	-2.0	1.1	-	1.1	-1.2	-
NM_003120.2	*SPI1*			-1.2	-1.2	-1.2	-1.2	-1.5	-2.1	-1.2	-1.0	-1.3	-1.4	1.1	-1.3	-1.1	-1.2	-	-1.1	-1.3	-
NM_000582.2	*SPP1*			-1.4	-2.8	-2.0	-1.6	-1.9	-2.9	-1.4	-1.4	-2.2	-3.2	-3.4	-5.4	-1.6	1.0	-	-1.4	-1.7	-
NM_003380.2	*VIM*			-1.0	-1.5	-1.5	-1.1	-1.8	-3.2	-1.3	-1.2	-1.4	-1.5	-1.9	-1.8	1.1	-1.1	-	-1.1	-1.4	-
NM_003183.4	*ADAM17*			-1.1	-1.0	-1.3	1.0	1.2	-2.4	-1.1	1.0	-1.2	-1.0	1.1	-1.2	-1.5	-1.1	-	-1.0	1.1	-
NM_001134.1	*AFP*			-1.1	-1.3	1.1	-1.7	-2.6	4.6	1.1	1.3	1.1	1.1	1.1	1.1	2.9	-1.1	-	1.1	-1.3	-
NM_152641.2	*ARID2*			1.1	-1.0	-1.2	1.2	1.0	-2.3	-1.1	-1.1	-1.1	1.0	-1.1	1.1	1.0	1.0	-	1.1	-1.0	-
NM_001166.3	*BIRC2*			1.1	-1.4	-1.2	-1.0	-1.3	-2.1	-1.3	-1.3	1.1	-1.1	-1.3	1.2	-1.2	-1.4	-	1.1	-1.5	-
NM_053056.2	*CCND1*			1.2	-1.3	1.0	-1.2	-1.3	-1.7	1.1	-1.3	-1.0	-1.4	-2.1	1.2	1.1	1.2	-	-1.3	-1.4	-
NM_001024844.1	*CD82*	Liver Hyper-plasia/ Hyper-proliferation		-1.4	-1.0	-1.2	-1.3	-1.4	-2.2	1.0	1.0	1.1	-1.1	1.0	-1.3	-1.4	-1.1	-	-1.7	-1.2	-
NM_004358.3	*CDC25B*			-1.4	1.2	-1.4	-1.6	-1.2	-3.9	-1.5	-1.2	-1.4	-1.7	-1.7	-1.7	-2.3	-1.1	-	-1.5	-1.5	-
NM_176096.1	*CDK5RAP3*			-1.5	-1.0	1.1	-1.5	-1.2	2.2	-1.0	-1.4	-1.1	1.3	-1.5	-1.0	1.1	-1.1	-	-1.1	-1.4	-
NM_012242.2	*DKK1*			1.1	-1.0	-1.1	1.2	1.0	-1.1	-1.1	-1.0	-1.0	-1.0	-1.2	-2.5	1.0	-1.1	-	-1.0	-1.1	-
NM_013352.2	*DSE*			-1.0	1.1	-1.7	1.1	-1.5	-3.0	-1.2	-1.1	1.2	-1.3	-1.1	-1.0	-1.3	-1.0	-	-1.1	-1.1	-
NM_018098.4	*ECT2*		Cancer	2.1	1.2	1.0	1.8	1.3	-5.6	-1.2	-1.1	-1.2	-1.0	-1.2	-1.5	-2.1	1.1	-	-1.3	-1.4	-
NM_001040092.1	*ENPP2*			-1.2	-1.4	-1.1	-1.3	-1.8	1.4	-1.1	-1.4	-1.1	-1.2	-1.8	1.2	2.1	-1.1	-	-1.1	-1.1	-
NM_004448.2	*ERBB2*			-1.5	-1.2	-1.0	-1.5	-1.3	-1.2	1.2	-1.4	-1.1	-1.0	-2.4	-1.1	1.5	-1.1	-	-1.1	-2.2	-
NM_000125.2	*ESR1*			-1.4	-2.4	-1.2	-1.4	-4.5	1.2	1.3	-1.0	-1.1	-1.1	-1.5	-1.3	1.6	-1.0	-	-1.4	-1.7	-
NM_005252.2	*FOS*			1.1	-1.1	1.2	-1.3	2.3	-1.9	1.2	1.0	1.4	-1.1	-1.3	-1.2	-1.8	-1.1	-	-1.9	-1.8	-
NM_033260.3	*FOXQ1*			-1.1	1.0	-1.8	-1.4	1.5	-2.4	1.3	-1.0	1.3	-1.7	1.2	1.0	1.3	-1.0	-	1.0	-1.4	-
NM_001924.2	*GADD45A*			1.0	-1.1	2.1	-1.0	-1.1	4.6	1.2	-1.0	-1.5	-1.1	1.3	-1.5	-1.0	1.0	-	-1.3	-1.1	-
NM_000597.2	*IGFBP2*			-1.8	-2.1	-1.4	-1.9	-1.9	-2.4	-1.4	-1.1	-1.9	-2.1	-2.4	-2.4	-1.4	-1.4	-	-2.3	-3.0	-
NM_000598.4	*IGFBP3*			-1.0	1.2	-1.5	1.3	3.0	-1.6	-1.4	-1.1	-1.2	-1.8	-1.6	-2.6	-1.4	-1.0	-	-1.1	-1.2	-
NM_057159.2	*LPAR1*			1.3	1.0	-1.5	1.2	1.1	-2.4	-1.3	1.0	1.0	-1.1	1.2	-1.1	1.0	-1.2	-	1.1	1.0	-
NM_000245.2	*MET*			2.0	1.3	-1.2	2.2	1.6	-1.9	-1.2	-1.1	-1.1	-1.1	1.1	-1.2	-1.5	-1.3	-	1.0	-1.6	-

Table 61 (continued)

RefSeq	Symbol	IPA® Tox function	Function	Donor 1						Donor 2						Donor 3					
				0.7 µM CsA			7 µM CsA			0.7 µM CsA			7 µM CsA			0.7 µM CsA			7 µM CsA		
				d01	d03	d14	d01	d03	d14	d01	d03	d14	d01	d03	d14	d01	d03	d14	d01	d03	d14
NM_004994.2	*MMP9*			-1.3	-1.6	-1.9	-1.4	-2.8	-8.5	-1.3	-1.0	-1.7	-1.7	-1.8	-4.6	-2.2	-1.1	-	-1.1	-2.4	-
NM_002467.3	*MYC*			-1.1	1.5	1.6	-1.3	1.6	1.4	-1.1	-1.2	-1.4	-1.8	1.1	-2.7	-1.7	-1.0	-	-1.3	1.5	-
NM_006096.2	*NDRG1*			-1.2	1.2	-1.6	1.2	2.3	-1.0	-1.3	1.4	1.1	-1.1	1.3	1.0	2.0	1.2	-	1.2	-1.4	-
NM_153292.1	*NOS2*			1.1	1.0	-6.8	1.3	1.1	-7.1	1.1	1.1	1.1	-1.1	1.0	-1.1	-1.4	1.3	-	-1.4	1.1	-
NM_006206.3	*PDGFRA*			1.2	-1.3	-2.2	1.2	-1.7	-2.8	1.0	-1.1	1.1	-1.0	-1.1	-1.2	-2.0	-1.0	-	-1.5	-1.3	-
NM_006218.2	*PIK3CA*			2.3	-1.1	-1.3	2.4	-1.1	-1.5	-1.1	-1.1	-1.1	1.0	1.0	-1.2	-1.0	-1.0	-	-1.1	1.0	-
NM_052880.3	*PIK3IP1*			-1.7	-1.2	-1.4	-1.6	-2.8	1.3	1.0	-1.0	-1.1	-1.2	-1.2	1.3	-1.2	-1.0	-	-1.6	-1.2	-
NM_001005376.1	*PLAUR*			-1.3	-1.2	-2.0	-1.3	1.1	-4.3	-1.2	1.0	-1.2	-1.5	-1.6	-1.4	-1.4	-1.0	-	-1.2	-1.3	-
NM_000301.1	*PLG*			-1.7	-1.1	1.1	-2.2	-2.3	1.5	1.0	1.1	-1.0	-1.2	1.3	1.5	1.3	-1.0	-	-1.3	1.1	-
NM_002763.3	*PROX1*			1.6	-1.7	-1.3	1.9	-2.2	-1.7	1.0	1.1	1.1	-1.3	-1.0	1.0	-1.3	1.0	-	-1.1	-1.3	-
NM_000964.2	*RARA*			-1.4	-1.1	1.0	-1.2	-1.1	-2.3	-1.1	-1.1	-1.1	-1.1	-1.3	-1.2	1.0	-1.1	-	-1.1	-1.6	-
NM_019554.2	*S100A4*		Cancer	-1.4	-1.5	-1.0	-1.6	-2.7	-2.1	-1.0	1.1	-1.1	-1.1	-1.0	1.0	1.3	-1.1	-	-1.1	-1.1	-
NM_003107.2	*SOX4*	Liver Hyper-plasia/ Hyper-proliferation		-1.4	-1.3	-1.1	-2.7	-1.2	-1.7	-1.3	-1.1	-1.5	-1.9	-1.1	-1.9	1.3	-1.1	-	-1.4	-1.5	-
NM_003118.2	*SPARC*			-1.4	-1.4	-1.6	-1.6	-2.6	-2.4	-1.2	-1.1	-1.0	-1.9	-1.9	-2.1	-1.1	1.1	-	-1.4	-1.3	-
NM_139276.2	*STAT3*			-1.3	-1.3	-1.5	-1.3	-1.4	-2.0	1.0	-1.1	1.1	-1.0	1.0	-1.1	-1.8	1.1	-	-1.3	-1.4	-
NM_002353.1	*TACSTD2*			-1.2	-1.1	-1.2	-1.9	1.2	-4.0	1.0	-1.3	-2.0	1.0	-2.4	-3.7	-1.2	-1.0	-	-1.3	-2.0	-
NM_005651.1	*TDO2*			-1.5	-2.2	-1.4	-2.8	-3.2	1.3	-1.1	-1.1	1.0	-1.6	-1.4	-1.1	-1.4	-1.1	-	-1.4	-1.0	-
NM_014220.2	*TM4SF1*			-1.2	-1.2	-1.3	-1.5	-1.0	-3.5	1.1	-1.0	-1.3	-1.0	-2.5	-2.7	-1.2	-1.1	-	-1.7	-2.0	-
NM_000594.2	*TNF*			-1.1	-1.2	1.1	-1.1	1.0	-4.1	1.2	-1.2	1.1	1.0	-1.3	1.1	-1.7	1.1	-	-1.5	-1.2	-
NM_003810.2	*TNFSF10*			-1.4	-1.8	-1.5	-1.6	-2.9	-4.0	1.1	-1.1	-1.0	-1.0	-2.0	1.2	-2.2	-1.3	-	-1.7	-2.7	-
NM_030912.2	*TRIM8*			-1.6	-1.1	-1.1	-1.9	-1.3	-2.2	-1.0	1.2	1.1	-1.4	-1.0	-1.3	-2.0	1.1	-	-1.5	-1.2	-
NM_005429.2	*VEGFC*			1.2	-1.1	-1.5	1.2	-1.3	-2.5	-1.1	-1.1	1.0	1.1	-1.2	-1.3	-1.2	1.1	-	-1.2	1.0	-
NM_152415.1	*VPS37A*			2.0	1.1	-1.5	2.4	1.4	1.6	-1.2	-1.1	1.1	-1.2	1.3	1.1	-1.2	1.1	-	1.3	1.3	-
NM_001614.2	*ACTG1*			-1.3	-2.0	1.1	-2.1	1.1	-1.0	-1.0	1.0	-1.1	-1.1	1.1	-1.1	1.0	1.0	-	-1.0	-1.3	-
NM_033257.2	*DGCR6L*			-1.1	1.5	1.1	-1.1	1.0	2.2	-1.0	1.3	1.1	1.1	1.3	-1.0	1.4	-1.1	-	1.0	1.5	-
NM_014800.9	*ELMO1*		ECM organisation	-1.4	-1.5	-1.1	-2.0	-1.4	-1.3	-1.1	-1.1	-1.1	-1.0	-1.6	1.1	-1.1	-1.2	-	-1.0	-1.4	-
NM_006633.2	*IQGAP2*			-1.6	1.2	1.0	-1.9	-1.5	2.2	-1.1	1.0	-1.1	-1.1	1.1	-1.5	1.5	-1.1	-	-1.1	1.0	-
NM_052972.2	*LRG1*			-1.5	-1.3	1.5	-2.1	-2.3	-1.2	1.3	1.4	1.3	1.5	1.1	-1.5	-2.1	1.3	-	-1.2	1.0	-

Table 61 (continued)

RefSeq	Symbol	IPA® Tox function	Function	Donor 1						Donor 2						Donor 3					
				0.7 µM CsA			7 µM CsA			0.7 µM CsA			7 µM CsA			0.7 µM CsA			7 µM CsA		
				d01	d03	d14	d01	d03	d14	d01	d03	d14	d01	d03	d14	d01	d03	d14	d01	d03	d14
NM_018454.5	*NUSAP1*		ECM organisation	-1.0	-1.2	-1.2	-1.1	-1.6	-2.0	-1.3	-1.0	-1.4	-1.2	-1.4	-1.4	-2.4	1.0	-	-1.7	-1.3	-
NM_003255.4	*TIMP2*			-1.9	-1.2	-1.5	-2.0	-1.5	-1.6	-1.2	-1.4	-1.6	-1.3	-1.7	-2.2	1.1	-1.1	-	-1.1	-1.4	-
NM_012385.1	*NUPR1*		Xenobiotic response	-1.3	1.3	-1.3	-1.6	1.0	2.9	1.0	1.1	1.1	-1.1	1.7	-1.1	1.1	1.3	-	-1.2	1.4	-
NM_012238.3	*SIRT1*			1.9	1.5	-1.3	2.2	1.1	-1.3	-1.4	-1.0	1.6	-1.4	1.2	1.4	-1.1	-1.0	-	1.0	1.1	-
NM_006472.2	*TXNIP*			1.3	2.0	-1.3	2.7	1.0	-2.5	1.2	-1.3	1.2	1.4	-1.8	-1.4	1.2	1.0	-	1.2	-1.1	-
NM_001011645.1	*AR*	Liver Hyper-plasia/ Hyper-proliferation	Other and unknown functions	-1.4	-1.1	1.3	-1.2	-2.0	1.7	1.1	-1.1	1.0	1.2	-1.2	1.4	2.2	1.1	-	1.3	1.3	-
NM_001497.2	*B4GALT1*			1.3	-1.0	-1.4	1.4	-1.1	-1.6	-1.2	-1.1	-1.3	-1.1	1.1	-2.1	-1.5	1.0	-	-1.4	-1.4	-
NM_001713.1	*BHMT*			-1.8	-1.5	-1.1	-3.9	-3.6	16.6	-1.2	1.1	1.0	-1.7	-1.3	1.6	4.5	-1.3	-	-1.3	1.0	-
NM_014670.2	*BZW1*			2.3	-1.4	-1.2	2.3	-1.2	-1.2	-1.2	-1.1	-1.1	-1.2	1.1	-1.0	-1.0	-1.4	-	1.2	-1.1	-
NM_032649.5	*CNDP1*			1.0	1.2	-1.0	-1.1	1.1	-3.2	1.2	1.2	1.1	-1.6	1.2	1.3	1.3	1.3	-	1.0	1.7	-
NM_000096.1	*CP*			1.3	-2.1	1.0	1.1	-1.6	-1.9	-1.2	1.1	1.1	-1.2	1.2	-1.1	-1.6	1.1	-	-1.4	-1.3	-
NM_024324.2	*CRELD2*			-1.9	2.2	1.3	-1.2	1.5	2.0	1.0	-1.0	1.1	3.1	-1.4	1.2	-1.2	-1.0	-	1.5	1.3	-
NM_001356.3	*DDX3X*			1.2	-1.0	1.0	1.3	-1.0	-2.5	-1.0	-1.1	-1.0	-1.1	1.2	1.1	-1.4	1.0	-	-1.1	1.0	-
NM_001412.3	*EIF1AX*			2.2	-1.2	1.0	2.2	1.0	-1.2	-1.0	-1.1	-1.2	-1.1	-1.1	-1.1	-1.0	-1.2	-	1.1	-1.3	-
NM_000137.1	*FAH*			-1.6	-1.2	1.0	-2.0	-1.7	2.1	-1.1	1.1	-1.1	-1.3	-1.1	-1.9	1.4	1.1	-	-1.0	-1.0	-
NM_030919.2	*FAM83D*			-1.0	-1.6	1.2	-1.2	-2.2	1.1	1.2	-1.1	-1.4	-1.1	-1.4	1.0	-1.5	-1.3	-	-1.5	-1.4	-
NM_000508.3	*FGA*			-1.6	-1.4	-1.0	-1.6	-5.4	-1.2	-1.6	-1.2	-1.1	-1.8	-1.1	-2.6	-2.0	-1.3	-	-1.5	-2.2	-
NM_000166.4	*GJB1*			-1.5	-1.0	1.1	-1.9	-1.5	3.5	-1.1	1.1	1.1	-1.1	1.1	-1.2	1.5	-1.2	-	-1.0	-1.2	-
NM_018960.4	*GNMT*			-2.1	1.0	1.8	-2.2	-4.3	7.3	-1.1	1.2	1.5	-1.5	1.2	1.7	1.2	1.0	-	-1.2	1.7	-
NM_021175.2	*HAMP*			-1.2	-1.5	1.2	-1.5	-7.9	-1.4	1.5	1.1	1.9	2.5	1.9	-3.0	-3.0	-1.1	-	-1.2	-1.3	-
NM_001530.2	*HIF1A*			2.4	-2.3	-1.4	1.8	-1.9	-4.6	-1.1	-1.4	-1.3	-1.4	-1.1	-1.5	-2.5	-1.4	-	-1.2	-1.7	-
NM_002150.2	*HPD*			-1.2	1.0	1.3	-1.7	-1.2	2.8	1.0	1.3	-1.3	-1.4	1.0	1.0	1.2	1.3	-	-1.5	1.2	-
NM_005347.2	*HSPA5*			-3.6	1.7	-1.1	-2.3	-1.2	1.8	-1.1	1.1	1.2	1.7	1.5	1.6	-1.1	1.3	-	1.2	1.5	-
NM_002205.2	*ITGA5*			-1.4	1.1	-1.6	-1.4	1.7	-2.3	1.0	-1.2	-1.1	-1.0	-2.1	-2.2	-1.0	1.2	-	1.0	-1.3	-
NM_002302.2	*LECT2*			-2.0	-5.4	-1.6	-2.4	-11.7	-1.7	1.6	1.0	-1.0	-1.5	-1.1	-1.3	1.4	-1.2	-	1.0	-2.0	-
NM_000240.2	*MAOA*			-1.1	1.3	1.3	-1.2	-1.2	4.8	1.1	1.1	1.0	-1.1	1.0	1.1	1.3	1.2	-	1.1	1.4	-
NM_005911.4	*MAT2A*			-1.2	1.2	2.1	-1.9	1.0	-2.2	1.1	-1.1	-1.3	1.1	-1.3	-2.1	-1.1	1.1	-	-1.6	-1.4	-
NM_002447.2	*MST1R*			-1.1	1.0	-1.4	-1.3	1.7	-3.2	1.0	-1.0	1.3	1.1	-1.4	1.3	1.0	-1.1	-	1.0	-1.3	-

Table 61 (continued)

RefSeq	Symbol	IPA® Tox function	Function	Donor 1						Donor 2						Donor 3					
				0.7 µM CsA			7 µM CsA			0.7 µM CsA			7 µM CsA			0.7 µM CsA			7 µM CsA		
				d01	d03	d14	d01	d03	d14	d01	d03	d14	d01	d03	d14	d01	d03	d14	d01	d03	d14
NM_003998.2	*NFKB1*			-1.3	-1.2	-1.3	-1.8	1.2	-2.7	1.0	-1.1	-1.2	1.0	-1.2	-1.2	-1.4	1.1	-	-1.3	-1.0	-
NM_052890.3	*PGLYRP2*			-1.3	-1.6	1.3	-1.6	-3.5	1.5	-1.1	1.3	-1.1	-1.7	-1.0	-1.1	1.2	1.2	-	-2.3	1.0	-
NM_006623.2	*PHGDH*			-1.0	2.5	1.3	-1.4	1.9	3.0	1.0	1.0	1.3	-1.1	1.1	1.8	1.6	1.6	-	1.2	2.3	-
NM_006813.1	*PNRC1*			1.1	1.0	-1.1	1.1	1.1	-2.9	1.1	1.1	-1.1	-1.3	1.1	-1.4	-1.9	-1.0	-	-1.2	-1.0	-
NM_002692.2	*POLE2*			1.1	1.3	-1.1	1.3	1.4	2.0	1.0	1.1	1.2	1.6	1.3	1.3	1.3	-1.0	-	1.9	1.3	-
NM_002693.1	*POLG*			-1.3	-1.0	-1.4	-1.4	1.2	-2.6	-1.1	-1.2	-1.2	-1.1	-1.3	-1.1	-1.1	1.1	-	-1.3	1.3	-
NM_000941.2	*POR*			-1.2	1.2	-1.1	-1.2	1.2	2.1	-1.1	1.0	-1.2	-1.1	1.2	-1.0	1.2	1.1	-	-1.2	1.1	-
NM_000021.2	*PSEN1*			1.5	-1.2	-1.4	1.2	1.2	-2.0	-1.0	-1.1	-1.4	1.2	-1.0	1.0	-1.3	-1.0	-	-1.3	-1.2	-
NM_002800.4	*PSMB9*			-1.5	-1.3	-1.4	-1.6	-1.1	-3.0	-1.2	1.0	-1.1	-1.4	-1.5	-1.1	-2.8	-1.2	-	-2.0	-1.3	-
NM_021975.2	*RELA*			-1.6	-1.2	-2.1	-1.7	-1.0	-2.0	-1.2	1.2	-1.0	-1.1	1.1	1.2	-1.3	-1.1	-	-1.2	-1.0	-
NM_006509.2	*RELB*	Liver Hyper-plasia/ Hyper-proliferation	Other and unknown functions	-1.2	-1.4	-1.0	-1.2	1.1	-2.2	-1.1	-1.3	-1.3	-1.6	-1.7	-1.3	-2.7	-1.0	-	-1.6	-1.4	-
NM_152703.2	*SAMD9L*			1.5	1.1	-1.8	1.3	1.2	-3.3	1.0	-1.1	-1.1	1.2	-1.5	1.0	-1.4	-1.0	-	-1.5	-1.2	-
NM_001002236.1	*SERPINA1*			-1.0	-1.2	-1.4	-1.1	-1.3	-1.6	-1.0	-1.0	-1.2	-1.1	1.0	-2.4	-1.4	-1.2	-	-1.2	-1.2	-
NM_001756.3	*SERPINA6*			-1.7	-1.5	1.1	-2.4	-3.5	1.4	-1.0	1.2	1.3	-1.3	1.3	1.2	1.0	-1.1	-	-1.3	-1.3	-
NM_000602.1	*SERPINE1*			-1.6	-1.2	-1.4	-2.6	1.9	-1.8	-1.3	-1.3	1.3	-1.4	-1.6	1.3	-1.5	1.2	-	-1.8	-1.4	-
NM_080866.2	*SLC22A9*			-1.5	-1.7	1.3	-1.9	-2.0	2.8	1.1	1.3	1.1	-1.4	-1.0	1.1	1.4	1.1	-	-1.1	1.0	-
NM_018389.3	*SLC35C1*			-1.4	1.2	1.1	-1.2	1.3	-2.4	1.0	-1.3	-1.1	1.2	-1.4	-1.7	-2.1	1.2	-	1.0	-1.2	-
NM_000346.2	*SOX9*			-1.7	-1.1	-1.7	-1.6	1.2	-3.4	1.1	-1.1	-1.1	-1.5	1.2	-1.2	-1.2	1.0	-	-1.1	1.5	-
NM_006288.2	*THY1*			-1.4	-1.4	-1.5	-1.7	-3.0	-2.5	-1.1	-1.1	-1.2	-1.7	-1.6	-2.8	-1.0	1.1	-	-1.2	-1.0	-
NM_001068.2	*TOP2B*			-1.3	1.1	-1.1	-1.3	-1.0	-2.1	-1.1	-1.2	-1.0	-1.1	-1.2	1.0	1.1	1.2	-	1.0	-1.1	-
NM_001113756.1	*TYMP*			-1.9	-1.4	-1.4	-1.9	1.5	-3.6	-1.1	1.3	-1.1	-1.4	1.3	-1.2	-2.0	-1.1	-	-1.4	-1.6	-
NM_004181.3	*UCHL1*			1.1	1.6	1.0	1.7	2.4	1.6	-1.0	1.2	-1.4	1.1	1.1	-1.8	1.1	1.0	-	1.3	-1.2	-
NM_012479.2	*YWHAG*			1.9	-1.1	-1.1	2.2	1.0	-1.5	-1.2	1.0	-1.2	-1.3	1.2	-1.4	-1.1	-1.1	-	1.0	-1.3	-
NM_000668.3	*ADH1B*	Hepato-cellular Carcinoma	Fatty acid and lipid metabolism	-1.1	1.5	1.7	1.0	-5.9	10.4	-1.6	1.0	1.3	-1.4	1.2	2.7	1.5	-1.2	-	-1.2	1.2	-
NM_000669.3	*ADH1C*			1.1	1.2	1.7	-1.1	-4.3	9.7	-1.0	-1.2	1.0	-1.3	-1.2	1.9	1.8	1.2	-	1.1	1.1	-
NM_003742.2	*ABCB11*		Bile acid metabolism	-1.0	1.1	1.0	-1.0	-1.3	2.5	1.3	1.4	1.5	1.5	1.4	3.3	-1.0	-1.0	-	-1.4	1.2	-
NM_005989.2	*AKR1D1*			1.2	-1.1	-1.3	-1.3	-2.6	-1.0	1.2	1.1	-1.4	-1.3	-1.0	1.0	-1.3	1.0	-	-1.1	1.3	-
NM_003049.2	*SLC10A1*			-2.0	-1.4	1.5	-5.2	-2.6	10.3	-1.0	1.1	-1.4	-1.7	-1.3	1.3	2.6	-1.1	-	-1.7	-1.3	-

Table 61 (continued)

RefSeq	Symbol	IPA® Tox function	Function	Donor 1						Donor 2						Donor 3					
				0.7 µM CsA			7 µM CsA			0.7 µM CsA			7 µM CsA			0.7 µM CsA			7 µM CsA		
				d01	d03	d14	d01	d03	d14	d01	d03	d14	d01	d03	d14	d01	d03	d14	d01	d03	d14
NM_006446.3	*SLCO1B1*		Bile acid metabolism	1.2	-1.1	1.1	1.3	-1.3	3.0	-1.2	1.2	-1.8	-1.5	1.4	1.0	1.6	-1.2	-	1.4	1.0	-
NM_019844.2	*SLCO1B3*			2.8	1.3	1.1	3.0	1.6	1.1	-1.1	1.0	1.3	-1.4	1.3	2.8	1.5	1.0	-	1.1	1.3	-
NM_001249.1	*ENTPD5*		Carbo-hydrate metabolism	-1.0	-1.4	1.1	-1.4	-1.6	3.3	1.1	1.4	-1.3	-1.4	1.2	-1.0	1.7	-1.1	-	-1.1	-1.1	-
NM_002612.3	*PDK4*			1.4	1.6	-1.7	3.0	-1.8	3.2	1.1	1.1	-1.7	-1.0	1.0	-1.1	2.8	-1.8	-	1.2	-1.8	-
NM_000291.2	*PGK1*			-1.2	-1.2	-1.5	-1.2	-1.2	-2.5	-1.2	1.1	1.0	-1.0	-1.1	-1.2	-1.5	-1.2	-	-1.1	-1.1	-
NM_003183.4	*ADAM17*			-1.1	-1.0	-1.3	1.0	1.2	-2.4	-1.1	1.0	-1.2	-1.0	1.1	-1.2	-1.5	-1.1	-	-1.0	1.1	-
NM_001134.1	*AFP*			-1.1	-1.3	1.1	-1.7	-2.6	4.6	1.1	1.3	1.1	1.1	1.1	1.1	2.9	-1.1	-	1.1	-1.3	-
NM_152641.2	*ARID2*			1.1	-1.0	-1.2	1.2	1.0	-2.3	-1.1	-1.1	-1.1	1.0	-1.1	1.1	1.0	1.0	-	1.1	-1.0	-
NM_001166.3	*BIRC2*			1.1	-1.4	-1.2	-1.0	-1.3	-2.1	-1.3	-1.3	1.1	-1.1	-1.3	1.2	-1.2	-1.4	-	1.1	-1.5	-
NM_001024844.1	*CD82*			-1.4	-1.0	-1.2	-1.3	-1.4	-2.2	1.0	1.0	1.1	-1.1	1.0	-1.3	-1.4	-1.1	-	-1.7	-1.2	-
NM_004358.3	*CDC25B*			-1.4	1.2	-1.4	-1.6	-1.2	-3.9	-1.5	-1.2	-1.4	-1.7	-1.7	-1.7	-2.3	-1.1	-	-1.5	-1.5	-
NM_176096.1	*CDK5RAP3*			-1.5	-1.0	1.1	-1.5	-1.2	2.2	-1.0	-1.4	-1.1	1.3	-1.5	-1.0	1.1	-1.1	-	-1.1	-1.4	-
NM_012242.2	*DKK1*			1.1	-1.0	-1.1	1.2	1.0	-1.1	-1.1	-1.0	-1.0	-1.0	-1.2	-2.5	1.0	-1.1	-	-1.0	-1.1	-
NM_013352.2	*DSE*	Hepato-cellular Carcinoma		-1.0	1.1	-1.7	1.1	-1.5	-3.0	-1.2	-1.1	1.2	-1.3	-1.1	-1.0	-1.3	-1.0	-	-1.1	-1.1	-
NM_018098.4	*ECT2*			2.1	1.2	1.0	1.8	1.3	-5.6	-1.2	-1.1	-1.2	-1.0	-1.2	-1.5	-2.1	1.1	-	-1.3	-1.4	-
NM_001040092.1	*ENPP2*			-1.2	-1.4	-1.1	-1.3	-1.8	1.4	-1.1	-1.4	-1.1	-1.2	-1.8	1.2	2.1	-1.1	-	-1.1	-1.1	-
NM_000125.2	*ESR1*		Cancer	-1.4	-2.4	-1.2	-1.4	-4.5	1.2	1.3	-1.0	-1.1	-1.1	-1.5	-1.3	1.6	-1.0	-	-1.4	-1.7	-
NM_033260.3	*FOXQ1*			-1.1	1.0	-1.8	-1.4	1.5	-2.4	1.3	-1.0	1.3	-1.7	1.2	1.0	1.3	-1.0	-	1.0	-1.4	-
NM_000598.4	*IGFBP3*			-1.0	1.2	-1.5	1.3	3.0	-1.6	-1.4	-1.1	-1.2	-1.8	-1.6	-2.6	-1.4	-1.0	-	-1.1	-1.2	-
NM_057159.2	*LPAR1*			1.3	1.0	-1.5	1.2	1.1	-2.4	-1.3	1.0	1.0	-1.1	1.2	-1.1	1.0	-1.2	-	1.1	1.0	-
NM_000245.2	*MET*			2.0	1.3	-1.2	2.2	1.6	-1.9	-1.2	-1.1	-1.1	-1.1	1.1	-1.2	-1.5	-1.3	-	1.0	-1.6	-
NM_004994.2	*MMP9*			-1.3	-1.6	-1.9	-1.4	-2.8	-8.5	-1.3	-1.0	-1.7	-1.7	-1.8	-4.6	-2.2	-1.1	-	-1.1	-2.4	-
NM_002467.3	*MYC*			-1.1	1.5	1.6	-1.3	1.6	1.4	-1.1	-1.2	-1.4	-1.8	1.1	-2.7	-1.7	-1.0	-	-1.3	1.5	-
NM_153292.1	*NOS2*			1.1	1.0	-6.8	1.3	1.1	-7.1	1.1	1.1	1.1	-1.1	1.0	-1.1	-1.4	1.3	-	-1.4	1.1	-
NM_006206.3	*PDGFRA*			1.2	-1.3	-2.2	1.2	-1.7	-2.8	1.0	-1.1	1.1	-1.0	-1.1	-1.2	-2.0	-1.0	-	-1.5	-1.3	-
NM_006218.2	*PIK3CA*			2.3	-1.1	-1.3	2.4	-1.1	-1.5	-1.1	-1.1	-1.1	1.0	1.0	-1.2	-1.0	-1.0	-	-1.1	1.0	-
NM_001005376.1	*PLAUR*			-1.3	-1.2	-2.0	-1.3	1.1	-4.3	-1.2	1.0	-1.2	-1.5	-1.6	-1.4	-1.4	-1.0	-	-1.2	-1.3	-
NM_000964.2	*RARA*			-1.4	-1.1	1.0	-1.2	-1.1	-2.3	-1.1	-1.1	-1.1	-1.1	-1.3	-1.2	1.0	-1.1	-	-1.1	-1.6	-

Table 61 (continued)

RefSeq	Symbol	IPA® Tox function	Function	Donor 1						Donor 2						Donor 3					
				0.7 µM CsA			7 µM CsA			0.7 µM CsA			7 µM CsA			0.7 µM CsA			7 µM CsA		
				d01	d03	d14	d01	d03	d14	d01	d03	d14	d01	d03	d14	d01	d03	d14	d01	d03	d14
NM_019554.2	*S100A4*	Hepato-cellular Carcinoma	Cancer	-1.4	-1.5	-1.0	-1.6	-2.7	-2.1	-1.0	1.1	-1.1	-1.1	-1.0	1.0	1.3	-1.1	-	-1.1	-1.1	-
NM_213662.1	*STAT3*			-1.3	-1.3	-1.5	-1.3	-1.4	-2.0	1.0	-1.1	1.1	-1.0	1.0	-1.1	-1.8	1.1	-	-1.3	-1.4	-
NM_014220.2	*TM4SF1*			-1.2	-1.2	-1.3	-1.5	-1.0	-3.5	1.1	-1.0	-1.3	-1.0	-2.5	-2.7	-1.2	-1.1	-	-1.7	-2.0	-
NM_000594.2	*TNF*			-1.1	-1.2	1.1	-1.1	1.0	-4.1	1.2	-1.2	1.1	1.0	-1.3	1.1	-1.7	1.1	-	-1.5	-1.2	-
NM_003810.2	*TNFSF10*			-1.4	-1.8	-1.5	-1.6	-2.9	-4.0	1.1	-1.1	-1.0	-1.0	-2.0	1.2	-2.2	-1.3	-	-1.7	-2.7	-
NM_030912.2	*TRIM8*			-1.6	-1.1	-1.1	-1.9	-1.3	-2.2	-1.0	1.2	1.1	-1.4	-1.0	-1.3	-2.0	1.1	-	-1.5	-1.2	-
NM_012238.3	*SIRT1*			1.9	1.5	-1.3	2.2	1.1	-1.3	-1.4	-1.0	1.6	-1.4	1.2	1.4	-1.1	-1.0	-	1.0	1.1	-
NM_006988.3	*ADAMTS1*		In-flammation	-1.2	-1.0	-1.5	-1.3	-1.3	-3.0	1.1	-1.5	1.1	-1.2	1.0	-3.3	-2.3	-1.1	-	-1.5	-1.2	-
NM_001679.2	*ATP1B3*			-1.0	-1.5	-1.2	-1.2	-1.2	-2.0	-1.3	-1.2	-1.2	-1.6	-1.1	-1.9	-1.1	-1.2	-	1.0	-1.6	-
NM_032607.1	*CREB3L3*			1.6	1.7	-1.2	2.5	-1.1	-2.8	1.1	-1.1	1.1	1.7	-1.6	-2.6	-3.9	1.1	-	-1.4	1.1	-
NM_002341.1	*LTB*			-1.2	-1.3	-2.0	-1.2	-1.9	-8.3	1.0	-1.1	-1.1	-1.7	-1.6	-1.7	-3.5	-1.1	-	-2.1	-1.8	-
NM_000963.1	*PTGS2*			1.0	1.0	-1.7	1.2	-1.1	-9.7	-1.1	-1.2	-1.0	-1.2	-1.2	-1.0	-1.2	-1.2	-	1.0	-1.3	-
NM_003745.1	*SOCS1*			-1.1	-1.4	-1.1	1.0	-1.0	-3.5	1.3	1.1	1.3	1.3	1.5	-1.9	-4.2	1.1	-	-1.3	-1.1	-
NM_003955.3	*SOCS3*			-1.2	1.0	-1.1	-1.3	-1.0	-1.8	1.0	-1.2	-1.2	1.1	-1.0	-1.3	-4.9	1.0	-	-1.0	-1.1	-
NM_001737.2	*C9*		Immune response	2.6	-1.6	1.1	2.7	-4.2	-2.1	-1.1	1.4	-1.1	-1.3	1.6	-1.4	-1.3	1.1	-	1.1	-1.3	-
NM_021023.3	*CFHR3*			-1.0	-2.7	1.2	1.0	-7.3	1.4	-1.1	1.2	1.3	1.1	1.9	-1.0	-1.7	-1.3	-	-1.3	-1.4	-
NM_006684.2	*CFHR4*			1.3	-1.5	1.1	1.3	-2.5	1.4	1.4	-1.1	1.5	1.4	1.0	1.2	-1.3	1.0	-	-1.0	1.2	-
NM_003665.2	*FCN3*			-1.6	-1.7	-1.1	-2.2	-3.0	-1.5	1.1	-1.3	-2.7	-1.5	-2.8	-10.1	-1.1	1.1	-	-1.7	-1.6	-
NM_000201.1	*ICAM1*			-1.7	-1.4	-1.6	-1.8	1.1	-2.1	-1.0	2.2	-1.2	-1.2	1.5	-1.5	-3.9	1.2	-	-1.8	-1.4	-
NM_207585.1	*IFNAR2*			-1.2	-1.6	-1.2	1.0	1.0	-2.8	-1.1	-1.3	1.1	-1.2	-1.1	-1.2	-1.6	-1.2	-	-1.4	-1.4	-
NM_000600.1	*IL6*			-1.1	-1.0	-1.4	-1.1	-1.1	-6.6	-1.0	-1.1	1.2	1.1	1.1	-1.4	-2.8	1.1	-	-1.2	1.1	-
NM_000584.2	*IL8*			-1.2	-1.8	-1.1	-1.7	1.6	-1.5	1.0	1.0	-2.0	-1.5	-1.6	-2.3	-3.6	-1.2	-	-1.2	-2.0	-
NM_003999.1	*OSMR*			1.3	-1.1	-1.4	1.3	1.1	-3.1	-1.0	1.1	1.1	1.4	1.1	-1.4	-2.0	1.1	-	1.1	-1.2	-
NM_000582.2	*SPP1*			-1.4	-2.8	-2.0	-1.6	-1.9	-2.9	-1.4	-1.4	-2.2	-3.2	-3.4	-5.4	-1.6	1.0	-	-1.4	-1.7	-
NM_003380.2	*VIM*			-1.0	-1.5	-1.5	-1.1	-1.8	-3.2	-1.3	-1.2	-1.4	-1.5	-1.9	-1.8	1.1	-1.1	-	-1.1	-1.4	-
NM_006633.2	*IQGAP2*		ECM organisation	-1.6	1.2	1.0	-1.9	-1.5	2.2	-1.1	1.0	-1.1	-1.1	1.1	-1.5	1.5	-1.1	-	-1.1	1.0	-
NM_018454.5	*NUSAP1*			-1.0	-1.2	-1.2	-1.1	-1.6	-2.0	-1.3	-1.0	-1.4	-1.2	-1.4	-1.4	-2.4	1.0	-	-1.7	-1.3	-
NM_003255.4	*TIMP2*			-1.9	-1.2	-1.5	-2.0	-1.5	-1.6	-1.2	-1.4	-1.6	-1.3	-1.7	-2.2	1.1	-1.1	-	-1.1	-1.4	-

Table 61 (continued)

RefSeq	Symbol	IPA® Tox function	Function	Donor 1						Donor 2						Donor 3					
				0.7 µM CsA			7 µM CsA			0.7 µM CsA			7 µM CsA			0.7 µM CsA			7 µM CsA		
				d01	d03	d14	d01	d03	d14	d01	d03	d14	d01	d03	d14	d01	d03	d14	d01	d03	d14
NM_000499.2	*CYP1A1*			1.2	2.2	1.2	-1.1	-1.0	6.6	6.8	2.6	2.8	5.0	3.3	3.3	2.8	1.8	-	1.5	6.0	-
NM_000771.2	*CYP2C9*			-1.5	-1.1	1.4	-2.1	-1.7	2.4	1.1	1.2	1.2	-1.1	1.8	1.1	1.4	-1.2	-	1.1	1.2	-
NM_003725.2	*HSD17B6*			-1.4	1.1	2.0	-1.3	-1.4	2.4	1.1	1.1	1.2	1.3	1.5	1.8	1.5	1.0	-	1.4	1.3	-
NM_006169.2	*NNMT*			-1.1	1.2	-1.0	-1.0	-1.4	-2.1	1.1	1.3	1.0	1.1	1.4	-1.8	-2.4	1.7	-	-1.1	1.1	-
NM_000463.2	*UGT1A1*		Xenobiotic metabolism	-1.1	-1.5	1.5	-1.9	-1.4	2.8	1.2	1.5	1.3	1.0	1.5	1.9	1.4	1.2	-	-1.2	1.4	-
NM_007120.2	*UGT1A4*			1.6	-1.7	1.5	1.1	-1.1	4.0	1.2	1.2	-1.0	1.1	1.5	1.8	1.1	1.0	-	1.1	1.9	-
NM_001072.3	*UGT1A6*			1.0	-1.9	-1.1	-1.4	-1.1	1.7	-1.2	-1.1	-1.1	1.0	-1.1	2.0	1.1	-1.0	-	1.0	-1.0	-
NM_019075.2	*UGT1A9*			1.1	-2.6	1.7	-1.3	-1.3	6.6	1.0	1.3	-1.2	-1.0	1.8	2.6	1.5	1.1	-	-1.0	1.7	-
NM_019075.2	*UGT1A9*			1.1	-2.6	1.7	-1.3	-1.3	6.6	1.0	1.3	-1.2	-1.0	1.8	2.6	1.5	1.1	-	-1.0	1.7	-
NM_000478.3	*ALPL*			1.1	1.5	1.6	1.1	-1.2	1.1	1.3	1.2	1.7	1.4	1.0	1.3	-3.4	1.4	-	-1.6	1.4	-
NM_001011645.1	*AR*			-1.4	-1.1	1.3	-1.2	-2.0	1.7	1.1	-1.1	1.0	1.2	-1.2	1.4	2.2	1.1	-	1.3	1.3	-
NM_001713.1	*BHMT*			-1.8	-1.5	-1.1	-3.9	-3.6	16.6	-1.2	1.1	1.0	-1.7	-1.3	1.6	4.5	-1.3	-	-1.3	1.0	-
NM_032649.5	*CNDP1*			1.0	1.2	-1.0	-1.1	1.1	-3.2	1.2	1.2	1.1	-1.6	1.2	1.3	1.3	1.3	-	1.0	1.7	-
NM_024324.2	*CRELD2*	Hepato-cellular Carcinoma		-1.9	2.2	1.3	-1.2	1.5	2.0	1.0	-1.0	1.1	3.1	-1.4	1.2	-1.2	-1.0	-	1.5	1.3	-
NM_000137.1	*FAH*			-1.6	-1.2	1.0	-2.0	-1.7	2.1	-1.1	1.1	-1.1	-1.3	-1.1	-1.9	1.4	1.1	-	-1.0	-1.0	-
NM_000508.3	*FGA*			-1.6	-1.4	-1.0	-1.6	-5.4	-1.2	-1.6	-1.2	-1.1	-1.8	-1.1	-2.6	-2.0	-1.3	-	-1.5	-2.2	-
NM_000166.4	*GJB1*			-1.5	-1.0	1.1	-1.9	-1.5	3.5	-1.1	1.1	1.1	-1.1	1.1	-1.2	1.5	-1.2	-	-1.0	-1.2	-
NM_018960.4	*GNMT*			-2.1	1.0	1.8	-2.2	-4.3	7.3	-1.1	1.2	1.5	-1.5	1.2	1.7	1.2	1.0	-	-1.2	1.7	-
NM_021175.2	*HAMP*		Other and unknown functions	-1.2	-1.5	1.2	-1.5	-7.9	-1.4	1.5	1.1	1.9	2.5	1.9	-3.0	-3.0	-1.1	-	-1.2	-1.3	-
NM_001530.2	*HIF1A*			2.4	-2.3	-1.4	1.8	-1.9	-4.6	-1.1	-1.4	-1.3	-1.4	-1.1	-1.5	-2.5	-1.4	-	-1.2	-1.7	-
NM_002150.2	*HPD*			-1.2	1.0	1.3	-1.7	-1.2	2.8	1.0	1.3	-1.3	-1.4	1.0	1.0	1.2	1.3	-	-1.5	1.2	-
NM_002205.2	*ITGA5*			-1.4	1.1	-1.6	-1.4	1.7	-2.3	1.0	-1.2	-1.1	-1.0	-2.1	-2.2	-1.0	1.2	-	1.0	-1.3	-
NM_000240.2	*MAOA*			-1.1	1.3	1.3	-1.2	-1.2	4.8	1.1	1.1	1.0	-1.1	1.0	1.1	1.3	1.2	-	1.1	1.4	-
NM_003998.2	*NFKB1*			-1.3	-1.2	-1.3	-1.8	1.2	-2.7	1.0	-1.1	-1.2	1.0	-1.2	-1.2	-1.4	1.1	-	-1.3	-1.0	-
NM_001042483.1	*NUPR1*			-1.3	1.3	-1.3	-1.6	1.0	2.9	1.0	1.1	1.1	-1.1	1.7	-1.1	1.1	1.3	-	-1.2	1.4	-
NM_152341.2	*PAQR4*			-1.6	-1.3	-1.3	-1.7	1.1	-1.2	-1.2	1.7	-1.3	-1.5	-1.8	-1.4	1.1	1.3	-	-1.2	-1.9	-
NM_002692.2	*POLE2*			1.1	1.3	-1.1	1.3	1.4	2.0	1.0	1.1	1.2	1.6	1.3	1.3	1.3	-1.0	-	1.9	1.3	-
NM_000941.2	*POR*			-1.2	1.2	-1.1	-1.2	1.2	2.1	-1.1	1.0	-1.2	-1.1	1.2	-1.0	1.2	1.1	-	-1.2	1.1	-

Table 61 (continued)

RefSeq	Symbol	IPA® Tox function	Function	Donor 1						Donor 2						Donor 3					
				0.7 µM CsA			7 µM CsA			0.7 µM CsA			7 µM CsA			0.7 µM CsA			7 µM CsA		
				d01	d03	d14	d01	d03	d14	d01	d03	d14	d01	d03	d14	d01	d03	d14	d01	d03	d14
NM_000021.2	*PSEN1*			1.5	-1.2	-1.4	1.2	1.2	-2.0	-1.0	-1.1	-1.4	1.2	-1.0	1.0	-1.3	-1.0	-	-1.3	-1.2	-
NM_002800.4	*PSMB9*			-1.5	-1.3	-1.4	-1.6	-1.1	-3.0	-1.2	1.0	-1.1	-1.4	-1.5	-1.1	-2.8	-1.2	-	-2.0	-1.3	-
NM_021975.2	*RELA*			-1.6	-1.2	-2.1	-1.7	-1.0	-2.0	-1.2	1.2	-1.0	-1.1	1.1	1.2	-1.3	-1.1	-	-1.2	-1.0	-
NM_006509.2	*RELB*			-1.2	-1.4	-1.0	-1.2	1.1	-2.2	-1.1	-1.3	-1.3	-1.6	-1.7	-1.3	-2.7	-1.0	-	-1.6	-1.4	-
NM_152703.2	*SAMD9L*	Hepato-cellular Carcinoma	Other and unknown functions	1.5	1.1	-1.8	1.3	1.2	-3.3	1.0	-1.1	-1.1	1.2	-1.5	1.0	-1.4	-1.0	-	-1.5	-1.2	-
NM_000346.2	*SOX9*			-1.7	-1.1	-1.7	-1.6	1.2	-3.4	1.1	-1.1	-1.1	-1.5	1.2	-1.2	-1.2	1.0	-	-1.1	1.5	-
NM_001068.2	*TOP2B*			-1.3	1.1	-1.1	-1.3	-1.0	-2.1	-1.1	-1.2	-1.0	-1.1	-1.2	1.0	1.1	1.2	-	1.0	-1.1	-
NM_001113756.1	*TYMP*			-1.9	-1.4	-1.4	-1.9	1.5	-3.6	-1.1	1.3	-1.1	-1.4	1.3	-1.2	-2.0	-1.1	-	-1.4	-1.6	-
NM_012479.2	*YWHAG*			1.9	-1.1	-1.1	2.2	1.0	-1.5	-1.2	1.0	-1.2	-1.3	1.2	-1.4	-1.1	-1.1	-	1.0	-1.3	-

Table 62. Absolute fold changes of genes deregulated at least 2-fold compared to the time matched vehicle treated control in primary human hepatocytes from three different donors treated with 0.5 or 5 µM amiodarone (AMI) for 1, 3 or 14 days. The categorisation of the genes into IPA® tox functions was evaluated manually which is indicated as the additional "function" category. The genes are in alphabetic order within each IPA® tox function and full gene names are given in Table 63.

RefSeq	Symbol	IPA® Tox function	Function	Donor 1						Donor 2						Donor 3					
				0.5 µM AMI			5 µM AMI			0.5 µM AMI			5 µM AMI			0.5 µM AMI			5 µM AMI		
				d01	d03	d14	d01	d03	d14	d01	d03	d14	d01	d03	d14	d01	d03	d14	d01	d03	d14
NM_001086.2	*AADAC*	Liver Hyperplasia/ Hyperproliferation	Fatty acid and lipid metabolism	1.1	1.0	1.0	1.0	1.2	1.1	-1.4	1.1	-1.0	-1.3	1.1	-3.4	-1.2	1.1	-	-1.0	1.0	-
NM_000668.3	*ADH1B*			1.1	1.1	1.1	1.2	-1.1	-1.4	-1.8	-1.3	1.3	-1.4	1.1	-6.0	-3.2	-1.0	-	-1.1	-1.1	-
NM_000669.3	*ADH1C*			1.2	1.1	1.2	1.2	1.0	-1.2	-1.2	-1.4	1.3	-1.5	-1.2	-2.4	-2.1	1.0	-	-1.0	-1.0	-
NM_052968.3	*APOA5*			1.1	-1.1	-1.0	-1.0	-1.3	1.1	1.4	-1.5	1.2	1.4	1.1	1.6	-2.4	-1.1	-	-1.2	1.0	-
NM_002979.3	*SCP2*			1.6	1.1	1.0	1.5	1.1	1.3	-1.3	-1.0	1.3	-1.2	-1.0	-1.0	-2.0	-1.2	-	-1.3	-1.1	-
NM_000618.2	*IGF1*		Carbohydrate metabolism	1.2	1.1	-1.1	-1.0	-1.0	1.0	-1.0	-1.0	-1.3	-1.0	1.1	-2.4	-1.1	1.0	-	1.0	-1.1	-
NM_002612.3	*PDK4*			-1.0	-1.0	1.1	-1.2	-1.2	1.4	1.2	-1.7	-1.3	1.1	-1.2	-3.0	-3.4	-1.1	-	-1.2	-1.2	-
NM_000291.2	*PGK1*			1.1	1.1	-1.1	1.1	-1.0	-1.3	1.5	-1.3	1.0	1.5	1.1	2.2	1.1	1.0	-	1.1	-1.1	-
NM_181523.1	*PIK3R1*			-1.0	1.0	-1.1	1.0	1.1	-1.2	-1.1	-1.3	1.2	-1.1	-1.1	2.0	-1.4	1.0	-	-1.1	1.1	-
NM_005398.4	*PPP1R3C*			1.2	-1.1	-1.3	1.2	-1.1	1.1	1.2	-1.1	1.4	1.2	1.1	2.4	-1.9	1.1	-	-1.1	1.0	-
NM_006516.1	*SLC2A1*			1.2	-1.1	-1.3	1.0	-1.0	1.1	1.6	-1.3	1.2	2.1	-1.1	4.1	1.2	1.1	-	1.1	-1.1	-
NM_003742.2	*ABCB11*		Bile acid metabolism	1.1	1.1	-1.2	1.1	1.1	-1.2	-1.1	1.0	-1.0	-1.1	-1.1	-2.0	-2.2	1.1	-	-1.2	-1.1	-
NM_005989.2	*AKR1D1*			1.3	1.1	1.2	1.2	-1.2	-1.0	-1.5	1.6	1.3	-1.7	1.1	5.7	1.0	1.1	-	1.1	-1.1	-
NM_003049.2	*SLC10A1*			-1.0	1.1	1.1	-1.0	-1.2	1.0	-1.0	-1.3	2.0	-1.2	-1.3	1.7	-2.5	-1.2	-	-1.1	-1.0	-
NM_001171.3	*ABCC6*		Xenobiotic metabolism	-1.1	1.1	1.0	-1.1	-1.0	-1.0	1.0	-1.0	1.0	-1.1	-1.0	2.2	-1.4	-1.1	-	-1.0	-1.2	-
NM_001266.4	*CES1*			1.5	1.2	-1.3	1.5	1.1	-1.3	1.1	1.3	1.5	-1.1	1.5	-2.6	1.0	-1.1	-	1.3	-1.6	-
NM_000499.2	*CYP1A1*			2.1	2.0	2.7	2.0	1.9	2.3	6.3	2.1	2.3	4.2	1.9	9.7	-1.2	1.8	-	1.7	2.2	-
NM_000771.2	*CYP2C9*			1.1	1.0	1.0	-1.0	1.1	1.5	1.2	-1.0	3.0	1.3	1.0	5.9	-1.2	1.4	-	1.1	1.2	-
NM_006169.2	*NNMT*			1.0	-1.2	1.1	1.1	1.1	1.0	-1.0	-1.1	-1.0	1.0	-1.0	-1.0	2.5	1.0	-	1.2	-1.0	-
NM_001077475.1	*NR1I3*			1.2	-1.0	-1.2	1.1	-1.1	-1.2	1.1	1.1	1.6	1.1	1.1	3.0	-1.4	1.2	-	-1.1	1.3	-
NM_003708.3	*RDH16*			-1.0	-1.2	1.1	1.0	-1.5	-1.4	-1.3	2.2	1.9	-1.3	1.5	2.7	1.0	-1.0	-	1.0	1.0	-
NM_003057.2	*SLC22A1*			1.2	1.1	1.1	1.1	-1.3	-1.2	-1.1	-1.2	1.7	-1.0	-1.1	2.5	-1.7	1.0	-	-1.0	1.0	-
NM_007120.2	*UGT1A4*			1.4	1.9	1.2	1.5	1.4	1.7	1.2	1.3	1.3	1.2	1.7	2.1	-1.3	1.3	-	-1.1	1.2	-
NM_006988.3	*ADAMTS1*		Inflammation	-1.1	1.0	1.3	-1.1	-1.0	1.1	1.1	1.1	-2.3	1.2	1.0	-1.1	1.2	-1.2	-	-1.1	-1.4	-
NM_002982.3	*CCL2*			-1.0	1.4	1.2	-1.1	1.2	-1.1	1.0	1.2	-1.9	1.0	-1.1	-3.3	3.8	-1.0	-	1.7	-1.0	-
NM_032607.1	*CREB3L3*			1.2	-1.5	-1.1	1.1	-1.3	-1.2	1.1	-1.0	-1.4	1.1	-1.0	-1.4	3.0	1.0	-	1.2	1.3	-

Table 62 (continued)

RefSeq	Symbol	IPA® Tox function	Function	Donor 1						Donor 2						Donor 3					
				0.5 µM AMI			5 µM AMI			0.5 µM AMI			5 µM AMI			0.5 µM AMI			5 µM AMI		
				d01	d03	d14	d01	d03	d14	d01	d03	d14	d01	d03	d14	d01	d03	d14	d01	d03	d14
NM_000567.2	*CRP*			1.0	1.1	-1.1	1.1	1.4	-1.1	1.1	1.1	-1.0	1.1	1.0	-1.0	2.4	-1.2	-	1.4	-1.1	-
NM_005211.2	*CSF1R*			-1.0	-1.2	1.2	1.0	-1.4	1.4	1.1	-1.1	-1.2	1.0	-1.1	2.2	1.1	-1.3	-	-1.0	-1.3	-
NM_173843.1	*IL1RN*		In-flammation	1.1	1.2	-1.1	1.2	-1.0	-1.2	1.1	1.1	-1.1	1.2	1.1	-2.3	1.6	-1.1	-	-1.2	-1.0	-
NM_002341.1	*LTB*			1.0	-1.1	1.2	-1.1	-1.2	-1.1	-1.1	-1.0	-2.9	1.1	-1.2	-3.6	2.9	1.1	-	1.4	1.0	-
NM_003745.1	*SOCS1*			1.1	-1.1	1.3	-1.0	-1.1	-1.6	-1.1	1.3	-1.7	-1.1	1.2	-1.1	3.9	-1.1	-	1.3	-1.2	-
NM_003955.3	*SOCS3*			1.0	-1.0	1.0	-1.1	-1.1	-1.3	1.3	1.1	-1.9	1.0	1.0	-1.8	3.0	1.1	-	1.0	1.4	-
NM_000064.2	*C3*			1.3	1.3	-1.0	1.4	1.2	-1.1	1.1	1.5	1.1	1.1	1.0	6.4	1.3	-1.0	-	-1.1	-1.3	-
NM_001737.2	*C9*			1.3	1.7	-1.0	1.2	-1.1	-1.7	1.2	-1.0	2.5	1.0	1.2	1.0	1.5	1.2	-	1.3	-1.1	-
NM_001001392.1	*CD44*			1.2	-1.2	-1.2	1.1	1.1	-1.3	-1.0	1.1	-1.3	1.2	1.0	-2.5	1.3	1.2	-	-1.1	1.3	-
NM_199168.2	*CXCL12*			1.0	1.0	-1.1	1.0	-1.2	1.1	-1.2	-1.1	-1.3	-1.3	-1.1	-3.3	1.1	-1.1	-	-1.3	-1.1	-
NM_003467.2	*CXCR4*			1.5	1.0	-1.1	1.5	1.1	1.5	-1.0	1.1	1.0	-1.0	1.2	2.5	-1.1	1.3	-	1.0	1.1	-
NM_003665.2	*FCN3*			-1.2	-1.2	1.3	-1.1	1.0	1.6	-1.1	1.3	1.3	-1.1	1.0	2.7	1.3	1.1	-	-1.0	1.4	-
NM_000201.1	*ICAM1*		Immune response	-1.1	-1.1	-1.4	-1.2	-1.4	-1.4	1.0	1.3	-1.3	1.2	1.0	-2.9	3.8	-1.1	-	1.1	-1.3	-
NM_000576.2	*IL1B*			-1.1	1.4	-1.2	-1.1	-1.1	-1.2	1.2	-1.0	-1.1	1.2	1.0	2.2	3.9	-1.1	-	1.3	-1.1	-
NM_000600.1	*IL6*			-1.2	-1.0	-1.0	-1.2	-1.1	1.2	-1.0	1.1	-1.1	1.1	1.0	-1.6	2.0	-1.1	-	1.0	-1.0	-
NM_000584.2	*IL8*			1.3	1.0	1.1	1.4	1.3	1.2	1.1	1.3	-1.1	-1.0	1.0	-2.1	2.9	1.0	-	1.5	-1.1	-
NM_001879.4	*MASP1*			1.1	-1.0	-1.1	1.1	-1.2	-1.0	1.3	-1.0	1.2	1.6	-1.1	2.3	-1.5	1.0	-	-1.0	-1.0	-
NM_000582.2	*SPP1*			1.0	1.1	-1.4	1.2	1.3	1.3	-1.2	-1.2	-1.4	-1.2	-1.2	-4.5	1.1	-1.0	-	-1.0	-1.1	-
NM_020299.3	*AKR1B10*			1.1	1.0	-1.0	-1.0	1.1	1.0	-1.2	1.3	1.3	-1.1	-1.0	-7.5	-1.5	-1.1	-	-1.0	-1.1	-
NM_001216.1	*CA9*			-1.1	1.1	-1.2	-1.1	-1.1	1.2	2.2	-2.8	1.2	3.3	-1.3	5.9	-1.4	-1.0	-	1.0	-1.1	-
NM_153768.1	*CABYR*			1.4	-1.0	1.1	1.1	1.1	1.3	1.0	-1.0	-1.4	1.1	1.1	-2.6	-1.0	-1.0	-	-1.1	-1.1	-
NM_078487.2	*CDKN2B*			-1.1	1.1	-1.4	-1.1	1.4	-1.3	-1.2	-1.0	1.1	-1.1	1.1	-2.1	1.1	-1.0	-	1.1	1.0	-
NM_001827.1	*CKS2*			1.2	1.1	-1.2	1.1	-1.0	1.1	-1.1	-1.2	1.0	-1.1	-1.0	-2.4	1.0	-1.0	-	1.1	1.1	-
NM_012242.2	*DKK1*		Cancer	-1.0	1.3	-1.0	1.0	1.3	1.2	1.0	1.1	-1.3	-1.1	1.1	-3.5	1.2	1.1	-	1.0	1.6	-
NM_004467.3	*FGL1*			1.2	1.5	1.1	1.2	1.4	-1.0	-1.0	-1.2	2.5	-1.3	-1.0	-1.4	1.5	-1.1	-	1.1	-1.7	-
NM_005252.2	*FOS*			-1.1	1.2	1.3	-1.1	1.2	1.5	1.3	1.3	-1.4	1.4	1.1	-3.8	-2.2	1.2	-	-1.4	-1.0	-
NM_033260.3	*FOXQ1*			1.3	1.1	-1.9	1.2	1.2	-1.4	-1.0	1.9	1.1	-1.1	1.3	3.0	-2.0	1.0	-	-1.0	-1.4	-
NM_001924.2	*GADD45A*			-1.0	-1.1	-1.4	1.0	-1.2	2.0	-1.0	2.2	1.2	-1.2	1.3	1.1	-1.2	1.0	-	-1.1	1.1	-

Table 62 (continued)

RefSeq	Symbol	IPA® Tox function	Function	Donor 1						Donor 2						Donor 3					
				0.5 µM AMI			5 µM AMI			0.5 µM AMI			5 µM AMI			0.5 µM AMI			5 µM AMI		
				d01	d03	d14	d01	d03	d14	d01	d03	d14	d01	d03	d14	d01	d03	d14	d01	d03	d14
NR_002196.1	*H19*			1.3	1.2	-1.4	1.2	1.3	1.4	1.9	-1.0	1.1	3.2	-1.2	1.9	-5.9	1.1	-	-1.3	-1.1	-
NM_001093772.1	*KIT*			1.3	1.2	-1.1	1.3	1.1	1.5	-1.0	1.2	-1.2	-1.2	1.1	2.3	-1.1	1.0	-	1.0	1.0	-
NM_004994.2	*MMP9*			1.1	1.1	-1.4	-1.1	-1.1	1.2	-1.1	-1.0	-2.3	1.0	1.0	-4.3	2.2	-1.0	-	1.2	1.0	-
NM_006096.2	*NDRG1*			-1.0	-1.0	-1.3	-1.1	-1.1	-1.0	1.6	-2.1	1.0	2.3	-1.5	3.2	-2.0	-1.1	-	-1.1	-1.0	-
NM_153292.1	*NOS2*			-1.0	1.1	-1.1	-1.1	1.1	-2.7	1.1	-1.1	1.1	1.1	1.0	-1.0	-1.0	-1.2	-	1.1	-1.2	-
NM_006206.3	*PDGFRA*			1.1	1.2	-1.1	1.2	-1.0	-1.1	1.1	-1.2	1.1	-1.1	-1.1	-3.3	1.4	1.0	-	1.4	-1.0	-
NM_052880.3	*PIK3IP1*		Cancer	1.1	-1.1	-1.4	1.1	-1.1	-1.0	-1.0	-1.1	1.0	1.1	-1.2	-5.0	-1.2	-1.2	-	1.1	-1.1	-
NM_080591.1	*PTGS1*			1.3	1.5	1.1	1.3	1.3	1.5	1.1	-1.2	-1.3	-1.0	-1.1	-2.3	-1.2	-1.1	-	1.1	-1.0	-
NM_182664.2	*RASSF5*			1.0	-1.0	-1.4	-1.1	-1.0	-2.2	1.0	1.2	-1.0	1.1	1.1	1.8	1.1	1.0	-	-1.0	-1.1	-
NM_003118.2	*SPARC*			1.1	1.1	-1.2	-1.2	1.0	1.2	-1.1	-1.2	1.1	-1.1	-1.1	-5.7	-1.2	-1.1	-	1.0	-1.1	-
NM_002353.1	*TACSTD2*			1.0	-1.2	-1.1	1.1	1.2	1.3	1.1	-1.2	-1.3	1.1	1.0	-5.3	1.5	1.0	-	1.3	-1.1	-
NM_003376.4	*VEGFA*			-1.0	-1.9	1.1	-1.0	-1.5	1.7	1.1	1.2	-1.3	1.2	-1.1	3.9	1.2	-1.1	-	1.0	1.1	-
NM_005429.2	*VEGFC*			-1.1	1.0	-1.0	-1.2	1.1	1.3	1.1	1.1	-1.3	-1.0	1.0	-4.1	-1.1	-1.1	-	-1.2	1.0	-
NM_000088.3	*COL1A1*	Liver Hyper-plasia/ Hyper-proliferation		1.1	-1.0	1.1	1.1	1.0	1.7	-1.1	-1.2	1.1	-1.1	-1.2	-10.5	1.1	-1.2	-	1.2	-1.4	-
NM_001901.1	*CTGF*		ECM organisation	-1.2	-1.2	-1.0	-1.1	-1.0	1.4	1.1	-1.2	-1.1	1.0	-1.1	-5.0	-1.9	-1.1	-	1.2	-1.3	-
NM_003255.4	*TIMP2*			-1.2	1.0	-1.2	-1.2	-1.0	1.1	-1.2	-1.0	-1.1	-1.1	-1.1	-2.5	-1.1	-1.1	-	1.1	-1.3	-
NM_001713.1	*BHMT*			1.2	-1.1	-1.5	1.1	-1.3	-1.1	-1.1	-1.1	1.9	1.1	1.1	8.7	-3.2	-1.0	-	-1.1	-1.1	-
NM_000071.1	*CBS*			1.0	-1.2	1.2	-1.0	-1.3	-1.3	1.3	1.0	1.3	1.3	-1.1	2.9	-1.0	-1.1	-	1.0	-1.0	-
NM_006079.3	*CITED2*			1.1	1.3	1.0	1.2	-1.0	1.4	1.6	-1.8	-1.1	1.7	-1.2	2.7	-1.6	-1.1	-	1.0	-1.1	-
NM_004379.2	*CREB1*			-1.3	1.3	-1.3	-1.3	1.1	-1.1	-1.0	-1.1	-1.0	-1.1	-1.3	-2.0	1.1	1.3	-	-1.2	1.8	-
NM_024324.2	*CRELD2*			1.0	-1.2	1.0	-1.0	-1.2	1.3	-1.1	-1.4	-1.3	-1.2	-1.1	-2.1	1.8	1.1	-	1.0	1.0	-
NM_013409.1	*FST*		Other and unknown functions	-1.2	1.2	-1.4	-1.1	1.1	1.3	1.0	-1.1	1.0	1.6	-1.0	-2.6	-1.3	1.1	-	-1.0	1.1	-
NM_000166.4	*GJB1*			1.0	-1.1	-1.1	-1.0	-1.2	1.3	1.2	-1.0	2.0	1.2	-1.1	1.2	-1.3	1.0	-	-1.2	1.4	-
NM_021175.2	*HAMP*			-1.0	-1.4	1.1	-1.0	-1.0	1.2	1.1	1.1	-2.6	1.0	1.2	1.2	3.6	-1.1	-	1.3	1.1	-
NR_003249.1	*HNRPDL*			1.0	-1.5	-1.2	1.0	-1.4	-1.0	-1.0	1.5	-1.4	1.1	-1.1	2.9	1.3	1.2	-	-1.0	1.6	-
NM_002150.2	*HPD*			1.1	-1.1	1.0	-1.0	1.1	1.3	-1.2	1.1	1.3	-1.0	1.2	2.3	-1.1	-1.0	-	1.1	-1.0	-
NM_005347.2	*HSPA5*			1.1	-1.1	1.1	-1.1	-1.4	1.2	1.1	-1.8	-1.1	-1.1	-1.2	-2.1	1.6	1.1	-	1.2	-1.1	-
NM_000596.2	*IGFBP1*			1.3	1.3	1.1	1.5	1.1	1.5	1.7	1.5	1.8	1.5	1.4	2.1	1.1	-1.2	-	1.4	-1.2	-

Table 62 (continued)

RefSeq	Symbol	IPA® Tox function	Function	Donor 1						Donor 2						Donor 3					
				0.5 µM AMI			5 µM AMI			0.5 µM AMI			5 µM AMI			0.5 µM AMI			5 µM AMI		
				d01	d03	d14	d01	d03	d14	d01	d03	d14	d01	d03	d14	d01	d03	d14	d01	d03	d14
NM_002302.2	*LECT2*	Liver Hyper-plasia/ Hyper-proliferation	Other and unknown functions	-1.0	1.4	1.0	1.1	1.1	-1.6	-1.1	1.3	1.4	-1.2	-1.0	5.6	-1.3	-1.1	-	-1.0	-1.2	-
NM_005911.4	*MAT2A*			-1.2	-1.4	1.2	-1.2	-1.0	1.2	-1.1	1.1	-1.2	-1.0	1.2	2.1	1.3	1.1	-	-1.0	1.3	-
NM_175617.2	*MT1E*			-1.2	-1.0	1.2	-1.1	1.1	1.2	-1.1	-1.1	-1.2	1.2	-1.2	-2.1	1.2	1.0	-	-1.0	1.3	-
NM_003204.1	*NFE2L1*			-1.1	-1.3	-1.1	-1.1	-1.2	-1.2	-1.1	1.5	1.0	1.0	1.0	2.1	1.1	1.0	-	-1.2	1.1	-
NM_152341.2	*PAQR4*			-1.2	-1.3	-1.0	-1.0	-1.1	-1.5	1.6	-2.4	1.5	1.7	-1.5	1.6	-1.7	-1.0	-	-1.2	1.1	-
NM_006623.2	*PHGDH*			1.0	-1.5	-1.0	-1.1	-1.2	-1.4	-1.1	1.1	1.2	-1.1	1.0	2.3	-1.2	-1.0	-	-1.0	-1.0	-
NM_002800.4	*PSMB9*			-1.0	-1.2	-1.2	-1.1	-1.3	-1.4	-1.0	1.0	1.2	-1.1	-1.0	1.5	2.0	1.0	-	-1.0	1.0	-
NM_006507.2	*REG1B*			-1.0	-1.1	1.2	-1.1	-1.1	2.1	1.0	-1.9	-3.1	1.1	-1.2	-33.3	1.5	1.0	-	1.1	1.1	-
NM_001024921.2	*RPL9*			-1.1	2.0	-1.1	1.0	1.4	1.2	1.1	-1.2	1.9	-1.1	1.0	-1.0	1.0	1.1	-	1.2	-1.2	-
NM_000602.1	*SERPINE1*			-1.0	1.0	-1.3	-1.1	1.0	-1.1	1.4	1.4	1.1	2.0	1.1	2.5	1.2	-1.1	-	-1.0	-1.1	-
NM_018389.3	*SLC35C1*			-1.3	-1.1	1.2	-1.1	1.1	1.3	-1.0	1.1	-1.2	-1.1	-1.0	-1.8	2.1	1.0	-	1.1	1.0	-
NM_003486.5	*SLC7A5*			1.1	-1.2	-1.3	1.0	-1.1	1.1	-1.0	2.2	1.2	-1.0	1.4	2.4	-1.1	1.0	-	-1.1	-1.0	-
NM_000346.2	*SOX9*			1.1	-1.0	1.1	-1.1	1.0	-1.2	-1.1	1.3	-1.1	1.0	1.0	3.3	-1.1	1.2	-	-1.2	-1.3	-
NM_003246.2	*THBS1*			1.0	-1.0	1.3	-1.0	1.3	1.3	1.0	1.2	1.0	-1.1	1.0	-2.3	-1.4	1.1	-	-1.1	1.1	-
NM_006288.2	*THY1*			-1.1	1.1	-1.1	-1.2	-1.0	1.4	-1.2	1.0	-1.1	-1.1	-1.1	-5.7	1.0	1.1	-	1.0	1.2	-
NM_006472.2	*TXNIP*			-1.1	-1.1	-1.0	-1.1	-1.2	-1.8	1.1	-1.1	-1.4	1.0	-1.1	-3.4	-1.4	1.1	-	1.0	1.1	-
NM_004181.3	*UCHL1*			-1.2	-1.1	1.2	-1.3	-1.0	1.7	-1.1	-1.0	-1.1	-1.3	1.1	-2.8	-1.1	1.2	-	-1.0	-1.0	-
NM_000668.3	*ADH1B*	Hepato-cellular Carcinoma	Fatty acid and lipid metabolism	1.1	1.1	1.1	1.2	-1.1	-1.4	-1.8	-1.3	1.3	-1.4	1.1	-6.0	-3.2	-1.0	-	-1.1	-1.1	-
NM_000669.3	*ADH1C*			1.2	1.1	1.2	1.2	1.0	-1.2	-1.2	-1.4	1.3	-1.5	-1.2	-2.4	-2.1	1.0	-	-1.0	-1.0	-
NM_003742.2	*ABCB11*		Bile acid metabolism	1.1	1.1	-1.2	1.1	1.1	-1.2	-1.1	1.0	-1.0	-1.1	-1.1	-2.0	-2.2	1.1	-	-1.2	-1.1	-
NM_005989.2	*AKR1D1*			1.3	1.1	1.2	1.2	-1.2	-1.0	-1.5	1.6	1.3	-1.7	1.1	5.7	1.0	1.1	-	1.1	-1.1	-
NM_003049.2	*SLC10A1*			-1.0	1.1	1.1	-1.0	-1.2	1.0	-1.0	-1.3	2.0	-1.2	-1.3	1.7	-2.5	-1.2	-	-1.1	-1.0	-
NM_002612.3	*PDK4*		Carbo-hydrate metabolism	-1.0	-1.0	1.1	-1.2	-1.2	1.4	1.2	-1.7	-1.3	1.1	-1.2	-3.0	-3.4	-1.1	-	-1.2	-1.2	-
NM_000291.2	*PGK1*			1.1	1.1	-1.1	1.1	-1.0	-1.3	1.5	-1.3	1.0	1.5	1.1	2.2	1.1	1.0	-	1.1	-1.1	-
NM_181523.1	*PIK3R1*			-1.0	1.0	-1.1	1.0	1.1	-1.2	-1.1	-1.3	1.2	-1.1	-1.1	2.0	-1.4	1.0	-	-1.1	1.1	-
NM_020299.3	*AKR1B10*		Cancer	1.1	1.0	-1.0	-1.0	1.1	1.0	-1.2	1.3	1.3	-1.1	-1.0	-7.5	-1.5	-1.1	-	-1.0	-1.1	-
NM_153768.1	*CABYR*			1.4	-1.0	1.1	1.1	1.1	1.3	1.0	-1.0	-1.4	1.1	1.1	-2.6	-1.0	-1.0	-	-1.1	-1.1	-
NM_001827.1	*CKS2*			1.2	1.1	-1.2	1.1	-1.0	1.1	-1.1	-1.2	1.0	-1.1	-1.0	-2.4	1.0	-1.0	-	1.1	1.1	-

Table 62 (continued)

RefSeq	Symbol	IPA® Tox function	Function	Donor 1						Donor 2						Donor 3					
				0.5 µM AMI			5 µM AMI			0.5 µM AMI			5 µM AMI			0.5 µM AMI			5 µM AMI		
				d01	d03	d14	d01	d03	d14	d01	d03	d14	d01	d03	d14	d01	d03	d14	d01	d03	d14
NM_012242.2	*DKK1*	Hepato-cellular Carcinoma	Cancer	-1.0	1.3	-1.0	1.0	1.3	1.2	1.0	1.1	-1.3	-1.1	1.1	-3.5	1.2	1.1	-	1.0	1.6	-
NM_004467.3	*FGL1*			1.2	1.5	1.1	1.2	1.4	-1.0	-1.0	-1.2	2.5	-1.3	-1.0	-1.4	1.5	-1.1	-	1.1	-1.7	-
NM_033260.3	*FOXQ1*			1.3	1.1	-1.9	1.2	1.2	-1.4	-1.0	1.9	1.1	-1.1	1.3	3.0	-2.0	1.0	-	-1.0	-1.4	-
NM_001093772.1	*KIT*			1.3	1.2	-1.1	1.3	1.1	1.5	-1.0	1.2	-1.2	-1.2	1.1	2.3	-1.1	1.0	-	1.0	1.0	-
NM_004994.2	*MMP9*			1.1	1.1	-1.4	-1.1	-1.1	1.2	-1.1	-1.0	-2.3	1.0	1.0	-4.3	2.2	-1.0	-	1.2	1.0	-
NM_153292.1	*NOS2*			-1.0	1.1	-1.1	-1.1	1.1	-2.7	1.1	-1.1	1.1	1.1	1.0	-1.0	-1.0	-1.2	-	1.1	-1.2	-
NM_006206.3	*PDGFRA*			1.1	1.2	1.2	1.0	-1.0	1.1	-1.0	-1.1	-1.5	-1.1	1.0	-3.4	1.6	-1.1	-	1.1	-1.1	-
NM_080591.1	*PTGS1*			1.3	1.5	1.1	1.3	1.3	1.5	1.1	-1.2	-1.3	-1.0	-1.1	-2.3	-1.2	-1.1	-	1.1	-1.0	-
NM_003376.4	*VEGFA*			-1.0	-1.9	1.1	-1.0	-1.5	1.7	1.1	1.2	-1.3	1.2	-1.1	3.9	1.2	-1.1	-	1.0	1.1	-
NM_006988.3	*ADAMTS1*		In-flammation	-1.1	1.0	1.3	-1.1	-1.0	1.1	1.1	1.1	-2.3	1.2	1.0	-1.1	1.2	-1.2	-	-1.1	-1.4	-
NM_032607.1	*CREB3L3*			1.2	-1.5	-1.1	1.1	-1.3	-1.2	1.1	-1.0	-1.4	1.1	-1.0	-1.4	3.0	1.0	-	1.2	1.3	-
NM_005211.2	*CSF1R*			-1.0	-1.2	1.2	1.0	-1.4	1.4	1.1	-1.1	-1.2	1.0	-1.1	2.2	1.1	-1.3	-	-1.0	-1.3	-
NM_002341.1	*LTB*			1.0	-1.1	1.2	-1.1	-1.2	-1.1	-1.1	-1.0	-2.9	1.1	-1.2	-3.6	2.9	1.1	-	1.4	1.0	-
NM_003745.1	*SOCS1*			1.1	-1.1	1.3	-1.0	-1.1	-1.6	-1.1	1.3	-1.7	-1.1	1.2	-1.1	3.9	-1.1	-	1.3	-1.2	-
NM_003955.3	*SOCS3*			1.0	-1.0	1.0	-1.1	-1.1	-1.3	1.3	1.1	-1.9	1.0	1.0	-1.8	3.0	1.1	-	1.0	1.4	-
NM_001737.2	*C9*		Immune response	1.3	1.7	-1.0	1.2	-1.1	-1.7	1.2	-1.0	2.5	1.0	1.2	1.0	1.5	1.2	-	1.3	-1.1	-
NM_003665.2	*FCN3*			-1.2	-1.2	1.3	-1.1	1.0	1.6	-1.1	1.3	1.3	-1.1	1.0	2.7	1.3	1.1	-	-1.0	1.4	-
NM_000201.1	*ICAM1*			-1.1	-1.1	-1.4	-1.2	-1.4	-1.4	1.0	1.3	-1.3	1.2	1.0	-2.9	3.8	-1.1	-	1.1	-1.3	-
NM_000584.2	*IL8*			1.3	1.0	1.1	1.4	1.3	1.2	1.1	1.3	-1.1	-1.0	1.0	-2.1	2.9	1.0	-	1.5	-1.1	-
NM_001040058.1	*SPP1*			1.3	1.1	-1.4	1.2	1.3	1.3	-1.4	-1.3	-1.3	-1.1	-1.2	-5.0	1.0	-1.0	-	-1.1	-1.1	-
NM_003255.4	*TIMP2*		ECM organisation	-1.2	1.0	-1.2	-1.2	-1.0	1.1	-1.2	-1.0	-1.1	-1.1	-1.1	-2.5	-1.1	-1.1	-	1.1	-1.3	-
NM_000499.2	*CYP1A1*		Xenobiotic metabolism	2.1	2.0	2.7	2.0	1.9	2.3	6.3	2.1	2.3	4.2	1.9	9.7	-1.2	1.8	-	1.7	2.2	-
NM_000771.2	*CYP2C9*			1.1	1.0	1.0	-1.0	1.1	1.5	1.2	-1.0	3.0	1.3	1.0	5.9	-1.2	1.4	-	1.1	1.2	-
NM_006169.2	*NNMT*			1.0	-1.2	1.1	1.1	1.1	1.0	-1.0	-1.1	-1.0	1.0	-1.0	-1.0	2.5	1.0	-	1.2	-1.0	-
NM_007120.2	*UGT1A4*			1.4	1.9	1.2	1.5	1.4	1.7	1.2	1.3	1.3	1.2	1.7	2.1	-1.3	1.3	-	-1.1	1.2	-
NM_019075.2	*UGT1A9*			1.4	1.2	1.1	1.2	1.3	1.7	1.1	1.2	2.0	1.1	1.2	-1.4	-1.4	-1.1	-	1.1	-1.0	-

Table 62 (continued)

RefSeq	Symbol	IPA® Tox function	Function	Donor 1						Donor 2						Donor 3					
				0.5 µM AMI			5 µM AMI			0.5 µM AMI			5 µM AMI			0.5 µM AMI			5 µM AMI		
				d01	d03	d14	d01	d03	d14	d01	d03	d14	d01	d03	d14	d01	d03	d14	d01	d03	d14
NM_001713.1	*BHMT*			1.2	-1.1	-1.5	1.1	-1.3	-1.1	-1.1	-1.1	1.9	1.1	1.1	8.7	-3.2	-1.0	-	-1.1	-1.1	-
NM_004379.2	*CREB1*			-1.3	1.3	-1.3	-1.3	1.1	-1.1	-1.0	-1.1	-1.0	-1.1	-1.3	-2.0	1.1	1.3	-	-1.2	1.8	-
NM_024324.2	*CRELD2*			1.0	-1.2	1.0	-1.0	-1.2	1.3	-1.1	-1.4	-1.3	-1.2	-1.1	-2.1	1.8	1.1	-	1.0	1.0	-
NM_000166.4	*GJB1*			1.0	-1.1	-1.1	-1.0	-1.2	1.3	1.2	-1.0	2.0	1.2	-1.1	1.2	-1.3	1.0	-	-1.2	1.4	-
NM_021175.2	*HAMP*			-1.0	-1.4	1.1	-1.0	-1.0	1.2	1.1	1.1	-2.6	1.0	1.2	1.2	3.6	-1.1	-	1.3	1.1	-
NM_002150.2	*HPD*	Hepato-cellular Carcinoma	Other and unknown functions	1.1	-1.1	1.0	-1.0	1.1	1.3	-1.2	1.1	1.3	-1.0	1.2	2.3	-1.1	-1.0	-	1.1	-1.0	-
NM_005347.2	*HSPA5*			1.1	-1.1	1.1	-1.1	-1.4	1.2	1.1	-1.8	-1.1	-1.1	-1.2	-2.1	1.6	1.1	-	1.2	-1.1	-
NM_152341.2	*PAQR4*			-1.2	-1.3	-1.0	-1.0	-1.1	-1.5	1.6	-2.4	1.5	1.7	-1.5	1.6	-1.7	-1.0	-	-1.2	1.1	-
NM_002800.4	*PSMB9*			-1.0	-1.2	-1.2	-1.1	-1.3	-1.4	-1.0	1.0	1.2	-1.1	-1.0	1.5	2.0	1.0	-	-1.0	1.0	-
NM_001024921.2	*RPL9*			-1.1	2.0	-1.1	1.0	1.4	1.2	1.1	-1.2	1.9	-1.1	1.0	-1.0	1.0	1.1	-	1.2	-1.2	-
NM_000602.1	*SERPINE1*			-1.0	1.0	-1.3	-1.1	1.0	-1.1	1.4	1.4	1.1	2.0	1.1	2.5	1.2	-1.1	-	-1.0	-1.1	-
NM_000346.2	*SOX9*			1.1	-1.0	1.1	-1.1	1.0	-1.2	-1.1	1.3	-1.1	1.0	1.0	3.3	-1.1	1.2	-	-1.2	-1.3	-
NM_007292.3	*ACOX1*		Fatty acid and lipid metabolism	1.5	1.0	1.0	1.4	1.2	1.3	-1.1	1.1	1.3	1.0	1.1	1.1	-1.8	-1.2	-	-1.2	-2.0	-
NM_002979.3	*SCP2*			1.6	1.1	1.0	1.5	1.1	1.3	-1.3	-1.0	1.3	-1.2	-1.0	-1.0	-2.0	-1.2	-	-1.3	-1.1	-
NM_003742.2	*ABCB11*		Bile acid metabolism	1.1	1.1	-1.2	1.1	1.1	-1.2	-1.1	1.0	-1.0	-1.1	-1.1	-2.0	-2.2	1.1	-	-1.2	-1.1	-
NM_003049.2	*SLC10A1*			-1.0	1.1	1.1	-1.0	-1.2	1.0	-1.0	-1.3	2.0	-1.2	-1.3	1.7	-2.5	-1.2	-	-1.1	-1.0	-
NM_000592.4	*C4A*			1.3	1.1	-1.3	1.3	1.0	1.0	-1.0	1.6	1.0	1.1	1.1	4.1	1.1	-1.3	-	-1.3	-1.8	-
NM_002982.3	*CCL2*			-1.0	1.4	1.2	-1.1	1.2	-1.1	1.0	1.2	-1.9	1.0	-1.1	-3.3	3.8	-1.0	-	1.7	-1.0	-
NM_001001437.3	*CCL3L1*	Liver In-flammation/ Hepatitis		-1.2	-1.1	-1.3	-1.2	-1.2	-1.2	-1.3	1.0	-1.4	-1.1	-1.2	1.3	2.7	1.1	-	1.1	-1.2	-
NM_021006.4	*CCL3L1*			-1.1	1.1	-1.3	1.1	-1.0	1.0	-1.4	1.1	-1.1	-1.3	-1.2	1.4	2.7	-1.2	-	-1.0	-1.2	-
NM_005623.2	*CCL8*			-1.3	1.1	1.1	-1.1	-1.1	-2.3	1.1	1.0	-1.5	-1.1	-1.2	-1.1	4.3	-1.2	-	1.6	-2.2	-
NM_001511.1	*CXCL1*		In-flammation	1.3	1.0	1.1	-1.1	1.1	-1.1	1.5	1.1	1.1	1.7	-1.0	-2.1	3.6	-1.0	-	1.8	-1.1	-
NM_001565.2	*CXCL10*			-1.7	1.3	1.0	-1.8	-1.2	-1.0	1.6	-2.1	1.5	1.0	-1.9	-1.1	2.2	-1.0	-	1.4	-1.0	-
NM_002089.3	*CXCL2*			-1.2	1.2	1.4	1.1	1.2	1.3	1.1	1.2	-1.1	1.2	1.1	1.4	2.1	1.1	-	1.4	1.2	-
NM_173842.1	*IL1RN*			1.2	-1.1	-1.3	1.1	1.1	-1.1	-1.0	1.2	-1.1	1.1	1.2	-2.2	1.9	1.0	-	-1.0	1.0	-
NM_002341.1	*LTB*			1.0	-1.1	1.2	-1.1	-1.2	-1.1	-1.1	-1.0	-2.9	1.1	-1.2	-3.6	2.9	1.1	-	1.4	1.0	-
NM_003745.1	*SOCS1*			1.1	-1.1	1.3	-1.0	-1.1	-1.6	-1.1	1.3	-1.7	-1.1	1.2	-1.1	3.9	-1.1	-	1.3	-1.2	-

Table 62 (continued)

RefSeq	Symbol	IPA® Tox function	Function	Donor 1						Donor 2						Donor 3					
				0.5 µM AMI			5 µM AMI			0.5 µM AMI			5 µM AMI			0.5 µM AMI			5 µM AMI		
				d01	d03	d14	d01	d03	d14	d01	d03	d14	d01	d03	d14	d01	d03	d14	d01	d03	d14
NM_000064.2	*C3*	Liver In-flammation/ Hepatitis	Immune response	1.3	1.3	-1.0	1.4	1.2	-1.1	1.1	1.5	1.1	1.1	1.0	6.4	1.3	-1.0	-	-1.1	-1.3	-
NM_000592.4	*C4A*			1.3	1.1	-1.3	1.3	1.0	1.0	-1.0	1.6	1.0	1.1	1.1	4.1	1.1	-1.3	-	-1.3	-1.8	-
NM_002985.2	*CCL5*			1.0	-1.4	-1.0	1.1	-1.4	-2.2	1.0	1.0	-2.2	1.1	-1.1	-2.0	1.5	1.1	-	1.0	-1.0	-
NM_001001391.1	*CD44*			1.1	1.0	-1.1	1.0	-1.0	-1.3	1.0	-1.1	-1.5	-1.0	1.0	-2.8	1.7	-1.1	-	1.2	-1.1	-
NM_000574.2	*CD55*			1.2	1.7	-1.5	1.6	1.1	-2.0	-1.2	2.2	1.7	1.1	1.1	2.3	1.3	1.1	-	1.0	1.2	-
NM_002993.2	*CXCL6*			-1.2	1.2	-1.1	-1.1	1.2	-1.3	-1.0	1.1	-1.1	-1.3	1.1	-4.0	2.5	-1.1	-	1.4	1.1	-
NM_004843.2	*IL27RA*			1.0	1.4	-1.1	1.0	1.2	1.1	1.0	-1.1	-1.0	-1.0	1.1	-2.2	-1.1	1.0	-	-1.2	-1.1	-
NM_000600.1	*IL6*			-1.2	-1.0	-1.0	-1.2	-1.1	1.2	-1.0	1.1	-1.1	1.1	1.0	-1.6	2.0	-1.1	-	1.0	-1.0	-
NM_000584.2	*IL8*			1.3	1.0	1.1	1.4	1.3	1.2	1.1	1.3	-1.1	-1.0	1.0	-2.1	2.9	1.0	-	1.5	-1.1	-
NM_001040058.1	*SPP1*			1.3	1.1	-1.4	1.2	1.3	1.3	-1.4	-1.3	-1.3	-1.1	-1.2	-5.0	1.0	-1.0	-	-1.1	-1.1	-
NM_001561.4	*TNFRSF9*			1.1	1.0	-1.2	1.5	1.0	-1.3	1.3	1.4	1.4	1.4	-1.0	2.5	1.2	-1.4	-	1.1	-1.2	-
NM_001964.2	*EGR1*		Cancer	-1.1	-1.0	1.2	-1.2	-1.0	1.2	-1.1	1.5	-1.2	-1.0	1.1	-6.5	-1.1	-1.0	-	-1.0	-1.0	-
NM_152877.1	*FAS*			-1.1	1.2	-1.1	1.1	-1.1	-1.6	1.0	-1.1	1.2	-1.3	1.1	1.3	1.3	1.1	-	1.5	-2.1	-
NM_004994.2	*MMP9*			1.1	1.1	-1.4	-1.1	-1.1	1.2	-1.1	-1.0	-2.3	1.0	1.0	-4.3	2.2	-1.0	-	1.2	1.0	-
NM_000636.2	*SOD2*		Stress response	1.7	1.3	1.1	1.5	1.4	1.1	1.1	1.2	1.5	1.3	1.3	1.0	2.3	1.0	-	1.4	-1.3	-
NM_000090.3	*COL3A1*		ECM or-ganisation	1.2	1.6	-1.1	1.1	1.3	1.2	-1.7	-1.3	-1.1	-1.5	-1.4	-10.4	1.1	-1.2	-	1.1	-1.2	-
NM_005309.1	*GPT*		Carbo-hydrate metabolism	-1.0	-1.4	1.1	1.0	-1.2	1.9	-1.0	1.1	1.3	-1.2	1.0	3.1	-1.2	1.0	-	1.2	1.1	-
NM_005100.2	*AKAP12*		Other and unknown functions	-1.1	1.2	-2.0	-1.3	1.1	-1.4	1.0	-1.0	-1.0	-1.0	-1.2	1.0	-1.1	1.0	-	1.0	1.2	-
NM_000071.1	*CBS*			1.0	-1.2	1.2	-1.0	-1.3	-1.3	1.3	1.0	1.3	1.3	-1.1	2.9	-1.0	-1.1	-	1.0	-1.0	-
NM_000799.2	*EPO*			1.1	1.1	-1.0	-1.0	1.2	1.2	1.2	-2.3	-1.2	1.3	-1.3	1.9	-1.1	-1.2	-	-1.2	-1.1	-
NM_000596.2	*IGFBP1*			1.3	1.3	1.1	1.5	1.1	1.5	1.7	1.5	1.8	1.5	1.4	2.1	1.1	-1.2	-	1.4	-1.2	-
NM_002302.2	*LECT2*			-1.0	1.4	1.0	1.1	1.1	-1.6	-1.1	1.3	1.4	-1.2	-1.0	5.6	-1.3	-1.1	-	-1.0	-1.2	-
NM_003204.1	*NFE2L1*			-1.1	-1.3	-1.1	-1.1	-1.2	-1.2	-1.1	1.5	1.0	1.0	1.0	2.1	1.1	1.0	-	-1.2	1.1	-
NM_000602.1	*SERPINE1*			-1.0	1.0	-1.3	-1.1	1.0	-1.1	1.4	1.4	1.1	2.0	1.1	2.5	1.2	-1.1	-	-1.0	-1.1	-

Table 62 (continued)

RefSeq	Symbol	IPA® Tox function	Function	Donor 1						Donor 2						Donor 3					
				0.5 µM AMI			5 µM AMI			0.5 µM AMI			5 µM AMI			0.5 µM AMI			5 µM AMI		
				d01	d03	d14	d01	d03	d14	d01	d03	d14	d01	d03	d14	d01	d03	d14	d01	d03	d14
NM_000668.3	*ADH1B*	Liver Cholestasis	Fatty acid and lipid metabolism	1.1	1.1	1.1	1.2	-1.1	-1.4	-1.8	-1.3	1.3	-1.4	1.1	-6.0	-3.2	-1.0	-	-1.1	-1.1	-
NM_000669.3	*ADH1C*			1.2	1.1	1.2	1.2	1.0	-1.2	-1.2	-1.4	1.3	-1.5	-1.2	-2.4	-2.1	1.0	-	-1.0	-1.0	-
NM_052968.3	*APOA5*			1.1	-1.1	-1.0	-1.0	-1.3	1.1	1.4	-1.5	1.2	1.4	1.1	1.6	-2.4	-1.1	-	-1.2	1.0	-
NM_002979.3	*SCP2*			1.6	1.1	1.0	1.5	1.1	1.3	-1.3	-1.0	1.3	-1.2	-1.0	-1.0	-2.0	-1.2	-	-1.3	-1.1	-
NM_006759.3	*UGP2*		Carbo-hydrate metabolism	1.3	2.0	-1.0	1.3	1.4	1.1	1.1	-1.2	2.6	1.1	-1.2	1.1	-1.6	-1.1	-	1.0	-1.3	-
NM_003742.2	*ABCB11*		Bile acid metabolism	1.1	1.1	-1.2	1.1	1.1	-1.2	-1.1	1.0	-1.0	-1.1	-1.1	-2.0	-2.2	1.1	-	-1.2	-1.1	-
NM_005989.2	*AKR1D1*			1.3	1.1	1.2	1.2	-1.2	-1.0	-1.5	1.6	1.3	-1.7	1.1	5.7	1.0	1.1	-	1.1	-1.1	-
NM_003049.2	*SLC10A1*			-1.0	1.1	1.1	-1.0	-1.2	1.0	-1.0	-1.3	2.0	-1.2	-1.3	1.7	-2.5	-1.2	-	-1.1	-1.0	-
NM_152672.4	*SLC51A*			1.1	-1.0	-1.2	-1.0	-1.0	-1.5	1.4	-1.2	1.1	1.6	-1.1	-1.0	-2.0	1.1	-	-1.0	-1.1	-
NM_001216.1	*CA9*		Cancer	-1.1	1.1	-1.2	-1.1	-1.1	1.2	2.2	-2.8	1.2	3.3	-1.3	5.9	-1.4	-1.0	-	1.0	-1.1	-
NM_152877.1	*FAS*			-1.1	1.2	-1.1	1.1	-1.1	-1.6	1.0	-1.1	1.2	-1.3	1.1	1.3	1.3	1.1	-	1.5	-2.1	-
NM_052880.3	*PIK3IP1*			1.1	-1.1	-1.4	1.1	-1.1	-1.0	-1.0	-1.1	1.0	1.1	-1.2	-5.0	-1.2	-1.2	-	1.1	-1.1	-
NM_000064.2	*C3*		Immune response	1.3	1.3	-1.0	1.4	1.2	-1.1	1.1	1.5	1.1	1.1	1.0	6.4	1.3	-1.0	-	-1.1	-1.3	-
NM_000600.1	*IL6*			-1.2	-1.0	-1.0	-1.2	-1.1	1.2	-1.0	1.1	-1.1	1.1	1.0	-1.6	2.0	-1.1	-	1.0	-1.0	-
NM_000584.2	*IL8*			1.3	1.0	1.1	1.4	1.3	1.2	1.1	1.3	-1.1	-1.0	1.0	-2.1	2.9	1.0	-	1.5	-1.1	-
NM_139125.2	*MASP1*			1.0	1.1	-1.1	-1.0	1.0	-1.0	1.1	-1.4	1.1	1.3	-1.1	2.4	-1.1	1.1	-	1.1	1.2	-
NM_001077475.1	*NR1I3*		Xenobiotic metabolism	1.2	-1.0	-1.2	1.1	-1.1	-1.2	1.1	1.1	1.6	1.1	1.1	3.0	-1.4	1.2	-	-1.1	1.3	-
NM_003708.3	*RDH16*			-1.0	-1.2	1.1	1.0	-1.5	-1.4	-1.3	2.2	1.9	-1.3	1.5	2.7	1.0	-1.0	-	1.0	1.0	-
NM_153187.1	*SLC22A1*			1.1	-1.1	-1.1	-1.1	-1.5	-1.1	-1.1	-1.2	2.0	-1.2	-1.2	2.3	-1.2	1.0	-	1.1	-1.0	-
NM_001075.3	*UGT2B10*			1.1	1.1	1.2	1.0	-1.2	-1.1	-1.3	1.1	1.8	-1.2	-1.1	-2.1	-2.7	1.1	-	-1.1	1.1	-
XM_001127829.1	*UGT2B15*			1.6	1.3	1.4	1.5	1.0	-1.1	1.3	-1.2	1.7	1.3	1.1	1.1	-2.1	1.1	-	1.1	-1.0	-
NM_001752.2	*CAT*		Stress response	-1.0	1.5	-1.0	1.1	1.1	-1.1	1.1	-1.0	2.0	-1.1	1.1	-1.2	-1.6	1.1	-	1.2	-1.2	-
NM_005265.2	*GGT1*			-1.3	-1.1	-1.3	-1.2	-1.2	1.1	-1.0	1.6	1.1	1.1	1.1	2.7	-1.2	1.2	-	-1.2	2.2	-
NM_000846.3	*GSTA2*			1.1	-1.2	-1.1	1.0	-1.2	1.1	-1.2	-1.1	3.6	-1.3	-1.2	15.3	-3.2	1.1	-	-1.3	-1.0	-
NM_005689.1	*ABCB6*		Other and unknown functions	-1.1	1.1	-1.2	1.0	1.1	1.2	1.2	-1.2	1.2	1.2	-1.1	2.5	1.2	-1.1	-	1.3	-1.1	-
NM_000670.3	*ADH4*			1.1	-1.2	-1.2	1.1	-1.4	-1.4	-1.4	-1.1	1.9	-1.5	1.1	2.7	-2.9	1.0	-	-1.2	1.2	-
NM_000672.2	*ADH6*			1.3	1.0	1.1	1.2	-1.1	-1.0	-1.0	-1.1	1.5	-1.2	-1.0	1.4	-2.0	-1.0	-	-1.2	-1.2	-

Table 62 (continued)

RefSeq	Symbol	IPA® Tox function	Function	Donor 1						Donor 2						Donor 3					
				0.5 µM AMI			5 µM AMI			0.5 µM AMI			5 µM AMI			0.5 µM AMI			5 µM AMI		
				d01	d03	d14	d01	d03	d14	d01	d03	d14	d01	d03	d14	d01	d03	d14	d01	d03	d14
NM_001713.1	*BHMT*	Liver Cholestasis	Other and unknown functions	1.2	-1.1	-1.5	1.1	-1.3	-1.1	-1.1	-1.1	1.9	1.1	1.1	8.7	-3.2	-1.0	-	-1.1	-1.1	-
NM_000166.4	*GJB1*			1.0	-1.1	-1.1	-1.0	-1.2	1.3	1.2	-1.0	2.0	1.2	-1.1	1.2	-1.3	1.0	-	-1.2	1.4	-
NM_002083.2	*GPX2*			1.0	-1.1	1.0	1.0	1.1	1.0	-1.0	-1.1	-1.2	-1.0	-1.0	1.1	2.4	1.0	-	-1.1	1.2	-
NM_021969.1	*NR0B2*			1.1	1.0	-1.3	1.1	1.1	1.4	-1.1	1.2	-1.1	1.1	1.0	-2.5	-1.6	1.0	-	-1.2	1.1	-
NM_000277.1	*PAH*			1.2	2.0	1.2	1.3	1.4	1.1	-1.1	-1.3	1.9	-1.1	1.1	-1.1	-1.2	-1.0	-	1.2	-1.2	-
NM_005074.2	*SLC17A1*			-1.2	-1.1	-1.0	-1.1	-1.2	1.1	-1.1	1.2	1.1	-1.0	1.2	3.6	1.1	1.1	-	1.1	1.2	-
NM_000544.3	*TAP2*			1.0	1.2	-1.2	-1.0	1.1	-2.0	-1.2	-1.0	-1.1	-1.2	1.1	-1.0	1.7	1.1	-	-1.0	-1.4	-
NM_000016.2	*ACADM*	Liver Steatosis	Fatty acid and lipid metabolism	1.3	1.3	1.1	1.2	1.0	-1.0	1.1	1.0	1.1	1.2	1.1	-2.2	-1.7	-1.3	-	-1.0	-1.1	-
NM_000018.2	*ACADVL*			-1.2	-1.2	-1.3	-1.2	-1.3	-1.1	1.1	-1.0	-1.2	1.3	-1.0	-2.1	-1.2	-1.1	-	-1.5	1.5	-
NM_007292.3	*ACOX1*			1.5	1.0	1.0	1.4	1.2	1.3	-1.1	1.1	1.3	1.0	1.1	1.1	-1.8	-1.2	-	-1.2	-2.0	-
NM_004458.1	*ACSL4*			1.2	1.4	1.0	1.1	1.6	-1.1	-1.1	1.1	1.3	-1.4	1.2	-2.3	1.6	-1.1	-	1.4	-1.2	-
NM_000778.2	*CYP4A11*			1.1	1.1	1.1	-1.1	1.1	-1.1	1.2	-1.1	1.3	1.4	-1.1	-2.3	-1.5	1.1	-	1.0	1.0	-
NM_001442.1	*FABP4*			1.0	-1.1	-1.1	1.0	-1.4	-1.2	-1.3	1.1	-1.4	-1.5	1.1	-7.6	-1.4	-1.5	-	1.1	-1.7	-
NM_004104.4	*FASN*			-1.1	-1.1	1.3	-1.2	1.0	2.3	-1.2	1.3	1.3	1.1	1.0	-1.9	-2.1	1.1	-	-1.4	1.2	-
NM_198336.1	*INSIG1*			1.2	1.2	1.0	1.3	1.3	1.2	-1.0	-1.2	1.1	1.0	1.0	-2.2	-1.8	1.1	-	-1.1	-1.0	-
NM_145693.1	*LPIN1*			1.2	-1.0	1.0	1.1	1.4	1.4	1.1	1.2	-1.0	1.1	1.2	-2.1	-1.1	1.0	-	1.0	1.0	-
NM_000237.2	*LPL*			1.1	-1.0	-1.3	-1.1	-1.2	-1.2	1.1	1.0	-1.2	-1.0	1.1	-2.8	1.1	-1.2	-	-1.2	1.0	-
NM_002982.3	*CCL2*		Inflammation	-1.0	1.4	1.2	-1.1	1.2	-1.1	1.0	1.2	-1.9	1.0	-1.1	-3.3	3.8	-1.0	-	1.7	-1.0	-
NM_004089.3	*TSC22D3*			1.2	1.0	-1.2	1.1	1.1	1.2	-1.0	1.3	1.0	-1.0	1.2	2.3	-2.2	1.2	-	-1.1	-1.0	-
NM_000064.2	*C3*		Immune response	1.3	1.3	-1.0	1.4	1.2	-1.1	1.1	1.5	1.1	1.1	1.0	6.4	1.3	-1.0	-	-1.1	-1.3	-
NM_005408.2	*CCL13*			1.1	1.1	-1.1	1.0	1.1	-1.3	-1.2	1.2	-2.1	-1.1	1.0	-3.4	1.3	-1.1	-	1.1	-1.2	-
NM_001001391.1	*CD44*			1.1	1.0	-1.1	1.0	-1.0	-1.3	1.0	-1.1	-1.5	-1.0	1.0	-2.8	1.7	-1.1	-	1.2	-1.1	-
NM_000576.2	*IL1B*			-1.1	1.4	-1.2	-1.1	-1.1	-1.2	1.2	-1.0	-1.1	1.2	1.0	2.2	3.9	-1.1	-	1.3	-1.1	-
NM_000600.1	*IL6*			-1.2	-1.0	-1.0	-1.2	-1.1	1.2	-1.0	1.1	-1.1	1.1	1.0	-1.6	2.0	-1.1	-	1.0	-1.0	-
NM_001040058.1	*SPP1*			1.3	1.1	-1.4	1.2	1.3	1.3	-1.4	-1.3	-1.3	-1.1	-1.2	-5.0	1.0	-1.0	-	-1.1	-1.1	-

Table 62 (continued)

RefSeq	Symbol	IPA® Tox function	Function	Donor 1						Donor 2						Donor 3					
				0.5 µM AMI			5 µM AMI			0.5 µM AMI			5 µM AMI			0.5 µM AMI			5 µM AMI		
				d01	d03	d14	d01	d03	d14	d01	d03	d14	d01	d03	d14	d01	d03	d14	d01	d03	d14
NM_000151.2	*G6PC*	Liver Steatosis	Carbo-hydrate metabolism	1.2	-1.1	1.2	-1.0	-1.1	-1.3	1.0	-1.2	-1.5	1.1	-1.1	-4.3	-3.9	-1.2	-	-1.1	-1.2	-
NM_005309.1	*GPT*			-1.0	-1.4	1.1	1.0	-1.2	1.9	-1.0	1.1	1.3	-1.2	1.0	3.1	-1.2	1.0	-	1.2	1.1	-
NM_005544.1	*IRS1*			1.1	1.1	1.3	1.0	-1.1	1.1	1.2	-1.2	-1.2	1.3	1.1	1.3	-2.2	-1.1	-	-1.2	-1.2	-
NM_001752.2	*CAT*		Stress response	-1.0	1.5	-1.0	1.1	1.1	-1.1	1.1	-1.0	2.0	-1.1	1.1	-1.2	-1.6	1.1	-	1.2	-1.2	-
NM_000636.2	*SOD2*			1.7	1.3	1.1	1.5	1.4	1.1	1.1	1.2	1.5	1.3	1.3	1.0	2.3	1.0	-	1.4	-1.3	-
NM_006472.2	*TXNIP*			-1.1	-1.1	-1.0	-1.1	-1.2	-1.8	1.1	-1.1	-1.4	1.0	-1.1	-3.4	-1.4	1.1	-	1.0	1.1	-
NM_003742.2	*ABCB11*		Other and unknown functions	1.1	1.1	-1.2	1.1	1.1	-1.2	-1.1	1.0	-1.0	-1.1	-1.1	-2.0	-2.2	1.1	-	-1.2	-1.1	-
NM_001713.1	*BHMT*			1.2	-1.1	-1.5	1.1	-1.3	-1.1	-1.1	-1.1	1.9	1.1	1.1	8.7	-3.2	-1.0	-	-1.1	-1.1	-
NM_000071.1	*CBS*			1.0	-1.2	1.2	-1.0	-1.3	-1.3	1.3	1.0	1.3	1.3	-1.1	2.9	-1.0	-1.1	-	1.0	-1.0	-
NM_022094.2	*CIDEC*			-1.1	-1.2	1.1	-1.2	-1.0	1.1	-1.1	1.2	-1.2	-1.4	1.2	-9.3	1.2	-1.1	-	-1.1	-1.2	-
NM_005860.2	*FSTL3*			-1.2	-1.0	-1.6	-1.2	1.2	-1.5	-1.0	1.1	1.1	-1.1	-1.2	-1.0	2.2	1.4	-	1.2	1.1	-
NM_005525.2	*HSD11B1*			1.5	-1.0	1.1	1.3	1.0	-1.0	1.1	1.1	-1.1	1.3	-1.0	-2.2	-1.3	-1.1	-	1.1	-1.2	-
NM_000596.2	*IGFBP1*			1.3	1.3	1.1	1.5	1.1	1.5	1.7	1.5	1.8	1.5	1.4	2.1	1.1	-1.2	-	1.4	-1.2	-
NM_018433.3	*KDM3A*			-1.1	1.2	-1.1	-1.1	1.2	-1.0	1.6	-1.1	1.1	1.5	1.2	2.2	-1.1	1.1	-	1.2	-1.0	-
NM_003204.1	*NFE2L1*			-1.1	-1.3	-1.1	-1.1	-1.2	-1.2	-1.1	1.5	1.0	1.0	1.0	2.1	1.1	1.0	-	-1.2	1.1	-
NM_001077475.1	*NR1I3*			1.2	-1.0	-1.2	1.1	-1.1	-1.2	1.1	1.1	1.6	1.1	1.1	3.0	-1.4	1.2	-	-1.1	1.3	-
NM_152869.2	*RGN*			1.2	-1.0	-1.0	1.1	1.0	-1.0	-1.0	1.1	1.3	-1.3	1.2	1.2	-2.0	1.2	-	-1.1	1.1	-
NM_080792.2	*SIRPA*			1.0	-1.2	-1.1	-1.1	-1.1	-1.5	-1.1	1.4	-1.0	1.0	-1.0	2.6	1.4	-1.0	-	1.0	-1.0	-
NM_002982.3	*CCL2*	Liver Fibrosis and Cirrhosis	In-flammation	-1.0	1.4	1.2	-1.1	1.2	-1.1	1.0	1.2	-1.9	1.0	-1.1	-3.3	3.8	-1.0	-	1.7	-1.0	-
NM_005623.2	*CCL8*			-1.3	1.1	1.1	-1.1	-1.1	-2.3	1.1	1.0	-1.5	-1.1	-1.2	-1.1	4.3	-1.2	-	1.6	-2.2	-
NM_001565.2	*CXCL10*			-1.7	1.3	1.0	-1.8	-1.2	-1.0	1.6	-2.1	1.5	1.0	-1.9	-1.1	2.2	-1.0	-	1.4	-1.0	-
NM_002341.1	*LTB*			1.0	-1.1	1.2	-1.1	-1.2	-1.1	-1.1	-1.0	-2.9	1.1	-1.2	-3.6	2.9	1.1	-	1.4	1.0	-
NM_003745.1	*SOCS1*			1.1	-1.1	1.3	-1.0	-1.1	-1.6	-1.1	1.3	-1.7	-1.1	1.2	-1.1	3.9	-1.1	-	1.3	-1.2	-
NM_003955.3	*SOCS3*			1.0	-1.0	1.0	-1.1	-1.1	-1.3	1.3	1.1	-1.9	1.0	1.0	-1.8	3.0	1.1	-	1.0	1.4	-
NM_005408.2	*CCL13*		Immune response	1.1	1.1	-1.1	1.0	1.1	-1.3	-1.2	1.2	-2.1	-1.1	1.0	-3.4	1.3	-1.1	-	1.1	-1.2	-
NM_002985.2	*CCL5*			1.0	-1.4	-1.0	1.1	-1.4	-2.2	1.0	1.0	-2.2	1.1	-1.1	-2.0	1.5	1.1	-	1.0	-1.0	-
NM_001001391.1	*CD44*			1.1	1.0	-1.1	1.0	-1.0	-1.3	1.0	-1.1	-1.5	-1.0	1.0	-2.8	1.7	-1.1	-	1.2	-1.1	-
NM_001025159.1	*CD74*			-1.2	-1.2	-1.2	-1.1	-1.0	-1.7	-1.0	1.2	-1.1	1.0	-1.1	-2.7	-1.1	-1.1	-	-1.3	-1.2	-

Table 62 (continued)

RefSeq	Symbol	IPA® Tox function	Function	Donor 1						Donor 2						Donor 3					
				0.5 µM AMI			5 µM AMI			0.5 µM AMI			5 µM AMI			0.5 µM AMI			5 µM AMI		
				d01	d03	d14	d01	d03	d14	d01	d03	d14	d01	d03	d14	d01	d03	d14	d01	d03	d14
NM_199168.2	*CXCL12*	Liver Fibrosis and Cirrhosis	Immune response	1.0	1.0	-1.1	1.0	-1.2	1.1	-1.2	-1.1	-1.3	-1.3	-1.1	-3.3	1.1	-1.1	-	-1.3	-1.1	-
NM_003467.2	*CXCR4*			1.5	1.0	-1.1	1.5	1.1	1.5	-1.0	1.1	1.0	-1.0	1.2	2.5	-1.1	1.3	-	1.0	1.1	-
NM_000584.2	*IL8*			1.3	1.0	1.1	1.4	1.3	1.2	1.1	1.3	-1.1	-1.0	1.0	-2.1	2.9	1.0	-	1.5	-1.1	-
NM_001040058.1	*SPP1*			1.3	1.1	-1.4	1.2	1.3	1.3	-1.4	-1.3	-1.3	-1.1	-1.2	-5.0	1.0	-1.0	-	-1.1	-1.1	-
NM_003265.2	*TLR3*			1.1	1.1	1.1	1.0	1.1	1.1	1.3	-1.1	1.3	1.3	-1.0	2.5	-1.4	-1.1	-	-1.1	-1.2	-
NM_000088.3	*COL1A1*		ECM organisation	1.1	-1.0	1.1	1.1	1.0	1.7	-1.1	-1.2	1.1	-1.1	-1.2	-10.5	1.1	-1.2	-	1.2	-1.4	-
NM_000089.3	*COL1A2*			1.2	1.0	1.0	1.2	1.1	1.4	-1.2	-1.3	-1.0	-1.0	-1.2	-13.5	1.2	1.0	-	1.0	-1.1	-
NM_000090.3	*COL3A1*			1.2	1.6	-1.1	1.1	1.3	1.2	-1.7	-1.3	-1.1	-1.5	-1.4	-10.4	1.1	-1.2	-	1.1	-1.2	-
NM_001901.1	*CTGF*			-1.2	-1.2	-1.0	-1.1	-1.0	1.4	1.1	-1.2	-1.1	1.0	-1.1	-5.0	-1.9	-1.1	-	1.2	-1.3	-
NM_001998.2	*FBLN2*			1.1	-1.0	-1.0	-1.1	1.0	1.4	-1.2	-1.1	-1.2	-1.3	-1.0	-2.3	-1.0	-1.0	-	1.1	1.1	-
NM_002026.2	*FN1*			1.1	1.2	-1.1	1.1	1.2	-1.1	-1.1	1.1	1.2	1.2	-1.0	3.5	-1.8	-1.2	-	-1.3	-1.3	-
NM_003255.4	*TIMP2*			-1.2	1.0	-1.2	-1.2	-1.0	1.1	-1.2	-1.0	-1.1	-1.1	-1.1	-2.5	-1.1	-1.1	-	1.1	-1.3	-
NM_001964.2	*EGR1*		Cancer	-1.1	-1.0	1.2	-1.2	-1.0	1.2	-1.1	1.5	-1.2	-1.0	1.1	-6.5	-1.1	-1.0	-	-1.0	-1.0	-
NM_004994.2	*MMP9*			1.1	1.1	-1.4	-1.1	-1.1	1.2	-1.1	-1.0	-2.3	1.0	1.0	-4.3	2.2	-1.0	-	1.2	1.0	-
NM_003376.4	*VEGFA*			-1.0	-1.9	1.1	-1.0	-1.5	1.7	1.1	1.2	-1.3	1.2	-1.1	3.9	1.2	-1.1	-	1.0	1.1	-
NM_003742.2	*ABCB11*		Bile acid metabolism	1.1	1.1	-1.2	1.1	1.1	-1.2	-1.1	1.0	-1.0	-1.1	-1.1	-2.0	-2.2	1.1	-	-1.2	-1.1	-
NM_152672.4	*SLC51A*			1.1	-1.0	-1.2	-1.0	-1.0	-1.5	1.4	-1.2	1.1	1.6	-1.1	-1.0	-2.0	1.1	-	-1.0	-1.1	-
NM_178859.2	*SLC51B*			-1.1	1.2	-1.4	-1.0	1.6	1.1	-1.0	1.4	-1.1	-1.1	-1.0	-1.1	-2.5	1.1	-	-1.2	1.1	-
NM_001030004.1	*HNF4A*		Carbo-hydrate metabolism	1.2	-1.4	-1.1	1.1	-1.1	1.1	1.1	1.3	1.1	1.2	1.2	2.3	-1.3	1.1	-	-1.2	1.3	-
NM_000618.2	*IGF1*			1.2	1.1	-1.1	-1.0	-1.0	1.0	-1.0	-1.0	-1.3	-1.0	1.1	-2.4	-1.1	1.0	-	1.0	-1.1	-
NM_017460.3	*CYP3A4*		Xenobiotic metabolism	-1.1	1.1	1.3	1.1	3.1	5.0	-1.1	1.4	1.5	-1.3	1.4	-1.0	-3.2	-1.1	-	1.5	-1.0	-
NM_000024.4	*ADRB2*		Other and unknown functions	1.0	-1.1	1.0	1.0	-1.2	-1.4	1.0	-1.0	1.0	1.1	-1.1	2.2	-1.4	-1.1	-	-1.1	1.1	-
NM_000071.1	*CBS*			1.0	-1.2	1.2	-1.0	-1.3	-1.3	1.3	1.0	1.3	1.3	-1.1	2.9	-1.0	-1.1	-	1.0	-1.0	-
NM_001958.2	*EEF1A2*			-1.1	-1.1	1.0	1.0	1.1	-1.1	-1.0	1.4	1.5	-1.1	1.3	-2.0	1.0	-1.1	-	1.1	-1.1	-
NM_001992.2	*F2R*			1.3	-1.0	1.1	1.1	-1.0	1.4	1.1	-1.1	-1.0	-1.1	-1.2	-4.0	-1.2	1.3	-	1.1	1.0	-
NM_000131.3	*F7*			-1.0	-1.3	1.0	-1.1	-1.3	-1.3	-1.0	1.1	1.5	-1.0	-1.1	2.8	-1.0	-1.1	-	-1.0	1.0	-
NM_013409.1	*FST*			-1.2	1.2	-1.4	-1.1	1.1	1.3	1.0	-1.1	1.0	1.6	-1.0	-2.6	-1.3	1.1	-	-1.0	1.1	-

Table 62 (continued)

RefSeq	Symbol	IPA® Tox function	Function	Donor 1						Donor 2						Donor 3					
				0.5 µM AMI			5 µM AMI			0.5 µM AMI			5 µM AMI			0.5 µM AMI			5 µM AMI		
				d01	d03	d14	d01	d03	d14	d01	d03	d14	d01	d03	d14	d01	d03	d14	d01	d03	d14
NM_005265.2	*GGT1*	Liver Fibrosis and Cirrhosis	Other and unknown functions	-1.3	-1.1	-1.3	-1.2	-1.2	1.1	-1.0	1.6	1.1	1.1	1.1	2.7	-1.2	1.2	-	-1.2	2.2	-
NM_005534.2	*IFNGR2*			1.0	1.1	-1.0	-1.0	1.1	-1.0	-1.1	-1.2	-1.2	-1.0	-1.1	-2.1	1.2	-1.1	-	1.0	-1.1	-
NM_003204.1	*NFE2L1*			-1.1	-1.3	-1.1	-1.1	-1.2	-1.2	-1.1	1.5	1.0	1.0	1.0	2.1	1.1	1.0	-	-1.2	1.1	-
NM_000602.1	*SERPINE1*			-1.0	1.0	-1.3	-1.1	1.0	-1.1	1.4	1.4	1.1	2.0	1.1	2.5	1.2	-1.1	-	-1.0	-1.1	-

Table 63. Full gene names of the appropriate RefSeqs and Symbols given in Table 59 - Table 62 (alphabetical order).

RefSeq	Symbol	Gene name
NM_001086.2	*AADAC*	arylacetamide deacetylase
NM_005502.2	*ABCA1*	ATP-binding cassette, sub-family A (ABC1), member 1
NM_000927.3	*ABCB1*	ATP-binding cassette, sub-family B (MDR/TAP), member 1
NM_003742.2	*ABCB11*	ATP-binding cassette, sub-family B (MDR/TAP), member 11
NM_018850.2	*ABCB4*	ATP-binding cassette, sub-family B (MDR/TAP), member 4
NM_005689.1	*ABCB6*	ATP-binding cassette, sub-family B (MDR/TAP), member 6
NM_000392.1	*ABCC2*	ATP-binding cassette, sub-family C (CFTR/MRP), member 2
NM_001171.3	*ABCC6*	ATP-binding cassette, sub-family C (CFTR/MRP), member 6
NM_016818.2	*ABCG1*	ATP-binding cassette, sub-family G (WHITE), member 1
NM_016006.3	*ABHD5*	abhydrolase domain containing 5
NM_198836.1	*ACACA*	acetyl-CoA carboxylase alpha
NM_000016.2	*ACADM*	acyl-CoA dehydrogenase, C-4 to C-12 straight chain
NM_001033859.1	*ACADVL*	acyl-CoA dehydrogenase, very long chain
NM_000018.2	*ACADVL*	acyl-CoA dehydrogenase, very long chain
NM_018473.2	*ACOT13*	acyl-CoA thioesterase 13
NM_007292.4	*ACOX1*	acyl-CoA oxidase 1, palmitoyl
NM_007292.3	*ACOX1*	acyl-CoA oxidase 1, palmitoyl
NM_003500.2	*ACOX2*	acyl-CoA oxidase 2, branched chain
NM_001995.2	*ACSL1*	acyl-CoA synthetase long-chain family member 1
NM_004458.1	*ACSL4*	acyl-CoA synthetase long-chain family member 4
NM_001614.2	*ACTG1*	actin, gamma 1
XM_001124642.1	*ACY1*	aminoacylase 1
NM_003183.4	*ADAM17*	ADAM metallopeptidase domain 17
NM_006988.3	*ADAMTS1*	ADAM metallopeptidase with thrombospondin type 1 motif, 1
NM_000668.3	*ADH1B*	alcohol dehydrogenase 1B (class I), beta polypeptide
NM_000669.3	*ADH1C*	alcohol dehydrogenase 1C (class I), gamma polypeptide
NM_000670.3	*ADH4*	alcohol dehydrogenase 4 (class II), pi polypeptide
NM_000672.2	*ADH6*	alcohol dehydrogenase 6 (class V)
NM_001123.2	*ADK*	adenosine kinase
NM_000675.3	*ADORA2A*	adenosine A2a receptor
NM_000024.4	*ADRB2*	adrenoceptor beta 2, surface
NM_001134.1	*AFP*	alpha-fetoprotein
NM_001012727.1	*AGPAT2*	1-acylglycerol-3-phosphate O-acyltransferase 2
NM_006412.3	*AGPAT2*	1-acylglycerol-3-phosphate O-acyltransferase 2
NM_005100.2	*AKAP12*	A kinase (PRKA) anchor protein 12
NM_020299.3	*AKR1B10*	aldo-keto reductase family 1, member B10 (aldose reductase)
XM_943415.1	*AKR1C2*	aldo-keto reductase family 1, member C2
NM_005989.2	*AKR1D1*	aldo-keto reductase family 1, member D1
NM_000035.2	*ALDOB*	aldolase B, fructose-bisphosphate
NM_000478.3	*ALPL*	alkaline phosphatase, liver/bone/kidney
NM_001633.2	*AMBP*	alpha-1-microglobulin/bikunin precursor

Table 63 (continued)

RefSeq	Symbol	Gene name
NM_031917.2	*ANGPTL6*	angiopoietin-like 6
NM_000700.1	*ANXA1*	annexin A1
NM_001002857.1	*ANXA2*	annexin A2
NM_052968.3	*APOA5*	apolipoprotein A-V
NM_000041.2	*APOE*	apolipoprotein E
NM_001011645.1	*AR*	androgen receptor
NM_173454.1	*AR*	androgen receptor
NM_152641.2	*ARID2*	AT rich interactive domain 2 (ARID, RFX-like)
NM_000047.1	*ARSE*	arylsulfatase E (chondrodysplasia punctata 1)
NM_001679.2	*ATP1B3*	ATPase, Na+/K+ transporting, beta 3 polypeptide
NM_198434.1	*AURKA*	aurora kinase A
NM_181050.1	*AXIN1*	axin 1
NM_001497.2	*B4GALT1*	UDP-Gal:betaGlcNAc beta 1,4- galactosyltransferase, polypeptide 1
NM_004281.3	*BAG3*	BCL2-associated athanogene 3
NM_001713.1	*BHMT*	betaine--homocysteine S-methyltransferase
NM_001166.3	*BIRC2*	baculoviral IAP repeat containing 2
NM_198590.1	*BSG*	basigin (Ok blood group)
NM_014670.2	*BZW1*	basic leucine zipper and W2 domains 1
NM_201442.1	*C1S*	complement component 1, s subcomponent
NM_001734.2	*C1S*	complement component 1, s subcomponent
NM_000064.1	*C3*	complement component 3
NM_000064.2	*C3*	complement component 3
NM_000592.4	*C4A*	complement component 4B (Chido blood group)
NM_000715.3	*C4BPA*	complement component 4 binding protein, alpha
NM_001737.2	*C9*	complement component 9
NM_001216.1	*CA9*	carbonic anhydrase IX
NM_153768.1	*CABYR*	calcium binding tyrosine-(Y)-phosphorylation regulated
NM_001080125.1	*CASP8*	caspase 8, apoptosis-related cysteine peptidase
NM_001752.2	*CAT*	catalase
NM_001753.3	*CAV1*	caveolin 1, caveolae protein, 22kDa
NM_000071.1	*CBS*	cystathionine-beta-synthase
NM_005408.2	*CCL13*	chemokine (C-C motif) ligand 13
NM_002982.3	*CCL2*	chemokine (C-C motif) ligand 2
NM_001001437.3	*CCL3L1*	chemokine (C-C motif) ligand 3-like 1
NM_021006.4	*CCL3L1*	chemokine (C-C motif) ligand 3-like 1
NM_002985.2	*CCL5*	chemokine (C-C motif) ligand 5
NM_005623.2	*CCL8*	chemokine (C-C motif) ligand 8
NM_053056.2	*CCND1*	cyclin D1
NM_001238.1	*CCNE1*	cyclin E1
NM_000591.2	*CD14*	CD14 molecule
NM_001001392.1	*CD44*	CD44 molecule (Indian blood group)
NM_031917.2	*ANGPTL6*	angiopoietin-like 6

Table 63 (continued)

RefSeq	Symbol	Gene name
NM_001001391.1	*CD44*	CD44 molecule (Indian blood group)
NM_000574.2	*CD55*	CD55 molecule, decay accelerating factor for complement (Cromer blood group)
NM_001025159.1	*CD74*	CD74 molecule, major histocompatibility complex, class II invariant chain
NM_001024844.1	*CD82*	CD82 molecule
NM_004358.3	*CDC25B*	cell division cycle 25B
NM_004360.2	*CDH1*	cadherin 1, type 1, E-cadherin (epithelial)
NM_000075.2	*CDK4*	cyclin-dependent kinase 4
NM_176096.1	*CDK5RAP3*	CDK5 regulatory subunit associated protein 3
NM_078467.1	*CDKN1A*	cyclin-dependent kinase inhibitor 1A (p21, Cip1)
NM_004064.2	*CDKN1B*	cyclin-dependent kinase inhibitor 1B (p27, Kip1)
NM_078487.2	*CDKN2B*	cyclin-dependent kinase inhibitor 2B (p15, inhibits CDK4)
NM_004364.2	*CEBPA*	CCAAT/enhancer binding protein (C/EBP), alpha
NM_001266.4	*CES1*	carboxylesterase 1
NM_021023.3	*CFHR3*	complement factor H-related 3
NM_021023.4	*CFHR3*	complement factor H-related 3
NM_006684.2	*CFHR4*	complement factor H-related 4
NM_022094.2	*CIDEC*	cell death-inducing DFFA-like effector c
NM_006079.3	*CITED2*	Cbp/p300-interacting transactivator, with Glu/Asp-rich carboxy-terminal domain, 2
NM_001826.1	*CKS1B*	CDC28 protein kinase regulatory subunit 1B
NM_001827.1	*CKS2*	CDC28 protein kinase regulatory subunit 2
NM_032649.5	*CNDP1*	carnosine dipeptidase 1 (metallopeptidase M20 family)
NM_000088.3	*COL1A1*	collagen, type I, alpha 1
NM_000089.3	*COL1A2*	collagen, type I, alpha 2
NM_000090.3	*COL3A1*	collagen, type III, alpha 1
NM_000096.1	*CP*	ceruloplasmin (ferroxidase)
NM_001031847.1	*CPT1A*	carnitine palmitoyltransferase 1A (liver)
NM_004379.2	*CREB1*	cAMP responsive element binding protein 1
NM_032607.1	*CREB3L3*	cAMP responsive element binding protein 3-like 3
NM_024324.2	*CRELD2*	cysteine-rich with EGF-like domains 2
NM_000567.2	*CRP*	C-reactive protein, pentraxin-related
NM_005211.2	*CSF1R*	colony stimulating factor 1 receptor
NM_001901.1	*CTGF*	connective tissue growth factor
NM_138455.2	*CTHRC1*	collagen triple helix repeat containing 1
NM_001511.1	*CXCL1*	chemokine (C-X-C motif) ligand 1 (melanoma growth stimulating activity, alpha)
NM_001565.2	*CXCL10*	chemokine (C-X-C motif) ligand 10
NM_199168.2	*CXCL12*	chemokine (C-X-C motif) ligand 12
NM_002089.3	*CXCL2*	chemokine (C-X-C motif) ligand 2
NM_002993.2	*CXCL6*	chemokine (C-X-C motif) ligand 6
NM_003467.2	*CXCR4*	chemokine (C-X-C motif) receptor 4

Table 63 (continued)

RefSeq	Symbol	Gene name
NM_000499.2	*CYP1A1*	cytochrome P450, family 1, subfamily A, polypeptide 1
NM_000771.2	*CYP2C9*	cytochrome P450, family 2, subfamily C, polypeptide 9
NM_000773.3	*CYP2E1*	cytochrome P450, family 2, subfamily E, polypeptide 1
NM_017460.3	*CYP3A4*	cytochrome P450, family 3, subfamily A, polypeptide 4
NM_000778.2	*CYP4A11*	cytochrome P450, family 4, subfamily A, polypeptide 11
NM_004820.2	*CYP7B1*	cytochrome P450, family 7, subfamily B, polypeptide 1
NM_000790.2	*DDC*	dopa decarboxylase (aromatic L-amino acid decarboxylase)
NM_001356.3	*DDX3X*	DEAD (Asp-Glu-Ala-Asp) box helicase 3, X-linked
NM_032564.2	*DGAT2*	diacylglycerol O-acyltransferase 2
NM_033257.2	*DGCR6L*	DiGeorge syndrome critical region gene 6-like
NM_012242.2	*DKK1*	dickkopf WNT signaling pathway inhibitor 1
NM_013352.2	*DSE*	dermatan sulfate epimerase
NM_004417.2	*DUSP1*	dual specificity phosphatase 1
NM_018098.4	*ECT2*	epithelial cell transforming sequence 2 oncogene
NM_001958.2	*EEF1A2*	eukaryotic translation elongation factor 1 alpha 2
NM_198156.1	*EGLN3*	egl-9 family hypoxia-inducible factor 3
NM_001964.2	*EGR1*	early growth response 1
NM_001966.2	*EHHADH*	enoyl-CoA, hydratase/3-hydroxyacyl CoA dehydrogenase
NM_001412.3	*EIF1AX*	eukaryotic translation initiation factor 1A, X-linked
NM_001968.2	*EIF4E*	eukaryotic translation initiation factor 4E
NM_014800.9	*ELMO1*	engulfment and cell motility 1
NM_021814.3	*ELOVL5*	ELOVL fatty acid elongase 5
NM_001040092.1	*ENPP2*	ectonucleotide pyrophosphatase/phosphodiesterase 2
NM_001098175.1	*ENTPD1*	ectonucleoside triphosphate diphosphohydrolase 1
NM_001249.1	*ENTPD5*	ectonucleoside triphosphate diphosphohydrolase 5
NM_004431.2	*EPHA2*	EPH receptor A2
NM_000799.2	*EPO*	erythropoietin
NM_004448.2	*ERBB2*	v-erb-b2 erythroblastic leukemia viral oncogene homolog 2, neuro/glioblastoma derived oncogene homolog (avian)
NM_001005915.1	*ERBB3*	v-erb-b2 erythroblastic leukemia viral oncogene homolog 3 (avian)
NM_000125.2	*ESR1*	estrogen receptor 1
NM_001992.2	*F2R*	coagulation factor II (thrombin) receptor
NM_001993.2	*F3*	coagulation factor III (thromboplastin, tissue factor)
NM_000131.3	*F7*	coagulation factor VII (serum prothrombin conversion accelerator)
NM_001442.1	*FABP4*	fatty acid binding protein 4, adipocyte
NM_000137.1	*FAH*	fumarylacetoacetate hydrolase (fumarylacetoacetase)
NM_001033030.1	*FAIM*	Fas apoptotic inhibitory molecule
NM_030919.2	*FAM83D*	family with sequence similarity 83, member D
NM_152877.1	*FAS*	Fas cell surface death receptor
NM_004104.4	*FASN*	fatty acid synthase
NM_001998.2	*FBLN2*	fibulin 2
NM_033632.2	*FBXW7*	F-box and WD repeat domain containing 7, E3 ubiquitin protein ligase

Table 63 (continued)

RefSeq	Symbol	Gene name
NM_003665.2	*FCN3*	ficolin (collagen/fibrinogen domain containing) 3 (Hakata antigen)
NM_000508.3	*FGA*	fibrinogen alpha chain
NM_002006.3	*FGF2*	fibroblast growth factor 2 (basic)
NM_019113.2	*FGF21*	fibroblast growth factor 21
NM_004467.3	*FGL1*	fibrinogen-like 1
NM_002026.2	*FN1*	fibronectin 1
NM_005252.2	*FOS*	FBJ murine osteosarcoma viral oncogene homolog
NM_033260.3	*FOXQ1*	forkhead box Q1
NM_013409.1	*FST*	follistatin
NM_005860.2	*FSTL3*	follistatin-like 3 (secreted glycoprotein)
NM_000151.2	*G6PC*	glucose-6-phosphatase, catalytic subunit
NM_001924.2	*GADD45A*	growth arrest and DNA-damage-inducible, alpha
NM_001482.2	*GATM*	glycine amidinotransferase (L-arginine:glycine amidinotransferase)
NM_005265.2	*GGT1*	gamma-glutamyltransferase 1
NM_000163.2	*GHR*	growth hormone receptor
NM_000166.4	*GJB1*	gap junction protein, beta 1, 32kDa
NM_000167.3	*GK*	glycerol kinase
NM_203391.1	*GK*	glycerol kinase
NM_018960.4	*GNMT*	glycine N-methyltransferase
NM_177937.1	*GOLM1*	golgi membrane protein 1
NM_003801.3	*GPAA1*	glycosylphosphatidylinositol anchor attachment 1
NM_005276.2	*GPD1*	glycerol-3-phosphate dehydrogenase 1 (soluble)
NM_001083112.1	*GPD2*	glycerol-3-phosphate dehydrogenase 2 (mitochondrial)
NM_004489.4	*GPS2*	G protein pathway suppressor 2
NM_005309.1	*GPT*	glutamic-pyruvate transaminase (alanine aminotransferase)
NM_002083.2	*GPX2*	glutathione peroxidase 2 (gastrointestinal)
NM_000846.3	*GSTA2*	glutathione S-transferase alpha 2
NM_000561.2	*GSTM1*	glutathione S-transferase mu 1
NR_002196.1	*H19*	H19, imprinted maternally expressed transcript (non-protein coding)
NM_004132.2	*HABP2*	hyaluronan binding protein 2
NM_000182.4	*HADHA*	hydroxyacyl-CoA dehydrogenase/3-ketoacyl-CoA thiolase/enoyl-CoA hydratase (trifunctional protein), alpha subunit
NM_021175.2	*HAMP*	hepcidin antimicrobial peptide
NM_001945.1	*HBEGF*	heparin-binding EGF-like growth factor
NM_004712.3	*HGS*	hepatocyte growth factor-regulated tyrosine kinase substrate
NM_001530.2	*HIF1A*	hypoxia inducible factor 1, alpha subunit (basic helix-loop-helix transcription factor)
NM_002128.4	*HMGB1*	high mobility group box 1
NM_000859.1	*HMGCR*	3-hydroxy-3-methylglutaryl-CoA reductase
NM_000545.4	*HNF1A*	HNF1 homeobox A
NM_178850.1	*HNF4A*	hepatocyte nuclear factor 4, alpha
NM_001030004.1	*HNF4A*	hepatocyte nuclear factor 4, alpha

Table 63 (continued)

RefSeq	Symbol	Gene name
NR_003249.1	*HNRPDL*	heterogeneous nuclear ribonucleoprotein D-like
NM_000666.1	*HPX*	hemopexin
NM_005525.2	*HSD11B1*	hydroxysteroid (11-beta) dehydrogenase 1
NM_003725.2	*HSD17B6*	hydroxysteroid (17-beta) dehydrogenase 6
NM_005347.2	*HSPA5*	heat shock 70kDa protein 5 (glucose-regulated protein, 78kDa)
NM_000867.3	*HTR2B*	5-hydroxytryptamine (serotonin) receptor 2B, G protein-coupled
NM_000201.1	*ICAM1*	intercellular adhesion molecule 1
NM_207585.1	*IFNAR2*	interferon (alpha, beta and omega) receptor 2
NM_005534.2	*IFNGR2*	interferon gamma receptor 2 (interferon gamma transducer 1)
NM_006531.3	*IFT88*	intraflagellar transport 88 homolog (Chlamydomonas)
NM_000618.2	*IGF1*	insulin-like growth factor 1 (somatomedin C)
NM_000596.2	*IGFBP1*	insulin-like growth factor binding protein 1
NM_000597.2	*IGFBP2*	insulin-like growth factor binding protein 2, 36kDa
NM_000598.4	*IGFBP3*	insulin-like growth factor binding protein 3
NM_001099856.1	*IKBKG*	inhibitor of kappa light polypeptide gene enhancer in B-cells, kinase gamma
NM_000576.2	*IL1B*	interleukin 1, beta
NM_173843.1	*IL1RN*	interleukin 1 receptor antagonist
NM_173842.1	*IL1RN*	interleukin 1 receptor antagonist
NM_004843.2	*IL27RA*	interleukin 27 receptor, alpha
NM_000600.1	*IL6*	interleukin 6 (interferon, beta 2)
NM_002184.2	*IL6ST*	interleukin 6 signal transducer (gp130, oncostatin M receptor)
NM_000584.2	*IL8*	interleukin 8
NM_198336.1	*INSIG1*	insulin induced gene 1
NM_016133.2	*INSIG2*	insulin induced gene 2
NM_006391.1	*IPO7*	importin 7
NM_006633.2	*IQGAP2*	IQ motif containing GTPase activating protein 2
NM_005544.1	*IRS1*	insulin receptor substrate 1
NM_003749.2	*IRS2*	insulin receptor substrate 2
NM_002205.2	*ITGA5*	integrin, alpha 5 (fibronectin receptor, alpha polypeptide)
NM_002218.3	*ITIH4*	inter-alpha-trypsin inhibitor heavy chain family, member 4
NM_004972.2	*JAK2*	Janus kinase 2
NM_018433.3	*KDM3A*	lysine (K)-specific demethylase 3A
NM_001093772.1	*KIT*	v-kit Hardy-Zuckerman 4 feline sarcoma viral oncogene homolog
NM_000893.2	*KNG1*	kininogen 1
NM_000527.2	*LDLR*	low density lipoprotein receptor
NM_002302.2	*LECT2*	leukocyte cell-derived chemotaxin 2
NM_001003679.1	*LEPR*	leptin receptor
NM_005577.2	*LPA*	lipoprotein, Lp(a)
NM_057159.2	*LPAR1*	lysophosphatidic acid receptor 1
NM_145693.1	*LPIN1*	lipin 1
NM_000237.2	*LPL*	lipoprotein lipase

Table 63 (continued)

RefSeq	Symbol	Gene name
NM_052972.2	*LRG1*	leucine-rich alpha-2-glycoprotein 1
NM_002341.1	*LTB*	lymphotoxin beta (TNF superfamily, member 3)
NM_002342.1	*LTBR*	lymphotoxin beta receptor (TNFR superfamily, member 3)
NM_000240.2	*MAOA*	monoamine oxidase A
NM_012325.1	*MAPRE1*	microtubule-associated protein, RP/EB family, member 1
NM_001879.4	*MASP1*	mannan-binding lectin serine peptidase 1 (C4/C2 activating component of Ra-reactive factor)
NM_139125.2	*MASP1*	mannan-binding lectin serine peptidase 1 (C4/C2 activating component of Ra-reactive factor)
NM_000429.2	*MAT1A*	methionine adenosyltransferase I, alpha
NM_005911.4	*MAT2A*	methionine adenosyltransferase II, alpha
NM_002392.2	*MDM2*	MDM2 oncogene, E3 ubiquitin protein ligase
NM_000245.2	*MET*	met proto-oncogene (hepatocyte growth factor receptor)
NM_004958.2	*MGMT*	O-6-methylguanine-DNA methyltransferase
NM_004994.2	*MMP9*	matrix metallopeptidase 9 (gelatinase B, 92kDa gelatinase, 92kDa type IV collagenase)
NM_002447.2	*MST1R*	macrophage stimulating 1 receptor (c-met-related tyrosine kinase)
NM_175617.2	*MT1E*	metallothionein 1E
NM_005957.2	*MTHFR*	methylenetetrahydrofolate reductase (NAD(P)H)
NM_006623.2	*MTOR*	mechanistic target of rapamycin (serine/threonine kinase)
NM_000253.2	*MTTP*	microsomal triglyceride transfer protein
NM_000255.1	*MUT*	methylmalonyl CoA mutase
NM_002467.3	*MYC*	v-myc myelocytomatosis viral oncogene homolog (avian)
NM_198055.1	*MZF1*	myeloid zinc finger 1
NM_006096.2	*NDRG1*	N-myc downstream regulated 1
NM_003204.1	*NFE2L1*	nuclear factor, erythroid 2-like 1
NM_003998.2	*NFKB1*	nuclear factor of kappa light polypeptide gene enhancer in B-cells 1
NM_198175.1	*NME1*	NME/NM23 nucleoside diphosphate kinase 1
NM_006169.2	*NNMT*	nicotinamide N-methyltransferase
NM_153292.1	*NOS2*	nitric oxide synthase 2, inducible
NM_000271.3	*NPC1*	Niemann-Pick disease, type C1
NM_000903.2	*NQO1*	NAD(P)H dehydrogenase, quinone 1
NM_021969.1	*NR0B2*	nuclear receptor subfamily 0, group B, member 2
NM_005693.1	*NR1H3*	nuclear receptor subfamily 1, group H, member 3
NM_001077469.1	*NR1I3*	nuclear receptor subfamily 1, group I, member 3
NM_001077475.1	*NR1I3*	nuclear receptor subfamily 1, group I, member 3
NM_002524.2	*NRAS*	neuroblastoma RAS viral (v-ras) oncogene homolog
NM_000613.1	*NUPR1*	nuclear protein, transcriptional regulator, 1
NM_001042483.1	*NUPR1*	nuclear protein, transcriptional regulator, 1
NM_018454.5	*NUSAP1*	nucleolar and spindle associated protein 1
NM_022073.3	*OMA1*	OMA1 zinc metallopeptidase
NM_003999.1	*OSMR*	oncostatin M receptor

Table 63 (continued)

RefSeq	Symbol	Gene name
NM_000277.1	*PAH*	phenylalanine hydroxylase
NM_148978.1	*PANK1*	pantothenate kinase 1
NM_152341.2	*PAQR4*	progestin and adipoQ receptor family member IV
NM_030593.1	*PARG*	poly (ADP-ribose) glycohydrolase
NM_001618.2	*PARP1*	poly (ADP-ribose) polymerase 1
NM_002591.2	*PCK1*	phosphoenolpyruvate carboxykinase 1 (soluble)
NM_000922.2	*PDE3B*	phosphodiesterase 3B, cGMP-inhibited
NM_002600.3	*PDE4B*	phosphodiesterase 4B, cAMP-specific
NM_001083.3	*PDE5A*	phosphodiesterase 5A, cGMP-specific
NM_145243.3	*PDE8A*	phosphodiesterase 8A
NM_006206.3	*PDGFRA*	platelet-derived growth factor receptor, alpha polypeptide
NM_002609.3	*PDGFRB*	platelet-derived growth factor receptor, beta polypeptide
NM_002612.3	*PDK4*	pyruvate dehydrogenase kinase, isozyme 4
NM_007169.2	*PEMT*	phosphatidylethanolamine N-methyltransferase
NM_000291.2	*PGK1*	phosphoglycerate kinase 1
NM_052890.3	*PGLYRP2*	peptidoglycan recognition protein 2
NM_001037537.1	*PHYH*	phytanoyl-CoA 2-hydroxylase
NM_006218.2	*PIK3CA*	phosphatidylinositol-4,5-bisphosphate 3-kinase, catalytic subunit alpha
NM_052880.3	*PIK3IP1*	phosphoinositide-3-kinase interacting protein 1
NM_181523.1	*PIK3R1*	phosphoinositide-3-kinase, regulatory subunit 1 (alpha)
NM_001005376.1	*PLAUR*	plasminogen activator, urokinase receptor
NM_000301.1	*PLG*	plasminogen
NM_001122.2	*PLIN2*	perilipin 2
NM_020376.2	*PNPLA2*	patatin-like phospholipase domain containing 2
NM_006813.1	*PNRC1*	proline-rich nuclear receptor coactivator 1
NM_017761.2	*PNRC2*	proline-rich nuclear receptor coactivator 2
NM_002692.2	*POLE2*	polymerase (DNA directed), epsilon 2, accessory subunit
NM_002693.1	*POLG*	polymerase (DNA directed), gamma
NM_000941.2	*POR*	P450 (cytochrome) oxidoreductase
NM_001001928.2	*PPARA*	peroxisome proliferator-activated receptor alpha
NM_015869.4	*PPARG*	peroxisome proliferator-activated receptor gamma
NM_013261.3	*PPARGC1A*	peroxisome proliferator-activated receptor gamma, coactivator 1 alpha
NM_005398.4	*PPP1R3C*	protein phosphatase 1, regulatory subunit 3C
NM_004156.2	*PPP2CB*	protein phosphatase 2, catalytic subunit, beta isozyme
NM_002734.3	*PRKAR1A*	protein kinase, cAMP-dependent, regulatory, type I, alpha
NM_002763.3	*PROX1*	prospero homeobox 1
NM_000021.2	*PSEN1*	presenilin 1
NM_002800.4	*PSMB9*	proteasome (prosome, macropain) subunit, beta type, 9
NM_005789.2	*PSME3*	proteasome (prosome, macropain) activator subunit 3 (PA28 gamma; Ki)
NM_000958.2	*PTGER4*	prostaglandin E receptor 4 (subtype EP4)

Table 63 (continued)

RefSeq	Symbol	Gene name
NM_080591.1	*PTGS1*	prostaglandin-endoperoxide synthase 1 (prostaglandin G/H synthase and cyclooxygenase)
NM_000963.1	*PTGS2*	prostaglandin-endoperoxide synthase 2 (prostaglandin G/H synthase and cyclooxygenase)
NM_000964.2	*RARA*	retinoic acid receptor, alpha
NM_007182.4	*RASSF1*	Ras association (RalGDS/AF-6) domain family member 1
NM_182664.2	*RASSF5*	Ras association (RalGDS/AF-6) domain family member 5
NM_003708.3	*RDH16*	retinol dehydrogenase 16 (all-trans)
NM_006507.2	*REG1B*	regenerating islet-derived 1 beta
NM_021975.2	*RELA*	v-rel avian reticuloendotheliosis viral oncogene homolog A
NM_006509.2	*RELB*	v-rel avian reticuloendotheliosis viral oncogene homolog B
NM_020630.4	*RET*	ret proto-oncogene
NM_152869.2	*RGN*	regucalcin (senescence marker protein-30)
NM_001024921.2	*RPL9*	ribosomal protein L9
NM_019554.2	*S100A4*	S100 calcium binding protein A4
NM_152703.2	*SAMD9L*	sterile alpha motif domain containing 9-like
NM_002979.3	*SCP2*	sterol carrier protein 2
NM_001002236.1	*SERPINA1*	serpin peptidase inhibitor, clade A (alpha-1 antiproteinase, antitrypsin), member 1
NM_001756.3	*SERPINA6*	serpin peptidase inhibitor, clade A (alpha-1 antiproteinase, antitrypsin), member 6
NM_000602.1	*SERPINE1*	serpin peptidase inhibitor, clade E (nexin, plasminogen activator inhibitor type 1), member 1
NM_080792.2	*SIRPA*	signal-regulatory protein alpha
NM_012238.3	*SIRT1*	sirtuin 1
NM_012385.1	*SIRT1*	sirtuin 1
NM_002150.2	*SIRT2*	sirtuin 2
NM_032637.2	*SKP2*	S-phase kinase-associated protein 2, E3 ubiquitin protein ligase
NM_003049.2	*SLC10A1*	solute carrier family 10 (sodium/bile acid cotransporter family), member 1
NM_001046.2	*SLC12A2*	solute carrier family 12 (sodium/potassium/chloride transporter), member 2
NM_005074.2	*SLC17A1*	solute carrier family 17 (organic anion transporter), member 1
NM_003057.2	*SLC22A1*	solute carrier family 22 (organic cation transporter), member 1
NM_153187.1	*SLC22A1*	solute carrier family 22 (organic cation transporter), member 1
NM_003060.2	*SLC22A5*	solute carrier family 22 (organic cation/carnitine transporter), member 5
NM_080866.2	*SLC22A9*	solute carrier family 22 (organic anion transporter), member 9
NM_012254.1	*SLC27A5*	solute carrier family 27 (fatty acid transporter), member 5
NM_006516.1	*SLC2A1*	solute carrier family 2 (facilitated glucose transporter), member 1
NM_018389.3	*SLC35C1*	solute carrier family 35 (GDP-fucose transporter), member C1
NM_018242.2	*SLC47A1*	solute carrier family 47, member 1
NM_152672.4	*SLC51A*	solute carrier family 51, alpha subunit
NM_178859.2	*SLC51B*	solute carrier family 51, beta subunit

Table 63 (continued)

RefSeq	Symbol	Gene name
NM_003486.5	*SLC7A5*	solute carrier family 7 (amino acid transporter light chain, L system), member 5
NM_006446.3	*SLCO1B1*	solute carrier organic anion transporter family, member 1B1
NM_019844.2	*SLCO1B3*	solute carrier organic anion transporter family, member 1B3
NM_003745.1	*SOCS1*	suppressor of cytokine signaling 1
NM_003955.3	*SOCS3*	suppressor of cytokine signaling 3
NM_000636.2	*SOD2*	superoxide dismutase 2, mitochondrial
NM_003107.2	*SOX4*	SRY (sex determining region Y)-box 4
NM_000346.2	*SOX9*	SRY (sex determining region Y)-box 9
NM_003118.2	*SPARC*	secreted protein, acidic, cysteine-rich (osteonectin)
NM_004684.2	*SPARCL1*	SPARC-like 1 (hevin)
NM_003120.2	*SPI1*	spleen focus forming virus (SFFV) proviral integration oncogene
NM_000582.2	*SPP1*	secreted phosphoprotein 1
NM_001040058.1	*SPP1*	secreted phosphoprotein 1
NM_004176.3	*SREBF1*	sterol regulatory element binding transcription factor 1
NM_001005291.1	*SREBF1*	sterol regulatory element binding transcription factor 1
NM_139276.2	*STAT3*	signal transducer and activator of transcription 3 (acute-phase response factor)
NM_213662.1	*STAT3*	signal transducer and activator of transcription 3 (acute-phase response factor)
NM_002353.1	*TACSTD2*	tumor-associated calcium signal transducer 2
NM_000544.3	*TAP2*	transporter 2, ATP-binding cassette, sub-family B (MDR/TAP)
NM_005651.1	*TDO2*	tryptophan 2,3-dioxygenase
NM_003236.1	*TGFA*	transforming growth factor, alpha
NM_003246.2	*THBS1*	thrombospondin 1
NM_006288.2	*THY1*	Thy-1 cell surface antigen
NM_003255.4	*TIMP2*	TIMP metallopeptidase inhibitor 2
NM_003265.2	*TLR3*	toll-like receptor 3
NM_138554.2	*TLR4*	toll-like receptor 4
NM_014220.2	*TM4SF1*	transmembrane 4 L six family member 1
NM_000594.2	*TNF*	tumor necrosis factor
NM_001561.4	*TNFRSF9*	tumor necrosis factor receptor superfamily, member 9
NM_003810.2	*TNFSF10*	tumor necrosis factor (ligand) superfamily, member 10
NM_001068.2	*TOP2B*	topoisomerase (DNA) II beta 180kDa
NM_015905.2	*TRIM24*	tripartite motif containing 24
NM_030912.2	*TRIM8*	tripartite motif containing 8
NM_004089.3	*TSC22D3*	TSC22 domain family, member 3
NM_006088.5	*TUBB4B*	tubulin, beta 4B class IVb
NM_006472.2	*TXNIP*	thioredoxin interacting protein
NM_002412.2	*TXNIP*	thioredoxin interacting protein
NM_001113756.1	*TYMP*	thymidine phosphorylase
NM_004181.3	*UCHL1*	ubiquitin carboxyl-terminal esterase L1 (ubiquitin thiolesterase)
NM_006759.3	*UGP2*	UDP-glucose pyrophosphorylase 2

Table 63 (continued)

RefSeq	Symbol	Gene name
NM_000463.2	*UGT1A1*	UDP glucuronosyltransferase 1 family, polypeptide A1
NM_019093.2	*UGT1A3*	UDP glucuronosyltransferase 1 family, polypeptide A3
NM_007120.2	*UGT1A4*	UDP glucuronosyltransferase 1 family, polypeptide A4
NM_001072.3	*UGT1A6*	UDP glucuronosyltransferase 1 family, polypeptide A6
NM_019075.2	*UGT1A9*	UDP glucuronosyltransferase 1 family, polypeptide A8
NM_001075.3	*UGT2B10*	UDP glucuronosyltransferase 2 family, polypeptide B10
XM_001127829.1	*UGT2B15*	UDP glucuronosyltransferase 2 family, polypeptide B15
NM_003376.4	*VEGFA*	vascular endothelial growth factor A
NM_005429.2	*VEGFC*	vascular endothelial growth factor C
NM_003380.2	*VIM*	vimentin
NM_152415.1	*VPS37A*	vacuolar protein sorting 37 homolog A (S. cerevisiae)
NM_012479.2	*YWHAG*	tyrosine 3-monooxygenase/tryptophan 5-monooxygenase activation protein, gamma polypeptide

Appendix 11: MitoXpress results.

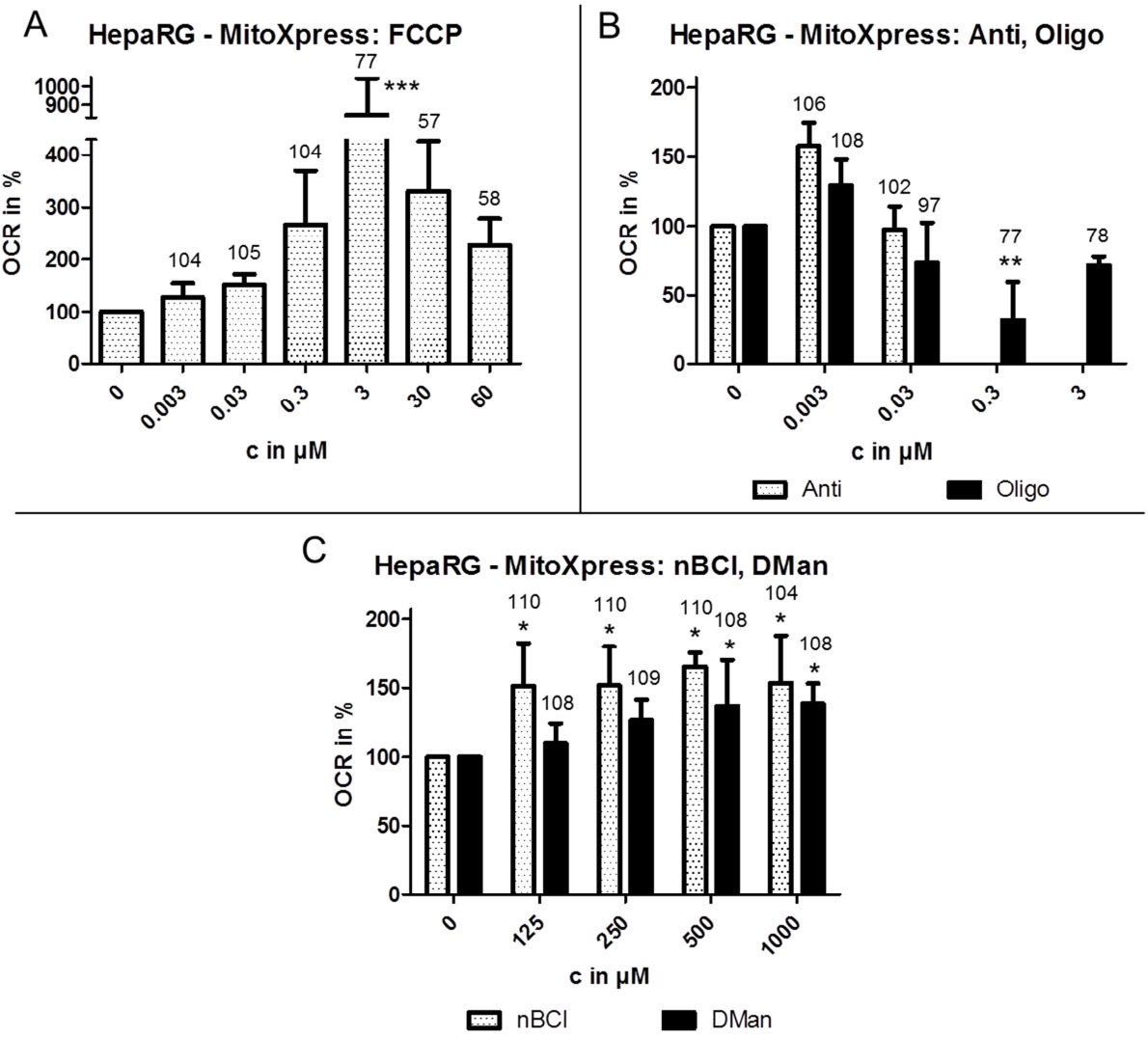

Figure 59. Oxygen consumption rate (OCR) in percent in HepaRG cells after treatment with different concentrations of the applied positive (A: carbonyl cyanide 4-(trifluoromethoxy)phenylhydrazone (FCCP), B: antimycin (Anti), oligomycin (Oligo)) and negative (C: n-butyl chloride (nBCl), D-mannitol (DMan)) controls. The percentages refer to the slope of the vehicle treated control, in relative fluorescence units per minute (RFU/min), set to 100%; corresponding to ~ 120 RFU/min. Values are given as mean of 3 biological replicates +SD. Numbers above columns represent viabilities in percent taken from the 1 h ATP test. Statistical significance is expressed in p-value ≤ 0.05 (*), ≤ 0.01 (**) and ≤ 0.001 (***) and was calculated by one-way repeated-measures analysis of variance (ANOVA) of a treatment towards the vehicle control and application of the Dunnett's post test.

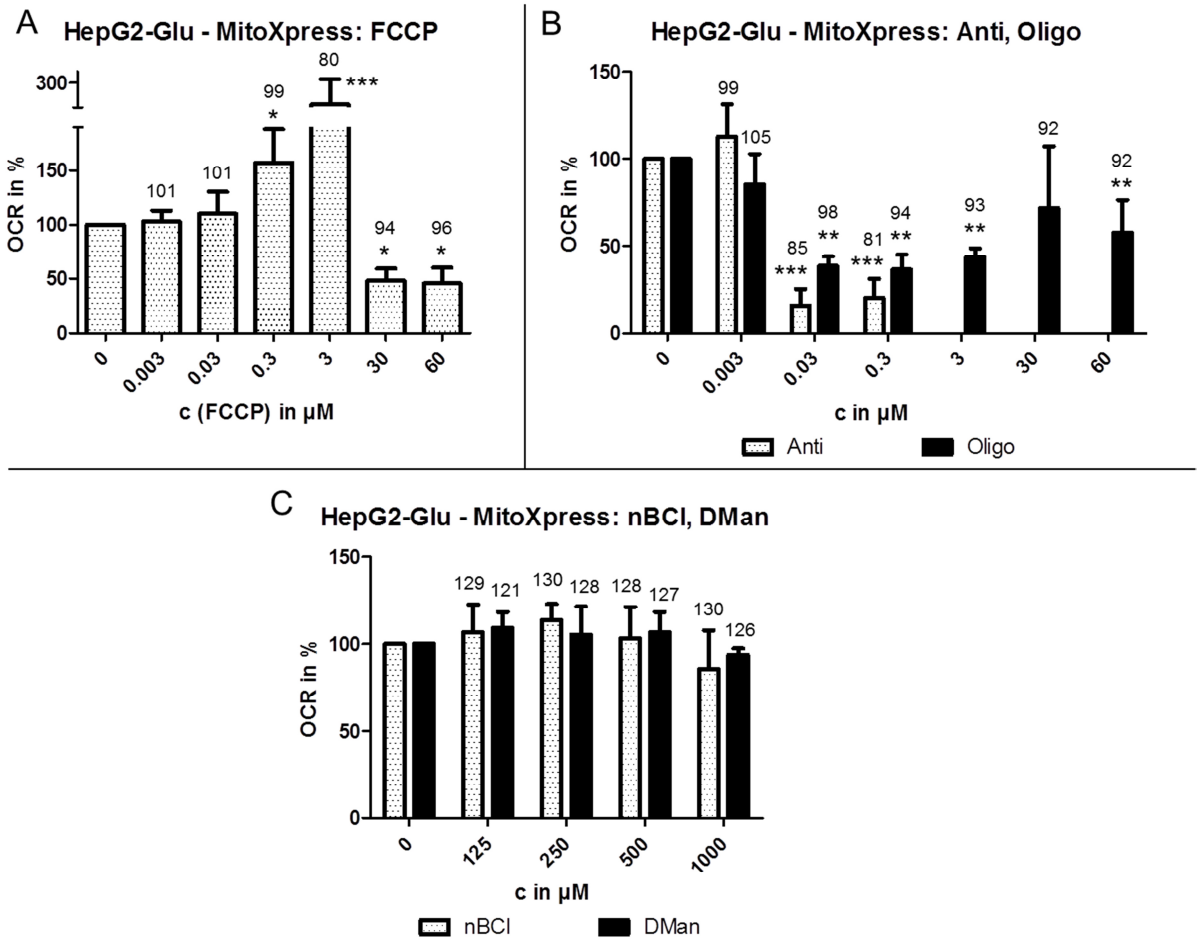

Figure 60. Oxygen consumption rate (OCR) in percent in HepG2 cells cultured in regular glucose-containing medium (HepG2-Glu) after treatment with different concentrations of the applied positive (A: carbonyl cyanide 4-(trifluoromethoxy)phenylhydrazone (FCCP), B: antimycin (Anti), oligomycin (Oligo)) and negative (C: n-butyl chloride (nBCl), D-mannitol (DMan)) controls. The percentages refer to the slope of the vehicle treated control, in relative fluorescence units per minute (RFU/min), set to 100%; corresponding to ~ 100 RFU/min. Values are given as mean of 3 biological replicates +SD. Numbers above columns represent viabilities in percent taken from the 1 h ATP test. Statistical significance is expressed in p-value ≤ 0.05 (*), ≤ 0.01 (**) and ≤ 0.001 (***) and was calculated by one-way repeated-measures analysis of variance (ANOVA) of a treatment towards the vehicle control and application of the Dunnett's post test.

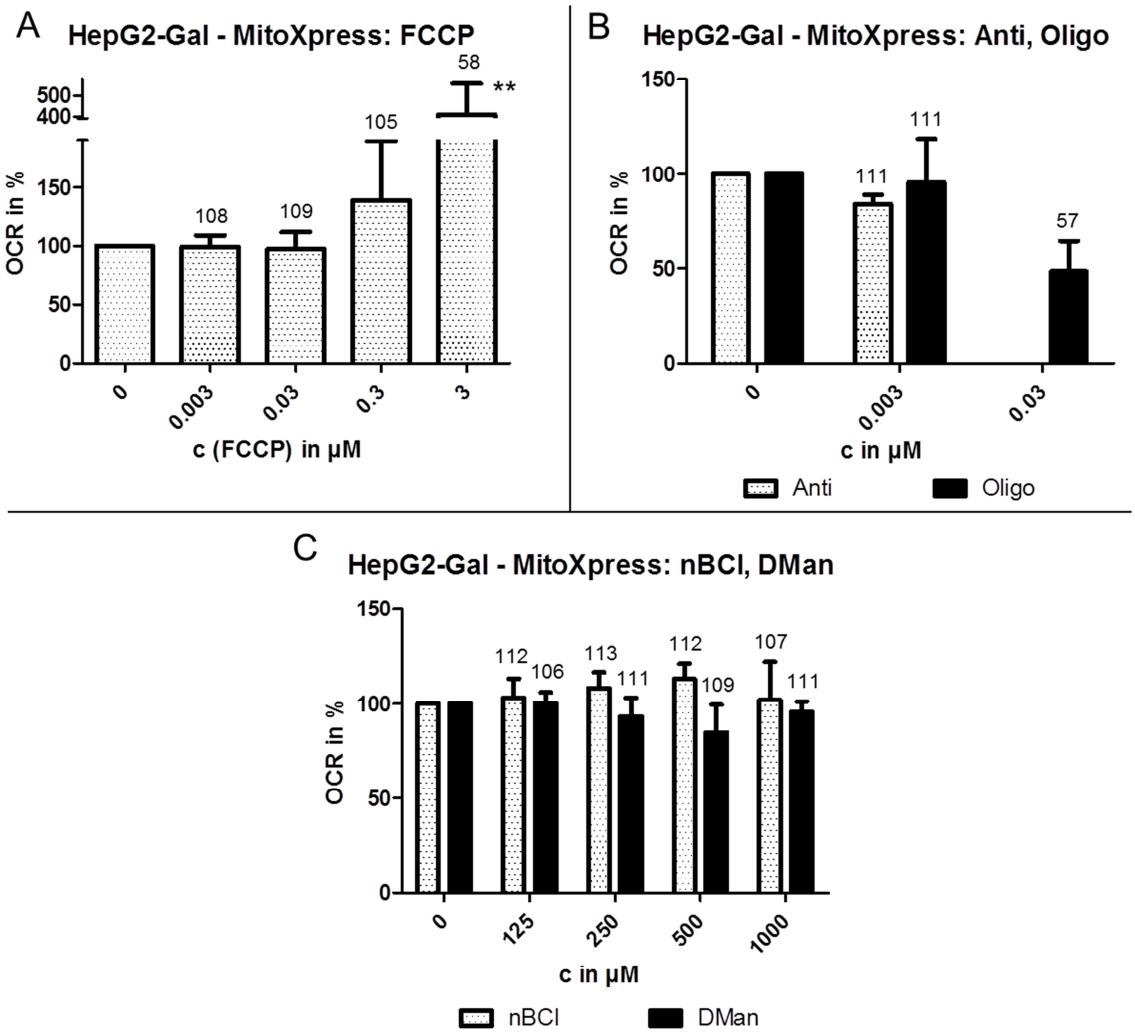

Figure 61. Oxygen consumption rate (OCR) in percent in HepG2 cells adapted to galactose-containing medium (HepG2-Gal) after treatment with different concentrations of the applied positive (A: carbonyl cyanide 4-(trifluoromethoxy)phenylhydrazone (FCCP), B: antimycin (Anti), oligomycin (Oligo)) and negative (C: n-butyl chloride (nBCl), D-mannitol (DMan)) controls. The percentages refer to the slope of the vehicle treated control, in relative fluorescence units per minute (RFU/min), set to 100%; corresponding to ~ 150 RFU/min. Values are given as mean of 3 biological replicates +SD. Numbers above columns represent viabilities in percent taken from the 1 h ATP test. Statistical significance is expressed in p-value ≤ 0.05 (*), ≤ 0.01 (**) and ≤ 0.001 (***) and was calculated by one-way repeated-measures analysis of variance (ANOVA) of a treatment towards the vehicle control and application of the Dunnett's post test.

Appendix 12: Seahorse results.

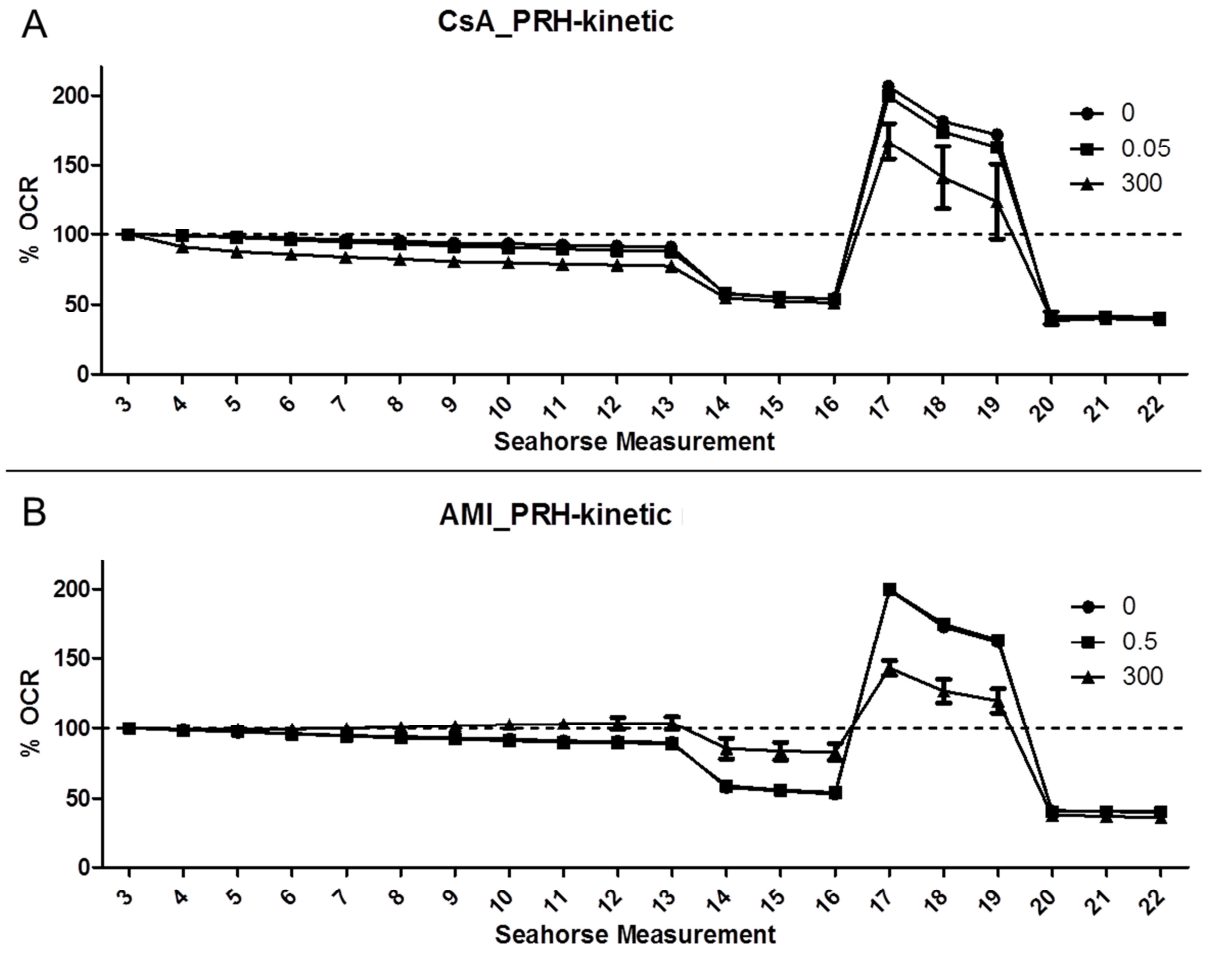

Figure 62. Oxygen consumption rate (OCR) in percent measured in primary rat hepatocytes (PRH) treated with cyclosporine A (CsA) (A; 0.05 and 300 µM), amiodarone (AMI) (B; 0.5 and 300 µM) or DMSO vehicle control (0 µM) at the indicated Seahorse measurements ("3 min mix/3 min measure" cycles). The percentages refer to the basal (3rd measurement) OCR in pmol/min set to 100%; corresponding to ~ 140 pmol/min or 150 pmol/min for CsA or AMI treated PRH, respectively. Compound or DMSO was injected after the 3rd measurement, while 1 µM oligomycin, 0.6 µM carbonyl cyanide 4-(trifluoromethoxy)phenylhydrazone (FCCP) and 1 µM antimycin/ 1 µM rotenone were injected after measurement 13, 16 and 19, respectively. Values are given as mean of 3 biological replicates ±SD.

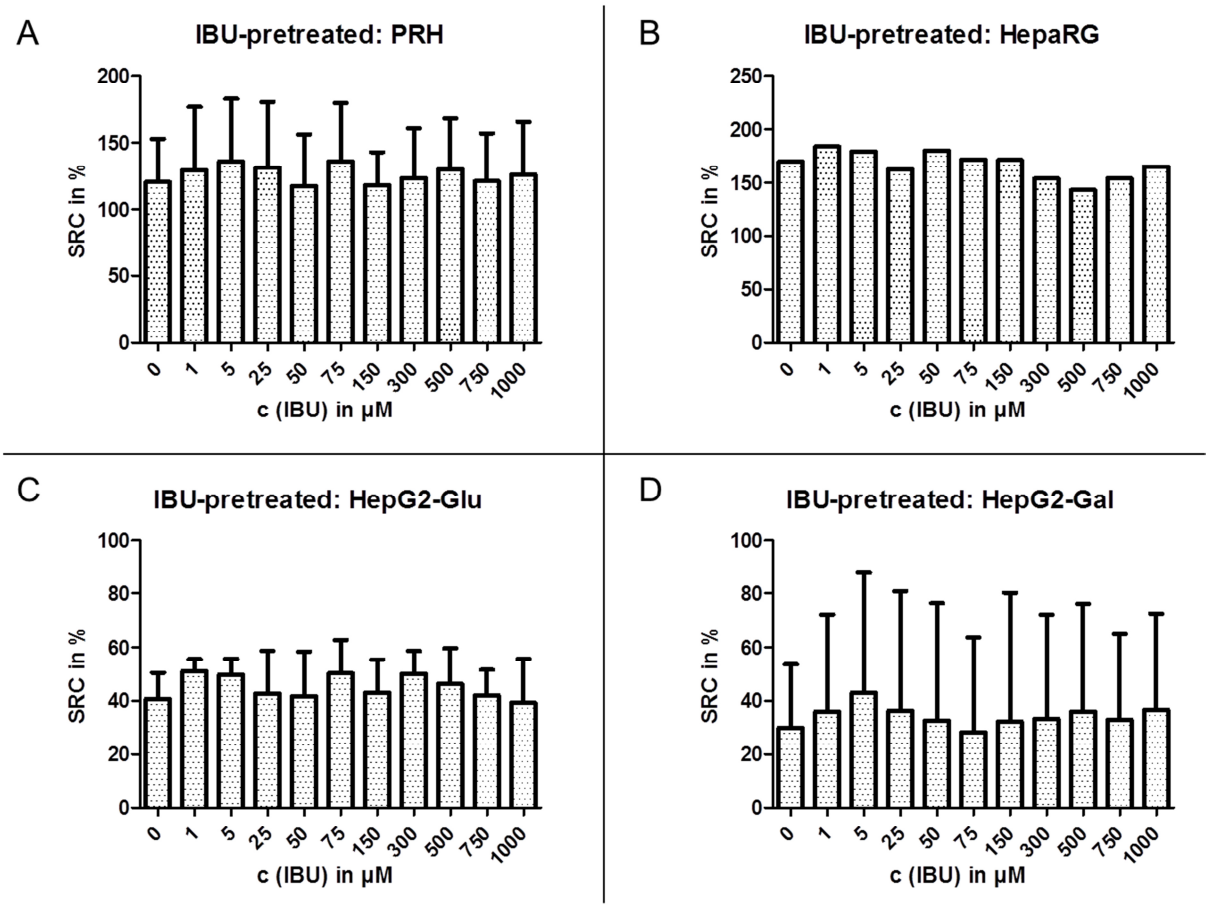

Figure 63. Spare respiratory capacity (SRC) in percent in the different hepatic systems (primary rat hepatocytes (PRH) (A), HepaRG (B), HepG2 cultured in regular glucose-containing medium (HepG2-Glu) (C) and HepG2 adapted to galactose-containing medium (HepG2-Gal) (D)) after pre-treatment for 24 h with the indicated concentrations of ibuprofen (IBU). The raw data curves of the single biological replicates were normalised to the corresponding basal (3rd measurement) oxygen consumption rate in pmol/min set to 100%. The percentages refer to the difference between basal (100%) and maximum (1st measurement after carbonyl cyanide 4-(trifluoromethoxy)phenylhydrazone (FCCP) injection) respiration. Values are given as mean of 2 (HepaRG) or 3 biological replicates +SD. Statistical significance is expressed in p-value ≤ 0.05 (*), ≤ 0.01 (**) and ≤ 0.001 (***) and was calculated by one-way repeated-measures analysis of variance (ANOVA) of a treatment towards the vehicle control and application of the Dunnett's post test. A detailed description of the compound treatment and SRC calculation is given in the Materials and Methods.

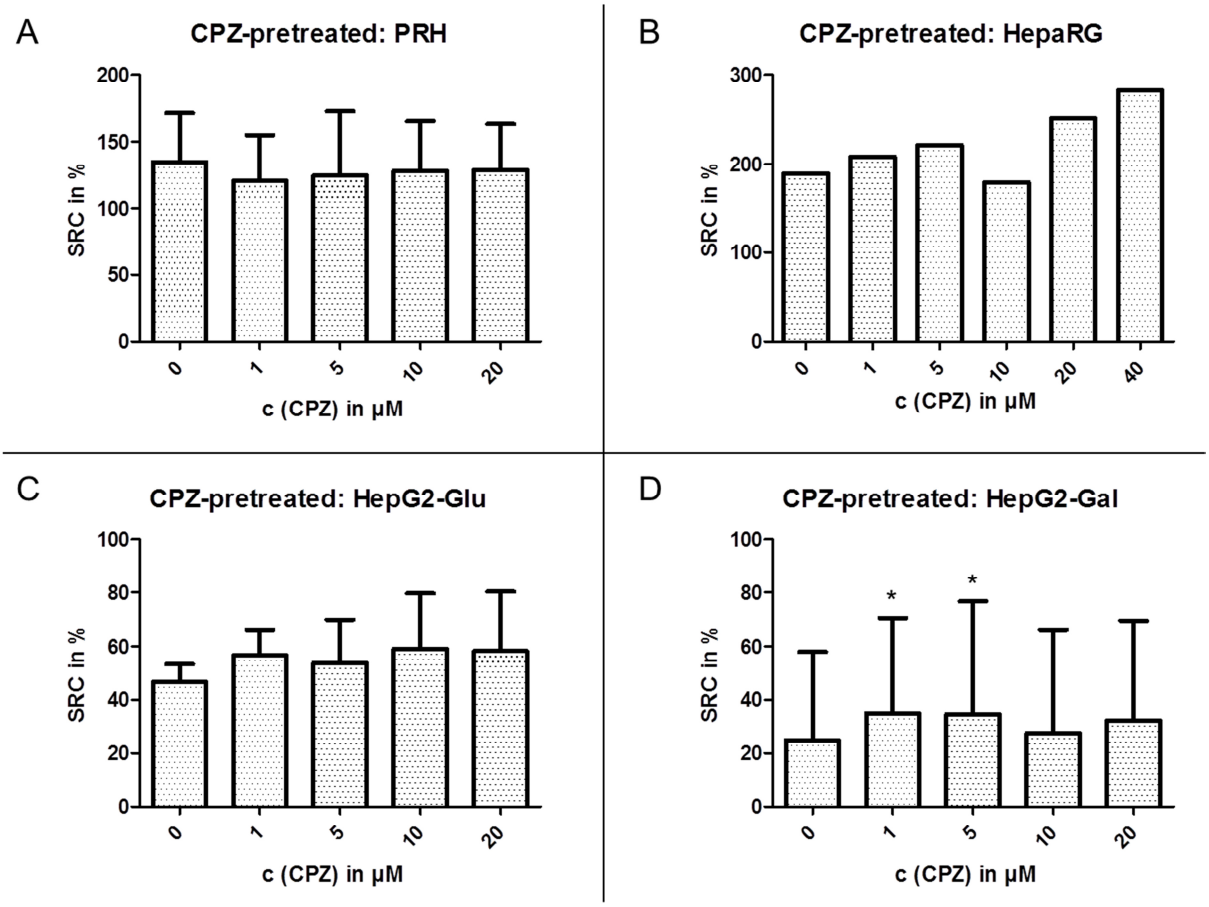

Figure 64. Spare respiratory capacity (SRC) in percent in the different hepatic systems (primary rat hepatocytes (PRH) (A), HepaRG (B), HepG2 cultured in regular glucose-containing medium (HepG2-Glu) (C) and HepG2 adapted to galactose-containing medium (HepG2-Gal) (D)) after pre-treatment for 24 h with the indicated concentrations of chlorpromazine (CPZ). The raw data curves of the single biological replicates were normalised to the corresponding basal (3rd measurement) oxygen consumption rate in pmol/min set to 100%. The percentages refer to the difference between basal (100%) and maximum (1st measurement after carbonyl cyanide 4-(trifluoromethoxy)phenylhydrazone (FCCP) injection) respiration. Values are given as mean of 2 (HepaRG) or 3 biological replicates +SD. Statistical significance is expressed in p-value ≤ 0.05 (*), ≤ 0.01 (**) and ≤ 0.001 (***) and was calculated by one-way repeated-measures analysis of variance (ANOVA) of a treatment towards the vehicle control and application of the Dunnett's post test. A detailed description of the compound treatment and SRC calculation is given in the Materials and Methods.

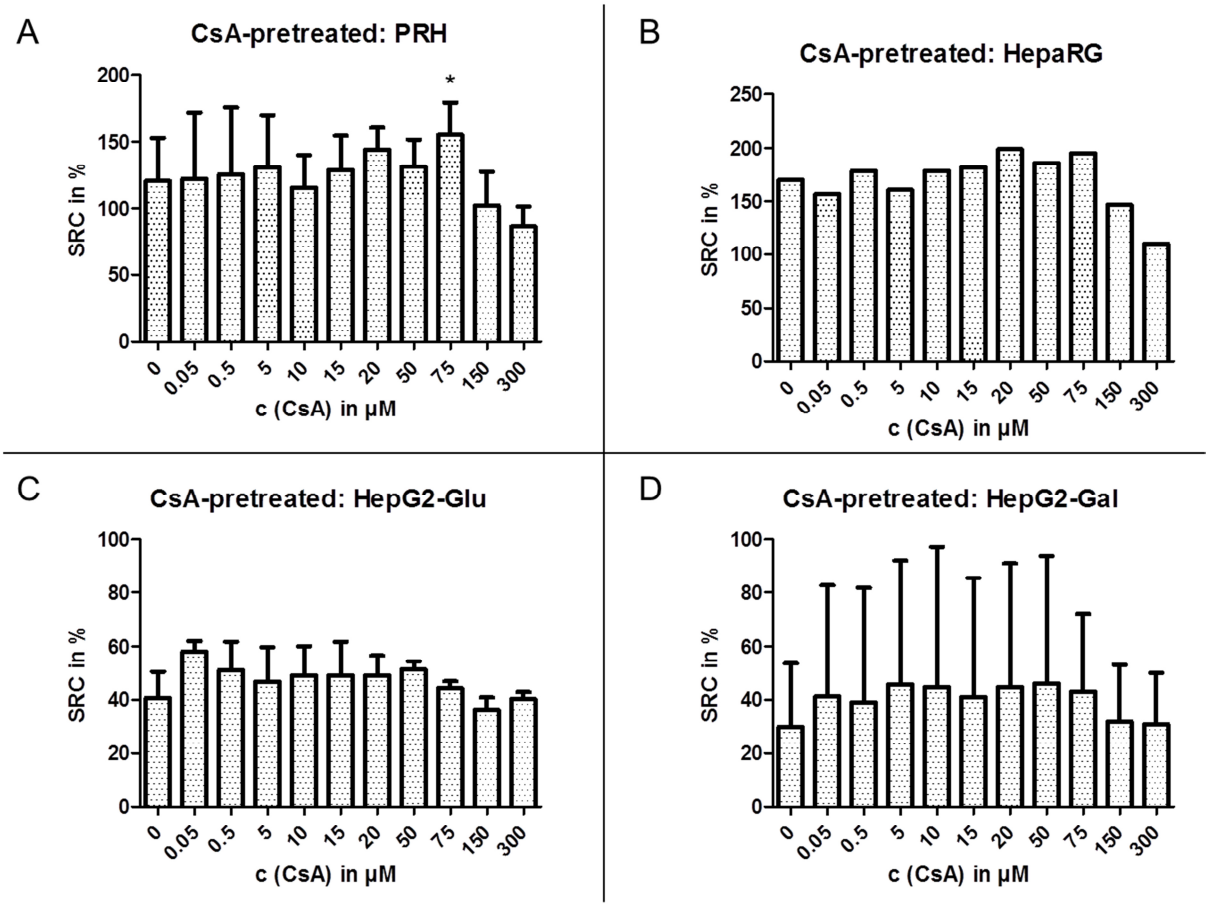

Figure 65. Spare respiratory capacity (SRC) in percent in the different hepatic systems (primary rat hepatocytes (PRH) (A), HepaRG (B), HepG2 cultured in regular glucose-containing medium (HepG2-Glu) (C) and HepG2 adapted to galactose-containing medium (HepG2-Gal) (D)) after pre-treatment for 24 h with the indicated concentrations of cyclosporine A (CsA). The raw data curves of the single biological replicates were normalised to the corresponding basal (3rd measurement) oxygen consumption rate in pmol/min set to 100%. The percentages refer to the difference between basal (100%) and maximum (1st measurement after carbonyl cyanide 4-(trifluoromethoxy)phenylhydrazone (FCCP) injection) respiration. Values are given as mean of 2 (HepaRG) or 3 biological replicates +SD. Statistical significance is expressed in p-value ≤ 0.05 (*), ≤ 0.01 (**) and ≤ 0.001 (***) and was calculated by one-way repeated-measures analysis of variance (ANOVA) of a treatment towards the vehicle control and application of the Dunnett's post test. A detailed description of the compound treatment and SRC calculation is given in the Materials and Methods.

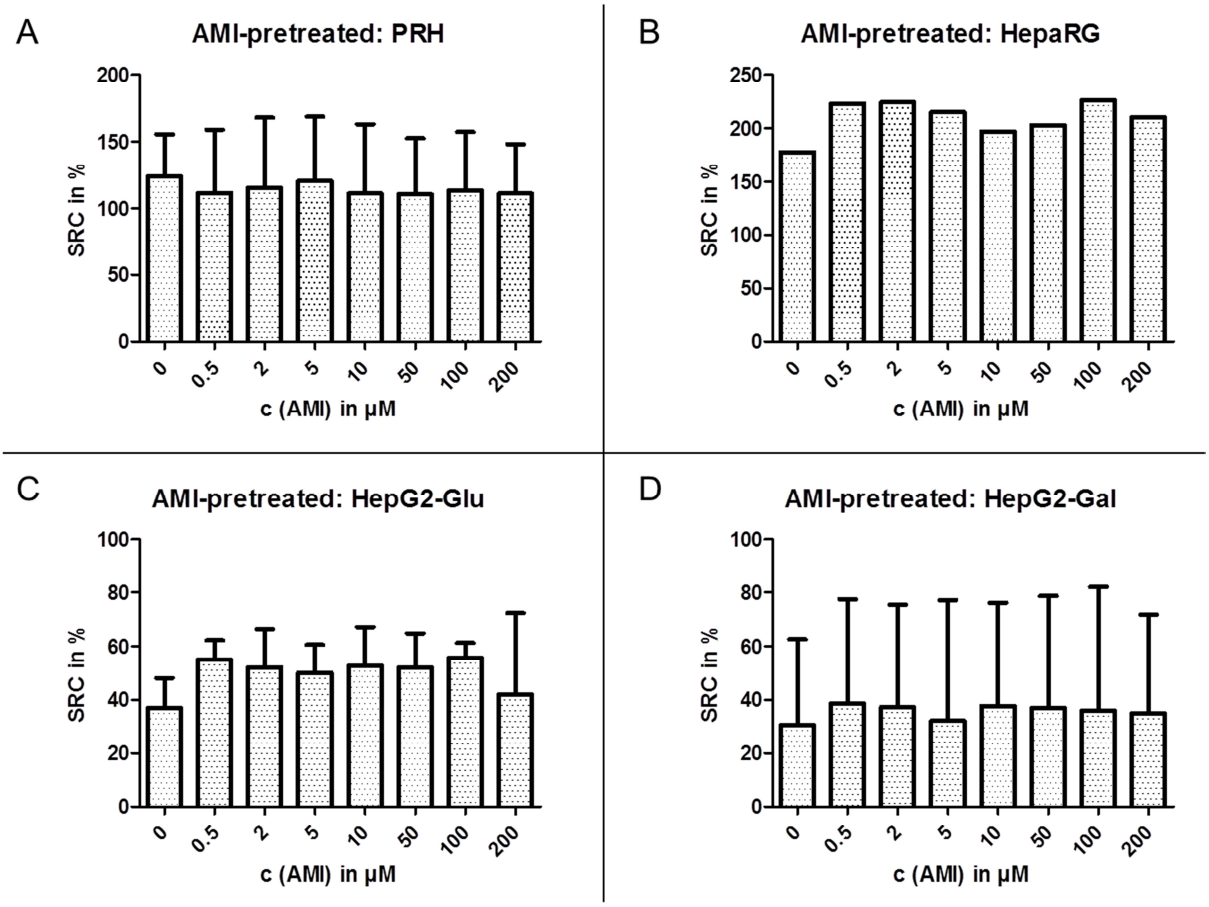

Figure 66. Spare respiratory capacity (SRC) in percent in the different hepatic systems (primary rat hepatocytes (PRH) (A), HepaRG (B), HepG2 cultured in regular glucose-containing medium (HepG2-Glu) (C) and HepG2 adapted to galactose-containing medium (HepG2-Gal) (D)) after pre-treatment for 24 h with the indicated concentrations of amiodarone (AMI). The raw data curves of the single biological replicates were normalised to the corresponding basal (3rd measurement) oxygen consumption rate in pmol/min set to 100%. The percentages refer to the difference between basal (100%) and maximum (1st measurement after carbonyl cyanide 4-(trifluoromethoxy)phenylhydrazone (FCCP) injection) respiration. Values are given as mean of 2 (HepaRG) or 3 biological replicates +SD. Statistical significance is expressed in p-value ≤ 0.05 (*), ≤ 0.01 (**) and ≤ 0.001 (***) and was calculated by one-way repeated-measures analysis of variance (ANOVA) of a treatment towards the vehicle control and application of the Dunnett's post test. A detailed description of the compound treatment and SRC calculation is given in the Materials and Methods.

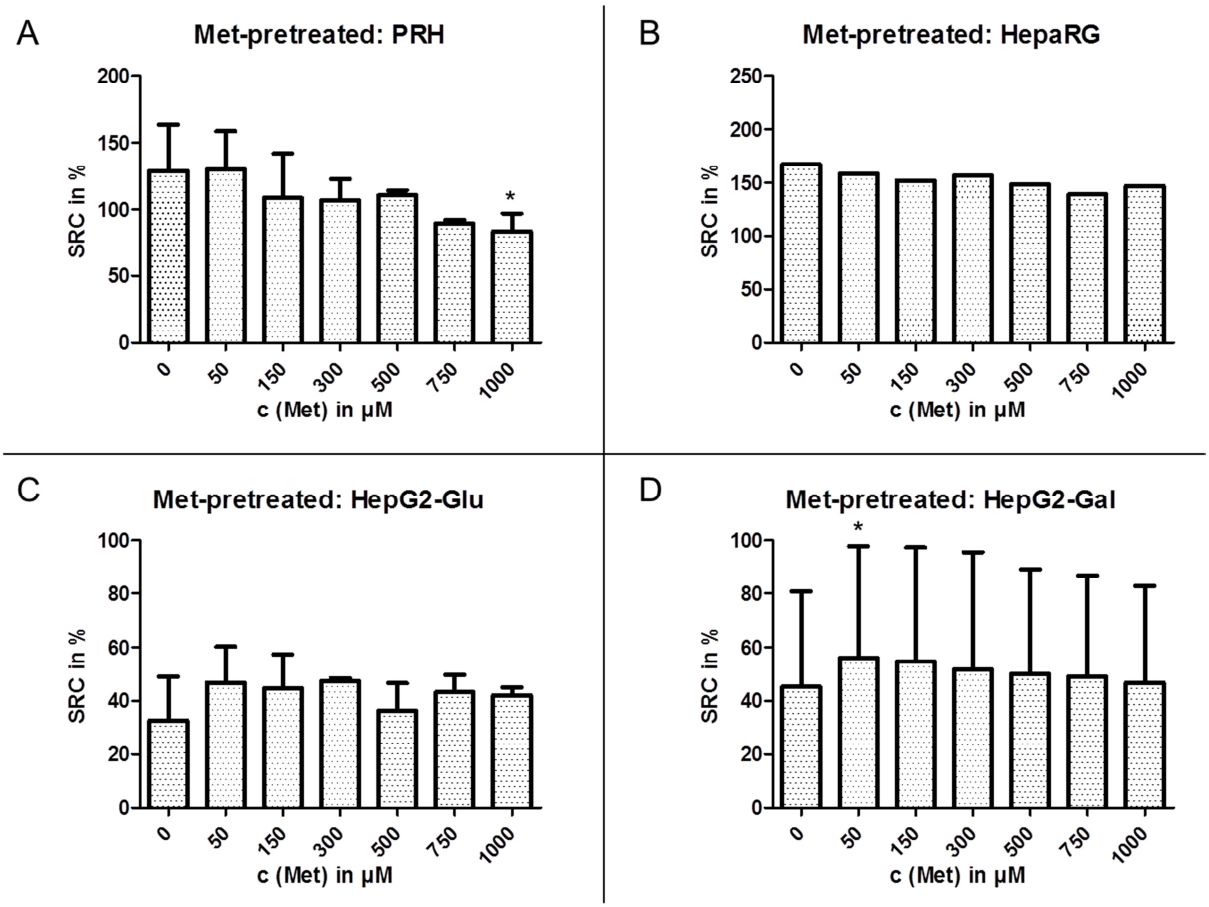

Figure 67. Spare respiratory capacity (SRC) in percent in the different hepatic systems (primary rat hepatocytes (PRH) (A), HepaRG (B), HepG2 cultured in regular glucose-containing medium (HepG2-Glu) (C) and HepG2 adapted to galactose-containing medium (HepG2-Gal) (D)) after pre-treatment for 24 h with the indicated concentrations of metformin (Met). The raw data curves of the single biological replicates were normalised to the corresponding basal (3rd measurement) oxygen consumption rate in pmol/min set to 100%. The percentages refer to the difference between basal (100%) and maximum (1st measurement after carbonyl cyanide 4-(trifluoromethoxy)phenylhydrazone (FCCP) injection) respiration. Values are given as mean of 2 (HepaRG) or 3 biological replicates +SD. Statistical significance is expressed in p-value ≤ 0.05 (*), ≤ 0.01 (**) and ≤ 0.001 (***) and was calculated by one-way repeated-measures analysis of variance (ANOVA) of a treatment towards the vehicle control and application of the Dunnett's post test. A detailed description of the compound treatment and SRC calculation is given in the Materials and Methods.

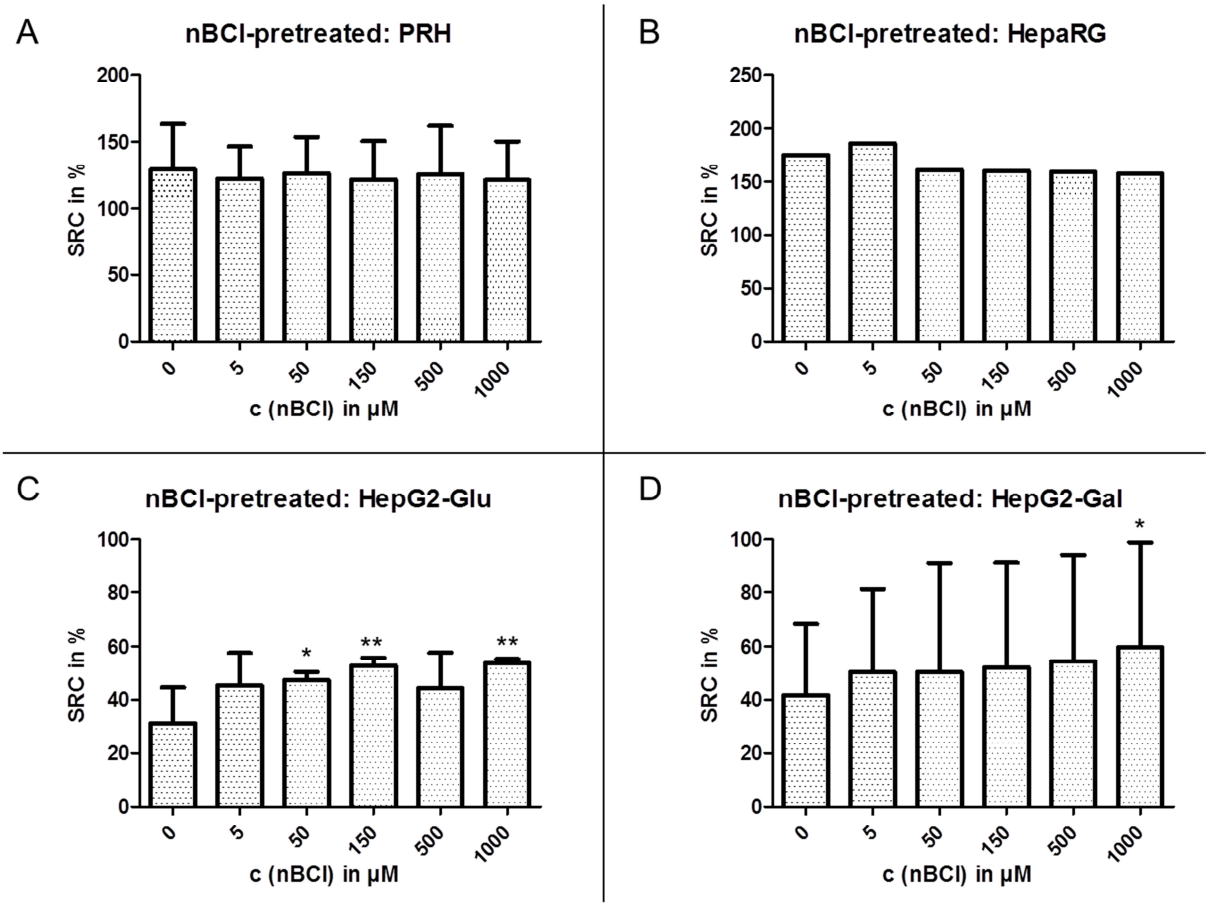

Figure 68. Spare respiratory capacity (SRC) in percent in the different hepatic systems (primary rat hepatocytes (PRH) (A), HepaRG (B), HepG2 cultured in regular glucose-containing medium (HepG2-Glu) (C) and HepG2 adapted to galactose-containing medium (HepG2-Gal) (D)) after pre-treatment for 24 h with the indicated concentrations of n-butyl chloride (nBCl). The raw data curves of the single biological replicates were normalised to the corresponding basal (3rd measurement) oxygen consumption rate in pmol/min set to 100%. The percentages refer to the difference between basal (100%) and maximum (1st measurement after carbonyl cyanide 4-(trifluoromethoxy)phenylhydrazone (FCCP) injection) respiration. Values are given as mean of 2 (HepaRG) or 3 biological replicates +SD. Statistical significance is expressed in p-value ≤ 0.05 (*), ≤ 0.01 (**) and ≤ 0.001 (***) and was calculated by one-way repeated-measures analysis of variance (ANOVA) of a treatment towards the vehicle control and application of the Dunnett's post test. A detailed description of the compound treatment and SRC calculation is given in the Materials and Methods.

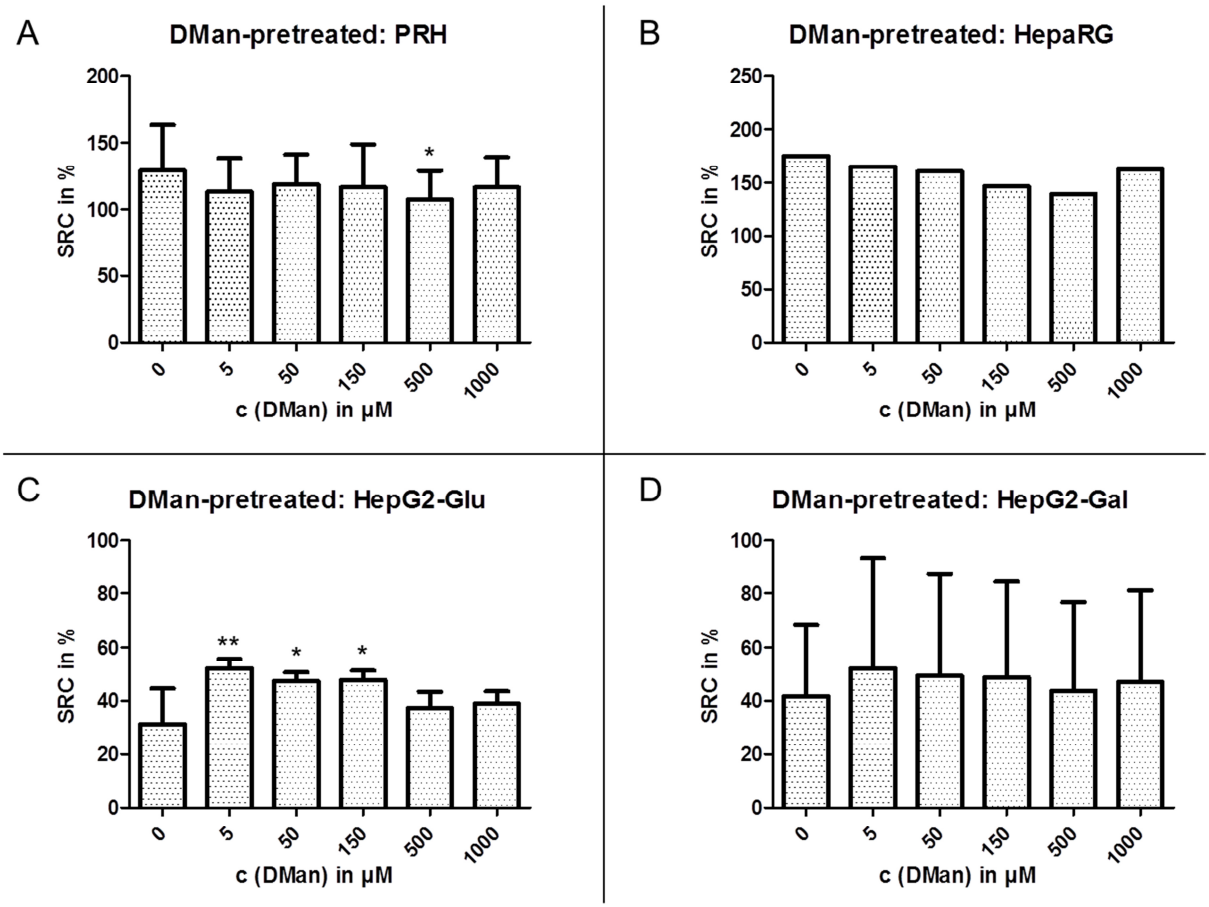

Figure 69. Spare respiratory capacity (SRC) in percent in the different hepatic systems (primary rat hepatocytes (PRH) (A), HepaRG (B), HepG2 cultured in regular glucose-containing medium (HepG2-Glu) (C) and HepG2 adapted to galactose-containing medium (HepG2-Gal) (D)) after pre-treatment for 24 h with the indicated concentrations of D-mannitol (DMan). The raw data curves of the single biological replicates were normalised to the corresponding basal (3rd measurement) oxygen consumption rate in pmol/min set to 100%. The percentages refer to the difference between basal (100%) and maximum (1st measurement after carbonyl cyanide 4-(trifluoromethoxy)phenylhydrazone (FCCP) injection) respiration. Values are given as mean of 2 (HepaRG) or 3 biological replicates +SD. Statistical significance is expressed in p-value ≤ 0.05 (*), ≤ 0.01 (**) and ≤ 0.001 (***) and was calculated by one-way repeated-measures analysis of variance (ANOVA) of a treatment towards the vehicle control and application of the Dunnett's post test. A detailed description of the compound treatment and SRC calculation is given in the Materials and Methods.